Functional characterization of Regulator of Cyclin A1 (Rca1) as an APC/C substrate and inhibitor

DISSERTATION ZUR ERLANGUNG DES
DOKTORGRADES DER NATURWISSENSCHAFTEN (DR. RER. NAT.)
DER FAKULTÄT FÜR BIOLOGIE UND VORKLINISCHE MEDIZIN
DER UNIVERSITÄT REGENSBURG

vorgelegt von
Jan, Polz

aus
Landshut

Im Jahr
2021

Das Promotionsgesuch wurde eingereicht am:
17.03.2021

Die Arbeit wurde angeleitet von:
Prof. Dr. Frank Sprenger

Unterschrift:

Für Verena und Ferdinand

Table of Contents

1. Abstract

The cell division cycle is regulated by the timely degradation of cell cycle regulators leading to an abrupt and irreversible change of protein concentration. At the centre of this system are E3 ubiquitin ligases that mark substrates for degradation by the 26S proteasome at precise time points during cell cycle progression. The anaphase promoting complex or cyclosome (APC/C) is a multi-subunit E3 ubiquitin ligase that targets a multitude of different proteins during mitosis and G1-phase in a strict order, thereby triggering mitotic events. APC/C activity is supressed during S- and G2-phase through inhibitory phosphorylation of the co-activator subunit Cdh1/Fzr and the simultaneous action of potent APC/C inhibitor proteins, allowing re-accumulation of mitotic cyclins. In *Drosophila*, Regulator of Cyclin A1 (Rca1) inhibits APC/C^{Fzr} in S- and G2-phase, whereas its degradation during G1-phase submits APC/C^{Fzr} activity required for the establishment and maintenance of G1-phase. This thesis focuses on the degradation pathway, inhibitory function, and regulation of Rca1 during cell cycle progression. Initially, Rca1 degradation during G1-phase and the involved E3 ubiquitin ligase were investigated. Therefore, an *in vivo* high-throughput method to analyze the stability of selected proteins during the cell cycle in single cells using flow cytometry of asynchronous cell populations in *Drosophila* S2R+ cells was established and verified using known substrates of the APC/C and $CRL4^{Cdt2}$ ligases. Using this "relative protein stability" (RPS) system, it was shown that Rca1 is degraded with similar kinetics like the APC/C target Geminin and that its degradation depends on APC/C^{Fzr} activity. Furthermore, several APC/C degrons and the C-terminal RL-tail were found to confer Rca1 destruction, demonstrating that Rca1 also constitutes an APC/C substrate besides being an APC/C inhibitor. Next, the functional domains of Rca1 mediating APC/C inhibition were characterized. Rca1 shares a similar arrangement of protein domains like the vertebrate APC/C inhibitor Emi1, which other than canonical pseudosubstrate inhibitors supresses APC/C activity mainly through regulation of E2 binding and only to a lesser extent by blocking substrate recruitment. Using an *in vivo* APC/C activity assay, several protein domains including a C-terminal KEN- and D-box, a ZBR, and a RL-tail that confer APC/C inhibition by Rca1 were identified. The requirement of similar protein domains for sufficient APC/C inhibition like Emi1 suggests that Rca1 also restricts APC/C activity by a more sophisticated mechanism than just acting as a pseudosubstrate competitive inhibitor. Finally, the molecular mechanisms turning Rca1 from an APC/C inhibitor to substrate were explored. It could be demonstrated that phosphorylation of Rca1 at the C-terminal inhibitory domains increased its ability to inhibit the APC/C and in parallel phosphorylation of N-terminal residues caused a stabilization of Rca1. Just as phosphorylation, nuclear localization of Rca1 was shown to be essential for sufficient degradation during G1-phase. Additionally, a phospho-dependent interaction with 14-3-3 was discovered that is probably involved in Rca1 sequestration by enhancing its nuclear export, thereby providing a first hint linking Rca1 phosphorylation and localization as potential regulatory mechanisms converting Rca1 from an APC/C inhibitor to substrate.

2. Introduction

2.1. The eukaryotic cell cycle – a fundamental aspect of life

The cell cycle is a series of highly coordinated events through which a cell duplicates its genome, grows, and divides. Cell reproduction constitutes a fundamental aspect of live allowing the formation of highly specialized tissues or organs, sexual reproduction, growth, development, and replacement of dead or damaged cells. The eukaryotic cell cycle is commonly divided in four phases: G1-, S-, G2- and M-phase. After cell division each cell cycle begins with a period of growth, called G1-phase. Cellular macromolecules including RNAs, proteins and membranes are synthesized that are required for DNA replication. Cells can also enter a transient non-dividing state called G0-phase that is either induced by external signalling or unfavourable environmental conditions like low amounts of mitogens or growth factors. However, cells can re-enter cell cycle progression out of the quiescence state upon mitogen stimulation (Dong et al., 1997)(Pollard et al., 2017). The genetic material is replicated during S-phase resulting in chromosomes that consist of two identical sister chromatids. S-phase is followed by another gap phase G2 where cell growth and synthesis of proteins required for M-phase takes place. The first three phases (G1-, S-and G2-phase) are also called interphase, as taken together they represent by far the longest part of the cell cycle and constitute the period between the M-phase of successive cell cycles. The last stage of the cell cycle, M-Phase is divided into mitosis, the nuclear division and separation of daughter chromosomes, and cytokinesis the division of the cell into two new cells (Figure 1)(Cooper, 2000; Morgan, 2007; Walker, 2016).

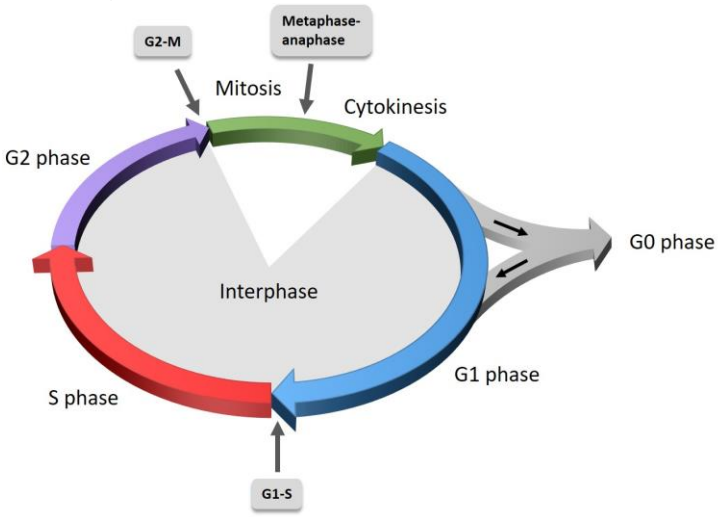

Figure 1| The eukaryotic cell cycle

The standard eukaryotic cell cycle consists of G1-, S-, G2- and M-phase. In S-phase DNA is replicated. During M-phase, the replicated DNA is equally distributed into two new cells, by a series of highly regulated events. M-phase is comprised of mitosis (nuclear division and chromosome separation) and cytokinesis (cell division). M- and S-phase are separated by two gap phases, G1- and G2-phase that prepare the cell for the upcoming cell cycle stages. G1-, S- and G2-phase are collectively called interphase that is by far the longest part of the cell cycle and provides time for cell growth. Cells can also remain in a quiescent, non-proliferative state called G0. The cell cycle is highly regulated and contains three major transitions: Entry into a new cell cycle is marked by the G1/S transition that regulates the start of S-phase. Initiation of mitosis is governed by the G2/M transition. After onset of mitosis, separation of sister chromatids is halted by the metaphase to anaphase transition until correct spindle attachment. (Figure adapted from Hochegger et al., 2008).

Mitosis consists of five highly regulated consecutive stages: prophase, prometaphase, metaphase, anaphase, and telophase. Prophase begins with initial chromosome condensation followed by centrosome separation and the initiation of mitotic spindle assembly. During prometaphase, nuclear envelope breakdown takes place allowing attachment of sister chromatids to the mitotic spindle at the kinetochore. The attached chromatids begin to move towards the centre of the cell. Prometaphase is followed by metaphase, where the sister chromatids completely align at the metaphase plate, the centre of the mitotic spindle. In anaphase the cohesion complex of the chromosome is dissolved after correct attachment to the spindle and the single chromatids are pulled in opposite directions towards the poles of the mitotic spindle. In the last stage of mitosis, telophase, the mitotic spindle is disassembled, chromatids are condensed, and nuclear components are repackaged into two newly formed nuclei. M-phase is completed by cytokinesis, the division of the cytoplasm resulting in two daughter cells sharing the same genetic information (Cooper, 2000; Morgan, 2007).

2.2. Cell cycle progression is defined by distinct transitions

The events of the cell cycle must be tightly controlled in a spatio-temporal manner ensuring the correct timing and order of events. Each phase can only occur after successful completion of the preceding phase and under advantageous environmental conditions. There are three major switch-like transitions that behave in an all-or-non response. Once activated, irreversible cellular processes are induced providing a unidirectionality to the cell cycle. Before entering a new cell cycle, a cell must pass the Start (yeast) or restriction point (mammals) in late G1. Once crossed, cells commit to mitogen-independent cell cycle progression (Johnson et al., 2013). After the restriction point cells pass the G1-S transition and DNA replication is induced. The second, G2-M transition regulates initiation and entry into mitosis. The third transition, metaphase to anaphase, monitors sister chromatid segregation and includes completion of mitosis and cytokinesis (Figure 1). Cell cycle progression is halted at the corresponding transition if the previous events have not been completed successfully or if inconvenient conditions force a cell cycle arrest. This regulatory system is under control of an oscillatory network driven by changes in protein phosphorylation and ubiquitin-dependent protein degradation. Central to this system are the cyclin-dependent protein kinases (Cdks) and different E3 ubiquitin ligases mediating proteasomal protein degradation (Morgan, 2007; Teixeira et al., 2013).

2.3. Cyclin dependent kinases, master regulators of the cell cycle

Cyclin dependent kinases (Cdks) are master regulators of cell division controlling cell cycle progression through posttranslational modification of a vast number of key regulatory proteins. Cdks are serine/threonine kinases that are characterized by a conserved catalytic core comprised of an ATP-binding pocket, a PSTAIRE-like cyclin binding domain and the T-loop or activation loop. Cdks alone are inactive and are activated by a two-step process. In a first activation step, Cdks interact with their regulatory

subunit called cyclins (Cyc). In a second step, full activation is catalyzed through phosphorylation of a conserved threonine residue in the T-loop mediated by Cdk-activating kinases (CAKs). Substrate recognition and phosphorylation by activated Cdks is driven by three interactions (Figure 2 A): First, Cdk active site recognizes substrates on the minimal consensus motif S/TP with the optimal sequence S/TPxR/K (x represent any amino acid) (Suryadinata et al., 2010). Alternative non S/TP motifs with the minimal sequence S/TxxR/K and a more favourable (P)xS/Tx[R/K]$_{2\text{-}5}$ are also recognized and phosphorylated by Cdks (Suzuki et al., 2015). Second, cyclins target substrates via short linear motifs (SLiMs). In mammals, E- and A-type cyclins interact with a short RxL motif also called the cy motif (cyclin binding motif) via a hydrophobic patch (MRAIL). Whereas, D-type cyclins possess a N-terminal LxCxE motif mediating interaction with members of the pocket protein family (Dowdy et al., 1993; Ewen et al., 1993; Landis et al., 2007; Topacio et al., 2019). Recent studies *in S.cerevisiae* completed a set of specific interaction motifs for the four classes of major cyclins by discovering the missing M- and G2-Cdk motifs: G1 cyclins use a LP motif (Bhaduri et al., 2011) and S-and G2-cyclins share the RxL motif (Kõivomägi et al., 2011 a). The recently found PxF (PxxPxF) and LxF (ExLxF) motifs are unique for G2- and M-cyclins, respectively (Örd et al., 2019 a, 2020)(Figure 2 B). Third, cyclin dependent kinase subunits (Cks) interact with cyclin-Cdk complexes and a phosphorylated TP site in the substrate thereby directing multisite phosphorylation (Kõivomägi et al., 2011 b; McGrath et al., 2013). Cks have originally been discovered in yeast and are expressed in all eukaryotic lineages (Hayles et al., 1986; Hadwiger et al., 1989). For instance, mammals possess two highly conserved Cks proteins Cks1 and Cks2 (Cks85A and Cks30a in Drosophila)(Swan et al., 2005).

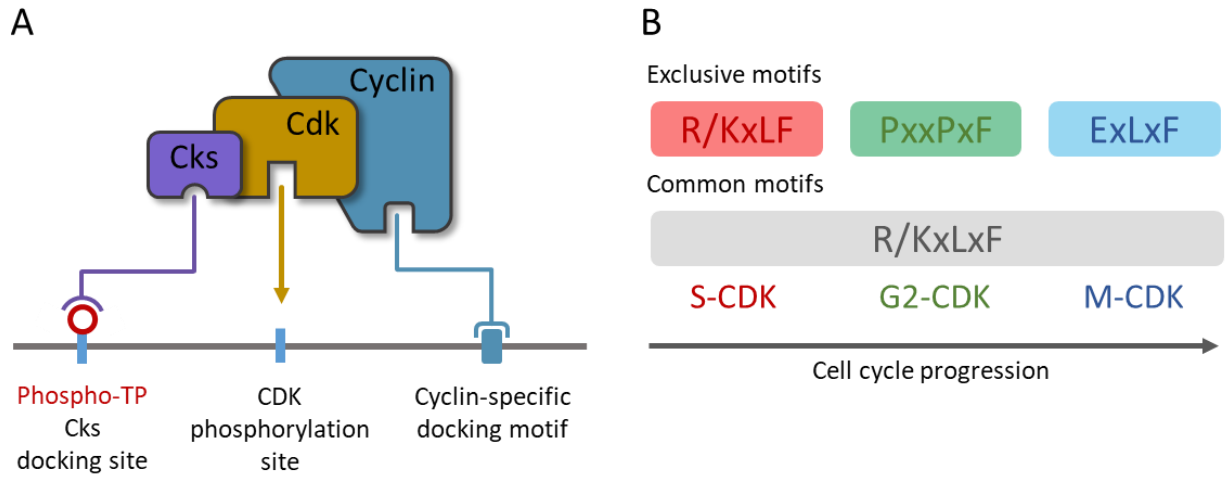

Figure 2| Cdk substrate recognition mediated by specific docking motifs

(**A**) Cdk substrate phosphorylation is mediated by the combination of Cdk, cyclin and Cks interaction with the substrate. Cdks recognize specific phosphorylation sites within the substrate and the cyclin interacts with a cyclin specific docking motif. The cyclin dependent kinase subunit (Cks) interacts with a phosphorylated TP site promoting multisite phosphorylation of the substrate. (**B**) The common RxL motif shared by S-, G2-, and M-cyclins is complemented by unique interactions motifs for each cyclin class in *S.cerevisiae*.(Figure adopted from Örd et al., 2020)

Cdk activity oscillates during cell cycle progression due to changes in the concentration of cyclins, whereas their own abundance stays relatively constant during the cell cycle. The formation of specific cyclin-Cdk complexes at distinct time points is responsible for cell cycle progression by triggering key cell cycle events. In yeast, only a single Cdk, Cdc28 (*S. pombe*) or Cdc2 (*S. cerevisiae*), drives cell cycle progression in combination with different cyclins that are expressed at certain cell cycle stages. During evolution, there has been an expansion in the number of Cdks and cyclins. For example, in humans there are 20 Cdks and 13 cyclin groups, but only Cdk 2, 4 and 6 (interphase Cdks) and Cdk1 (mitotic Cdk) in combination with ten cyclins belonging in four different classes (D-type: CycD1, D2 and D3; E-type: CycE1, E2; A-type: CycA1, A2; B-type: CycB1, B2 and B3) are directly involved in control of the cell division cycle (Morgan, 2007; Malumbres, 2014; Whittaker et al., 2017; Roskoski, 2019). The number of cyclin subtypes varies among species even though cyclins are well conserved in their function among eukaryotes. For instance, in *Drosophila* there is only one version of A-, D-, and E-type cyclins and two versions of B-type cyclins (CycB and CycB3).

Based on their occurrence and function cyclins and Cdks can be divided in four classes: G1-, G1/S-, S-, and M-cyclin-Cdk complexes. A classical cyclin specificity model of cell cycle regulation is based on the sequential activation of different cyc-Cdk complexes due to oscillating cyclin levels. The G1 cyclin, CycD in combination with Cdk4/6 coordinates cell growth and is essential for the entry in a new cell cycle by regulation of the restriction point. Initiation of S-phase depends on CycE-Cdk2 activity whereas maintenance and completion of S-phase depend on CycA-Cdk2. Both CycA and CycB can form complexes with Cdk1 and are required for mitosis. CycA-Cdk1 is active during G2-phase and early stages of mitosis promoting mitotic entry. Whereas CycB-Cdk1 is responsible for different mitotic vents, especially mitotic spindle assembly and alignment of sister chromatids at the metaphase plate. The decline of CycB-Cdk1 activity after anaphase causes mitotic exit and cytokinesis (Figure 3 A).

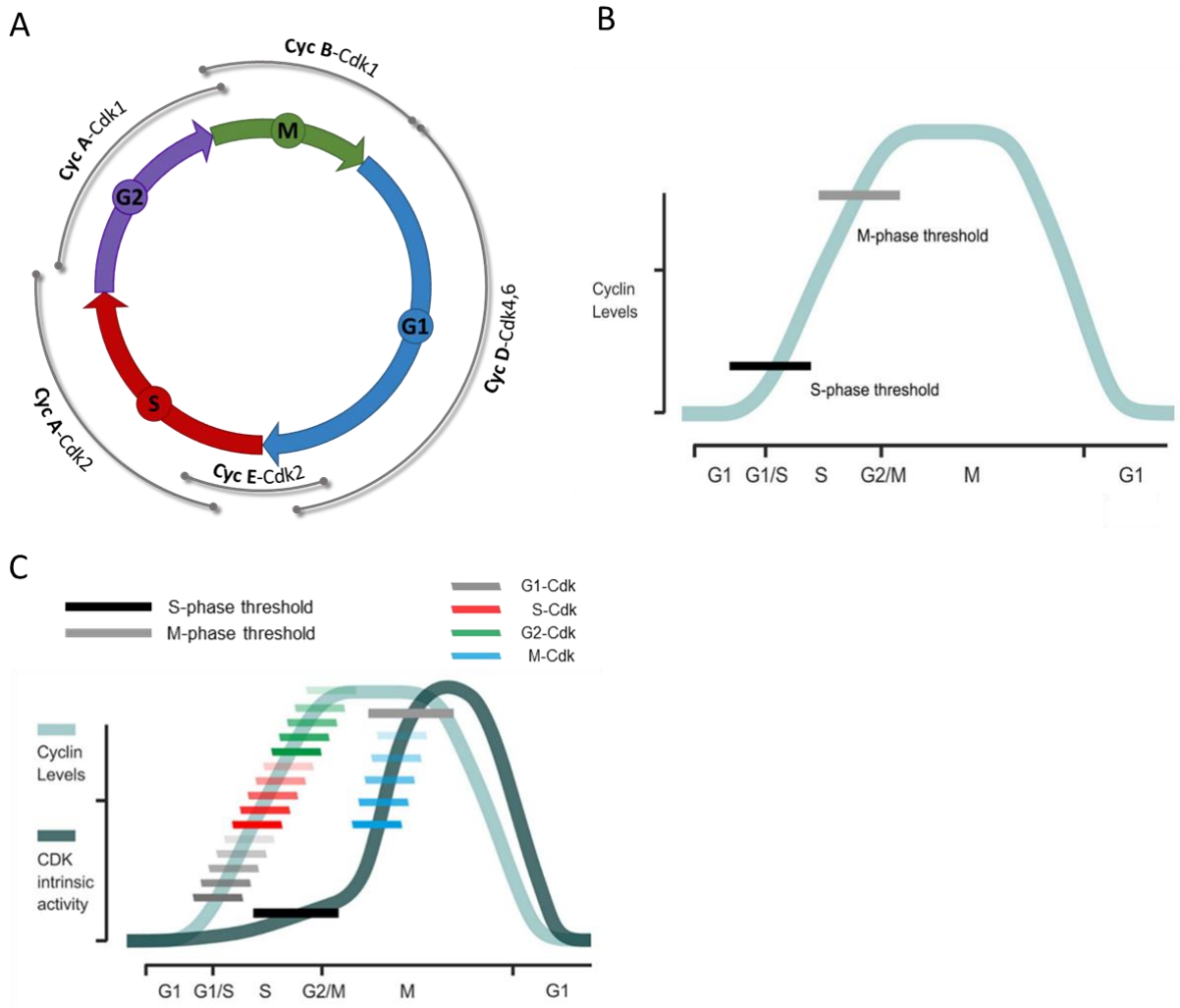

Figure 3| Different models of Cdk function

(**A**) The cyclin specificity model explains Cdk function by sequential Cdk activation caused by waves of different cyclins. CycD levels rise in response to cell growth and extracellular growth factors during G1 promoting entry into a new cell cycle in combination with Cdk4, 6. S-phase entry is initiated by CycE-Cdk2 followed by CycA-Cdk2 activity maintaining S-phase progression. Cdk1 interacts with CycA and CycB triggering key events of mitosis. (**B**) The quantitative model is based on accumulating Cdk activity resulting in different thresholds triggering stage specific events. (**C**) The quantitative model of specificity combines different Cdk threshold levels and the sequential occurrence of cyclins resulting in changing specificities but also a common baseline specificity. Specific cyclin interaction motifs in combination with the linear encoded multisite phosphorylation code allows a broader dynamic range of threshold modulation. As Cdk complexes specificity increases sequentially, the intrinsic CDK activity has a delayed response compared to cyclin-Cdk complexes. (Figure B and C adopted from Örd et al., 2019 b)

However, a difficulty to this classical model proposing that temporal ordering of the cell cycle depends on the formation of distinct cyclin-Cdk complexes at certain time points and their biochemical specificity towards different substrates arose as different lines of evidence in murine cells (Geng et al., 2003; Kozar et al., 2004; Santamaría et al., 2007; Kalaszczynska et al., 2009), *Xenopus* egg extracts (Moore et al., 2003) and fission yeast (Coudreuse et al., 2010) demonstrated that specific cyclin-Cdks can be eliminated without major impact on the cell cycle. G1- and S-cyclins are dispensable and can be compensated by mitotic cyclin-Cdk complexes, but not the other way round (reviewed in Uhlmann et al., 2011).

An alternative quantitative model, already postulated in 1996 by Nurse and Stern (Stern et al., 1996) states that different thresholds of Cdk activity based on increasing cyclin accumulation lead to phosphorylation of different targets at individual threshold levels, thereby driving cell cycle progression (Figure 3 B). This model is supported by the findings that a single chimeric cyclin-Cdk fusion protein can maintain sequential temporal ordering of the cell cycle in fission yeast (Coudreuse et al., 2010). Furthermore, it was shown that early and late substrates have different phosphorylation rates in dependence on rising Cdk activity levels (Swaffer et al., 2016). Recently, a mechanistic explanation has been postulated how different threshold levels and cell cycle execution time can be encoded into cyclin-Cdk complexes and their substrates by a linear multisite phosphorylation code. The rate of multisite phosphorylation is influenced by the relative distance of the phosphorylation site to the Cks- and cyclin docking sites, the distribution of SP and TP sites within the substrate, consensus motif elements around the phosphorylation site and other parameters like dephosphorylation specificity (Kõivomägi et al., 2013; Örd et al., 2019 c; b). This individual barcode determines the sequential ordering of several substrates that are phosphorylated by a single cyclin-Cdk complex.

With the recent discovery of so far missing M- and G2-Cdk specific docking mechanisms in yeast a new model was proposed, combining the cyclin specificity and the quantitative model. The unified quantitative model of specificity is based on the findings that each class of M-, G1/S-, S-, and G2- cyclins possess a unique linear docking motif in the correlating set of substrates increasing Cdk substrate specificity. Cdk substrate specificity is also increased by cyclins in the order of their expression during the cell cycle (Kõivomägi et al., 2011 a). Taken together cyclin specificity in addition to Cks1 binding provides a wider range of thresholds and switching orders allowing fine tuning of cell cycle events (Figure 3 C). Also, the single mitotic cyclin system can be explained as M-cyclins have a key to all threshold levels thereby providing a robust and safe system that can maintain cell cycle progression alone. However, fine tuning of the threshold levels by different cyclins and the multisite phosphorylation code would be especially important for competitive fitness (Örd et al., 2019 a; b).

Due to their important functions, dysregulation of cyclin-Cdk activity can culminate in severe defects ranging from unrestrained proliferation to genomic instability or even cell death. There are several regulatory mechanisms ensuring correct Cdk function. Cdk activity can be regulated on the level of cyclins by increased cyclin degradation in combination with decreased cyclin gene expression mediated by inhibitory gene regulatory proteins. Another regulatory mechanism is the Wee1-Cdc25 circuit. Besides activation promoting phosphorylation in the T-loop, activated cyclin-Cdk complexes can be inactivated by phosphorylation of a tyrosine or threonine residue (Tyr15 in all Cdks, Tyr15 and Thr14 in Cdks of higher eukaryotes) within the ATP-binding site mediated by members of the Wee1 kinase family. This inhibitory phosphorylation is opposed by dephosphorylation carried out by members of the Cdc25 phosphatase family providing a switch like feature of Cdk activation (Morgan, 1997, 2007; Pavletich, 1999). A further regulatory mechanism is the inhibition by cyclin dependent kinase inhibitors

(CKI). In mammals, there exist several CKIs belonging to either the class of INK4-family or the Cdk interacting protein/kinase inhibitor protein (CIP/KIP) family. The members of the INK4 CKIs (p15, p16, p18 and p19) are specific inhibitors for Cdk4 and Cdk6 in G1-phase. In contrast to this, CIP/KIP members (p21, p27 and p57) are capable to inhibit all Cdks. They are all characterized by a Cdk inhibitory domain (CDI) and a short RxL motif that mediates interactions with both, the cyclin and the Cdk (Morgan, 2007). In Drosophila, only two CKIs are present, Roughex (Rux) and the CIP/KIP member Dacapo (Dap). Rux is important for G1 establishment and maintenance by inhibiting S- and M-Cdk complexes but not G1/S-Cdk complexes (Foley et al., 1999; Avedisov et al., 2000). Dap instead was shown to specifically inhibit CycE-Cdk2 preventing a premature G1/S transition (De Nooij et al., 1996; Lane et al., 1996).

2.4. Protein degradation mediated by the ubiquitin proteasome pathway

Besides phosphorylation, protein degradation is a further key regulatory mechanism in the course of the cell cycle. The fast and irreversible proteolysis of cell cycle regulators in a spatiotemporal manner is crucial for proper cell cycle progression and results in a unidirectional order of molecular events (Bassermann et al., 2014). In eukaryotes, protein degradation is regulated by a major proteolytic system called the ubiquitin proteasome pathway (UPP). The UPP is based on the post-translational modification called ubiquitination, the attachment of a small protein ubiquitin (Ub) to a substrate (Figure 4 A). Typically, Ub is linked via a covalent bond between the α-carboxyl group of its C-terminal glycine residue to the ε-amino group of an internal lysine residue or the α-amino group of the N-terminal residue of the substrate (Ciechanover et al., 2004). Alternative attachment to cysteine, serine and threonine residues have also been discovered, expanding the combinatorial possibilities and biological functions even further (McDowell et al., 2016). Ubiquitination can occur in diverse forms with completely different outcomes, which is usually referred to as “ubiquitin code”. The linkage of a single (monoubiquitination) or multiple single Ub molecules (multi-monoubiquitination) are the most abundant modifications that regulate various processes from endocytosis, DNA repair, signal transduction to even proteasomal degradation (Braten et al., 2016; reviewed in Hicke, 2001; Pickart, 2001; Livneh et al., 2016). Polyubiquitination, the sequential addition of further Ub molecules to one of the eight amino groups (M1, K6, K11, K27, K29, K33, K48, and K63) of the previously attached Ub results in the formation of polyubiquitin chains of variable length, linkage type and configuration (homo- and heterotypic/branched Ub chains) (Figure 4).

Depending on the linkage type, polyubiquitination is involved in diverse molecular processes. K11, K29 and K48 linked chains serve as proteolytic signals, whereas K48 is the most abundant linkage in all organisms subjected to proteomics serving as the primary mediator for protein degradation mediated by the UPP (Komander et al., 2012). K63-linked chains were initially accounted to “proteasome-independent” processes such as inflammatory signal transduction (Ohtake et al., 2016), DNA repair (Spence et al., 1995), protein trafficking (reviewed in Erpapazoglou et al., 2014), and selective autophagy (Kirkin

et al., 2009). However, K63 linked or mixed chains were also found in the context of proteolytic degradation (Saeki et al., 2009; Ohtake et al., 2016). The function of K6-linked polyUb chains is still elusive but they have been found to be indirectly linked to DNA repair (Morris et al., 2004) and mitochondrial quality control mechanisms (Ordureau et al., 2015). K27 linkages are involved in DNA damage response (Gatti et al., 2015) and innate immunity (Wang et al., 2014). Mixed K29/33 chains are implicated in kinase modification (e.g. inhibition of Wnt signalling; T cell receptors)(Huang et al., 2010; Fei et al., 2013). More recently K33 chains have also been found to be involved in anterograde protein trafficking (Yuan et al., 2014) and innate immune response (Liu et al., 2018). PolyUb chains formed via M1 have regulatory functions in NF-κB signalling (reviewd in Spit et al., 2019). Finally, Ub molecules themselves can be subjected to different forms of posttranslational modifications, including phosphorylation (reviewed in Swatek et al., 2016), acetylation (Ohtake et al., 2015), SUMOylation (Hendriks et al., 2015), Neddylation (Hjerpe et al., 2012), ADP-ribosylation (Yang et al., 2017), phosphoribosylation (Bhogaraju et al., 2016), succinylation (Weinert et al., 2013), and deamidation (Cui et al., 2010), yet adding another layer of complexity to the ubiquitin code (Figure 4 B). Ubiquitination is carried out by the consecutive action of a three-enzyme cascade composed of an E1- (ubiquitin activating), an E2- (ubiquitin conjugating), and an E3-enzyme (ubiquitin ligase). In a first step, the C-terminal glycine of ubiquitin is activated in an ATP dependent reaction by the E1 enzyme.

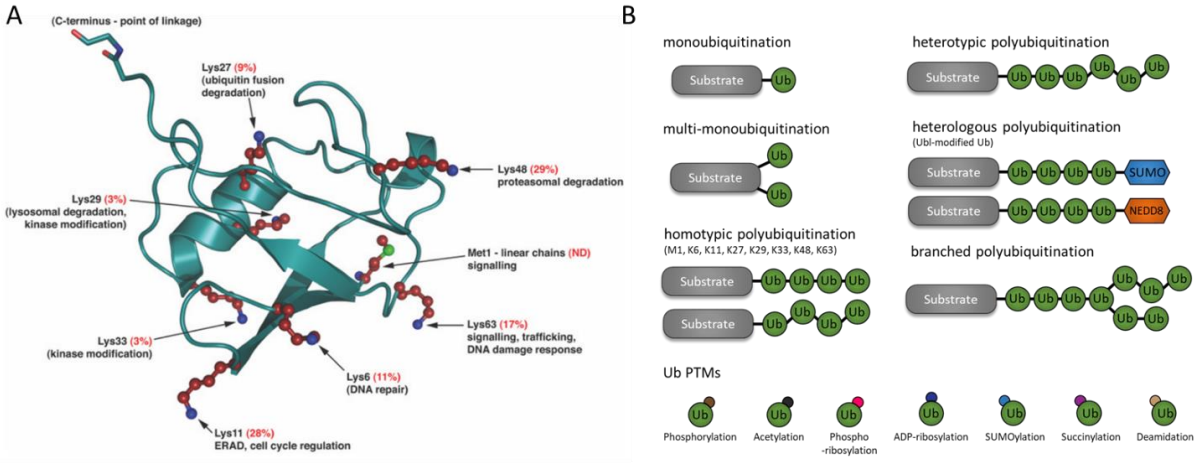

Figure 4| The ubiquitin code

(**A**) Structure of the 76 amino-acid protein ubiquitin. The seven lysine residues (red, with blue nitrogen atoms) and the Met1 (red with green sulfur atom) can be linked to further Ub molecules, creating polyubiquitin chains. Depending on the linkage type, polyUb chains are involved in diverse processes. The red numbers represent the relative abundance of the linkage type in S. cerevisiae, with K48 being the most abundant linkage form (Xu et al., 2009) (Figure adopted from Komander, 2009). (**B**) Different forms of ubiquitination. Substrates can be either modified with a single or several single Ub molecules (mono- or multi-monoubiquitination respectively). Elongated polyUb chains can be formed either homotypic with just one linkage type or heterotypic with mixed forms. Ub chains can be linked to ubiquitin like proteins (Ubl) such as Small Ubiquitin-Related Modifier (SUMO) or neural-precursor-cell-expressed developmentally down-regulated 8 (Nedd8). Ubiquitin itself can also be subjected to different post-translational modification (PTM).(Figure adopted and modified from Kliza et al., 2020)

Adenylation of the carboxy terminal glycine residue results in a ubiquitin adenylate intermediate, releasing pyrophosphate, followed by the formation of a covalent high energy thioester bond (~) between Ub and a catalytic cysteine in E1 (E1~Ub) along with the release of AMP (Haas et al., 1983). Most species contain only a single E1 enzyme, for example in *Drosophila* Uba1 is the sole E1 (Lee et al., 2007), whereas in humans there are two forms, UBE1 and UBEL2 (Pelzer et al., 2007).

In a next step, the activated Ub is transferred from the E1 enzyme to a catalytic cysteine residue of the E2 enzyme by transthiolation (E2~Ub) (reviewed in Olsen et al., 2013). Compared to E1 enzymes, E2 ubiquitin conjugating enzymes comprise a larger superfamily divided in 17 families based on comprehensive phylogenetic analysis. All E2s are characterized by conserved ubiquitin conjugating (Ubc) domain harbouring the catalytic cysteine residue. In *Drosophila* 32 members were identified, while in humans 37 E2 enzymes exist (Michelle et al., 2009).

In a last step, an E3 ubiquitin ligase mediates the final step of Ub transfer from a selected E2~Ub to a specific substrate forming an isopeptide bond between the C-terminal Gly^{76} and the lysine ε-amino group carried out by a nucleophilic attack. In contrast to E1 and E2, E3 ligases represent the biggest part with more than 600 E3 ligase genes in humans and several hundred in Drosophila. E3 ubiquitin ligases are divided into three classes based on different catalytic domains and the ubiquitin transfer mechanism: Really Interesting New Gene (RING), Homologous to E6-AP Carboxyl Terminus (HECT), or Ring-Between-Ring (RBR). RING E3s are characterized by a RING or U-box-fold catalytic domain. They act as scaffolding platforms, binding both the E2 enzyme and the substrate simultaneously, thereby promoting direct transfer of the Ub molecule from the E2 onto the substrate via their RING domain (reviewed in Deshaies et al., 2009). The class of RING E3s is further divided into single- and multi-subunit E3 ligases based on their structure (reviewed in Hegde, 2010). Distinct from RING E3 ligases, HECT E3s ubiquinate their substrates in a two-step reaction. After binding the E2~Ub complex via the C-terminal HECT domain, a catalytic cysteine within the domain accepts the Ub molecules, forming an E3~Ub thioester intermediate, before transferring them onto the substrate (reviewed in Rotin et al., 2009; Zheng et al., 2017). The RBR proteins constitute a unique family of RING-HECT hybrids sharing features of both the RING and HECT E3 ligases. RBR E3s are characterized by three domains consisting of two RING finger domains, RING1 and RING2, separated by a central in between-RINGs (IBR) zinc binding domain. The RING1 domain is responsible for interaction with the Ub-loaded E2 enzyme, whereas the RING2 domain catalyzes the transthioesterfication via a catalytic cysteine residue (E3~Ub intermediate) receiving the Ub molecule from RING1 which is then transferred to the target substrate (Wenzel et al., 2011; Walden et al., 2018). The ubiquitination cascade has a hierarchical structure with only one or very few E1, several E2 and hundreds of E3 enzymes, whereas E2s determine the type of Ub linkage and the vast number of E3s is responsible for substrate selection.

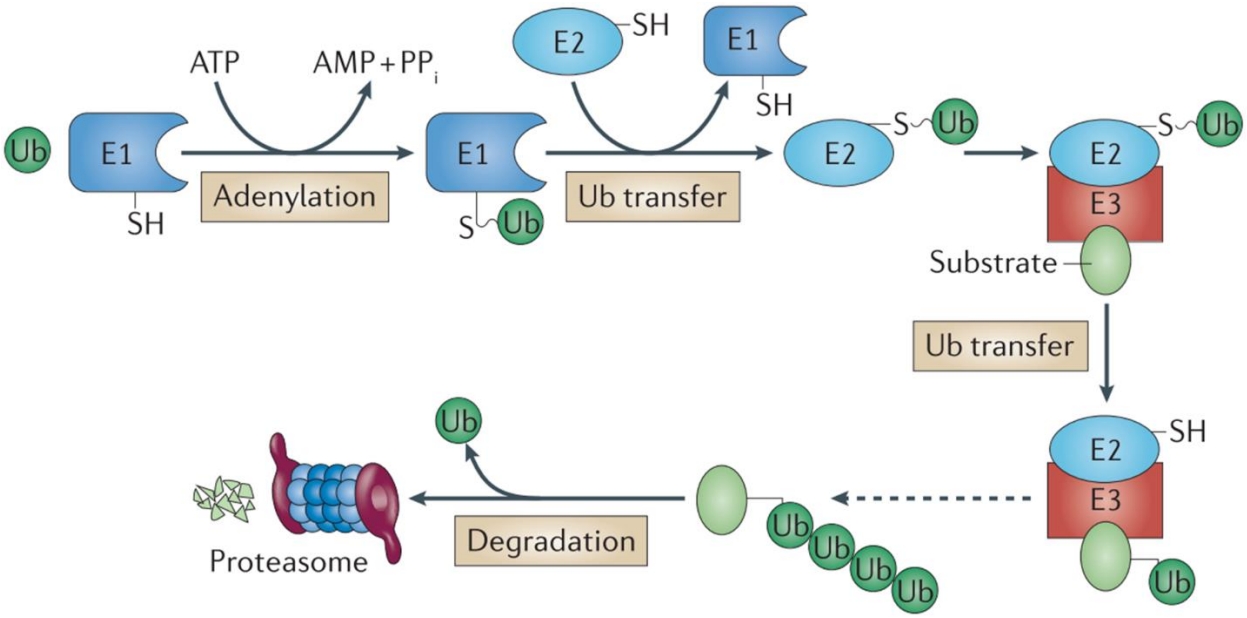

Figure 5| The ubiquitin proteasome pathway

The ubiquitin proteasome pathway marks substrates via polyubiquitination (mainly K48 and K11 linked polyub chains) for protein degradation by the 26S proteasome. Ubiquitination is carried out by the sequential activity of three enzymes: The E1 Ub-activating enzyme, the E2 Ub-conjugating enzyme, and the E3 Ub-protein ligase. Ub is activated in an ATP consuming reaction mediated by the E1 enzyme. First an Ub adenylate intermediate (adenylation) is formed which is then transferred to a catalytic cysteine in the E1 creating a high energy thioester bond, releasing AMP and pyrophosphate (PPi). The activated Ub is further transferred onto the E2 enzyme. Finally, the E3 ubiquitin ligase catalyzes the transfer of Ub to the substrate forming an isopeptide bond. Repeated addition of Ub molecules to the previously attached Ub results in the formation of poly-Ub chains that are recognized by the 26S proteasome, marking the substrate for degradation (Maupin-Furlow, 2011).

The substrates marked with polyubiquitin chains, especially K48- and K11- linkages, are recognized and degraded by the 26S proteasome, a large protein complex composed of two functionally distinct subcomplexes: The 20S core particle (CP) that houses peptidase activities and is capped at either one or both sides by the 19S regulatory particle (RP) that is responsible for identification, binding, deubiquitination, unfolding, and translocation of substrates to the CP (Figure 6 A). The CP has a barrel shape formed by four axial stacked heteroheptameric rings, two outer α-rings and two inner β-rings, each consisting of seven distinct subunits $\alpha_{1\text{-}7}$ and $\beta_{1\text{-}7}$, respectively. The outer α-rings create opposing pores gating the entrance of substrates and the removal of degradation products via N-terminal extensions of several α-subunits. The two inner β-rings generate a central chamber containing six catalytic sites for peptide bond cleavage, provided by the β_1, β_2 and β_5 subunits. The RP is divided into two sub-complexes the lid and the base. The base directly contacts the CP and is composed of a ring of six AAA-ATPase subunits, named regulatory particle triple-A protein 1-6 (Rpt1-6) and 4 non ATPase subunits Rpn1, Rpn2, Rpn10 and Rpn13 (regulatory particle non-ATPase). The ring of Rpt subunits is required for ATP dependent unfolding of the substrate and opening the axial pore by repositioning the extensions of the CP α-subunits. The lid is constituted of 9 non-ATPase subunits (Rpn3, Rpn5-Rpn9, Rpn11, Rpn12, and Rpn15) and is required for the de-ubiquitination of the captured substrates (Figure 6 B)

(reviewed in Marshall et al., 2019). Rpn11 serves as an integral deubiquitination enzyme (DUB) accompanied by transiently associated DUBs, UCH37 and Ubp6, releasing the attached polyUb chains (Verma et al., 2002; Hamazaki et al., 2006; Aufderheide et al., 2015). Free polyUb chains are further recycled into single Ub moieties by the action of a unique DUB called isopeptidase T (isoT) (Wilkinson et al., 1995). Recognition and selection of ubiquinated substrates is mediated by either intrinsic receptors of the non-ATPase subunits Rpn1, Rpn10, Rpn13, and possibly Rpn15 or extra-proteasomal ubiquitin binding proteins (Dsk2, Rad23, and Ddi1) (Marshall et al., 2019). These shuttle proteins bind Ub via one or more C-terminal ubiquitin-associated (UBA) domains (Hofmann et al., 1996; Wilkinson et al., 2001) coupled to a N-terminal ubiquitin-like (UBL) domain that interacts with the 19S CP ubiquitin receptors shuttling the cargo to the proteasome (Elsasser et al., 2002, 2004; Walters et al., 2002; Chen et al., 2019). Fully assembled 26S proteasomes are spread throughout the nucleus and the cytoplasm, albeit often they are predominantly found in the nucleus accumulating especially at the inner nuclear membrane in close proximity to nuclear core complexes (Pack et al., 2014; Albert et al., 2017). Surprisingly, proteasome activity in yeast nuclei was drastically reduced compared to cytosolic localized proteasomes (Dang et al., 2016; Enam et al., 2018).Curiously, less proteasomes were detected in the nucleus compared to the cytoplasm in this study, contradicting the observation of enriched nuclear localization in vivo (reviewed in Chowdhury et al., 2015). Till now proteasome activity measurements in the two compartments has varied greatly and the impact of proteasome localization in parallel with its activity remains elusive (Dang et al., 2016; Kito et al., 2020).

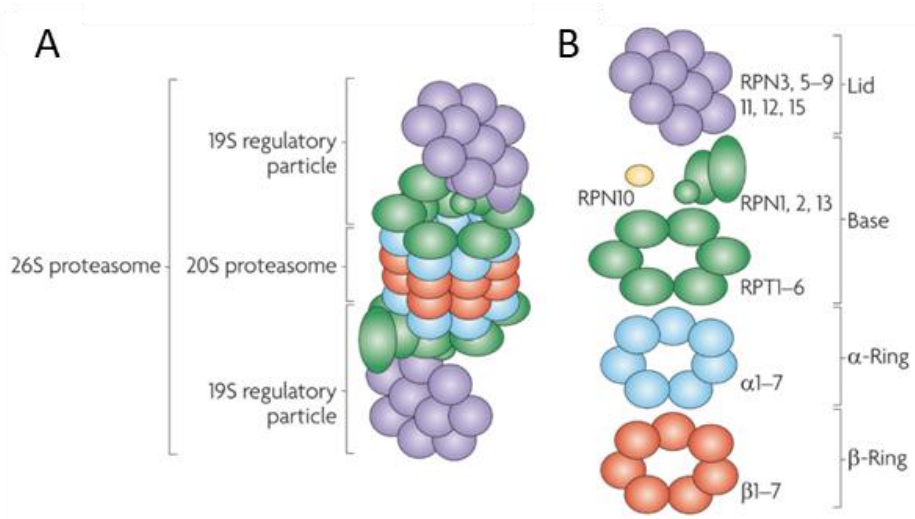

Figure 6| Structure of the 26S proteasome

(**A**) The 26S proteasome is composed of two subcomplexes, the 19S regulatory particle (RP) and the catalytic 20S core particle (CP). (**B**) The RP is divided into lid and base; the lid consists of 9 subunits, Rpn3, 5-9, 11, 12, and 15. The base is made up of six AAA-ATPase proteins (Rpt1-6) and four non ATPase subunits Rpn1, 2, 13 and 10. Rpn10 exist in a proteasome bound and free form, making it unique among the proteasome subunits. The CP is composed of two outer α -rings and two inner β-rings, each consisting of seven distinct subunits (α_{1-7} and β_{1-7}). (Figure adopted from Murata et al., 2009)

2.5. The CRL4^{Cdt2} E3 ubiquitin ligase

The CRL4^{Cdt2} ubiquitin ligase belongs to the E3 cullin RING ligases (CRLs) and functions during S-phase and after DNA damage targeting a wide spectrum of proteins that are crucial for cell cycle regulation and DNA damage response (reviewed in Panagopoulos et al., 2020). CRL4^{Cdt2} comprises a cullin scaffold (Cul4), an adaptor protein DNA damage-binding protein 1 (DDB1), a RING domain protein Rbx1 that recruits the E2 enzyme, and a substrate recognition factor, in this case Cdt2 (Cdc10-dependent transcript 2) (Figure 7) (Havens et al., 2011). Substrate recognition by Cdt2 and subsequent ubiquitination by CRL4 requires the substrate to be bound to DNA associated proliferating cell nuclear antigen (PCNA) trimer. PCNA functions as a processivity factor for DNA polymerases and its requirement limits CRL4^{Cdt2} activity to S-phase and DNA damage response (Abbas et al., 2011). CRL4^{Cdt2} substrates contain a "PIP degron" composed of a PCNA interacting protein (PIP) box, an eight amino acid linear motif with four essential residues QxxΨxxϑϑ (Ψ is any hydrophobic amino acid L, V, I or M and ϑ is an aromatic residue, Y or F) and a basic residue four amino acids downstream of the PIP box, also called "B+4"(Havens et al., 2009, 2011, 2012; Abbas et al., 2010; Tsanov et al., 2014). The PIP degron together with an acidic residue on PCNA forms a bipartite binding interface that is recognized by Cdt2 ensuring that only PCNA associated substrates are ubiquitinated (Havens et al., 2012). Recently, it was shown that Cdt2 itself also binds PCNA via a C-terminal PIP box in combination with a DNA binding domain ensuring that only substrates bound to DNA associated and not free PCNA are targeted for degradation (Hayashi et al., 2018; Leng et al., 2018; Mazian et al., 2019).

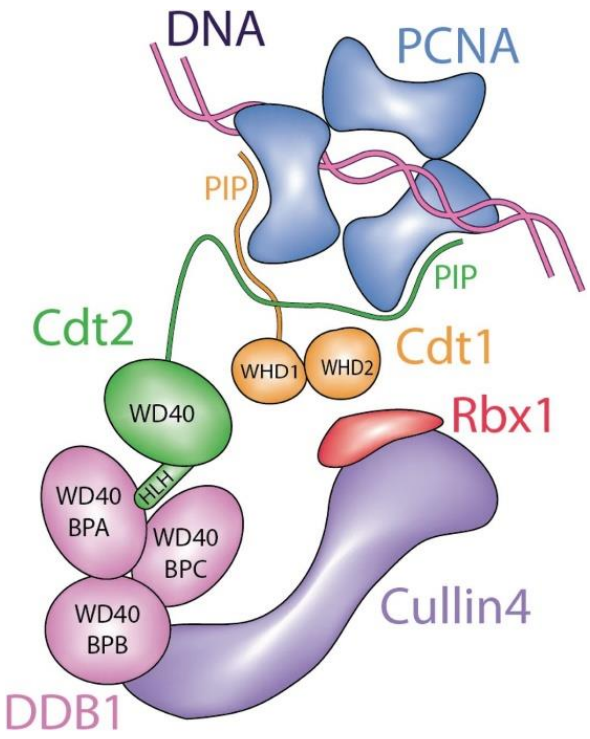

Figure 7| Model of CRL4^{Cdt2} and Cdt1 bound to PCNA

Illustration of CRL4^{Cdt2} and its substrate Cdt1 bound to DNA associated PCNA. CRL4^{Cdt2} is composed of the scaffold subunit Cul4, the RING domain protein Rbx1, and the adaptor protein DDB1. The substrate recognition factor Cdt2 interacts with CRL4 via DDB1. The substrates (here Cdt1) interact with PCNA via a PIP degron. Cdt2 interacts with DNA bound PCNA via a PIP box and a DNA binding domain, ensuring degradation of only substrates associated with DNA bound PCNA. (Figure adopted from Hayashi et al., 2018)

Different substrates of CRL4Cdt2 haven been identified that are directly linked to cell cycle regulation, especially to the G1-S transition. The replication licensing factor Cdt1, responsible for MCM2-7 recruitment to the origin of replication during G1- phase is targeted by CRL4Cdt2 during S-phase. Cdt1 proteolysis prevents a de novo licensing of DNA replication and prevents re-replication (Arias et al., 2006; Jin et al., 2006; Lovejoy et al., 2006). Further substrates include the Drosophila transcription factor E2F1 (Shibutani et al., 2008), the CKI p21 (Abbas et al., 2008; Kim et al., 2008) and the Drosophila CKI homologue Dacapo (Swanson et al., 2015).

2.6. The Anaphase promoting complex / cyclosome (APC/C)

2.6.1. APC/C and its role in cell cycle regulation

The anaphase promoting complex/cyclosome (APC/C) is an E3 ubiquitin ligase that governs cell cycle progression by controlling mitotic entry in particular the metaphase to anaphase transition, mitotic exit, and establishment and maintenance of G1-phase (reviewed in Castro et al., 2005; Bansal et al., 2019). APC/C activity depends to a vast extent on the temporal interaction with its two co-activators Cdc20 (cell division cycle protein 20 homolog) and Cdh1 (Cdc20-homologue 1), represented by Fizzy (Fzy) and Fizzy-related (Fzr) in *Drosophila*, respectively (Morgan, 2007). The two co-activators have opposing activity profiles associating with the APC/C in different cell cycle stages. The switching between APC/C^{Cdc20} and APC/C^{Cdh1} enables the degradation of different substrates at distinct cell cycle stages, even though Cdc20 and Cdh1 have a partially overlapping substrate specificity. Furthermore, they provide a broader level of APC/C regulation as they are subjected to different regulatory mechanisms, discussed in more detail later. Cdc20 stimulates APC/C activity during early mitosis when kinase activity is high, as APC/C-Cdc20 interaction requires phosphorylation of the APC/C at several sites (Qiao et al., 2016). On the contrary, Cdh1 is held in an inactive state during this period, since phosphorylated Cdh1 is unable to interact with the APC/C. The main targets of APC/C^{Cdc20} are CycA, Nek2A, CycB, and Securin. CycB-Cdk1 activity is required for mitotic spindle assembly and Securin inhibits the enzyme separase that cleaves the cohesion complex holding together the sister chromatids. Degradation of both proteins must be prevented until all chromatids are correctly attached to the mitotic spindle during metaphase, which is achieved through the action of the spindle assembly checkpoint (SAC) (reviewed in Lara-Gonzalez et al., 2012). After correct attachment of all chromosomes monitored by the SAC, the two targets are degraded, and the cohesion complex is dissolved by separase resulting in the transition from metaphase to anaphase. Interestingly, CycA and Nek2A are subjected to proteolysis right after nuclear envelope breakdown independent of the SAC. With the Cdc20 dependent destruction of mitotic cyclins, phosphorylation activity drops resulting in the dephosphorylation of Cdh1. APC/C^{Cdh1} is activated and initially ubiquinates Cdc20 followed by Plk1, Aurora kinase A and B after they have fulfilled their function during telophase and cytokinesis, leading to mitotic exit. Further degradation of Securin and the mitotic cyclins is mediated by APC/C^{Cdh1} until the end of G1-phase, ensuring low

kinase activity during G1-phase. Premature entry into S-phase is inhibited by the ubiquitination of several targets required for the start of DNA replication, for instance Orc1, Cdc6, and Geminin. Once all substrates are degraded, APC/C is inactivated through autoubiquitination of the E2 enzymes UbcH10 and held in an inactive state through Cdh1 phosphorylation and the activity of specific APC/C inhibitor proteins during S and G2-phase upon entry into the next mitosis (Figure 8) (reviewed in Zhou et al., 2016; Bansal et al., 2019). Besides its function in cell cycle regulation, the APC/C is also involved in a multitude of cell cycle independent processes including differentiation, developmental processes, function of nervous system, genomic stability, tumor suppression, apoptosis, senescence, energy metabolism, and cell motility (reviewed in Zhou et al., 2016; Bansal et al., 2019).

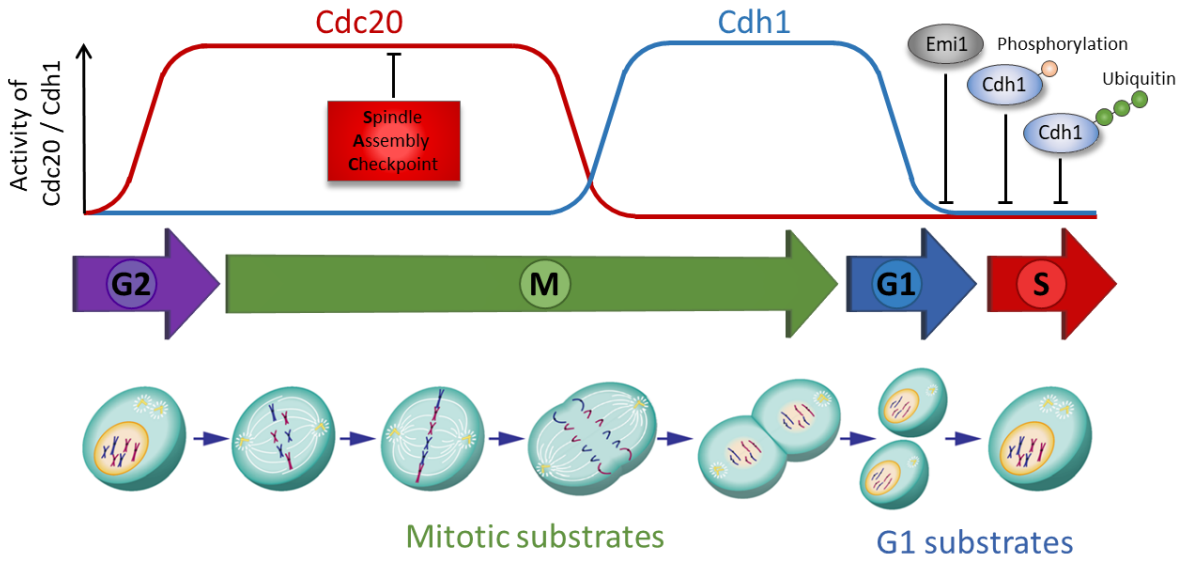

Prometaphase	Metaphase	Anaphase – Telophase			
Nek2A	Cyclin B	Aurora A	EYA1	Cdc25A	FoxM1
Cyclin A	Securin	Aurora B	Geminin	Skp2	Orc1
	Cyclin B3	Cdc20	Anillin	Ndd1	Est2
		PLK1	Kip1	Cks1	Id1/4
		Tpx2	Cln8/Rg5	Geminin	Id2
		JNL	Ase1/Prc1	Cdc6	Tome-1
		HEC1	Sgo1	UbcH10	CDCA3
		Bard1		Cdh1	Clb2
		Hmmr		TMPK1	CyclinA
		HURP		TK1	Cyclin B
		NuSAP		RRM2	Clapsin
				USP37	

Figure 8| APC/C in cell cycle regulation.

APC/C^{Cdc20} is activated during early mitosis upon APC/C phosphorylation. The substrates Cyclin A and NIMA-related kinase 2A (Nek2A) are ubiquinated in prometaphase independent of the spindle assembly checkpoint (SAC). Cyclin B and Securin destruction is halted by the SAC until correct attachment of the mitotic spindle in metaphase. APC/C mediated proteolysis of Securin and cyclin B after SAC inactivation results in anaphase onset. Cdh1 is activated through reduced Cdk activity and Cdc14 dependent dephosphorylation at the end of mitosis. APC^{Cdh1} targets all APC/C^{Cdc20} targets and an array of further individual targets including Cdc20. During G1-phase, APC/C^{Cdh1} degrades mitotic cyclins as well as proteins required for DNA replication (e.g., Geminin, Orc1, Cdc6, etc.) preventing premature entry into S-phase. After G1-phase APC/C activity is inhibited through several mechanisms including Cdh1 phosphorylation, Cdh1 degradation, and the action of APC/C specific inhibitors, e.g., vertebrate early mitotic inhibitor 1 (Emi1). (Figure adopted and modified from Zhou et al., 2016)

Recently, APC/C activity was also found to modulate gene expression and cell identity by an ubiquitin-mediated mechanism (Oh et al., 2020). Due to its diverse functions, the APC/C was subjected to immense research in the last 25 years since its discovery, regarding its structural composition, catalytic activity, substrate recruitment, and the multitude of regulatory mechanisms controlling APC/C activity.

2.6.2. APC/C structure and subunit composition

The APC/C is an unusually large multi-subunit cullin-RING E3 ubiquitin ligase with a mass of approximately 1.2 MDa. The APC/C core complex is composed of 14 individual subunits (13 subunits in yeast) with 5 subunits forming homodimers, making a total of 19 subunits (Table S 2). Active APC/C requires the interaction with one of its two interchangeable co-activator subunits, Cdc20 or Cdh1. The whole complex adopts a triangular or asymmetric heart-shape (V-shape) and is organized in three sub-complexes based on the function and structure of the respective subunits: the catalytic module, the substrate recognition module and the scaffolding module (Figure 9 A)(reviewed in Alfieri et al., 2017).

The catalytic module consists of the RING domain subunit Apc11 ($Apc11^{RING}$) and the cullin subunit Apc2. An Apc11-Apc2 heterodimer is formed by the interaction of the Apc11 N-terminal β-strand with the Apc2 C-terminal domain (CTD). The $Apc11^{RING}$ and Apc2 WHB domain ($Apc2^{WHB}$), both required for interaction with the E2 enzyme, are bound to the Apc2 CTD via flexible linkers. The minimal module of Apc11-Apc2 heterodimer is already active but only with poor substrate specificity (Gmachl et al., 2000; Leverson et al., 2000; Tang et al., 2001). The substrate recognition module is composed of Apc10 and the co-activator subunit (either Cdc20 or Cdh1) (Carroll et al., 2002; Passmore et al., 2003; Fonseca et al., 2011). Together, the catalytic and the substrate recognition module represent only 15% of the total complex mass, even though they are the key functional subcomplexes. The remaining 85% APC/C mass are attributed to the scaffolding module including the seven subunits (Apc1, Apc3, Apc4, Apc5-8) and four additional accessory subunits (Apc12, Apc13, Apc15 and Apc16). Particularly, the scaffolding subunits are all characterized by multiple repeat motifs. The subunits Apc3, Apc6, Apc7, Apc8 and Apc5 are tetratricopeptide (TPR) proteins containing 13-14 continuous TPR motifs. Apc4 and Apc1 both contain WD40 β-propeller domains, though Apc1 features a further array of four proteasome-cyclosome motifs (PC). The scaffolding module is organized in two substructures, the platform and the TPR lobe, forming a lattice like shell surrounding an inner cavity. Homodimers of Apc3, Apc6, Apc7, and Apc8 together with the TPR accessory subunits Apc12, Apc13 and Apc16 constitute the TPR lobe representing the back and the top of the structure (reviewed in Alfieri et al., 2017; Yamano, 2019; Barford, 2020). The N-terminal TPR helix serves as the homo-dimer interface, while the C-terminal TPR helix creates a protein binding groove. The Apc6 dimer interacts with two copies of Apc12 via its protein binding groove, stabilizing Apc6 (Wang et al., 2009). Apc3 and Apc8 homodimers use one of their grooves for interaction with the co-activator subunits (Cdh1 or Cdc20). The TPR lobe is further stabilized by the binding of accessory subunits Apc13 and Apc16 to sites on seven of the eight TPR domains. Besides

stabilization these interactions are also crucial in the process of APC/C assembly (reviewed in Chang et al., 2014). Interestingly, the APC/C of higher eukaryotes contains an additional TPR subunit Apc7 that only interacts with Apc3. The precise function of Apc7 is still ambiguous, as the deletion of Apc7 only resulted in a slightly reduction of ubiquitination activity with no major defects in mitotic timing, CycB1 degradation, and response to spindle assembly defects (Wild et al., 2018). The platform is made up of Apc4, Apc5 and two non-PC domains of Apc1. The accessory subunit Apc15 binds the TPR groove of Apc5, bridging it to Apc8. Apc1 PC domain extends from the platform interacting with the TPR lobe, creating a central cavity (Chang et al., 2014, 2015). The substrate recognition module (Apc10 and Cdc20/Cdh1) interacts with the Apc1 PC domain positioning it at the top of the cavity. Furthermore, APC10 and the coactivator interact with TPR motif of Apc3 with their C-terminal Ile-Arg residues (IR tail). Cdc20 and Cdh1 contain a further N-terminal C-box motif mediating interactions with Apc8. The catalytic module (Apc11-Apc2) is situated in the periphery of the platform subcomplex in such a way that Apc2 CTD and the associated Apc11 are at the front right below the substrate recognition module (Figure 9 B).

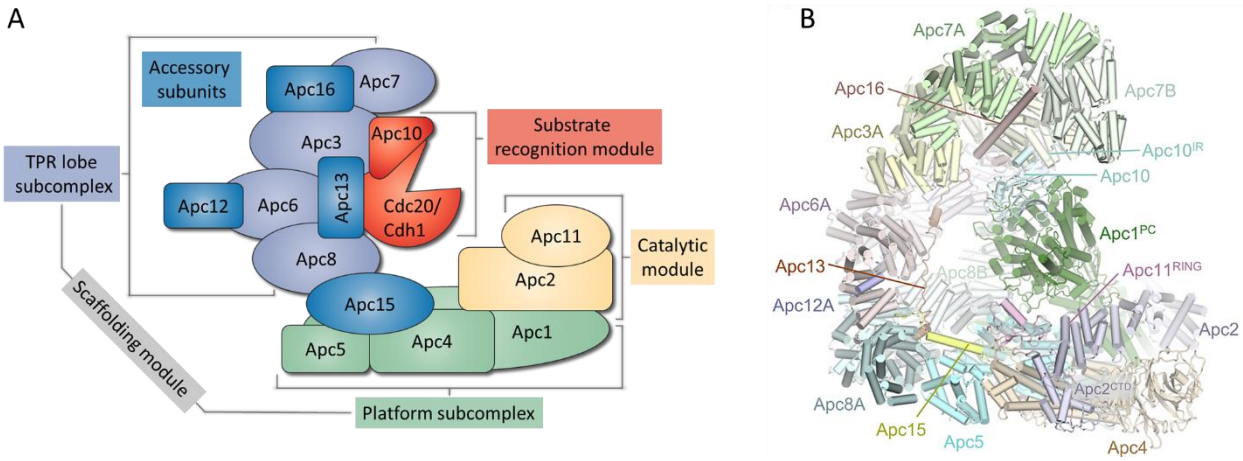

Figure 9| Subunit organization of the APC/C

(**A**) Schematic of the anaphase promoting complex/cyclosome (APC/C). The APC/C is organized in three modules: The catalytic module, the substrate recognition module, and the scaffolding module. The latter is divided into the TPR lobe and platform subcomplexes. The substrate recognition module is composed of Apc10 and one of the two interchangeable WD40 co-activator subunits, Cdh1 or Cdc20. The catalytic module is represented by a heterodimer of Apc11 and Apc2. The scaffolding module consisting of the TPR lobe subcomplex made up of the subunits Apc3, Apc6, Apc7, and Apc8 (all forming homodimers; not shown here) with three stabilizing accessory subunits (Apc12, Apc13, and Apc16) and the platform subcomplex composed of Apc1, Apc4, and Apc5. The Apc1 PC domain and the accessory subunit Apc15 connect the platform and the TPR lobe. The substrate recognition and the catalytic module interact with the scaffolding module at different sites, positioning them in close proximity for substrate ubiquitination (Figure A adopted and modified from Sivakumar et al., 2015). (**B**) Overall structure of an apo-APC/C, without co-activator; APC/C subunits are represented as cartoons. The Apc1 PC, Apc2 CTD, Apc10 IR and APC11 RING domain are also shown (Figure B adopted from Barford, 2020).

2.6.3. APC/C employs two E2 to catalyze polyubiquitination

The ubiquitination of a substrate by the APC/C requires the activity of two E2 enzymes that interact at different sites within the catalytic module. Their collaborating activities result in either monoubiquitination, multi-monoubiquitiniation or the assembly of polyubiquitin chains. In case of human APC/C, chain formation is initiated by the E2 enzyme UbcH10 (also termed Ube2C) or UbcH5, whereas chain elongation is catalyzed by another E2 called Ube2S. In *Drosophila*, UbcD1/Effete and Vihar represent the homologous of UbcH5 and UbcH10, respectively (Treier et al., 1992; Máthé et al., 2004). Interestingly, yeast APC/C uses canonical K48 linked Ub chains as signal for proteolysis, while metazoan APC/C-Ube2S utilizes atypical K11 linkages (Rodrigo-Brenni et al., 2007). The priming monoubiquitination by UbcH10 is mediated by the interaction with the RING domain of Apc11 that is dependent on a conformational change mediated by the co-activator (Brown et al., 2015; Chang et al., 2015). Without co-activator, $Apc11^{RING}$ is in contact with Apc5 blocking the UbcH10 binding site being in an inactive state referred to as “down position”. Co-activator binding leads to a conformational change in the high flexible catalytic module resulting in an active “up position” with the exposure of UbcH10 binding sites on $Apc11^{RING}$-$Apc2^{WHB}$ increasing APC/C-UbcH10 affinity by more than ten-fold (Chang et al., 2014; Li et al., 2016; Zhang et al., 2016). The co-activators are therefore not only responsible for substrate recognition but are also important for stimulating APC/C catalytic activity (Kimata et al., 2008). Binding of UbcH10 to the RING domain via its Ubc domain leads to a closed E2∼Ub conformation presenting the thioester bond for nucleophilic attack by the substrate lysine. A second interaction between $Apc2^{WHB}$ and the backside of UbcH10 results in a rigidification of the WHB domain that increases the catalytic activity of UbcH10 more than 100-fold and further enhances the APC/C-UbcH10 affinity (Brown et al., 2015). Interaction with $Apc2^{WHB}$ also promotes closed UbcH10∼Ub conformation, although the mechanism behind this is still unknown (Barford, 2020). After the attachment of the priming Ub moiety, UbcH10 can further ubiquinate the substrate in a process called processive affinity amplification, whereby the attached Ub molecule enhances the substrate-APC/C affinity increasing the rate of ubiquitination (Lu et al., 2015 a). UbcH10 has the capacity to either generate mixed K11-, K48- and K63-polyubiquitin chains or ubiquitinate a different lysine residue leading to multi-monoubiquitination.

Alternatively, further assembly of K11-polyubiquitin chains on the previous attached Ub molecules is catalyzed by Ube2S. Unusually for an E2 enzyme, Ube2S does not interact with the RING domain of Apc11 and is consequently not in competition for binding sites with UbcH10. Instead a C-terminal LRRL motif (RL-tail) mediates interaction with the APC/C at a site between Apc2 and Apc4 (Chang et al., 2015). Ube2S catalytic activity is intensely increased by the APC/C as the already substrate-bound Ub molecule engages an exosite on $Apc11^{RING}$ leading to a conformational change of the RING domain presenting the K11 residue of the substrates Ub for further linkage with the Ube2S∼Ub (Brown et al., 2016). Interestingly, the same exosite was also required for multi-ubiquitination events catalyzed by UbcH10 (Brown et al., 2015). Ube2S does not simply extend a ubiquitin chain but creates mixed or

branched K11/K48-linkages in cooperation with UbcH10, which serve as a more potent degradation signal compared to homotypic K11- or K48-linked chains (Meyer et al., 2014; Rana et al., 2017; Yau et al., 2017). The underlying mechanisms orchestrating the loading and switching between UbcH10 and Ube2S activity are still elusive. However, two recent discoveries provided new insight into possible regulatory mechanisms regarding Ube2S and UbcH10 activity. First, Ube2S autoubiquitination of a conserved lysine, located five residues upstream of the active site of the UBC domain, impaired E1-mediated ubiquitin reloading. This autoinhibitory process controlling Ube2S activity is also regulated in the context of the cell cycle, with reduced ubiquitination levels at this site during mitotic exit (Liess et al., 2019). Second, the discovery of Apc2^{WHB} being also an Ub-binding domain for K48-linked ubiquitin chains, gave rise to a possible regulatory mechanism for UbcH10, as binding of K48-linked ubiquitin at this site would compete for UbcH10. However, the function is yet unknown and the cryptic K48-linked ubiquitin binding site could contribute to switching between the two E2 activities or other processes modulating APC/C activity and further studies will be required to definitively determine the basis of E2 regulation (Watson et al., 2019 a).

2.6.4. APC/C substrate recognition is mediated by short linear degrons

The APC/C is responsible for the degradation of over 100 proteins across different eukaryotic species and it is of great importance that these targets are recognized with high specificity to assure proper proteolysis in a spatio-temporal context (Davey et al., 2016). APC/C substrate recognition is mainly mediated by interactions of the seven blade β-propeller WD40 repeat domain in the C-terminal half of the co-activator subunits with short degrons (derived from degradation motif) located in unstructured, intrinsically disordered regions of the target substrate. Degron localization to these flexible and accessible regions is important to adopt a defined conformation upon binding to the co-activator and for efficient interaction of nearby lysines or attached Ub molecules with the E2 enzyme (He et al., 2013; Guharoy et al., 2016). The WD40 domains of the co-activator subunits contain different binding pockets for the recognition of APC/C degrons, of which there are three major types: The destruction box (D-box) (Glotzer et al., 1991), the KEN-box (Pfleger et al., 2000) and the ABBA motif (Burton et al., 2011; DiFiore et al., 2015) (Figure 10 A).

The D-box was first discovered in B-type cyclins and the majority of characterized D-boxes follows the consensus RxxLxx[ILV], although there are variations with strong preferences outside of the consensus. Even the +1 arginine and +4 leucine residue are not strictly necessary, for instance *Drosophila* Pimpels lacks arginine at the +1 position (Leismann et al., 2003) and a phenylalanine substitution of the leucine residue is found in *Drosophila* cyclin A and *H. sapiens* Cyclin B3 (Nguyen et al., 2002; Ramachandran et al., 2007). The D-box consensus is a bipartite degron comprised of a N-terminal motif (RxxLx[D/E][Ψ]) for co-activator interaction at a site of the β-propeller between β-blades 1 and 7 and a hydrophilic C-terminal segment for binding Apc10 (Buschhorn et al., 2011; Da Fonseca et al., 2011) (Figure 10 B).

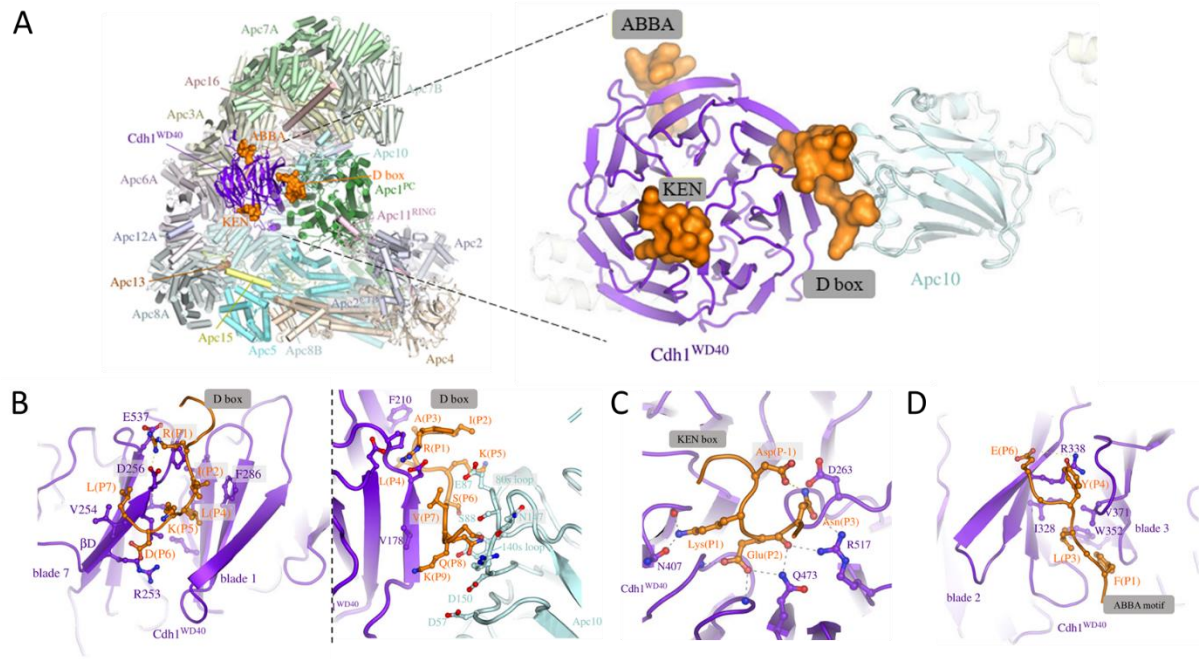

Figure 10| APC/C co-activator recognize substrates via APC/C specific degrons

(**A**) APC/C co-activators (Cdh1 shown here) interact with Apc1 and Apc3 and provide different binding sites for specific APC/C degrons, the D-box, KEN-box, and the ABBA motif (structure based on APC/C^{Cdh1}-Emi1 complex [PDB 4UI9] with the KEN box and ABBA motif modeled on *S. cerevisiae* Cdh1-Acm1 complex [PDB: 4BH6])(Chang et al., 2015). The D-box binding pocket is comprised of an interaction site between β-sheet blade 1 and 7 together with Apc10. The KEN receptor site is situated on the top surface of the WD40 co-activator with the ABBA motif binding site on the opposite side in an inter-blade groove between β-blades 2 and 3. (**B**) The D-box receptor of Cdh1 interacts with the D-box peptide together with Apc10. (**C**) The bound KEN peptide forms a 3_{10} helix with the three consecutive KEN residues facing in the same orientation interacting with the KEN receptor. (**D**) The ABBA residues +1 and +3 are deeply buried in the ABBA receptor site, whereas position +4 rests against β-blade 3. The +6 position contacts the side of the WD 40 domain outside of the binding pocket (He et al., 2013). (B left panel, C,D are based on *S. cerevisiae* Cdh1-Acm1 complex [PDB: 4BH6] ; B right panel is based on APC/C^{Cdh1}-Emi1 complex [PDB 4UI9]) (Figures adopted and modified form Alfieri et al., 2017).

The +1 arginine of the RxxL motif contacts an acidic patch on the activator subunit, whereas +4 leucine anchors the D-box within an aliphatic pocket (He et al., 2013). The +3 position has a preference for proline and alanine and +5 for small residues, both attributed to a tight turn after the +4 leucine that imposes strong constraints. The +6 residue interacts with an invariant arginine residue on the activator surface, explaining the preference for acidic amino acids at this position. A hydrophobic residue at +7 is preferred for the interaction with a non-polar surface on the β-propeller. The C-terminal hydrophilic residues mediate interactions with the hydrophilic surface of Apc10 preferring small polar residues at this site, with a high preference of serine, threonine, and asparagine at +8 and asparagine at +9 and +10 positions (Chang et al., 2015) (Figure 11 A).

The KEN-box, named after its core consensus sequence [DNE]KENxxP, is commonly present in APC/C substrates often in addition to the D-box. Degradation and efficient ubiquitination of substrates containing both D- and KEN-box peptides, is most commonly dependent on both degrons (Burton et al., 2001). The short motif is strictly defined and especially the glutamic acid and asparagine residues rarely deviate, whereas the lysine position allows other residues (e.g. aspartate, glutamine, or asparagine).

The substitution of the +1 lysine is often compensated by a glycine residue at the -1 position (GxEN) which has usually a preference for asparagine or aspartate that stabilize the KEN conformation via a hydrogen bond to the asparagine of the KEN consensus (He et al., 2013) (Figure 11 B).The bound KEN-box peptide forms a 3_{10} helix conformation that positions all three residues facing in the same orientation engaging the surface of the KEN-box binding pocket situated on the top surface of the activator subunit WD 40 domain (Tian et al., 2012; He et al., 2013). Amino acids one or two residues C-terminal of the KEN box are often prolines that direct the exiting peptide away from the domain surface (Figure 10 C).

A more recent degron, the ABBA motif was initially discovered as the A-motif in the yeast APC/C inhibitor Acm1 and further characterization led to a general class with the six-residue consensus [FILV]x[ILMVP][FHY]x[DE] including the degrons of its eponymous representatives vertebrate cyclin **A** (S. cerevisiae Clb5), **B**ubR1, **B**ub1, and **A**cm1 (DiFiore et al., 2015) (Figure 11 C). However, there is only a limited number of validated ABBA motifs available at this point and thus the consensus will probably change in the future. The ABBA motif was originally thought to be exclusively specific for Cdh1 but variation of a single residue in the flanking regions of the ABBA motif can switch the specificity from Cdh1 to Cdc20 (Davey et al., 2016). The ABBA motif binding pocket is situated in the inter-blade groove of blades 2 and 3 on the opposite surface of the WD40 domain from the KEN-box binding pocket (Figure 10 A). The three non-polar residues at positions +1, +3, and +4 anchor the motif to the binding groove. The +6 residue reaches out of the pocket contacting an arginine residue of blade 2 (Figure 10 D) (He et al., 2013; Davey et al., 2016). Interestingly, the ABBA binding motif seems to be lost from animal Cdh1, as neither the ABBA motifs of Cyclin A, Bub1 or BubR1 can bind human Cdh1 and no ABBA motif that binds to metazoan Cdh1 has been found ,yet (DiFiore et al., 2015). Besides the canonical degrons, other non-canonical degrons have also been described (e.g. Cry-box or O-box). However, in some cases it turned out that these new degrons were only variants of the D-box and KEN-box. For instance the degrons discovered in *Drosophila* abnormal spindle (Asc), *S. pombe* Securin (Cut2), and the O-box identified in *Drosophila* Orc1 are all non-canonical D-box degrons but do not represent novel classes of APC/C degrons (reviewed in Davey et al., 2016). The high divergence

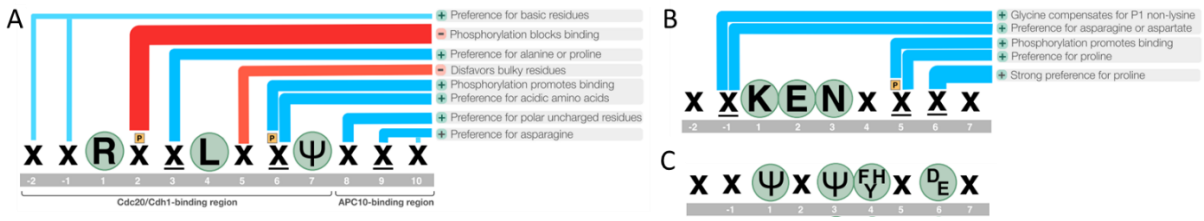

Figure 11| Consensus sequence of the D-box, KEN-box, and ABBA motif

(**A**) Preferences of the D-box binding pocket, (**B**) KEN-box binding pocket and (**C**) ABBA motif binding pocket. "x" indicates any residue, "x" means any residue but with strong preferences based on characterized degrons. Green circles highlight the consensus residues. Ψ stands for a leucine, isoleucine, or valine residue at this position. An orange "P" marks a site for phosphorylation. The blue bars indicate a preferred residue, whereas the red bars indicate disfavored residues. (Figure adopted from Davey et al., 2016)

outside the key residues of the degrons could be responsible for differences in specificity, affinity and selectivity of activator binding among the vast number of substrates (Van Roey et al., 2014). It is also important to consider that most simplified APC/C degron consensus peptides (RxxL or KEN) are unlikely to be functional, as for instance about 70% of human proteins contain these minimal D- and KEN-box sequences. This considerable number of instances makes it rather unlikely that all are actual APC/C targets and most of these motifs will not fit the different requirements of being accessible in intrinsically disordered regions of the protein, to co-localize with the APC/C nor exhibit the complex sequence preferences of the corresponding binding pocket (Lu et al., 2015 b).

2.6.5. Regulation of APC/C activity during the cell cycle

The fidelity of the cell cycle requires the degradation of the regulatory proteins in a defined and strict temporal order which applies to a vast number of substrates in case of the APC/C. The spatio-temporal regulation of protein degradation mediated by this large single holoenzyme and its two substrate recognition co-activators is not simply mediated by a single mechanism but instead by variety of cooperating molecular processes. Some of these are sequence encoded within the substrates, whereas others are cell state dependent mechanisms altering APC/C activity.

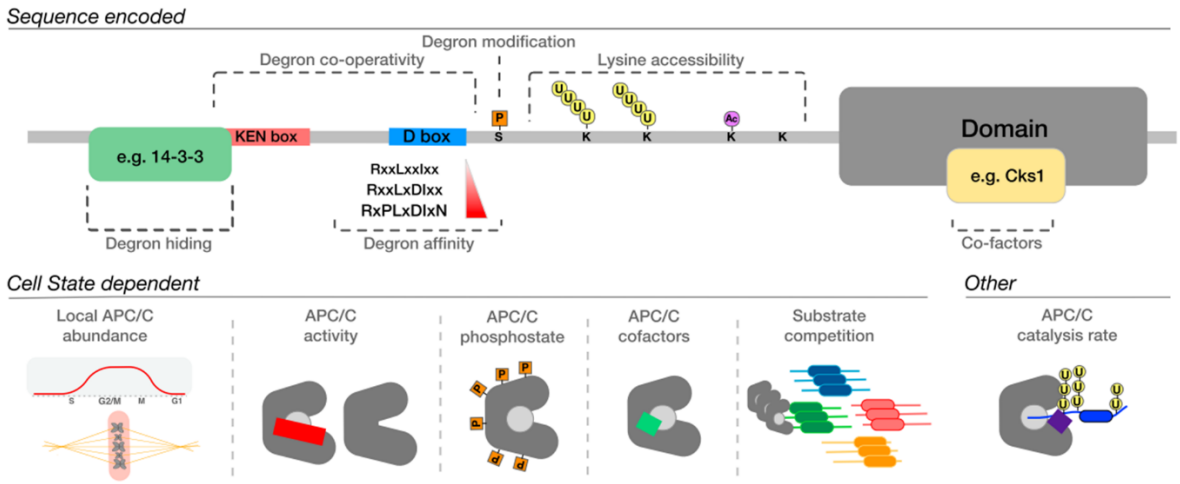

Figure 12| Principles of APC/C regulation

The APC/C can be regulated by a myriad of collaborating mechanisms. Some of these, for example degron hiding, degron cooperativity, degron modification especially phosphorylation, degron affinity, lysine accessibility and modification, and interaction with co-factors are encoded within the substrate sequence. Other processes are cell state dependent comprising spatial abundance of the APC/C, co-activator dependent APC/C activation, regulation through phosphorylation of core APC/C subunits, substrate competition, and APC/C catalysis rate. (Figure adopted from Davey et al., 2016) .

2.6.6. Substrate encoded regulatory mechanism

Degron affinity and cooperativity - The binding affinity, or more precisely the dissociation rate, and the resulting abundance time on the APC/C together with its processivity determines the rate of ubiquitination and consequently the degradation efficiency of a substrate. The different APC/C degron binding

affinities have not been systematically tested to this point, but different lines of evidence indicate that differences in the degron consensus have an impact on the individual affinity to the respective binding pockets. The Hsl1 protein from *S. pombe* contains the D-box with the highest affinity (also called super D-box) tested in competition based assays, whereas metazoan cyclin A has a rather weak D-box and the cyclin B D-box sequence does not even represent a transplantable degradation signal (Klotzbücher et al., 1996; Burton et al., 2001; Frye et al., 2013). The differences of the binding affinities can be explained by the sequence preferences of the D-box consensus, whereby less preferred residues at critical positions can decrease the degron affinity. Cooperativity of multiple degrons must also be taken in consideration, since the D-box, KEN-box, and ABBA motif binding pockets can be occupied at the same time (He et al., 2013) reflected by the presence of multiple degrons in potent APC/C pseudosubstrate inhibitors as well as in many APC/C substrates (reviewed in Davey et al., 2016). For instance, the degradation of the early targets human cyclin A and Nek2A depends on multiple degrons together with other cooperating APC/C interactions. Cyclin A harbours a canonical D-box (D1) as well as a second non canonical D-box (D2), an ABBA motif and a degenerate KEN-box and further employs Cks1 that can enhance binding affinity towards the APC/C besides its function in Cdk phosphorylation. Cooperative binding of the D2 together with the KEN-box and ABBA motif enables Cyclin A degradation in the presence of activated SAC. Surprisingly, cyclin A can engage the APC/C by two distinct binding modes, one with high activity mediated by D2 and KEN-boxes and a mode of lower activity via D1- and KEN-boxes and the ABBA motif. This highlights that different degron combinations of a single substrate can alter their own affinity towards the APC/C (Lu et al., 2014; DiFiore et al., 2015; Zhang et al., 2019). Efficient ubiquitination of Nek2A relies on a KEN- and a D-box and additional interaction with the APC/C mediated by a C-terminal MR tail motif that resembles the IR motif of the co-activators (Hames et al., 2001; Sedgwick et al., 2013). The cooperativity of these interaction sites strongly enhances Nek2A affinity towards the APC/C and enables the degradation in the presence of activated SAC. Interestingly, multivalent degrons are often located in close proximity, which might reflect the relative distance of the degron interaction sites on the WD40 domains of the co-activators. The appearance of multiple degrons of the same type (e.g., multiple D-box motifs in *S. pombe* Dfb4 or human Sgo1) might provide an extra layer of fine tuning in avidity or specificity towards a co-activator. However, these possible modes of function have not systematically been tested and need further studies.

Lysine position and accessibility - The APC/C does not prefer a distinct lysine residue but utilizes several lysines for ubiquitination as multiple lysine substitutions are required for stabilization of a target substrate. The position of lysines is probably important as the degron binding pockets in the substrate recognition module are about 20-40 Å distant from the E2 active site within the catalytic module. This would correspond five to ten residues in an unfolded polypeptide chain and ubiquitination of a lysine residue is only possible beyond this distance (Chang et al., 2015; Brown et al., 2016). However, there

is no strict necessity for acceptor lysines to be located in the same region as the degrons, since the preferred location of potential lysine residues in intrinsic disordered regions of the protein provides a high degree of flexibility also allowing interactions with further separated residues. Sequence context of ubiquitinated lysines (Williamson et al., 2011; Min et al., 2013; Mattiroli et al., 2014) and the various PTMs of lysine residues that can block lysine accessibility provide further mechanisms to control substrate degradation (Zee et al., 2012).

Degron phosphorylation - Post translational modification of degrons through phosphorylation can result in completely opposing outcomes. Cdk1 mediated phosphorylation of a serine residue at the +2 position of the Dbf4 and KIF1C D-box and phosphorylation of the +3 position of the Geminin D-box sequence by Aurora kinase A results in substrate stabilization (Rape et al., 2006; Tsunematsu et al., 2013; Lu et al., 2014). Consequently, dephosphorylation of these residues promotes ubiquitin dependent proteolysis. On the contrary, phosphorylation of human Securin at the D-box +6 position enhances the rate of degradation (Hellmuth et al., 2014). These opposing effects can be rationalized by the sequence preference of the D-box degrons. The +2 and +3 position prefer non bulky residues and a negatively charged phosphate at this position interferes with D-box binding, whereas +6 position favours acidic residues and a phosphate thus increases D-box avidity towards its receptor site (see Figure 11 A). KEN-box affinity can also be influenced by phosphorylation. The KEN motif of Acm1 bound to Cdh1 includes a phosphorylated serine residue (Hall et al., 2008; He et al., 2013) and phosphorylation in close vicinity of the D- and KEN-box of Cdc6 results in stabilization (Mailand et al., 2005). Substrate stability can likewise be altered through phosphorylation outside the degron sequence as seen in the case of *S. cerevisiae* Securin. Cdk1 phosphorylation 17 residues C-terminal of the KEN-box and 14 residues N-terminal of the D-box reduces the ubiquitination rate drastically by 5-10-fold. Reversely, dephosphorylation of these sites by Cdc14 promotes Securin degradation (Holt et al., 2008; Lu et al., 2014). Another example, the destruction of Mcl1 during mitotic arrest requires phosphorylation of a critical site over 100 residues N-terminal of the D-box degron (Harley et al., 2010). Phosphorylation is a powerful regulatory mechanism that integrates the current state of mitosis into ordering of APC/C substrates, as it is a direct response to the decline of kinase activity due to APC/C dependent degradation of mitotic cyclins.

Motif hiding – Association with a protein that blocks the access of one or several degrons can protect a substrate from APC/C dependent degradation. For instance, human kinase Aurora A is protected from APC/C^{Cdh1} degradation through the interaction with TPX2 and depletion of TPX2 caused a premature degradation of Aurora A in prometaphase (Giubettini et al., 2011). The spindle assembly factors HURP and NuSAP are protected through binding of the importin subunit β that blocks APC/C degrons. Release of importin β through the action of Ran^{GTP} exposes the degrons leading to APC/C dependent proteolysis. Several APC/C targets also interact with importin β (e.g. Cyclin B), but none was stabilized

by this association indicating a unique regulatory mechanism restricted to the process of spindle assembly (Song et al., 2010). Phosphorylation and degron hiding can also be a cooperative process. The F-box protein NIPA is protected from APC/C^{Cdh1} dependent degradation though its interaction with the SCF subunit Skp1 (von Klitzing et al., 2011). Phosphorylation of NIPA dissolves Skp1 interaction and promotes its destruction by the APC/C. Another example is the yeast APC/C inhibitor Acm1. Cdc28 dependent phosphorylation of Acm1 promotes binding of the 14-3-3 family members Bmh1 and Bmh2 stabilizing Acm1. Opposing dephosphorylation by the action of phosphatase Cdc14 results in 14-3-3 dissociation and rapid Acm1 degradation (Hall et al., 2008; Qin et al., 2019).

2.6.7. Phosphorylation of core APC/C and the co-activators regulates APC/C activity

The major cell state dependent factor regulating APC/C activity from the beginning of mitosis through G1-phase is the interaction with its two co-activator subunits Cdc20 and Cdh1. The association between the APC/C and the co-activators is regulated through phosphorylation of both the core APC/C and the co-activators (reviewed in Alfieri et al., 2017; Yamano, 2019). APC/C activity is stimulated through cyclin-Cdk phosphorylation of core APC/C subunits at the beginning of mitosis and even remains active after mitotic cyclin destruction due to the different modes of activation mediated by Cdc20 and Cdh1. Phosphorylation of the APC/C is necessary for Cdc20 association, whereas Cdh1 does not require phosphorylated APC/C for interaction, but Cdh1 phosphorylation itself completely renders it unable to bind APC/C during interphase and early mitosis. The decline of Cdk activity after destruction of mitotic cyclins mediated by APC/C^{Cdc20} results in APC/C and Cdh1 dephosphorylation, thereby activating APC/C^{Cdh1} and simultaneously inactivating APC/C^{Cdc20}. After its functions in late mitosis and G1-phase, APC/C^{Cdh1} is inactivated at the end of G1-phase through the action of APC/C inhibitor proteins (e.g. Acm1 in yeast, Emi1 in vertebrates, and Rca1 in *Drosophila*) and Cdk dependent Cdh1 phosphorylation (Lahav-Baratz et al., 1995; Shteinberg et al., 1999; Kramer et al., 2000; Rudner et al., 2000; Golan et al., 2002; Kraft et al., 2003).

The molecular mechanism behind APC/C^{Cdc20} activation involves phosphorylation of multiple APC/C subunits, but especially two hyperphosphorylated regions in Apc1 and Apc3, and the consequences for Cdc20 interaction motif sites (Kraft et al., 2003; Herzog et al., 2005; Steen et al., 2008; Hegemann et al., 2011). Cdc20 association with the APC/C is mediated by three interaction motifs located in the N-terminus (similar applies for Cdh1); the C box together with the KILR motif interact with Apc8B, the IR tail with Apc3A and a third region with Apc1 PC domain. The first hyperphosphorylated region is the 300s loop of the WD40 domain in Apc1 (Apc1^{300s} loop) that contains an auto-inhibitory segment (AI). The AI segment mimics the Cdc20 C-box motif and binds to the C box binding site on Apc8B in an unphosphorylated state blocking Cdc20 association. Hyperphosphorylation of the Apc1^{300s} loop leads to displacement of the AI segment and relives the auto-inhibition allowing Cdc20 binding. The second hyperphosphorylated region is a 300-residue segment in Apc3 that functions in regulation of Apc1^{300s}

loop phosphorylation. Apc3 directly interacts with Cks and initial phosphorylation of Apc3 enhances cyclin-Cdk-Cks association with the APC/C and consequently stimulates Apc1^{300s} loop phosphorylation. The relay mechanisms via the Apc3 kinase recruitment loop is required for efficient intra-molecular phosphorylation of the Apc1 AI segment that is only accessible for Cdk phosphorylation when transiently displaced from the C-box binding site on Apc8 (Figure 13) (Herzog et al., 2005; Steen et al., 2008; Qiao et al., 2016).

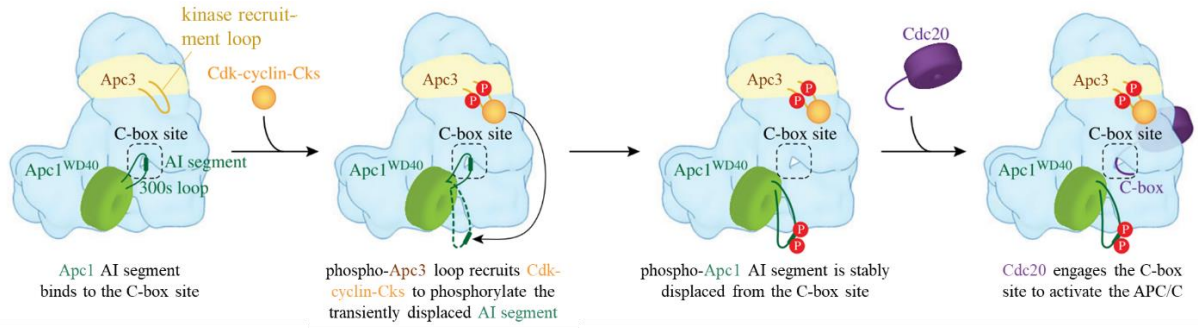

Figure 13| APC/C activation through hyperphosphorylation of Apc3 and Apc1

Unphosphorylated AI segment of Apc1 mimics the C-box of Cdc20 and occupies the C-box binding site. Cdk-cyclin-Cks1 dependent phosphorylation of the kinase recruitment loop of Apc3 displaces the AI segment followed by AI segment phosphorylation. Stably displaced AI releases the C-box binding site and Cdc20 association activates the APC/C. (Figure adopted and modified from Alfieri et al., 2017).

Only Cdc20 interaction requires phosphorylation of the APC/C, albeit Cdh1 and Cdc20 bind to common sites on the APC/C via their N-terminal domains. This can be explained by the fact that Cdh1 simply overcomes the need of phosphor-dependent release of the Apc1 AI segment through an increased affinity towards unphosphorylated apo APC/C resulting from more extensive contacts between Cdh1 and APC/C compared to Cdc20 (Alfieri et al., 2017).

Besides phosphorylation of the apo APC/C both Cdh1 and Cdc20 are negatively regulated through Cdk phosphorylation. Human Cdh1 contains four phosphorylation sites Ser40, Thr121, Ser151, and Ser163 flanking its N-terminal C box domain. Ser40 is proximately N-terminal to the core C box consensus, whereas Ser151 and Ser163 flank the C box augmenting the KLLR motif. Phosphorylation at all four sides sterically hinders Cdh1 to associate with the APC/C (Chang et al., 2015). Interaction of Cdc20 with the APC/C is also inhibited by Cdk mediated phosphorylation of its N-terminus in proximity to its C box (Thr55, Thr59, and Thr 70 in human Cdc20) (Golan et al., 2002; Hein et al., 2016; Zhang et al., 2016). However, the mechanism behind Cdc20 inhibition through phosphorylation is not clear. The phosphorylation sites of Cdc20 are largely disordered and not directly connected to APC/C-Cdc20 interactions making it rather unlikely to resemble C box inhibition reminiscent to Cdh1. Another possible model is that phosphorylation results in a conformational change leading to a closed conformation, whereby the N-terminal domain interacts with the WD 40 domain of Cdc20 inhibiting interaction between the C box and Apc8 (Alfieri et al., 2017; Barford, 2020). The contradiction that Cdk phosphorylation of the apo-APC/C is required for APC/C^{Cdc20} activation and simultaneously inhibits Cdc20 can be explained by the differences in the rate of dephosphorylation. Cdc20 phosphorylation sites are phosphothreonines,

whereas Cdh1 and APC/C contain to a greater extent phosphoserine residues. The responsible phosphatase PP2A-B55 has a much strong preference for pTP than pSP sites and therefore dephosphorylates Cdc20 before Cdh1 and APC/C (Meghini et al., 2016). Similar observations were made for PP2A-B56 and for PP1 in *C. elegans* (Kim et al., 2017; Lee et al., 2017). In conclusion, phosphorylation alters APC/C activity on multiple levels: substrate phosphorylation that can either enhance or inhibit affinity towards the APC/C, phosphorylation of the core APC/C that removes the AI segment for co-activator recruitment and inhibitory phosphorylation of the co-activators themselves.

2.6.8. The SAC inhibits APC/C at the metaphase to anaphase transition

At the beginning of mitosis, activated APC/C^{Cdc20} must be inhibited until correct bipolar attachment of the sister chromatids to the mitotic spindle. APC/C inactivation is mediated by the spindle assembly checkpoint that coordinates the metaphase to anaphase transition and is exerted by a tetrameric protein complex called the mitotic checkpoint complex (MCC) (Lara-Gonzalez et al., 2012; Musacchio, 2015). The MCC consists of the four proteins BubR1, Bub3, Mad2 and Cdc20 and is generated at the outer regions of unattached kinetochores (Pesenti et al., 2016; Faesen et al., 2017). Open state Mad2 (O-Mad2) is converted into a closed state conformation (C-Mad2) within seconds through a template-mechanisms at the unattached kinetochores that is only partially understood. C-Mad2 associated to the kinetochores via Mad1 interacts with free O-Mad2 and converts it to C-Mad2 catalyzed by Mps1 (De Antoni et al., 2005; Faesen et al., 2017; Ji et al., 2017). C-Mad2 binds the N-terminus of Cdc20 forming a binary complex that interacts with BubR1 and Bub3 generating the tetrameric MCC complex (C-Mad2-Cdc20-BubR1-Bub3) that targets and inactivates the APC/C (Sudakin et al., 2001). The structure of MCC bound to the APC/C (APC/C^{MCC}) involves two versions of Cdc20, one bound to the APC/C ($Cdc20^{APC/C}$) and one associated with the MCC ($Cdc20^{MCC}$). The MCC docks into the central cavity of the APC/C contacting $Cdc20^{APC/C}$ and the $Apc2^{WHB}$ domain of the catalytic module and inactivates the APC/C on different levels. Substrate recognition is blocked through the interaction of BubR1 with the two Cdc20 molecules. BubR1 harbours two D-box, two KEN-box and three ABBA motifs that interact with the six degron recognition sites on the Cdc20 molecules inhibiting substrate recruitment. In addition, binding of the MCC causes a conformational change of the APC/C rotating $Cdc20^{APC/C}$ away from Apc10 disrupting the D-box binding site (DiFiore et al., 2015; Davey et al., 2016; Di Fiore et al., 2016; Yamaguchi et al., 2016). Priming ubiquitination by UbcH10 is also inhibited by BubR1 contacting $Apc2^{WHB}$ obstructing the UbcH10 binding site (Alfieri et al., 2016). The inhibitory APC/$C^{MCC\text{-}closed}$ conformation also induces an ordered to disordered transition of the accessory subunit Apc15 disrupting interactions between domains of Apc15 with Apc4 and Apc5 accompanied by an upward movement of Apc4 and Apc5. An open conformation, APC/$C^{MCC\text{-}open}$ is generated by the opposing disordered to ordered transition of Apc15 resulting in MCC rotation away from the catalytic centre exposing the

UbcH10 binding site on Apc2^{WHB}. This movement allows a Apc15 and UbcH10 dependent auto-ubiquitination of two lysine residues of Cdc20^{MCC}, releasing the MCC from the APC/C (Eytan et al., 2013). The competing actions of MCC repressing the APC/C and simultaneous MCC disassembly through APC/C auto-ubiquitination generates a reciprocal mechanism. As long as correct attachment to the mitotic spindle is not completed, SAC remains active. New MCC is continuously generated at the unattached kinetochores inhibiting the APC/C, exceeding APC/C dependent MCC disassembly. Once all kinetochores are associated to the mitotic spindle the SAC is shut off, APC/C auto-ubiquination prevails MCC inhibition and induces anaphase onset. Thus, only unattached kinetochores signal to halt APC/C activity via the SAC. However, the molecular processes and factors underlying the Apc15 dependent transition from APC/C^{MCC} closed to open state are unknown. Cdc20 phosphorylation, action of p31^{Comet} that promotes Cdc20^{MCC} autoubiquitination, and Cdc20^{MCC} deubiquitination mediated by the DUB USP44 have been implicated as possible candidates (Stegmeier et al., 2007; Varetti et al., 2011; Alfieri et al., 2016). More recently, SUMOylation of Apc4 during mitosis was shown to be critical for timely APC/C activation and anaphase onset, likely at the level of the SAC. Further functional SUMO interacting motifs have also been found on Apc2, but the detailed function and mechanisms behind SUMOylation and SAC regulation are still unknown (Eifler et al., 2018; Lee et al., 2018).

Non-APC/C-associated MCC is disassembled in a second pathway by the joint actions of the adaptor protein p31^{Comet} and the AAA+ ATPase TRIP13. p31^{comet} interacts with C-Mad2 displacing BubR1 by competing for the same binding interface and recruits the C-Mad2-Cdc20 binary complex to TRIP13. C-Mad2 is remodelled to O-Mad2 in an ATP consuming reaction catalyzed by TRIP13 (Eytan et al., 2014; Ye et al., 2015, 2017; Alfieri et al., 2018). The p31-TRIP13 mediated MCC disassembly pathway was found to be inhibited through p31 phosphorylation by Plk1 that strengthens the SAC.

SAC regulation and anaphase onset is driven by the combination of Apc15-dependent Cdc20^{MCC} autoubiquitination and p31^{Comet}-TRIP13 MCC disassembly of free MCC complexes (Kim et al., 2018). However, the detailed mechanisms coordinating both processes are yet to be elucidated.

2.6.9. Spatial regulation of the APC/C

The localization of the APC/C and its co-activators to specific intracellular compartments has gained less attention compared to the other regulatory mechanisms and is little understood. The APC/C is thought to be localized mainly within the nucleus (Kraft et al., 2003; Hubner et al., 2010) and was shown to concentrate at microtubules, chromosomes, centromeres, and kinetochores but also at centrosomes outside the nucleus (Sivakumar et al., 2015). In human cell culture, APC/C was shown to be anchored to the mitotic spindle poles by the END network (**E**mi1-**N**uMA/**D**ynein-dynactin) recruited through Cyclin B-Cdk1 activity. The END network spatially restricts APC/C activity stabilizing spindle-associated Cyclin B creating a positive feedback loop that sustains CycB-Cdk2 activity at the spindle poles in order to maintain prometaphase (Ban et al., 2007). Furthermore, the interaction between the

APC/C and an uncharacterized human protein KIAA 1430 was shown to recruit an APC/C sub fraction to the centrosomes to facilitate mitotic progression (Hein et al., 2015). Another example is the interaction with Ska3 that also influences APC/C association to the chromosomes, timing Cyclin B destruction and mitotic exit (Ohta et al., 2010; Sivakumar et al., 2014). Besides localization of the whole APC/C complex, spatial abundance of the co-activator can also influence APC/C activity. In yeast, Cdh1 export from the nucleus at the end of G1-phase is regulated by Cdk dependent phosphorylation of N-terminal residues contributing to APC/C inactivation (Höckner et al., 2016). Localization of the *Drosophila* Cdh1 homologue Fzr to the centrioles directed by interaction with Spd2 is essential for efficient degradation of Aurora A (Meghini et al., 2016). Nevertheless, there is no uniform picture of spatial APC/C regulation at this time although the so far provided evidence highlight the critical importance of subcellular APC/C pools and their local activity in cell cycle progression.

2.6.10. Vertebrate Emi1 inhibits APC/C during S- and G2-phase

After the successful completion of mitosis and G1-phase, APC/C activity must be inactivated during S- and G2-phase to allow a cell to commit to DNA replication and to re-accumulate cyclins for a next round of cell division. Besides inhibitory phosphorylation of Cdh1, this is achieved through the action of potent APC/C inhibitor proteins since initial Cdk activity is too low after preceding APC/C dependent cyclin destruction. The vertebrate protein early mitotic inhibitor 1 (Emi1) can inhibit both APC/C^{Cdc20} and APC/C^{Cdh1} in vitro (Reimann et al., 2001 a; b), but in vivo data suggest that it is mainly responsible for APC/C^{Cdh1} inhibition during S- and G2-phase also supported by a higher affinity towards APC/C^{Cdh1} compared to APC^{Cdc20} in vitro (Di Fiore et al., 2007; Machida et al., 2007). Consistent with its function as APC/C^{Cdh1} inhibitor, knockdown of Emi1 resulted in impaired mitotic entry due to increased Cyclin A and B degradation. Emi1 overexpression in *Xenopus* egg extracts induced a mitotic block, which was attributed to decreased cyclin and Securin destruction caused by Emi1 dependent APC/C^{Cdc20} inhibition (Reimann et al., 2001 a; Margottin-Goguet et al., 2003). However, this effect is only observed at super-physiological Emi1 levels and did not significantly alter timing or degradation of Cyclin A, Cyclin B, or Securin in human cell culture, opposing an Emi1 inhibitory mechanism for APC/C^{Cdc20} at mitotic entry (Di Fiore et al., 2007). More importantly, Emi1 expression at the G1-S transition induced by E2F transcription factors allows the accumulation of APC/C substrates after APC/C^{Cdh1} inactivation. In this function, Emi1 is crucial in preventing re-replication by stabilizing the APC/C targets Cyclin A and Geminin that are re-replication inhibitors (Reimann et al., 2001 b; a; Hsu et al., 2002; Di Fiore et al., 2007; Machida et al., 2007). Emi1 is divided in three functional domains, the N-terminal domain (Emi1-NT) and the C-terminal domain (Emi1-CT) separated by a central localized F-box domain (Frye et al., 2013). Emi1-CT is required for APC/C inhibition and was initially proposed to inactivate the APC/C via a pseudosubstrate mechanism primarily mediated by a C-terminal located D-box degron (Miller et al., 2006).

However, intensive Cryo-EM, NMR and quantitative biochemical analysis have provided a more sophisticated inhibition mechanism that involves the combined action of four inhibitory domains: a D-box, Linker, zinc binding region (ZBR), and a C-terminal RL-tail (Frye et al., 2013; Wang et al., 2013; Chang et al., 2015). Association of the Emi1 D-box with the receptor sites on Cdh1 and Apc10 occludes substrate recognition (Chang et al., 2015). The linker situated between the D-box and ZBR is not a simple connector since deletion of 20 aa within the linker impaired APC/C inhibition and the effect was not rescued by simple replacement with a glycine rich sequence. Furthermore, substitutions of three highly conserved residues in the linker region were sufficient to impair Emi1 inhibition towards the APC/C, demonstrating that specific side chains contribute inhibition (Frye et al., 2013). The ZBR resembles an in between Ring domain that complexes two zinc ions. Linker together with the ZBR interact with the UbcH10 binding site on $Apc11^{RING}$ and elements of Apc2 and Apc1, blocking UbcH10 association. The ZBR preferentially inhibits UbcH10 chain elongation and only to a lesser extent priming mono- or multi-monoubiquitiniation (Frye et al., 2013; Wang et al., 2013). The C-terminal RL-tail resembles the sequence of Ube2S RL-tail and competes for the same binding groove localized between $Apc2^{CTD}$ and $Apc4^{WD40}$ and antagonizes Ube2S mediated polyubiquitin chain assembly (Figure 14) (Wang et al., 2013; Chang et al., 2015; Watson et al., 2019 b). Together, linker, ZBR, and RL-tail can even prevent polyubiquitination of already bound APC/C substrates (Wang et al., 2013). The individual elements only weakly interact with the APC/C, but synergetic binding to several APC/C subunits strongly increases Emi1 avidity towards APC/C^{Cdh1}. The joint association with several APC/C domains results in an inhibition mechanism on the level of substrate recruitment, UbcH10 ubiquitination and Ube2S dependent chain elongation, making Emi1 a very potent APC/C inhibitor.

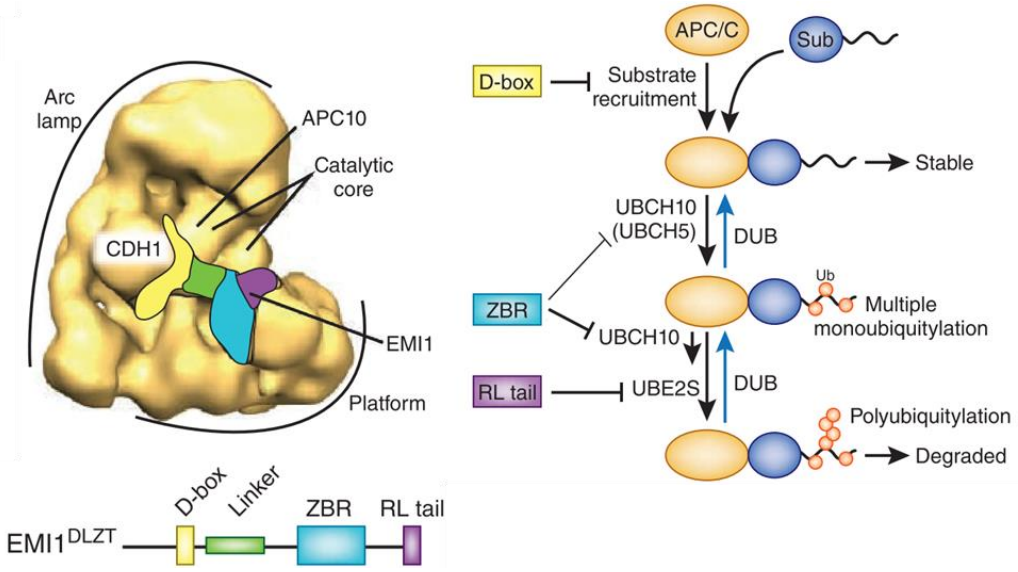

Figure 14| C-terminal Emi1 domains inhibit the APC/C^{Cdh1}

The D-box, Linker, ZBR, and RL-tail of Emi1 bind to different APC/C subunits and domains. Synergetic actions of different inhibitory functions inhibit APC/C^{Cdh1} activity. The D-box (yellow) blocks substrate recruitment occupying the D-box receptor, the Linker (green) together with the ZBR (cyan) inhibits priming substrate ubiquitination catalyzed by UbcH10 and UbcH5. The C-terminal RL-tail competes for the same binding site with Ube2S, abolishing ubiquitin chain elongation. (Figure adopted and modified from Yamano, 2013)

Emi-NT does not contribute to APC/C inhibition since the N-terminal moiety is not able to bind and inhibit the APC/C, but is involved in regulatory processes including APC/C localization via the END network (see section 2.6.9) and its degradation at the onset of mitosis (Reimann et al., 2001 a; Miller et al., 2006). APC/C inhibition by Emi1 must be resolved at the beginning of mitosis to allow destruction of mitotic APC/C targets. This is achieved through Emi1 degradation mediated by another E3 ubiquitin ligase, the Skp-Cullin-F-box containing complex $SCF^{\beta TrCP}$, whereby the adaptor protein β-TrCP recruits Emi1 via its N-terminal DSGxxS motif in a phosphorylation dependent mechanism (Margottin-Goguet et al., 2003). β-TrCP interaction with the DSGxxS motif requires both serine residues to be phosphorylated, which is mediated by Plk1 and is enhanced by the action of CycB-Cdk1 (Hansen et al., 2004; Moshe et al., 2004; Lau et al., 2012). Consistent with the $SCF^{\beta TrCP}$ degradation pathway, overexpression of a nondegradable Emi1 version with a mutated DSG motif caused mitotic arrest in human cell culture accompanied by severe spindle abnormalities, chromosome overcondensation, and chromosome missegregation that can be rationalized by constitutive APC/C inhibition (Margottin-Goguet et al., 2003). During S- and G2-phase, Emi1 degradation is prevented by the interaction with Evi5 that binds close to the DSG motif and inhibits both, Plk1 phosphorylation and β-TrCP binding. Evi5 itself is phosphorylated in early mitosis by Plk1 and degraded by a so far unknown E3 ligase (Eldridge et al., 2006).

Additionally, to the $SCF^{\beta TrCP}$ degradation pathway, Emi1 was suspected to be also an APC/C substrate besides its function as APC/C inhibitor. This hypothesis was supported since Emi1 with a non-functional ZBR was degraded in vivo in human cell culture and was also ubiquinated in vitro in and additional mutation of the D-box prevented both effects indicating that Emi1 is degraded in an APC/C dependent manner (Miller et al., 2006). Opposed to this, overexpression of Cdh1 in interphase Xenopus egg extracts did not promote Emi1 degradation. APC/C inhibition in mitotic extracts did not stabilize Emi1 and mutation of a putative KEN box motif in the Emi1-NT displayed no stabilizing effect in mitotic extracts. Finally, in this study Emi1 was not ubiquinated in vitro which indeed could be explained by the presence of a functional ZBR, however the explanation to this discrepancies is elusive (Reimann et al., 2001 a; b; Margottin-Goguet et al., 2003). A more recent study in different human cell types has in turn provided several lines of evidence supporting the hypothesis of APC/C dependent Emi1 degradation. First, Emi1 protein levels are relatively low in G1-phase compared to S- and G2-phase due to proteolytic degradation and first begin to rise concurrent to APC/C^{Cdh1} inactivation. Emi1 degradation during G1 is unlikely to be mediated by $Plk1/SCF^{\beta TrCP}$ as their activity is restricted to pro-metaphase. Furthermore, Emi1 was stabilized in G1-phase by the addition of a specific APC/C inhibitor proTAME. Second, transcriptional regulation was excluded since mRNA levels of Emi1 and other E2F transcription targets rise directly after anaphase onset, however protein accumulation of Emi1 and the APC/C^{Cdh1} target Geminin were delayed compared to the control proteins. Emi1 and Geminin accumulation is first observed contemporary to APC/C^{Cdh1} inactivation at the end of G1-phase. Third, recombinant Emi1 is ubiquinated in vitro but only at low concentrations. Together, the results strongly indicate a second

APC/C^{Cdh1} dependent degradation pathway keeping Emi1 protein levels in check during G1-phase after initial degradation by $SCF^{\beta TrCP}$ at mitotic entry. Curiously, the conversion from inhibitor to substrate was shown to be dependent on Emi1 concentration; at low concentrations Emi1 is a APC/C target whereas at high concentrations Emi1 functions as APC/C inhibitor (Cappell et al., 2018). To date, this dose dependent dual-negative feedback loop is the first and only mechanistic explanation for the switch converting Emi1 from a potent APC/C inhibitor to an APC/C substrate.

Emi1 contains an F-box domain situated between Emi-NT and -CT that mediates association with a SCF complex via the Skp1 component. Emi1 has been shown to direct interact with Skp1 indicating a further function by recruiting substrates targeted for ubiquitination by a SCF^{Emi1} complex (Reimann et al., 2001 a). However, so far there is only a single instance for a direct SCF^{Emi1} target. The protein Rad51 that is involved in homologous recombination repair is targeted by Emi1 for degradation, keeping free cellular Rad51 protein at homeostatic levels. Furthermore, Emi1 downregulation in BRCA1 deficient breast cancer cells is responsible for the resistance to therapeutic PAP inhibitors caused by elevated Rad51 levels, emphasising the importance proper SCF^{Emi1} function in breast cancer (Marzio et al., 2019).

2.6.11. Rca1, the *Drosophila* APC/C^{Fzr} inhibitor

Regulator of Cyclin A1 (Rca1), the *Drosophila* homologue of Emi1 was first discovered in a screen for dominant suppressors of the *rux[3]* phenotype in the developing eye of *Drosophila*. Rux is a CKI specific for Cdk1 and thus contributes to the establishment and maintenance of G1-phase (Foley et al., 1999; Avedisov et al., 2000). In *rux[3]* mutants, cells of the developing eye fail to establish a stable G1-phase and enter precocious into S-phase caused by premature CycA-Cdk1 activity. The rux phenotype is characterized by defects in pattern formation and morphological abnormalities in the eye, also referred to as rough eye phenotype. Heterozygous mutations in rca1, cycA, string and twine (Cdc25 homologues in *Drosophila*) suppressed the cell cycle defects in *rux[3]* mutant eye discs and were able to restore a normal G1 phase. A genetic interaction between *rca1* and *cycA* was postulated since Rca1 overexpression resulted in the rough eye phenotype with elevated Cyclin A levels and premature entry into S-phase. Homozygous *rca1* mutants arrest in G2-phase accompanied by reduced CycA protein levels and failed to complete mitosis of embryonic cell cycle 16 and to establish the first G1-phase during embryogenesis, similar to CycA loss of function mutants (Dong et al., 1997; Grosskortenhaus et al., 2002). Hence, the protein was named regulator of cyclin A1. Nevertheless, Rca1 is not responsible for direct regulation of Cyclin A, but the observed effects are attributable to its function as a potent APC/C^{Fzr} inhibitor during S- and G2-phase, similar to Emi1, which has been demonstrated by different findings. Embryos mutant for *rca1* exhibit premature degradation of the mitotic Cyclins A and B, and cells consequently failed to enter mitosis displayed by a reduced cell number compared to wild type. The observed phenotype is reminiscent to Fzr overexpression also causing premature cyclin destruction that can be blocked by additional Rca1 overexpression. Analysis of *rca1/fzr* double mutants ascertain that

the effects are specific for APC/C^{Cdh1} and not attributed to inhibition of the core APC/C. This was further supported by direct interaction of Rca1 with Fzr and Apc3 (Cdc27) seen in co-immunoprecipitation experiments (Grosskortenhaus et al., 2002). Besides the same APC/$C^{Cdh1/Fzr}$ inhibitory function, Rca1 and Emi1 possess a similar arrangement of functional domains, even though they shares only 16% sequence identity (Reimann et al., 2001 a). Rca1 is also divided into three domains: The N-terminal moiety (Rca1-NT), a centrally located F-box domain and the C-terminal part (Rca1-CT) (Figure 15).

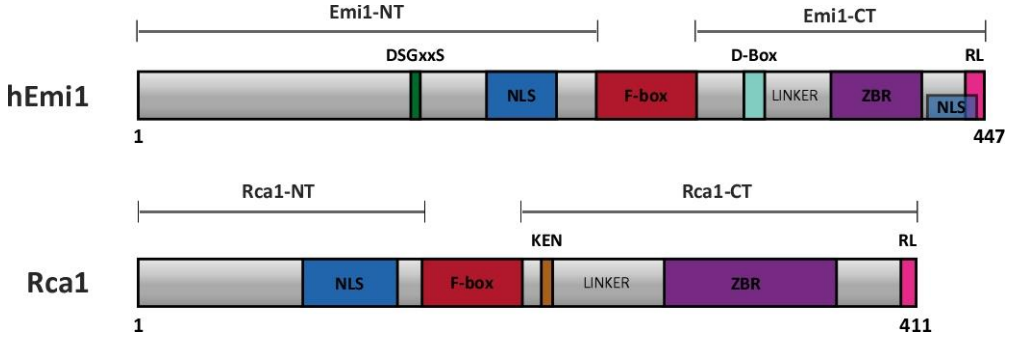

Figure 15| Illustration of human Emi1 and Rca1 protein domains

Rca1 and hEmi1 share a similar arrangement of functional domains and are both divided into an N-terminal domain (Emi1-NT/Rca1-NT), a centrally localized F-box domain, and a C-terminal domain (Emi1-CT/Rca1-CT). Emi1-NT harbors a nuclear localization sequence (NLS) and a DSG motif required for $SCF^{\beta TrCP}$ mediated degradation in mitosis. Emi1 and Rca1 are both incorporated into a SCF complex via an F-box domain. Emi1-CT contains APC/C inhibitory domains D-box, Linker, zinc binding region (ZBR) and the C-terminal RL-tail. A second NLS sequence is also predicted in Emi1-CT. Rca1 also contains a central F-box domain and a NLS in Rca1-NT. Rca1-CT shares similar domains to hEmi1-CT, a KEN-box instead of a D-box, a potential Linker region, a ZBR and a RL tail.

Rca1-NT contains a functional bipartite NLS since HA-Rca1 expressed in the embryo was nuclear (Grosskortenhaus et al., 2002). Rca1-CT harbours several functional domains like Emi1; a KEN-box degron instead of a D-box, a potential linker region, a ZBR and a C-terminal RL-tail. Rca1-CT was shown to be sufficient for APC/C^{Fzr} inhibition, since additional expression of Rca1-CT rescued the Rca1 phenotype in *rca1* mutants and restored mitosis 16 during embryogenesis. However, Rca1 with a non-functional ZBR (C351S) was not able to inhibit the APC/C, implying a similar mode of inhibition like Emi1 (Zielke et al., 2006).

APC/C inhibition was independent of the F-box domain, however Rca1 overexpression accelerates G1-S transition in an F-box dependent manner. Consistent to this, cells expressing Rca1 with an F-box deletion instead of endogenous Rca1 exhibit a delayed entry into S-phase. The F-box was found to be required for the interaction with the *Drosophila* Skp1 homologue SkpA together with the SCF component Cul1, indicating that Rca1 is incorporated into a SCF^{Rca1} complex, serving as a substrate recruiting F-box protein. A potential SCF^{Rca1} target is the *Drosophila* CKI Dacapo, identified by mass spectrometry experiments for Rca1 interaction partners that could explain the F-box dependent S-phase induction. Dap is a CKI specific for CycE-Cdk2 that prevails premature Cdk activity before S-phase entry and is first degraded via $CRL4^{Cdt2}$ E3 ligase complex at the beginning of DNA replication. SCF^{Rca1} mediated Dap degradation at the end of G1 would allow initial CycE-Cdk2 activity required for S-phase onset. Rca1 and

Dap interaction was verified by co-IP experiments, but the direct influence on the G1-S transition is still under investigation (Zielke et al., 2006; Frank, 2013; Kies, 2017).

Rca1 degradation takes place during G1-phase, since HA-Rca1 is no longer detectable in embryonic cells that entered the first G1-phase of the 17th cell cycle. Same results were observed in live cell imaging experiments with a Rca1-GFP reporter construct in whole embryos as well as in single cultured S2R+ cells (Grosskortenhaus et al., 2002; Morgenthaler, 2013). First attempts to get deeper insight into Rca1 degradation and the responsible protein domains, identified the central localized KEN-box motif to be responsible for degradation of a small Rca1 fragment (amino acids 204-299) and Rca1 degradation curves resembled those of an APC/C^{Fzr} substrate. These evidence gave rise to the hypothesis, that Rca1 destruction in G1-phase might be mediated by APC/C^{Fzr} (Morgenthaler, 2013). In summary, it can be stated that initial experiments regarding the APC/C^{Fzr} inhibitory mechanism and a potential degradation pathway have been described. However, more attempts in a uniform and robust system must be performed to further elucidate the molecular mechanisms behind Rca1 inhibition of APC/C^{Fzr}, Rca1 degradation in G1, and regulatory events that are responsible for turning Rca1 from an APC/C inhibitor to a possible APC/C substrate.

3. Results

3.1. The RPS system, a versatile tool to measure protein degradation in vivo

3.1.1. Aim

Rca1 is degraded during G1-phase and first attempts indicate that its degradation might be mediated by APC/C^{Fzr}. To further investigate Rca1 degradation a new high throughput analysis method to determine protein degradation in asynchronous, single cell populations using flow cytometry was established and named **R**elative **P**rotein **S**tability system (RPS). This method should enable quick, robust, and reproducible measurement of relative protein stability levels of selected proteins in *Drosophila* S2R+ cells after transient transfection *in vivo*. The system is based on a set of expression plasmids that allow the stoichiometric co-expression of a stable fluorescent reference and a fluorescent reporter fusion with the protein of interest (POI) from a single mRNA, using a viral 2A sequence. The stoichiometric translation of both proteins allows inference on relative protein levels by comparing the POI reporter to the reference signal. Based on the DNA content of each single cell, relative protein stability of the POI can be assigned to the respective cell cycle phase and thereby cell cycle phase specific degradation of the POI can be identified.

To establish the RPS system for the measurement of protein degradation *in vivo*, in a first step the stoichiometric protein co-expression, skipping efficiency, and cell cycle assignment based on the DNA content were analyzed. In the next step, a well known APC/C substrate, Cyclin B, which is degraded during G1-phase of the cell cycle, was examined in this RPS-system. Using an N-terminal Cyclin B fragment that contains APC/C degron sequences, the RPS system was used to determine the expression level range that allows detection of degradation. Furthermore, it was tested if this degradation is mediated by the proteasome and how unsuccessful ribosome skipping could potentially influence the results (see 3.1.5.1). Evaluation of putative APC/C degrons was performed by mutating the predicted degron consensus sequences. Furthermore, changes in protein stability levels were also analyzed after overactivation or knockdown of APC/C activity. Protein degradation during S-phase was analyzed using the $CRL4^{Cdt2}$ substrates that are typically degraded with the onset of DNA replication (see 3.1.6).

3.1.2. The RPS expression system allows stoichiometric protein co-expression

The measurement of relative protein stability levels relies on the stoichiometric co-expression of a fluorescent reference and reporter protein that are relatively stable during cell cycle progression. The decline of reporter-POI fusion intensities compared to the reference signals that is caused through the instability of the POI should be utilized as read out of protein degradation with the kinetics of the protein of interest. The stoichiometric expression of the two proteins which is achieved through the RPS expression plasmids was already tested in a preceding work (Polz, 2017). Since the initial analysis, further improvements of the data acquisitions settings on the flow cytometer could be established and the analysis of stoichiometric expression was repeated. The basic expression plasmids RPS-1 to RPS-8

contain the two fluorophores mCherry (CHE) (Shaner et al., 2004) and the enhanced green fluorescent protein (EGFP = GFP)(Cormack et al., 1996) either as reference or reporter separated by a modified viral T2A sequence (ddT2A = T2A) for ribosome skipping that has been optimized for the use in *Drosophila* (see Table S 3) (Polz, 2017). Both proteins contain an additional human influenza epitope (HA-tag; YPYDVPDY) and a nuclear localization signal derived from the SV40 nuclear Large T-antigen (NLS; PKKKRKV) at their N-terminus. Cloning sites at different positions allow the insertion of the POI either N- or C-terminal to the reporter protein and up- or downstream of the T2A site (Figure 16 A). The application of ribosome skipping mediated by 2A sequences enables the translation of the proteins from a single mRNA encoded by one expression plasmid. Protein expression is under the control of a strong constitutive active actin promotor derived from the *Drosophila* actin-5C gene (Cormack et al., 1996). To be suitable for the analysis of relative protein stability levels, the RPS plasmids must fulfill two basic criteria: First, protein co-expression must exhibit a high degree of co-linearity over a broad expression range. Second, a high skipping efficiency must be achieved to mainly translate the two desired proteins. To investigate the stoichiometric expression of the two proteins, cells were transiently transfected with the RPS plasmids and the GFP and CHE signals were detected via flow cytometry. The logarithmic CHE and GFP intensity values of each cell are displayed in a scatter plot with each cell being represented by a single point. The expression of the two fluorophores occurred with a high degree of co-linearity over the detected expression range verified by regression analysis with R^2 values between 0.98 and 0.99. The CHE/GFP quotients were also analyzed in different cell cycle stages using the DNA content of each cell that was recorded by the Hoechst 33342 fluorescence. The quotients were relatively stable in dependency of the DNA content of the measured cells, shown by a linear correlation in cells with different Hoechst intensities representing cells of different cell cycle phases. This indicates that the stoichiometric expression was independent of the cell cycle progression (Figure 16 B).

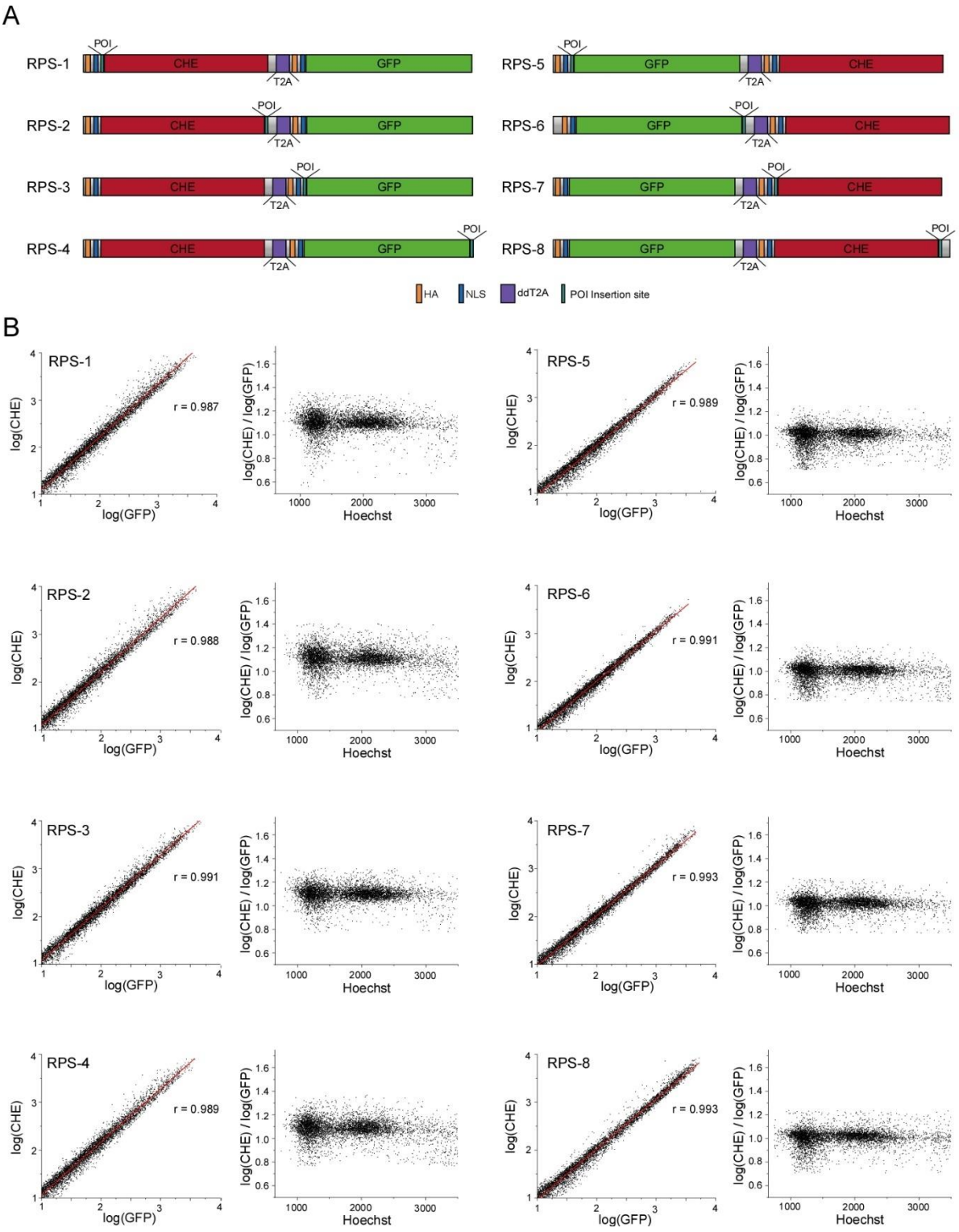

Figure 16| The RPS expression system enable stoichiometric co-expression of CHE and GFP

(**A**) Schematic illustration of the RPS expression constructs. The RPS plasmids contain the two fluorescent proteins mCherry (CHE - red) and green fluorescent protein (GFP - green) separated by a modified T2A sequence (purple). N-terminal of CHE and GFP, an HA-tag (orange) and a nuclear localization signal (NLS - blue) were inserted. POI insertion sites (cyan) are situated at different positions allowing N- and C-terminal tagging of the POI to GFP or CHE either up or downstream of the T2A site, respectively. (**B**) Scatter plots (n=5800) of CHE and GFP intensities detected by flow cytometry of cells transfected with the respective RPS plasmid. Regression lines (red) and resulting R^2 values (r) are indicated. The log(CHE)/log(GFP) quotient was plotted against the Hoechst intensities representing the cellular DNA content.

3.1.3. Ribosome skipping at the T2A site results with high efficiency

The second criterion regards the skipping efficiency mediated by the modified T2A site. In general, ribosome skipping mediated by 2A sequences can generally result in three outcomes (Liu et al., 2017): (1) Translational stop at the 2A site and dissociation of the ribosome from the mRNA resulting in the translation of only the protein upstream of the 2A sequence. (2) Successful ribosome skipping and translation of both proteins. (3) Failed skipping and ribosome read-through creating a full-length polyprotein (FLP). To test the skipping efficiency of the RPS plasmids, the translated proteins were quantified via Western blot analysis of S2R+ cell lysates after transfection with the RPS plasmids. Three major protein bands were detected using a HA-antibody representing HA-NLS-GFP and HA-NLS-CHE as well as FLP with a high molecular mass caused through failed ribosome skipping. After ribosome skipping 17 aa of the T2A sequence remain on the C-terminus of the upstream protein (T2A) and 3 aa at the N-terminus of the downstream protein (*). Quantification of the relative Western blot intensities resulted in a skipping efficiency of 92-97%, consequently only 3-8% of the translated protein are FLP (Figure 17 A,B,C) (Polz, 2017).

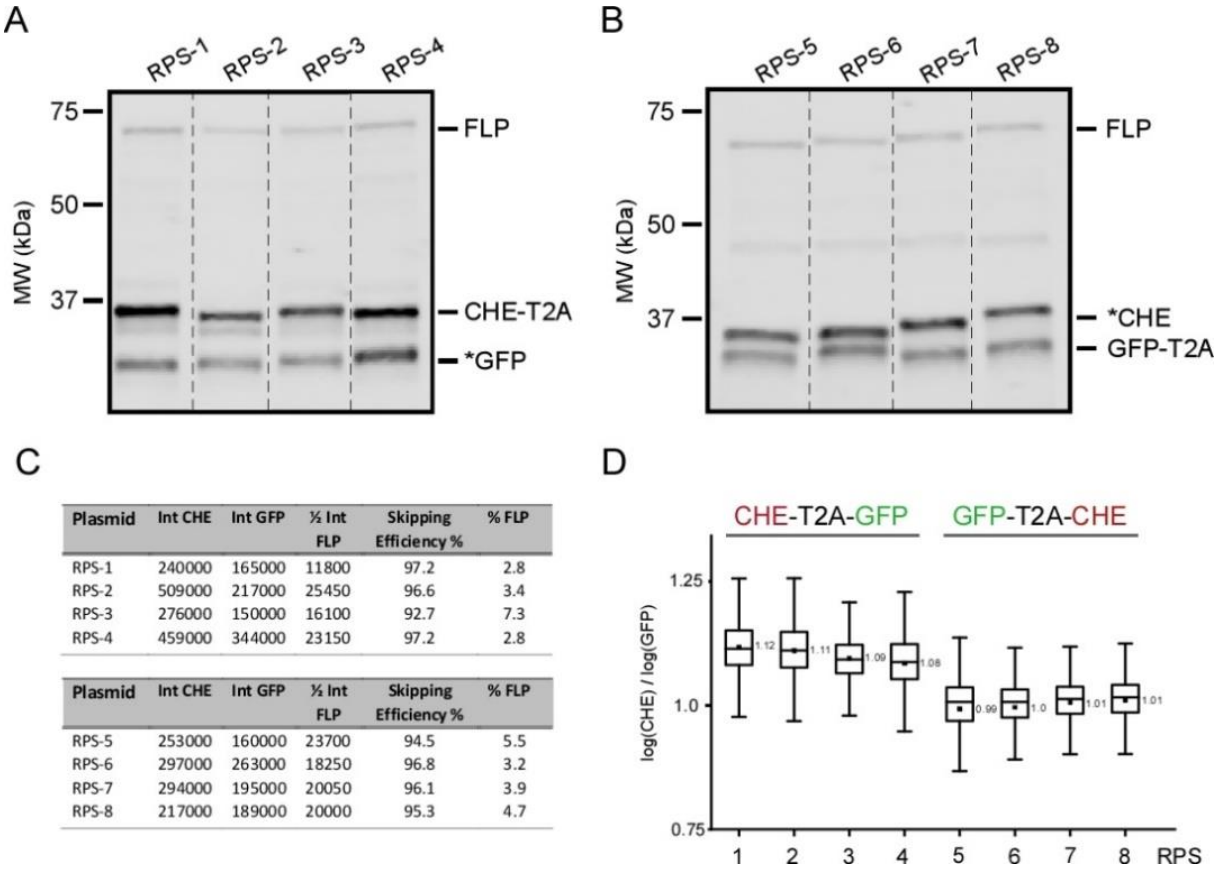

Plasmid	Int CHE	Int GFP	½ Int FLP	Skipping Efficiency %	% FLP
RPS-1	240000	165000	11800	97.2	2.8
RPS-2	509000	217000	25450	96.6	3.4
RPS-3	276000	150000	16100	92.7	7.3
RPS-4	459000	344000	23150	97.2	2.8

Plasmid	Int CHE	Int GFP	½ Int FLP	Skipping Efficiency %	% FLP
RPS-5	253000	160000	23700	94.5	5.5
RPS-6	297000	263000	18250	96.8	3.2
RPS-7	294000	195000	20050	96.1	3.9
RPS-8	217000	189000	20000	95.3	4.7

Figure 17| Quantification of the skipping efficiency of the T2A site

(**A**, **B**) Western blot analysis of the eight RPS plasmids. Three major protein bands are detected using an HA-antibody. The upstream protein with 17 aa of the T2A sequence (T2A) remaining on the C-terminus and 3 aa on the N-terminus of the upstream protein (*). A band with high molecular weight represents the full-length polyprotein (FLP) translated by a read through after failed ribosome skipping. (**C**) Quantification of the detected protein band intensities. Skipping efficiency was calculated by the formula Int^{CHE}+Int^{GFP}/ (0.5xInt^{FLP} + Int^{CHE}+Int^{GFP})x100. *Int*: integrated intensities of the HA-signal. The FLP contains two HA-tags; therefore, the integrated intensities were halved. (**D**) Analysis of the RPS plasmids with CHE set as reporter displayed higher CHE/GFP quotients with CHE being upstream of the T2A site compared to downstream.

To test if more upstream protein was translated, the CHE/GFP quotient of the RPS plasmids with either CHE up or downstream of the T2A site were compared via flow cytometry. The quotient was slightly higher when CHE was situated upstream of the T2A site indicating that more upstream protein is expressed because of a translational stop and dissociation of the ribosome at the T2A site. In accordance, intensities of the upstream protein were higher compared to the downstream protein in the Western blot quantification (Figure 17 C, D). In conclusion, the RPS plasmids allow the stoichiometric co-expression of the reporter and reference protein over a broad expression range. Ribosome skipping occurred with high efficiency with only a small proportion of full-length polyprotein being present. Since termination of translation at the T2A site caused a difference in translation between the up- and downstream protein, the insertion of the POI should be tested and compared at both positions.

3.1.4. Selection of cell populations “G1”, “S”, and “G2”

Assignment of relative protein stability levels to the respective cell cycle phase was implemented by defining cell populations based on the cellular DNA content. Cells were treated with the cell permeable DNA stain Hoechst 33342 that was detected during flow cytometric analysis in parallel to the GFP and CHE fluorescent signals. Plotting the Hoechst intensity values in a histogram results in a curve that represents the distribution of the cell population over the cell cycle, which can be inferred from the cellular DNA content. The first peak contains cells with lower DNA content, e.g. G1-cells (1C). After DNA-replication, cells contain a double DNA-content (2C), and these can be found under the second peak that also contains mitotic cells. In between are cells with intermediate DNA content, e.g. cells that undergo DNA-replication. To diminish overlap of different cell cycle phases, three cell populations “G1”, “S”, and “G2” were defined based on the two peak maxima and the minimum value between G1 and G2 peak. Cells in the range from the first maximum to values -200 are assigned as “G1”, cells in the range -150 to +100 from the minimum values are assigned “S”, and cells in the section +300 from the second maximum are referred to as “G2. The“G2” population will also contain mitotic cells in lower amount (less than 2% of cells are positive for the mitotic marker Ser10-phophorylated Histone 3) that cannot be distinguished fromG2-phase based on Hoechst fluorescence (personal communication Frank Sprenger). Analysis of cells transfected with RPS-8 in the defined G1, S, and G2 populations display a relatively constant CHE/GFP ratio since both proteins are not degraded in a cell cycle dependent manner (Figure 18 A, B). To validate this subdivision, S-phase cells were detected by EdU incorporation using the Click-It EdU Kit. Flow cytometric analysis of glyoxal fixated cells stained with Edu and Hoechst enabled the simultaneous detection of EdU positive S-phase cells and the Hoechst-DNA signal (Figure 18 C, D). The EdU positive cells (red line) are displayed in a histogram in combination with a Hoechst histogram of all cells (black line) (Figure 18 E). In total, 20.5% of the measured cells were EdU positive. Analysis of the cell cycle distribution using the MultiCycle AV DNA analysis tool built in FCS express software predicted a proportion of 25.7% of S-phase cells based on a mathematical model. Due to

background in the Edu detecting channel, cells with lower EdU incorporation level or insufficient click-chemistry will be missed, underestimating the number of S-phase cells slightly (compare Figure 18 E and F). The defined “G1” population contained 8.6%, the “G2” cells 7.8%, and the “S”-phase population 40.5% EdU positive cells (Figure 18 C). This indicates that all population contain cells in different cell cycle phase, but the majority of cells in the “G1” population has not entered S-phase. Similarly, the “S” population does contain G1 and G2 cells, as predicted by the mathematical model as well. In the “G2” population, S-phase cells as well as mitotic cells will be present, but the majority will be cells in G2 phase.

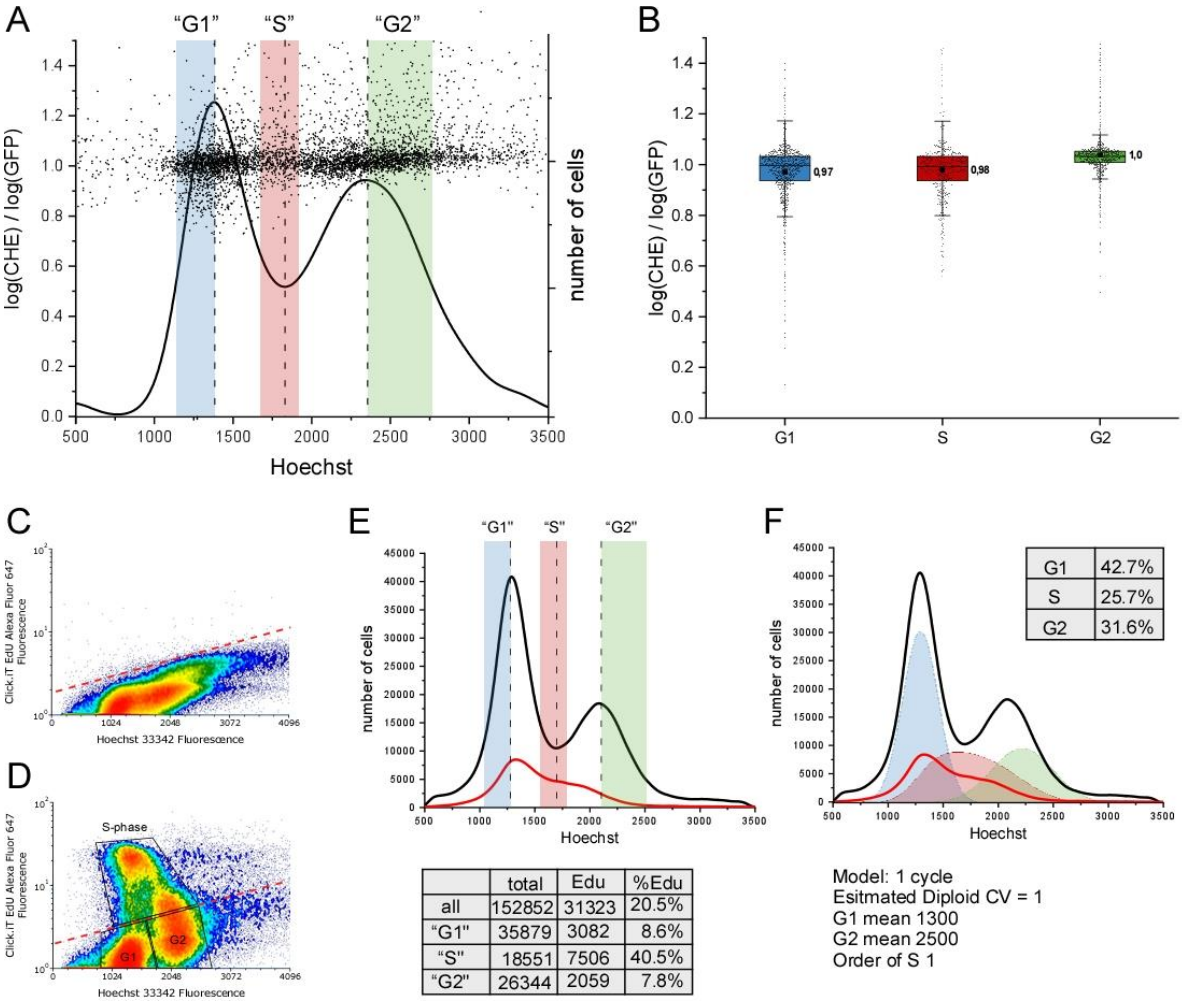

	total	Edu	%Edu
all	152852	31323	20.5%
“G1”	35879	3082	8.6%
“S”	18551	7506	40.5%
“G2”	26344	2059	7.8%

Figure 18| Determination of the "G1", "S", and "G2" cell populations

(**A**) Combination of DNA histogram (Hoechst x-axis and number of cells right y-axis) and scatter plot of CHE/GFP ratios of cells transfected with RPS-8 NLS-GFP-T2A-NLS-CHE-B/X (CHE/GFP left y-axis and Hoechst x-axis). The two maxima and the minimum value between are displayed by a dashed line. “G1” cells are defined by the area from the G1 peak to -200 (blue area), “S” cells in the range -150/+100 from the minimum value (red area), and “G2” cells from the G2-peak +300 (green area). (**B**) Box plot of the cells analyzed in the G1, S, and G2 cell populations display a fairly constant expression of GFP and CHE with G1 mean 0.97, S mean 0.98, and G2 mean 1.0. (**C**) Density plot of control cells without EdU treatment. The red dashed line marks the threshold of background signal. (**D**) Density plot of EdU and Hoechst 33342 stained cells. The two populations below the EdU threshold are G1 and G2 cells the EdU positive cells represent S-phase cells. (**E**) DNA histogram of glyoxal fixated cells after EdU incorporation (red line). Quantification of the EdU positive cells compared to the total cell number and for the defined G1, S, and G2 cell population. (**F**) Calculation of cells in G1- (blue area), S- (red area), and G2-phase (green area) by a mathematical model.

3.1.5. Degradation analysis of known APC/C substrates in G1-phase

To test if protein degradation of a POI can be detected using the RPS method and that cell cycle phase assignment is sufficient to allocate POI proteolysis to a respective cell cycle stage, known E3-ligase substrates were analyzed with the RPS system. Protein degradation in G1-phase was tested using the well characterized APC/C targets Cyclin B and Geminin. To simplify the analysis, only RPS plasmids with GFP as reference and CHE as reporter were used for the following analysis, except for the analysis of the mutated T2A site (see section 3.1.5.1.4). Additionally, the omnipresent HA-tag and the NLS (HA-NLS) were omitted from the names to allow an easier nomenclature (except in the localization analysis see section 3.4.4). For instance, HA-NLS-GFP-T2A-HA-NLS-CHE-POI will be termed GFP-T2A-CHE-POI.

3.1.5.1. Analysis of Cyclin B

Cyclin B is important for mitotic entry, regulating several mitotic events by activating Cdk1. Decline of Cdk1 activity after anaphase is important to trigger mitotic exit and cytokinesis that is in large part achieved through proteolytic destruction of Cyclin B. Degradation of Cyclin B is initiated by APC/C^{Fzy} dependent ubiquitination after SAC inactivation at the beginning of anaphase and continued by APC/C^{Fzr} throughout G1-phase.

3.1.5.1.1. Cyclin B degradation is impaired at high expression level rates

For the analysis of cell cycle stage dependent Cyclin B degradation, an N-terminal fragment CycB_Del_286-530 (CycB-NT^{285}) was used. CycB-NT^{285} contains the N-terminal located D-box required for APC/C dependent degradation (Sigrist et al., 1995) but the deletion of the C-terminal cyclin boxes renders it unable to bind and activate Cdk1 (Figure 19 A). Thus, no artificial Cdk1 activity will be added when using this CycB version. CycB-NT^{285} was cloned into RPS-5 to RPS-8 to determine relative protein stability levels by flow cytometry of transiently transfected S2R+ cells. However, transient transfection results in heterogeneous cell populations with different expression rates of the target proteins due to varying numbers of absorbed plasmids. To test which expression levels are compatible with normal degradation of CycB in this system, CHE/GFP ratios were analyzed with increasing expression levels visualized by increasing GFP values. Cyclin B degradation takes place from mitosis to G1-phase, consequently low CHE/GFP ratios are expected for G1 cells. Analysis of the G1 population of cells transfected with GFP-T2A-CHE-CycB-NT^{285} displayed the expected low CHE/GFP ratios in a range of low GFP-reference values but the CHE/GFP quotient showed a sudden increase at higher expression levels (Figure 19 B). Analysis of G1 cells with different expression level ranges (exp.lvl.) displayed a strong increase of the mean CHE/GFP ratios at higher expression levels: 0.03 (exp.lvl. 1.0 - 1.75), 0.13 (exp.lvl. 1.75 - 2.5), and 0.50 (exp.lvl. 2.5 - 3.25) (Figure 19 D).

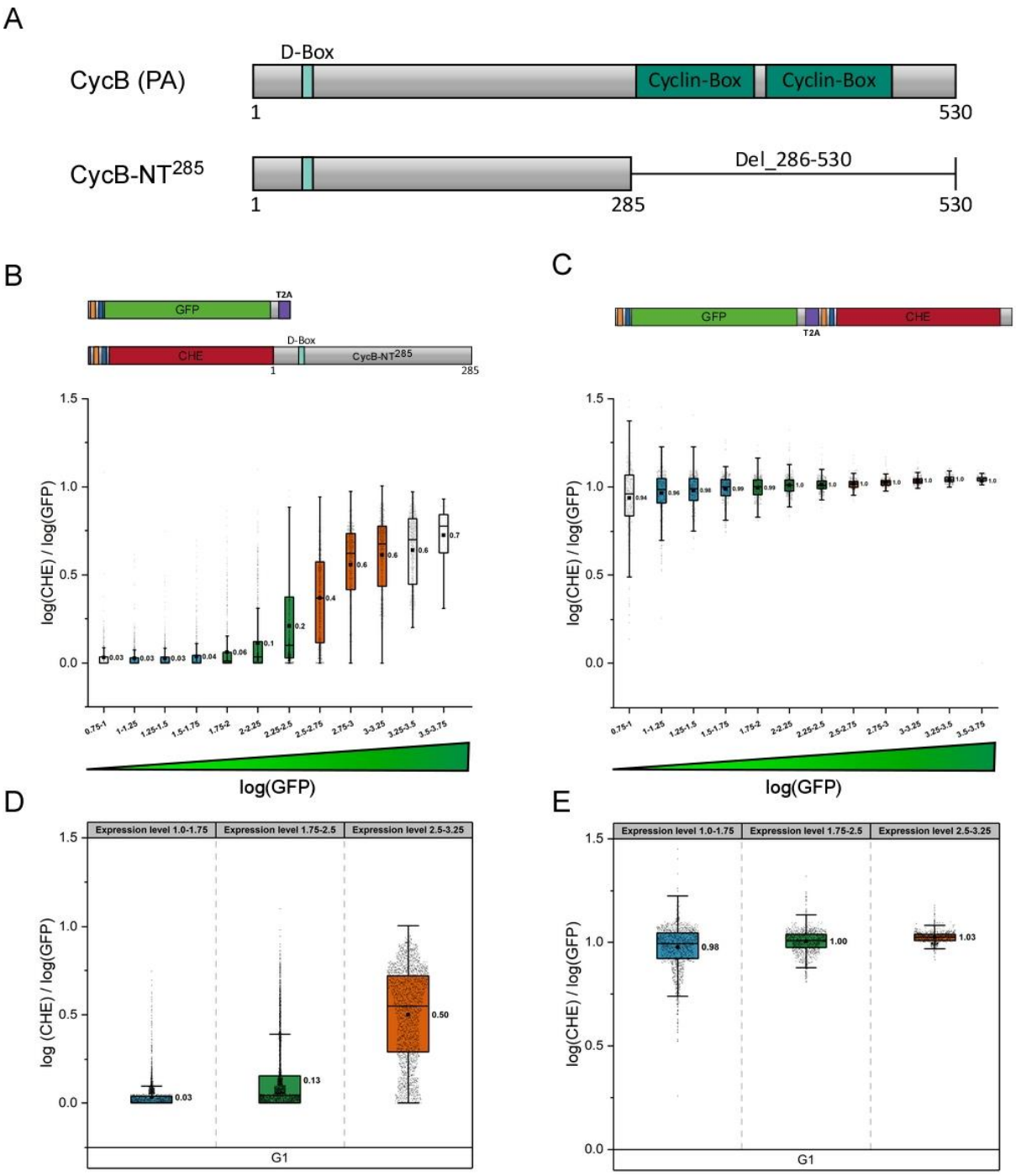

Figure 19| Selection of expression levels ranges based on the reference intensity

(**A**) Schematic illustration of Cyclin B (isoform PA) and CycB-NT^{285}. (**B, C**) Flow cytometric analysis of CycB-NT^{285} and the RPS-8 control showing CHE/GFP values of transfected cells with increasing GFP reference values. Cells have been summarized in box plots with increasing GFP values with an increment of 0.25. CHE/GFP quotients begin to rise at higher expression levels in case of GFT-T2A-CHE-CycB-NT^{285}, whereas the control plasmid GFP-T2A-CHE remains stable with increasing GFP reference intensities. (**D, E**) Analysis of the G1-population with defined expression level ranges 1.0 - 1.75, 1.75 - 2.5, and 2.5 - 3.25 displayed increasing CHE/GFP values for CycB-NT^{285} compared to the stable RPS control plasmid (RPS-8).

In control cells transfected with GFP-T2A-CHE (RPS-8) the CHE/GFP ratio of G1 cells remained constant over the whole expression range compared to CycB-NT^{285} (Figure 19 C, E). The increase of relative protein stability levels in dependence on increasing expression levels is most pronounced in G1 when Cyclin B degradation takes place, however the same effect can be observed in the S- and G2-population to a minor extent, for all RPS-CycB-NT^{285} variants (data not shown). The observed stabilization of CycB with increasing expression levels is probably referable to a saturation of the endogenous degradation system caused by the overexpression of the target protein. Consequently, selection of the appropriate expression levels is essential to determine relative protein stability levels of a protein of interest and suitable ranges have been individually determined for each substrate and are noted in the figure legend.

3.1.5.1.2. N- and C-terminal CycB-NT^{285} reporter fusion are degraded in G1 cells

After determination of an appropriate expression level range, CycB-NT^{285} relative protein stability levels were analyzed for the G1-, S-, and G2- population. Decreased CHE/GFP values are expected for G1-cells compared to S- and G2-cells due to Cyclin B degradation in G1 and subsequent inactivation of APC/C^{Fzr} at the onset of S-phase. Flow cytometric analysis of cells transfected with GFP-T2A-CHE-CycB-NT^{285} displayed a significant reduction in the CHE/GFP ratio for cells with lower DNA content compared to control cells (compare Figure 18 A and Figure 20 A). Analysis of the defined cell cycle phase populations resulted in low CHE/GFP values with a mean value of 0.03 in G1-cells compared to mean values of 0.2 and 0.5 in S- and G2-cells, respectively (Figure 20 B). The decrease of relative protein stability in G1 and increasing values in S and G2 are in accordance with APC/C dependent Cyclin B degradation during M- and G1-phase followed by Cyclin B accumulation. Relative protein stability levels of C-terminal tagged constructs GFP-T2A-CycB-NT^{285}-CHE and CycB-NT^{285}-CHE-T2A-GFP and N-terminal tagged constructs GFP-T2A-CHE-CycB-NT^{285} and CHE-CycB-NT^{285}-T2A-GFP were compared to confirm if the different reporter fusions influence CycB-NT^{285} degradation. Mean values of independent replicates conducted in different weeks were summarized in box plots. The mean values were normalized to the mean values of the respective RPS control of the same cell cycle phase. No difference was observed between N- and C-terminal tagged CycB-NT^{285}. All four constructs are significantly destabilized in G1 cells compared to S- and G2-cells with similar mean values in the respective cell cycle populations (Figure 20 C). Thus, CycB-NT^{285} degradation is not impaired by either N- or C-terminal reporter fusions and both variants result in similar outcomes.

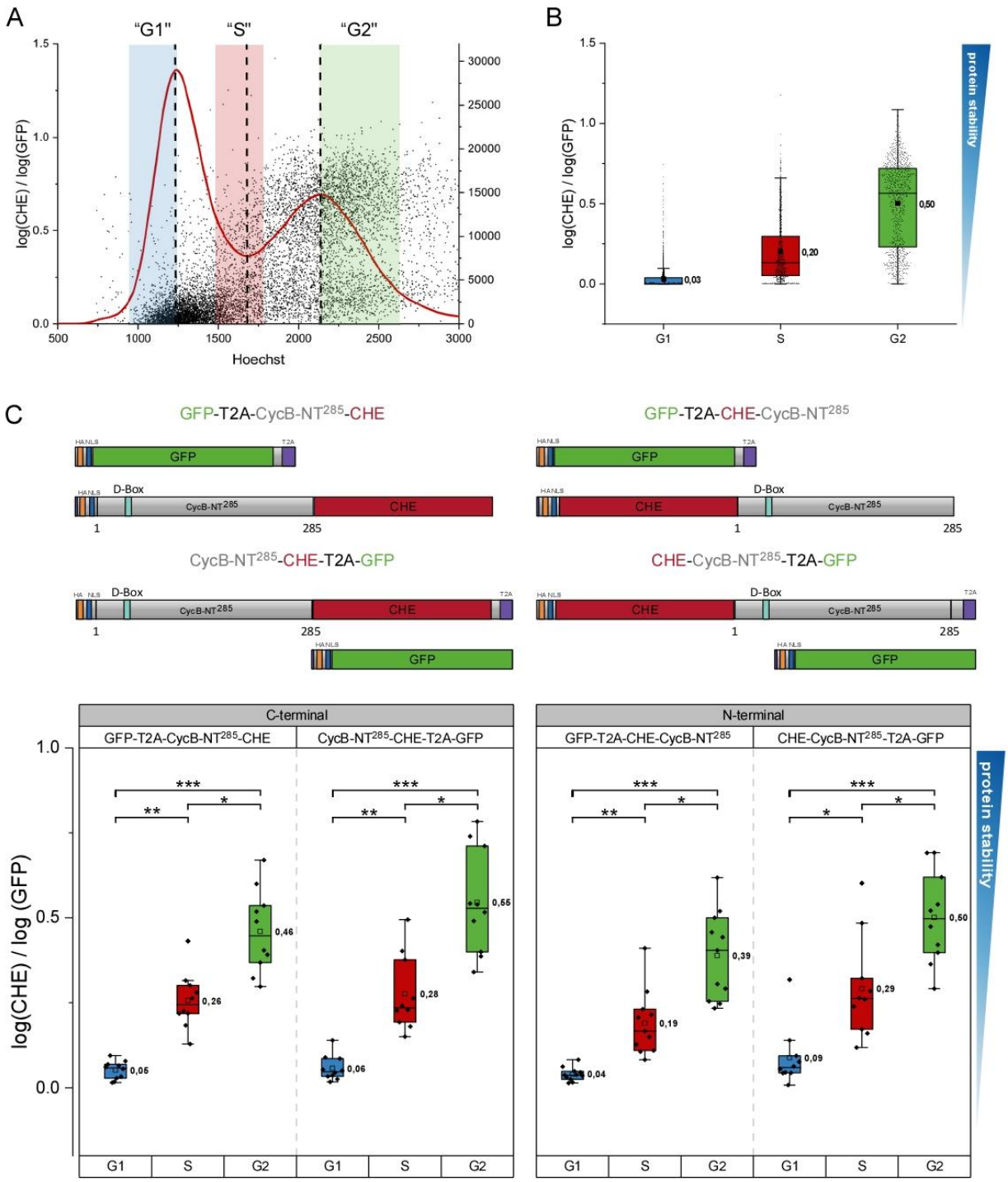

Figure 20| CycB-NT^{285} degradation in G1-phase

(**A**) Combination of DNA histogram and scatter plot of cells transfected with GFP-T2A-CHE-CycB-NT^{285}. Cells with lower DNA content display decreased CHE/GFP values compared to cells with higher DNA content. (**B**) Analysis of the G1-, S-, and G2-population displays a decrease of relative protein stability in G1 and increasing levels in S and G2. (**C**) Comparison of N- and C-terminal reporter fusions of CycB-NT^{285}. Illustration of the analyzed N- and C-terminal tagged CycB-NT^{285} RPS variants. Box plot (exp.lvl. 1.0 - 1.75) summarizing the mean quantification of CHE/GFP ratios of independent replicates normalized to the RPS control values. Statistics performed by t-test with Welch´s correction, * ≤ 0.05, ** ≤ 0.01, ***≤ 0.001.

3.1.5.1.3. RPS analysis reflects proteasomal degradation

The readout of relative protein stability levels is based on the difference of fluorescent intensities between the stable reference and the reporter-POI fusions fluorescent intensities. Ideally, any change in

the reporter-POI fluorescent intensities is caused by the proteolysis of the fusion protein with the kinetics of the POI. To confirm that low protein stability level of CHE-CycB-NT^{285}/GFP values in G1 is caused by degradation in the 26S proteasome and not by any other changes that might influence the fluorescence of the POI-fusion protein, relative protein stability levels were analyzed with simultaneous inhibition of proteasomal degradation. Relative protein stability of GFP-T2A-CHE-CycB-NT^{285} was measured in cells treated with the proteasome inhibitor Bortezomib (100 nM, 8h) or DMSO, 48 h after transient transfection. Mean values of the cell cycle phases were normalized to the RPS control treated the same way either with DMSO or Bortezomib. Control cells treated with DMSO displayed a decrease of relative protein stability levels in G1-cells and increasing levels in S- and G2-cells similar to untreated cells (compare Figure 20 C and Figure 21). Cells treated with the proteasome inhibitor Bortezomib exhibit elevated CHE/GFP ratios in all three cell cycle populations compared to the control cells. Thus, the observed differences in the CHE/GFP ratios are attributed to proteasomal degradation of the CHE-POI fusion protein.

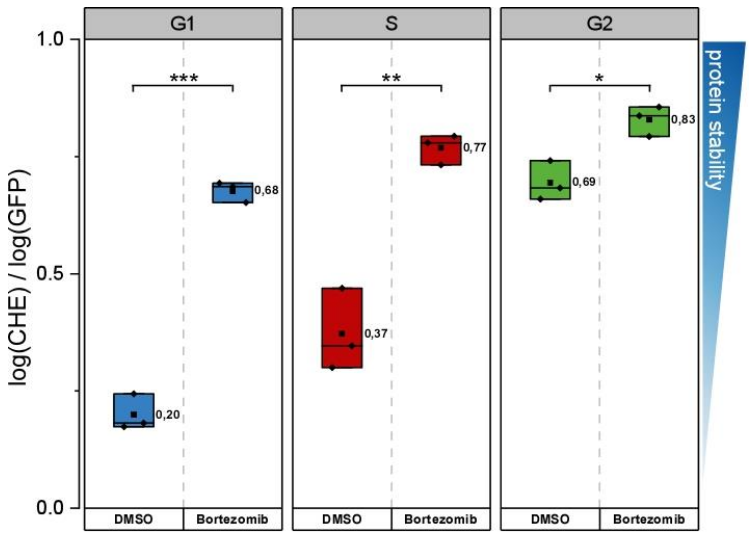

Figure 21| CycB-NT^{285} RPS levels increased in S2R+ cells treated with Bortezomib

RPS analysis of GFP-T2A-CHE-CycB-NT^{285} transfected S2R+ cells (n=3; exp.lvl 2.0 - 3.0). Comparison of control cells treated with DMSO and cells treated with Bortezomib. Normalized CHE/GFP quotients to RPS control treated either with DMSO or Bortezomib. Cells treated with Bortezomib display an increase in protein stability of CHE-CycB-NT^{285} in all three cell cycle populations. Statistics performed by t-test with Welch´s correction, * ≤ 0.05, ** ≤ 0.01, ***≤ 0.001.

3.1.5.1.4. FLP-CycB-NT^{285} is degraded during cell cycle progression

Protein expression of the cells transfected with the CycB-NT^{285} was analyzed in cell lysates separated by SDS PAGE and following Western blot analysis using a HA-antibody for protein detection. The RPS controls displayed three major protein bands representing the up- and downstream fluorescent protein and unskipped FLP that have already been observed (see 3.1.2, Figure 17). Analysis of the RPS-CycB-NT^{285} variants, using the example of GFP-T2A-CHE-CycB-NT^{285} detected the HA-NLS-GFP-T2A reference protein (32.07 kDa), the reporter-POI fusion HA-NLS-CHE-CycB-NT^{285} (61.06 kDa) and a third protein band with high molecular weight representing the unskipped polyprotein FLP-CycB-NT^{285} (93.13 kDa) (Figure 22). The same protein bands were detected for all Cyclin B RPS constructs (data not shown).

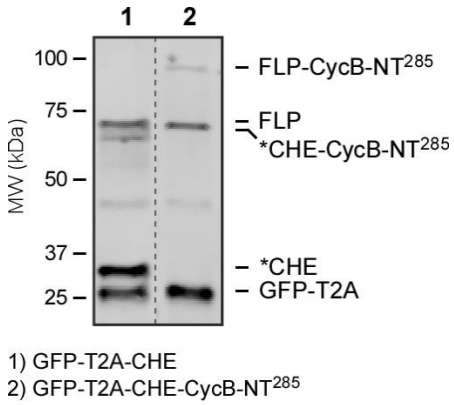

Figure 22| Protein expression of RPS-CycB-NT^{285} plasmids

Western blot analysis of cell lysates after transient transfection with RPS-8 (GFP-T2A-CHE) and RPS-8-CycB-NT^{285} (GFP-T2A-CHE-CycB-NT^{285}) using an anti HA-antibody. CHE*, GFP-T2A and FLP are detected for RPS-8. Analysis of RPS-8-CycB-NT^{285} shows the protein band of the GFP reference and the *CHE-CycB-NT^{285} fusion protein (61.06 kDa). An additional protein band with high molecular weight representing the FLP-CycB-NT^{285} (93.13 kDa) is detected.

In the case that the FLP-CycB-NT^{285} polyprotein is still fluorescent but stable throughout the cell cycle, this would bias the results towards more stable POI protein levels. To analyse, if the FLP-CycB-NT^{285} is still degraded or constitutes a stable fusion of the two fluorescent proteins together with the POI, a RPS expression vector with a mutated T2A site (mT2A) was established. Mutation of proline 17 and glycine 18 to alanine of the T2A sequence that are critical for ribosome skipping should impair protein co-expression resulting in exclusive expression of FLP (see Table S 3) (Doronina et al., 2008; Brown, Jeremy; Ryan, 2010). The mT2A site was introduced into RPS-4 that has been used for Cyclin B RPS analysis with similar results to the RPS plasmids with CHE reporters (Polz, 2017) (Figure 23 A). Western blot analysis of the expressed proteins from CHE-mT2A-GFP showed a prominent FLP band but no expression of the two skipped proteins CHE-T2A and *GFP compared to the RPS-4 control (Figure 23 B compare lane 1 and 2). Thus, mutation of the T2A site was successful and only FLP was expressed. Signals for both, CHE and GFP were detected by microscopy and flow cytometry showing that the CHE-GFP fusion protein still fluoresces in the GFP and CHE channel (data not shown). Expression of CycB-NT^{285} from the mT2A vector resulted exclusively in translation of only FLP-CycB-NT^{285} protein (compare lane 2 and 3 Figure 23 B). To determine if FLP-CycB-NT^{285} is still degraded in a cell cycle dependent manner, cells were co-transfected with CHE-mT2A-GFP-CycB-NT^{285} and 4xFLAG-CHE and analyzed via flow cytometry. Co-transfection of additional 4xFLAG-CHE was necessary since the reference signal would also disappear when the FLP protein is degraded. The mean values of cell populations were normalized to the mean of mT2A control also co-transfected with additional CHE (Figure 23 C). A decrease of GFP/CHE quotient in G1 compared to S and G2 is observed, showing that the FLP protein is still degraded in G1-phase in the expected Cyclin B pattern. The analysis of relative protein stability levels with the co-transfection of CHE reference protein is not as precise as using the RPS plasmids alone and a direct comparison of CHE-CycB-NT^{285} and FLP-CycB-NT^{285} is therefore not possible. However, only a small percentage of FLP is translated (see section 3.1.2) and the FLP-CycB-NT^{285} degradation patter corresponds to the expected Cyclin B degradation indicating a degradation of the FLP-POI. Thus, any bias caused by failed ribosome skipping can be assumed to be insignificant for the analysis.

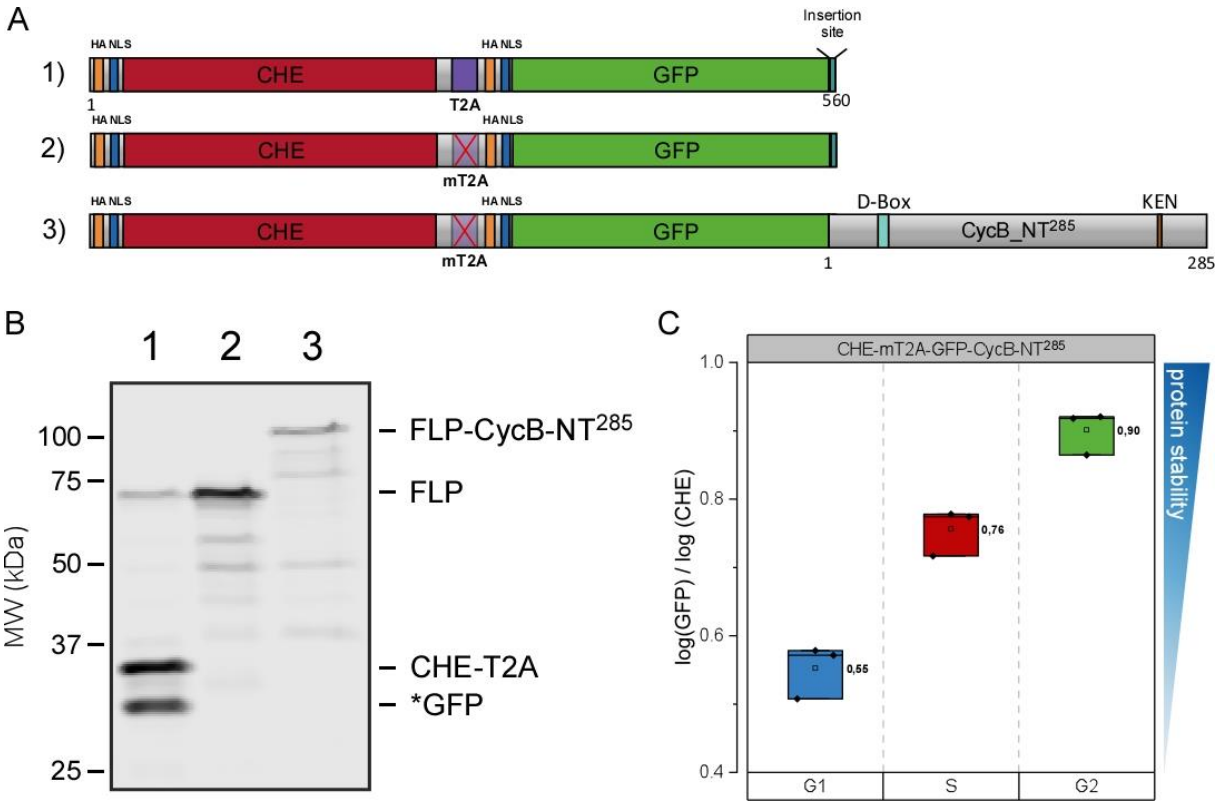

Figure 23| FLP-CycB-NT^{285} degradation occurs in a cell cycle dependent manner

(**A**) Schematic illustration of 1) CHE-T2A-GFP (RPS-4), 2) CHE-mT2A-GFP, and 3) CHE-mT2A-GFP-CycB-NT^{285}. (**B**) Western blot analysis of cell lysates using anti HA-antibody for protein detection. CHE-T2A (32.1 kDa), *GFP (30.1 kDa), and FLP (62.1 kDa) are detected for RPS-4 (lane 1). Only FLP is detected after mutation of P17A and G18A of the T2A site (mT2A) (lane 2). A high molecular band is detected for the FLP-CycB-NT^{285} (CHE-mT2A-GFP-CycB-NT^{285}; 88.67 kDa) (lane 3). (**C**) RPS analysis of cells co-transfected with CHE-mT2A-GFP-CycB-NT^{285} and 4xFLAG-CHE (exp.lvl. 1.0 - 1.75). Data has been normalized to respective mean values of cells transfected with CHE-mT2A-GFP and 4xFLAG-CHE. In G1 lower GFP/CHE ratios indicate cell cycle specific destabilization.

3.1.5.1.5. CycB-NT degradation depends on a D-box and KEN-box degron

APC/C dependent degradation of *Drosophila* Cyclin B was suggested to rely on a N-terminal D-box degron (aa 35-46), since deletion of 144 amino acids including the D-box consensus and a concurrent insertion of an HA-tag interfered with mitotic destruction and prevented exit from mitosis when expressed in *Drosophila* embryo (Sigrist et al., 1995). To test whether the RPS system can be utilized for the identification of putative degrons, protein stability of Cyclin B with a mutated D-box (mDB) was analyzed in S2R+ cells by flow cytometry. The two essential residues of the D-box consensus RxxL were mutated to alanine (AxxA) and introduced in the N-terminal Cyclin B fragment (CycB-NT^{285}_mDB). Analysis of relative protein stability levels of CycB-NT^{285}_mDB (CHE/GFP: 0.09) resulted only in a minor increase in G1 cells compared to the CycB-NT^{285} (CHE/GFP: 0.06) (Figure 24 A). Even though the effect was significant, a stronger stabilization was expected since S- and G2-cells display more elevated protein stability levels after APC/C inactivation at the end of G1 (Figure 20 C). Recruitment of APC/C substrates often depends on multiple degrons that interact with the co-activator at different interaction sites (see 2.6.4) and mutation of a single degron might not be sufficient for protein stabilization. In yeast, efficient degradation of the B-type cyclin Clb2 was shown to depend on both a N-terminal D-

and KEN-box motif (Hendrickson et al., 2001). However, no KEN-box motif has been described so far for *Drosophila* Cyclin B. Therefore, the protein sequence was scanned for additional APC/C degrons with the APC/C degron repository online tool. Besides the already known D-box at position 35-46, two additional putative D-box and three KEN-box degrons were identified in the first 258 aa of Cyclin B (Figure 24 B). However, the degrons displayed low similarity scores and consensus similarity, except for the KEN-box at position 247-253 with a high similarity score (0.97). To test, if the KEN-box is required for Cyclin B degradation in G1-phase, the N-terminal Cyclin B fragment was further truncated to amino acid 247 resulting in a deletion of the KEN-box (CycB-NT^{247}_ΔKEN). Analysis of CycB-NT^{247}_ΔKEN resulted in a more pronounced stabilization (CHE/GFP: 0.15) in G1 cells compared to the mutation of the D-box. Analysis of the D- and KEN-box double mutant CycB-NT^{247}_mDB_ΔKEN showed an even stronger stabilization (CHE/GFP: 0.63) of Cyclin B in G1 cells

A

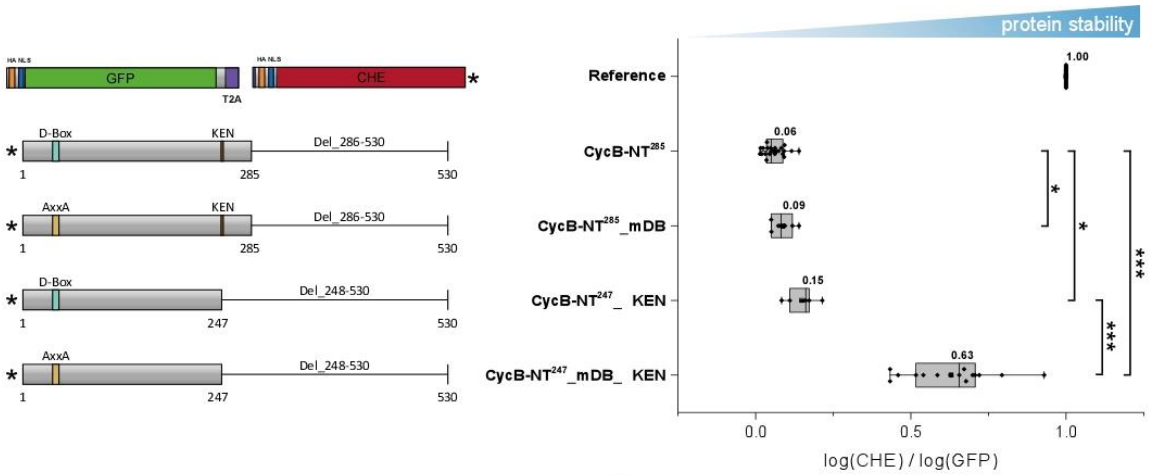

B

Degron	Motif sequence	Position	Similarity score	Consensus similarity	Disordered score
D-box	TKRAALGDLQNR	35-46	0.94	High	0.66
D-box	KLRAALAKPVMG	160-171	0.76	Low	0.48
D-box	ATRMPLIRGNSA	207-218	0.77	Low	0.58
KEN-box	GDENASE	10-16	0.64	Low	0.62
KEN-box	SSENVNE	137-143	0.46	Low	0.79
KEN-box	DKENLVL	247-253	0.97	High	0.19

C

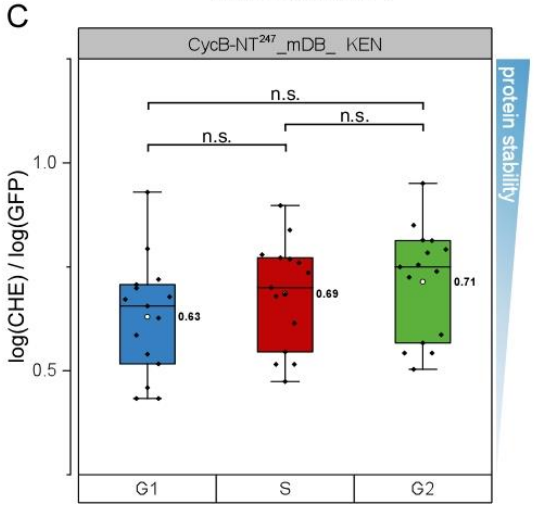

Figure 24| Analysis of the N-terminal D- and KEN-box motif of Cyclin B

(**A**) Analysis of relative protein stability levels of CycB-NT degron mutants. Illustration of the corresponding CycB mutant (left panel) and the normalized CHE/GFP ratios in G1-cells (right panel) (exp.lvl. 1.0 - 1.75). Mutation of the D-box consensus to AxxA (mDB) and deletion of the KEN-box (ΔKEN) increased CycB-NT stability in G1-phase. The double mutant CycB-NT^{247}_mDB_ΔKEN was strongly stabilized in G1-cells compared to the single D- and KEN-box mutants. (**B**) Summary of putative APC/C degrons located in Cyclin B N-terminus determined by the APC degron repository online tool. (**C**) Flow cytometry analysis of CycB-NT^{247}_mDB_mKEN in G1-, S-, and G2-cells. No significant destabilization in G1 can be detected. Statistics performed by t-test with Welch´s correction, n.s. > 0.05, * ≤ 0.05, ** ≤ 0.01, ***≤ 0.001.

compared to the single mutations (Figure 24 A). Analysis of the protein stability levels of CycB-NT^{247}_mDB_ΔKEN in the G1, S, and G2 cell populations displayed no significant difference in protein levels during cell cycle progression, indicating a complete stabilization of the N-terminal Cyclin B fragment (Figure 24 C). Thus, degradation of CycB-NT^{285} is not only dependent on the D-box degron but requires in addition the N-terminal KEN-box degron for proper proteolytic degradation in G1-phase.

3.1.5.1.6. Degradation of CycB-NT can be modified through altered APC/C activity

Mutation of the APC/C specific degrons of Cyclin B resulted in complete stabilization of the N-terminal CycB fragment that should be allocated to impaired APC/C recruitment and ubiquitination. This leads to the question if altered APC/C activity can modify protein stability levels of putative APC/C substrates. Hyperactivation of the APC/C can be obtained by overexpression of Fzr (Listovsky et al., 2000; Zur et al., 2001). This should lead to an increased degradation of CycB-NT^{285}, even in cell cycle phases when the APC/C^{Fzr} is normally inactive (Figure 25 A). To test this assumption, stability of CycB-NT^{285} was analyzed in S2R+ cells co-transfected with GFP-T2A-CHE-CycB-NT^{285} and 4xFLAG-Fzr. Protein expression of 4xFLAG-Fzr was detected via Western blot analysis of cell lysates using a FLAG-antibody, resulting in similar Fzr expression levels for the analyzed samples (data not shown). Overexpression of Fzr resulted in a strong destabilization of CycB-NT^{285} in S- and G2-cells compared to the control cells (S: 0.43 to 0.19; G2: 0.74 to 0.17). In G1-cells only a minor destabilization was observed (G1: 0.21 to 0.14) since APC/C is already active in G1-phase under normal conditions. The observed changes in protein levels caused by Fzr overexpression were much more pronounced at high expression levels compared to low expression levels (data not shown). This is effect is probably attributable to the amount of additional Fzr protein that is required to overcome inhibitory Cdk dependent phosphorylation and to hyperactivate the APC/C. CycB-NT^{247}_mDB_ΔKEN lacks the identified APC/C degron motifs and should thereby be refractory to elevated APC/C activity. Accordingly, stability of GFP-T2A-CHE-CycB-NT^{247}_mDB_ΔKEN with additional Fzr overexpression was constant in G1- and S- cells. A decline in G2 stability was observed (Figure 25 B). However, we did not follow up this observation but noted that Fzr overexpression can result in severe over-replication and this can result in an abnormal cellular status (Sigrist et al., 1997).

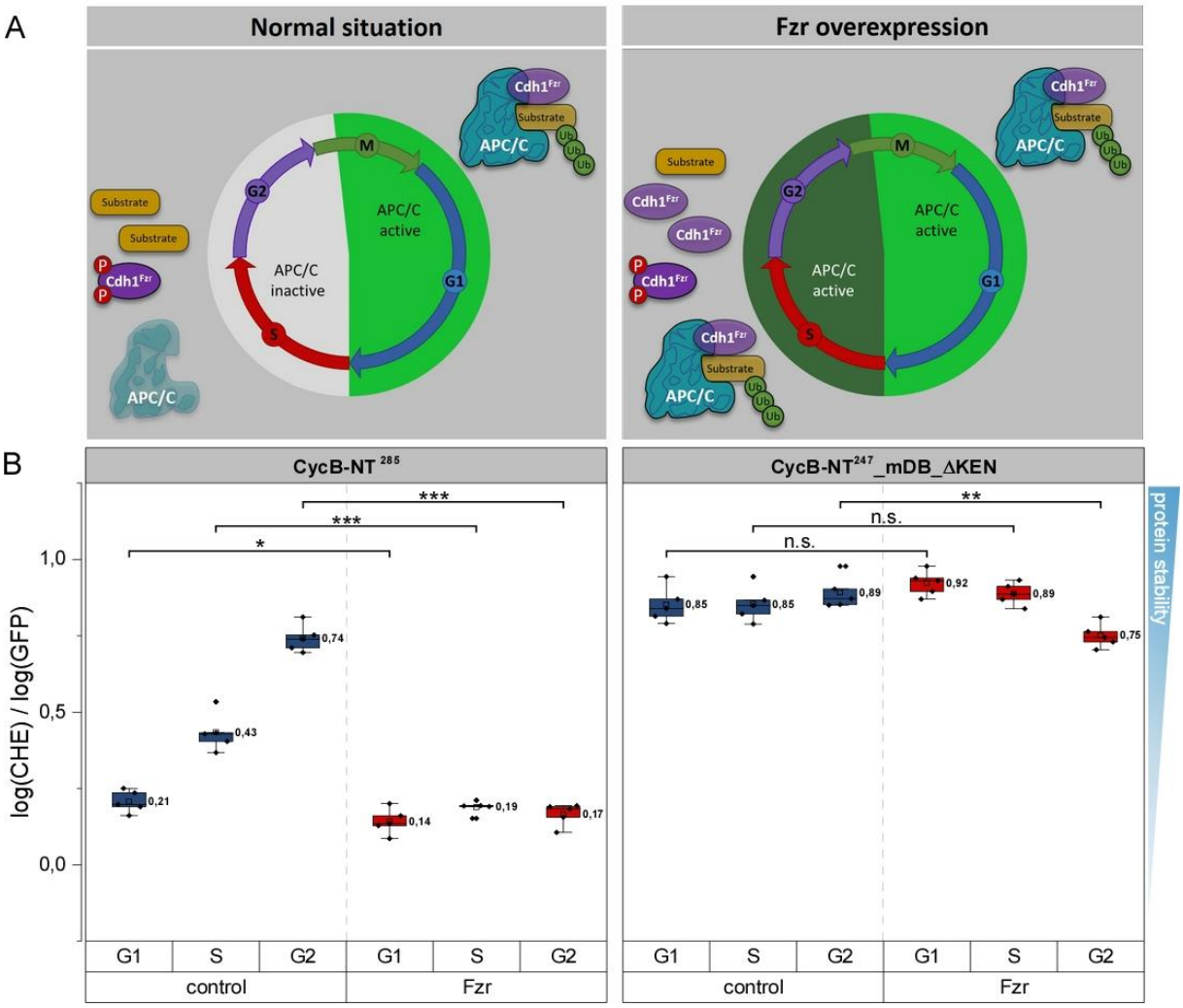

Figure 25| CycB-NT^{285} degradation with Fzr overexpression

(**A**) Schematic of APC/C activity during the cell cycle. Fzr overexpression leads to an unnatural activation of APC/C^{Fzr} in S- and G2-phase. (**B**) Flow cytometric analysis of GFP-T2A-CHE-CycB-NT^{285} and GFP-T2A-CHE-CycB-NT^{247}_mDB_mKEN (exp.lvl. 2.0 - 3.0). Fzr overexpression leads to a significant decrease of CycB-NT^{285} protein stability levels (red boxes) in all three cell cycle populations compared to control cells (blue boxes). CycB-NT^{247}_mDB_mKEN is only destabilized in G2-cells upon Fzr overexpression compared to the control and no changes are observed in G1- and S-cells. Statistics performed by t-test with Welch´s correction, n.s. > 0.05, * ≤ 0.05, ** ≤ 0.01, ***≤ 0.001.

On the contrary, downregulation of APC/C^{Fzr} activity should lead to an increase of CycB-NT stability levels. Impaired APC/C^{Fzr} activity should be most visible in G1-phase when APC/C^{Fzr} activity drives protein degradation under normal conditions (Figure 26 A). Fzr protein levels were decreased by using dsRNA (dsRNA Fzr) against part of the Fzr coding sequence (aa 231-478) to test the effects of reduced APC/C activity on CycB-NT stability levels. Cells were treated with a mock dsRNA directed against a part of the sequence of the hygromycin-resistance gene (Hygro dsRNA) to exclude unspecific off target effects caused by cell treatment with dsRNA and activated RISC/DICER system in the cell. Treatment with the mock Hygro dsRNA had no effect on CycB-NT^{285} nor CycB-NT^{247}_mDB_ΔKEN stability levels in G1-, S-, or G2-cells. Knockdown of *fzr* resulted in a stabilization of CycB-NT^{285} in G1- and S-cells (G1: 0.12 to 0.54; S: 0.30 to 0.59) and did not affect G2 cells (G2: 0.58 to 0.59). CycB-NT^{247}_mDB_ΔKEN levels were

increased in all three cell cycle populations in cells treated with Fzr dsRNA (G1: 0.72 to 0.9; S: 0.75 to 0.9; G2: 0.79 to 0.9) (Figure 26 B).

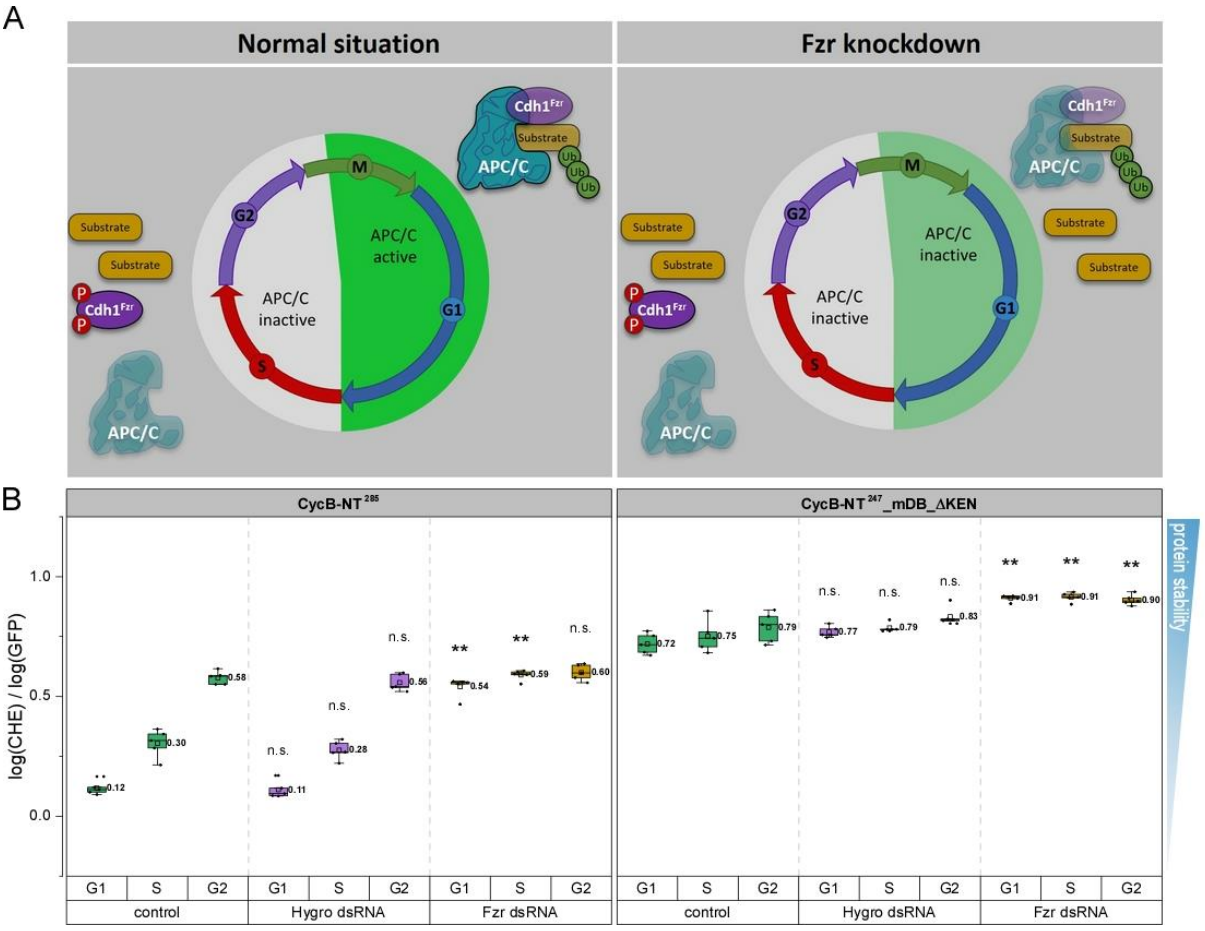

Figure 26| CycB-NT^{285} degradation with Fzr knockdown

(**A**) Schematic of APC/C activity during the cell cycle. Fzr knockdown leads to an inactivation of APC/C^{Fzr} in M- and G1-phase. (**B**) Flow cytometric analysis (exp.lvl. 1.75 - 2.5) of GFP-T2A-CHE-CycB-NT^{285} and GFP-T2A-CHE-CycB-NT^{247}_mDB_mKEN under normal conditions (green boxes) or treated either with mock Hygro dsRNA (purple boxes) or Fzr dsRNA (brown boxes). CycB-NT^{285} stability increased in G1- and S-cells but not G2-cells upon Fzr knockdown. Treatment with Hygro dsRNA had no effect on relative protein stability levels. Fzr knockdown stabilized CycB-NT^{247}_mDB_mKEN in all three cell cycle populations. Statistics performed by t-test with Welch´s correction, n.s. > 0.05, * ≤ 0.05, ** ≤ 0.01, ***≤ 0.001. The samples were compared to the control cells of the respective cell cycle phase and symbols for p-values displayed above the box.

In conclusion, changed Cyclin B degradation caused by altered APC/C^{Fzr} activity was detectable and reflected the expected changes in the respective cell cycle stages. Surprisingly, relative protein stability levels of the stabilized D- and KEN-box mutant were increased after downregulation of Fzr protein levels in all three cell cycle populations. Possibly, unnatural APC/C activity is able to target proteins that display only weak interactions with the APC/C co-activator subunit under physiological conditions. Therefore, a possible explanation is that further functional degrons could be located in the N-terminus that are capable of APC/C^{Fzr} interaction, even though to a much lesser extent than the analyzed D- and KEN-box and effects are only observed under unnatural APC/C activity profiles. However, this issue was not further investigated in this thesis.

3.1.5.2. Analysis of Geminin

The *Drosophila* protein Geminin (Gem) was used as a second APC/C model substrate for the analysis of protein degradation in G1-phase. Geminin is an important regulator of DNA replication, prohibiting premature start of DNA replication and re-replication during S-phase by blocking the formation of prereplication complexes (pre-RC) (McGarry et al., 1998). Geminin directly interacts and inhibits the licensing factor Cdt1 (double-parked in *Drosophila*) via its C-terminal coiled coil domain that is required for the formation of pre-RCs (Wohlschlegel et al., 2000; Tada et al., 2001; Benjamin et al., 2004). Geminin accumulates during S-, G2-, and M-phase followed by its degradation from late mitosis throughout G1-phase mediated by the APC/C, releasing Cdt1 and allowing pre-RC formation and establishment of S-phase (McGarry et al., 1998; Zielke et al., 2008).

3.1.5.2.1. Gem-NT^{101} degradation is impaired by C-terminal reporter fusions

For the analysis of Geminin degradation, a degron containing but otherwise inert Geminin fragment composed of amino acid residues 1-101 (Gem-NT^{101}) was inserted into the RPS expression plasmids. Deletion of the coiled coil region renders Gem-NT^{101} unable to interact with Cdt1 but the fragment still contains an N-terminal D-box degron sequence like *Xenopus* and human Geminin where it has been shown to be recognized by the APC/C (McGarry et al., 1998; Sakaue-Sawano et al., 2008; Clijsters et al., 2013). Besides the D-box, putative KEN-box sequences can be found in *Xenopus*, *Drosophila*, and human Geminin which have not been investigated in regard of Geminin degradation, yet. In case of *Drosophila* Gem-NT^{101} the putative KEN-box is located in close proximity to the D-box degron (Figure 27 A, B). Gem-NT^{101} was inserted into RPS-5 to RPS-8 to analyse protein stability of N- and C-terminal CHE fusions by flow cytometry, similar to the experiments conducted for Cyclin B (see 3.1.5.1.2)(Figure 27 C). C-terminal Geminin fusions, GFP-T2A-Gem-NT^{101}-CHE and Gem^{101}-CHE-T2A-GFP, confirmed that this fragment behaves like an APC/C target. A decrease of CHE/GFP ratio in G1-phase allocated to APC/C^{Fzr} dependent degradation (G1: 0.30 /0.49) and increasing values in S- and G2-cells representing re-accumulation (S: 0.60/0.69; G2: 0.63/0.80) were observed. On the contrary, N-terminal tagging of Geminin showed no cell cycle dependent degradation of Gem-NT^{101}. No difference of relative protein stability levels was detectable between G1-, S-, and G2-cells anymore. Thus, in contrast to CycB-NT^{285}, degradation of Geminin can be completely impaired depending on the position of the reporter fusion. Furthermore, the insertion up- or downstream of the T2A site in case of the two N-terminal fusion also displayed differences in stability levels. Flow cytometric analysis of GFP-T2A-CHE-Gem-NT^{101} resulted in mean CHE/GFP ratios of 0.69 in G1- and 0.77 in G2-phase, whereas CHE-Gem-NT^{101}-T2A-GFP displayed ratios around 1.0. This indicates a complete stabilization of CHE-Gem-NT^{101} with similar extent to a stable RPS control (Figure 27 D). Increased CHE/GFP ratios were also observed for constructs with the GFP reference downstream of the T2A site in case of CycB-NT^{285} (Figure 20 C) and the C-terminal Gem-NT^{101} fusions (Figure 27 D). This effect is most likely attributed to a decreased expression of the

downstream GFP reference protein resulting in an increased CHE/GFP quotient (see 3.1.3). Thus, the difference between the N-terminal Gem-NT^{101} constructs can be explained by an additive effect of impaired Gem-NT^{101} degradation caused by N-terminal fusion and a decreased expression of the GFP reference expression in case of CHE-Gem-NT^{101}-T2A-GFP.

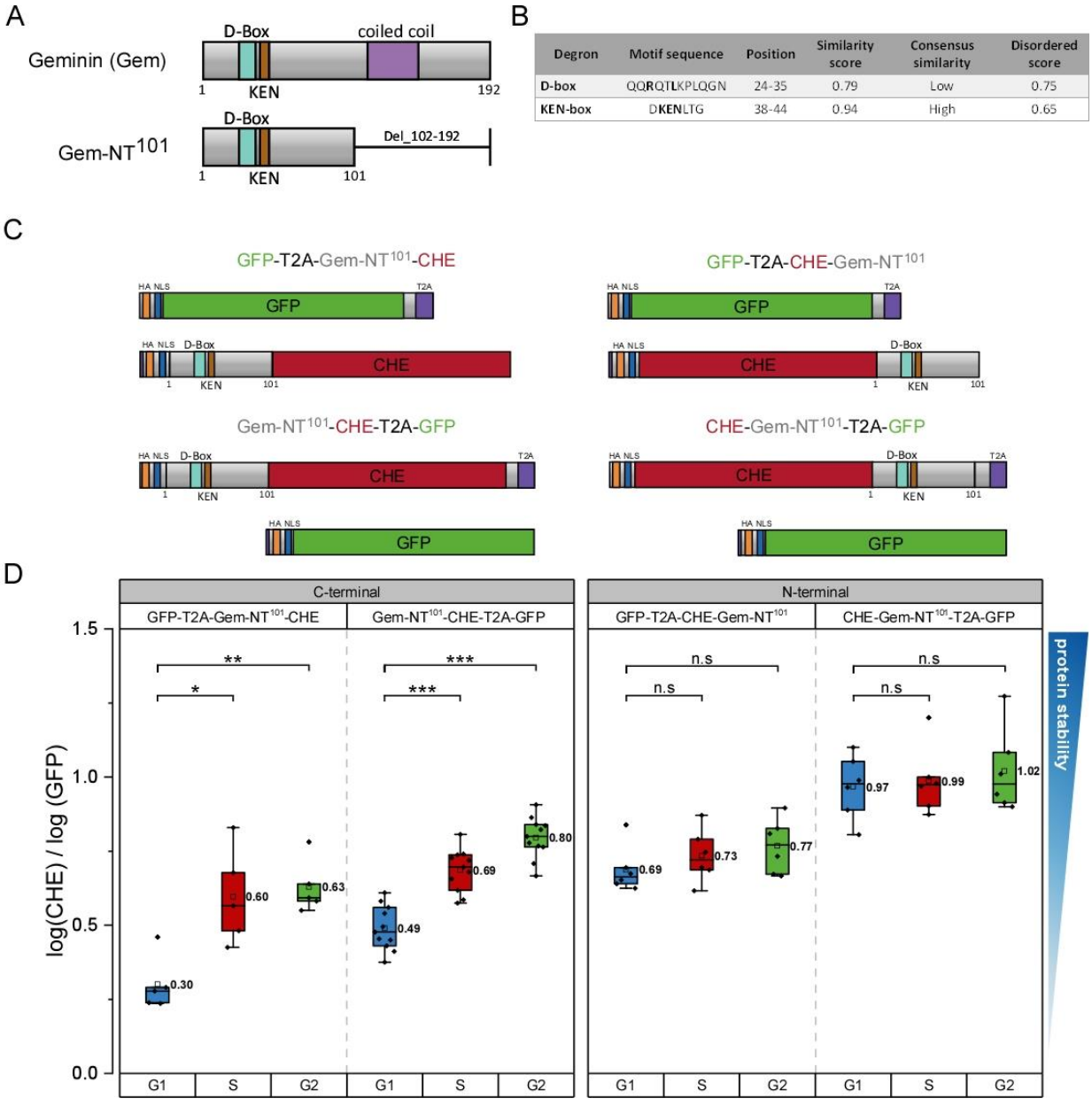

Figure 27| Gem-NT^{101} degradation is impaired by N-terminal reporter fusions

(**A**) Illustration of *Drosophila* Geminin and the truncated N-terminal fragment Gem-NT^{101}. (**B**) Summary of putative APC/C degrons located in Geminin N-terminus determined by the APC degron repository online tool. (**C**) Illustration of the N- and C-terminal reporter fusions of Gem-NT^{101} of the RPS expression plasmids. (**D**) Comparison of relative protein levels of the N- and C-terminal tagged Gem-NT^{101} variants shown in a box plot (exp.lvl. 1.0 - 1.75). C-terminal fusions show decreased mean values of G1-cells compared to the S- and G2-populations. N-terminal fusions result in a stabilization with no significant difference between G1-, S-, and G2-cells. Statistics performed by t-test with Welch´s correction, n.s. > 0.05, * ≤ 0.05, ** ≤ 0.01, ***≤ 0.001.

3.1.5.2.2. Mutation of either the D- or KEN-box degron stabilize Geminin in G1-phase

Recognition of Geminin by the APC/C was suggested to be dependent on an N-terminal located D-box motif in case of *Xenopus* and human Geminin. Mutation of the arginine and leucine residues to alanine (RxxL to AxxA) resulted in an non-degradable Geminin mutant that was completely stable in G1-phase (McGarry et al., 1998; Clijsters et al., 2013). Besides the D-box, *Drosophila* Geminin contains an additional putative KEN-box degron sequence in the N-terminal region. To test if either one or both degrons are required for Geminin degradation in G1-phase, single D- or KEN-box mutants and the double mutant were analyzed using the RPS system. Mutation of the D-box consensus to AxxA (mDB) caused a strong stabilization of Gem-NT^{101}_mDB in G1-phase (CHE/GFP: 0.79) compared to Gem-NT^{101} control (CHE/GFP: 0.54). However, mutation of the KEN-box consensus sequence to KAA (mKEN) also resulted in a stabilization in G1-cells (CHE/GFP: 0.83) similar to the increase observed for the D-box mutant. A Geminin mutant containing mutations in both degrons Gem-NT^{101}_mDB_mKEN was only slightly more stabilized (CHE/GFP: 0.89) compared to the single D- or KEN-box mutants, though the statistical analysis of the observed effect was only just significant (p-value: 0.042) (Figure 28). Based on the obtained results, it is not possible to clearly estimate if only a single or both degrons mediate APC/C dependent destruction of Geminin.

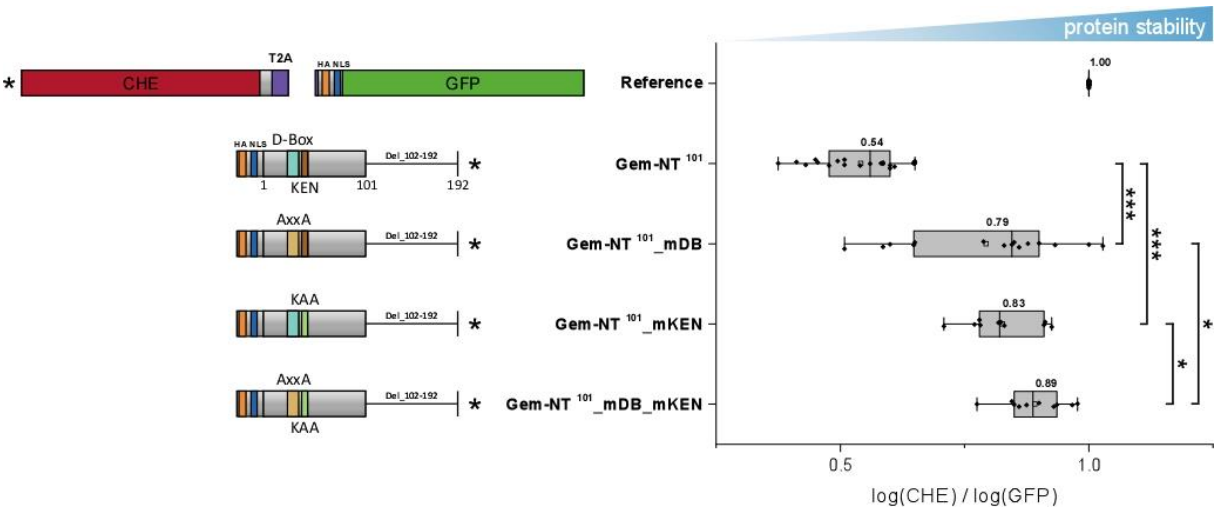

Figure 28| Mutation of the D- or KEN-box degron stabilized Gem-NT^{101} in G1-cells

Analysis of relative protein stability levels of Gem-NT^{101} degron mutants using RPS-5. Schematic illustration of the corresponding Gem mutant (left panel) and a box plot of the normalized CHE/GFP ratios in G1-cells (right panel) (exp.lvl. 1.0 - 1.75). Mutation of the D-box consensus to AxxA (mDB) and the KEN-box consensus to KAA (mKEN) stabilized Gem-NT^{101} in G1-phase. The double mutant Gem-NT^{101}_mDB_mKEN was only slightly more stabilized in G1-cells compared to the single degron mutants. Statistics performed by t-test with Welch´s correction, n.s. > 0.05, * ≤ 0.05, ** ≤ 0.01, ***≤ 0.001.

3.1.5.2.3. Geminin degradation depends on APC/C^{Fzr} activity

Several studies suggested that Geminin degradation relies solely on APC/C$^{Cdh1/Fzr}$ activity, in such a way that proteolysis of Cyclin B after SAC inactivation reduces Cdk1 activity, thus triggering APC/C$^{Cdh1/Fzr}$ activity which subsequently targets Geminin (Narbonne-Reveau et al., 2008; Zielke et al., 2008;

Colombo et al., 2010). On the contrary, human Geminin degradation in U2OS cells was found to be independent of APC/C^{Cdh1} activity since Cdh1 knockdown did not impair Geminin protein degradation (Clijsters et al., 2013). To test if Geminin degradation in *Drosophila* relies on APC/C^{Fzr} activity, Gem-NT^{101} degradation was analyzed under conditions of either hyperactivated or downregulated APC/C^{Fzr} activity, similar to the experiments conducted for Cyclin B (see 3.1.5.1.6). S2R+ cells were co-transfected with 4xFLAG-Fzr and Gem-NT^{101}-CHE-T2A-GFP and analyzed by flow cytometry. As seen in Fzr overexpression experiments with Cyclin B the effects caused by Fzr overexpression were most pronounced in G2 cells with high expression levels. Analysis of relative protein stability levels of Gem-NT^{101} in the G2-cell population with ectopic APC/C^{Fzr} activation resulted in a significant destabilization compared to the control. Additionally, we tested the three degron mutants under the same conditions with the result that none of the mutants was affected by elevated APC/C^{Fzr} activity (Figure 29 A). Reversely, downregulation of APC/C^{Fzr} activity via Fzr knockdown led to a stabilization of Gem-NT^{101} in G1-cells, whereas the D-box mutant Gem-NT^{101}_mDB was not affected by the treatment with Fzr dsRNA (Figure 29 B). In conclusion, degradation of *Drosophila* Geminin depends on APC/C^{Fzr} activity opposed to the findings for human Geminin in Clijsters et al. (2013). Furthermore, analysis of the Geminin degron mutants with hyperactivated APC/C activity did not display any destabilization for any of the mutants and mutation of either the D- or KEN-box made Gem-NT^{101} completely refractory to altered APC/C^{Fzr} activity.

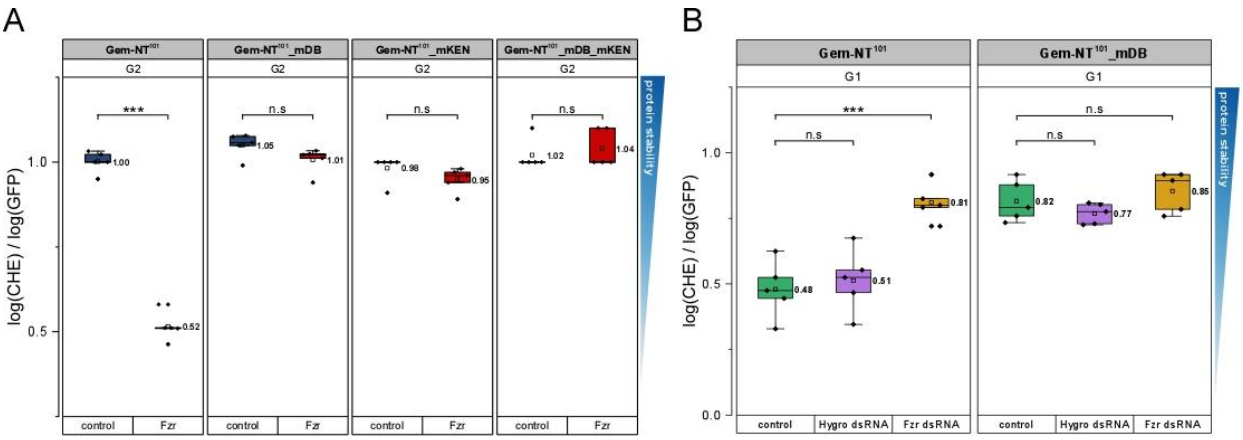

Figure 29| Gem-NT^{101} degradation with Fzr overexpression and knockdown

(**A**) Flow cytometric analysis of Gem-NT^{101}-CHE-T2A-GFP and the respective degron mutants (exp.lvl. 2.0 - 3.0) with elevated APC/C^{Fzr} activity. Fzr overexpression leads to a significant decrease of Gem-NT^{101} protein stability levels (red box) compared to the control (blue box) in G2-phase. The degron mutants Gem-NT^{101}_mDB, Gem-NT^{101}_mKEN, and Gem-NT^{101}_mDB_mKEN were not affected by additional 4xFLAG-Fzr overexpression in G2-cells. (**B**) Flow cytometric analysis of Gem-NT^{101}-CHE-T2A-GFP and Gem-NT^{101}_mDB-CHE-T2A-GFP under normal conditions (green boxes) or treated either with mock Hygro dsRNA (purple boxes) or Fzr dsRNA (brown boxes) (exp.lvl. 1.0 - 1.75). Gem-NT^{101} was significantly stabilized by Fzr knockdown in G1-cells. Treatment with Hygro dsRNA had no effect on relative protein stability levels. Gem-NT^{101}_mDB was not affected by Fzr knockdown. Statistics performed by t-test with Welch´s correction, n.s. > 0.05, * ≤ 0.05, ** ≤ 0.01, ***≤ 0.001.

3.1.5.2.4. Geminin and Cyclin B are degraded with different kinetics

Degradation of human Geminin was also found to take place at the same time and with similar kinetics as Cyclin B1 degradation (Clijsters et al., 2013), contradicting previous findings in *Xenopus* egg extracts in which Geminin protein levels were only reduced by 50% after exit from mitosis (Li et al., 2004). In case of *Drosophila*, it is still unknown if Geminin degradation happens at the same time and with similar kinetics to Cyclin B. While flow cytometric analysis enables a static determination of protein degradation in different cell cycle stages it does not provide information of degradation kinetics within a certain cell cycle phase. Therefore, Geminin and Cyclin B degradation was examined via live cell imaging experiments using time lapse microscopy to compare their degradation kinetics. Cells transfected with either the control RPS construct GFP-T2A-CHE, GFP-T2A-CHE-CycB-NT^{285}or Gem-NT^{101}-CHE-T2A-GFP were recorded with 15 min intervals for three channels, brightfield (BF), GFP, and CHE. Cells undergoing mitosis were selected in the brightfield channel defined by the formation of two new nuclei in telophase (T= 0 min). The nuclear CHE and GFP signals were selected by threshold settings and quantified and the CHE/GFP quotient was calculated for one of the newly born cells for each individual time frame using the software ImageJ. The CHE/GFP ratios were normalized to the mean CHE/GFP value of three time frames prior to telophase (G2-phase). Based on the single cell traces, a mean degradation curve was calculated by the average value from the single cells for each time point. As expected, analysis of the RPS control resulted in stable CHE and GFP signals over the whole timeframe, since both fluorescent proteins are stable during cell cycle progression (Figure 30 A, B). In case of CHE-CycB-NT^{285}, the CHE signal starts to decline rapidly after the formation of the new nucleus and is already clearly decreased at the beginning of G1-phase (see Figure 30 C; t=45 min). Opposed to this, the decline of Gem-NT^{101}-CHE signals was delayed compared to Cyclin B and the Gem-NT^{101}-CHE signal slowly decreases during G1-phase (compare Figure 30 C and E).

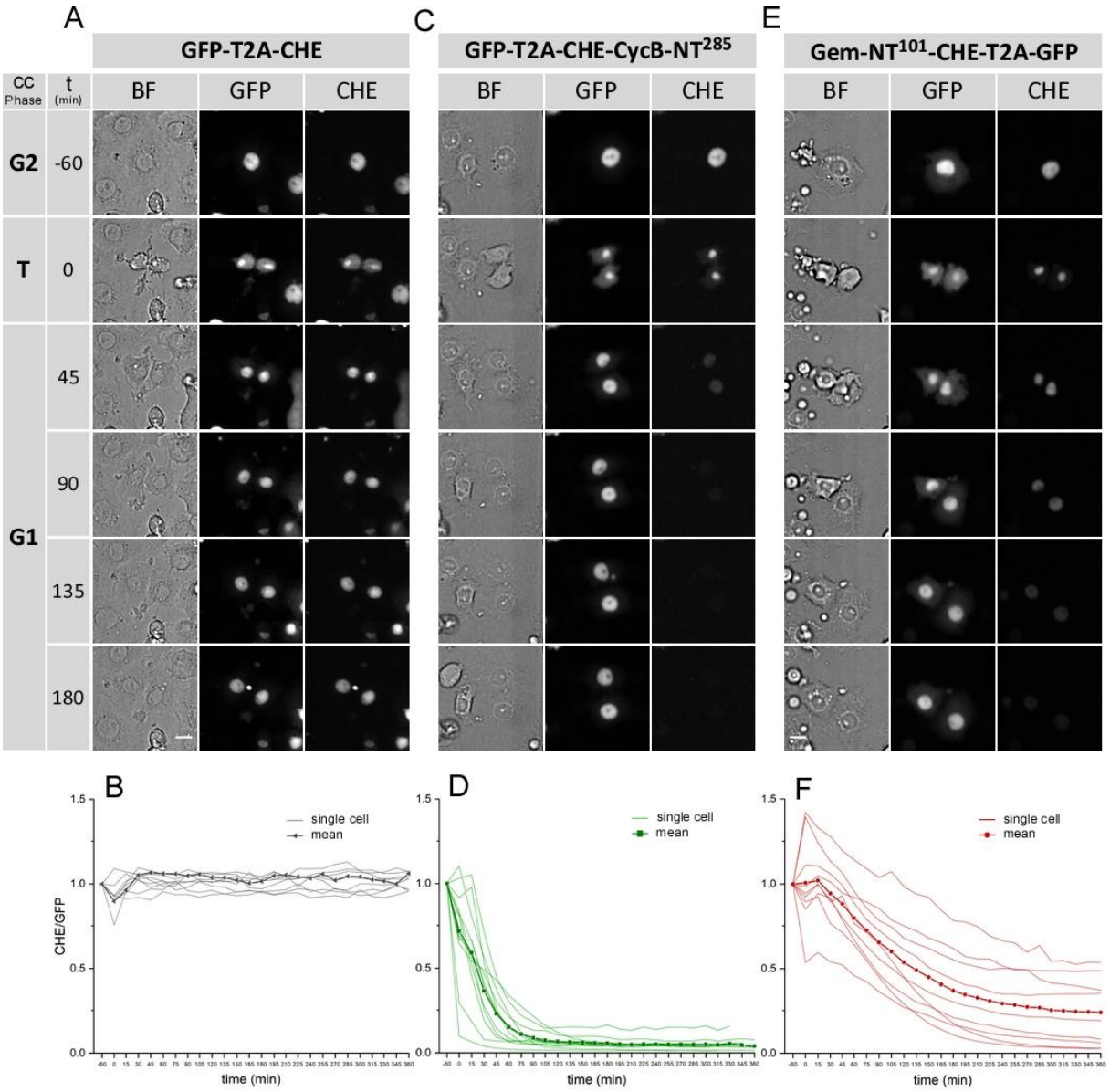

Figure 30| Live cell imaging of Cyclin B and Geminin

(**A**, **C**, **E**) Images of S2R+ cells transfected with either GFP-T2A-CHE, GFP-T2A-CHE-CycB-NT^{285}, and Gem-NT^{101}-CHE-T2A-GFP in the brightfield (BF), GFP-, and CHE-channel. Images were taken with a time interval of 15 min. Telophase cells determined by the formation of new nuclei were set as starting point (t= 0min). Time point 60 min earlier was set as G2-phase. G1 was defined by the formation of two new cells after cytokinesis. (**B**, **D**, **F**) One of the daughter cells was tracked for 360 min (30 time frames) and the CHE/GFP was calculated for each time point. Single cell traces were created for each cell and a mean degradation curve calculated based on the average value for each time point.

The mean degradation curve derived from the average values from the single cells also displays completely different degradation kinetics for Cyclin B and Geminin. Cyclin B is degraded earlier and with faster kinetics compared to Geminin, where degradation starts 15 min after telophase and with much slower kinetics (compare Figure 30 D and F). These results show that *Drosophila* Geminin and Cyclin B are degraded at different time points of the cell cycle and that both proteins are degraded with different kinetics opposed to the report for human Geminin and Cyclin B (Clijsters et al., 2013). This could also indicate that Geminin degradation relies solely on APC/C^{Fzr} activity and not APC/C$^{Fzy/Fzr}$ like Cyclin B. Since Fzy/Cdc20 itself is a target of APC/C$^{Cdh1/Fzr}$ after SAC inactivation at the anaphase to metaphase

transition (see 2.6.1), it is rather unlikely that APC/$C^{Cdc20/Fzy}$ mediates Geminin degradation. However, this issue was not further investigated in this thesis. Nevertheless, it was shown that the RPS reporter system is also well suited for live cell imaging analysis in addition to static readout via flow cytometry. Live cell imaging allows an accurate determination of protein degradation within specific cell cycle phases with a dynamic inference on degradation kinetics compared to flow cytometry. However, it is a more time-consuming technique especially compared to the high throughput analysis via flow cytometry which instead allows a quick determination of protein degradation during cell cycle progression.

3.1.6. Degradation analysis of known $CRL4^{Cdt2}$ substrates in S-phase

Protein degradation in G1-phase was clearly detectable in case of the two APC/C substrates Cyclin B and Geminin using the RPS system. In a next step, protein degradation during S-phase was analyzed via flow cytometry. To test how degradation in S-phase can be captured by the RPS-system, the substrates of the E3 cullin RING ligase $CRL4^{Cdt2}$, Dacapo, E2F1, and Cdt1 that are degraded at the beginning of S-phase were analyzed.

3.1.6.1. Analysis of Dacapo

Dacapo (Dap) is the *Drosophila* CKI homologue of the mammalian CIP/KIP proteins $p21^{Cip1}$, $p27^{Kip1}$ and $p57^{Kip2}$ with highest homology to rat $p21^{Cip1}$ (De Nooij et al., 1996; Lane et al., 1996). Dap functions as a CKI exclusively for CycE-Cdk2 and has important functions during *Drosophila* embryogenesis contributing to G1 cell cycle arrest in different tissues including the embryonic epidermis, mesoderm, and the nervous system (Swanson et al., 2015; Stadler et al., 2019). Dap inhibits CycE-Cdk2 activity during G1-phase when low Cdk activity is required for replication origin licensing. $CRL4^{Cdt2}$ dependent degradation of Dap during S-phase resolves CycE-Cdk2 inhibition, thereby increasing Cdk activity necessary for origin firing (Swanson et al., 2015).

3.1.6.1.1. Flow cytometric analysis of Dap_dCDI and Dap_dCDI_dPIPa degradation

Dap overexpression causes a cell cycle arrest with an enrichment of cells in G1-phase and thus not suited for the analysis of protein levels during cell cycle progression (Frank, 2013; Swanson et al., 2015; Rössler, 2019). Hence, Dap mutants with a disrupted CDK inhibitor domain (CDI) required for CycE-Cdk2 interaction were used for relative protein stability analysis, that have already been established in the Sprenger group. The mutant form Dap_dCDI still contains the PIP degron required for $CRL4^{Cdt2}$ dependent degradation in S-Phase, but deletions/insertions in the Cdk2 binding domain (Del_103-105G) and the cyclin binding site (Del_38-44RAR) that were chosen based on the structural data from p27 and CycA-Cdk2 complex, render it unable to bind and inhibit CycE-Cdk2. Furthermore, a Dap mutant with an additional deletion in the PIP degron (dPIPa = Del_184-188), referred to as Dap_dCDI_dPIPa, which should be refractory to $CRL4^{Cdt2}$ mediated proteolysis was tested and compared with Dap_dCDI

using the RPS system (Figure 31 A). Flow cytometric analysis of GFP-T2A-CHE-Dap_dCDI resulted in a decreased CHE/GFP quotient in the S-population (CHE/GFP: 0.31) compared to the G1-population (CHE/GFP: 0.45), in agreement with Dap degradation by $CRL4^{Cdt2}$ during S-phase (see 2.5). In the G2-population, only a slight stabilization of Dap_dCDI was observed (CHE/GFP: 0.35) compared to S-phase (Figure 31 B). Reaccumulation of the proteins after the turn-off of the $CRL4^{Cdt2}$ degradation at the end of S-phase and fluorescent maturation require substantial time. Fluorescent protein maturation times vary between different fluorescent proteins and these times also differ between cell lines and are dependent on the temperature. For instance, half maturation for GFP and CHE in E.coli at 32°C show values of 22 min and 46 min, respectively (Balleza et al., 2018). In S2R+-cells, faster maturation of GFP has also been seen (F. Sprenger, personal communication). Thus, at the beginning of G2-phase, GFP-fluorescence will come up quicker than CHE, causing lower CHE/GFP values. Furthermore, similar results were obtained with N- and C-terminal fusions using RPS-5 to RPS-7 indicating that this effect is not due to any issues with the different reporter fusions to Dap (Figure S 1).

Compared to Dap_dCDI, analysis of Dap_dCDI_dPIPa showed no cell cycle specific degradation and overall higher stability values (G1: 0.79, S: 0.76, and G2: 0.74) (Figure 31 B). To test, if the observed decrease in protein levels of Dap_dCDI were directly allocated to $CRL4^{Cdt2}$ dependent ubiquitination, protein levels were analyzed with additional downregulation of $CRL4^{Cdt2}$ activity. This was achieved by RNAi gene knockdown of the $CRL4^{Cdt2}$ scaffold subunit Cul4 by using dsRNA against exon 10 of *cul4* (Cul4 dsRNA). Dap_dCDI protein stability levels were significantly increased in cells treated with Cul4 dsRNA in the three cell cycle phase populations (G1: 0.45 to 0.65; S: 0.31 to 0.52; G2: 0.36 to 0.53), whereas treatment with the control Hygro dsRNA had no effect on Dap_dCDI protein stability levels. In accordance with Dap_dCDI_dPIPa being refractory to $CRL4^{Cdt2}$ activity, knockdown of Cul4 had no effect on its protein levels in any cell cycle phase (G1: 0.78 to 0.76; S: 0.74 to 0.75; G2: 0.73 to 0.72) (Figure 31 C). The stabilization of Dap_dCDI in G1 cells upon $CRL4^{Cdt2}$ inactivation could be explained by the presence of early S-phase cells in this population and the lack of $CRL4^{Cdt2}$ dependent degradation in these cells. This issue was further investigated and discussed in more detail below (see 3.1.6.3.2). In conclusion, $CRL4^{Cdt2}$ dependent Dap_dCDI degradation in S-phase was detectable via flow cytometric analysis. To test, if similar results are obtained for other $CRL4^{Cdt2}$ substrates, the degradation of E2F1 and Cdt1 were investigated in the following.

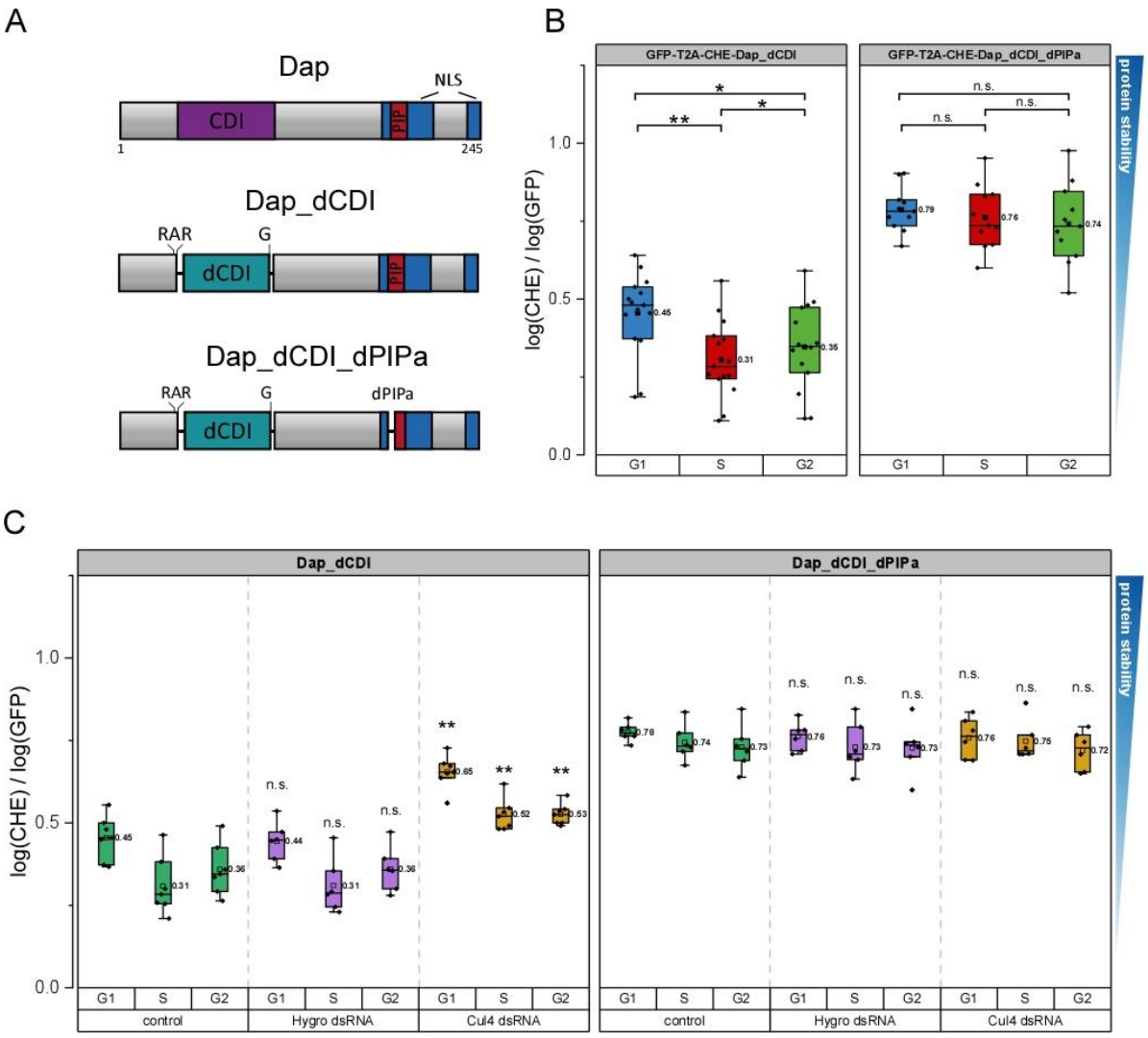

Figure 31| Flow cytometric analysis of Dap_dCDI and Dap_dCDI_dPIPa degradation

(**A**) Illustration of Dacapo (Dap), Dap_dCDI and Dap_dCDI_dPIPa. (**B**) Box plot of relative protein stability levels of Dap_dCDI and Dap_dCDI_dPIPa in G1-, S-, and G2-cells (exp.lvl. 1.0 - 1.75) summarizing the mean quantification of CHE/GFP ratios of independent replicates normalized to the RPS control. Dap_dCDI is destabilized in S-phase compared to G1-phase and stabilization is observed in G2-phase. Dap_dCDI_dPIPa is fairly stable during cell cycle progression. Statistics performed by t-test with Welch´s correction, n.s. > 0.05, * ≤ 0.05, ** ≤ 0.01. (**C**) Analysis of Dap_dCDI and Dap_dCDI_dPIPa with Cul4 knockdown (Cul4 dsRNA) and mock control (Hygro dsRNA) (exp.lvl. 1.5 - 2.5). Dap_dCDI is stabilized in cells treated with Cul4 dsRNA in G1-, S-, and G2-cells. Dap_dCDI_dPIPa was not affected by Cul4 knockdown. Treatment with Hygro dsRNA had no effect on both proteins. Statistics performed by Mann-Whitney U-Test, n.s. > 0.05, * ≤ 0.05, ** ≤ 0.01. The samples were compared to the control cells of the respective cell cycle phase and symbols for p-values displayed above the box.

3.1.6.2. Analysis of E2F1

E2 promotor binding factor 1 (E2F1) is a transcription factor belonging to E2F protein family and is involved in the regulation of the restriction point and the G1/S transition by inducing the expression of several G1/S genes including *cycE* and *cycA* (reviewed in Bertoli et al., 2013). E2F1 is inhibited during G1-phase by the pocket protein retinoblastoma (pRB). Mitogen stimulated CycD-Cdk4/6 phosphorylation of pRB causes inhibitory release of E2F1 and allows transcription of E2F1 target genes required for S-phase (Morgan, 2007). In *Drosophila*, E2F1 is inactivated during early S-phase via $CRL4^{Cdt2}$ dependent degradation mediated by an N-terminal located PIP degron (Shibutani et al., 2008).

3.1.6.2.1. Flow cytometric analysis of E2F1-NT^{230} degradation

For the analysis of E2F1 degradation a truncated protein fragment consisting of the amino acid residues 1-230 (E2F1-NT^{230}) was used similar to the applied E2F1 reporter in the *Drosophila* fluorescent ubiquitination-based cell cycle indicator system (Fly-FUCCI) (Zielke et al., 2014). E2F1-NT^{230} contains the PIP degron that confers CRL4^{Cdt2} mediated degradation in S-phase but lacks the DNA binding and coiled coil - marked box (CC-MB) domain and is thus unable to bind DNA or activate gene transcription. Since an N-terminal GFP-E2F1-NT^{230} fusion protein was successfully established as an S-phase marker in the FLY-FUCCI system, E2F1-NT^{230} was inserted into RPS-8 and investigated in S2R+ cells after transient transfection via flow cytometry (Figure 32 A). GFP-T2A-CHE-E2F1-NT^{230} displayed a decrease of protein levels in S-phase compared to the G1-population similar to the results of Dap_dCDI, but no increase in protein levels was observed in the G2-cell population (CHE/GFP ratios - G1: 0.80; S: 0.67; G2: 0.60) (Figure 32 B).

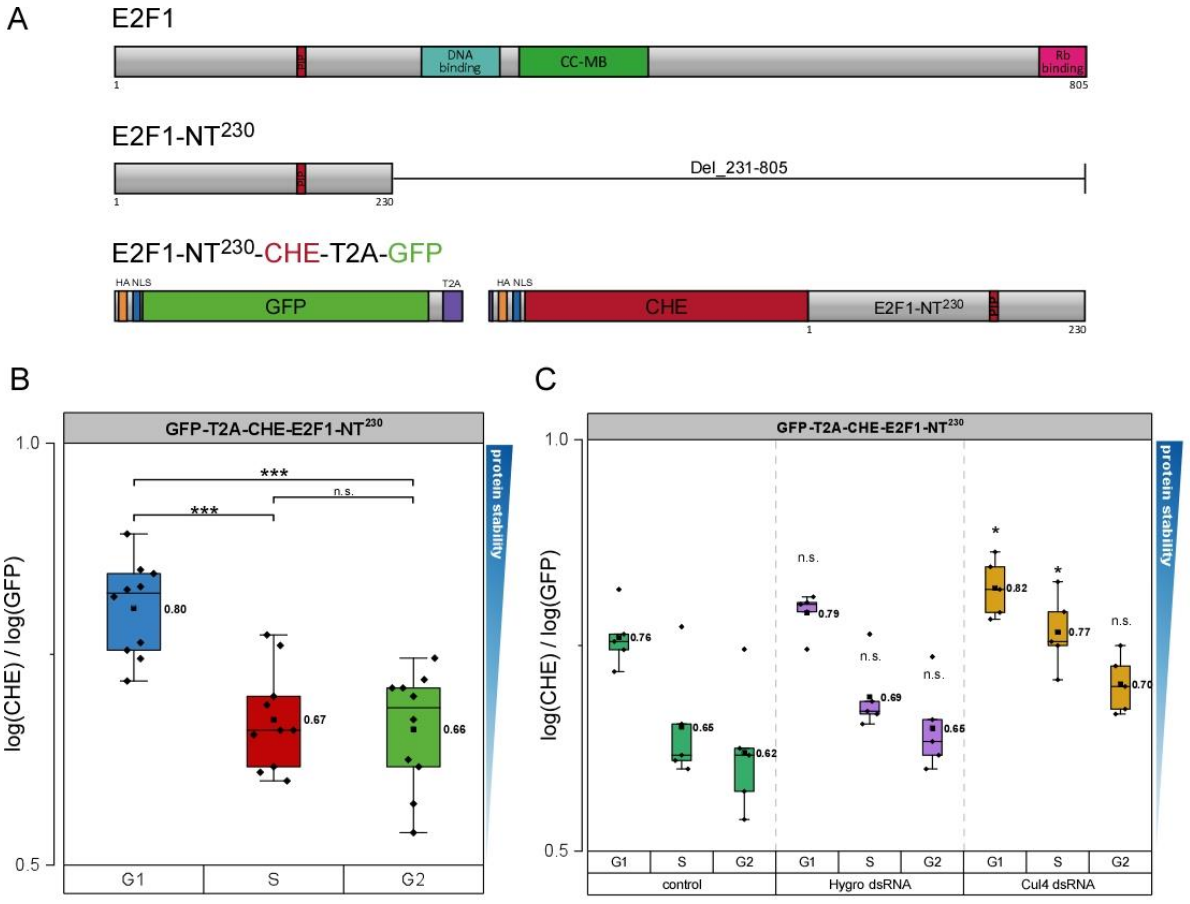

Figure 32| Flow cytometric analysis of E2F1-NT^{230} degradation

(**A**) Illustration of E2F1, E2F1-NT^{230} and the applied E2F1 RPS reporter construct. (**B**) Box plot of relative protein stability levels of GFP-T2A-CHE-E2F1-NT^{230} in G1-, S-, and G2-cells (exp.lvl. 1.5 - 2.5) summarizing the mean quantification of CHE/GFP ratios of independent replicates normalized to the RPS control. E2F1-NT^{230} is significantly destabilized in S-phase compared to G1-phase, but no reaccumulation is detected in G2-phase. Statistics performed by t-test with Welch´s correction, n.s. > 0.05, * ≤ 0.05, ** ≤ 0.01, *** ≤ 0.01. (**C**) Analysis of E2F1-NT^{230} with Cul4 knockdown (Cul4 dsRNA) and mock control (Hygro dsRNA) (exp.lvl. 1.5 - 2.5). E2F1-NT^{230} was stabilized significantly in cells treated with Cul4 dsRNA in G1-, S-, and in G2-cells, albeit not being significantly. Statistics performed by Mann-Whitney U-Test, n.s. > 0.05, * ≤ 0.05. The samples were compared to the control cells of the respective cell cycle phase and symbols for p-values displayed above the box.

Additionally, E2F1-NT^{230} degradation was also tested with downregulated CRL4^{Cdt2} activity implemented via Cul4 knockdown. Flow cytometric analysis of cells treated with Cul4 dsRNA resulted in significant stabilization of E2F1-NT^{230} in G1- and S-cells (G1: 0.76 to 0.82; S: 0.65 to 0.77) and also a stabilization in G2-cells (G2: 0.62 to 0.70), albeit not statistically significant (Figure 32 C). In conclusion, the results of E2F1-NT^{230} degradation analysis are similar to the findings for Dap_dCDI. E2F1-NT^{230} degradation in S-phase is detectable but CRL4^{Cdt2} dependent degradation is also observed in the G1- and G2-populations.

3.1.6.3. Analysis of Cdt1

As a third CRL4^{Cdt2} substrate, the *Drosophila* Cdt1 homologue Double parked (hereafter referred to as Cdt1) was investigated. Cdt1 is involved in pre-RC assembly in the course of origin licensing by recruiting the mini-chromosome maintenance complex (MCM) to the DNA (Wohlschlegel et al., 2000). Cdt1 is regulated by different mechanisms involving inhibitory binding by Geminin (see 3.1.5.2) and proteasomal degradation. Previous work in the Sprenger group showed that Cdt1 is targeted by the E3 ligase SCF^{Skp2} by a phosphorylation dependent mechanism (Thomer et al., 2004; Rössler, 2019). Furthermore, Cdt1 is also degraded by a phosphorylation independent mechanism mediated by CRL4^{Cdt2} via a N-terminal PIP degron (Lin et al., 2009; Lee et al., 2010).

3.1.6.3.1. Flow cytometric analysis of Cdt1-NT^{101} degradation

Degradation analysis of Cdt1 was performed using an cell cycle inert N-terminal fragment (aa 1-101) that has been already established as a S-phase marker in the Sprenger group (Heimbucher, 2017). Cdt1-NT^{101} represents an inactive protein fragment due to the deletion of the MCM binding domain but is still targeted via its PIP degron by CRL4^{Cdt2}. The truncated version should also not be targeted by SCF^{Skp2} due to the lack of phosphorylation sites in this region based on mass spectrometry data of the ISB Phosphopep database (Bodenmiller et al., 2007). Cdt1-NT^{101} was inserted into RPS-5 to avoid disturbance of its degradation by blocking the PIP degron by a bulky N-terminal fusion (Figure 33 A). Flow cytometric analysis of Cdt1-NT^{101}-CHE-T2A-GFP displayed similar results to Dap_dCDI and E2F1-NT^{230} with a destabilization in S-cells compared to G1-cells and no measurable protein reaccumulation in G2-cells (G1: 0.60; S: 0.43; G2: 0.45) (Figure 33 B). To test, if CRL4^{Cdt2} inactivation would have the same stabilizing effect in the assigned cell cycle populations as observed for Dap and E2F1, Cdt1-NT^{101} stability was investigated with additional Cul4 knockdown. Gene knockdown was achieved via co-transfection of a mir1-shRNA (short hairpin RNA) plasmid (Nguyen et al., 2006; Haley et al., 2008) directed against *cul4* exon 8 (mir1-Cul4) that has been established in the meantime in the Sprenger lab (Heidrich, 2020). The mir1-Cul4 shRNA was expressed from a pVALIUM20 plasmid under the control of a *hsp70* core promotor regulated by two pentamers of upstream activating sequence (UAS) as described in Ni et al. (2006). Expression was induced by additional co-transfection of Gal4 from a strong

polyubiquitin promotor (Brand et al., 1993), resulting in similar knockdown efficiency as achieved by RNAi knockdown implemented by dsRNA treatment (F. Sprenger, personal communication). Cdt1-NT^{101} was stabilized upon Cul4 knockdown with significant effects in the S- and G2- cell population (S: 0.43 to 0.61; G2: 0.44 to 0.59). A stabilization was also observed in G1-cells (G1: 0.59 to 0.70), albeit not being statistically significant (Figure 33 C). In summary it can be stated that degradation of Dap_dCDI, E2F1-NT^{230}, and Cdt1-NT^{101} during S-phase can be detected via flow cytometric measurement.

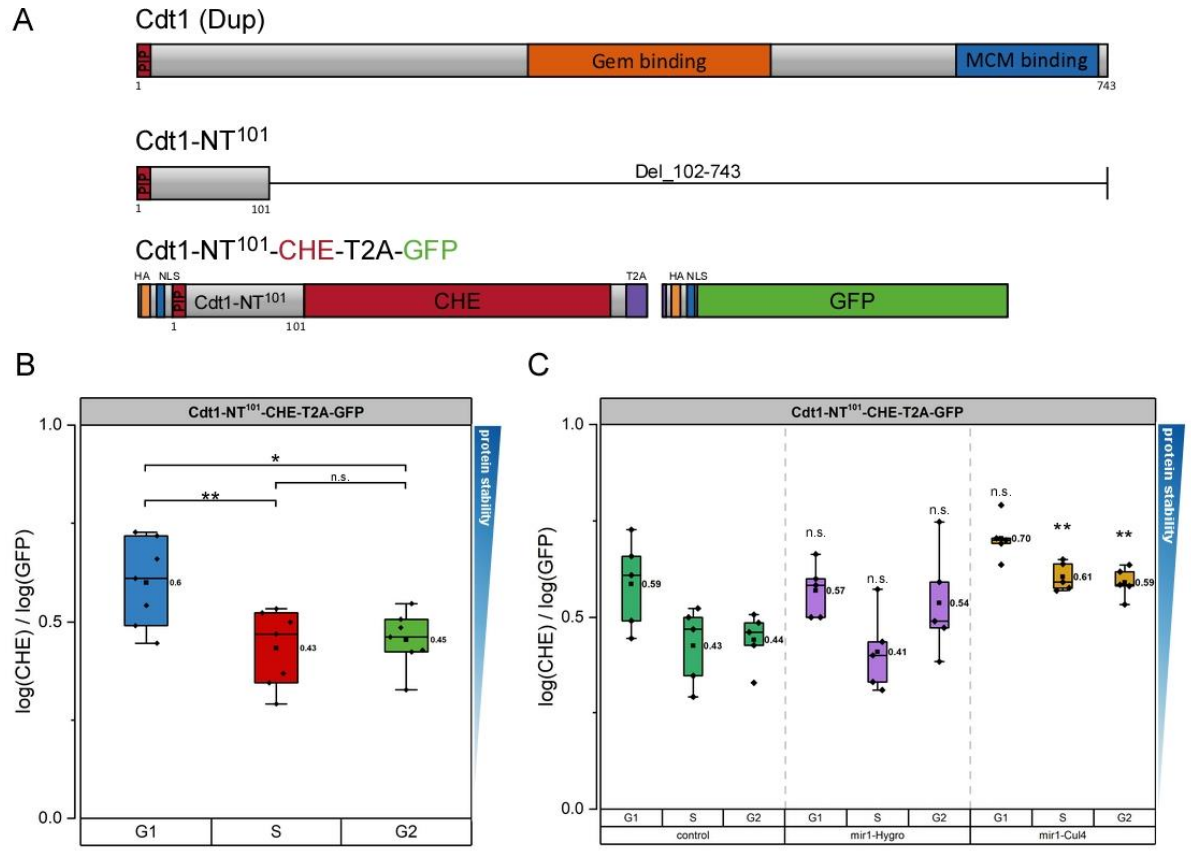

Figure 33| Flow cytometric analysis of Cdt1-NT^{101} degradation

(**A**) Illustration of *Drosophila* homologue Cdt1 (Double parked (Dup)), the N-terminal fragment Cdt1-NT^{101} and the applied Cdt1-NT^{101} RPS reporter construct. (**B**) Box plot summarizing the mean quantification of CHE/GFP ratios of independent replicates normalized to the RPS control of Cdt1-NT^{101}-CHE-T2A-GFP in G1-, S-, and G2-cells (exp.lvl. 1.25 - 2.0). Cdt1-NT^{101} is significantly destabilized in S-phase compared to G1-phase, but no reaccumulation is detected in G2-phase. (**C**) Mir1-based shRNA knockdown of Cul4 caused stabilization of Cdt1-NT^{101} in S- and G2- cells. A not significant increase of CHE/GFP quotient was also observed in G1- cells (exp.lvl. 1.5 - 2.5). Statistics performed by t-test with Welch´s correction, n.s. > 0.05, * ≤ 0.05, ** ≤ 0.01. The samples were compared to the control cells of the respective cell cycle phase and symbols for p-values displayed above the box.

3.1.6.3.2. Cdt1 subpopulations in the assigned G1-, S-, and G2- cell cycle populations

The stabilizing effect caused by Cul4 knockdown in the G1- and G2- cells is most likely attributed to the presence of “early” and “late” S-phase cells, respectively. Additionally, the slower maturation of CHE compared to GFP will cause decreased CHE/GFP ratios in the G2-population (see 3.1.6.1.1). Scatter plots of the cells transfected with Cdt1-NT^{101}-CHE-T2A-GFP displayed two subpopulations within the assigned cell cycle phases based on the CHE/GFP ratios. The G1-population is composed of cells with

high CHE/GFP quotients in the range 0.50 to 1.25, representing G1 cells (69.2%) and a second subpopulation with lower quotients in the area from 0.00 to 0.50 probably constituting early S-phase cells (29.6%). Using the same areas for the S-population showed a population consisting of cells that are either in G1- or already in G2-phase with high CHE/GFP values (35.7%) and an S-phase population in the lower range (60.8%). The G2 population consist of cells in the area of high CHE/GFP ratios representing G2 cells (45.3%) and cells in the area of lower area that are most likely late S-phase cells or cells that just entered G2 and just begun CHE-Cdt1-NT^{101} synthesis (52.7%) (Figure 34).

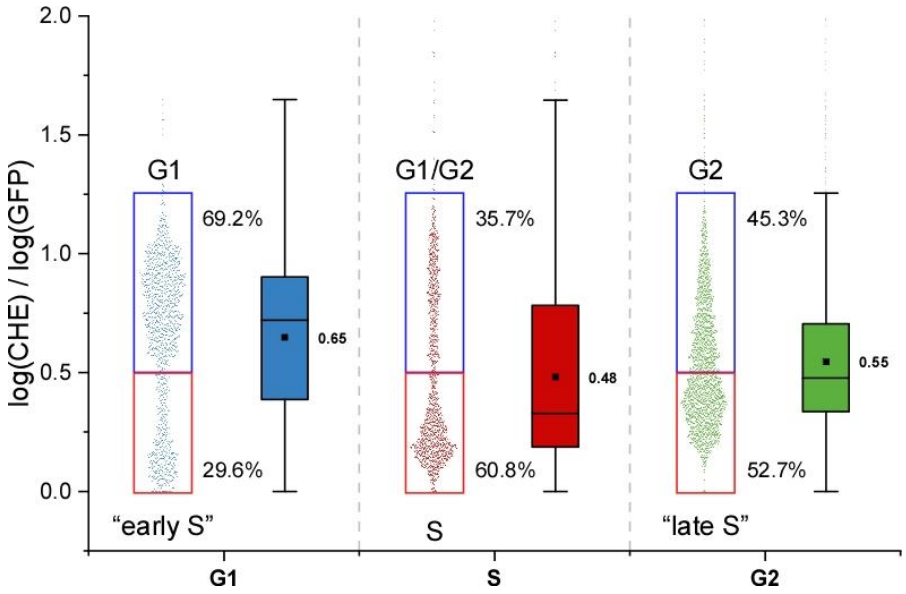

Figure 34| Cell subpopulations within the G1-, S-, and G2- cell populations

Scatter plot and the corresponding box plot of CHE/GFP ratios of cells transfected with Cdt1-NT^{101}-CHE-T2A-GFP detected by flow cytometry. The G1-, S-, and G2- populations contain subpopulations based on high CHE/GFP ratios in the range from 0.5 - 1.25 (blue box) and low ratios in the range 0.0 - 0.5 (red box). Percentage of the cells in the respective range were calculated for each cell cycle population and displayed next to the box. Cells in the higher CHE/GFP range have not degraded Cdt1-NT^{101} and are either G1 or G2 cells respectively, cells in the low range are assigned as S-phase or "early S" and "late S" if present within the G1 or G2 population, respectively.

Similar subpopulations have been observed for Dap_dCDI and E2F1 (data not shown). On should mention that the assignment of the subpopulations was only based on the reference/reporter signals of Cdt1-NT^{101}-CHE-T2A-GFP which are not comparable to precise cell cycle phase assignments based on EdU incorporation or other specific cell cycle markers. Also, the example shown here only represents a single replicate and the occurrence and characteristics of the subpopulations were subjected to variations among the replicates and were not always this pronounced. Summarizing the obtained data for Dap, E2F1, and Cdt1 shows that the cell cycle phase assignment via Hoechst DNA stain is not ideal for the analysis of protein degradation in S-phase due to heterogeneity of cells in the defined cell cycle populations. Nevertheless, S-phase degradation can be detected using the RPS system via flow cytometry, but with less accuracy compared to degradation in G1-phase. In general, this problem could be overcome by more accurate definition of S-phase cells, which though must be carried out *in vivo* avoiding cell fixation that causes loss of the GFP and CHE signal. This could for instance be implemented by

in vivo EdU incorporation as described in Salic et al. (2008) in addition to the Hoechst 33342 DNA stain. Alternatively, utilization of a fluorescent S-phase marker in addition to the GFP and CHE signals of the RPS system would also enable a more accurate determination of S-phase cells (Grant et al., 2018). However, due to the limited number of detectors it was not possible to measure further parameters with the existing CyFlow Space flow cytometer at the genetics department and consequently it was not possible to further improve the method in this regard.

3.1.6.3.3. Live cell imaging analysis of Cdt1-NT^{101}

To confirm that the degradation of the selected S-phase substrates is only initiated once S-phase starts, the flow cytometry analysis setup is not suited because early S-phase cells are present in the "G1" gate since they contain nearly identical DNA-content which cannot be distinguished by Hoechst stain of cell populations. Following individual cells by live cell imaging allows more precise determination of cell cycle stages and should enable an even more accurate measurement of protein degradation of the targets with the onset of S-phase. Time lapse microscopy analysis of Cdt1-NT^{101}-CHE-T2A-GFP have already been conducted in the course of a bachelor thesis in the Sprenger group (Heidrich, 2020). Since the initial analysis, further improvements in the data evaluation could be established and the raw data was reanalyzed (Figure 35). Protein levels of Cdt1-NT^{101}-CHE and the GFP reference were detected in single cells during cell cycle progression via live cell imaging and allocated to the different cell cycle phases. Starting with telophase (T = - 30 min) which was visually defined in the brightfield, G2-phase was assigned 60 min prior to telophase (G2 = -90 min). After formation of two nuclei, cells reside in G1-phase (t = 0 - 210 min) upon a sudden decrease of Cdt1-NT^{101}-CHE intensities which was defined as the beginning of S-phase (t = 225 - 255 min) (Figure 35 A). The nuclear CHE/GFP values were normalized to telophase and single cell traces were calculated and summarized in a line chart. Since cells were analyzed under unperturbed proliferation conditions, cell cycle phase durations vary among single cells (Chiorino et al., 2001; Snijder et al., 2011). This is clearly visible by the different time points of the sudden decline of Cdt1-NT^{101}-CHE fluorescence intensities marking S-phase, attributable to differing G1-durations (Figure 35 B). To adjust for cell-to-cell variations the single cell traces were interpolated using the multiple interval-based curve alignment (MICA) software (Mann et al., 2018). Based on the MICA aligned single cell traces a consensus trace was calculated representing Cdt1-NT^{101} protein levels in G1- and S-phase (Figure 35 C). Live cell imaging analysis of Cdt1-NT^{101}-CHE-T2A-GFP resulted in fairly stable reference/reporter signals during G1-phase, followed by a rapid decline of Cdt1-NT^{101}-CHE signals allocated to CRL4^{Cdt2} dependent degradation in S-phase. Hence, protein degradation in S-phase was more accurately determined using the RPS expression system via microscopic analysis compared to flow cytometric measurement.

In summary, it was possible to determine proteolysis of known APC/C targets, Cyclin B and Geminin, during G1-phase and degradation of the CRL4^{Cdt2} substrates Dacapo, E2F1, and Cdt1 in S-phase. Thus,

the RPS-system allows fast, accurate, and reproducible determination of the degradation of a selected protein interest within a certain cell cycle phase using flow cytometry. Verification of putative degradation motifs and detection of changes of relative protein stability levels in dependence of E3 ligase activity were successfully implemented using the RPS-system. Therefore, in a next step degradation of Rca1 was investigated using the established method.

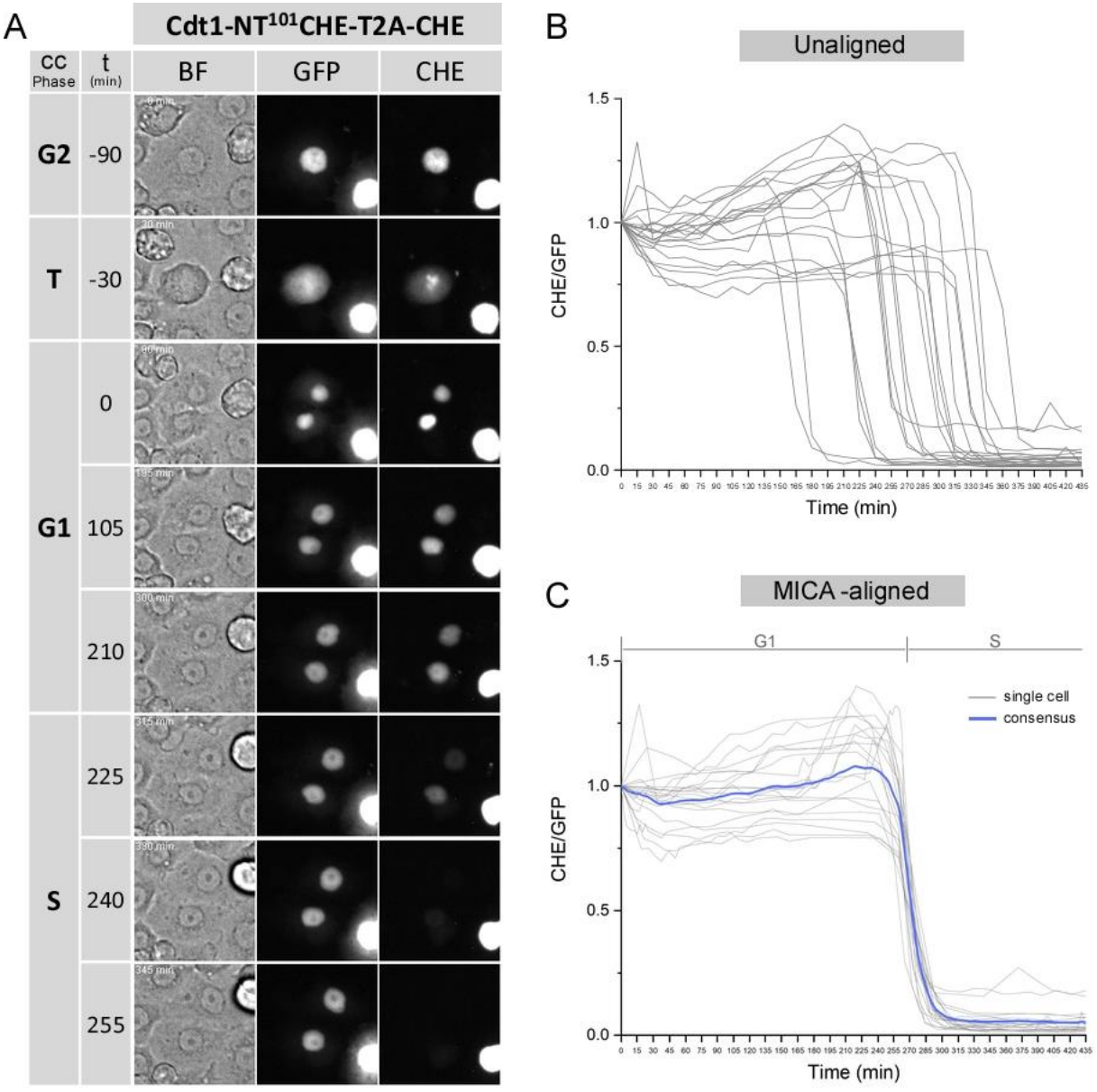

Figure 35| Live cell imaging of Cdt1-NT^{101}

(**A**) Images of S2R+ cells transfected with Cdt1-NT^{101}-CHE-T2A-GFP in the brightfield (BF), GFP-, and CHE-channel. Images were taken with a time interval of 15 min. Telophase was determined by the formation of new nuclei (t= -30 min). G2-phase was set 60 min prior to telophase (t= -90 min). G1 was defined by the formation of two new cells after cytokinesis (t= 0). Sudden decline of Cdt1-NT^{101}-CHE signal was as beginning of S-phase (t= 225 min) (**B**) Single cell traces of unaligned cells with different G1-durations. CHE/GFP ratios were normalized to telophase (-30 min) (**C**) Interpolated single cell traces via the MICA software (MICA aligned). Based on the interpolated traces, a consensus trace (blue line) was calculated. The Cdt1-NT^{101}-CHE reporter construct remains relatively stable during G1-phase and sudden drop in CHE intensities marks the beginning of S-phase and CRL4^{Cdt2} mediated degradation of Cdt1-NT^{101}-CHE. Raw data from Heidrich (2020).

3.2. Rca1 - an APC/C^{Fzr} target in G1-phase

3.2.1. Aim

According to previous studies, Rca1 is degraded during G1-phase. Detection of HA-Rca1 in embryos displayed degradation of Rca1 during the first G1-phase of the 17th cell cycle of *Drosophila* embryogenesis (Grosskortenhaus et al., 2002). In parallel, time lapse microscopy analysis of fluorescent labelled Rca1 in embryos and S2R+ also showed a decrease of Rca1 protein levels during G1-phase (Morgenthaler, 2013). An APC/C^{Fzr} dependent degradation of Rca1 was suggested based on biochemical interaction with Fzr (Grosskortenhaus et al., 2002) and similar degradation kinetics of Rca1 in comparison to known APC/C substrates (Morgenthaler, 2013). However, to this point there is only anecdotal evidence and no uniform picture of the E3 ubiquitin ligases and the degrons responsible for Rca1 degradation.

To further elucidate the degradation pathway of Rca1, protein levels were initially analyzed via flow cytometry using the RPS system to test if Rca1 degradation can be detected in G1-cells. In a next step, Rca1 degradation kinetics in G1-phase were measured via time lapse microscopy and compared to the results already obtained for the APC/C substrates Cyclin B and Geminin. Next, the influence of APC/C^{Fzr} activity on Rca1 protein levels was tested by either downregulation or hyperactivation of the APC/C^{Fzr}. Lastly, several putative degrons in Rca1 protein sequence were identified in a bioinformatic screen and validated via flow cytometric analysis of different Rca1 mutants.

3.2.2. Rca1, Rca1-NT, and Rca1-CT is degraded in S2R+ cells during G1-phase

Studies in *Drosophila* embryo and S2R+ cells showed that both, N- and C-terminal Rca1 moieties display decreased protein levels in G1-phase similar to Rca1 (Zielke, 2006; Morgenthaler, 2013). Hence, full-length Rca1, an N-terminal fragment Rca1_Del_204-411 (Rca1_1-203), and a C-terminal fragment Rca1_Del_1-203 (Rca1_204-411) were used for flow cytometric analysis to test if degradation in G1-phase can be detected in S2R+ cells via the RPS system. Preceding experiments demonstrated that C-terminal but not N-terminal fusions to Rca1 impaired Rca1 degradation as well as APC/C inhibition by Rca1 (Morgenthaler, 2013). Therefore, the Rca1 fragments were inserted into RPS-8 (GFP-T2A-CHE-POI) with an N-terminal fusion of the CHE-reporter (Figure 36 A). Flow cytometric analysis of GFP-T2A-CHE-Rca1 resulted in decreased protein levels in G1-cells and reaccumulation in the S- and G2-populations (CHE/GFP - G1: 0.26, S: 0.45, G2: 0.53). Similar results with decreased protein levels in G1-cells were obtained for the N-terminal part of Rca1, GFP-T2A-CHE-Rca1_1-203 (CHE/GFP - G1: 0.24, S: 0.43, G2: 0.51) and the C-terminal Rca1 fragment GFP-T2A-CHE-Rca1_204-411 (CHE/GFP - G1: 0.32, S: 0.46, G2: 0.50). However, the CHE/GFP quotient of C-terminal Rca1 was slightly elevated in G1-cells compared to Rca1 and Rca1_1-203 (Figure 36 B).Thus, Rca1 degradation during G1-phase was detectable using the RPS-system and the N-terminal fusion did not impair protein degradation.

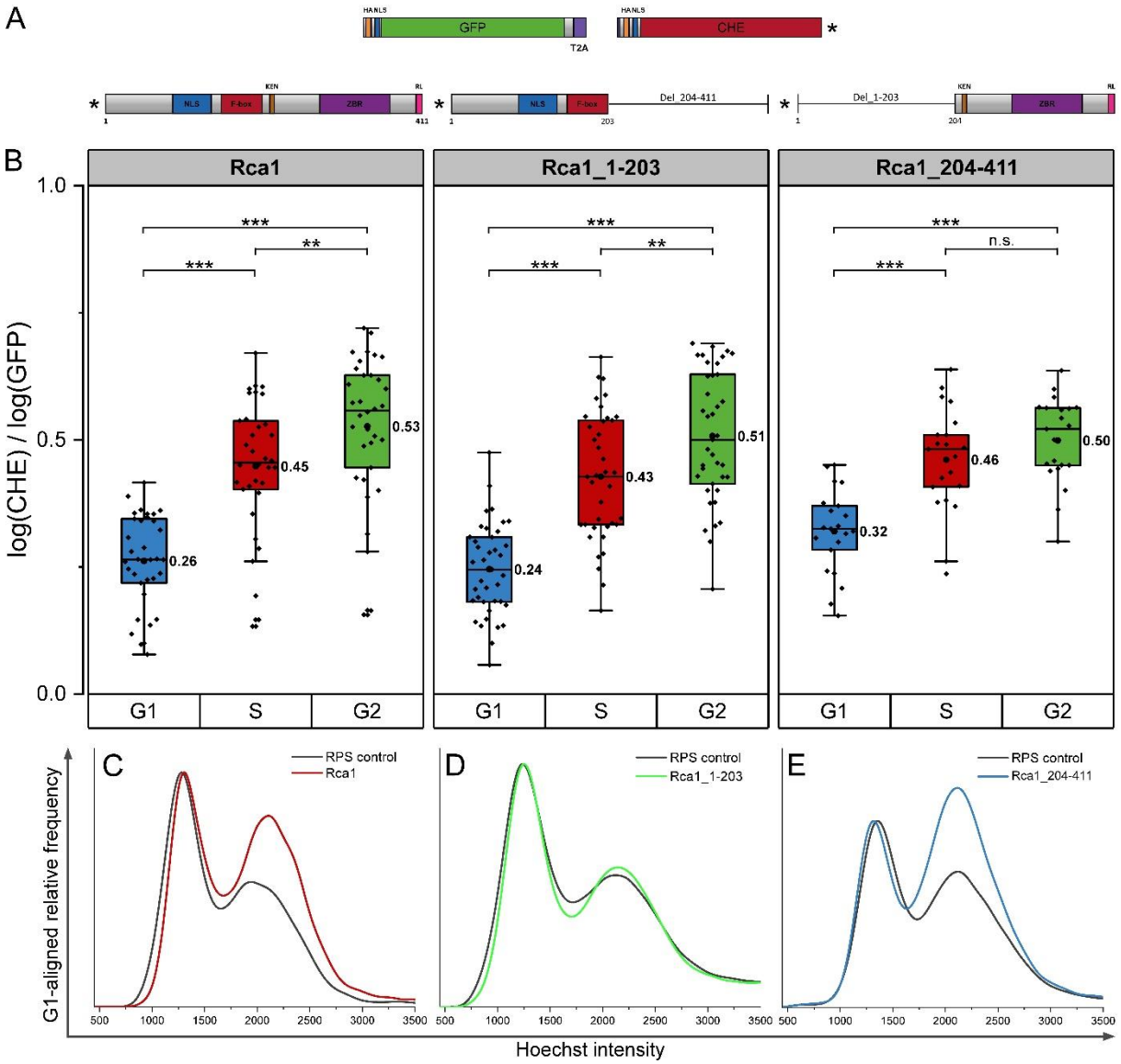

Figure 36| Rca1, Rca1_1-203 and Rca1_204-411 are degraded in G1-phase

A) Illustration of Rca1, Rca1_1-203, and Rca1_204-411 inserted into RPS-8. (**B**) Box plot summarizing the mean quantification of CHE/GFP ratios of independent replicates normalized to the RPS control of GFP-T2A-CHE-Rca1, GFP-T2A-CHE-Rca1_1-203, and GFP-T2A-CHE-Rca1_204-411 in G1-, S-, and G2-cells (exp.lvl. 1.0 - 1.75). G1-cells display decreased CHE/GFP ratios compared to the S- and G2-population. Statistics performed by Mann-Whitney U-Test, n.s. > 0.05, * ≤ 0.05, ** ≤ 0.01, ***≤ 0.001. (**C**, **D**, **E**) G1-aligned DNA histograms of the GFP positive cells transfected with the RPS control (black line) or the respective RPS-Rca1 construct. Overexpression of GFP-T2A-CHE-Rca1 (**C** - red line) and GFP-T2A-CHE-Rca1_204-411 (**E** - blue line) display an increased G2-peak. GFP-T2A-CHE-Rca1_1-203 (**D** - green line) did not cause a cell cycle shift compared to the control.

Previous studies demonstrated that overexpression of HA-Rca1 induced ectopic S-phase entry in eye imaginal discs and also overexpression in wing imaginal discs accelerates the G1/S transition (Zielke, 2006). In agreement, overexpression of 4xFLAG-Rca1 in S2R+ cells resulted in premature entry into S-phase accompanied by a shortened G1-phase (Frank, 2013). To test if the overexpression of the RPS-Rca1 constructs altered cell cycle progression, cell cycle distributions based on the Hoechst intensities of the GFP positive cells were analyzed (Figure 36 C, D, E). Premature S-phase induction and shortened G1-phase would result in a compensatory accumulation in G2-phase. Cells transfected with GFP-T2A-

CHE-Rca1 and GFP-T2A-CHE-Rca1_204-411 indeed displayed an increase of G2-cells compared to cells transfected with the RPS control seen by an exalted G2-peak in the Hoechst histogram (Figure 36 C, E). In contrast, expression of the N-terminal Rca1 fragment GFP-T2A-CHE-Rca1_1-203 did not cause an increase of G2-cells. This indicates that the N-terminal part with a present F-box domain was not able to induce premature S-phase entry, whereas C-terminal fragment with intact ZBR domain but missing F-box was able to cause acceleration of the G1/S transition.

In summary, the N-terminal fusion of the CHE reporter did neither impair Rca1 degradation nor its functionality. In accordance to previous studies (Grosskortenhaus et al., 2002; Morgenthaler, 2013), both the N- and C-terminal part of Rca1 are degraded in a cell cycle specific context to a similar extent as full-length Rca1, indicating that protein domains that confer Rca1 degradation are located in both protein regions.

3.2.3. Rca1 degradation has similar kinetics to Geminin

To investigate the degradation kinetics of Rca1 during G1-phase, live cell imaging experiments were conducted as implemented for Cyclin B and Geminin (see 3.1.5.2.4). Cells were transfected with either GFP-T2A-CHE-Rca1, the N-terminal fragment GFP-T2A-CHE-Rca1_1-203 or the C-terminal part, GFP-T2A-CHE-Rca1_204-411 and recorded by time lapse microscopy. Live cell imaging analysis of cells transfected with GFP-T2A-CHE-Rca1_1-203 showed a decrease of CHE/GFP ratio during G1-phase resulting from Rca1 degradation (Figure 37 A). Overexpression of GFP-T2A-CHE-Rca1 or GFP-T2A-CHE-Rca1_204-411 leads to a change in cell cycle distribution whereby G1-phase is significantly shortened, which is caused by their APC/C inhibition activity (see 3.3.3). Most cells that express sufficient levels of CHE-Rca1 (or CHE-Rca1_204-411) that is required for quantitative live cell imaging show no degradation after exit from mitosis, likely caused by the rapid entry into S-phase. To circumvent this problem, a point mutation in the ZBR of Rca1 (Rca1_204-411_A344T) was used for live cell imaging. The mutation A344T was original found in the *rca1*^{2} allele first described in Dong et al., 1997 that resulted in a phenotype of reduced cell number in embryos due to the lack of APC/C inhibition, which will also be discussed in more detail later (see 3.3.4 and 3.3.5). Flow cytometric analysis of the cell cycle distribution of cells transfected with GFP-T2A-CHE-Rca1_204-411_A344T showed no G2-accumulation anymore, in accordance with the lack of APC/C inhibition (compare Figure 36 E and Figure 37 C). Live cell imaging analysis of GFP-T2A-CHE-Rca1_204-411_A344T resulted in a decrease of CHE intensity with the onset of G1-phase similar to Rca1_1-203 (compare Figure 37 A and B). The respective single cell traces were summarized by mean degradation curves (Figure 37 D, E). To assess whether the Rca1 fragments are degraded with similar kinetics like other APC/C substrates, the mean degradation curves of Rca1_1-203 and Rca1_204-411_A344T were compared to the results obtained for CycB-NT^{285} and Gem-NT^{101} (see 3.1.5.2.4). These showed very similar degradation kinetics of the N- and C-terminal Rca1 fragments to Gem-NT^{101}, whereas CycB-NT^{285} degradation begins at an earlier time point and with faster kinetics (Figure 37 F).

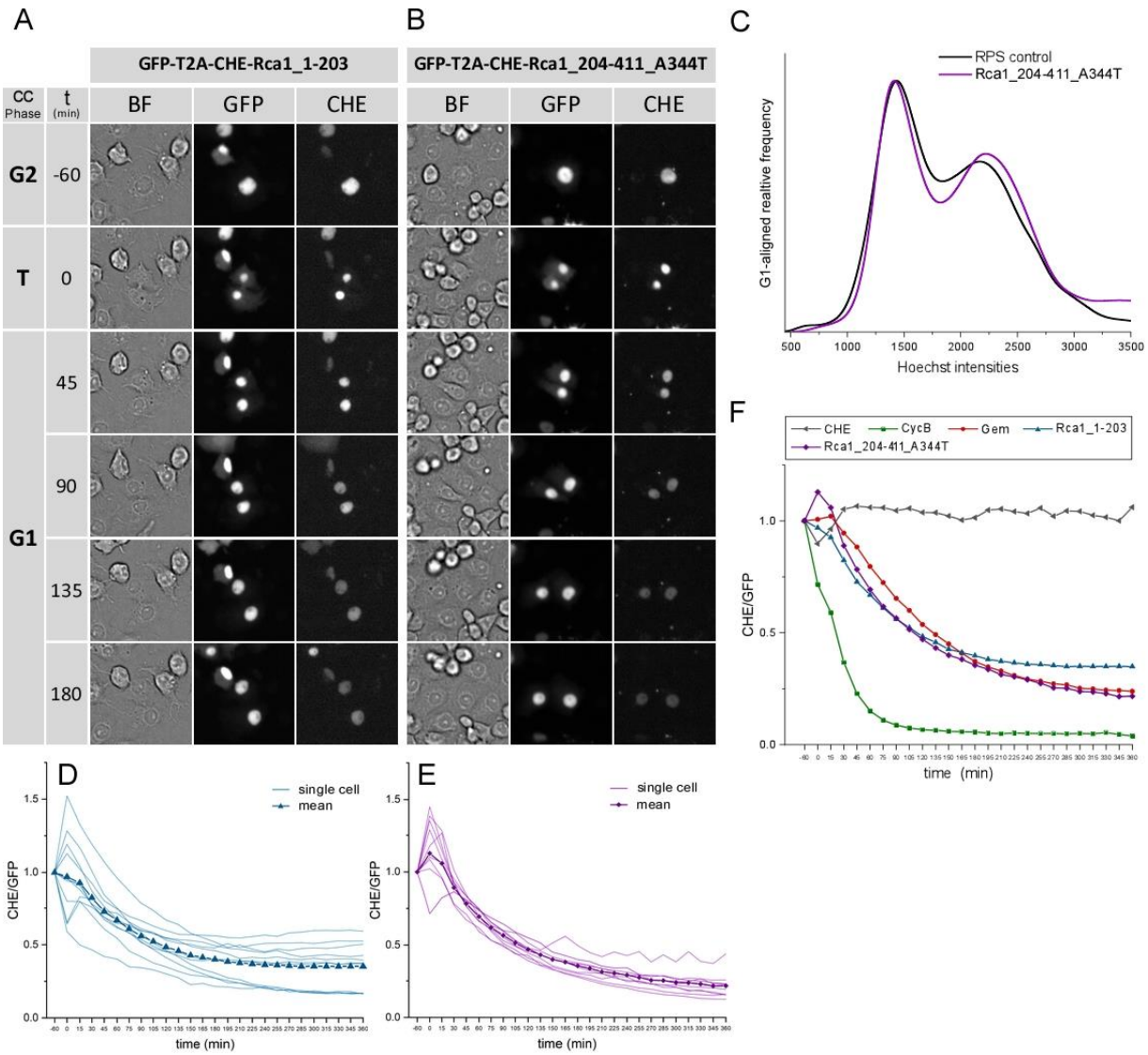

Figure 37| Rca1_1-203 and Rca1_204-411_A344T are degraded with similar kinetics like Gem-NT^{101}

(**A**, **B**) Images of S2R+ cells transfected with GFP-T2A-CHE-Rca1_1-203 or GFP-T2A-CHE-Rca1_204-411_A344T in the brightfield (BF), GFP-, and CHE-channel. Images were taken with a time interval of 15 min. Telophase cells determined by the formation of new nuclei were set as starting point (t= 0min). Time point 60 min earlier was set as G2-phase. G1 was defined by the formation of two new cells after cytokinesis. (**C**) G1-aligned DNA histograms of the GFP positive cells transfected with the RPS control (black line) and GFP-T2A-CHE-Rca1_204-411_A344T (purple line). Overexpression of Rca1_204-411_A344T does not cause a shift into G2-phase. (**D**, **E**) Telophase cells were tracked for 360 min (30 time frames) and the CHE/GFP ratios were calculated for each time point. Single cell traces are displayed and a mean degradation curve calculated based on the average value for each time point. (**F**) Comparison of the mean degradation curves of the GFP-T2A-CHE (CHE - gray), GFP-T2A-CHE-CycB-NT^{285} (CycB - green), Gem-NT101-CHE-T2A-GFP (Gem - red), GFP-T2A-CHE-Rca1_1-203 (Rca1_1-203 - blue), and GFP-T2A-CHE-Rca1_204-411_A344T (Rca1_204-411_A344T - purple).

In conclusion, the degradation kinetics of Rca1_1-203 and Rca1_204-411_A344T are very similar and resemble degradation of Gem-NT^{101} but not CycB-NT^{285} which indicates that Rca1 is also targeted by the APC/C^{Fzr} during G1-phase like Geminin.

3.2.4. Rca1 degradation depends on APC/C^{Fzr} activity

To further examine if Rca1 degradation is mediated by the APC/C^{Fzr}, Rca1 protein levels were investigated under conditions of hyperactivated and downregulated APC/C^{Fzr} activity, as implemented in the

analysis of Cyclin B and Geminin (see 3.1.5.1.6 and 3.1.5.2.3). In a first attempt, protein levels of GFP-T2A-CHE-Rca1 were measured by flow cytometry with additional overexpression of 4xFLAG-Fzr. CHE-Rca1 protein levels were analyzed in the G2-cell population, in which elevated activation of the APC/C^{Fzr} caused by 4xFLAG-Fzr overexpression is most pronounced as already seen in case of Cyclin B and Geminin (Figure 38 A). However, 4xFLAG-Fzr overexpression had no effect on CHE-Rca1 protein stability levels in G2 cells (CHE/GFP - G2: 0.63 to 0.62) (Figure 38 B). This can be explained by the inhibitory function of Rca1 since overexpression of HA-Rca1 was shown to be able to supress the effect of Fzr overexpression in *Drosophila* embryo (Grosskortenhaus et al., 2002). Hence, Rca1 is a potent APC/C inhibitor and consequently its overexpression can suppress the effect of Fzr overexpression and compensate the hyperactivated APC/C activity thereby inhibiting its own potential degradation mediated by the APC/C (Figure 38 A). Previous experiments have shown that the C-terminal part of Rca1 was sufficient for APC/C inhibition in *Drosophila* embryo (Zielke et al., 2006) and consequently the N-terminal part should not be able to restrain APC/C activity. Therefore, GFP-T2A-CHE-Rca1_1-203 was analyzed in a next step. Indeed, GFP-T2A-CHE-Rca1_1-203 protein levels were significantly decreased in G2 cells after simultaneous 4xFLAG-Fzr co-overexpression compared to the control (CHE/GFP - G2: 0.64 to 0.47). Surprisingly, Fzr overexpression also caused a decrease of relative protein stability levels of the C-terminal part of Rca1, GFP-T2A-CHE-Rca1_204-411 (CHE/GFP - G2: 0.64 to 0.52) similar to Rca1_1-203 (Figure 38 B). This was not expected since the C-terminal region of Rca1 was sufficient to restrict APC/C^{Fzr} activity in *Drosophila* embryo in Zielke et al. (2006), which will also later be shown to be the case in S2R+ cells (see 3.3.3), and consequently its overexpression should be able to restrain the ectopic APC/C activity similar to full-length Rca1. Nevertheless, this indicates that the Rca1 C-terminus can inhibit the APC/C but probably not to the same extent as Rca1.

Reversely, CHE-Rca1 stability was also measured with downregulated APC/C^{Fzr} activity implemented by Fzr RNAi knockdown. Flow cytometric analysis of Rca1 relative protein stability levels in cells treated with dsRNA against Fzr showed a stabilization of CHE-Rca1 (CHE/GFP: 0.20 to 0.39), CHE-Rca1_1-203 (CHE/GFP: 0.24 to 0.45), and CHE-Rca1_204-411 (CHE/GFP: 0.27 to 0.59) in the G1-cell population. Treatment with mock Hygro-dsRNA had no effect on protein stability levels in none of the conducted experiments (Figure 38 C).

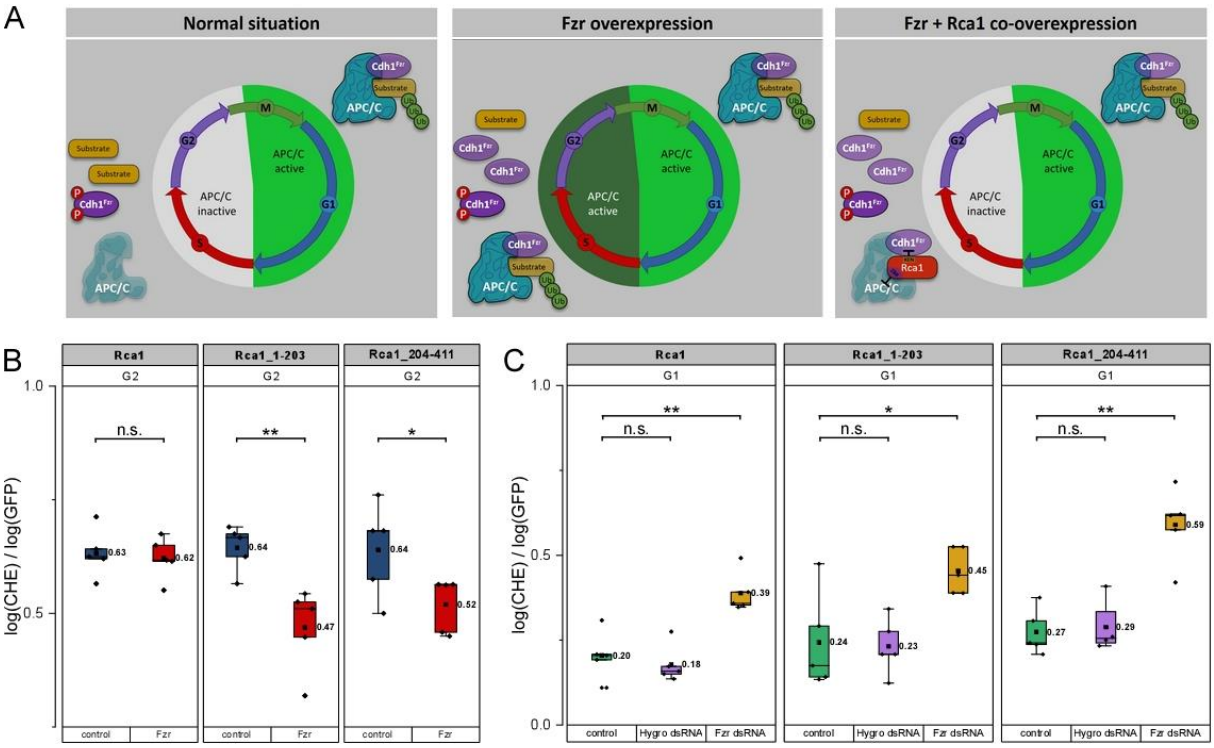

Figure 38| Rca1 degradation is dependent on APC/C^{Fzr} activity

(**A**) Schematic illustration of APC/C activity during the cell cycle. Fzr overexpression leads to an unnatural activation of APC/C^{Fzr} in S- and G2-phase. Simultaneous co-overexpression of Fzr and Rca1 leads to a suppression of elevated APC/C^{Fzr} activity by Rca1 in S- and G2-phase, restoring the normal situation. (**B**) Flow cytometric analysis of G2-cells transfected with either GFP-T2A-CHE-Rca1, GFP-T2A-CHE-Rca1_1-203 or GFP-T2A-CHE-Rca1_204-411 (exp.lvl. 1.0 - 1.75) with elevated APC/C^{Fzr} activity through 4xFLAG-Fzr overexpression. Fzr overexpression has no effect on Rca1 protein stability levels. Rca1_1-203 and Rca1-204-411 are significantly destabilized by Fzr overexpression (red box) compared to the control (blue box). (**B**) Flow cytometric analysis of the G1-population of cells transfected with GFP-T2A-CHE-Rca1, GFP-T2A-CHE-Rca1_1-203 or GFP-T2A-CHE-Rca1_204-411 under normal conditions (green boxes), treated with mock Hygro dsRNA (purple boxes) or Fzr dsRNA (brown boxes) (exp.lvl. 1.0 - 1.75). Rca1, Rca1_1-203, and Rca1_204-411 relative protein stability levels were significantly increased by Fzr knockdown in G1-cells. Treatment with Hygro dsRNA had no effect on relative protein stability levels. Statistics performed by Mann-Whitney U-Test, n.s. > 0.05, * ≤ 0.05, ** ≤ 0.01.

Taken together, increased APC/C^{Fzr} activity caused a destabilization of the N- and C-terminal part of Rca1 whereas full-length Rca1 overexpression suspends the effects of 4xFLAG-Fzr overexpression by suppressing the ectopic APC/C^{Fzr} activity. Downregulation of APC/C^{Fzr} activity caused an increase of relative protein stability levels of full-length, N- and C-terminal Rca1 during G1-phase. Hence, Rca1 relative stability levels are dependent on APC/C^{Fzr} activity.

3.2.5. Identification and validation of APC/C degrons mediating Rca1 degradation

The observed changes of Rca1 protein stability levels in dependence on APC/C^{Fzr} activity do not inevitably imply that Rca1 is a direct substrate of the APC/C. The effects could also be indirect, referable to an APC/C substrate that either protects Rca1 from degradation or is required for the activity of another E3-ligase actually targeting Rca1. In the case that Rca1 is a direct APC/C substrate, it should consistently contain APC/C specific degrons mediating APC/C recruitment. Therefore, the Rca1 protein sequence was scanned for putative degradation motifs in a bioinformatic screen. Initially, analysis with the GPS-

ARM: *Predictor for APC/C Recognition Motif* tool (Liu et al., 2012) identified three putative D-box degrons besides the already known KEN-box (Zielke, 2006; Morgenthaler, 2013). A search using the Eukaryotic Linear Motif (ELM) prediction tool detected a potential ABBA motif and a $SCF^{\beta TrCP}$-diphospho degron that is also present in Emi1. Furthermore, a manual search using the Scan Prosite tool (de Castro et al., 2006) for non-canonical and less characterized degrons including the CRY-box (CRYxPS) (Reis et al., 2006), the TEK-box (R/KxxTxKT) (Jin et al., 2008), the destruction sequence found in budding yeast Spo13 (LxExxxN) (Sullivan et al., 2007), and the minimal consensus of the O-box motif (LxxxN) (Araki et al., 2005) showed three putative O-box sequences within Rca1 (Figure 39). A further sequence analysis using the APC/C degron repository online tool discovered an additional non-canonical KEN-box degron (Figure 41 C) that will also be investigated later (see 3.2.5.1).

A

Software / Database	Degron	Position	Sequence	Abbrevation
GPS-ARM	D-box	7-10	^{1}MSAYYR**RAAL**RKKSPSR^{18}	DB(1)
		207-210	^{207}LERLQNH**RLKL**NLTKENP^{223}	DB(2)
		384-387	^{275}PSKLMMP**RERL**TPPQRAQ^{394}	DB(3)
	KEN-box	214-216	^{207}RLKLNLT**KEN**PHVPKRC^{223}	KEN(2)
ELM resource	ABBA	135-140	^{129}KKSKKLL**LFPHIE**EPPKNRF^{147}	ABBA
	$SCF^{\beta TrCP}$-diphospho degron	252-257	^{245}NSAASLM**DSGNSS**IHLMDVD^{264}	DSGxxS
Scan ProSite	O-box	34-38	^{27}ESGYTSF**L**ALH**N**STAETPF^{45}	OB(1)
		212-216	^{205}NHRLKLN**L**TKE**N**PHVPKRC^{223}	OB(2)
		235-239	^{228}KANHTVP**L**QTS**N**HSSLANS^{246}	OB(3)

B

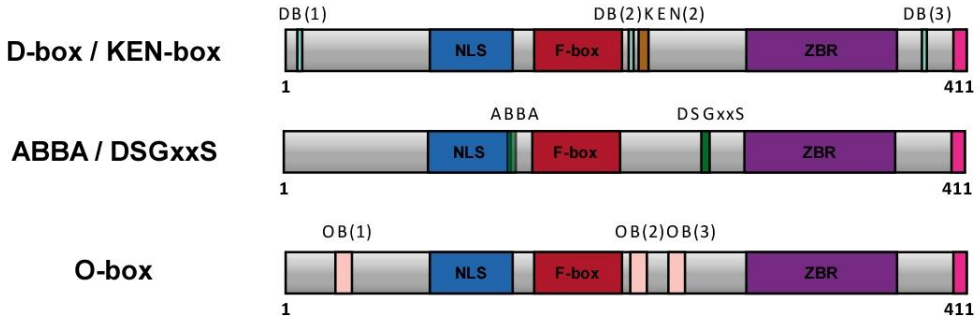

Figure 39| Bioinformatic screen for potential degradation motif in Rca1

(**A**) Table summarizing the results of a first bioinformatic screen for putative degradation motifs in Rca1. The essential amino acids of the respective consensus sequence are highlighted in red. (**B**) Illustration of the location of the potential degradation motifs in Rca1: D-box (cyan), KEN-box (brown), ABBA motif (green), DSGxxS (green) and O-box (pink).

In summary, Rca1 contains several putative degradation motifs, of which four types, the D-box, KEN-box, ABBA motif, and the O-box are directly attributed to APC/C dependent ubiquitination, whereas the DSGxxS motif mediates interaction with the E3 ligase $SCF^{\beta TrCP}$. To ascertain if the motifs are involved

in Rca1 degradation during G1-phase, several Rca1 mutants were analyzed via the RPS system in the following.

3.2.5.1. Flow cytometric analysis of Rca1_1-203

The N-terminal Rca1 fragment, Rca1_1-203, was destabilized in G1-cells similar to Rca1 (see 3.2.2) and based on the bioinformatic screen, this protein region contains a putative D-box, an O-box, and an ABBA motif. To assess whether degradation is mediated by one or a combination of these degrons, different mutants were tested for their relative protein stability levels in the G1-population. Analysis of the N-terminal located D-box degron by either mutation of the D-box consensus (RxxL mutated to AxxL as in GFP-T2A-CHE-Rca1_1-203_mDB(1)) or a deletion of the first ten amino acid residues along with the D-box (GFP-T2A-CHE-Rca1_1-203_ΔDB(1)) resulted in a significant stabilization in G1-cells. The D-box deletion, Rca1_1-203 _ΔDB(1), displayed a more pronounced stabilization (CHE/GFP - G1: 0.41) compared to the mutation of the D-box (CHE/GFP - G1: 0.32) (Figure 40 A). Due to cloning issues the mutation of the D-box consensus resulted only in a partial amino acid exchange from RxxL to AxxL instead of AxxA, which could explain the observed difference. In spite of the stabilization in G1-phase, analysis of protein stability levels of Rca1_1-203 _ΔDB(1) throughout the cell cycle populations still showed a statistically significant difference in protein levels between G1- and S-/G2-cells (CHE/GFP - G1: 0.41, S: 0.55, G2: 0.60) (Figure 40 B). The lower G1 levels indicate that mutation of the D-box only partially stabilized Rca1-NT and further motifs still cause its APC/C dependent degradation in G1-phase (Figure 40 B). Therefore, it was tested if the remaining G1-instability is mediated by the O-box or ABBA motif. Single mutation of the O-box consensus from LxxxN to AxxxA (as in GFP-T2A-CHE-Rca1_1-203_mOB(1)), had no effect on relative protein stability levels (CHE/GFP - G1: 0.23) and also the double mutation, Rca1_1-203_ΔDB(1)_mOB(1), was not further stabilized compared to the single deletion of the D-box (CHE/GFP - G1: 0.39). Consequently, the O-box had no influence on Rca1_1-203 stability. Single mutation of the ABBA motif by alanine substitutions of the consensus sequence from LxPHxE to AxAAxA (mABBA) caused a minor stabilization of GFP-T2A-Rca1_1-203_mABBA (CHE/GFP - G1: 0.29), albeit not being statistically significant compared to Rca1_1-203. Also the double mutant, Rca1_1-203 _ΔDB(1)_mABBA, showed slightly increased CHE/GFP ratios in G1-cells (CHE/GFP - G1: 0.49), but also missing statistical significance compared to Rca1_1-203 _ΔDB(1) (Figure 40 A). Thus, neither the O-box nor the ABBA motif caused the remaining G1 instability of Rca1_1-203_ΔDB(1). Since no further known short linear interaction motifs were found in the initial bioinformatic screen, different N-terminal truncations of Rca1_1-203 were analyzed in order to identify the protein region that mediates its degradation besides the N-terminal D-box. A sequence alignment of Rca1 from different *Drosophila* species displayed several conserved regions within the N-terminus, which were analyzed by progressive deletion (Figure 41 A).

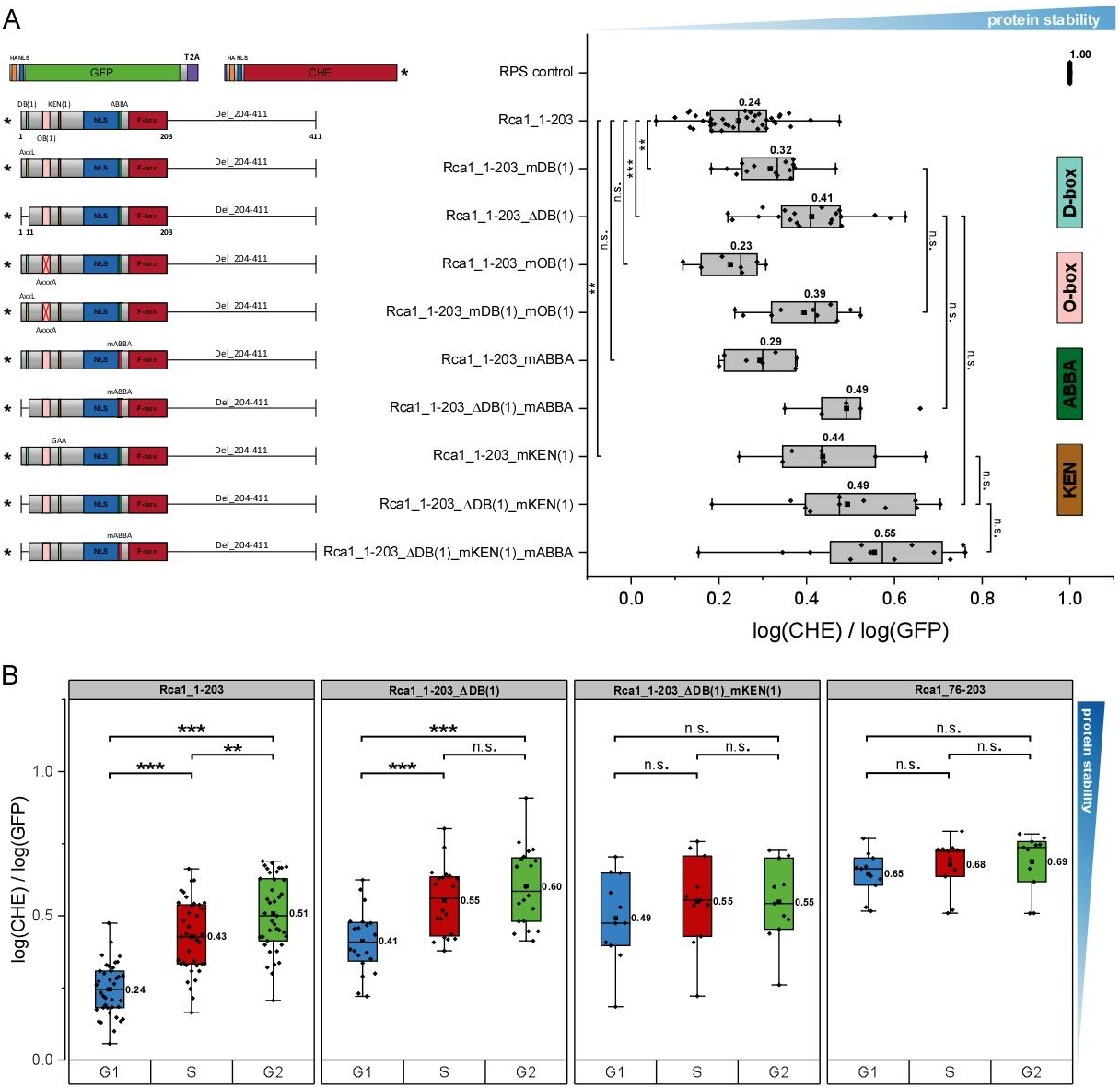

Figure 40| A D-box and a non-canonical KEN-box degron mediated Rca1_1-203 degradation

(**A**) Analysis of relative protein stability levels of Rca1_1-203 degron mutants. Illustration of the corresponding Rca1_1-203 mutant (left panel) and the normalized CHE/GFP ratios in G1-cells (right panel) (exp.lvl. 1.0 - 1.75). Mutation of the D-box consensus to AxxL (mDB(1)) and deletion of the first ten amino acid residues ΔDB(1) increased Rca1_1-203 stability in G1-phase. Single mutation of the O-box and in combination with mDB(1) had no effect on relative protein stability levels. Analysis of the ABBA motif caused only a slight stabilization in combination with ΔDB(1), albeit not being statistically significant. Mutation of the non-canonical KEN-box (mKEN(1)) resulted in significant stabilization of Rca1_1-203 in G1-cells. The double mutant Rca1_1-203_ΔDB(1)_mKEN(2) showed a weak additive but not significant effect. The triple mutant Rca1_1-203_ΔDB(1)_mKEN(2)_mABBA was slightly more stable in G1-cells, however missing statistical relevance. (**B**) Flow cytometry analysis of Rca1_1-203, Rca1_1-203_ΔDB(1), Rca1_1-203_ΔDB(1)_mKEN(1), and Rca1_76-203 in G1-, S-, and G2-cells (exp.lvl. 1.0 - 1.75). No significant destabilization in G1 can be detected for the D- and KEN-box mutant and also not for Rca1_76-203. Statistics performed by t-test with Welch´s correction, n.s. > 0.05, * ≤ 0.05, ** ≤ 0.01, ***≤ 0.001.

N-terminal truncations of the first 25 aa (Rca1_26-204) and 35 aa (Rca1_36-203) did not cause a further stabilization compared to Rca1_1-203_ΔDB(1) in G1-cells (CHE/GFP - G1: 0.48 and 0.37). First a deletion of the first 50 amino acid residues (Rca1_51-203) significantly increased relative protein stability (CHE/GFP - G1: 0.52) which was even increased after deletion of amino acid residues 1 to 75 (Rca1_76-

203; CHE/GFP - G1: 0.65) (Figure 41 B) and was also no longer degraded throughout the three cell cycle populations (CHE/GFP - G1: 0.65, S: 0.68, G2: 0.69) (Figure 40 B).

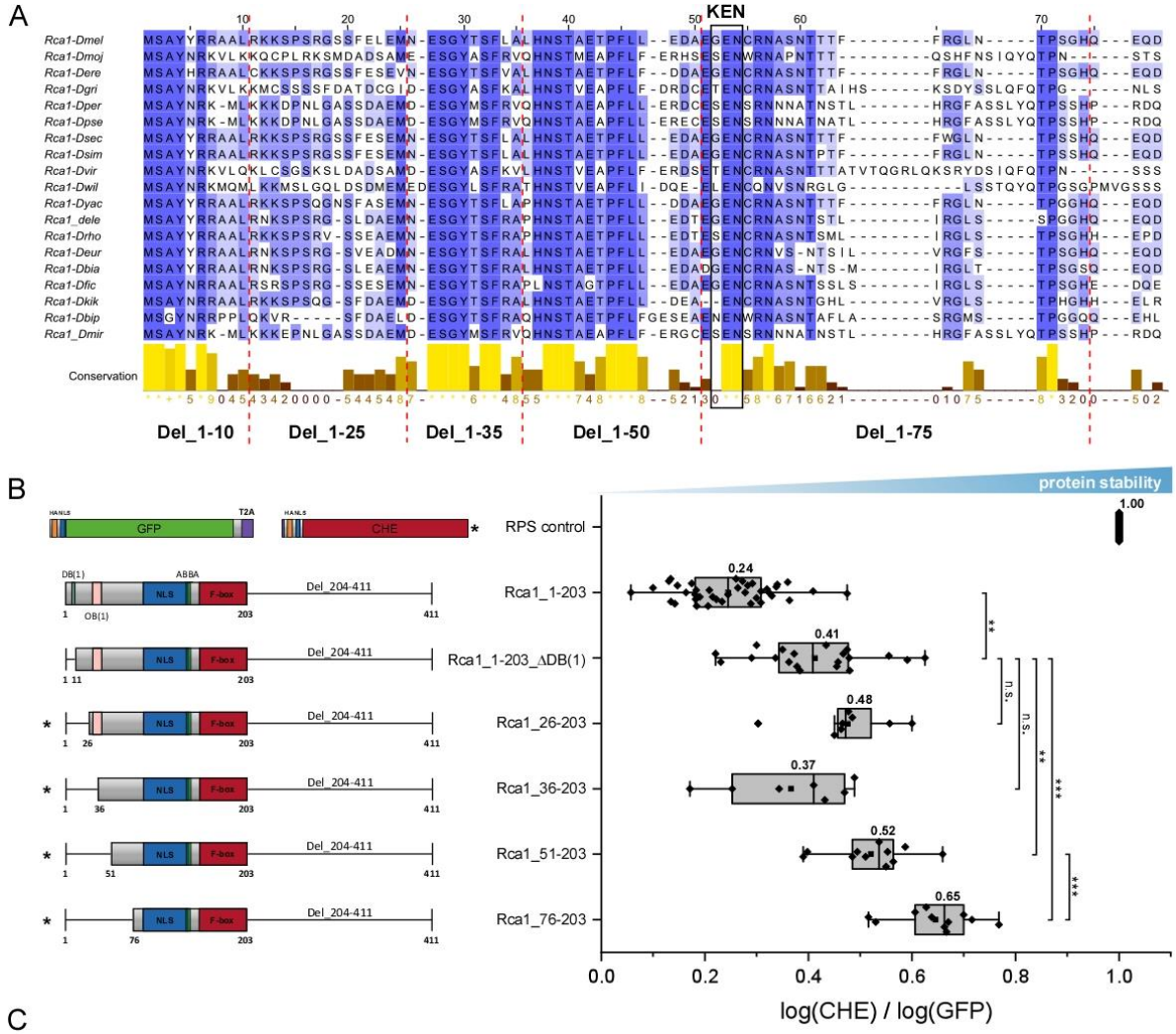

Software / Database	Degron	Position	Sequence	Abbrevation
APC/C degron repository	KEN-box	52-54	^{46}LLEDAE**GEN**CRNASNT^{61}	KEN(1)

Figure 41| Identification of the non-canonical KEN-box degron in Rca1 N-terminus

(**A**) Rca1 sequence alignment among different *Drosophila* species. N-terminal deletions are indicated by a red dashed line. The non-canonical KEN-box is marked by a black box. (**B**) Analysis of relative protein stability levels of successive truncations of Rca1_1-203 N-terminal region. Illustration of the corresponding proteins (left panel) and the normalized CHE/GFP ratios in G1-cells (right panel) (exp.lvl. 1.0 - 1.75). Deletion of the first 50 amino acids caused a significant stabilization in G1-cells. Further truncation up to position 75 further increased the relative protein stability of the N-terminal Rca1 mutant in G1-phase. Statistics performed by t-test with Welch´s correction, n.s. > 0.05, * ≤ 0.05, ** ≤ 0.01, ***≤ 0.001. (**C**) Identification of a non-canonical KEN-box degron using the APC/C degron repository online tool. The essential amino acids of the consensus sequence are highlighted in red.

This indicates a potential degradation motif located between amino acid positions 50 to 75 and indeed an additional non canonical KEN-box degron (E**GEN**CRN) at position 51-57 was identified in a second bioinformatic screen with the APC degron repository online tool (Figure 41 C). Flow cytometric analysis of GFP-T2A-CHE-Rca1_1-203_mKEN(1) containing a mutated KEN-box degron (GEN to GAA = mKEN(1))

displayed an increase of CHE/GFP ratio in G1-cells (CHE/GFP - G1: 0.44) similar to the deletion of the D-box. However, the simultaneous deletion of the D-box and mutation of the KEN-box, as in GFP-T2A-CHE-Rca1_1-203_ΔDB(1)_mKEN(1), resulted in a complete stabilization throughout the cell cycle populations (CHE/GFP - G1: 0.49, S: 0.55, G2: 0.55) similar to GFP-T2A-CHE-Rca1_76-203 (Figure 40 A, B). Since mutation of the ABBA motif caused a slight stabilization even though not being statistically significant, a triple mutant, Rca1_1-203_ΔDB(1)_mKEN(1)_mABBA, was also tested. The additional mutation of the ABBA motif resulted in weak stabilization compared to Rca1_1-203_ΔDB(1)_mKEN(1) (CHE/GFP - G1: 0.49 to 0.55) though missing statistically significance (Figure 40 A). Also, no significant effect was observed between D- and KEN-box double mutant and the triple mutant in the S- and G2-populations (data not shown). Thus, the minor but statistically insignificant effect observed for the different ABBA mutants, does not allow a proper evaluation on the functionality of the ABBA motif to this point. In summary, the N-terminal half of Rca1 contains at least two APC/C degrons, and inactivation of both prevents cell cycle degradation resulting in a complete stabilization of the N-terminal Rca1 fragment.

3.2.5.2. Flow cytometric analysis of Rca1_204-299

The central region of Rca1 (Rca1_204-299) contains a D-box, a KEN-box, and an O-box motif. The potential O-box sequence (OB(2)) was excluded from the analysis, since the essential amino acids are part of the KEN-box consensus (Figure 39 A). The KEN-box was already investigated in a preceding study, demonstrating that mutation of the KEN-box resulted in the stabilization of a small degradable Rca1 fragment, Rca1_204-299, in G1-phase (Morgenthaler, 2013). However, the D-box which is located in close proximity upstream of the KEN-box was not investigated to this point. Therefore, Rca1_204-299 was used for the analysis of the centrally located degradation motifs via the RPS system. In a first step, relative protein stability levels of GFP-T2A-CHE-Rca1_204-299 were analyzed via flow cytometry to test if the Rca1 fragment is still degraded in G1-phase. Cells transfected with GFP-T2A-CHE-Rca1_204-299 showed a destabilization in G1-cells compared to S- and G2-cells (CHE/GFP - G1: 0.51, S: 0.67, G2: 0.78), however the CHE/GFP quotient of G1 cells was increased compared to Rca1 and the N- and C-terminal Rca1 fragments (CHE/GFP - G1: 0.26; 0.24; 0.32) (compare Figure 36 B and Figure 42 A). To test if the destabilization in G1-cells is mediated by the D- or KEN-box, both degrons were mutated and analyzed by flow cytometry. Mutation of the D-box (RxxL to AxxA = mDB(2)) did not cause a stabilization of Rca1_204-299_mDB(2) (CHE/GFP - G1: 0.58). In contrast, a deletion of the D-box, Rca1_204-299_ΔDB(2), caused a significant stabilization in G1-cells (CHE/GFP - G1: 0.66) (Figure 42 B). However, neither mutation nor deletion of the D-box resulted in a complete stabilization of the central Rca1 fragment in the context of cell cycle progression, as both mutants were still destabilized in G1-cells compared to S- and G2-cells (Figure 42 A). Thus, in a next attempt, mutation of the KEN motif (KEN to KAA = mKEN(2)) was tested and compared to the D-box mutant. GFP-T2A-Rca1_204-

299_mKEN(2) was significantly stabilized in G1-cells (CHE/GFP - G1: 0.72) and also no difference was detectable compared to S- and G2-cells anymore, indicating a complete stabilization of the KEN-box mutant. A double D- and KEN-box mutant, Rca1_204-299_mDB(2)_mKEN(2) did not result in an additive effect and also no differences was observed in the S- and G2-cells compared to the single KEN-box mutation (Figure 42 A, B). One must mention, that Rca1_204-299 also contains the $SCF^{\beta TrCP}$ diphosphodegron (DSGxxS), which has not been investigated in this protein fragment, since mutation of the KEN-box already caused a complete stabilization. However, the DSGxxS motif will also be investigated in the following (see 3.2.5.4).

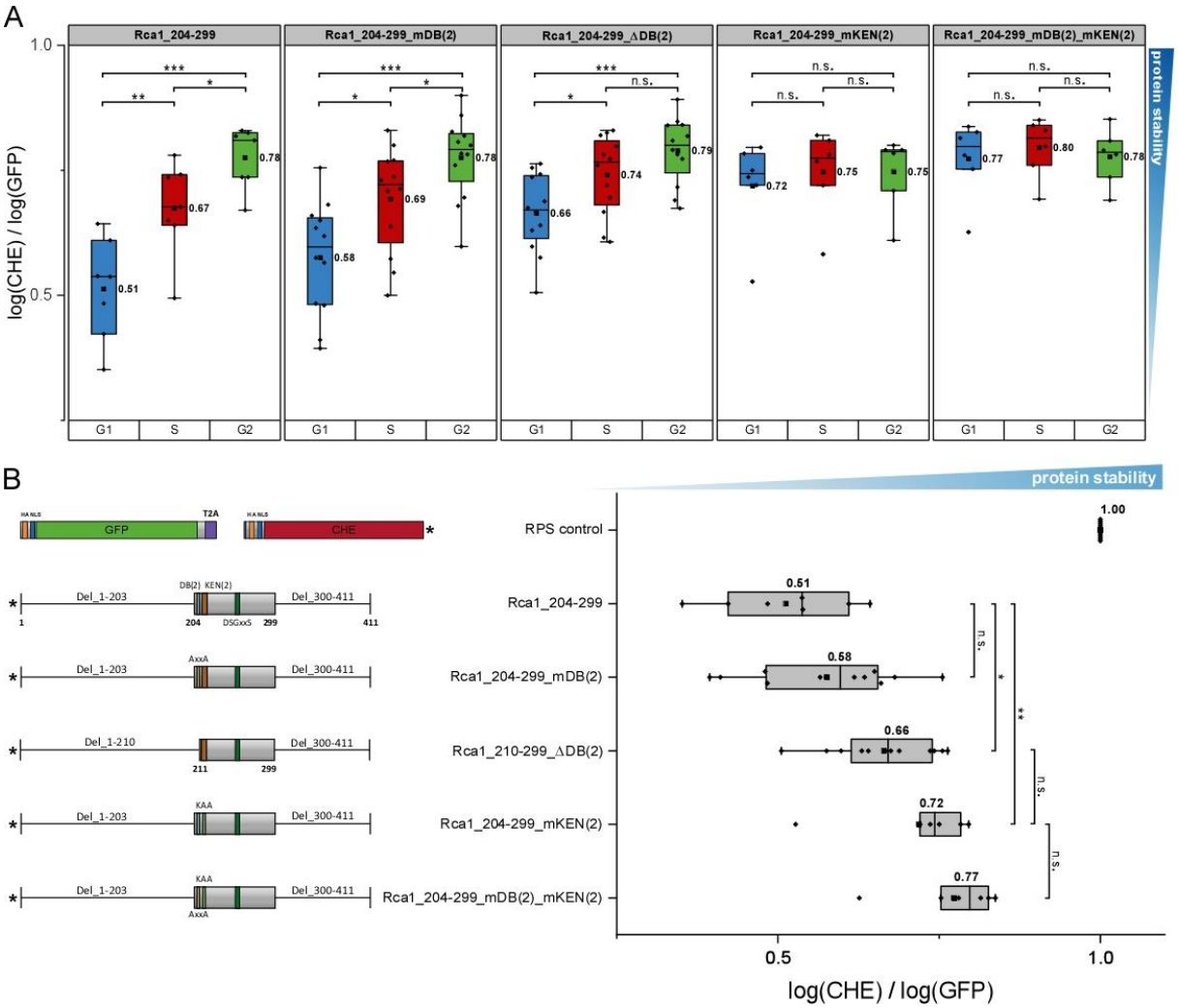

Figure 42| Rca1_204-299 degradation is mediated by a KEN-box degron

(**A**) Flow cytometric analysis of Rca1_204-299, Rca1_204-299_mDB(2), Rca1_204-299_ΔDB(2), Rca1_204-299_mKEN(2), and Rca1_204-299_mDB(2)_mKEN(2) inserted into RPS-8 in the G1-, S-, and G2-cell populations (exp.lvl. 1.0 - 1.75). Mutation of the KEN-box leads to a complete stabilization of Rca1_204-299. (**B**) Analysis of relative protein stability levels of Rca1_204-299 degron mutants. Illustration of the corresponding Rca1_204-299 mutants (left panel) and the normalized CHE/GFP ratios in G1-cells (right panel) (exp.lvl. 1.0 - 1.75). Deletion of the D-box (ΔDB(2)) but not mutation (mDB(2)) increased Rca1_204-299 stability in G1-phase. Mutation of the KEN-box (mKEN(2)) caused an even more pronounced increase in relative protein stability levels and a complete stabilization of Rca1_204-299 compared to ΔDB(2). The double mutation of the D- and KEN-box did not cause a further stabilization. Statistics performed by Mann-Whitney U-Test, n.s. > 0.05, * ≤ 0.05, ** ≤ 0.01, ***≤ 0.001.

To this point it can be stated that cell cycle dependent degradation of Rca1_204-299 requires the KEN-box degron. An additional contribution of the centrally located D-box degron on Rca1 stability cannot be fully excluded since only a deletion but not a mutation resulted in a stabilization. Furthermore, the limited spacing between the two degrons exacerbates the evaluation of the observed effects, since the results for Rca1_204-299_ΔDB(2) could thereby result of an impairment of the KEN-box. Additionally, the N-terminal CHE fusion could pose a problem due to the limited spacing to the degrons.

3.2.5.3. Flow cytometric analysis of Rca1_100-299

To test whether the close proximity of the N-terminal CHE-part in the GFP-T2A-CHE-Rca1_204-299 fusion protein impaired accessibility of the D-box, an Rca1 fragment with an N-terminal extension, Rca1_100-299, was analyzed. Flow cytometric analysis of GFP-T2A-CHE-Rca1_100-299 showed the expected decrease of the CHE/GFP ratio in G1- compared to S- and G2-cells (CHE/GFP - G1: 0.22, S: 0.42, G2: 0.52). Surprisingly, in contrast to Rca1_204-299 which was distinctly more stable in G1-cells (Figure 42; CHE/GFP - G1: 0.51) the decrease of the CHE/GFP ratio of Rca1_100-299 reflected the degradation of Rca1, Rca1_1-203, and Rca1_204-411 in G1-phase (CHE/GFP - G1: 0.26; 0.24; 0.32) (compare Figure 36 and Figure 43). To test if the D- and KEN-box degron in combination with the enhanced spacing to the CHE-fusion caused the intensified degradation of Rca1_100-299 in G1-phase, D- and KEN-box mutants were analyzed via the RPS system. The single mutation of the KEN-box as well as the D-box did not cause a stabilization of Rca1_100-299 (CHE/GFP - G1: 0.24; 0.18). Also the double mutant, Rca1_100-299_mDB(2)_mKEN(2), did not show an increased CHE/GFP quotient in G1-cells (CHE/GFP - G1: 0.17). The increased destabilization in G1-phase was consequently not caused by an enhanced accessibility of the D- and KEN-box. Thus, a protein domain within amino acid residues 100 to 204 must be responsible for the increased destabilization of Rca1_100-299. The ABBA motif is located in this region and mutation of the ABBA motif already displayed a minor stabilization of Rca1_1-203 (see 3.2.5.1). To test whether the ABBA motif is involved in Rca1_100-299 destruction a double mutation of the ABBA motif and KEN-box was tested, since Rca1_204-299 was stabilized by a mutation of the KEN-box (see 3.2.5.2). Rca1_100-299_mABBA_mKEN(2) exhibited only a slight increase of the CHE/GFP quotient in G1-cells (CHE/GFP - G1: 0.27) but did not result in a distinct stabilization of the Rca1 fragment (Figure 43 B). Hence, the observed effect was not caused by the presence of the ABBA motif. Besides the ABBA motif, the F-box and a major part of the NLS were also present in the N-terminal extension. To assess whether the F-box or the remaining part of the NLS have an impact on Rca1_100-299 degradation, a mutant with a disrupted F-box domain and a complete deletion of the NLS were tested. The point mutation M182T within the F-box, which obstructs interaction with the SCF subunit SkpA (Kies, 2017), had no stabilizing effect on G1-stability levels. In contrast, a complete deletion of the NLS, Rca1_134-299, caused a significant stabilization in G1-phase (CHE/GFP - G1: 0.52) (Figure 43

B), although the fragment was not completely stabilized in the context of cell cycle progression (CHE/GFP - G1: 0.52, S: 0.64, G2: 0.67) (Figure 43 A).

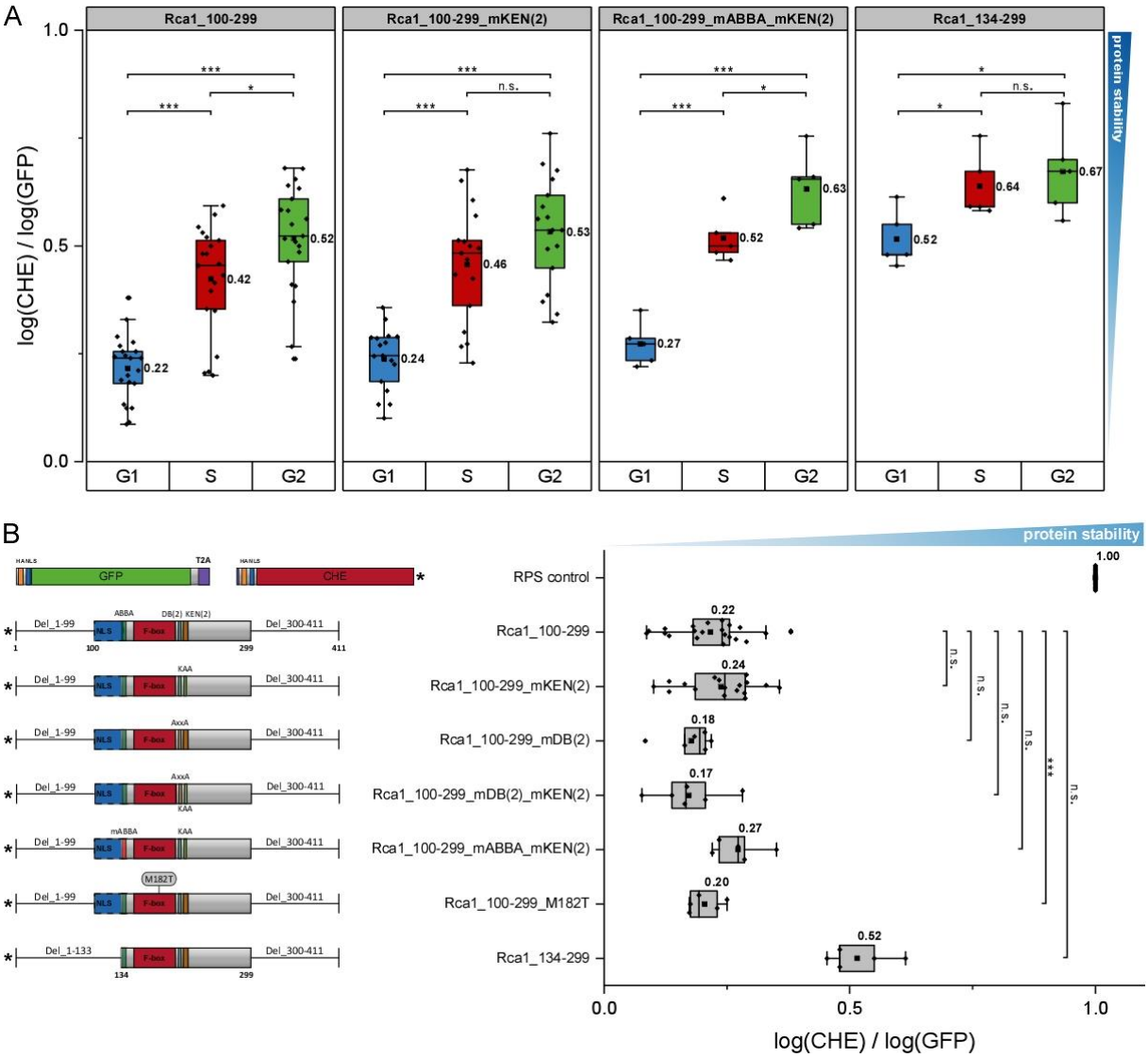

Figure 43| Deletion of the NLS causes stabilization of Rca1_100-299

(**A**) Flow cytometry analysis of Rca1_100-299, Rca1_100-299_mKEN(2), Rca1_100-299_mABBA_mKEN(2), Rca1_134-299 inserted in RPS-8 in the G1-, S-, and G2-cell populations. (**B**) Analysis of relative protein stability levels of Rca1_100-299 degron mutants in G1-cells. Illustration of the corresponding Rca1_100-299 mutants (left panel). Partial deletion of the NLS is shown by a dashed line. Normalized CHE/GFP ratios in G1-cells (right panel) (exp.lvl. 1.0 - 1.75). Mutation of the D- and KEN-box did not affect Rca1_100-299 degradation in G1-cells. Additional mutation of ABBA motif to the KEN-box had no stabilizing effect. The F-box mutation M182T did not cause stabilization, whereas deletion of the NLS caused an increase of the CHE/GFP quotient in G1-cells. Statistics performed by t-test with Welch´s correction, n.s. > 0.05, * ≤ 0.05, ** ≤ 0.01, ***≤ 0.001.

In summary, none of the mutations in the APC/C degrons or the F-box domain had an effect on Rca1_100-299 stability, only deletion of the NLS caused a significant stabilization. This is in contradiction to the findings for Rca1_204-299 degradation which was shown to be dependent on the KEN-box. There is no explanation for the KEN mutation having no effect in Rca1_100-299 to this point. However, mutation of the KEN-box was not tested in combination with a deleted NLS in this experiment. The results also indicate that the limited spacing between the CHE-reporter and Rca1_204-299 did not impair accessibility of the D- or KEN-box degron but it was not possible to further evaluate which degron

was responsible for the degradation of Rca1_204-299. Nevertheless, the increase of relative protein stability levels resulting from the deletion of the NLS could imply that localization of Rca1 and the presence of the endogenous NLS could be important for proper Rca1 degradation, even in presence of the exogenous SV40 nuclear Large T-antigen NLS of the RPS reporter, which will be investigated in more detail later (see 3.4.4).

3.2.5.4. Flow cytometric analysis of Rca1_221-411

The C-terminal fragment Rca1_204-411 was degraded in G1-cells similar to Rca1 (see 3.2.2). Besides the KEN-box, a putative O-box, a DSGxxS motif, and a D-box are located in this part of Rca1. For the validation of these degrons, a C-terminal fragment without the KEN-box, Rca1_221-411, was utilized.

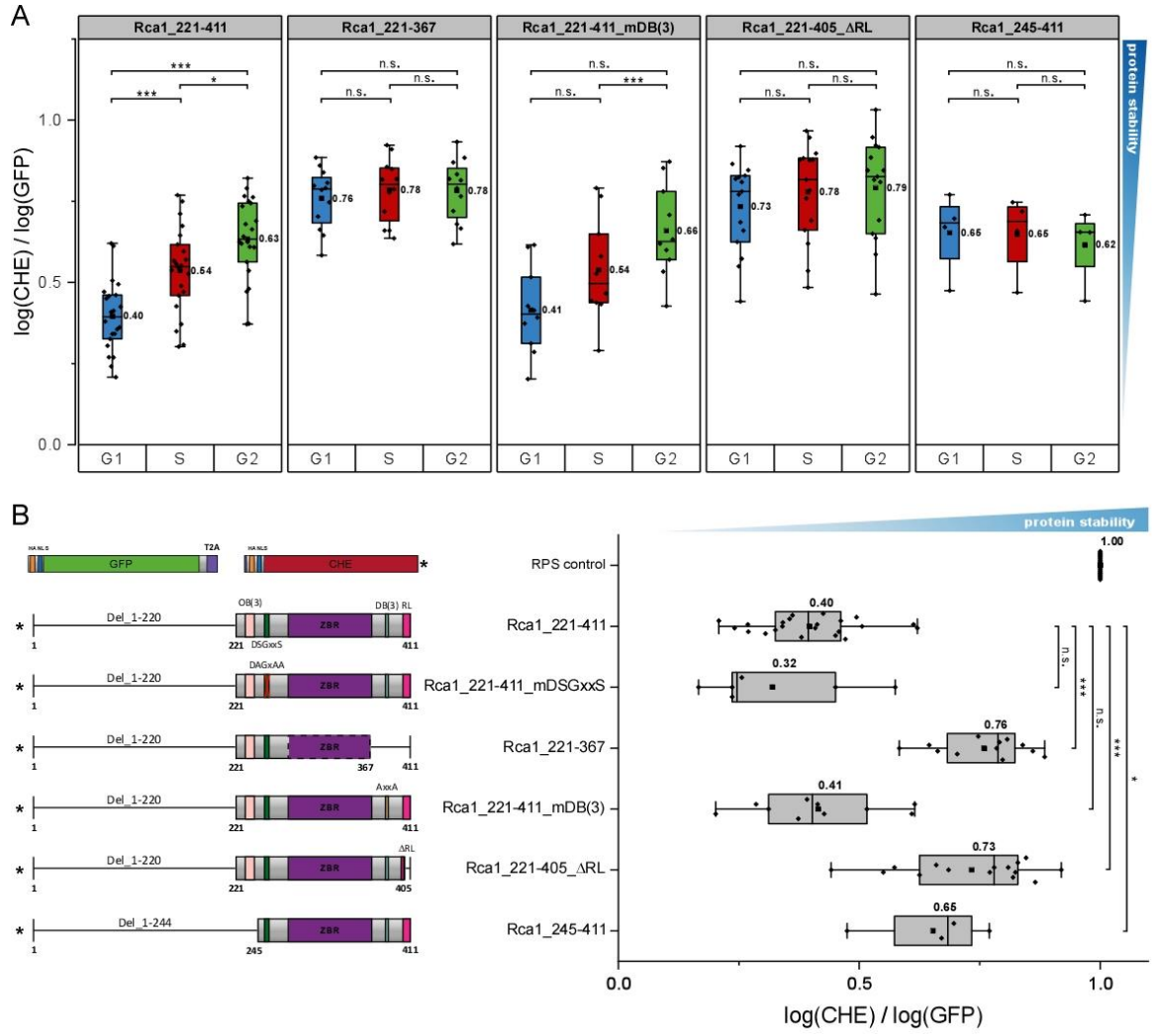

Figure 44| The C-terminal RL-tail is essential for degradation of Rca1_221-411

(**A**) Flow cytometric analysis of Rca1_221-411, Rca1_221-367, Rca1_221-411_mDB(3), Rca1_221-405_ΔRL, and Rca1_245-411 inserted in RPS-8 for the G1-, S-, and G2-cell populations. (**B**) Analysis of relative protein stability levels of Rca1_221-411 degron mutants in G1-cells. Illustration of the corresponding Rca1_221-411 mutants (left panel) and the corresponding normalized CHE/GFP ratios in G1-cells (right panel) (exp.lvl. 1.0 - 1.75). Mutation of the $SCF^{\beta TrCP}$ diphospho degron DSGxxS displayed an intrinsic destabilization of Rca1_221-411. Deletion of C-terminal residues resulted in a complete stabilization, which was referable to the deletion of the C-terminal RL-tail but not the D-box sequence. An N-terminal deletion including the O-box motif did cause a stabilization but as seen in (**A**) the deletion caused an unspecific intrinsic stabilization in all three cell cycle populations. Statistics performed by t-test with Welch´s correction, n.s. > 0.05, * ≤ 0.05, ** ≤ 0.01, ***≤ 0.001.

Flow cytometric analysis of GFP-T2A-CHE-Rca1_221-411 showed a decrease of relative protein stability in G1-cells (CHE/GFP - G1: 0.22, S: 0.42, G2: 0.52). In comparison to Rca1_204-411, the CHE/GFP quotient of Rca1_221-411 was increased in the G1-population (CHE/GFP - G1: 0.32 / 0.40) (compare Figure 36 and Figure 44). This can be explained by the deletion of the centrally located KEN-box, which is in concordance with the results of Rca1_204-299 (see 3.2.5.2). But the remaining instability in G1 suggest that the KEN motif was not exclusively responsible for the cell cycle dependent degradation of Rca1_204-411. To assess whether one of the remaining motifs, the DSGxxS, O-box or D-box is responsible for the destabilization, different C-terminal Rca1 mutants were analyzed in the following. The DSGxxS motif is involved in Emi1 degradation mediated by the E3 ligase $SCF^{\beta TrCP}$ in early mitosis (see 2.6.10). Phosphorylation of the serine residues of the DSGxxS diphospho degron by Plk1 leads to recruitment via the adaptor protein β-TrCP and subsequent degradation of Emi1 by $SCF^{\beta TrCP}$ (Hansen et al., 2004; Moshe et al., 2004). To test if the DSGxxS motif is also involved in Rca1 degradation the serine residues of the motif were mutated to alanine (DSGNSS to GAGNAA = mDSGxxS). Analysis of GFP-T2A-CHE-Rca1_221-411_mDSGxxS did not cause a stabilization in the G1-population but resulted in a decreased CHE/GFP quotient (CHE/GFP - G1: 0.32) (Figure 44 B). This effect was also observed in the S- and G2-population (data not shown) indicating an intrinsic destabilization caused by the mutation of the potential phosphorylation sites. Thus, in contrast to Emi1 the DSGxxS motif is not involved in cell cycle dependent Rca1 destruction. To test if the C-terminal D-box confers Rca1_221-411 degradation, an Rca1 mutant with an additional deletion of amino acids 368-411 was tested in the first place. GFP-T2A-CHE-Rca1_221-367 was completely stabilized in the three cell cycle populations (CHE/GFP - G1: 0.76, S: 0.78, G2: 0.78) (Figure 44 A, B). To further assess whether the stabilization was caused by the deletion of the D-box, Rca1_221-411 with a mutated D-box consensus was analyzed. However, Rca1_221-411_mDB(3) was not stabilized in G1-cells (CHE/GFP - G1: 0.41). The stabilization observed for Rca1_221-367 must then be caused by another C-terminal domain. Besides the D-box another domain, the RL-tail is located in this region. In Emi1, the RL-tail is required for APC/C inhibition by competing for the same binding site as the E2 enzyme Ube2S (see 2.6.10). To test if the RL-tail is involved in Rca1 degradation, an Rca1 mutant with a partial deletion of the RL-tail (ΔRL) removing the conserved LRRL residues (LKRL in Rca1) was analyzed via flow cytometry (Figure 45). Rca1_221-405_ΔRL was distinctly stabilized in G1-cells (CHE/GFP - G1: 0.73) and was also no longer destabilized in the context of cell cycle progression seen by similar CHE/GFP ratios in the three cell cycle populations (CHE/GFP - G1: 0.73, S: 0.78, G2: 0.79) (Figure 44 A, B). Thus, the observed stabilization of Rca1_221-367 can likely be

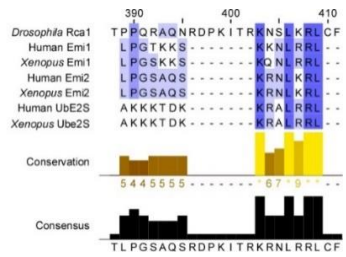

Figure 45| Alignment of C-terminal RL-tail of Rca1, Emi1, Emi2, and Ube2S

Alignment of the C-terminal regions of *Drosophila* Rca1, Emi1, Emi2, and Ube2S. Blue boxes highlight conserved residues. Numbers above refer to *Drosophila* Rca1 amino acid position.

attributed to the absence of the RL-tail. In addition, an N-terminal truncation of Rca1_221-411 causing the deletion of the O-box motif was also tested. Interestingly, Rca1_245-411 was also stabilized in G1-cells (CHE/GFP - G1: 0.65) but further analysis of the S- and G2-populations showed similar CHE/GFP values (CHE/GFP - S: 0.65; G2: 0.62) indicating an intrinsic stabilization (Figure 44). In summary, degradation of the C-terminal Rca1 fragment, Rca1_221-411, was not dependent on one of the putative APC/C degrons nor the $SCF^{\beta TrCP}$ degron, but the C-terminal RL-tail. This was rather surprising since the RL-tail in Emi1 comprises an inhibitory domain but not a degradation signal. The function of the RL-tail in APC/C inhibition by Rca1 will also be examined in more detail later (see 3.3.4).

3.2.5.5. Flow cytometric analysis of Rca1

Through the analysis of different Rca1 fragments, several degron sequences could be identified. The next goal was to test if mutation of these degrons would cause cell cycle dependent stabilization of the full-length Rca1 molecule. In a first step, Rca1 with mutations in the APC/C degrons identified in Rca1_1-203 and Rca1_100-299 was tested (see 3.2.5.1 and 3.2.5.2). Hence, Rca1 with a deletion of the N-terminal D-box and mutation of the two KEN-box degrons was analyzed using the RPS-8 reporter. Surprisingly, flow cytometric analysis of CHE-Rca1_ΔDB(1)_mKEN(1)_mKEN(2) showed no stabilization in G1-cells compared to CHE-Rca1 (CHE/GFP - G1: 0.26 / 0.24). Since the ABBA motif showed minor stabilizing effects in the analysis of Rca1_1-203 and Rca1_100-299, an additional mutation of the ABBA motif was introduced. However, relative protein stability levels of CHE-Rca1_ΔDB(1)_mKEN(1)_mABBA_mKEN(2) were only slightly increased in G1-cells (CHE/GFP - G1: 0.32). Nevertheless, the observed effect missed statistically significance compared to CHE-Rca1 and CHE-Rca1_ΔDB(1)_mKEN(1)_mKEN(2) (p-value: 0.2, not displayed in the figure). Since degradation of the C-terminal Rca1-fragment, Rca1_221-411, was dependent on the C-terminal RL-tail, additional deletion of the RL-tail was also investigated. Flow cytometric analysis of CHE-Rca1_ΔDB(1)_mKEN(1)_mABBA_mKEN(2)_ΔRL did also not result in a stabilization of Rca1 (CHE/GFP - G1: 0.31). Since deletion of the RL-tail, which actually constitutes an inhibitory domain in case of Emi1, caused a stabilization of Rca1_221-411 it could be possible that also the zinc binding region is also involved in Rca1 degradation besides its role in APC/C inhibition. To test whether the ZBR has an influence on Rca1 destruction in G1-phase, an Rca1 mutant with a disrupted ZBR domain was tested. The point mutation C351S of the conserved cysteine residues within the ZBR was shown to eliminate Rca1 activity in *Drosophila* embryo (Zielke et al., 2006). Flow cytometric analysis of CHE-Rca1_ΔDB(1)_mKEN(1)_mABBA_mKEN(2)_C351S_ΔRL showed no change in relative protein stability levels in G1-cells (CHE/GFP - G1: 0.29). This suggests that in contrast to the RL-tail, the ZBR does not constitute a degradation motif. As mutation of the validated degrons did not cause a stabilization of Rca1, degrons that did not show an effect in the Rca1 fragments were in part tested in full-length Rca1.

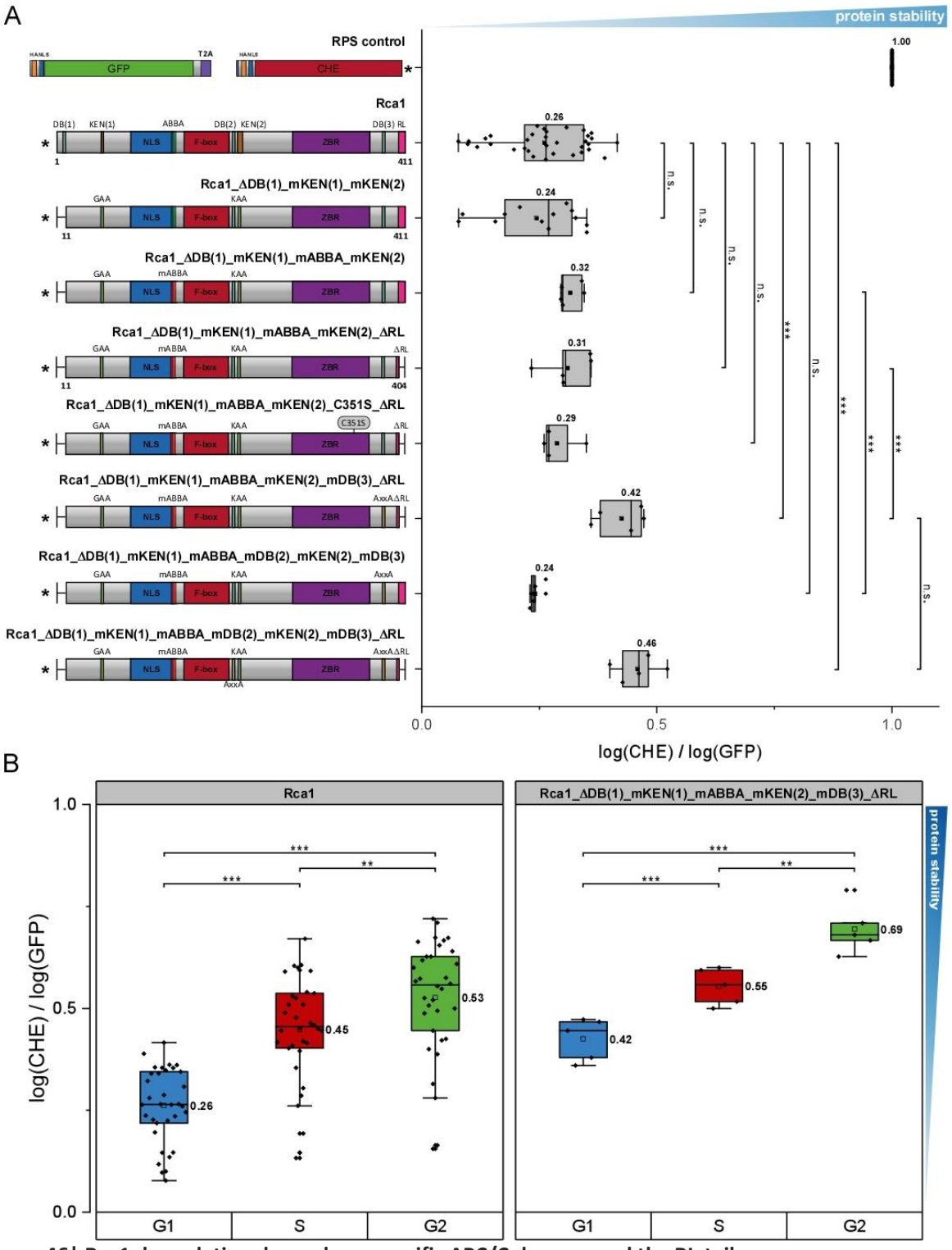

Figure 46| Rca1 degradation depends on specific APC/C degrons and the RL-tail

(**A**) Analysis of relative protein stability levels of Rca1 degron mutants in G1-cells. Illustration of the corresponding Rca1 mutants (left panel) and the corresponding normalized CHE/GFP ratios in G1-cells (right panel) (exp.lvl. 1.0 - 1.75). Mutation of the N-terminal APC/C degrons, DB(1),KEN(1), ABBA, and KEN(2), did not cause a stabilization of Rca1. First an additional mutation of the C-terminal D-box (mDB(3)) together with a deletion of the RL-tail resulted in a partial stabilization of Rca1 in G1-cells. (**B**) Flow cytometric analysis of Rca1 and Rca1_ΔDB(1)_mKEN(1)_mABBA _mKEN(2)_mDB(3)_ΔRL inserted in RPS-8 in the G1-, S-, and G2-cell populations. Mutation of the APC/C degrons together with the RL-tail caused a partial stabilization of Rca1. Statistics performed by Mann-Whitney U-Test, n.s. > 0.05, * ≤ 0.05, ** ≤ 0.01, ***≤ 0.001.

Additional mutation of the C-terminal D-box degron (mDB(3)) resulted in a significant stabilization of Rca1_ΔDB(1)_mKEN(1)_mABBA_mKEN(2)_mDB(3)_ΔRL (CHE/GFP - G1: 0.42). Interestingly, no stabilization was observed with intact RL-tail. Instead, Rca1_ΔDB(1)_mKEN(1)_mABBA_mKEN(2)_mDB(3) displayed a decreased CHE/GFP ratio in G1-cells (CHE/GFP - G1: 0.24) compared to Rca1_ΔDB(1)_mKEN(1)_mABBA_mKEN(2) (CHE/GFP - G1: 0.32). Nevertheless, Rca1_ΔDB(1)_mKEN(1)_mABBA_mKEN(2)_mDB(3)_ΔRL was stabilized in G1-cells but still displayed a decrease in comparison to the S- and G2-cell populations (CHE/GFP - G1: 0.42, S: 0.55, G2: 0.69) (Figure 46 B). To test if the central located D-box (DB(2)) would also be functional in context of the full-length Rca1 molecule, an additional mutation was introduced and tested. Albeit, Rca1_ΔDB(1)_mKEN(1)_mABBA_mDB(2)_mKEN(2)_mDB(3)_ΔRL was not further stabilized in G1-cells (CHE/GFP - G1: 0.46) (Figure 46 A).

Although it was not possible to completely stabilize Rca1, no further attempts were taken in this regard in the course of this thesis. Accordingly, not all protein domains that mediate degradation of Rca1 were found in the analysis of the different Rca1 fragments. The analysis of Rca1_100-299 indicated that the protein region from amino acid 100 to 134 contributes to Rca1 degradation (see 3.2.5.3), which could be involved in the remaining destabilization of full-length Rca1 protein. Nevertheless, it was shown that Rca1 degradation is mediated by APC/C specific degrons and also the C-terminal RL-tail. Together with the previous results, this strongly supports an APC/C^{Fzr} dependent degradation of Rca1 during G1-phase.

3.3. *In vivo* analysis of Rca1 domains required for APC/C^{Fzr} activity regulation

3.3.1. Aim

Rca1 was found as an APC/C inhibitor in *Drosophila* that restrains APC/C^{Fzr} activity in S- and G2-phase, thereby allowing re-accumulation of mitotic cyclins that are required for the next mitosis (see 2.6.11). In accordance, *rca1* mutant embryos displayed premature degradation of the mitotic cyclins, CycA and CycB, and cells failed to enter mitosis causing an embryonic phenotype with a reduced number of cells. Rca1 overexpression was also able to complement premature destruction of mitotic cyclins after Fzr overexpression (Grosskortenhaus et al., 2002). Previous studies have shown that the C-terminal part of Rca1 was sufficient for APC/C inhibition in *Drosophila* embryo (Zielke et al., 2006). Interestingly, the C-terminal moiety of Rca1 has a similar arrangement of functional domains like the vertebrate inhibitor Emi1 (see 2.6.11; Figure 15). Thus, Rca1 could inhibit the APC/C by a similar mechanism as Emi1.

To identify and characterize the protein domains involved in APC/C^{Fzr} activity regulation by Rca1, an *in vivo* APC/C activity assay was established that allows to monitor APC/C activity in S2R+ cells. Using this assay, different Rca1 mutants were tested for their capacity to inhibit APC/C^{Fzr} activity in G2-phase and the C-terminal domains that confer APC/C inhibition were identified.

3.3.2. Method for *in vivo* analysis of APC/C activity

In order to analyze APC/C activity regulation by Rca1, an *in vivo* method to determine APC/C activity in S2R+ cells was established. This assay is based on the measurement of relative protein stability levels of GFP-T2A-CHE-CycB-NT^{285} (see 3.1.5.1.2) with simultaneous co-overexpression of 4xFLAG-Fzr and 4xFLAG-Rca1 constructs (Figure 47 A). The inactive CycB fragment is degraded by the APC/C during mitosis and G1-phase, whereas it is stable in S- and G2-phase under normal conditions (see 3.1.5.1.2). Fzr overexpression causes activation of the APC/C in G2-phase resulting in an anomalous degradation of CycB-NT^{285} that can be measured via the RPS-system (see 3.1.5.1.6). Simultaneous co-overexpression of Rca1 is able to inhibit the overexpressed APC/C^{Fzr} activity due to its function as potent APC/C inhibitor (see 3.2.4), thereby inhibiting the unnatural destruction of CycB-NT^{285} reporter protein during G2-phase. Thus, the capacity of Rca1 to inhibit the APC/C can be quantified by the restitution of relative protein stability levels of CycB-NT^{285} in G2-cells after simultaneous Fzr and Rca1 co-overexpression (Figure 47 B). This means, the higher the CHE/GFP ratio of GFP-T2A-CHE-CycB-NT^{285} after Fzr and Rca1 overexpression, the lower the level of active APC/C^{Fzr} which is directly referable to Rca1 inhibition of the hyperactivated APC/C^{Fzr}.

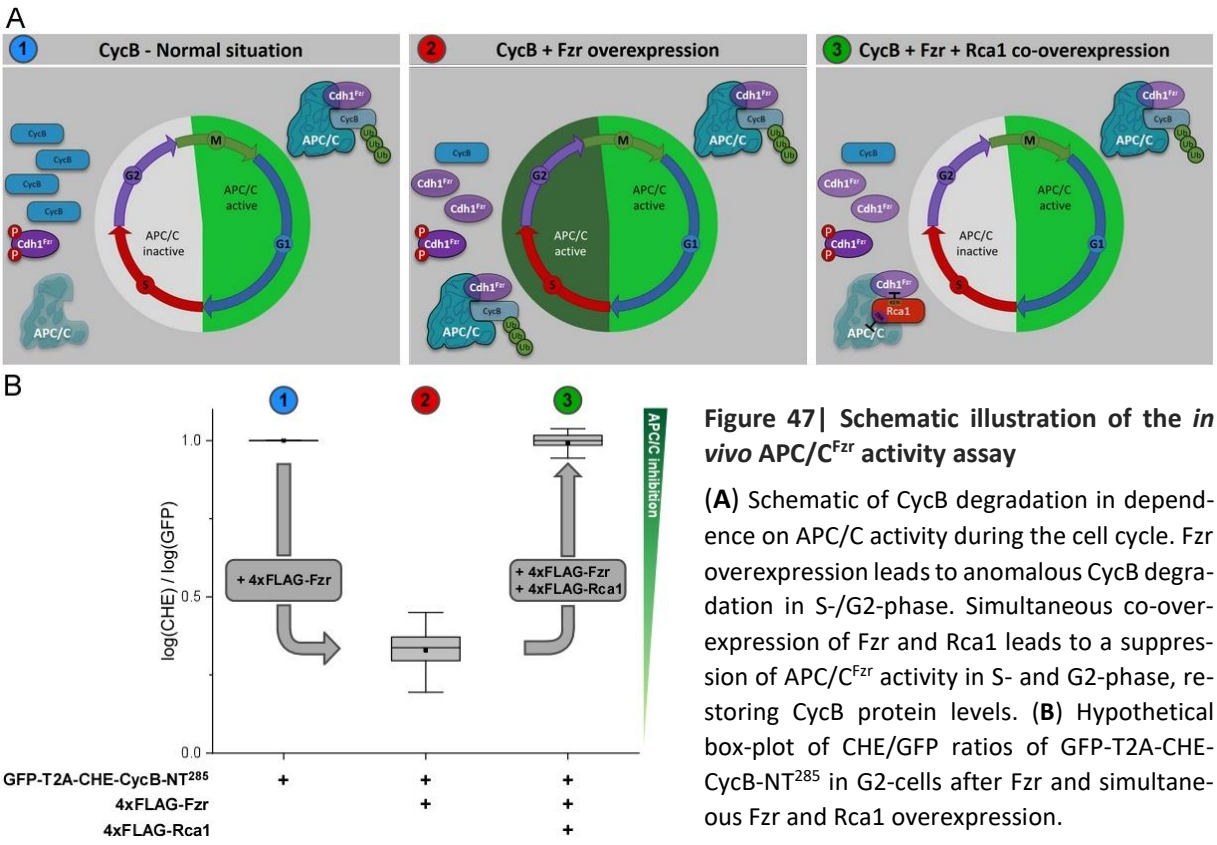

Figure 47| Schematic illustration of the *in vivo* APC/C^{Fzr} activity assay

(**A**) Schematic of CycB degradation in dependence on APC/C activity during the cell cycle. Fzr overexpression leads to anomalous CycB degradation in S-/G2-phase. Simultaneous co-overexpression of Fzr and Rca1 leads to a suppression of APC/C^{Fzr} activity in S- and G2-phase, restoring CycB protein levels. (**B**) Hypothetical box-plot of CHE/GFP ratios of GFP-T2A-CHE-CycB-NT^{285} in G2-cells after Fzr and simultaneous Fzr and Rca1 overexpression.

3.3.3. C-terminal Rca1 is sufficient for APC/C inhibition

To test whether the *in vivo* APC/C^{Fzr} activity assay is suited for the quantification of Rca1 functionality and can be further applied for the identification of the protein domains involved in APC/C inhibition,

Rca1, Rca1_1-203 and Rca1_204-411 were initially tested for their capacity to restrain APC/C activity. Relative protein stability levels of GFP-T2A-CHE-CycB-NT^{285} were measured in S2R+ cells via flow cytometry with either co-transfection of solely 4xFLAG-Fzr or additional co-expression of the respective NLS-4xFLAG-Rca1 construct (Figure 48 A). The Rca1 fragments were initially tagged with NLS-4xFLAG to compensate for the loss of the endogenous NLS in case of C-terminal Rca1 fragments. However, the influence of Rca1 localization in context of APC/C inhibition will also be investigated in more detail later (see 3.4.4.5). The CHE/GFP ratios of the G2-cell population were normalized to the control cells transfected solely with the CycB-RPS reporter construct. Overexpression of 4xFLAG-Fzr resulted in destruction of CycB-NT^{285} in the G2-population, seen by a strong decrease of the CHE/GFP ratio in the G2-population (CHE/GFP - G2: 0.29) (also see 3.1.5.1.6). Additional co-overexpression of NLS-4xFLAG-Rca1 caused a complete stabilization of the GFP-T2A-CHE-CycB-NT^{285} reporter with a CHE/GFP ratio that was even slightly increased compared to the control cells (CHE/GFP - G2: 1.10) (Figure 48 B). In order to exclude the possibility, that the effects were attributed to strong variations in Fzr or Rca1 expression after transient transfection, protein expression was always validated for the applied cell lysates separated by SDS PAGE and following Western blot analysis using a FLAG-antibody for protein detection (Figure S 2).

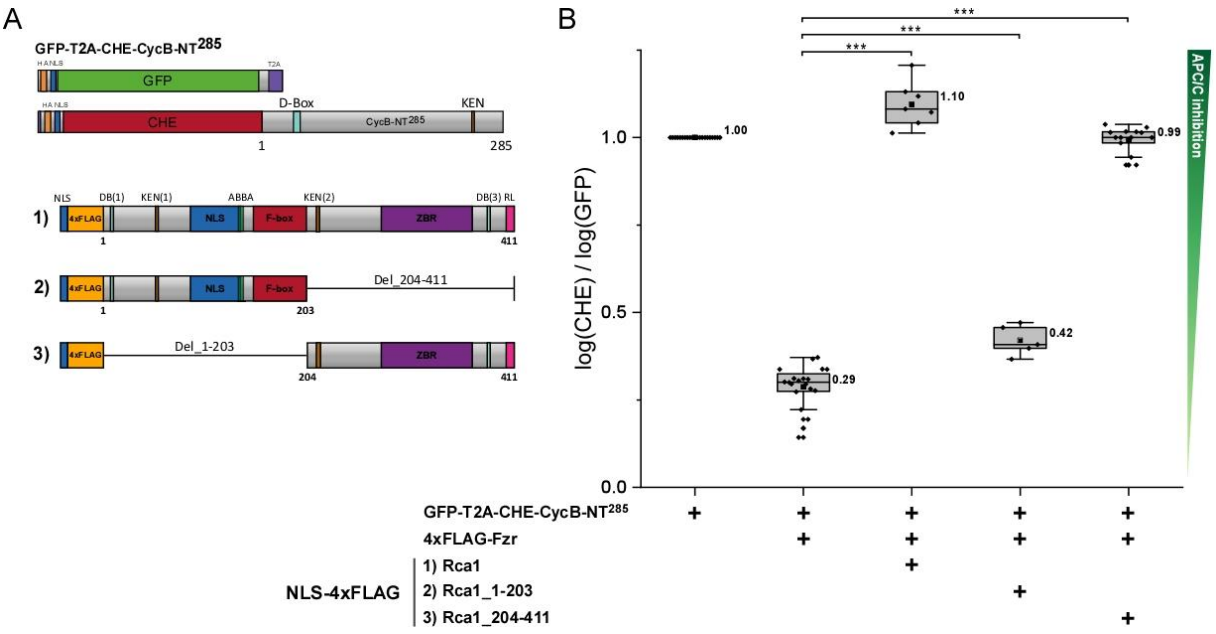

Figure 48| C-terminal but not N-terminal part of Rca1 is able to inhibit the APC/C

(**A**) Analysis of APC/C inhibition by Rca1. Illustration of the RPS-CycB sensor and the corresponding NLS-FLAG tagged Rca1 constructs. (**B**) Box plot of relative protein stability levels of GFP-T2A-CHE-CycB-NT^{285} with additional co-expression of 4xFLAG-Fzr and the corresponding NLS-4xFLAG-Rca1 mutants in G2-cells (exp.lvl. 2.0 - 3.0). Expression of NLS-4xFLAG-Rca1 and -Rca1_204-411 is able to compensate elevated APC/C activity after Fzr overexpression. N-terminal Rca1, NLS-4xFLAG-Rca1_1-203 is only capable to partially restore CycB protein levels after Fzr overexpression in G2-cells. Statistics performed by Mann-Whitney U-Test, n.s. > 0.05, * ≤ 0.05, ** ≤ 0.01, ***≤ 0.001.

In a next step, the N- and C-terminal part of Rca1 were tested for their functionality. Previous study in *rca1* mutant embryo have shown that expression of HA-Rca1_204-411 was able to complement the

rca1 phenotype and restore mitosis of cell cycle 16. Thus, Rca1-CT was sufficient for APC/C inhibition (Zielke et al., 2006). In concordance with these findings, analysis of NLS-4xFLAG-Rca1_1-203 resulted in only a minor stabilization of CycB relative protein stability levels (CHE/GFP - G2: 0.42), whereas NLS-4xFLAG-Rca1_204-411 completely restored CycB-NT^{285} protein stability levels (CHE/GFP - G2: 0.99) (Figure 48 B). The minor stabilization caused by NLS-4xFLAG-Rca1_1-203 expression, can be explained by a substrate competition between CycB and Rca1_1-203, since Rca1 itself is an APC/C substrate as demonstrated before (see section 3.2). In conclusion, the *in vivo* APC/C assay was suited to determine APC/C activity regulation by Rca1. It was shown that C-terminal Rca1 was sufficient to inhibit the APC/C similar to full-length Rca1, whereas the N-terminal part of Rca1 was not able to completely supress hyperactivated APC/C^{Fzr} activity.

3.3.4. Rca1 KEN-box, ZBR, D-box, and RL-tail mediate APC/C inhibition

Since the C-terminal part of Rca1 was sufficient for complete APC/C inhibition after Fzr overexpression, inhibitory protein domains that are involved in APC/C inactivation must be located in this region of Rca1. Interestingly, Rca1 C-terminal region shares a similar arrangement of protein domains like Emi1. APC/C inhibition by Emi1 is mediated by combined action of a C-terminal D-box, linker, ZBR, and RL-tail domain (Frye et al., 2013; Wang et al., 2013; Chang et al., 2015). These functional domains restrict APC/C activity by different mechanisms, blocking substrate recognition as well as UbcH10 and Ube2S interaction thereby inhibiting mono- and polyubiquitination reactions (see 2.6.10). Rca1 also contains a ZBR, a RL-tail and a KEN-box instead of a D-box and could consequently inhibit the APC/C by similar mechanisms like Emi1. To assess whether the C-terminal domains are involved in APC/C inhibition, different C-terminal Rca1 mutants were analyzed for their capacity to restrict APC/C activity (Figure 49 A). Analysis of a KEN-box mutant, NLS-4xFLAG-Rca1_204-411_mKEN(2), resulted in a slightly impaired APC/C inhibition seen by decreased CHE/GFP ratio compared to NLS-4xFLAG-Rca1_204-411 in the APC/C activity assay (CHE/GFP - G2: 0.85) (Figure 49 B). This indicates that KEN-box dependent interaction with the substrate recognition site is partially involved in APC/C inhibition by Rca1.

Next, the influence of the ZBR domain was investigated as previous studies were able to demonstrate that mutations within or near the ZBR led to a loss of function. Hence, three different point mutations (S285R, A344T, and C351S) within the ZBR domain were investigated in the following. The mutation A344T was originally discovered in the *rca1^{2}* allele (Dong et al., 1997) that resulted in the Rca1 phenotype due to the lack of APC/C inhibition. A further Rca1 allele was discovered in the work group of Manfred Frasch that caused a specific phenotype in muscle and respiratory cells which was attributed to an amino exchange of serine 285 to asparagine (S285N) (unpublished data). A more severe mutation to arginine at this position (S285R) was previously analyzed in *Drosophila* embryo resulting in a reduced number of epidermal cells similar to the phenotype observed in *rca1^{2}* mutants (Potzler, 2018). Likewise, mutation of one of the conserved cysteine residue (C351S) of the ZBR eliminated Rca1 function,

since HA-Rca1_C351S was not able to restore mitosis 16 in *rca1* mutant embryo (Zielke et al., 2006). Expression of NLS-4xFLAG-Rca1_204-411_S285R, NLS-4xFLAG-Rca1_204-411_A344T, and NLS-4xFLAG-Rca1_204-411_C351S resulted only in a minor stabilization of CycB-NT^{285} relative protein stability levels after Fzr overexpression (CHE/GFP - G2: 0.41, 0.45, 0.38, respectively) (Figure 49 B). This indicates that the ZBR mutations significantly impaired APC/C inhibition by Rca1 and that the ZBR has a crucial role in Rca1 function in concordance with the observed effects in *Drosophila* embryo.

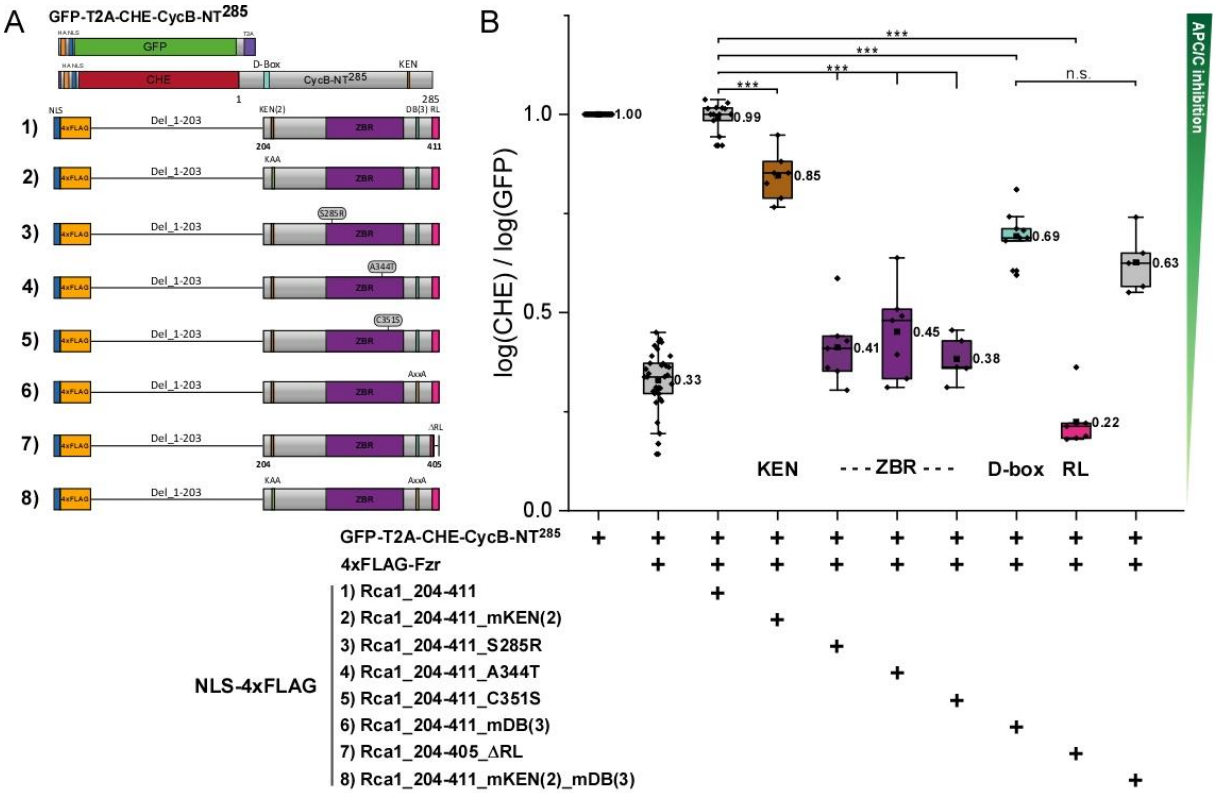

Figure 49| Functional analysis of C-terminal domains in APC/C inhibition

(**A**) Analysis of APC/C inhibition by C-terminal Rca1 mutants. Illustration of the RPS-CycB sensor and the corresponding NLS-4xFLAG tagged Rca1 constructs. (**B**) Box plot of relative protein stability levels of GFP-T2A-CHE-CycB-NT^{285} with additional co-overexpression of 4xFLAG-Fzr and the corresponding NLS-4xFLAG-Rca1_204-411 mutants in G2-cells (exp.lvl. 2.0 - 3.0). Mutation of the KEN-box and D-box degron partially decreased Rca1 function. No additive effect is observed for the double mutation of KEN- and D-box. Point mutations within the ZBR domain cause a nearly complete elimination of Rca1 function. Deletion of the RL-tail causes a complete loss of function. Statistics performed by Mann-Whitney U-Test, n.s. > 0.05, * ≤ 0.05, ** ≤ 0.01, ***≤ 0.001.

Since mutation of the KEN-box caused a partial decline in APC/C inhibition, it was also tested if the D-box degron located between the ZBR and the RL-tail is involved in APC/C inhibition besides its function in Rca1 degradation (see 3.2.5.5). Analysis of NLS-4xFLAG_Rca1_204-411_mDB(3) functionality in the APC/C activity assay displayed a decrease in APC/C inhibition (CHE/GFP - G2: 0.69), with an even more pronounced decline in CycB-NT^{285} stability compared to the KEN-box mutant (CHE/GFP - G2: 0.85). Thus, mutation of either the KEN- or the D-box partially impaired Rca1 function. It was also tested if the double mutation of both degrons would result in an additive effect. However, expression of

NLS-4xFLAG_Rca1_mKEN(2)_mDB(3) did not cause a further decline in APC/C inhibition compared to the D-box mutant (CHE/GFP - G2: 0.63).

Finally, the role of the C-terminal RL-tail in Rca1 function was examined. In Emi1, the RL-tail competes for the same APC/C binding site as Ube2S, thereby antagonizing Ube2S mediated polyubiquitin chain assembly (Wang et al., 2013; Chang et al., 2015; Watson et al., 2019 b). Interestingly, the RL-tail was also involved in Rca1 degradation as seen in the flow cytometric analysis of Rca1_221-411 and Rca1 (see 3.2.5.4 and 3.2.5.5). To assess whether the RL-tail is also required for APC/C inhibition, an Rca1 mutant with a partial deletion of the RL-tail was tested (see 3.2.5.4, Figure 45). Expression of NLS-4xFLAG_Rca1_204-405_ΔRL was not able to inhibit the hyperactivated APC/C^{Fzr} at all, since GFP-T2A-CHE-CycB-NT^{285} protein stability levels were not stabilized compared to cells solely co-transfected with 4xFLAG-Fzr (CHE/GFP - G2: 0.22). Thus, disruption of the RL-tail caused a complete elimination of Rca1 function.

In conclusion, the C-terminal KEN-box, ZBR, D-box, and RL-tail of Rca1 are involved in APC/C inhibition. This indicates that Rca1 might inhibit the APC/C by a similar mechanism as Emi1. The different protein domains have been shown to exert different impact on Rca1 function, as mutation of the KEN- and D-box degrons had only mediocre effects, whereas disruption of the ZBR and the RL-tail caused a loss of Rca1 function. It is worth mentioning that Emi1 also contained a linker region between the D-box and the ZBR that was shown to be essential for APC/C inhibition (Frye et al., 2013). Rca1 also contains a region with several highly conserved amino acid residues between the KEN-box and the ZBR that could constitute a further potential inhibitory domain. However, the linker region was not further investigated in the course of this thesis.

3.3.5. Characterization of Rca1 zinc binding region

As shown above, the ZBR domain was essential for Rca1 function. Interestingly, besides mutation of one of the conserved cysteine residues, point mutations of A344 and S285 also caused a loss of function. Due to its critical role in APC/C inhibition, the composition of the C-terminal ZBR in Rca1 was further investigated and compared to the ZBR domain of Emi1. NMR and electron microscopic analysis of the Emi1 ZBR domain displayed an In-Between-RING (IBR) domain topology resembling the IBR domain of RNF31 (Frye et al., 2013). Sequence alignment of Emi1 and Emi2 displayed a highly conserved array of cysteine residues following the typical IBR C6HC consensus pattern (Figure 50 A, B, C). A ZBR sequence alignment of Rca1 among different *Drosophila* species also showed a high conservation of the seven cysteine residues and the histidine residue of the C6HC consensus (Figure S 3). Typically, the first two cysteine residues of the C6H6 consensus are separated by 14-30 amino acids from the second array of cysteine and the histidine residues. This does also apply in case of Emi1 ZBR with a 14 amino acid long loop separating the second and the third cysteine residue of the IBR domain. In contrast, Rca1 contains an extended 63 amino acid long loop (ZBR loop) in this region. Thus, the question arose,

whether the first two cysteine residues are actually required for ZBR function due to untypically large spacing and if the extended loop has essential role in APC/C inhibition.

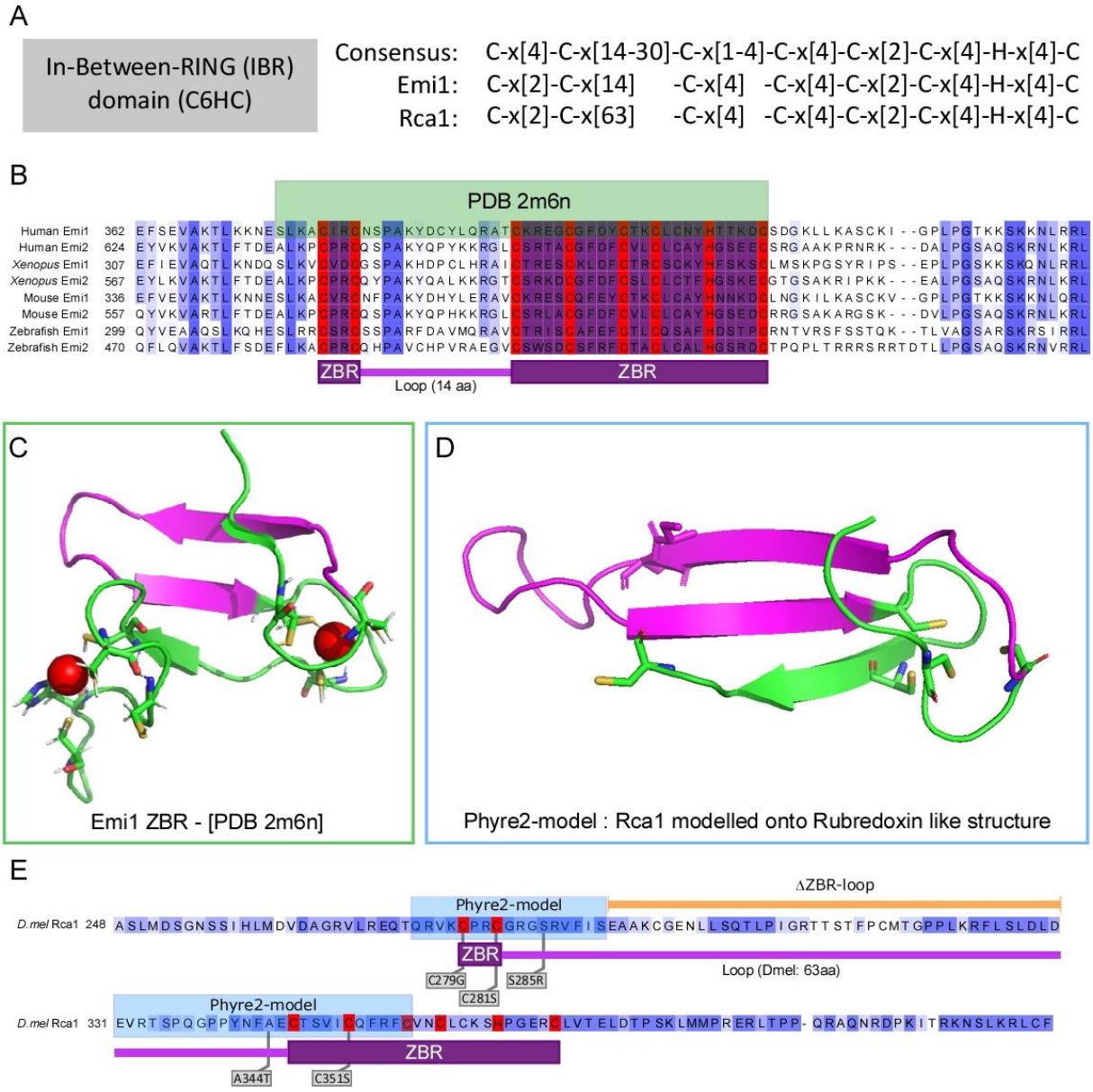

Figure 50| Comparison of Emi1 and Rca1 ZBR sequences

(**A**) Illustration of the typical consensus pattern of a C6HC In-Between-RING (IBR) domain, and the ZBR amino acid pattern of Emi1 and Rca1. (**B**) Sequence alignment of Emi1 and Emi2 ZBR sequences. The essential cysteine and histidine residues (highlighted in red) of the ZBR (purple) are highly conserved in Emi1 and Emi2. A 14 amino acid long loop (shown in pink) separates the second from the third cysteine residue of the IBR domain. (**C**) Cartoon representation of Emi1 ZBR [PDB 2m6n]; zinc atoms shown as red spheres and the 14 aa loop is shown in pink. (**D**) Cartoon representation of Rca1 ZBR predicted by the Phyre2 protein fold recognition server. Rca1 ZBR prediction by Phyre2 was closest to Rubredoxin-like fold of human transcription elongation factor A [PDB d1tfia]. The 63 aa acid long ZBR loop is shown in pink. (**E**) Sequence of Rca1 ZBR domain. Conserved C6HC residues are highlighted in red, the ZBR loop is represented by the pink bar and the ZBR point mutations are shown in gray boxes. The aligning parts of the Phyre2 model are highlighted by blue boxes.

To assess whether the cysteine residues C279 and C281 are essential for the integrity of the ZBR domain, both residues were mutated and the resulting Rca1 mutants were tested for their function as APC/C inhibitors. Analysis of NLS-4xFLAG-Rca1_204-411_C279G and NLS-4xFLAG-Rca1_204-

411_C281S resulted in impaired APC/C^{Fzr} inhibition, as the RPS-CycB-NT^{285} sensor was only partially stabilized (CHE/GFP - G2: 0.41 and 0.45). The observed effect was similar to the already tested ZBR mutations S285R, A344T, and C351S implying that C279 and C281 are functional part of Rca1 ZBR domain (Figure 51). Accordingly, Rca1 ZBR does indeed contain a long loop structure separating the two parts of the ZBR domain. To investigate if the ZBR loop is essential for ZBR function, a hypothetical protein fold model of the ZBR was predicted using the Phyre2 protein recognition server (Kelley et al., 2015). The Phyre2 model predicted a structure aligning closest to Rubredoxin-like fold of transcription elongation factor A (Figure 50 D). Based on the predicted model, the differing amino acids between the aligning part of the Rubredoxin-like fold protein domain and Rca1 ZBR loop were deleted (Figure 50 E). Co-overexpression of the ZBR_loop mutant, NLS-4xFLAG-Rca1_204-411_ΔZBR_loop in the APC/C activity assay resulted in a stabilization of CycB-NT^{285} after Fzr overexpression in the G2-cell population (CHE/GFP - G2: 0.84) (Figure 51). However, the ZBR_loop mutant was partially impaired in its inhibitory function, when compared to Rca1_204-411 (CHE/GFP - G2: 0.99). This indicates that the ZBR loop is required for full APC/C inhibition by Rca1 but the partial deletion of the ZBR_loop causes only a reduction but not elimination of Rca1 function.

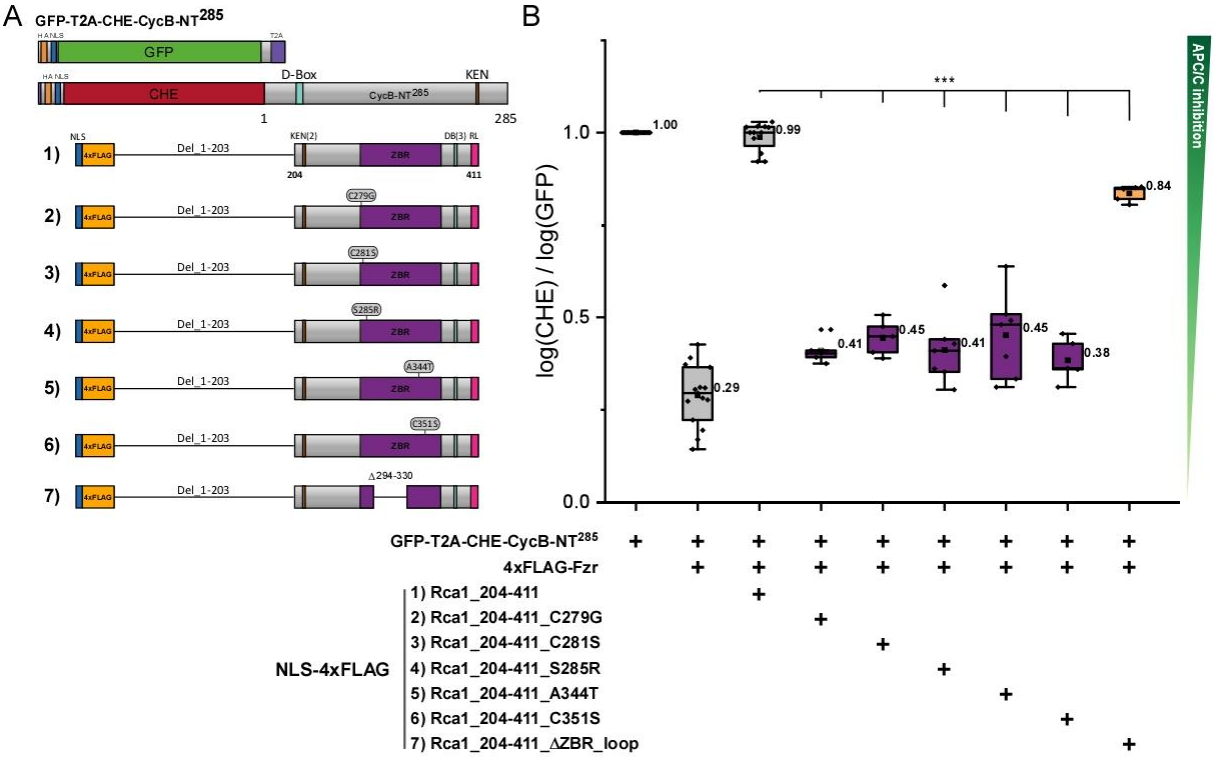

Figure 51| Deletion of the ZBR loop does not eliminate ZBR function

(**A**) Analysis of APC/C inhibition by Rca1 ZBR mutants. Illustration of the RPS-CycB sensor and the corresponding NLS-4xFLAG tagged Rca1 constructs with point mutations in the ZBR domain and a deletion of the ZBR loop. (**B**) Box plot of relative protein stability levels of GFP-T2A-CHE-CycB-NT^{285} with additional co-overexpression of 4xFLAG-Fzr and the corresponding NLS-4xFLAG-Rca1_204-411 mutants in G2-cells (exp.lvl. 2.0 - 3.0). The point mutations C278G, C281S, S285R, A344T, and C351S within the ZBR strongly impaired Rca1 function. Partial deletion of the ZBR_loop only reduced APC/C inhibition by Rca1. Statistics performed by Mann-Whitney U-Test, n.s. > 0.05, * ≤ 0.05, ** ≤ 0.01, ***≤ 0.001.

3.3.6. Impaired ZBR function destabilized Rca1

Loss of ZBR function strongly impaired APC/C inhibition by Rca1. Since Rca1 is also an APC/C^{Fzr} substrate, the question arose if impaired Rca1 function as an APC/C inhibitor would also influence its own degradation. To assess whether impaired ZBR function has an impact on Rca1 stability, the C-terminal part of Rca1 with a disrupted ZBR domain was analyzed via the RPS-system (Figure 52 A). Flow cytometric analysis of GFP-T2A-CHE-Rca1_204-411 containing one of the respective ZBR point mutations C278G, C281S, S285R, A344T, or C351S resulted in significant reduction of relative protein stability in the G1-, S- and G2-cell population compared to Rca1_204-411 with an intact ZBR domain (Figure 52 B). This suggests that a loss of ZBR function and impaired APC/C inhibitory function of Rca1 also causes a destabilization of Rca1. Accordingly, deletion of the ZBR loop which caused only a reduction of APC/C inhibition (see 3.3.5), resulted only a minor decrease of the CHE/GFP quotient for GFP-T2A-CHE-Rca1_204-411_ΔZBR_loop in G1-cells whereas no destabilization was observed in the S- and G2-populations (Figure 52 B).

The impact of impaired ZBR function was also analyzed in the context of full-length Rca1 that contains all of the degrons involved in APC/C dependent degradation (Figure 52 C). Analysis of GFP-T2A-CHE-Rca1_S285R, -Rca1_A344T and -Rca1_C351S also showed significantly reduced CHE/GFP ratios in the G1- and S-population compared to GFP-T2A-CHE-Rca1. Interestingly, elimination of ZBR function did not cause a destabilization in the G2-cell population in contrast to the results of Rca1_204-411. In conclusion, loss of APC/C inhibition caused by a disrupted ZBR domain is accompanied by a destabilization of Rca1. This could be either caused by an intrinsic instability due to impaired protein folding caused by the disrupted ZBR structure or indicate that loss of ZBR function has an impact on Rca1 degradation besides its function. Latter one could provide an indication for a potential molecular mechanism turning Rca1 from an APC/C^{Fzr} inhibitor during S-and G2-phase to an APC/C^{Fzr} substrate in G1-phase, which will be investigated in the following section.

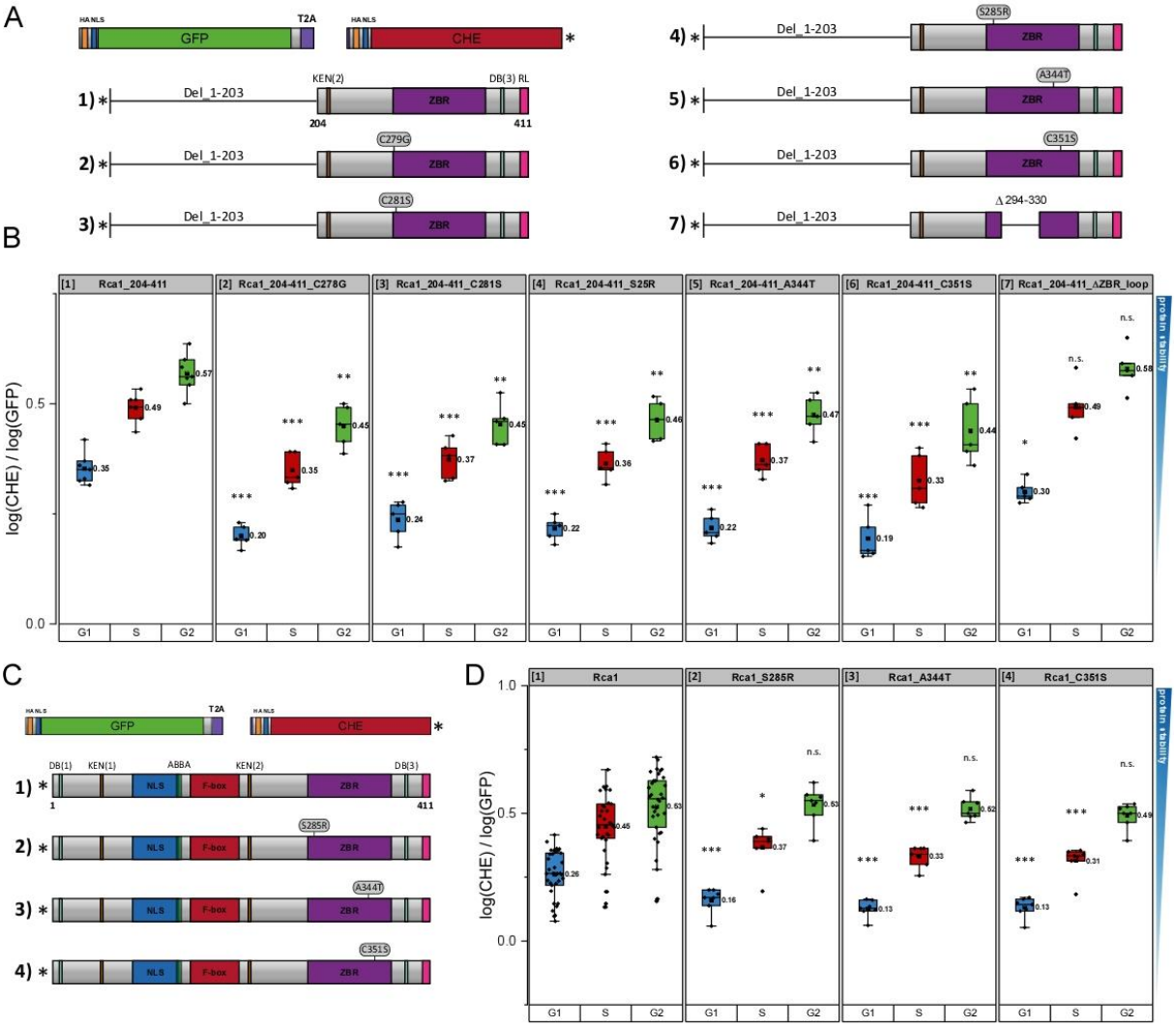

Figure 52| Impaired ZBR function causes a destabilization of Rca1

(**A**) Analysis of relative protein stability levels of Rca1_204-411 ZBR mutants. Illustration of the corresponding Rca1_204-411 ZBR mutants. (**B**) Box-plot of the normalized CHE/GFP ratios in G1-cells of the Rca1_204-411 ZBR mutants (exp.lvl. 1.0 - 1.75). The point mutations C278G, C281S, S285R, A344T, and C351S within the ZBR domain caused a significant decrease of relative protein stability levels of GFP-T2A-CHE_Rca1_204-411 in the G1-, S- and G2-population. Deletion of the ZBR_loop resulted only in a minor destabilization in G1-cells, whereas no effects were observed in the S- and G2-cell populations. The samples were compared to Rca1_204-411 of the respective cell cycle phase and symbols for p-values displayed above the box. (**C**) Analysis of relative protein stability levels of Rca1 ZBR mutants. Illustration of the corresponding Rca1 ZBR mutants. (**D**) Mutation of the ZBR (S285R, A344T, and C351S) caused a destabilization in the G1- and S-population whereas no difference was observed in the G2-population. The samples were compared to Rca1 of the respective cell cycle phase and symbols for p-values displayed above the box. Statistics performed by t-test with Welch´s correction, n.s. > 0.05, * ≤ 0.05, ** ≤ 0.01, ***≤ 0.001.

3.4. Investigation of potential "switches" turning Rca1 from an APC/C inhibitor to substrate

3.4.1. Aim

The experiments so far have shown that Rca1 is a potent APC/C inhibitor during S- and G2-phase that restrains APC/C activity via C-terminal domains including a KEN-box, a ZBR domain, a D-box degron, and a RL-tail (see section 3.3). Furthermore, it was demonstrated that besides its role as an APC/C inhibitor, Rca1 itself is targeted by APC/C^{Fzr} for proteasomal degradation during G1-phase (see section 3.2). Having established that Rca1 is an APC/C inhibitor during G2-phase and an APC/C substrate during G1-phase, the question arose how Rca1 is converted from an APC/C^{Fzr} inhibitor to substrate. In general, there is a multitude of regulatory mechanisms including post translational modifications, degron affinity, lysine accessibility, degron hiding, spatial regulations, etc. that can either influence substrate recruitment and the rate of ubiquitination as well as regulate protein function (see 2.6.6).

To elucidate the molecular switch converting Rca1 from an inhibitor to a substrate of the APC/C, three potential regulatory mechanisms were analyzed in the following section. First, the impact of Cdk phosphorylation in the regulation of Rca1 function and degradation was investigated. Second, a phosphorylation dependent protein interaction with the 14-3-3 protein mediated by a binding site within the ZBR_loop was discovered and examined for its role in Rca1 regulation. Finally, the influence of Rca1 localization on APC/C inhibition and Rca1 degradation was explored.

3.4.2. Phosphorylation of Rca1 influences its degradation and function as APC/C inhibitor

Post translational modification of proteins by phosphorylation is a versatile way to regulate protein activity. In case of APC/C substrates, it was shown that degron phosphorylation can result in opposing outcomes either resulting in substrate stabilization (e.g. Geminin, DBfk4, KIF1C) or enhanced substrate degradation (e.g. Securin) which can likewise be reversed by dephosphorylation (see 2.6.6, also reviewed in Davey et al., 2016). To assess whether Rca1 function or degradation is influenced by Cdk phosphorylation, the influence of potential phosphorylation sites should be analyzed. Thus, potential Cdk phosphorylation sites within Rca1 sequence were predicted using the algorithm of the Group-based Prediction system (GPS) 5.0 "*Predictor of Kinase-specific Phosphorylation sites*" (Wang et al., 2020). In total 17 putative Cdk phosphorylation sites were identified, of which ten contained the minimal consensus patter S/T-P (Figure 53). Two of the predicted Cdk phosphorylation sites, S123 and S127, together with an additional non Cdk phosphorylation site S326 were deposited in the iProteinDB online protein database (Hu et al., 2019). Interestingly, several of the S/T-P sites are located within or in close proximity to C-terminal domains required for APC/C inhibition (see 3.3), within the NLS, or the APC/C degrons mediating Rca1 degradation (see 3.2.5). Also, two Cks1 binding sites located in the N- and C-terminal part of Rca1 were predicted by the ELM database, which are essential for multisite

phosphorylation by Cdks (see 2.3). To test whether Rca1 activity or degradation is affected by phosphorylation of one of the predicted phosphorylation sites, Rca1 mutants for the ten putative S/T-P Cdk sites and the phosphorylation site S326 were investigated in the following.

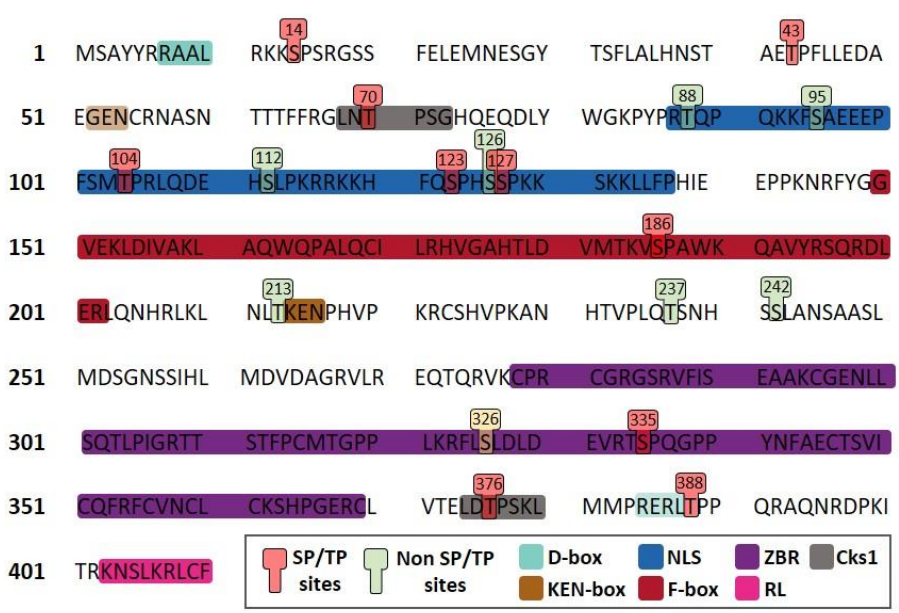

CDK phos. sites		
#	Amino acid	Position
1	S	14
2	T	43
3	T	70
4	T	88
5	S	95
6	T	104
7	S	112
8	S	123
9	S	126
10	S	127
11	S	186
12	T	213
13	T	237
14	S	242
15	S	335
16	T	376
17	T	388

Figure 53| Prediction of putative Cdk phosphorylation sites in Rca1

Illustration of the amino acid sequence of Rca1 with the functional domains and APC/C degrons highlighted in the respective color. The putative Cdk phosphorylation sites predicted using the GPS 5.0 algorithm are shown in the table (right) and are also highlighted in the sequence (left). S/T-P sites are shown in red, whereas non-S/T-P sites are shown in green, the number represents the position of the amino acid. The amino acid residue S326 within the ZBR was found as a phosphorylated site in the iProteinDB online database and is highlighted in yellow. Two Cks1 binding sites were found using the ELM database and are shown in gray.

3.4.2.1. Mutation of S/T-P sites changed Rca1 phosphorylation status

In order to investigate if Rca1 is regulated through phosphorylation, it was initially tested if phosphorylation of Rca1 was ascertainable and if mutation of the putative Cdk phosphorylation sites alters Rca1 phosphorylation status. Detection of phosphorylated Rca1 isoforms was implemented by Phos-tag SDS PAGE that enables mobility shift of phosphorylated proteins compared to their non-phosphorylated isoform, allowing inference on the level of phosphorylation, as well as on the amount of phosphorylated forms. Therefore, S2R+ cells were transfected with NLS-4xFLAG-Rca1 followed by Phos-tag SDS-PAGE of the cell lysate and Western blot analysis using an anti-FLAG antibody for protein detection. A control sample expressing the protein of interest was dephosphorylated using a Lambda phosphatase to compare the phosphorylated protein bands to the non-phosphorylated protein. Since molecular weight estimation using molecular weight markers is not possible in Phos-tag SDS-PAGE, the dephosphorylated sample was also used as a reference marker. Phos-tag SDS-PAGE analysis of NLS-4xFLAG-Rca1 resulted in detection of multiple phosphorylated Rca1 isoforms, seen by several mobility

shifts compared to the dephosphorylated Rca1 reference (Figure 54 B, sample 1). Since several phosphorylated Rca1 isoforms were detected, it can be assumed that Rca1 is phosphorylated at multiple sites. To test, if the putative Cdk phosphorylation sites are actually phosphorylated, an Rca1 mutant with alanine substitutions of the ten putative Cdk phosphorylation sites, referred to as Rca1_10A, was analyzed (also see Figure S 4). NLS-4xFLAG-Rca1_10A displayed less phosphorylated Rca1 isoforms compared to the control indicating that mutation of the S/T-P sites caused a reduction of Rca1 phosphorylation. Albeit not all phosphorylation sites were eliminated since some mobility shifts were still observed for the 10A mutant (Figure 54 A, B compare lane 1 and 2). Since phosphorylation sites S123 and S127 within the NLS were deposited in the iProteinDB database, an Rca1 mutant with alanine substitutions at these positions was also analyzed. In accordance with the reported phosphorylation at the two sites, NLS-4xFLAG-Rca1_S123A_S127A displayed a change in the pattern of the phosphorylated Rca1 isoforms (Figure 54 A, B compare lane 1 and 3).

Phosphorylation status of N- and C-terminal Rca1 was investigated to further estimate if both regions of Rca1 are subjected to phosphorylation. Post translational modification of either moiety of Rca1 could be involved in Rca1 regulation, since the protein domains that are involved in APC/C inhibition are located in the C-terminal region of Rca1, whereas the N-terminal part of Rca1 contains several of the APC/C degrons mediating its degradation. Phos-tag SDS PAGE analysis of NLS-4xFLAG-Rca1_1-203 showed multiple mobility shifts attributed to Rca1_1-203 phosphorylation. Mutation of the seven putative Cdk sites located in this Rca1 fragment (NLS-4xFLAG-Rca1_1-203_7A) caused a reduction in the amount of phosphorylated Rca1_1-203 isoforms (Figure 54 A, C compare lane 4 and 5). A mobility shift was also visible in the conventional SDS-PAGE, for both proteins. One must mention that no dephosphorylated reference protein is shown in Figure 54 for N- and C-terminal Rca1, since dephosphorylation of the samples was not successful for this replicate. However, based on the experience from other replicates, the lowest band constitutes the dephosphorylated protein and was therefore also indicated in Figure 54. Separation of S2R+ cell lysates of cells transfected with NLS-4xFLAG-Rca1_204-411 also showed multiple mobility shifts in the Phos-tag SDS-PAGE (Figure 54 D, lane 6). Mutation of the three C-terminal S/T-P sites (S335A, T376A, and T388A) caused a shift in the pattern of the phosphorylated Rca1 protein bands (Figure 54 D, compare lane 6 and 7). Since amino acid residue S326 was shown to be phosphorylated according to the iProteinDB database, NLS-4xFLAG-Rca1_S326A was additionally analyzed. The point mutation S326A caused a change in the pattern of phosphorylated Rca1_204-411 isoforms but it was not possible to clearly estimate which of the bands vanished (Figure 54 D, compare lane 6 and 8). Nevertheless, simultaneous mutation of the four C-terminal phosphorylation sites S326A, S335A, T376A, and T388A (Rca1_204-411_4A) resulted in a strong decline in phosphorylation of Rca1_204-411 and only a single phosphorylation band remained for NLS-4xFLAG-Rca1_204-411_4A (Figure 54 D, compare lane 6 and 9).

It was shown that Rca1 is mainly located within the nucleus (Grosskortenhaus et al., 2002) and it was therefore tested whether Rca1 phosphorylation is dependent on its subcellular localization. Thus, 4xFLAG-NES-Rca1_204-411 was compared to the NLS-4xFLAG tagged Rca1 version. However, Rca1 export from the nucleus had no effect on phosphorylation of the C-terminal Rca1-fragment, as no differences in the mobility shifts were detected for 4xFLAG-NES-Rca1_204-411 in the Phos-tag SDS PAGE (Figure 54 D, compare lane 6 and 10). In conclusion, it was shown that Rca1 is phosphorylated at multiple sites using Phos-tag SDS PAGE analysis for the detection of phosphorylated isoforms. Mutation of ten potential Cdk phosphorylation sites caused a change in Rca1 phosphorylation status, even though not all phosphorylation sites were eliminated.

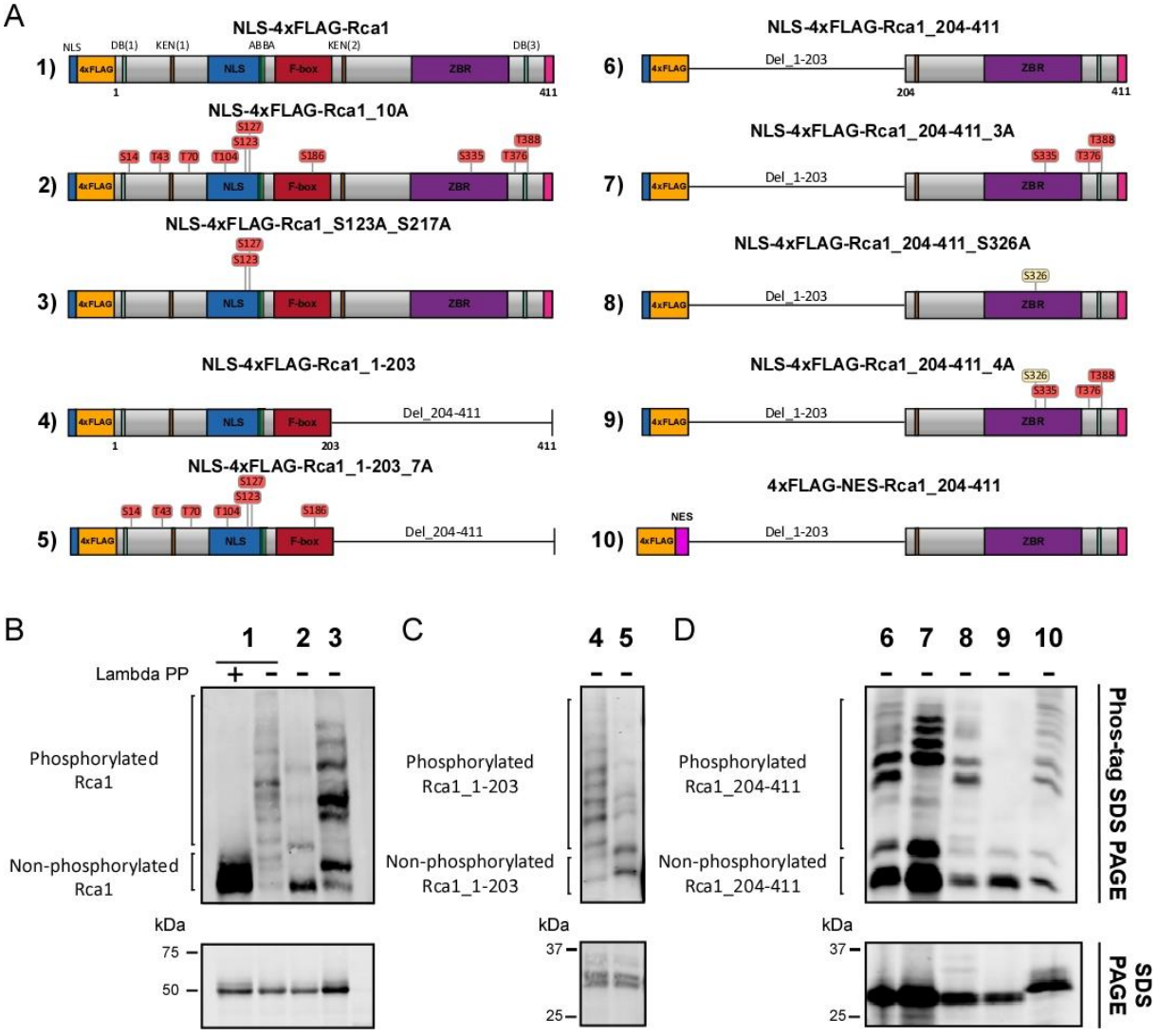

Figure 54| Phos-tag SDS-PAGE analysis of Rca1 reveals multisite phosphorylation of Rca1

(**A**) Illustration of the corresponding NLS-4xFLAG tagged Rca1 mutants analyzed by Phos-tag SDS-PAGE. The potential Cdk phosphorylation sites are shown in red boxes. The non Cdk phosphorylation site S326 is highlighted by a yellow box. (**B, C, D**) Phos-tag SDS PAGE conducted using a 10% SDS running gel containing 50 µM Phos-tag and 50 µM $MnCl_2$ after running time of 80 min. A conventional SDS-PAGE of the same samples was used to estimate similar protein expression. Protein detection on the Western blot membrane was carried out using an anti-FLAG antibody for immunostaining of the protein of interest. Mutation of the potential Cdk phosphorylation sites caused a loss of single Rca1 phosphorylation isoforms and shifts in the pattern of phosphorylated Rca1 isoforms were observed in the Phos-tag SDS PAGE.

Both moieties of Rca1 are phosphorylated, and mutation of the respective Cdk phosphorylation sites also caused a change in the phosphorylation status of N- and C-terminal Rca1. Interestingly, additional mutation of the amino acid residue S326 along with the three S/T-P sites resulted in strong reduction of Rca1_204-411 phosphorylation.

3.4.2.2. Mutation of putative N-terminal CDK phosphorylation sites destabilize Rca1

In a next step, it was tested whether changes in Rca1 phosphorylation status have an impact on its stability. Thus, relative protein stability levels of the phosphorylation site mutants that have been analyzed by Phos-tag SDS-PAGE (see 3.4.2.1) were determined using the RPS system. The Rca1 mutants were inserted in RPS-8 and analyzed via flow cytometry after transient transfection. GFP-T2A-CHE-Rca1_10A showed significantly decreased CHE/GFP quotients in the G1-, S-, and G2-cell populations (CHE/GFP - G1: 0.12, S: 0.23, G2: 0.38) compared to GFP-T2A-CHE-Rca1 control (CHE/GFP - G1: 0.21, S: 0.40, G2: 0.48) (Figure 55 A). However, only the decrease in the G1- and S-population was statistically significant. Analysis of N-terminal Rca1 containing alanine substitutions of the seven S/T-P sites also resulted in a strong decrease of relative protein stability levels in the three cell populations (CHE/GFP - G1: 0.06, S: 0.14, G2: 0.20) compared to the control (CHE/GFP - G1: 0.17, S: 0.30, G2: 0.37) (Figure 55 B).

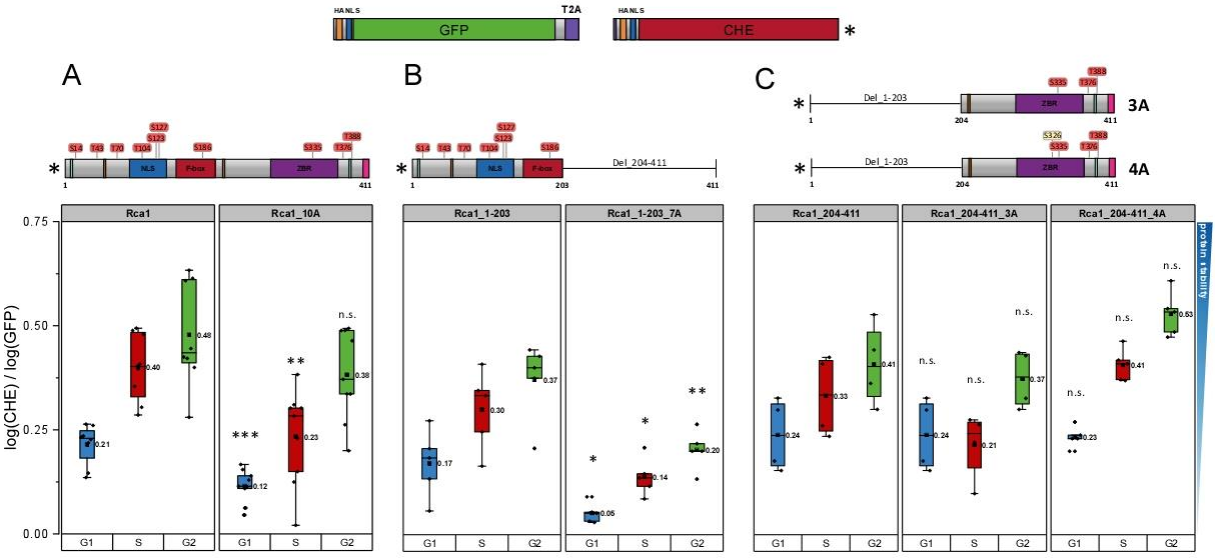

Figure 55| Mutation of the potential CDK phosphorylation destabilized Rca1 and Rca1_1-203

Flow cytometric analysis of the Rca1 phosphorylation site mutants in the G1, S- and G2-populations (exp.lvl. 1.0 - 1.75). The respective Rca1 mutant is displayed above the corresponding box plot. (**A**) Analysis of relative protein stability levels of GFP-T2A-CHE-Rca1_10A. Mutation of the ten potential Cdk phosphorylation sites caused a decrease of relative protein stability levels. (**B**) Relative protein stability of GFP-T2A-CHE-Rca1_1-203_7A was decreased compared to the control. (**C**) Mutation of the three S/T-P sites (GFP-T2A-CHE-Rca1_1-203_3A) and additional alanine substitution of S326 (GFP-T2A-CHE-Rca1_204-411_4A) had no influence on relative protein stability levels in the G1-, S-, and G2-population. Statistics performed by t-test with Welch´s correction, n.s. > 0.05, * ≤ 0.05. The samples were compared to the respective control of unmutated Rca1 of the respective cell cycle phase and symbols for p-values are displayed above the box.

Interestingly, flow cytometric analysis of GFP-T2A-CHE_Rca1_204-411_3A and GFP-T2A-CHE_Rca1_204-411_4A resulted in similar CHE/GFP ratios (CHE/GFP - G1: 0.24/0.23, S: 0.21/0.41, G2: 0.37/0.53) as observed for the control (CHE/GFP - G1: 0.24, S: 0.33, G2: 0.41) (Figure 55 C). Thus, mutation of the three potential Cdk phosphorylation sites, as well as the 4A mutant including phosphorylation site S326, did not result in a destabilization of C-terminal Rca1, even though the 4A mutant displayed a strong decline in the rate of phosphorylation as seen for NLS-4xFLAG-Rca1_204-411_4A in the Phos-tag SDS-PAGE analysis (see Figure 54 D).

Hence, mutation of the putative S/P-T phosphorylation sites in the N-terminal region of Rca1 had a destabilizing effect since relative protein stability levels of CHE-Rca1_10A and CHE-Rca1_1-203_7A were decreased, whereas mutation of the C-terminal phosphorylation sites including serine at position 326 (S326A) had no effect on relative protein stability of CHE-Rca1_204-411. Consequently, the destabilization caused by mutated phosphorylation sites is referable to the N-terminal located phosphorylation sites. However, decreased protein stability levels were observed in all three cell cycle populations and it must be considered that the effect could be attributed to an intrinsic misfolding of the protein caused by the introduced point mutations.

3.4.2.3. Destabilization of the CDK mutants is not caused by a negative intrinsic effect

To ascertain whether the mutation of the ten potential Cdk phosphorylation sites caused an unspecific intrinsic destabilization of the Rca1_10A mutant, protein stability levels were determined with additional inactivation of APC/C activity in cells that have also been enriched in G2-phase. If the destabilization of the 10A mutant is caused by increased APC/C dependent degradation, relative protein stability levels should increase under these conditions. Otherwise, the destabilizing effect would have an intrinsic cause. APC/C inactivation and enrichment of G2-cells was implemented by the simultaneous co-overexpression of NLS-4xFLAG-Rca1, HA-CycE, Cdk2-HA and SkpA in addition to GFP-T2A-CHE-Rca1_10A. Expression of the NLS-4xFLAG-Rca1 is able to restrain APC/C activity and additional CycE-Cdk2 activity causes an increase of cells in G2-phase (Herzinger, 2019). Protein stability levels of GFP-T2A-CHE-Rca1 and GFP-T2A-CHE-Rca1_10A (Figure 56 A) were determined in S2R+ cells via flow cytometry under normal conditions (control) or with the additional expression of NLS-4xFLAG tagged Rca1 and increased CycE-Cdk2 activity. Compared to the control, APC/C inhibition and enrichment of G2-cells had no effect on CHE-Rca1 protein levels (CHE/GFP - G1: 0.24/0.27, S: 0.49/0.57, G2: 0.62/0.65). Opposed to this, relative protein levels of CHE-Rca1_10A were significantly increased after additional overexpression of NLS-4xFLAG-Rca1 and CycE/Cdk2 (CHE/GFP - G1: 0.14/0.24, S: 0.32/0.53, G2: 0.48/0.58) reaching similar protein stability levels like the CHE-Rca1 control (Figure 56 B). The G2 enrichment caused by the NLS-4xFLAG-Rca1, HA-CycE, Cdk2-HA, and SkpA overexpression, was clearly detectable by an elevated G2-peak in the DNA histogram of the GFP-positive cells (Figure 56 C).

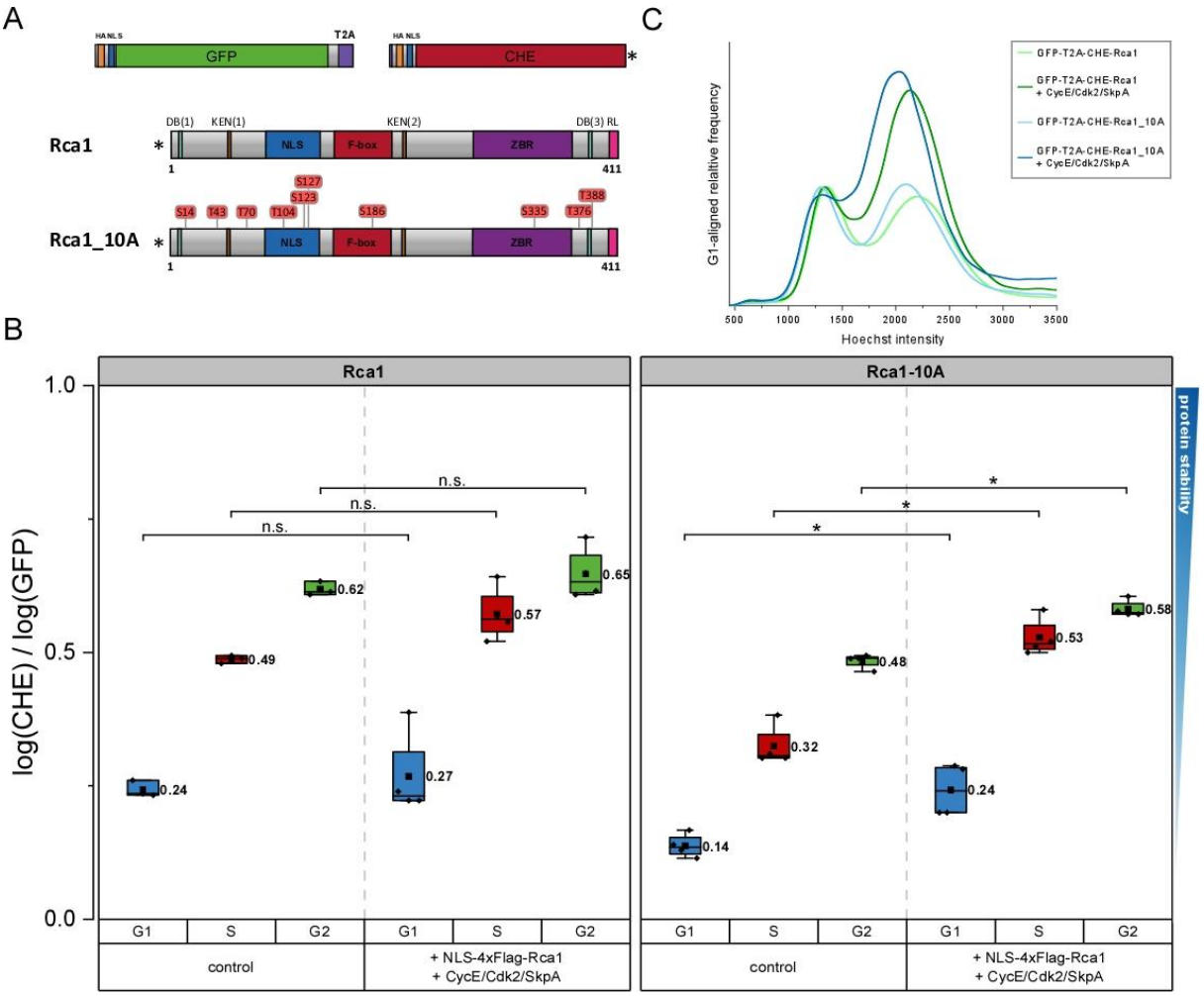

Figure 56| Rca1 is not intrinsically destabilized by the mutation of Cdk phosphorylation sites

Analysis of relative protein stability levels of GFP-T2A-CHE-Rca1 and GFP-T2A-CHE-Rca1_10A with decreased APC/C activity and G2-cell enrichment. (**A**) Illustration of the corresponding Rca1 and Rca1_10A mutant inserted into RPS-8. (**B**) Box-plot of the normalized CHE/GFP ratios in G1-, S-, and G2-cells (exp.lvl. 1.0 - 1.75) under normal conditions (control) or additional expression of NLS-4xFLAG-Rca1, HA-CycE, Cdk2-HA and SkpA. GFP-T2A-CHE-Rca1_10A relative protein stability levels were increased by additional Rca1 and CycE/Cdk2 expression. Statistics performed by Mann-Whitney U-Test, n.s. > 0.05, * ≤ 0.05. (**C**) G1-aligned DNA histograms of the GFP positive cells of the transfected cells. Additional expression NLS-4xFLAG-Rca1, HA-CycE, Cdk2-HA and SkpA resulted in an increase of G2-cells seen by an elevated G2-peak compared to the control (compare light to dark green and light to dark blue)

Thus, it can be assumed that the destabilization caused by the mutation of the N-terminal S/T-P sites is referable to increased Rca1 destruction mediated by the APC/C and is not due to an unspecific intrinsic destabilization.

3.4.2.4. C-terminal phosphorylation of Rca1 is required for full APC/C inhibition

Since mutation of the C-terminal phosphorylation sites resulted in a drastic change of NLS-4xFLAG-Rca1_204-411_4A phosphorylation status (see3.4.2.1) but had no effect on its relative protein stability levels (see 3.4.2.2), it was tested whether phosphorylation of the C-terminal Rca1 region is involved in regulation of Rca1 function. APC/C inhibition by Emi1 was shown to be negatively regulated by Cdk phosphorylation in mitosis. Mitotic phosphorylation of purified Emi1 and a C-terminal Emi1 fragment

(Emi1CT) was sufficient for inactivation of Emi1 function in a purified system. Mutation of the three C-terminal minimal consensus S/T-P sites rendered Emi1CT-3A refractory to mitotic phosphorylation and prevented its inactivation (Moshe et al., 2011). Since Rca1 also contains three S/T-P sites in its C-terminal region and utilizes similar domains for APC/C inhibition like Emi1 (see 3.3.4), it could also be regulated by Cdk dependent phosphorylation. To test this hypothesis, the Rca1_10A and Rac1_204-411_3A and 4A mutants (Figure 57 A) were analyzed for their capacity to restrict APC/C^{Fzr} activity in the established *in vivo* APC/C activity assay (see 3.3.2). Compared to NLS-4xFLAG-Rca1, expression of NLS-4xFLAG-Rca1_10A resulted only in a partial stabilization of GFP-T2A-CHE-CycB-NT^{285} in the G2-cell population after Fzr overexpression (CHE/GFP - G2: 1.10/0.7) (Figure 57 B). However as seen above, the 10A mutant was also destabilized in G2-cells which could cause the reduction in APC/C inhibition. To exclude this possibility, the C-terminal part of Rca1 which was sufficient for APC/C inhibition (see 3.3.3) was tested since both the 3A and 4A mutant did not display a destabilization of C-terminal Rca1 (see 3.4.2.2). Compared to NLS-4xFLAG-Rca1_204-411, both the 3A and 4A mutant were significantly impaired in their function as APC/C inhibitor. Expression of NLS-4xFLAG-Rca1_204-411_3A and NLS-4xFLAG-Rca1_204-411_4A only partially restored GFP-T2A-CHE-CycB-NT^{285} relative protein stability levels after Fzr overexpression in the G2-cell population (CHE/GFP - G2: 0.62/0.61) (Figure 57 B).

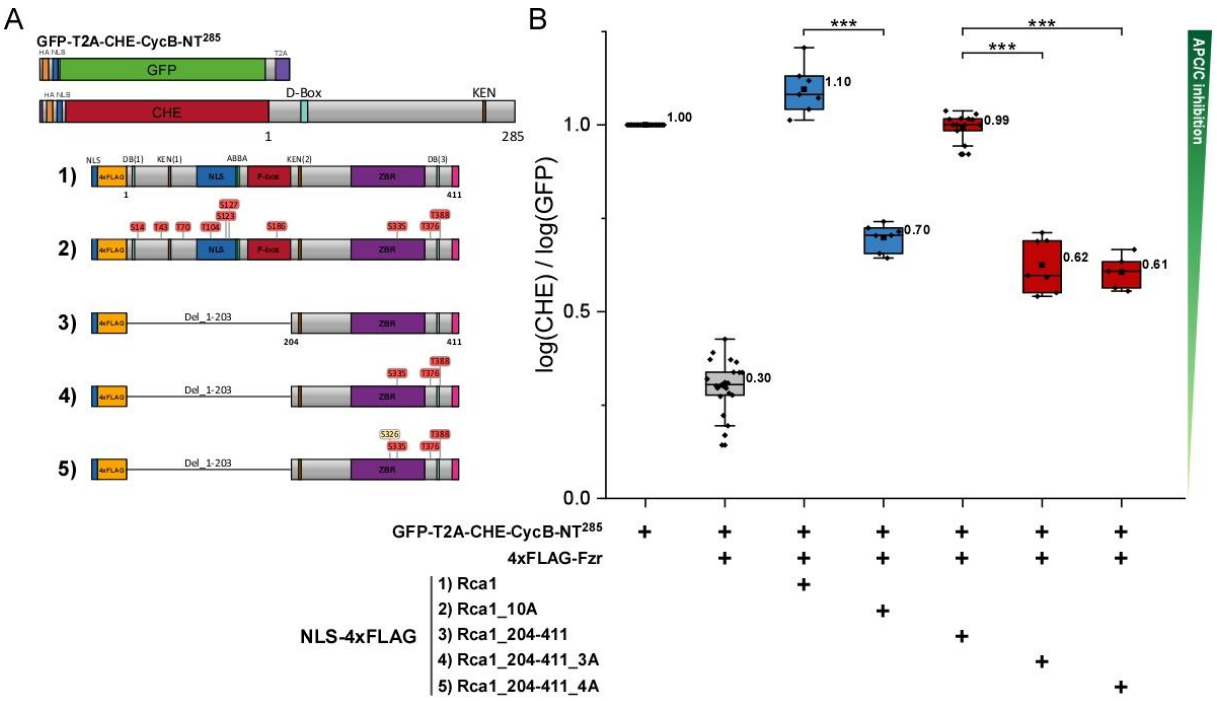

Figure 57| Rca1 function is impaired by mutation of C-terminal phosphorylation sites

Analysis of APC/C inhibition by Rca1 phosphorylation site mutants. (**A**) Illustration of the RPS-CycB sensor and the corresponding NLS-4xFLAG tagged Rca1 mutants. (**B**) Box plot of relative protein stability levels of GFP-T2A-CHE-CycB-NT^{285} with additional co-overexpression of 4xFLAG-Fzr and the corresponding NLS-4xFLAG-Rca1 mutants in G2-cells (exp.lvl. 2.0 - 3.0). Mutation of the ten potential S/T-P sites partially decreased Rca1 function (blue boxes). Mutation of the three potential Cdk phosphorylation sites (S335A, T376A, and T388A) impaired APC/C inhibition by NLS-4xFLAG-Rca1_204-411_3A. Additional mutation of S326A did not further impair NLS-4xFLAG-Rca1_204-411_4A function (red boxes). Statistics performed by Mann-Whitney U-Test, n.s. > 0.05, * ≤ 0.05, **≤ 0.01, ***≤ 0.001.

This indicates that mutation of the three S/T-P sites (S335A, T376A, and T388A) caused a partial inactivation of NLS-4xFLAG-Rca1_204-411 function. Interestingly, the additional point mutation S326A did not further enhance this effect, even though the 4A mutant displayed a strong decline in phosphorylation of NLS-4xFLAG-Rca1_204-411 compared to the 3A mutant (see 3.4.2.1). Furthermore, this suggests that the partial inactivation of Rca1_10A mutant was not necessarily caused by its decreased stability but could also be referable to the mutation of the C-terminal phosphorylation sites. However, decreased phosphorylation of Rca1 and Rca1_204-411 did not result in a complete elimination but only in a partial reduction of APC/C inhibition. This could be explained since Rca1 phosphorylation was not completely abolished by the introduced mutations, seen by remaining phosphorylated isoform in the Phos-tag SDS-PAGE, which was also the case for NLS-4xFLAG-Rca1_204-411_4A (see 3.4.2.1). Nevertheless, the obtained results indicate that phosphorylation of the C-terminal part of Rca1 is required for full APC/C inhibition, opposed to the mechanisms reported for Emi1 which is inactivated by mitotic phosphorylation of its three C-terminal S/P-T sites (Moshe et al., 2011).

3.4.2.5. Phosphorylation status of Rca1 in G1- and G2-arrested cells

Taken together, mutation of the putative N-terminal Cdk phosphorylation sites decreased Rca1 stability levels (see 3.4.2.2) and mutation of the C-terminal sites caused a reduction in Rca1 function (see 3.4.2.4). Thus, phosphorylated Rca1 should be more stable and also constitute a more potent APC/C inhibitor compared to dephosphorylated Rca1. Accordingly, in the context of cell cycle progression, Rca1 should be phosphorylated in S-phase and G2-phase in which it is stable and functions as an APC/C inhibitor, which could be initiated by high Cdk activity during S-phase and sustained by mediocre Cdk activity in G2-phase (see 2.3). On the contrary, Rca1 should be less or dephosphorylated during G1-phase, when Cdk activity is low and protein phosphatases cancel out Cdk substrate phosphorylation (Martín et al., 2020) and Rca1 is degraded by the APC/C. To test this hypothesis, phosphorylation of an N-terminal Rca1 fragment was analyzed in cells targeted to be enriched either in G2-phase, mitosis or G1-phase. The N-terminal Rca1 mutant, Rca1_1-203_ΔDB(1)_mKEN(1)_mABBA, which is refractory to APC/C dependent degradation was used for the analysis (see 3.2.5.1) since less phosphorylated Rca1 showed an increased destabilization and could therefore be missed or be underrepresented in the analysis. S2R+ cells were transiently transfected with NLS-4xFLAG-Rca1_1-203_ΔDB(1)_mKEN(1)_mABBA (Figure 58 A) and chemically treated to cause G2 phase, mitosis or G1-phase enrichment. The cell cycle progression arrest was induced by treating cells for at least 24 h with a final concentration of either 1.7 µM 20-hydroxyecdysone (for G2-arrest), 0.5 mM mimosine (for G1 arrest) or for 12h with 30 µM colchicine (for mitotic arrest) as described in Rogers et al. (2009) and Brownlee et al. (2011) (also see 6.3.5). Unfortunately, the proposed cell cycle changes were not very pronounced in the case of 20-hydroxyecdysone or mimosine treatment. Phos-tag SDS-PAGE followed

by Western blot analysis of the transfected cell lysates resulted in the detection of several phosphorylated isoforms of NLS-4xFLAG-Rca1_1-203_ΔDB(1)_mKEN(1)_mABBA in case of the control cells treated with DMSO. Dephosphorylation using a Lambda phosphatase resulted only in a partial dephosphorylation. Comparison of the cell lysates of G2- and G1-phase arrested cells displayed several phosphorylated isoforms similar to the control cells and no difference was detectable between the two samples. However, a complete cell cycle arrest in either G2- or G1-phase was not achieved and hence it is rather unlikely to detect a difference in Rca1 phosphorylation status in the applied experimental setup. Only mitotic arrested cells showed weaker signals compared to the DMSO control, G2- and G1-arrested cells (Figure 58 B). However, this was referable to a decreased input protein levels as seen in the conventional SDS-PAGE analysis. Most likely, colchicine treatment induced apoptosis, as a reduction in the overall cell number was visually observed in microscopic analysis that would explain the decreased protein levels in case of the mitotic arrested cells. The drug-induced cell cycle arrest was also verified by flow cytometry prior to cell lysis. Flow cytometric analysis of the cell cycle distribution of cells treated with 20-hydroxyecdysone or mimosine showed only a slight increase of G2-cells and G1-cells respectively, instead of a G2- or G1-phase arrest, whereas colchicine induced mitotic arrest was successful as only a single G2-peak was detectable in the Hoechst histogram (Figure 58 C). In summary, cell cycle enrichment for G2- and G1-phase was not achieved and no difference in the phosphorylation status of the applied N-terminal Rca1 fragment was discernible in the context of cell cycle progression using Phos-tag SDS-PAGE. To test the hypothesis, a strong arrest in the respective cell cycle stage is required but was unfortunately not achieved in the conducted experiments during this thesis. Thus, it was not possible to get further insight into cell cycle dependent phosphorylation of Rca1 and the experiment should be repeated:

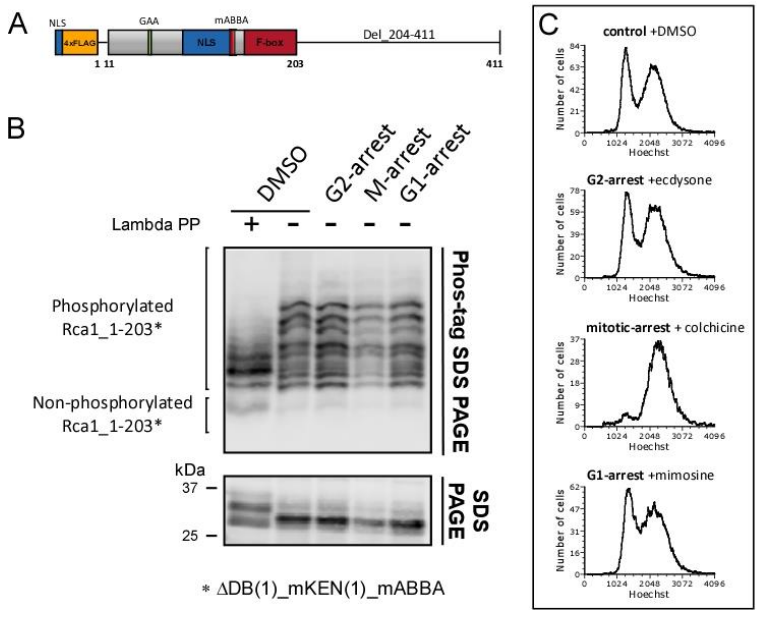

Figure 58| Rca1 phosphorylation in cell cycle stage arrested cells

(**A**) Illustration of NLS-4xFLAG-Rca1_1-203_ΔDB(1)_mKEN(1)_ mABBA. (**B**) Phos-tag SDS PAGE conducted using a 10% SDS running gel containing 50 µM Phos-tag and 50 µM $MnCl_2$ after running time of 55 min. A conventional SDS-PAGE of the same samples was used to estimate similar protein expression. An anti-FLAG-antibody was used for immunostaining. No difference was observed between the cells treated either with 20-Hydroxyecdysone, colchicine, or mimosine. (**C**) Hoechst histograms of the cell cycle arrested cells. G2- and G1-arrest was only partially achieved, whereas mitotic arrest is seen by a single peak.

3.4.3. Rca1 interaction with 14-3-3 protein

Rca1 sequence analysis with the ELM prediction tool identified five potential 14-3-3 binding sites that are either located in close proximity to the APC/C degrons or within the ZBR and RL-tail domain (Figure 59 A). In general, 14-3-3 proteins interact with a vast number of phosphorylated target proteins and thereby modulate their function in a variety of different mechanisms. Interestingly, Cdk1 phosphorylation dependent interaction of the budding yeast APC/C inhibitor Acm1 with the 14-3-3 members Bmh1 and Bmh2 results in a stabilization of Acm1. Vice versa, decreased Cdk1 activity and Acm1 dephosphorylation by the Cdc14 phosphatase inactivate phosphodependent 14-3-3 binding, allowing Acm1 degradation (Enquist-Newman et al., 2008; Hall et al., 2008; Ostapenko et al., 2008). To assess whether Rca1 is also modified by 14-3-3 binding, it was tested if Rca1 associates with 14-3-3 protein. Initially, the results of a mass spectrometric (MS) analysis for Rca1 interaction partners that was already implemented in a previous study (Kies, 2017) were searched for 14-3-3 protein. Indeed, 14-3-3 epsilon and 14-3-3 zeta proteins were both detected in the LC-MS/MS analysis of a 4xFLAG-Rca1 precipitate from S2R+ cells (see Table S 4).

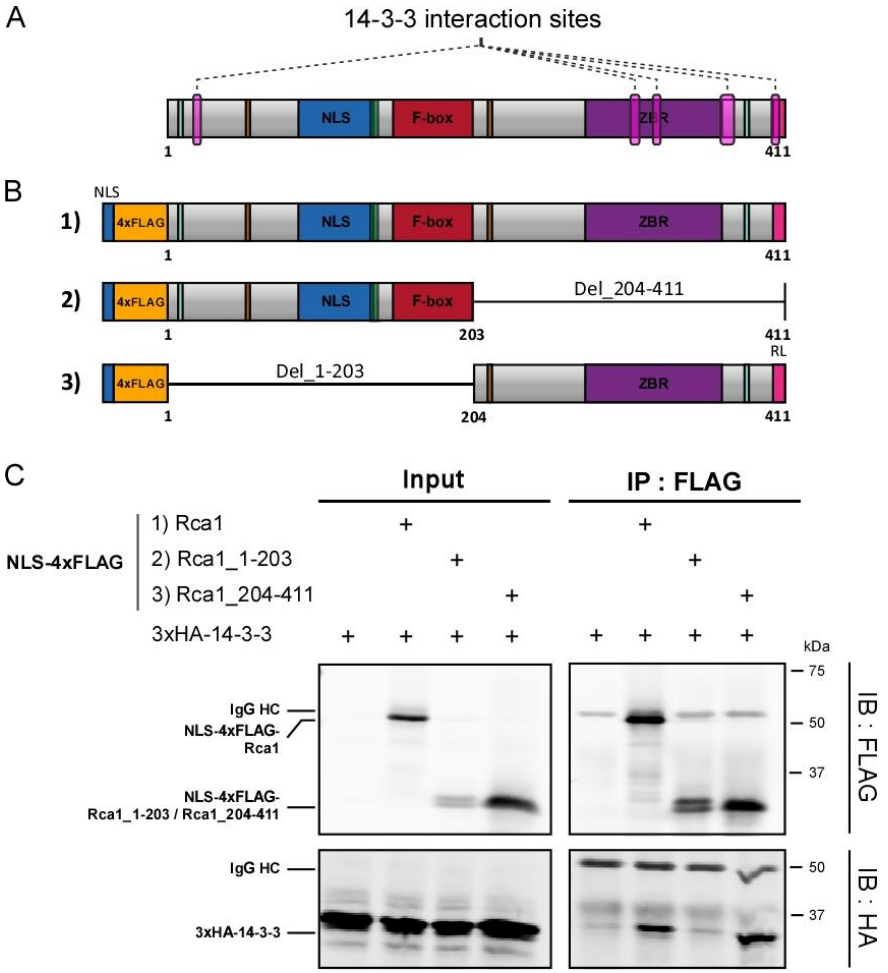

Figure 59| Rca1 binds 14-3-3 with its C-terminal part

(**A**) 14-3-3 binding sites predicted by the ELM prediction tool. (**B**) Illustration of the NLS-4xFLAG-Rca1 constructs for co-immunoprecipitation with 3xHA-14-3-3. (**C**) Co-IP between the different NLS-4xFLAG-Rca1 constructs and 3xHA-14-3-3. Rca1 and Rca1_204-411 interact with 14-3-3, whereas Rca1_1-203 fails to bind 3xHA-14-3-3.

To further assess whether Rca1 directly interacts with 14-3-3 and to narrow down the functional 14-3-3 binding site, the ability of 3xHA-14-3-3 to bind different 4xFLAG-Rca1 constructs was tested in S2R+ cell lysates by co-immunoprecipitations (co-IPs). For the analysis, 14-3-3 epsilon hereafter referred to as 14-3-3, was used since it displayed a higher sequence coverage and score in the MS analysis compared to 14-3-3 zeta (see Table S 4). Co-precipitation of 3xHA-14-3-3 was tested for NLS-4xFLAG-Rca1, -Rca1_1-203, and -Rca1_204-411 in S2R+ cell lysates after transient co-transfection. 3xHA-14-3-3 was able to bind NLS-4xFLAG-Rca1 and NLS-4xFLAG-Rca1_204-411 but failed to interact with the N-terminal fragment NLS-4xFLAG-Rca1_1-203 (Figure 59 B, C). Thus, consistent with the results of the MS analysis, a direct interaction between Rca1 and 14-3-3 was observed that requires the C-terminal part of Rca1.

3.4.3.1. Phosphorylation of S326 leads to 14-3-3 interaction

Since the C-terminal region of Rca1 was able to bind 14-3-3, it was further investigated which of the 4 remaining 14-3-3 binding sites, referred to as 14-3-3 site #1-4, is responsible for the interaction between Rca1 and 14-3-3 protein. A second bioinformatic analysis using the 14-3-3 Pred webserver (Madeira et al., 2015) displayed the highest consensus score for the site #2 which also contains the phosphorylation site S326 that was found in the iProteinDB database (see 3.4.2) (Figure 60). To test which of the 4 sites is responsible for 14-3-3 interaction with Rca1, 14-3-3 association was tested by co-IPs using different C-terminal Rca1 mutants (Figure 61 A). 3xHA-14-3-3 was still able to interact with NLS-4xFLAG-Rca1_204-405_ΔRL and NLS-4xFLAG-Rca1_204-368, excluding the binding sites #3 and #4 (Figure 61 B, lane 2 and 3). Mutation of the three Cdk phosphorylation sites did also

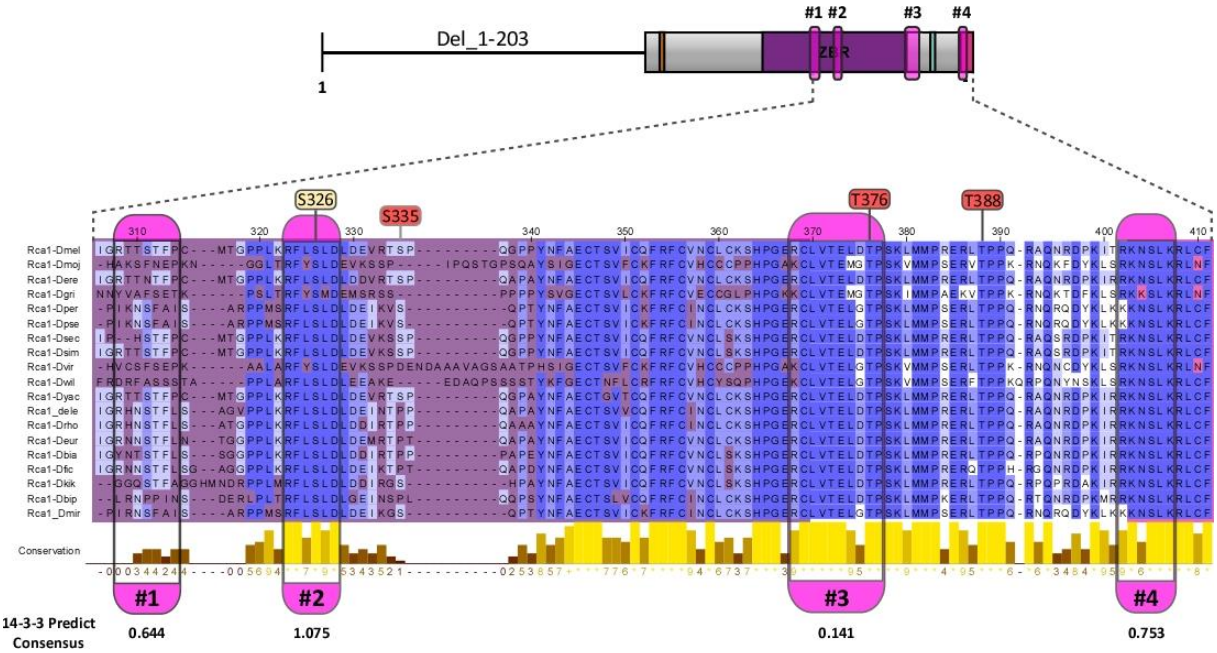

Figure 60| Bioinformatic analysis of the C-terminal Rca1 14-3-3 binding sites

Rca1 sequence alignment among different *Drosophila* species of the four C-terminal 14-3-3 binding sites. Site #2-4 are highly conserved and site #2 and #3 also contain phosphorylation sites, shown by the round boxes (Cdk sites in red, S326 in yellow). 14-3-3 binding site #2 has the highest score predicted by the 14-3-3 Pred webserver.

not impair 14-3-3 interaction with NLS-4xFLAG-Rca1_204-411_3A (Figure 61 B, lane 4). However, mutation of the phosphorylation site S326 to alanine caused a complete loss of 14-3-3 binding, as no co-precipitation was observed for NLS-4xFLAG-Rca1_204-411_S326A, anymore (Figure 61 B, lane 5). This indicates that Rca1 interaction with 14-3-3 is mediated by binding site #2 and also requires the phosphoserine at position 326 for interaction. It was also tested, if an aspartate substitution of the serine residue (S326D) would function as a phosphate mimic, however 14-3-3 also failed to bind to NLS-4xFLAG-Rca1_204-411_S326D (Figure 61 B, lane 6). Consistent with the requirement of phosphoserine S326, 14-3-3 interaction was completely abolished in case of the 4A mutant (NLS-4xFLAG_Rca1_204-411_4A) as well as the deletion of the ZBR_loop along with the 14-3-3 binding site (NLS-4xFLAG_Rca1_204-411_ΔZBR_loop) (Figure 61 B, lane 7 and 8).

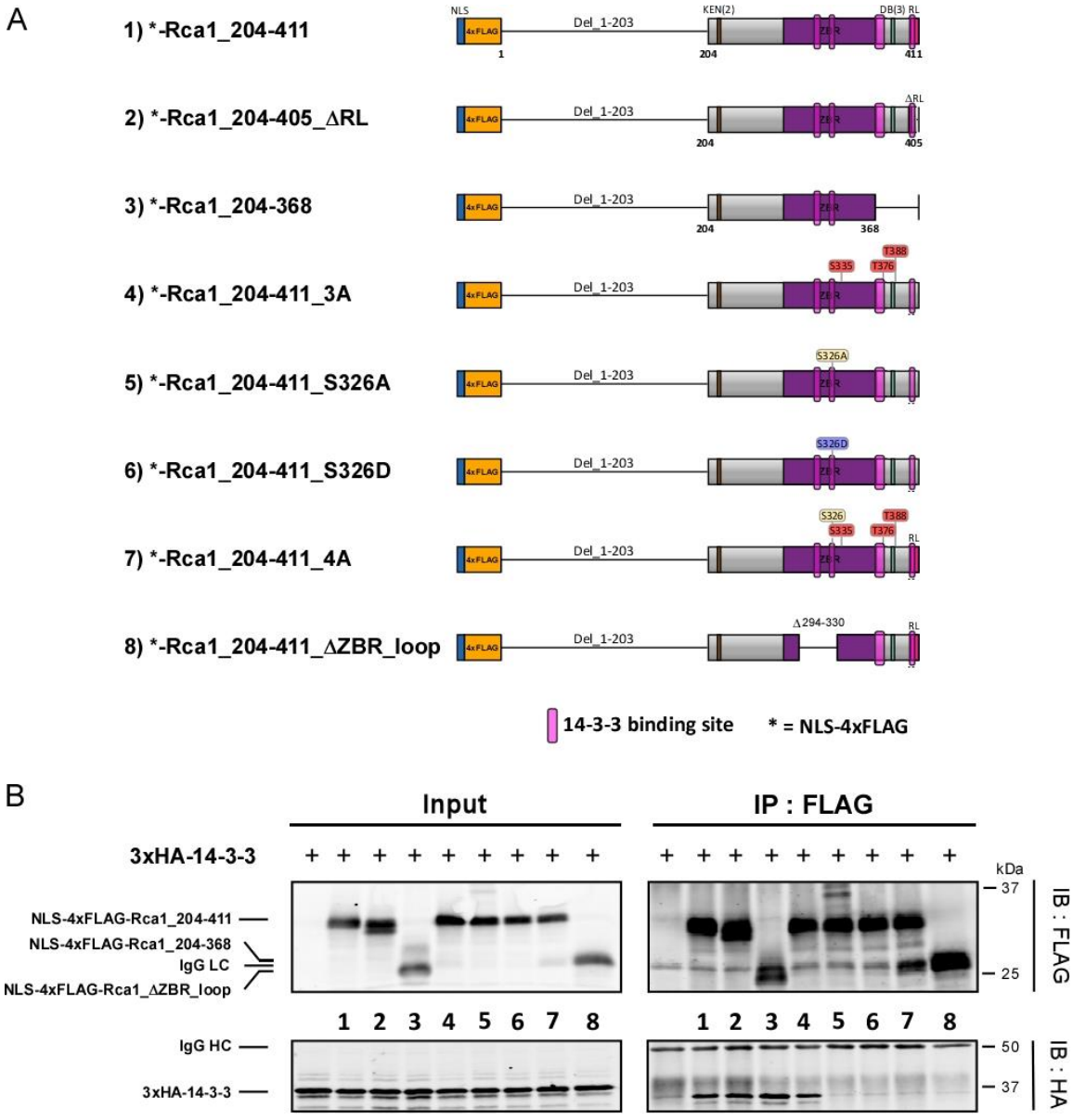

Figure 61| Interaction between Rca1 and 14-3-3 depends on the phosphoserine S326

(**A**) Illustration of the NLS-4xFLAG-Rca1_204-411 mutants for co-immunoprecipitation with 3xHA-14-3-3. (**B**) Co-IP between different NLS-4x-FLAG-Rca1_204-411 constructs and 3xHA-14-3-3. Mutation of S326 and deletion of the 14-3-3 binding site #2 caused a loss of 14-3-3 interaction.

In conclusion, it was shown that Rca1 associates with 14-3-3 via a C-terminal interaction site located within the ZBR_loop (see 3.3.5) and that the phosphorylation site S326 is essential for interaction with 14-3-3.

3.4.3.2. Loss of 14-3-3 interaction has no impact on Rca1 stability

Having established that Rca1 associates with 14-3-3 protein via its C-terminus, it was investigated if loss of 14-3-3 binding would influence Rca1 degradation by a similar mechanism as shown for budding yeast APC/C inhibitor Acm1. Therefore, relative protein stability levels were determined for a C-terminal Rca1 fragment containing the point mutation S326A or S326D that abolished 14-3-3 interaction. Flow cytometric analysis of GFP-T2A-CHE-Rca1_204-411_S326A showed no difference in the CHE/GFP ratios in the three cell populations (CHE/GFP - G1: 0.37, S: 0.50, G2: 0.57) compared to the control (CHE/GFP - G1: 0.35, S: 0.49, G2: 0.57). Also, substitution of serine 326 to aspartate, GFP-T2A-CHE-Rca1_204-411_S326D, did not cause a change in relative protein stability levels (CHE/GFP - G1: 0.40, S: 0.54, G2: 0.60) (Figure 62 A).

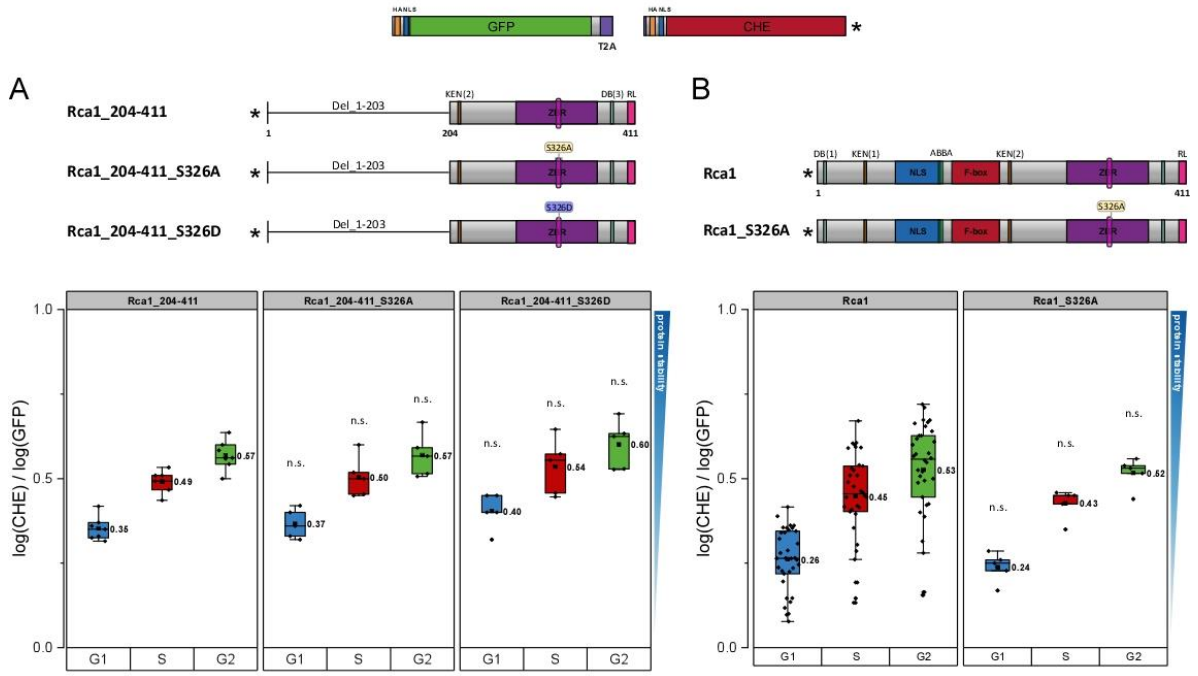

Figure 62| Loss of 14-3-3 interaction has no impact on Rca1 stability

Flow cytometric analysis of the Rca1 mutants unable to bind 14-3-3 protein in the G1, S- and G2-populations (exp.lvl. 1.0 - 1.75). The respective Rca1 mutants are displayed above the corresponding box plot. (**A**) Analysis of relative protein stability levels of GFP-T2A-CHE-Rca1_204-411-S326A or -S326D. Loss of 14-3-3 interaction had no influence on Rca1_204-411 stability levels. (**B**) Loss of 14-3-3 association did not cause a change in relative protein stability levels in case of full-length Rca1. Statistics performed by t-test with Welch´s correction, n.s. > 0.05. The samples were compared to the respective control of unmutated Rca1 of the respective cell cycle phase and symbols for p-values are displayed above the box.

3.4.3.3. Loss of 14-3-3 interaction has no impact on Rca1 function

Considering that the 14-3-3 binding site is located within the ZBR domain that is crucial for APC/C inhibition (see 3.3.5), it could also be possible that 14-3-3 binding is involved in regulation of Rca1 function instead of Rca1 degradation. To test this hypothesis, Rca1_204-411_S326A and -S326D were tested on their ability to inhibit APC/C^{Fzr} activity in the *in vivo* APC/C assay. Co-overexpression of either NLS-4xFLAG-Rca1_204-411_S326A or NLS-4xFLAG-Rca1_204-411_S326D was able to restore GFP-T2A-CHE-CycB-NT^{285} relative protein stability levels in the G2 cell population after 4xFLAG-Fzr overexpression to a similar extent as NLS-4xFLAG-Rca1_204-411 (Figure 63). Thus, interaction between Rca1 and 14-3-3 had no effect on Rca1 function as both mutants were fully capable of restraining APC/C^{Fzr} activity.

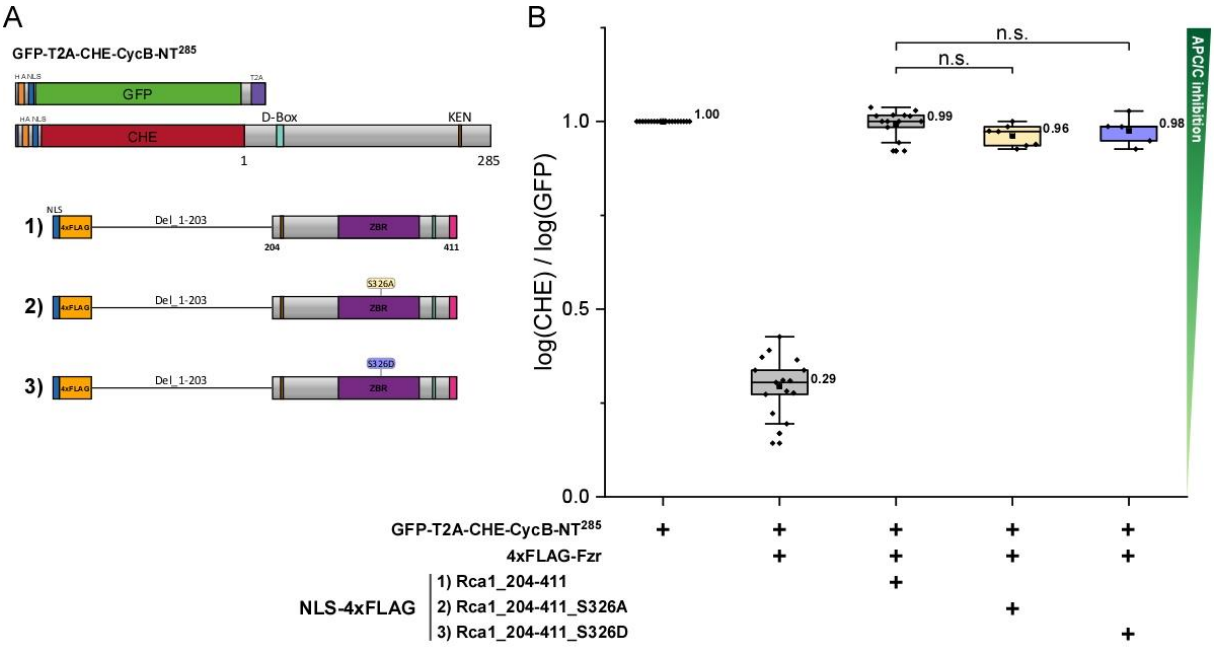

Figure 63| 14-3-3 binding is not involved in regulation of Rca1 function

Analysis of APC/C inhibition by Rca1_204-411 mutants unable to bind 14-3-3. (**A**) Illustration of the RPS-CycB sensor and the corresponding NLS-4xFLAG tagged Rca1_204-411 mutants. (**B**) Box plot of relative protein stability levels of GFP-T2A-CHE-CycB-NT^{285} with additional co-overexpression of 4xFLAG-Fzr and the corresponding NLS-4xFLAG-Rca1_204-411 mutants in G2-cells (exp.lvl. 2.0 - 3.0). Mutation of S326 to alanine (yellow box) or aspartate (blue box) had no effect on Rca1 function. Statistics performed by Mann-Whitney U-Test, n.s. > 0.05.

3.4.3.4. Cell cycle dependent interaction of Rca1 and 14-3-3

Loss of 14-3-3 interaction had no effect on Rca1 stability nor its function as an APC/C inhibitor. To further elucidate the function of 14-3-3 interaction with Rca1, it should be determined if the interaction takes place during a specific cell cycle phase. Therefore, 14-3-3 was tested for its ability to bind Rca1 by co-immunoprecipitations in S2R+ cell lysates that were attempted to be chemically enriched either in mitosis, G1-, S-, or G2-phase. Unfortunately, the proposed cell cycle changes were not very pronounced in the case of 20-hydroxyecdysone, mimosine, or aphidicolin/hydorxyurea treatment. NLS-4xFLAG-Rca1_204-405_ΔRL was used as bait protein since deletion of the RL-tail did not impair 14-3-3 binding (see 3.4.3.1) but abolished APC/C inhibition (see 3.3.4) and should thereby not cause a

undesired cell cycle shift into G2-phase caused by Rca1 overexpression (Figure 64 A). Cell cycle progression arrest was induced 24 h after transfection by treatment with a final concentration of either 1.7 µM 20-hydroxyecdysone (G2-arrest), 0.5 mM mimosine (G1 arrest), 1µM hydroxyurea and 10 µM aphidicolin (S-phase arrest) for at least 24 h or with 30 µM colchicine (mitotic arrest) for 12h. Co-precipitation of 3xHA-14-3-3 was observed for all samples to a similar extent and no difference in 14-3-3 binding to NLS-4xFLAG-Rca1_204-405_ΔRL was distinguishable between the different cell lysates (Figure 64 B). Nevertheless, flow cytometric analysis of the cell cycle distributions of Hoechst-stained cells applied for the co-IP assay showed that chemically induced cell cycle arrest was only successful in case of mitotic arrest, whereas G1-, S-, and G2-arrest was not achieved (Figure 64 C) Thus, chemically induced cell cycle arrest was not accomplished in this experiment and consequently it was not possible to predict if Rca1 interaction with 14-3-3 protein occurs during a specific cell cycle stage. Unfortunately, a successful execution of the experiment was not achieved in the course of this thesis.

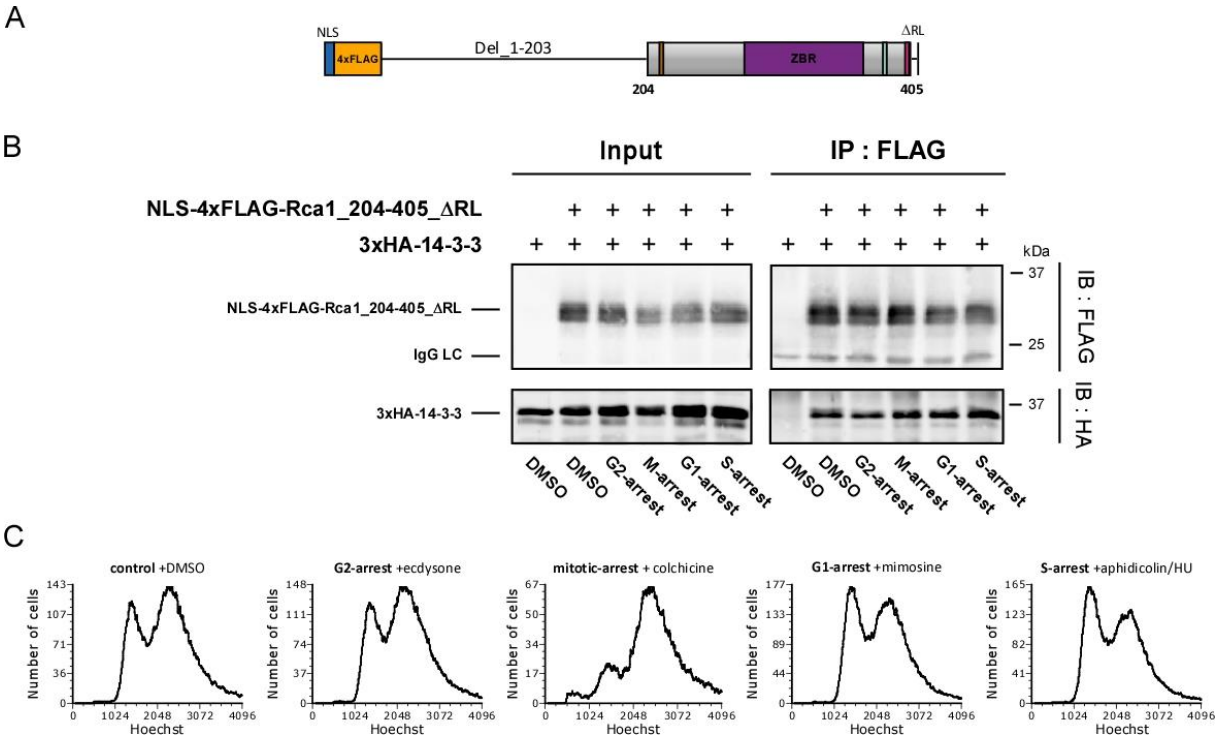

Figure 64| Temporal interaction of Rca1 and 14-3-3 during cell cycle progression

(**A**) Illustration of the NLS-4xFLAG-Rca1_204-405_ΔRL mutant for co-immunoprecipitation with 3xHA-14-3-3. (**B**) Co-IP between NLS-4xFLAG-Rca1_204-405_ΔRL and 3xHA-14-3-3 in cell lysates of cells treated either with 20-Hydroxyecdysone, colchicine, mimosine, or aphidicolin/hydroxyurea. 14-3-3 interaction was observed in all cases. (**C**) Flow cytometric analysis of the cell cycle distributions based on Hoechst intensities. Only mitotic arrest was observed by an elevated G2-peak.

In summary, an interaction between Rca1 and 14-3-3 was verified and it was possible to identify the 14-3-3 binding site within Rca1 C-terminal region that mediates 14-3-3 binding. It was further shown that 14-3-3 binding requires the phosphoserine residue at position 326 located within the 14-3-3 binding site. Nevertheless, loss of 14-3-3 interaction has not displayed any effect on Rca1 stability, nor did

it cause any change in Rca1 function. It was not possible to distinguish when interaction between 14-3-3 and Rca1 takes place in the course of cell cycle progression. Thus, the function of 14-3-3 interaction with Rca1 remains elusive up to this point.

3.4.4. Localization of Rca1 is essential for Rca1 degradation but not its function

Next, subcellular localization of Rca1 was investigated as a third potential regulatory mechanism converting Rca1 from an APC/C inhibitor to a substrate. Localization and partitioning of the APC/C, its two co-activators, and its substrates is likely to contribute to substrate recruitment and ordering (see 2.6.9, also reviewed in Bansal et al., 2019). For instance, the APC/C substrates Securin and Cyclin B are partially regulated in a spatio-temporal manner. Phosphorylated Securin that is mainly located in the cytoplasm is first targeted by APC/C^{Cdc20} followed by a small fraction of Separase bound Securin localized within the nucleus (Shindo et al., 2012). Human Cyclin B is rapidly translocated within the nucleus after Plk1 and MAPK dependent phosphorylation, where it is targeted by chromosome associated APC/C (Yuan et al., 2002). To assess whether spatial abundance of Rca1 contributes to either its degradation or its function as APC/C inhibitor, Rca1 degradation and function were investigated in the context of subcellular localization.

3.4.4.1. Establishment of RPS expression plasmids for localization analysis

Rca1 contains a nuclear localization sequence within its N-terminus and nuclear localization was also confirmed by immunostaining of HA-Rca1 in *Drosophila* embryo (Grosskortenhaus et al., 2002). To assess whether localization in the nucleus is essential for Rca1 degradation it should be tested if changes in the subcellular distribution of Rca1 would affect its relative protein stability levels. However, the RPS reporter constructs used in the previous experiments contained an NLS fusion to the CHE reporter in order to compensate for the loss of endogenous NLS sequences of the applied mutants. In order to investigate the impact of changed subcellular localization two further RPS expression constructs were established based on RPS-8. The N-terminal HA-tag and NLS sequence of the CHE-reporter were removed in case of RPS-9, NLS-GFP-T2A-CHE, whereas the NLS sequence was replaced with a nuclear export sequence (NES; LALKLAGLDI) derived from human kinase A inhibitor (Wen et al., 1995) in RPS-10, NLS-GFP-T2A-NES-CHE (Figure 65 A). The two new RPS constructs were tested for their stoichiometric co-expression of the GFP-reference and the CHE-reporter as conducted for the basic RPS expression plasmids (see 3.1.2).

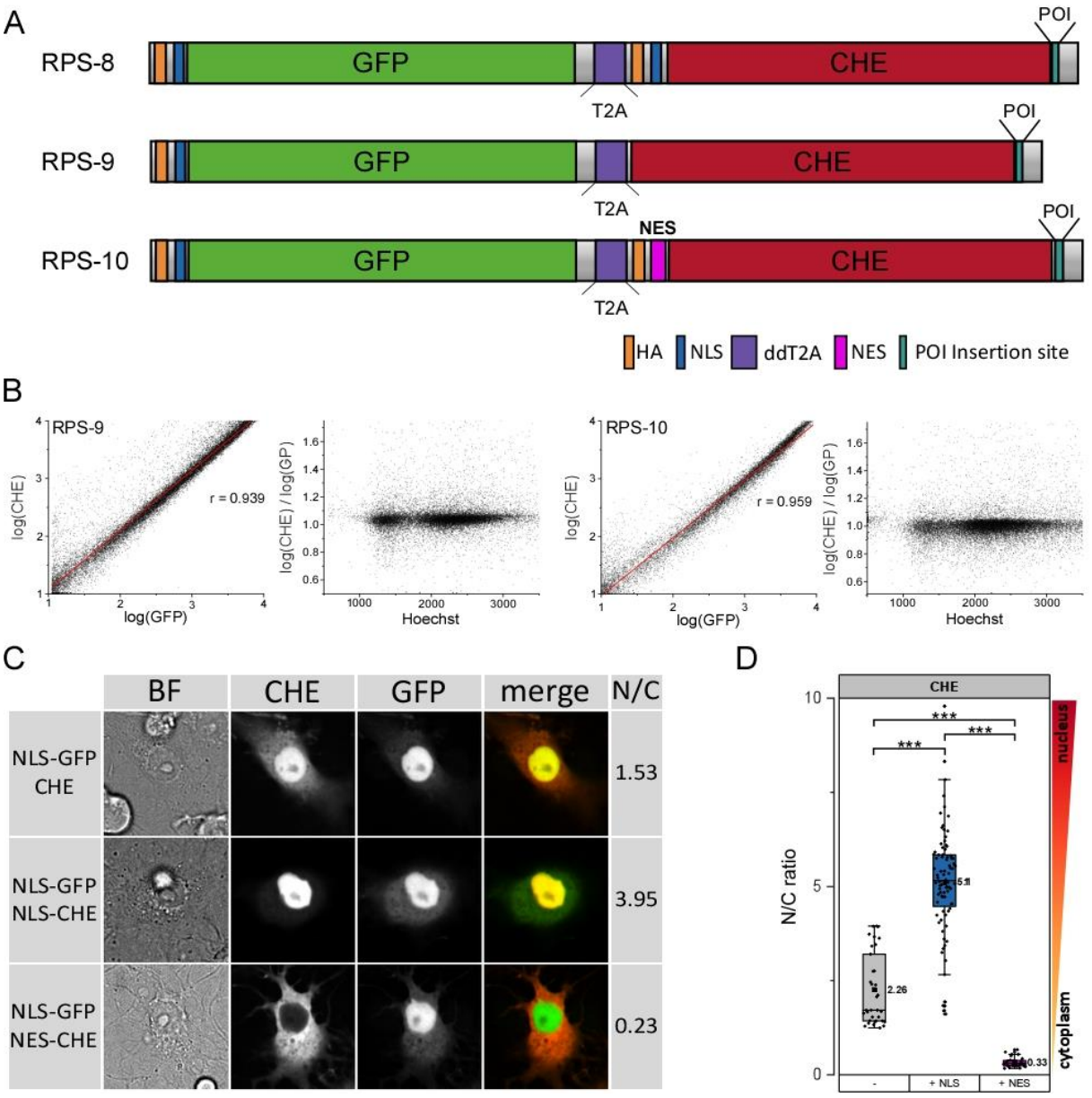

Figure 65| Establishment of RPS constructs for localization analysis

(**A**) Schematic illustration of the RPS expression constructs RPS-8 to -10. The HA-NLS tag N-terminal to the CHE reporter was removed in RPS-9 and replaced by an NES (pink) in RPS-10 (**B**) Scatter plots of CHE and GFP intensities of cells transfected with the respective RPS plasmid detected by flow cytometry. Regression lines (red) and resulting R^2 values (r) are indicated. The log(CHE)/log(GFP) quotient was plotted against the Hoechst intensities representing the cellular DNA content. (**C**) Exemplary illustration of a cell transfected with the respective expression construct depicted in the brightfield (BF), CHE- and GFP channel. The N/C ratio is indicated next to the microscopic picture. (**D**) Box plot summarizing the N/C ratios of the analyzed cells. CHE predominantly accumulates within the nucleus, whereas addition of a NLS increases nuclear accumulation and addition of a NES results in cytoplasmatic localization. Raw data of **C** and **D** from Bischof, 2020. Statistics performed by Mann-Whitney U-Test, n.s. > 0.05, * ≤ 0.05, **≤ 0.01, ***≤ 0.001.

Flow cytometric measurement of the GFP and CHE intensities of S2R+ cells transiently transfected with RPS-9 and RPS-10 displayed a high degree of co-linearity with R^2 values of 0.939 and 0.959, respectively. Analysis of the CHE/GFP quotient in dependence of the DNA content recorded by the Hoechst intensities also displayed relatively stable expression among cells of different cell cycle stages (Figure 65 B). Thus, protein co-expression using the new RPS constructs resulted in a stoichiometric production

of the two fluorescent proteins with a high degree of co-linearity, similar to the already established RPS constructs. This also indicates that the measurement procedure was not negatively biased by the nuclear accumulated GFP signal and the dispersed cytoplasmic CHE signal.

Protein localization was also verified and quantified by microscopic localization analysis that has been conducted in the course of a bachelor thesis (Bischof, 2020).In addition to the initial analysis, the obtained data was statistically evaluated and presented supplementary to the flow cytometric analysis. Based on threshold setting of the nuclear NLS-GFP reference signals, an inner region of the nucleus and a region representing the cytoplasm were defined (see 6.6.2). The CHE intensities were measured within these regions and a nucleus/cytoplasm (N/C) ratio of the CHE signal was calculated as a unit for nuclear localization for each cell (see 6.6.3). This means, an N/C ratio of 1.0 represents an equal distribution between the nucleus and cytoplasm of the CHE-POI, whereas values greater than 1.0 correspond to nuclear accumulation and ratios lower than 1.0 represent predominantly cytoplasmic accumulation of the CHE-POI. Localization analysis of RPS-8, RPS-9, and RPS-10 resulted in an N/C ratio of 2.26 for CHE (RPS-9), 5.11 for NLS-CHE (RPS-8) and 0.33 for NES-CHE (RPS-10) (Figure 65 C, D). Consequently, addition of an exogenous NLS significantly increased nuclear accumulation of NLS-CHE, whereas addition of a NES resulted in a strong cytoplasmic localization of NES-CHE. Surprisingly, CHE without an exogenous localisation signal was still predominately localized within the nucleus. This could be explained by the presence of two putative bipartite NLS sequences predicted by the cNLS mapper (Kosugi et al., 2008, 2009 a; b) that could cause a nuclear accumulation of CHE protein (Bischof, 2020). Additionally, a passive diffusion into the nucleus of CHE which has a molecular size of approximately 26.7 kDa cannot be excluded since passive diffusion through nuclear pore complexes is thought to just decrease beyond a 30-60 kDa size threshold (Timney et al., 2016). Nevertheless, in comparison to CHE, nuclear localization was either significantly increased with an additional NLS or nearly omitted by fusion of a NES. Hence, the three constructs were applied for localization analysis of Rca1 in the following.

3.4.4.2. Nuclear localization is required for sufficient Rca1 degradation

To assess whether Rca1 localization was altered using the established RPS-constructs, Rca1 was inserted into RPS-9 and RPS-10 in addition to RPS-8 which was already used in the previous experiments and localization of the different constructs was determined via microscopic analysis (Figure 66 A, B). Consistent with previous results (Grosskortenhaus et al., 2002), expression of NLS-GFP-T2A-CHE-Rca1 resulted in a nuclear accumulation of CHE-Rca1 (N/C: 3.00) which was also increased compared to just the CHE-reporter (N/C: 2.26) (compare Figure 65 D and Figure 66 C). The presence of an additional NLS sequence, as in NLS-GFP-T2A-NLS-CHE-Rca1 further increased translocation of NLS-CHE-Rca1 (N/C: 3.72) within the nucleus, whereas NLS-GFP-T2A-NES-CHE-Rca1 was exported from the nucleus, seen by a predominantly cytoplasmic accumulation of NES-CHE-Rca1 (N/C: 0.71) (Figure 66 B, C).

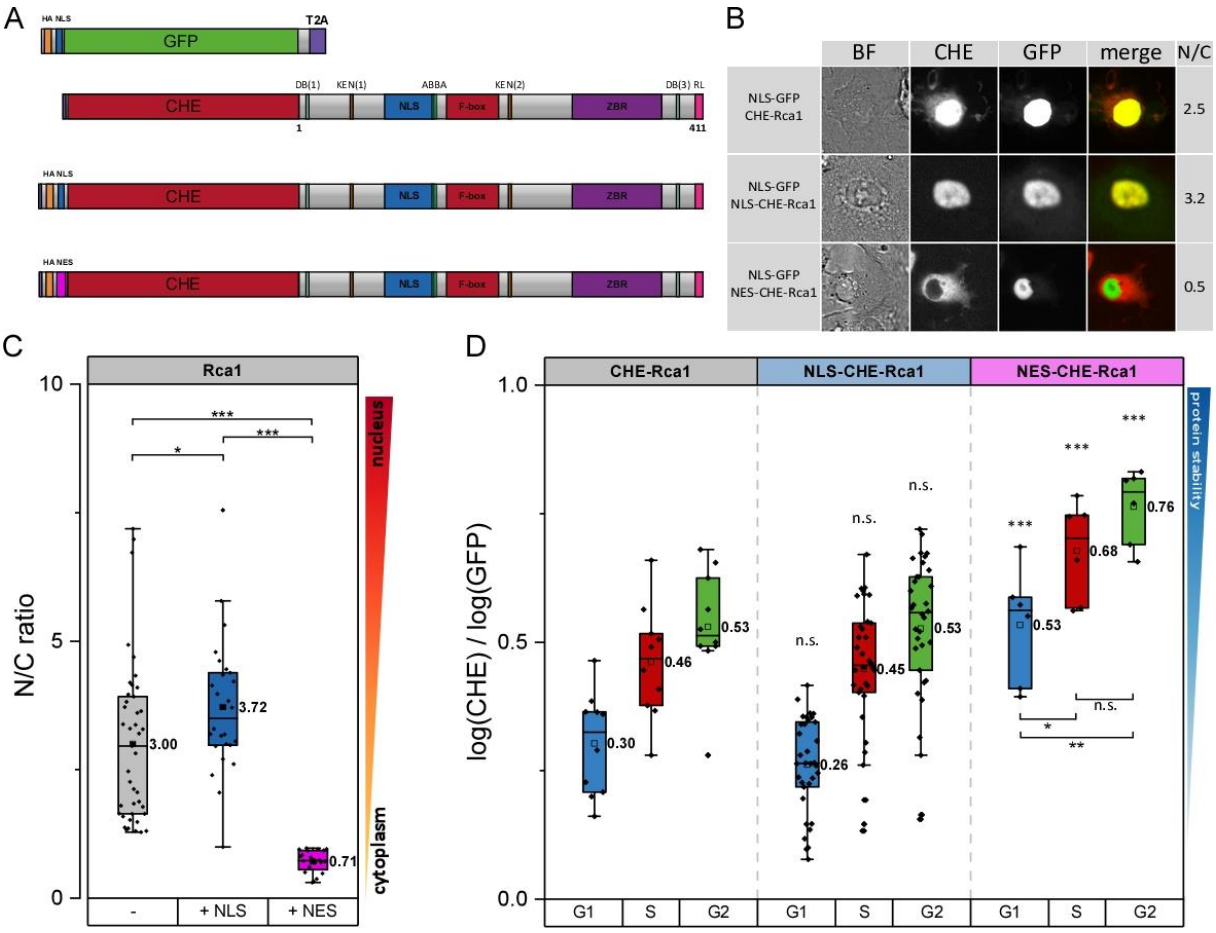

Figure 66| Nuclear localization of Rca1 is essential for its degradation

(**A**) Schematic illustration of CHE-, NLS-CHE-, and NES-CHE-Rca1 RPS constructs. (**B**) Exemplary illustration of a cell transfected with respective expression construct depicted in the brightfield (BF), CHE- and GFP-channel. The N/C ratio is indicated next to the microscopic picture. (**C**) Box plot summarizing the N/C ratios of the analyzed cells. CHE-Rca1 and NLS-CHE-Rca1 accumulate in the nucleus. NES-CHE-Rca1 is exported from the nucleus and is located in the cytoplasm. Raw data of **B** and **C** from Bischof, 2020. (**D**) Analysis of relative protein stability levels of CHE-, NLS-CHE-, and NES-CHE-Rca1 in G1-, S-, and G2-cells (exp.lvl. 1.0 - 1.75).Cytoplasmic localized NES-CHE-Rca1 is stabilized compared to CHE- and NLS-CHE-Rca1. Statistics performed by Mann-Whitney U-Test, n.s. > 0.05, * ≤ 0.05, **≤ 0.01, ***≤ 0.001. . The samples were compared to CHE-Rca1 of the respective cell cycle phase and symbols for p-values are displayed above the box. Comparison of the values within one group are indicated by bars below the boxes.

Thus, it was possible to alter Rca1 localization using the established expression system and either enhance or omit nuclear localization of Rca1. To test whether Rca1 degradation is modified in correlation to its subcellular localization, relative protein stability levels of the established constructs were determined via flow cytometry. Relative protein stability levels were not altered between NLS-GFP-T2A-CHE-Rca1 and NLS-GFP-T2A-NLS-CHE-Rca1 (CHE/GFP - G1: 0.30/0.26, S: 0.46/0.45, G2: 0.53/0.53). Thus, the slightly increased nuclear accumulation of NLS-CHE-Rca1 had no impact on its stability compared to CHE-Rca1. Opposed to this, fusion to NES-CHE (as in NLS-GFP-T2A-NES-CHE-Rca1) caused a significant stabilization in all three cell cycle populations (CHE/GFP - G1: 0.53, S: 0.68, G2: 0.76). However, the CHE/GFP ratio of the G1-cell population was still significantly decreased compared to the S- and G2-cell population, indicating that NES-CHE-Rca1 is still degraded during G1-phase (Figure 66 D).

Next, degradation of the C-terminal part of Rca1 in dependence on its subcellular localization was analyzed in the same way as conducted for Rca1 (Figure 67 A). NLS-GFP-T2A-CHE-Rca1_204-411 showed decreased nuclear accumulation (N/C: 1.56) compared to CHE-Rca1 (N/C: 3.00), which was expected due to the deletion of the N-terminal NLS sequence. Fusion to NLS-CHE (as in NLS-GFP-T2A-NLS-CHE-Rca1_204-411) caused a strong translocation into the nucleus (N/C: 3.90), whereas fusion to NES-CHE (as in NLS-GFP-T2A-NES-CHE-Rca1_204-411) resulted in a predominantly cytoplasmic localization (N/C: 0.65) consistent with the results obtained for full-length Rca1 (Figure 67 B, C). Surprisingly, CHE-Rca1_204-411 which lacks the endogenous NLS displayed N/C ratios greater than 1.0 and was consequently still localized within the nucleus although to a lesser

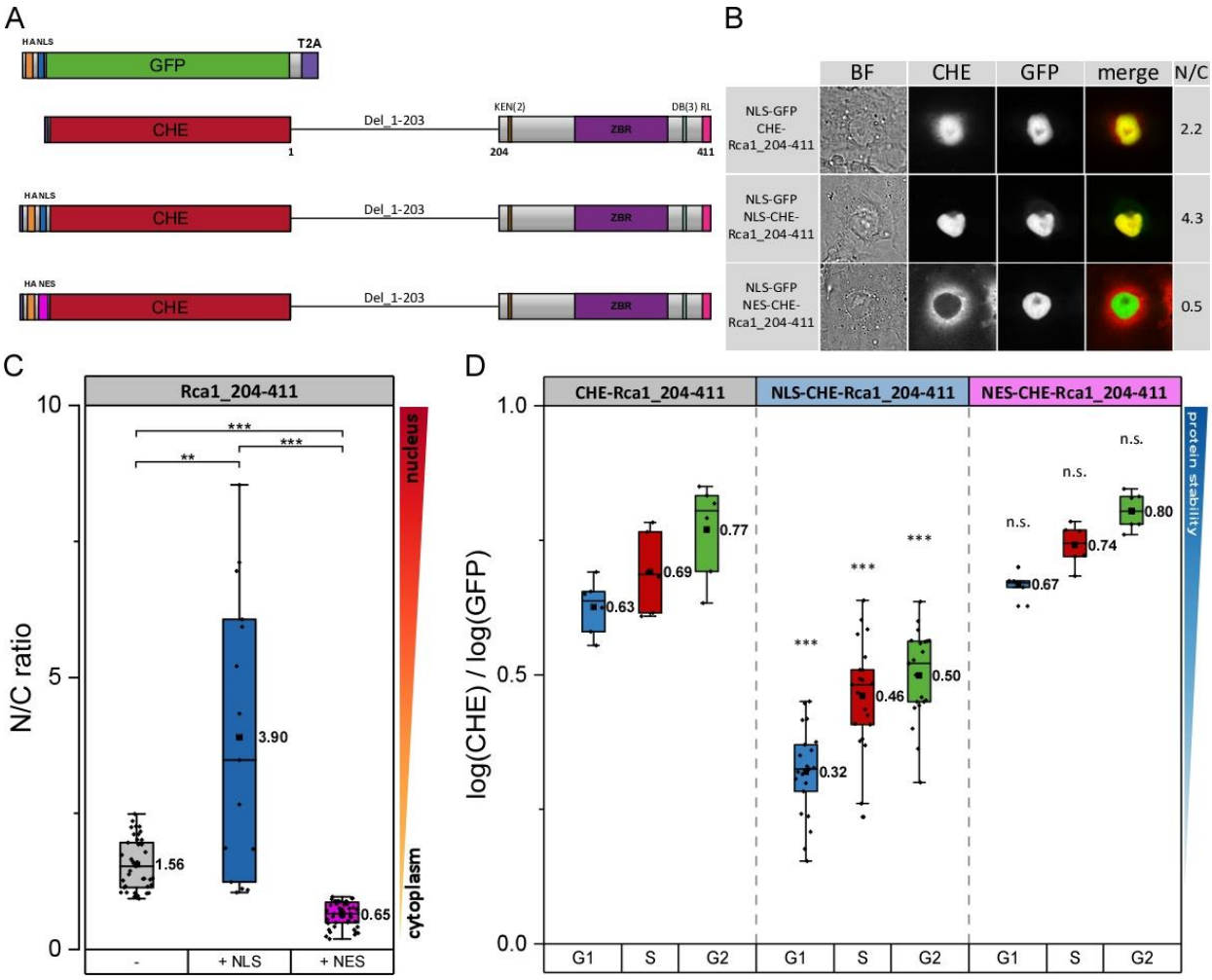

Figure 67| Cytoplasmic localization of Rca1_204-411 increases its stability

(**A**) Schematic illustration of CHE-, NLS-CHE-, and NES-CHE-Rca1_204-411 RPS constructs. (**B**) Exemplary illustration of a cell transfected with respective expression construct depicted in the brightfield (BF), CHE- and GFP channel. The N/C ratio is indicated next to the microscopic picture. (**C**) Box plot summarizing the N/C ratios of the analyzed cells. CHE-Rca1_204-411 is still localized within the nucleus. Fusion to NLS-CHE caused a significant increase of nuclear accumulation whereas NES-CHE fusion resulted in nuclear export. Statistics performed by Mann-Whitney U-Test, n.s. > 0.05, * ≤ 0.05, **≤ 0.01, ***≤ 0.001. Raw data of **B** and **C** from Bischof, 2020. (**D**) Analysis of relative protein stability levels of CHE-, NLS-CHE-, and NES-CHE-Rca1_204-411 in G1-, S-, and G2-cells (exp.lvl. 1.0 - 1.75).CHE- and NES-CHE-Rca1_204-411 were stabilized compared to NLS-CHE- Rca1_204-411. Statistics performed by t-test with Welch´s correction, n.s. > 0.05, * ≤ 0.05, ** ≤ 0.01, ***≤ 0.001. The samples were compared to CHE-Rca1_204-411 of the respective cell cycle phase and symbols for p-values are displayed above the box.

extent as CHE-Rca1. This was explained by the presence of a second bipartite NLS located in the C-terminal region of Rca1 (Figure 68), which will be discussed in more detail in the next section (see 3.4.4.3). Nevertheless, in accordance with its altered subcellular localization, relative protein stability levels of NLS-CHE-Rca1_204-411 (CHE/GFP - G1: 0.32, S: 0.46, G2: 0.50) were significantly reduced compared to CHE-Rca1_204-411 (CHE/GFP - G1: 0.63, S: 0.69, G2: 0.77), whereas NES-CHE-Rca1_204-411 was not further stabilized in the three cell populations (CHE/GFP - G1: 0.67, S: 0.74, G2: 0.80). The elevated CHE/GFP ratios of CHE-Rca1_204-411 indicate that nuclear localization of this construct was no longer sufficient for proper degradation. However, similar to the results of full-length Rca1, nuclear export of Rca1_204-411 caused a stabilization but CHE-Rca1_204-411 as well as NES-CHE-Rca1_204-411 were still destabilized in the G1-cell population compared to S- and G2-cells (Figure 67 D). In conclusion, the results of full-length and C-terminal Rca1 indicate that nuclear localization of Rca1 is essential for proper degradation of Rca1 during G1-phase, whereas ectopic cytoplasmic localization results in an enhanced although not complete stabilization of Rca1.

3.4.4.3. 14-3-3 interaction enhances Rca1 export from the nucleus

Having shown that subcellular localization of Rca1 has a distinct influence on its degradation, the Rca1 sequence was scanned for localization signals. Besides the known N-terminal bipartite NLS a potential NES sequence and a second NLS sequence in the C-terminal region of Rca1 were identified in a bioinformatic screen of the Rca1 sequence using the NetNES server (La Cour et al., 2004) and the cNLS mapper (Kosugi et al., 2008, 2009 a; b) (Figure 68). A recent study has shown that inactivation of the C-terminal NLS by the point mutation K322A enhances cytoplasmic accumulation of C-terminal Rca1 as well as full-length Rca1 with an additional deletion of the N-terminal NLS (Bischof, 2020). Thus, it can be assumed that the second NLS located in the C-terminal region of Rca1 is also functional. Since both the putative NES and the second NLS overlap with the 14-3-3 binding site, the question arose if 14-3-3 interaction could be involved in regulation of Rca1 localization. For instance, 14-3-3 binding to Cdc25 causes a cytoplasmic sequestration of Cdc25 by blocking its NLS at the G2/M transition (Kumagai et al., 1998; Gardino et al., 2011). Rapid export of the transcription factor FKHRL1 from the nucleus is achieved by a cooperative mechanism including phosphorylation dependent binding of 14-3-3 and a NES sequences within the bound ligand (Brunet et al., 2002). Furthermore, it was speculated that phosphorylation dependent 14-3-3 binding to Acm1 interferes with its nuclear import (Enquist-Newman et al., 2008). To test if 14-3-3 binding might function in regulation of Rca1 sequestration, the impact of 14-3-3 interaction was analyzed in dependence of Rca1 localization.

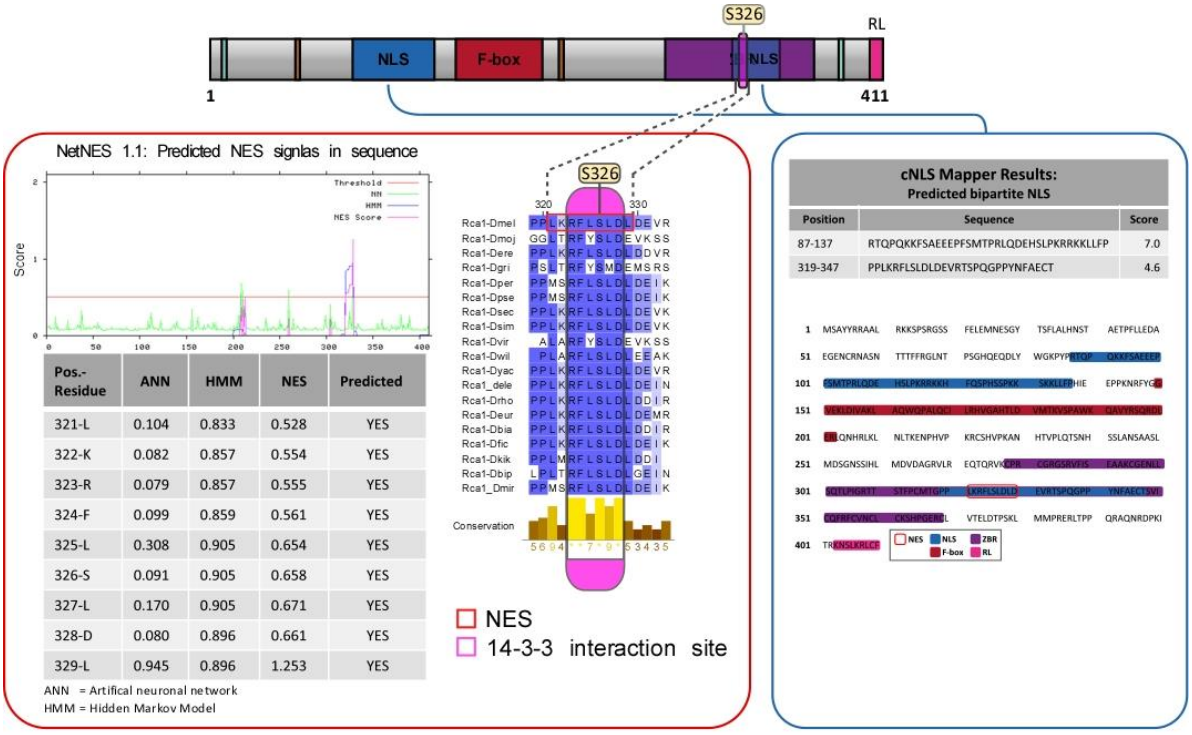

Pos.-Residue	ANN	HMM	NES	Predicted
321-L	0.104	0.833	0.528	YES
322-K	0.082	0.857	0.554	YES
323-R	0.079	0.857	0.555	YES
324-F	0.099	0.859	0.561	YES
325-L	0.308	0.905	0.654	YES
326-S	0.091	0.905	0.658	YES
327-L	0.170	0.905	0.671	YES
328-D	0.080	0.896	0.661	YES
329-L	0.945	0.896	1.253	YES

ANN = Artifical neuronal network
HMM = Hidden Markov Model

Figure 68| Prediction of NES and NLS signals of Rca1

Red box - Prediction of a potential NES using the NetNES server (La Cour et al., 2004). The predicted NES sequence (red box) overlaps with the 14-3-3 binding site (pink box). Blue box - Prediction of NLS sequences using the cNLS mapper (Kosugi et al., 2008, 2009 a; b). Besides the N-terminal NLS, a further NLS is located in the C-terminal region of Rca1 that overlaps with both, the 14-3-3 binding site and the putative NES.

Microscopic localization analysis of the C-terminal Rca1 fragment, Rca1_204-411_S326A, which is unable to bind 14-3-3 (see 3.4.3.1) displayed an increased nuclear accumulation of NLS-GFP-T2A-CHE-Rca1_204-411_S326A (N/C: 3.02) compared to CHE-Rca1_204-411 (N/C: 1.56). Surprisingly, NLS-GFP-T2A-NLS-CHE-Rca1_204-411_S326A (N/C: 2.60) displayed a less pronounced translocation into the nucleus compared to NLS-CHE-Rca1_204-411 (N/C: 3.90). However, the data of NLS-CHE-Rca1_204-411 displayed a high variability as seen by the broad spacing of the box plot and further replicates should be included to make a more reliable statement on NLS-CHE_Rca1_204-411 localization. Loss of 14-3-3 interaction had no effect on localization of NLS-GFP-T2A-NES-CHE-Rca1_204-411_S326A compared to the control, as both proteins were predominantly accumulated in the cytoplasm (N/C: 0.65) (Figure 69 A, B, C). Next, relative protein stability levels of the different constructs were determined via flow cytometry. Loss off 14-3-3 interaction had no effect on relative protein stability levels in the G1-cell population in case of CHE-Rca1_204-411_S326A (CHE/GFP - G1: 0.63 to 0.65) and NLS-CHE-Rca1_204-411_S326A (CHE/GFP - G1: 0.26 to 0.23) compared to the control. Opposed to this, stability of NES-CHE-Rca1_204-411_S326A was significantly decreased compared to NES-CHE-Rca1_204-411 (CHE/GFP - G1: 0.67 to 0.52) (Figure 69 D). This was rather surprising, since disruption of 14-3-3 interaction resulted in a significantly elevated nuclear accumulation of CHE-Rca1_204-411 but did not affect its relative protein stability levels. In contrast, NES-CHE-Rca1_204-411 localization was not altered by loss of

14-3-3 binding but relative protein stability levels were significantly decreased in the G1-cell population.

To assess whether similar effect would be observed for full-length Rca1, localization and stability analysis of Rca1_S326A was conducted in the same way. Microscopic analysis of NLS-CHE-Rca1_S326A showed an enhanced N/C ratio compared to NLS-CHE-Rca1 (N/C: 3.72 to 4.75), whereas no changes in subcellular localization of Rca1 were observed for CHE-Rca1_S326A (N/C: 3.00 to 3.01) and NES-CHE-Rca1_S326A (N/C: 0.71 to 0.80) (Figure 69 E, F, G). Thus, an increased nuclear accumulation of NLS-CHE-Rca1_S326A was observed similar to CHE-Rca1_204-411_S326A although the effect was not seen in case of CHE-Rca1_S326A .Consistent to the analysis of Rca1_204-411_S326A, flow cytometric analysis of the different Rca1_S326A constructs in the G1-population resulted only in a destabilization in case of NES-CHE-Rca1_S326 (CHE/GFP - G1: 0.53 to 0.46), albeit not being statistically significant, while no changes were observed for CHE-Rca1_S326A (CHE/GFP - G1: 0.30 to 0.33) and NLS-CHE-Rca1_S326A (CHE/GFP - G1: 0.26 to 0.23) (Figure 69 H).

In summary, increased nuclear accumulation of CHE-Rca1_204-411_S326A and NLS-CHE-Rca1_S326A suggest that 14-3-3 binding enhances nuclear export and translocation of Rca1 into the cytoplasm. In line with this hypothesis, the decreased relative stability of NES-CHE-Rca1_204-411_S326A and -Rca1_S326A suggests that loss of 14-3-3 binding causes an increased degradation, which could be explained by an enhanced translocation into the nucleus, albeit both constructs displayed a strong accumulation in the cytoplasm. However, one must mention that in the analysis of protein localization, G2- cells were preferentially chosen for the determination of the nuclear/cytoplasmic ratios since these cells were relatively bigger than G1 cells and were spread out on surface which allowed a better separation of nuclear and cytoplasmic staining. Consequently, the N/C ratios must not directly reflect the subcellular localization of Rca1 in G1-phase, in which protein stability was determined. However, taken into account that localization was determined prevalently for G2-cells, 14-3-3 might be required for cytoplasmic sequestration of Rca1 mainly during G2-phase, indicating a role in the regulation of Rca1 function, which will also be investigated in the following (see 3.4.4.5).

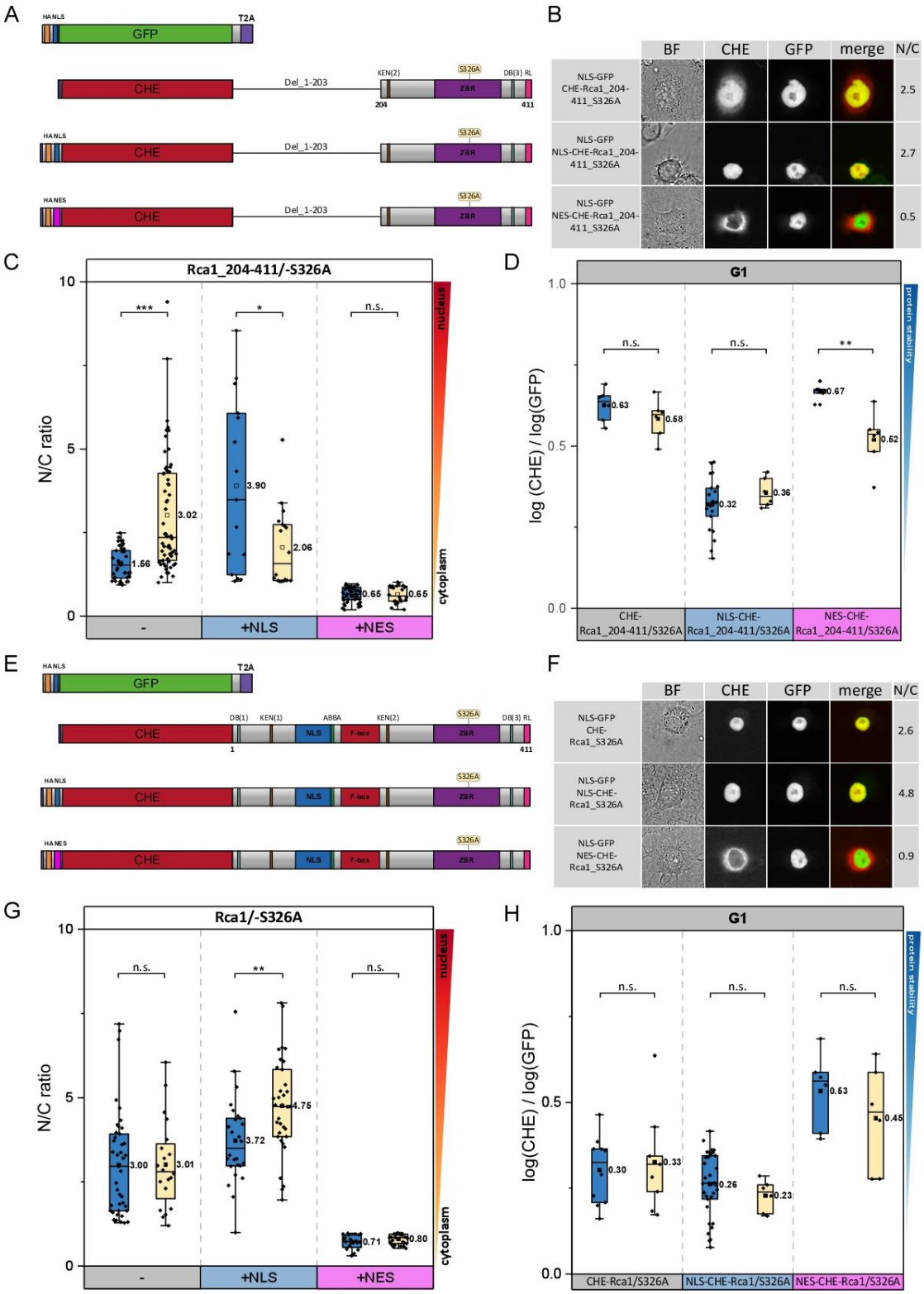

Figure 69| 14-3-3 binding enhances nuclear export of Rca1

(**A**) Schematic illustration of CHE-, NLS-CHE-, and NES-CHE-Rca1_204-411_S326A RPS constructs. (**B**) Exemplary illustration of a cell transfected with the respective expression construct (**C**) Box plot summarizing the N/C ratios of the analyzed cells. (**D**) Analysis of relative protein stability levels of CHE-, NLS-CHE-, and NES-CHE-Rca1_204-411_S326A in G1-cells (exp.lvl. 1.0 - 1.75). (**E**) Schematic illustration of CHE-, NLS-CHE-, and NES-CHE-Rca1_S326A RPS constructs. (**F**) Exemplary illustration of a cell transfected with respective expression construct. (**G**) Box plot summarizing the N/C ratios of the analyzed cells. (**H**) Analysis of relative protein stability levels of CHE-, NLS-CHE-, and NES-CHE-Rca1_S326A in G1-cells (exp.lvl. 1.0 - 1.75). Raw data of **B** ,**C**, **F**, **G** from Bischof, 2020. Statistics of **D** and **H** performed by t-test with Welch´s correction, n.s. > 0.05, * ≤ 0.05, ** ≤ 0.01. Statistics of **C** and **G** performed by Mann-Whitney U-Test, n.s. > 0.05, * ≤ 0.05, **≤ 0.01, ***≤ 0.001.

3.4.4.4. Cdk phosphorylation has an effect on Rca1 localization

Localization of a protein is often modulated through phosphorylation which can result in either an enhancing or inhibitory effect on nuclear import (reviewed in Nardozzi et al., 2010). Sequence analysis of Rca1 for Cdk phosphorylation sites identified 17 putative residues of which several are located within the two predicted NLS domains (Figure 53). As previous experiments have shown, mutation of the ten minimal consensus S/T-P sites resulted in both, a destabilization and a reduction of Rca1 function (see section 3.4.2). To assess whether phosphorylation of Rca1 is involved in regulation of its subcellular localization and whether the observed effects were attributed to changes in Rca1 sequestration, localization of the S/P-T site mutants was analyzed. The same constructs used for the analysis of Cdk-phosphorylation, which uniformly contained an HA-NLS fusion N-terminal to the CHE-reporter were used for the localization analysis for comparability with the already obtained results. Microscopic analysis of NLS-CHE-Rca1_10A displayed a nuclear accumulation (N/C: 3.37) which was not altered compared to NLS-CHE-Rca1 (N/C: 3.72). Opposed to this, nuclear localization of NLS-CHE-Rca1_1-203 (N/C: 3.50) was significantly reduced after mutation of the 7 Cdk sites, seen by more dispersed localization of NLS-CHE-Rca1_1-203_7A (N/C: 1.75). Subcellular localization of Rca1_204-411_3A (N/C: 4.09) was not altered compared to NLS-CHE_Rca1_204-411 (N/C: 3.90) (Figure 70 A, B, C).

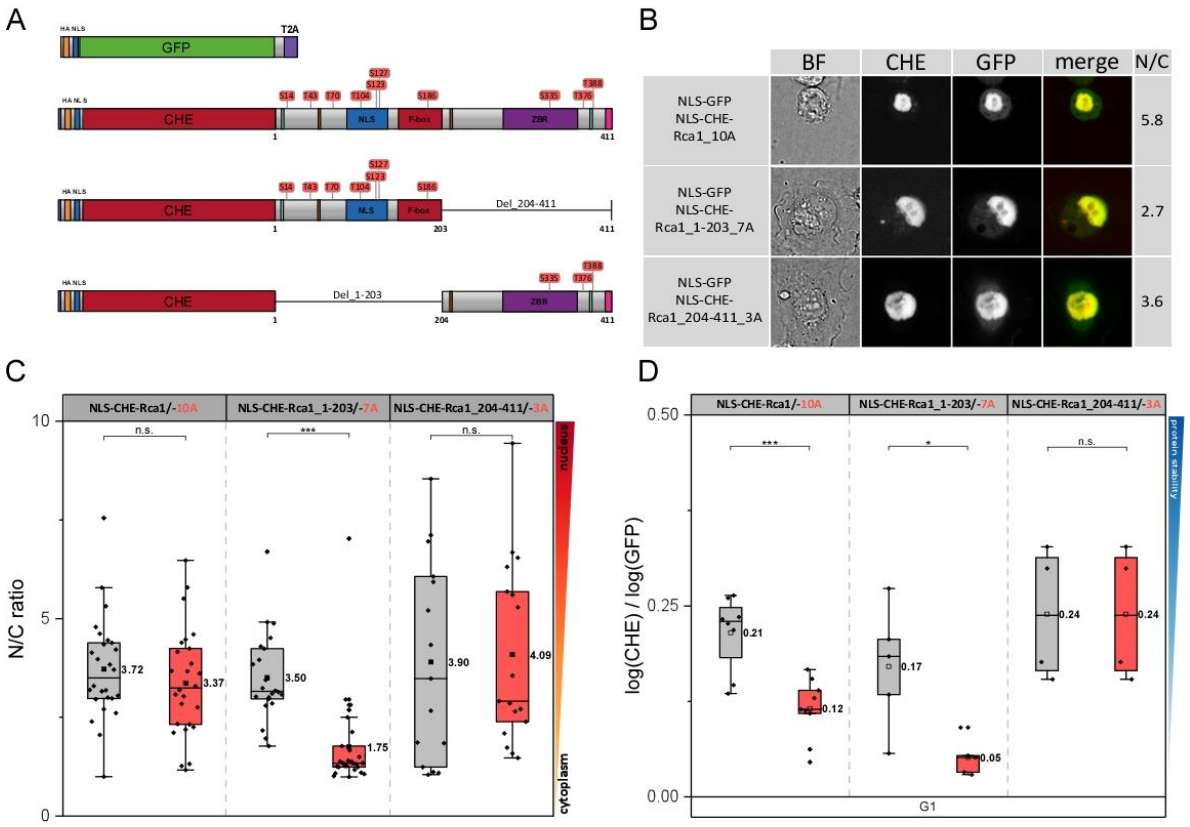

Figure 70| Localization analysis of Rca1 Cdk site mutants

(**A**) Schematic illustration of NLS-CHE-Rca1_10A, -Rca1_1-203_7A, and -Rca1_204-411_3A constructs. (**B**) Exemplary illustration of a cell transfected with respective expression construct depicted in the brightfield (BF), CHE- and GFP channel. (**C**) Box plot summarizing the N/C ratios of the analyzed cells. (**D**) Analysis of relative protein stability levels of the Rca1 Cdk site mutants in G1-cells (exp.lvl. 1.0 - 1.75). Statistics performed by t-test with Welch´s correction, n.s. > 0.05, * ≤ 0.05, ** ≤ 0.01, *** ≤ 0.001.

Stability analysis of the Cdk-site mutants displayed a strong destabilization of NLS-CHE-Rca1 and NLS-CHE-Rca1_1-203, whereas relative protein stability levels of the C-terminal part of Rca1, NLS-CHE-Rca1_204-411, was not affected by changes of its phosphorylation status (see 3.4.2 and Figure 70 D). Thus, decreased nuclear accumulation of NLS-CHE-Rca1_1-203_7A did not directly coincide with its increased destruction in G1-, S, and G2-cells (see 3.4.2.2; Figure 55), since it was shown that nuclear localization enhances Rca1 degradation (see 3.4.4.2) and consequently the 7A mutant should have been stabilized instead of destabilized compared to Rca1_1-203. It can also not be explained why no similar change in subcellular localization was observed for Rca1_10A. Thus, a proper evaluation if Cdk dependent phosphorylation is involved in regulation of Rca1 localization cannot be made with the obtained data, yet. However, the results of Rca1_1-203_7A gave a first hint towards a phosphorylation dependent localization of Rca1 in G2-phase that however must not compulsory be connected to Rca1 degradation.

Furthermore, it was tested if mutation of the two phosphorylation sites S123 and S127 that are located within the NLS and were also shown to be phosphorylated according to the iProteinDB database, would affect Rca1 stability in a localization dependent mechanism. Therefore, Rca1_S123A_S127A was inserted into RPS-8 to RPS-10 and analyzed via flow cytometry (Figure 71 A).

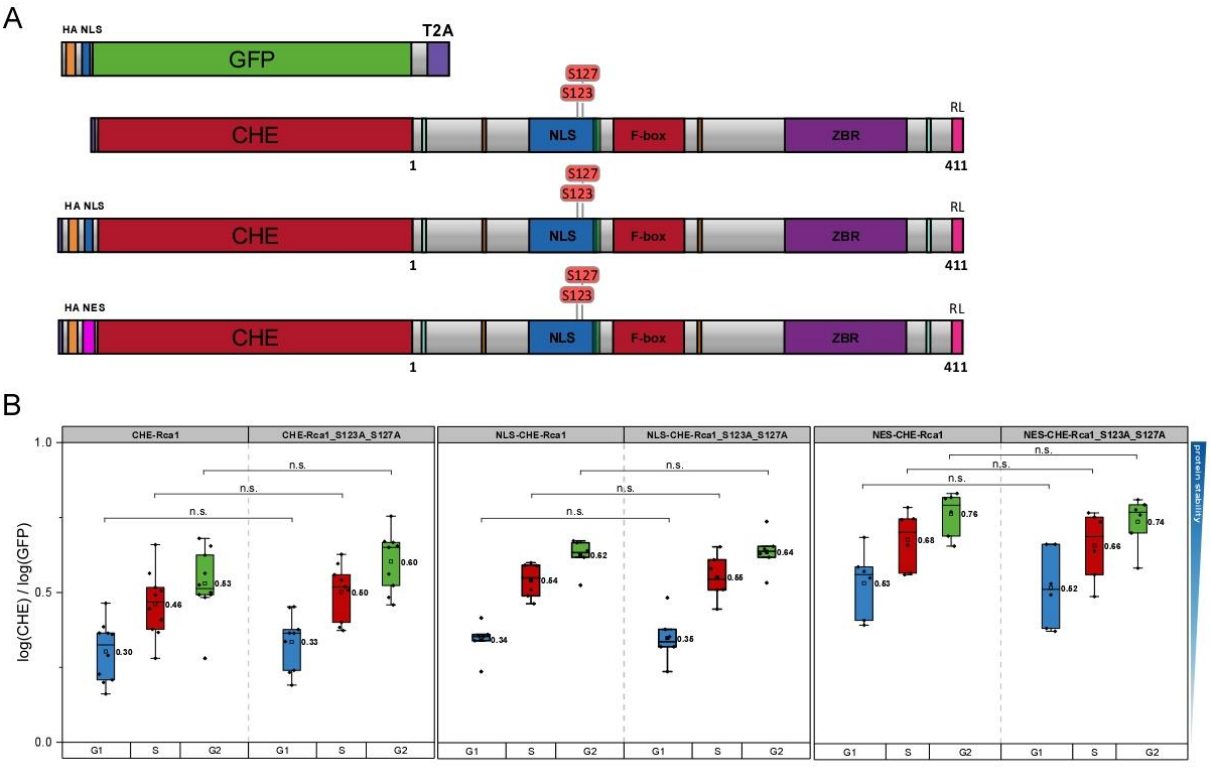

Figure 71| Mutation of S123 and S127 within the NLS does not influence Rca1 degradation

Analysis of relative protein stability levels of CHE-, NLS-CHE-, and NES-CHE-Rca1_S123A_S127A. (**A**) Illustration of the corresponding Rca1_S123A_S127A constructs. (**B**) Flow cytometric analysis of the Rca1_S123A_S127A constructs in the G1, S- and G2-populations (exp.lvl. 1.0 - 1.75). Mutation of the two serine residues only caused a minor stabilization in case of NLS-CHE-Rca1. Statistics performed by t-test with Welch´s correction, n.s. > 0.05, * ≤ 0.05.

However, mutation of the two phosphorylation sites had no effect on Rca1 stability in any of the tested expression constructs (Figure 71 B). Therefore, no microscopic localization analysis was conducted for these constructs. Nevertheless, these results show that these two phosphorylation sites are not causative for altered degradation and that other N-terminal phosphorylation sites must confer the stabilizing effect of Rca1 caused by phosphorylation, which is also consistent with the results of the Phos-tag SDS-PAGE analysis (see 3.4.2.1).

3.4.4.5. Nuclear localization of Rca1 is not essential for APC/C inhibition

Finally, it should also be tested if Rca1 localization constitutes a regulatory mechanism of Rca1 function as an APC/C inhibitor. In the previous analysis regarding Rca1 capacity to restrain APC/C activity, expression constructs containing an NLS-4xFLAG tag were used. To assess whether Rca1 function is altered in correlation with its localization, Rca1 function was analyzed in the APC/C *in vivo* activity assay using either NLS-4xFLAG, 4xFLAG, or a FLAG-NES tagged Rca1 construct. Additionally, the loss of 14-3-3 interaction was investigated since the results of the localization analysis indicated that 14-3-3 binding is probably involved in nuclear export of Rca1.

Analysis of Rca1_204-411 function showed APC/C inhibition was slightly decreased in case of 4xFLAG_Rca1_204-411 (CHE/GFP: G2 - 0.83) and 4xFLAG-NES-Rca1_204-411 (CHE/GFP: G2 - 0.83) compared to NLS-4xFLAG-Rca1_204-411 (CHE/GFP: G2 - 0.99) as both constructs were not able to fully restore NLS-CHE-CycB-NT^{285} levels after 4xFLAG-Fzr overexpression in the G2-cell population. Interestingly, the loss of 14-3-3 interaction completely restored APC/C inhibition in case of 4xFLAG-Rca1_204-411_S326A (CHE/GFP: G2 - 0.98), whereas no significant effect was observed for NLS-4xFLAG_Rca1_204-411_S326A (CHE/GFP: G2 - 0.96) or 4xFLAG-NES_Rca1_204-411_S326A (CHE/GFP: G2 - 0.88) (Figure 72 A, B). This observation can be explained by the additionally NLS or NES that likely masks the mediocre effect of 14-3-3 dependent Rca1 export. It was also tested if 14-3-3 binding has an effect on Rca1 function in the context of full-length Rca1. Since a 14-3-3 dependent effect was only observed for 4xFLAG-Rca1_204-411, Rca1 was just analyzed in that background. Co-overexpression of 4xFLAG-Rca1 did not result in any detectable deficiency of APC/C inhibition (CHE/GFP: G2 - 1.06) compared to NLS-4xFLAG-Rca1 (CHE/GFP: G2 - 1.10). Also, mutation of the 14-3-3 binding site did not show any change in Rca1 function, as seen for 4xFLAG-Rca1_S326A (CHE/GFP: G2 - 1.06) (Figure 72 C, D). This is likely attributed to the presence of the N-terminal NLS in Rca1 causing a stronger nuclear localization compared to C-terminal Rca1 (see 3.4.4.2), which probably masks the effect caused by loss of 14-3-3 interaction.

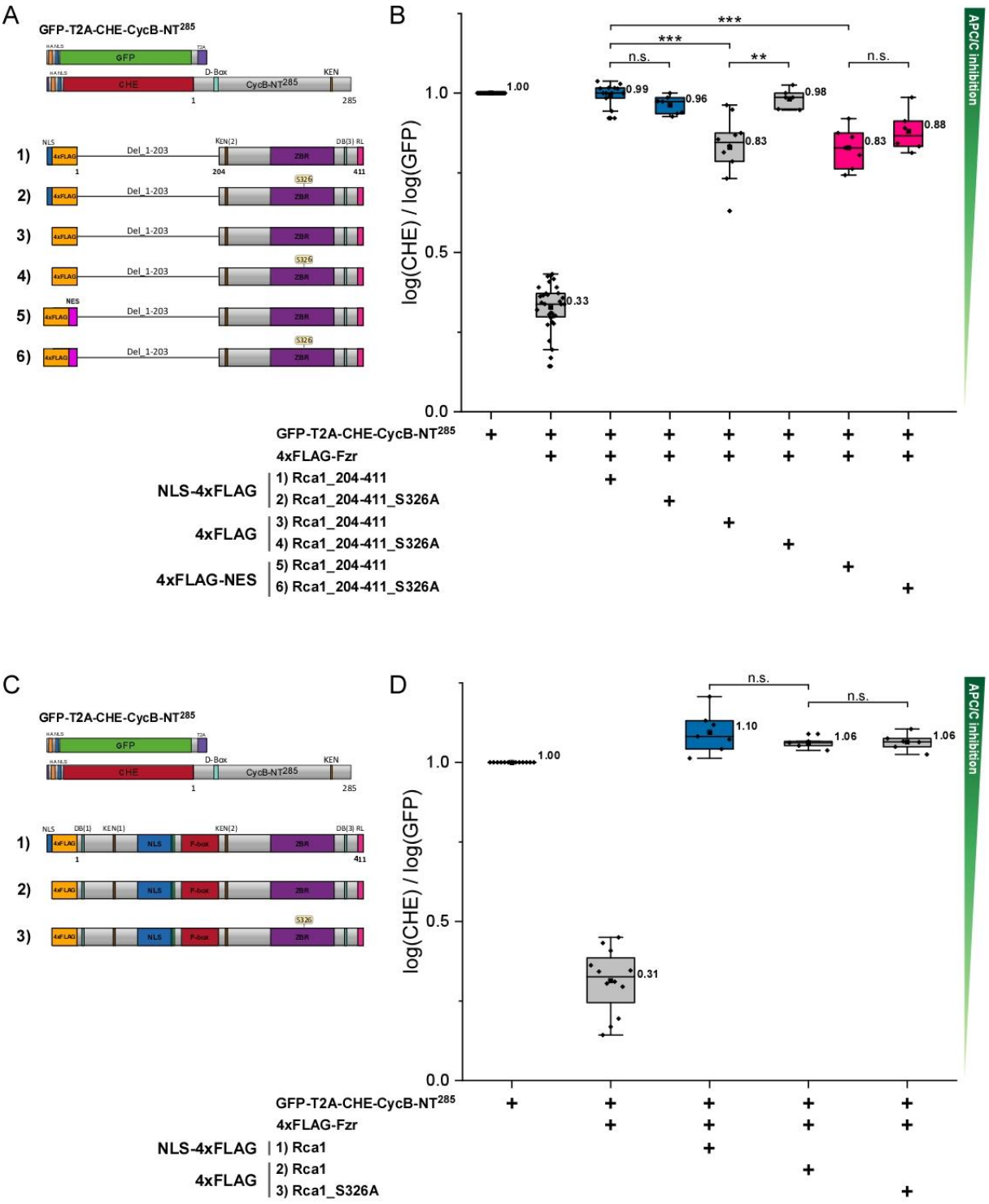

Figure 72| APC/C inhibition by Rca1 is only partially dependent on its nuclear localization

Analysis of APC/C inhibition by Rca1 in dependency of its subcellular localization. (**A**) Illustration of the RPS-CycB sensor and the different 4xFLAG tagged Rca1_204-411 constructs. (**B**) Box plot of relative protein stability levels of NLS-GFP-T2A-NLS-CHE-CycB-NT^{285} with additional co-overexpression of 4xFLAG-Fzr and the respective NLS-4xFLAG-(blue boxes), 4xFLAG- (grey boxes), and 4xFLAG-NES-tagged (pink boxes) Rca1_204-411 versions in G2-cells (exp.lvl. 2.0 - 3.0). C-terminal Rca1 displays a slight reduction of APC/C inhibition without an additional NLS sequence. Statistics performed by Mann-Whitney U-Test, n.s. > 0.05, * ≤ 0.05, ** ≤ 0.01, ***≤ 0.001. (**C**) Illustration of the RPS-CycB sensor and the different 4xFLAG tagged Rca1 constructs. (**D**) Box plot of relative protein stability levels of GFP-T2A-CHE-CycB-NT^{285} with additional co-expression of 4xFLAG-Fzr and NLS-4xFLAG- or 4xFLAG-Rca1. Rca1 function was not impaired without an additional NLS sequence. Statistics performed by t-test with Welch´s correction, n.s. > 0.05.

In conclusion, APC/C inhibition does not rely on a strict localization of Rca1, but analysis of Rca1_204-411 shows that nuclear localized Rca1 is more effective in APC/C inhibition. In addition, a contribution of 14-3-3 interaction can modulate the effectiveness of Rca1-204-411 inhibition, as mutating the 14-3-3 binding site can increase nuclear accumulation and APC/C inhibition.

3.4.4.6. Rca1 can inhibit degradation of nuclear and cytoplasmic Cyclin B

The APC/C is thought to be localized mainly within the nucleus (Kraft et al., 2003; Hubner et al., 2010) and it was shown that subcellular APC/C pools and their activity are essential for substrate ordering (see 3.4.4.6). Consistent with this assumption, APC/C dependent degradation of Rca1 was significantly decreased by a forced export of Rca1 from the nucleus in the cytoplasm (see 3.4.4.2). To further asses, if catalytic APC/C activity is mainly restricted to the nucleus it was also tested if Cyclin B degradation would be impaired in the cytoplasm. Therefore, CycB-NT^{285} that was already used in previous experiments (see 3.1.5.1) was inserted into RPS-10 and its cytoplasmic localization was validated by microscopic analysis.

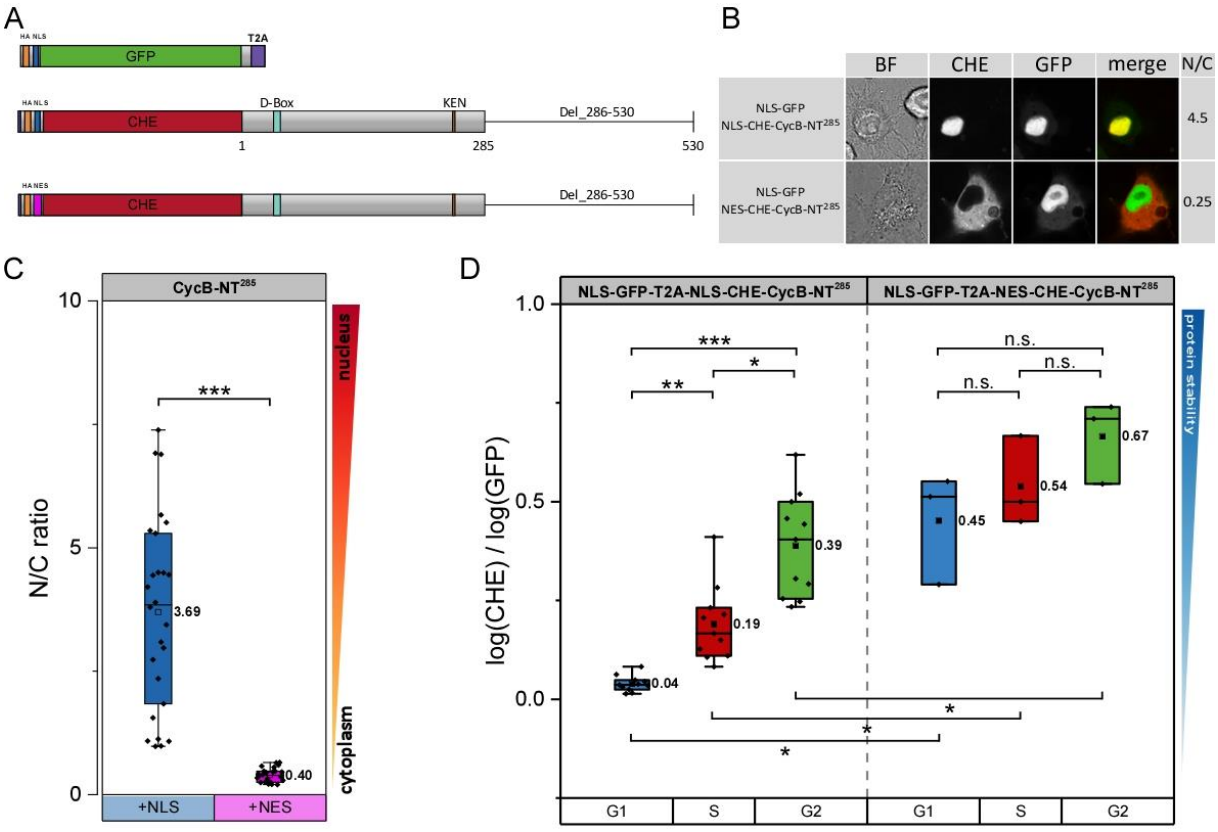

Figure 73| Localization analysis of NLS-CHE- and NES-CHE-CycB-NT^{285}

(**A**) Schematic illustration of NLS-CHE- and NES-CHE-CycB-NT^{285} RPS constructs. (**B**) Exemplary illustration of a cell transfected with respective expression construct depicted in the brightfield (BF), CHE- and GFP channel. (**C**) Box plot summarizing the N/C ratios of the analyzed cells. (**D**) Analysis of relative protein stability levels of NLS-CHE-CycB-NT^{285} and NES-CHE- CycB-NT^{285} in G1-, S-, and G2-cells (exp.lvl. 1.0 - 1.75). Statistics performed by t-test with Welch´s correction, n.s. > 0.05, * ≤ 0.05, ** ≤ 0.01, ***≤ 0.001.

As expected, fusion to NES-CHE (as in NLS-GFP-T2A-NES-CHE-CycB-NT^{285}) caused a strong nuclear export (N/C: 0.40) of Cyclin B compared to NLS-CHE-CycB-NT^{285} (N/C: 3.69) (Figure 73 A, B, C). Flow cytometric analysis of relative protein stability levels showed a stabilization of NLS-GFP-T2A-NES-CHE-CycB-NT^{285} (CHE/GFP - G1: 0.45, S: 0.54, G2: 0.67) compared to NLS-CHE-CycB-NT^{285} (CHE/GFP - G1: 0.04, S: 0.19, G2: 0.67). The CHE/GFP ratio of NLS-GFP-T2A-NES-CHE-CycB-NT^{285} of the G1-popuation was still decreased compared to S- and G2-cells, albeit not being statistically significant which should be treated with caution due to the limited number of replicates (n= 3). Nevertheless, the trend observed for NES-CHE-CycB-NT^{285} and the decreased G1 stability of NES-CHE-Rca1 indicate that the APC/C is also catalytic active in the cytoplasm, however to a much lesser extent as in the nucleus.

Having shown that the APC/C activity is likely higher within the nucleus, it was rather surprising that 4xFLAG-NES-Rca1 and -Rca1_204-411 were able to inhibit APC/C dependent degradation of the nuclear localized NLS-CHE-CycB-NT^{285} reporter. Thus, it was also tested if Rca1 would be able to inhibit degradation of cytoplasmic Cyclin B. Therefore, NLS-GFP-T2A-NES-CHE-CycB-NT^{285} was used in the *in vivo* APC/C activity assay instead of the NLS-CHE-CycB-NT^{285} reporter.

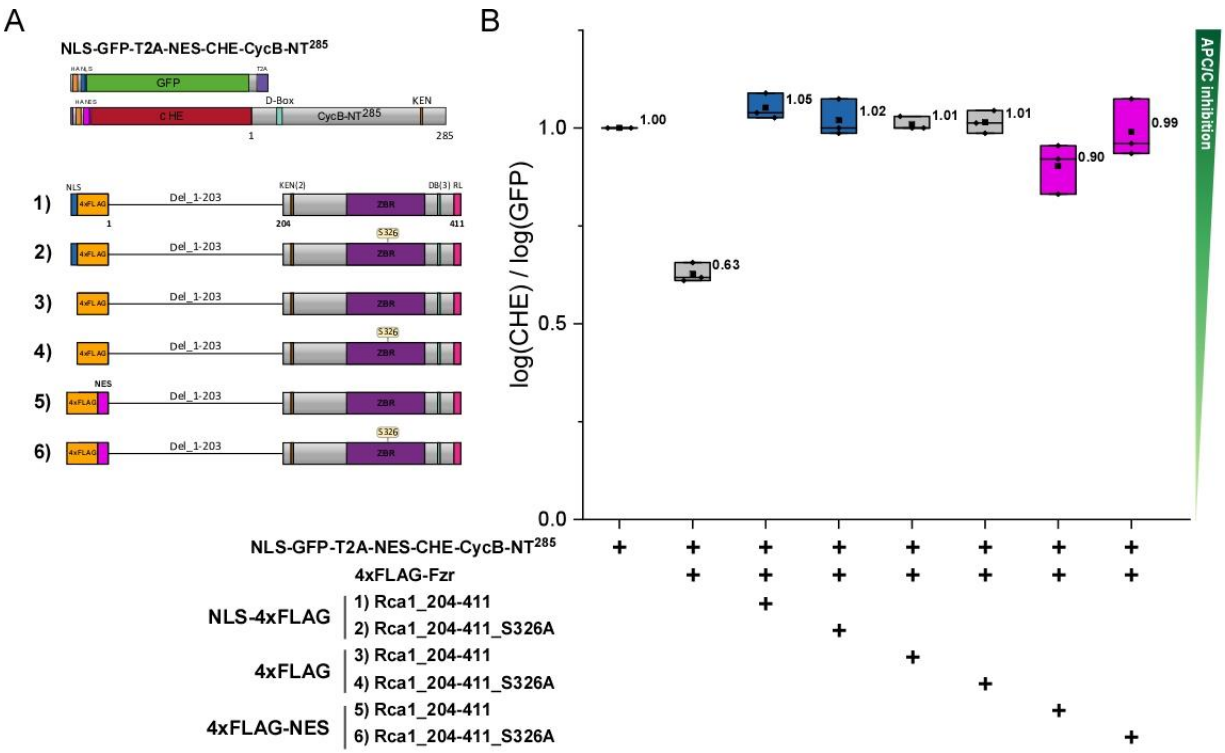

Figure 74|Nuclear Rca1 can inhibit APC/C dependent degradation of cytoplasmic Cyclin B

Analysis of APC/C inhibition by Rca1 in dependency of its subcellular localization using an NES-CHE-CycB-NT^{285} reporter. (**A**) Illustration of the NLS-GFP-T2A-NES-CHE-CycB-NT^{285} sensor and the different 4xFLAG tagged Rca1_204-411 constructs. (**B**) Box plot of relative protein stability levels of NLS-GFP-T2A-NLS-CHE-CycB-NT^{285} with additional co-overexpression of 4xFLAG-Fzr and the respective NLS-4xFLAG-(blue boxes), 4xFLAG- (grey boxes), and 4xFLAG-NES-tagged (pink boxes) Rca1_204-411 versions in G2-cells (exp.lvl. 2.0 - 3.0). C-terminal Rca1 is capable to inhibit APC/C dependent degradation of cytoplasmic CycB independent of its own subcellular localization. Statistics performed by Mann-Whitney U-Test, n.s. > 0.05, * ≤ 0.05, ** ≤ 0.01, ***≤ 0.001.

Additional 4xFLAG-Fzr overexpression caused a destabilization of NES-CHE-CycB-NT^{285} (CHE/GFP - G2: 0.63), consistent with our previous findings indicating catalytic APC/C activity in the cytoplasm. Co-overexpression of NLS-4xFLAG- and 4xFLAG-Rca1_204-411 were able to completely restore NES-CHE-CycB-NT^{285} relative protein stability levels (CHE/GFP - G2: 1.05/1.01), whereas 4xFLAG-NES-Rca1_204-411 displayed a slight reduction in APC/C inhibition (CHE/GFP - G2: 0.90). It was also tested if the loss of 14-3-3 interaction has an impact on Rca1 function under these conditions. Indeed, mutation of the 14-3-3 interaction caused a complete restitution of NES-CycB-NT^{285} stability in case of 4xFLAG-NES-Rca1_204-411_S326A, whereas no effect was observed for the other constructs (Figure 74 A, B). Since 14-3-3 is most likely involved in nuclear export of Rca1, 4xFLAG-NES-Rca1_204-411_S326A could display an enhanced nuclear accumulation, which although was not directly tested in this experiment, indicating that nuclear localized Rca1 would be a more potent APC/C inhibitor compared to cytoplasmic Rca1. Due to the limited number of replicates (n=3) no statistical analysis was performed and more replicates should be included in order to allow a more comprehensive evaluation of the results. Nonetheless, taken together the results of Rca1 function in dependency of its subcellular sequestration indicate that Rca1 can inhibit both cytoplasmic and nuclear APC/C activity independent of its localization.

4. Discussion

4.1. The RPS system - a versatile tool for the measurement of relative protein stability levels during cell cycle progression

4.1.1. Establishment of the RPS-expression system

Protein degradation constitutes a fundamental mechanism in regulation of cell cycle progression. The timely ordered synthesis and destruction of regulatory proteins at specific cell cycle stages is crucial for proper cell cycle progression and cell division (Morgan, 2007). It is therefore of great interest to understand the regulatory mechanisms that are involved in timely ordered protein degradation. Classical approaches to determine protein degradation are often time and cost exploiting techniques that often only allow estimation of overall protein degradation without providing information of the temporal context (reviewed in Eldeeb et al., 2019). Thus, the first aim of this thesis was to establish an *in vivo* high-throughput method that allows the quick and robust measurement of protein degradation of a selected protein during cell cycle progression in S2R+ cells, since our workgroup is focused on cell cycle regulation in the model organism *Drosophila melanogaster*. The relative protein stability (RPS) system enables measurement of protein degradation by monitoring the intensities of two fluorophores, a long-lived stable reference protein and a reporter-POI fusion, after transient transfection via flow cytometry. The decline of reporter-POI intensities in comparison to the stable reference correlates to degradation of the reporter-POI fusion with the kinetics of the selected protein of interest. A fundamental requirement of such a technique is the stoichiometric co-expression of the two fluorescent proteins. Bicistronic expression was obtained using a modified T2A sequence optimized for the use in *Drosophila* that causes ribosome skipping during translation. This overcomes the need of co-transfection with multiple vectors for protein co-expression, which results in undesired heterogeneous cell populations with different expression levels of the encoded proteins (Minskaia et al., 2015). However, protein co-expression mediated by viral 2A sequences also comes along with some general imperfections, as it was observed that ribosome skipping not always results in complete separation of both proteins and the production of the second protein can be reduced (De Felipe et al., 2010; Liu et al., 2017). Furthermore, it was shown that different 2A sequences have varying skipping efficiencies that also depend on the cell type as well as species specific modification of the 2A sequence (Kim et al., 2011; Lo et al., 2015). Nevertheless, the established RPS expression vectors showed a high degree of colinearity for the co-expression of the two fluorescent proteins GFP and CHE over a broad expression range (see 3.1.2; Figure 16) accompanied by a high skipping efficiency mediated by the modified T2A sequence (see 3.1.3; Figure 17). The impact of unskipped polyprotein using the model substrate Cyclin B still showed degradation of the FLP fusion with the known kinetics of Cyclin B (see 3.1.5.1.4; Figure 23). However, the experimental implementation required co-transfection of an additional CHE-reference protein which is less precise than the usual measurement using solely bicistronic RPS expression vectors. Moreover, degradation of the FLP-POI was only tested for this one substrate and it cannot

be excluded that failed ribosome skipping constitutes a more severe bias in case of other substrates. In any case, only a small proportion of unskipped polyprotein was observed in our experiments and in combination with the results of FLP-CycB, any bias caused by failed ribosome skipping was assumed to be insignificant for the analysis. Consistent with previous studies (Liu et al., 2017) the production of the protein at the second gene position downstream of the T2A was slightly reduced compared to the upstream position, albeit not being as drastic as reported in Liu et al. (2017). However, a stoichiometric co-expression of the two proteins was achieved and the slightly decreased expression of the second protein occurred constant and did consequently not constitute an issue for the measurement of relative protein stability levels (see 3.1.3; Figure 17). Nevertheless, insertion of the target protein up- or downstream of the T2A site should always be tested and compared to exclude unspecific effects caused by an undesired difference in protein expression levels depending on the position of the POI.

Expression of the RPS plasmids was implemented by transient transfection of S2R+ cells in order to facilitate a quick and simple analysis of different target proteins or mutant variants of a protein. However, transient transfection results in cell populations with different expression rates of the target proteins due to varying numbers of absorbed plasmids. It was demonstrated that relative protein stability levels, measured by the CHE-POI/GFP ratios, showed a sharp increase at high expression rates. This indicates that the protein degradation system was overwhelmed at high expression levels (see 3.1.5.1.1; Figure 19). This effect was observed for all tested substrates to varying degrees. Considering that protein expression was under control of a strong constitutive active actin promotor this observation was expected since high expression will likely result in levels exceeding endogenous protein levels. To analyse the degradation of a given protein, the expression level that allowed normal degradation had to be determined for each individual protein of interest.

In order to assign protein degradation to a specific cell cycle phase, three cell populations, “G1”, “S”, and “G2” were defined based on their DNA content detected by Hoechst incorporation (see 3.1.4; Figure 18). Consistent with a mathematical model of the cell cycle distribution, detection of S-phase cells by EdU incorporation showed that the designated cell populations were not exclusively made up of cells of the respective cell cycle stage but consist of cells of different cell cycle phases. Thus, cell cycle phase assignment is not absolute and must be considered under the aspect that the G1- and G2-population consist mainly of cells in G1- or G2- phase but also contain either early S-phase or late S-phase and mitotic cells, respectively. Similar, the S-phase cell population is made up of S-phase cells along with cells that are in G1- and G2-phase. More accurate implementation of cell cycle phase assignment would be challenging since most of the methods require cell fixation (e.g., EdU incorporation, pH3 histone staining, etc.) which causes a loss of the GFP and CHE fluorescence or require a more elaborate technical setup for the simultaneous measurement of fluorescent cell cycle markers as described for the Fly-FUCCI (Zielke et al., 2014) or PIP-FUCCI system (Grant et al., 2018), which however was not available at our facility. Anyway, using the RPS system with the described approach for cell

cycle assignment it was possible to successfully determine protein degradation of multiple cell cycle regulators during G1- and S-phase, which will be discussed in more detail in the following.

4.1.2. Protein degradation of APC/C substrates in G1-phase

The RPS system was designed to analyze protein degradation during cell cycle progression in *Drosophila* S2R+ cells. In a first attempt, APC/C dependent degradation of N-terminal Cyclin B and Geminin fragments were analyzed. G1-phase specific degradation of both proteins was detectable via flow cytometry using the RPS expression system. However, opposed to CycB, degradation of the Geminin fragment was completely impaired by N-terminal reporter fusions which was most severe by positioning the protein upstream of the T2A site. In general, attachment of a fluorescent protein can have drastic effects on protein function, structure, and its cellular localization, especially when proteins are overexpressed (reviewed in Crivat et al., 2012). The obtained results highlight the importance to test different fusions of the reporter and the positions respective to the T2A site to exclude undesired effects caused by unfavorable protein tagging.

Furthermore, it was shown that the test of the RPS system using established target proteins was not only is suited for the verification of degron sequences but also allowed the identification of new degrons. We were able to demonstrate that degradation of the N-terminal region of Cyclin B is not only dependent on a D-box degron as reported in previous studies (Sigrist et al., 1995) but additionally required a KEN-box for proper APC/C dependent degradation in G1-phase (see 3.1.5.1.5; Figure 24) similar to the reports for yeast Clb2 (Hendrickson et al., 2001). The two degrons most likely confer APC/C dependent degradation by a cooperative mechanism since a complete stabilization was only achieved by a simultaneous inactivation of both degrons.

Similar to Cyclin B, Geminin also harbors potential D- and KEN-box degrons in its N-terminal moiety, whereas only the D-box was reported to be involved in APC/C recruitment and Geminin degradation to this point (McGarry et al., 1998; Clijsters et al., 2013). Analysis of the N-terminal D- and KEN-box of *Drosophila* Geminin showed that mutation of either degron caused a strong stabilization of the applied Geminin fragment (see 3.1.5.2.2; Figure 28). However, due to the close proximity it cannot be distinguished which degron is involved in APC/C dependent degradation. A cooperative model which requires the simultaneous binding of both degrons to the respective D- and KEN-box receptor sites on the co-activator surface is rather unlikely taking the limited spacing of nine amino acid residues between the two degrons into account. Study of the structure of Cdc20 in *S.pombe* revealed that spacing of 17 residues in a KEN-/D-box arrangement would allow cooperative binding, whereas a D- /KEN-box arrangement permits only the interaction with one degron with the same spacing (Chao et al., 2012). Yet, there is no systematic data on the relative distance of APC/C degrons required for cooperative interaction but based on single evidence it is unlikely that both degrons function in a cooperative man-

ner in case of *Drosophila* Geminin. Furthermore, the additive stabilization effect observed in the double D- and KEN-box mutant was rather weak and only just significant, especially compared to the effects observed for Cyclin B, which further does not support a cooperative model. Nevertheless, single mutation of either the D- or KEN-box consensus was sufficient to completely stabilize the N-terminal moiety of Geminin. Therefore, either both degrons mediate APC/C interaction independently, in a non-cooperative mechanism to facilitate efficient and rapid Geminin degradation or the introduction of point mutations in a non-functional degron disrupts the functional degron due to its close proximity. Additional biophysical and/or biochemical methods (e.g. structural data) will be required to determine the precise interaction of this substrate with the APC/C. Besides this limitation, the RPS system is a fast and sensitive method for the evaluation of degron motifs, which constitutes an essential step in understanding the mechanisms behind targeting, competition and ordering of APC/C substrates

We also investigated the impact of altered APC/C activity on relative protein stability levels of the two APC/C substrates, which was implemented by Fzr overexpression or knockdown. Fzr overexpression resulted in a destabilization of the N-terminal CycB and Gem fragments which was most pronounced in G2-cells when APC/C activity is restrained under normal conditions. Vice versa, *fzr* knockdown resulted in a stabilization of the two substrates in accordance with an inactivation of APC/C^{Fzr} activity. Additionally, the cell cycle stabilized degron mutants of Cyclin B and Geminin were also analyzed under the same conditions. Unexpectedly, CycB-NT^{247}_mDB_ΔKEN was destabilized in the G2-population after simultaneous Fzr overexpression. Opposed to this, Gem-NT^{101}_mDB was completely refractory to hyperactivated or inactivated APC/C activity. The stabilization of the N-terminal CycB degron mutant after inactivation of APC/C^{Fzr} activity could indicate that one of the putative D- or KEN-box degrons that were found in a bioinformatic screen still confers APC/C^{Fzr} dependent degradation. However, this interaction would occur to a minor extent compared to the verified D- and KEN-box degrons since CycB-NT^{247}_mDB_ΔKEN was completely stabilized under normal conditions. Thus, the precise cause of the G2 decline of CycB-NT^{247}_mDB_ΔKEN after Fzr overexpression remains elusive to this point. As already mentioned, Fzr overexpression can cause severe over-replication accompanied by abnormal cellular status, which might affect CycB stability under this circumstances. As, this effect was not observed in case of Geminin, it is unlikely that it can be attributed to general side effects of Fzr overexpression. In overreplicating cells, Cyclin E activity fluctuates (Zielke et al., 2008) and this could cause Fzy-dependent APC/C activation for which Cyclin B, but not Geminin is a target.

In general, it can be challenging to interpret the effects of overexpression or knockdown experiments since both create unnatural cellular states which can cause deviation of the normal degradation mechanisms. Nevertheless, hyperactivation and downregulation of APC/C^{Fzr} activity were consistent with specific alterations of APC/C activity showing that the RPS system can also detect changes of relative protein stability in dependence of changes in the activity of responsible ubiquitin ligases.

In a further experiment, the degradation kinetics of CycB-NT^{258} and Gem-NT^{101} were compared using the RPS reporter system in live cell imaging experiments, since a study of human Geminin demonstrated similar degradation kinetics to Cyclin B, opposed to findings in *Xenopus* egg extracts that displayed slower degradation kinetics of Geminin compared to Cyclin B (Li et al., 2004; Clijsters et al., 2013). Our analysis showed a distinct difference between Cyclin B and Geminin degradation in S2R+ cells, in which Geminin is degraded to a later time point and with slower kinetics than Cyclin B. Thus, our findings in *Drosophila* coincide with the observations in *Xenopus* contradicting the results of Clijsters et al. (2013). Furthermore, having established that Geminin degradation in *Drosophila* S2R+ cells is dependent on APC/C^{Fzr} activity and that degradation begins later compared to Cyclin B support the hypothesis of several studies in re-replicating, endoreduplicating, and somatic cells that Geminin degradation solely relies on Fzr/Cdh1 (Diffley, 2004; Li et al., 2004; Di Fiore et al., 2007; Narbonne-Reveau et al., 2008; Sakaue-Sawano et al., 2008; Zielke et al., 2008). Since Fzy/Cdc20 itself is a target of APC/C$^{Cdh1/Fzr}$ after the anaphase to metaphase transition it is rather unlikely that APC/C$^{Cdc20/Fzy}$ mediates Geminin degradation in *Drosophila*. However, further experiments like *in vitro* ubiquitination of Geminin by APC/C^{Fzy} will be necessary to completely confirm this hypothesis.

4.1.3. Measuring S-phase degradation using the RPS system

In addition to G1-phase allocated protein degradation, proteolysis during S-phase was analyzed using the CRL4^{Cdt2} substrates Dacapo, E2F1, and Cdt1. Flow cytometric analysis displayed a decline of relative protein stability levels for S-phase cells compared to the G1-cell population that was uniformly observed for the three substrates. Direct allocation of the detected degradation to CRL4^{Cdt2} activity was verified by knockdown experiments and also shown by the analysis of a PIP degron mutant of Dacapo that was refractory to CRL4^{Cdt2} dependent degradation, demonstrating that S-phase specific protein degradation was distinguishable using the RPS system (see 3.1.6). However, flow cytometric measurement of protein degradation during S-phase also came along with two major limitations:

First, no or only little re-accumulation of the CHE-tagged S-phase substrates was detectable in the G2-population. This observation is likely due to a combination of different effects. CHE and GFP re-synthesis and fluorescent maturation after protein degradation requires a substantial time (Balleza et al., 2018) which may not be provided within the duration of G2-phase. Additionally, a faster maturation of GFP has been observed in S2R+ cells that causes an undesired decline in the CHE/GFP ratio. Additionally, the presence of late S-phase cells in the defined G2-gate also contributes to this issue, which will be discussed in more detail in the following.

Second, relative protein levels only partially reflect actual S-phase degradation due to the heterogeneity of the assigned cell populations. The presence of G1- and G2- cells within the S-phase gate causes an underrepresentation of the actual S-phase specific decline of the CHE-POI reporter fusion as shown

by the analysis of Cdt1 subpopulations within the three assigned cell cycle populations (3.1.6.3.2; Figure 34). Cdt1-NT^{101} degradation was likewise detectable in the G1- and G2-population, albeit to a lesser extent, which is likely to be attributable to the presence of early and late S-phase cells. This also explains the increase of stability levels in the two populations after Cul4 knockdown that was observed for the three tested substrates (e.g. Figure 33). This effect also contributes to the limited re-accumulation in G2-cells in addition to the already mentioned effects.

Thus, protein degradation during S-phase can be detected by flow cytometry using the RPS system similar to proteolysis during G1-phase as shown for Cyclin B and Geminin. In general, a statement of protein re-accumulation after turn off of E3-ligase mediated proteolysis is not possible in this setup. A further limitation of flow cytometric measurement of relative protein stability levels via the RPS system is that is does not provide information of the precise temporal order of substrate degradation within a cell cycle phase, but allows determination if a protein is degraded within a certain cell cycle stage and how it is degraded. A more accurate analysis of the degradation kinetics of a selected POI within either G1- or S-phase was achieved by live cell imaging analysis instead of flow cytometric measurement as shown for Cyclin B, Geminin (see 3.1.5.2.4; Figure 30), and Cdt1 (see 3.1.6.3.3; Figure 35).

In latter case, a challenging aspect was the adjustment of cell to cell variations in the duration of G1-phase of unsynchronized cells, which was compensated by an artificial interpolation of the raw data via the MICA alignment tool. Data manipulation should always be treated with caution since the obtained results no longer represent the direct output of an experiment which could lead to delusive interpretation of the data. To avoid interpolation, possible solutions for a more precise cell cycle phase assignment could for example be the use of *in vivo* EdU incorporation (Salic et al., 2008) or the use of fluorescent cell cycle markers (Grant et al., 2018), which in turn require a more elaborate technical setup.

In conclusion, the RPS system comes along with individual limitations as every other technique, but it provides a new versatile tool for the detection of relative protein stability during cell cycle progression in *Drosophila* S2R+ cells. We were able to demonstrate that the expression system provides a high degree of flexibility regarding protein tagging and also comes along with a high precision of protein co-expression. It was shown that the approach can address several different scientific questions, including detection of protein degradation in the course of cell cycle progression, evaluation of putative degron sequences, and identification of involved E3 ubiquitin ligases in the course of protein degradation.

4.2. Rca1 is a substrate of the APC/C^{Fzr} in G1-phase

Rca1 was found as a potent APC/C inhibitor in S- and G2-phase that is required for the first time during cell cycle 16 in *Drosophila* embryogenesis, restricting APC/C activity during G2-phase and allowing cells to enter mitosis followed by the first G1-phase (Grosskortenhaus et al., 2002). Consequently, APC/C inhibition by Rca1 must be resolved during mitosis to allow degradation of mitotic regulators and

proper execution of mitotic events, until Rca1 itself is degraded during G1-phase (Grosskortenhaus et al., 2002; Morgenthaler, 2013). Initial experiments indicated that Rca1 itself might be targeted by APC/C^{Fzr} for proteolytic destruction during G1-phase. Previous live cell imaging experiments showed that Rca1 was degraded with similar kinetics as other APC/C substrates during G1-phase and also a central located KEN-box degron was implicated in the degradation of a small Rca1 fragment (Morgenthaler, 2013). This gave rise to the hypothesis that after functioning as an APC/C inhibitor in G2-phase, Rca1 is inactivated during early mitosis by an unknown mechanisms converting Rca1 into an APC/C^{Fzr} substrate. To test this theory, in a first step the degradation pathway of Rca1 was examined using the RPS system. Consistent with previous studies (Grosskortenhaus et al., 2002; Morgenthaler, 2013), degradation of CHE tagged Rca1 as well as an N- and C-terminal Rca1 fragment during G1-phase was detected in S2R+ cells using the RPS system, demonstrating that our new method was suited for the analysis of Rca1 degradation (see 3.2.2; Figure 36). Hence, further experiments were conducted to test if Rca1 degradation is mediated by APC/C^{Fzr} activity. A large variety of experiments in this thesis supported an APC/C^{Fzr} dependent degradation of Rca1 during G1-phase:

First, investigation of degradation kinetics of an N-terminal and non-functional C-terminal Rca1 fragment via live cell imaging analysis displayed similar kinetics to Gem-NT^{101} but not CycB-NT^{285} (see 3.2.3; Figure 37). However, it must be considered that the degradation kinetics of the overexpressed substrate-reporter fusions might actually not directly reflect the degradation of the endogenous protein. As shown in the flow cytometric analysis of relative protein stability levels, the selection of adequate expression levels constitutes an essential aspect in the measurement of protein degradation since high expression levels displayed an unspecific stabilizing effect. Hence, only cells with moderate low expression levels were selected for image analysis. However, it cannot be excluded that the results were negatively influenced by the overexpression of the protein of interest. A further aspect that has to be considered is that the kinetics of Rca1 degradation might differ from the measured kinetics of the N- or C-terminal moieties. Both parts of Rca1 were degraded with similar kinetics and consequently full-length Rca1 could be degraded with even faster kinetics. This should be tested in future experiments to assess whether degradation kinetics of full-length Rca1 are also similar to Geminin. Nevertheless, the similar degradation kinetics to Gem-NT^{101} suggest that Rca1 might be targeted by the APC/C^{Fzr} similar to Geminin that is likely to be a sole APC/C^{Fzr} target (see 4.1.2).

Next, Rca1 stability was shown to be dependent on APC/C^{Fzr} activity. Augmented activation of the APC/C^{Fzr} by Fzr overexpression resulted in an unnatural degradation of Rca1_1-203 and Rca1_204-411 in G2-phase. Full-length, overexpressed Rca1 was not destabilized in G1 after simultaneous Fzr overexpression. This is likely caused by the APC/C inhibitory effect of Rca1 that counteracts the APC/C stimulation caused by Fzr overexpression. This observation is consistent with previous results showing

that overexpression of HA-Rca1 was able to supress the effects of Fzr overexpression in *Drosophila* embryo (Grosskortenhaus et al., 2002). Thus it was rather surprising that Rca1_204-411 was destabilized upon Fzr overexpression, as the C-terminal part of Rca1 was shown to be sufficient for APC/C inhibition in *Drosophila* embryo (Zielke et al., 2006). A possible explanation for this observation could be a difference in the expression levels between Rca1_204-411 and Fzr in this experiment. Since protein co-expression was implemented by transient co-transfection it cannot be excluded that Fzr expression levels exceeded CHE-Rca1_204-411 expression, which would consequently not be able to compensate the additional APC/C activity. To test this, a titration of different CHE-Rca1_204-411 amounts with constant 4xFLAG-Fzr expression should be applied in this setup, which has not been performed, yet. To generally circumvent this issue, protein co-expression could be implemented by a tricistronic expression vector containing two T2A sites that has recently been established in the Sprenger workgroup (Heidrich, 2020), avoiding the requirement of co-transfection. An alternative explanation could be the involvement of the N-terminal region in APC/C binding or APC/C inhibition, which will be discussed in more detail later (see 4.3). Reversely to the unnatural activation of the APC/C, downregulation of APC/C^{Fzr} activity by Fzr knockdown resulted in significantly increased relative stability levels of full-length, N- and C-terminal Rca1 in the G1-population. Taken together, Rca1 degradation was dependent on APC/C^{Fzr} activity further supporting an APC/C^{Fzr} dependent degradation of Rca1.

Finally, it was demonstrated that Rca1 degradation is mediated by several APC/C specific degrons. Previous investigations concerning the protein domains that confer Rca1 degradation have already identified a central located KEN-box motif that was involved in the degradation of a small Rca1 fragment (Morgenthaler, 2013). In this thesis, several putative degrons were identified in a bioinformatic screen and an extensive analysis of different Rca1 mutants via flow cytometry enabled the verification of several APC/C degrons that are required for Rca1 degradation, including two D-box degrons and a non-canonical N-terminal KEN-box degron besides the already known KEN-box. Furthermore, a potential ABBA motif was identified in the N-terminal region of Rca1 and mutation of the conserved amino acid residues in combination with the verified degrons displayed an additional but only minor stabilizing effect in case of Rca1_1-203 and in the context of full-length Rca1, albeit missing statistical significance. Due to the weakly pronounced effect it was not possible to properly evaluate the functionality of the ABBA motif in Rca1 degradation. Further interaction studies might be necessary to identify any interaction between the ABBA motif and Fzr. Besides the typical APC/C degrons, also the C-terminal RL-tail was shown to be required for the degradation of Rca1. A partial deletion of the RL-tail completely stabilized C-terminal Rca1 (see 3.2.5.4; Figure 44) and was also required for a partial stabilization of Rca1 (see 3.2.5.5; Figure 46). This finding was rather surprising, since the RL tail domain of Emi1 was implicated in APC/C inhibition by antagonizing chain elongation by Ube2S (Frye et al., 2013) but

was not reported to be involved in protein recruitment by the APC/C. The inhibitory function of the RL tail was further supported by a physical interaction of the C-terminal domain of Emi1 and Ube2S with Apc2, which however was only detected under low salt conditions (Wang et al., 2013). In concordance with these studies, the RL-tail domain of Rca1 was also shown to be essential in APC/C inhibition (see 3.3.4; Figure 49), indicating a dual role of the RL-tail in Rca1 degradation and function. However, an initial attempt to assess whether a RL-tail dependent interaction between the C-terminal part of Rca1 and Apc2 can be detected by co-immunoprecipitation, resulted in a RL-tail independent interaction of Rca1-CT and Apc2 albeit no interaction was observed for Ube2S opposed to the reports of Wang et al. (2013) (unpublished data). Interestingly, Emi2 was also shown to directly inhibit Ube2S binding to the APC/C via its C-terminal RL-tail but curiously both Emi2 and Ube2S directly bound to Apc10 instead of Apc2 via their RL-tail domain (Sako et al., 2014). Since Apc10 constitutes a subunit of the substrate recognition module providing a part of the docking platform of the D-box binding pocket, an RL-tail dependent interaction could also indicate a role in substrate recruitment that would correspond to our results. However, an interaction of Rca1 with Apc10 has not been tested yet and further experiments must be performed to ascertain this hypothesis and to unveil the molecular mechanism of the dual regulation of Rca1 degradation and function mediated by the RL-tail.

In addition to the evaluation of APC/C specific degrons, the C-terminal DSGxxS diphospho degron was analyzed. Mutations in the degron had no impact on Rca1 degradation (see 3.2.5.4; Figure 44) consistent with previous studies in *Drosophila* embryo and S2R+ cells (Zielke, 2006; Morgenthaler, 2013). Thus, a degradation pathway via $SCF^{\beta TrCP}$ as described for Emi1 that requires phosphorylation of the GSK motif by Plk1, can be excluded for Rca1 (Margottin-Goguet et al., 2003; Eldridge et al., 2006).

The analysis of Rca1 fragments revealed the presence of several degrons whose mutations resulted in the stabilization of the respective fragments. All these mutations were then introduced into the full-length Rca1 coding sequence. Surprisingly, simultaneous mutation of the evaluated degrons that caused a complete stabilization of the applied Rca1 fragments did only result in a minor stabilization of Rca1. An additional mutation the C-terminal D-box (DB(3)) that was initially excluded based on the results of Rca1_221-411, caused a more pronounced but still only partial stabilization of full-length Rca1 (see 3.2.5.5; Figure 46). Interestingly, mutation of the C-terminal D-box displayed only a stabilizing effect in combination with a deletion of the RL-tail. This could also indicate an interaction with Apc10 mediated by the RL-tail and the D-box. Furthermore, additional mutation of the central located D-box (DB(2)) had no further effect, contradicting a role in Rca1 degradation. The incomplete stabilization of the Rca1 degron mutant could be explained by the results of the N-terminal Rca1 fragment, Rca1_100-299. Degradation of this fragment was not impaired by simultaneous mutation of the ABBA motif and the central KEN-box that had both shown effects in overlapping Rca1 fragments. A further deletion of the NLS sequence (as in Rca1_134-299) resulted in a stabilization with similar stability levels to Rca1_204-299. This could indicate a further so far unidentified degradation motif located within the

region of amino acids 100 to 134 that could be responsible for the remaining instability of the Rca1 degron mutant during G1-phase.
Nevertheless, it was demonstrated that degradation of different N- and C-terminal Rca1 fragments was mediated by APC/C degrons and that mutations of these motifs resulted in a complete stabilization of these fragments, albeit not all protein domains mediating Rca1 degradation were identified in the course of this thesis.

In conclusion, the different results of the *in vivo* experiments conducted in this thesis strongly suggest an APC/C^{Fzr} dependent degradation of Rca1 during G1-phase. This is further supported by recent experiments using an *in vitro* APC/C ubiquitination assay that show a direct ubiquitination of CHE-Rca1_204-299 by APC/C^{Fzr} (unpublished data Manuel Saller). Thus, in accordance with the initial hypothesis it was demonstrated that besides being an APC/C inhibitor during S- and G2-phase, Rca1 also constitutes an APC/C substrate during G1-phase.

4.3. Rca1 utilizes similar C-terminal domains for APC/C inhibition like Emi1

Numerous APC/C pseudosubstrate inhibitors have been identified in different organisms (e.g., budding yeast Acm1, fission yeast Mes1, *Arabidopsis* protein PYM and GIG1, etc.) that bind to the APC/C with high affinity thereby inhibiting further substrate recruitment, which is often mediated by the cooperative action of several APC/C degrons (reviewed in Davey et al., 2016). In case of Emi1, a more sophisticated mechanism was described involving the action of a C-terminal D-box, Linker, ZBR and RL-tail domain that primarily restrain APC/C activity on the level of E2 enzyme binding and only to a lesser extent by blocking substrate recognition sites (Frye et al., 2013; Wang et al., 2013). Interestingly, Rca1 shares a similar arrangement of C-terminal domains and consequently a similar mechanism could also apply for Rca1. To test this hypothesis, an *in vivo* APC/C assay was established for the evaluation of the domains required for APC/C inhibition by Rca1. As a readout of APC/C inhibition relative protein stability levels of GFP-T2A-CHE-CycB-NT^{285} were monitored in the G2-cell population with additional Fzr overexpression that results in an unnatural degradation of the CycB sensor in this cell cycle phase due to hyperactivated APC/C^{Fzr} activity. Rca1 function was determined by simultaneous co-overexpression of 4xFLAG-tagged Rca1 constructs and the resulting stabilization of Cyclin B served as a unit of APC/C inhibition. Thus, it must be stated that all of the experiments regarding Rca1 function were conducted under this unnatural conditions and it cannot be assured that the results reflect the normal mode of Rca1 function as it would be under physiological conditions.

Using this approach it was demonstrated that Rca1 and C-terminal Rca1 were able to completely inhibit APC/C^{Fzr} activity, since both fully restored Cyclin B stability levels, which was in accordance with studies

in *Drosophila* embryo (Grosskortenhaus et al., 2002; Zielke et al., 2006). The expression of the N-terminal half of Rca1 alone resulted in some APC/C inhibition in G2 cells, as it was only able to partially allow Cyclin B stabilization (see 3.3.3; Figure 48). This could be explained by a simple substrate competition between the CycB sensor and Rca1_1-203, which itself is a good APC/C substrate, or indicate that the N-terminal residues confer a pseudosubstrate inhibition by partially blocking substrate recruitment. Latter possibility would also contribute to the findings that relative stability levels of C-terminal Rca1 were decreased after Fzr overexpression, which was not the case for Rca1 (see 4.2). The differences in APC/C inhibition between full-length and the C-terminal part of Rca1 could also be attributable to variations in the expression levels. However, similar expression of the 4xFLAG-tagged Rca1 constructs and Fzr were seen after Western blot analysis, but minor expression level differences cannot be excluded. However, further experiments will be needed to investigate the possible pseudosubstrate mechanism mediated by the N-terminal region of Rca1.

Since the C-terminal part of Rca1 was able to completely restore CycB-NT^{285} levels it was further investigated which protein domains are required for this inhibition. Analysis of different C-terminal Rca1 mutants showed that the KEN-box, ZBR, D-box, and the RL tail domain were involved in APC/C inhibition. Similar to Emi1, the KEN- and D-box had modest effects on APC/C inhibition. In contrast, the ZBR was shown to be crucial for Rca1 function, since mutations within the ZBR strongly impaired APC/C inhibition consistent with previous findings in *Drosophila* embryo (Zielke et al., 2006). A further dissection of the ZBR domain in Rca1 displayed an untypically long spacing (ZBR_loop) separating the two arrays of cysteine residues of the IBR C6HC consensus pattern. However, the ZBR loop had only minor influence on APC/C inhibition, since a deletion of the unique part of this loop resulted only in a modest decrease of APC/C inhibition in the *in vivo* APC/C activity assay (see 3.3.5; Figure 50). Interestingly, disruption of the ZBR domain also resulted in a destabilization of Rca1, which could imply that a turn off ZBR function could be involved in Rca1 conversion from an APC/C inhibitor to substrate (see 4.4). Although, it must be considered that the effect could also be attributed to an intrinsic destabilization caused by the disruption of the ZBR domain affecting the overall stability of Rca1, which should be excluded by further experiments in the first place. Compared to effects of the KEN-box, D-box, and ZBR domain, the most severe effect was observed for the deletion of the C-terminal RL-tail domain that totally abolished APC/C inhibition (see 3.3.4; Figure 49). Since deletion of the RL-tail completely stabilized C-terminal Rca1 and caused a complete loss of its function, it must also be considered that proper binding of Rca1 to the APC/C could be substantially impaired by the introduced deletion. However, an RL-tail independent interaction of C-terminal Rca1 and Apc2 was observed by co-immunoprecipitation (data not shown), hence deletion of the RL tail did at least not completely abolish APC/C-Rca1 binding. Thus, further experiments must be performed to elucidate the molecular function of the RL-tail domain in Rca1 degradation and function.

In conclusion, the results of this thesis provided new insights into the requirement of different C-terminal domains of Rca1 for APC/C inhibition, similar to the reports for the vertebrate homologue Emi1. APC/C inhibition by Rca1 was shown to depend on the synergetic action of these C-terminal elements, contradicting an exclusive pseudosubstrate inhibitory mechanisms, rather suggesting a similar inhibitory mechanism as shown for Emi1 that blocks APC/C activity by synergetic inhibition of ubiquitin ligation and chain elongation as well as blocking further substrate recruitment in a pseudosubstrate manner. However, the *in vivo* approach used in this thesis does not allow to further elucidate the molecular mechanisms mediated by the identified protein domains and further experiments similar to the *in vitro* single-encounter reaction assays presented in Wang et al. (2013) or elaborate EM reconstitutions of APC/C-Rca1 complex will be required to further dissect the detailed inhibitory mechanisms mediated by the individual domains..

4.4. Molecular switches converting Rca1 from an APC/C inhibitor to substrate

Having established that Rca1 constitutes an APC/C inhibitor and an APC/C substrate, a further aim of this thesis was to decipher the mechanism converting Rca1 from an APC/C inhibitor in G2-phase to a substrate in G1-phase. Recently, a regulatory mechanism for Emi1 was suggested in which Emi1 is regulated in dependence of its concentration. At high concentrations it functions as an APC/C inhibitor during S- and G2-phase, whereas at low concentrations, resulting from initial degradation by $SCF^{\beta TrCP}$ at the beginning of mitosis, Emi1 is targeted by the APC/C during G1-phase (Cappell et al., 2018). A similar regulation of Rca1 is very unlikely since a $SCF^{\beta TrCP}$ dependent degradation that would reduce Rca1 protein levels at the beginning of mitosis was excluded (see 3.2.5.4; Figure 44). Furthermore, the different Rca1 constructs were overexpressed in our experiments exceeding endogenous Rca1 levels, which should have resulted in constant APC/C inhibition and no Rca1 degradation during G1-phase, which was not the case. Thus, Rca1 function or degradation must be regulated by other mechanisms.

4.4.1. Phosphorylation of Rca1 is involved regulation of its function and degradation

A first molecular mechanism that was investigated in regard of Rca1 regulation was its post translational modification by phosphorylation. Since degron phosphorylation has been demonstrated as a regulatory mechanism of several APC/C substrates, including Geminin, Securin, Acm1, Cdc6, etc. (see 2.6.6), by either enhancing or reducing their degradation a similar regulation could also apply for Rca1. Initially it was demonstrated that Rca1 is phosphorylated at multiple sites in its N- and C-terminal region using Phostag SDS-PAGE. Next, mutation of ten putative Cdk phosphorylation S/T-P sites was shown to reduce Rca1 phosphorylation, indicating a Cdk dependent phosphorylation of Rca1. In addition, two potential Cks binding sites are present in the N- and C-terminal region of Rca1, respectively. These sites might allow Cks mediated Cdk recruitment and docking that can result in multisite phosphorylation as shown for other cell cycle regulated proteins (Örd et al., 2019 c).

Next, the impact of reduced Rca1 phosphorylation on its degradation and function were examined. It was demonstrated that impaired phosphorylation of N-terminal residues resulted in a destabilization of Rca1, opposed to previous analysis in *Drosophila* embryo (Zielke, 2006), which is likely referable to the less sensitive determination of Rca1 stability in these experiments. Furthermore, it was excluded that the destabilization resulted from an intrinsic effect caused by the introduced mutations (see 3.4.2.3; Figure 56). A similar regulatory mechanisms was described for budding yeast Acm1, that is stabilized by Cdc28 dependent phosphorylation that is opposed by Cdc14 activity resulting in Acm1 proteolysis (Hall et al., 2008). Consequently, a potential regulation of Rca1 degradation could be mediated by a phosphorylation dependent stabilization of Rca1 opposed by destabilizing dephosphorylation.

Furthermore, it was shown that impaired phosphorylation of C-terminal residues was required for sufficient Rca1 function. Interestingly, Cdk dependent phosphorylation of Emi1 in mitosis reduced the APC/C inhibitory function of Emi1 and mutation of three C-terminal S/T-P sites prevented this effect. Thus, our results indicate a completely opposed regulatory mechanisms for Rca1 function, in which phosphorylation at C-terminal inhibitory domains is required for full activation of Rca1 instead of its inactivation. Taken together, the results suggest a phosphorylation dependent regulation of Rca1 by which phosphorylation of Rca1 enhances its inhibitory function and simultaneously decreases its proteolysis. In such a model, Rca1 would be phosphorylated during S- and G2- phase when Cdk activity is high, whereas it is partially or even completely dephosphorylated during mitosis or G1-phase in which kinase activity is low and also opposed by high phosphatase activity (reviewed in Martín et al., 2020). To test this hypothesis, it was attempted to examine Rca1 phosphorylation status in cells arrested in either G2-, M- or G1-phase. Unfortunately, the experiments were unsuccessful as drug induced arrest in either G2- or G1- phase only resulted in a minor enrichment of cells in the respective cell cycle stage, although cell cycle arrest was successfully tested in preliminary tests. However, it must be stated that 20-Hydroxyecdysone induced G2-arrest was shown to result from decreased of Cyclin A and B expression in IAL-PID2 cell line from *Plodia interpunctella* (Mottier et al., 2004) and it can be assumed that similar applies for *Drosophila* cell lines. This would be a great disadvantage in this experiment, since the results could be negatively biased by a reduced Cdk activity caused by the treatment with 20-Hydroxyecdysone and consequently an alternative approach for a G2-phase arrest should be implemented instead.

In conclusion it can be stated that reduced phosphorylation of Rca1 had severe impact on its degradation and function supporting the hypothesis of a phosphorylation dependent regulation of Rca1. However several unanswered questions remain that could not be addressed with the applied approaches. First, not all phosphorylation sites were eliminated in the Rca1_10A mutant and the remaining phosphorylation sites must still be identified. Second, it cannot be easily determined by Phos-tag SDS-PAGE

which of the tested residues were actually phosphorylated and further attempts must be taken to decipher which of the amino acids residues of Rca1 were actually subjected to phosphorylation. Third, direct evidence of Cdk phosphorylation still has to be provided that also identifies the Cdk-Cyclin complexes that are involved in Rca1 phosphorylation. Fourth, evidence for differences in Rca1 phosphorylation status in the context of cell cycle progression must be obtained to prove the hypothesis of cell cycle stage dependent regulation of Rca1 by altered phosphorylation.

4.4.2. Rca1 stability and function is not influenced by 14-3-3 binding

A further regulatory mechanism that is often linked to phosphorylation, is motif hiding in which access of degrons or functional domains is blocked by phosphorylation dependent interaction with another protein. For instance, association of the F-box protein NIPA with Skp1 blocks APC/C^{Cdh1} dependent degradation, which is dissolved by phosphorylation dependent dissociation of Skp1 (von Klitzing et al., 2011). As Rca1 contains an F-box and was also shown to interact with *Drosophila* SkpA (Frank, 2013; Kies, 2017) a similar regulation could be assumed. However, abolished SkpA binding caused by a mutation within the F-box (M182T) had no effect on relative protein stability levels of Rca1_100-299 (see 3.2.5.3; Figure 43) and a destabilization would have been expected in case of a protective function of SkpA association. Hence, a regulation of Rca1 degradation by SkpA association is rather unlikely and was not further investigated in the course of this thesis.

Another well studied example is the protective interaction of budding yeast Acm1 with 14-3-3 proteins Bmh1 and Bmh2. Acm1 phosphorylation by Cdc28 triggers 14-3-3 binding thereby stabilizing Acm1 which is opposed by phosphatase Cdc14 activity causing a dissociation of 14-3-3 and Acm1 degradation (Hall et al., 2008; Qin et al., 2019). In this thesis, a so far unknown interaction of Rca1 with 14-3-3 protein was discovered that is mediated by a 14-3-3 binding site within the ZBR_loop (see 3.4.3; Figure 59). Furthermore, it was shown that 14-3-3 interaction was dependent on phosphorylation site S326 (see 3.4.3.1; Figure 61) which was shown to be phosphorylated consistent with the entry in the iProteinDB database (see 3.4.2.1; Figure 54). However, loss of 14-3-3 interaction had no impact on relative protein stability levels of Rca1 and Rca1_204-411 (see 3.4.3.2; Figure 62) contradicting a similar regulatory mechanism as reported for Acm1. Since the 14-3-3 binding site is located within the ZBR domain, it was also tested if 14-3-3 association enhances or inhibits Rca1 function. However, no changes were observed for Rca1 function in case of Rca1_204-411_S326A and the 4A mutant in the *in vivo* APC/C activity assay (see 3.4.3.3; Figure 63). Thus, loss of 14-3-3 interaction had no impact on Rca1 degradation nor its function as an APC/C inhibitor. Unfortunately, a replacement of serine 326 with an aspartic acid (S326D) did not result in a phosphomimetic of phospho-serine accompanied by constitutive 14-3-3 binding, which would have allowed to also asses the effects of enhanced 14-3-3 binding (see 3.4.3.1; Figure 61). Interestingly, subcellular localization of Acm1 was also influenced by Cdc28 dependent

phosphorylation and Cdc14 dependent dephosphorylation and it was speculated whether 14-3-3 binding could be involved in subcellular sequestration of Acm1 (Enquist-Newman et al., 2008). A localization dependent effect of 14-3-3 could have been concealed by the presence of an exogenous NLS in our experiments, hence the influence of 14-3-3 binding in the context of Rca1 localization was also investigated in this thesis and will be discussed in the next section.

4.4.3. Nuclear localization of Rca1 is essential for robust degradation

Rca1 was shown to be predominantly localized within the nucleus in Drosophila embryo (Grosskortenhaus et al., 2002) which was attributed to its N-terminal NLS sequence. To assess whether nuclear localization was essential for Rca1 degradation two new RPS constructs were established for localization dependent analysis of protein degradation either using CHE-, NLS-CHE, or NES-CHE as fluorescent reporters. However, initial analysis of CHE localization resulted in a mainly nuclear localization which was increased by an additional NLS sequence, whereas fusion of a NES sequence caused a nearly complete cytoplasmic sequestration. The nuclear localization of CHE must be taken into account for the interpretation of the obtained data as it is still unclear if it was caused by a passive diffusion or an active transport mediated by two putative NLS sequences within CHE. Thus, it cannot be excluded that fusion of just CHE to a protein of interest could alter subcellular localization and does not represent the regular localization of the POI. Nevertheless, marked differences in the localization of CHE-, NLS-CHE, and NES-CHE were detectable and thus it was focused on these distinctions.

Using the different reporter constructs it was demonstrated that Rca1 degradation was significantly impaired but not completely abolished by forced cytoplasmic accumulation. The N-terminal bipartite NLS mediates nuclear localization and CHE tagged C-terminal Rca1 that lacks this NLS was less localized within the nucleus causing a severe stabilization, which could be compensated by an exogenous NLS as used in the initial RPS analysis. A recent study (Bischof, 2020) showed that consistent with the results of this thesis, deletion of the N-terminal NLS in full-length Rca1 caused an increased cytoplasmatic accumulation and a stabilization of the Rca1 mutant. Furthermore, a second so far unknown NLS sequence in the C-terminal region was identified that explains the remaining nuclear import of C-terminal Rca1 (see 3.4.4.2; Figure 67). Hence, nuclear localization of Rca1 is mediated by an N-terminal and C-terminal NLS sequence, albeit latter one can be assumed to be less efficient, and nuclear localization is essential for robust Rca1 degradation. Consequently, a further potential regulatory mechanism of Rca1 degradation could be based on its subcellular localization.

Besides its role in motif hiding, 14-3-3 interaction has also been shown to interfere with nuclear localization as demonstrated for instance for Cdc25, whose nuclear import was inhibited by phosphorylation dependent binding of 14-3-3 (Gardino et al., 2011). Interestingly, the 14-3-3 binding site in the C-terminal part of Rca1 overlaps with the recently discovered C-terminal NLS sequence as well as a putative NES sequence (see 3.4.4.3; Figure 68), which could indicate a 14-3-3 regulated import or export of Rca1. Since initial analysis of the function of 14-3-3 interaction with Rca1 was conducted with a NLS-

CHE reporter, localization dependent effects could have been masked by the exogenous NLS. Examination of abolished 14-3-3 binding in the context of subcellular localization displayed an increased nuclear localization of CHE-Rca1_S326A and NLS-CHE-Rca1_S326A, indicating a nuclear export of Rca1 mediated by 14-3-3 binding (see 3.4.3.2; Figure 69). Furthermore, a decrease of Rca1_204-411_S326A and Rca1_S326A stability in G1-cells was observed when fused to NES-CHE indicating a less pronounced export from the nucleus without 14-3-3 interaction, although no discernible changes in the localization of these constructs was observed. However, the localization analysis mainly represents the situation in G2-phase and not G1-phase, in which Rca1 degradation was determined and subcellular localization of Rca1 in G1 may differ compared to G2-phase. Nevertheless, some of the data were contradictory to the 14-3-3 export mechanism. An increased nuclear localization of CHE-Rca1_S326A would have been expected but was just observed for NLS-CHE-Rca1_S326A. Moreover, a decline in nuclear localization of NLS-CHE-Rca1_204-411_S326A compared to NLS-CHE-Rca1_204-411 was observed. However, this is likely to be attributed to the strong variance of the data for NLS-CHE-Rca1_204-411 which did not allow a proper evaluation of its localization and should therefore be repeated.

Taken together, it can be stated that initial analysis of a 14-3-3 dependent regulation of Rca1 localization suggested a potential export mechanism of Rca1 mediated by phosphorylation dependent 14-3-3 binding. However, a major limitation of the conducted localization analysis that must be taken into account was that protein localization was quantified mainly for cells that resided in G2-phase. Though, a 14-3-3 mediated export of Rca1 was only measured during this cell cycle stage and it is not possible to evaluate the role of 14-3-3 binding during other cell cycle stage by the conducted experiments. A further attempt to additionally gain deeper insight into the temporal context of Rca1 and 14-3-3 interaction by co-immunoprecipitation assays using cell cycle arrested cells, failed due to unsuccessful cell cycle arrest (see3.4.3.2; Figure 62) and did not enable to gain deeper insight into the temporal context of this interaction. Additionally, strong protein overexpression were used in these experiments as protein expression was implemented by transient transfection, which can in general result in strong alterations of the regular localization of a protein. Furthermore, it cannot be excluded that the fusion to CHE and its intrinsic tendency to be predominately localized within the nucleus suppressed the effect of 14-3-3 binding and did not reflect actual localization of the applied Rca1 constructs. Thus, further experiments must be performed to ascertain a 14-3-3 dependent shuttling of Rca1.

As subcellular localization and protein trafficking between the cytoplasm and the nucleus is often intimately linked to protein phosphorylation (reviewed in Nardozzi et al., 2010), a cooperative regulation of Rca1 by phosphorylation dependent changes of its localization was also conceivable. To assess whether there is a link between the observed decreased stability of the Rca1 S/T-P site mutants and their subcellular localization, the NLS-CHE tagged mutants used for the stability analysis were analyzed upon changes of their subcellular localization. Since a destabilization in all three assigned cell cycle

populations was observed for the Rca1_10A and Rca1_1-203_7A mutant (see 3.4.2.2; Figure 55), an increased nuclear localization would be expected based on the previous results. However, the 10A mutant displayed no discernible changes in its nuclear localization whereas the N-terminal Rca1 7A mutant was distinctly more localized within the cytoplasm instead of an expected increased nuclear accumulation (see 3.4.4.4; Figure 70). This indicates that phosphorylation causes a stabilization of Rca1 and has also an influence on its localization in G2-phase, which however must not be linked to Rca1_1-203 degradation. Since no changes in the subcellular localization were observed for the Rca1_10A mutant, it can be assumed that also the C-terminal region of Rca1 has an impact on Rca1 localization, which would not be surprising due to the second NLS, the putative NES sequence, and the 14-3-3 binding site that was also involved in Rca1 localization. However further experiments must be performed to unveil the detailed mechanisms behind this observation. It must also be considered that the expression constructs contained an exogenous NLS sequence that could distort localization dependent effects and the experiments should be repeated using only a CHE reporter to exclude undesired effects caused by the additional NLS sequence.

As there are several reports for enhanced nuclear import by phosphorylation within a NLS sequence (reviewed in Nardozzi et al., 2010) an Rca1 mutant for the two verified phosphorylation sites S123 and S127, which are located within the N-terminal NLS, was analyzed upon changes in its relative protein stability levels using a CHE, NLS-CHE, and NES-CHE reporter. However, no changes in the degradation were observed by the introduced mutations (S123A_S127A) for any of the reporter constructs. This further contradicts a phosphorylation dependent regulation of Rca1 localization. However, localization of these mutants was not analyzed yet and also five further potential Cdk phosphorylation sites were identified within the bipartite NLS (T88, S95, T104, S112, and S126) that have not been analyzed so far. Thus, nuclear import may be regulated by phosphorylation but due to the incomplete identification of actual phosphorylation sites of Rca1 it was not possible to provide evidence for such a regulatory mechanism to this point. More data on the actual phosphorylated amino acid residues is required to determine if phosphorylation of the NLS sequence has a regulatory effect. Furthermore, it must also be considered that the C-terminal NLS and 14-3-3 binding are likely to be involved in the regulation of Rca1 localization, adding a further layer of complexity to this issue.

4.4.4. Rca1 function is independent of its subcellular localization

Besides the impact of localization on its degradation, it was also examined if nuclear localization is required for APC/C inhibition by Rca1. Analysis of Rca1 function in dependence of its localization was examined using either 4xFLAG-, NLS-4xFLAG-, or 4xFLAG-NES-tagged Rca1 constructs in the *in vivo* APC/C activity assay. Surprisingly, APC/C inhibition by Rca1_204-411 was only decreased to a minor extent without an additional NLS sequence (4xFLAG-Rca1_204-411) or an additional NES sequence (4xFLAG-NES-Rca1_204-411). Interestingly, abolishment of 14-3-3 binding, as in 4xFLAG-Rca1_204-

411_S326A, did no longer display impaired Rca1 function. This could be explained by an increased nuclear localization of the S326A mutant that would further support a 14-3-3 dependent export of Rca1 (see 3.4.4.5; Figure 72.). A similar effect was however not observed for 4xFLAG-Rca1, which could be explained by the presence of the N-terminal NLS, further indicating a complex regulation of Rca1 localization including N- and C-terminal domains of Rca1. Nevertheless, it was rather surprising that cytoplasmic Rca1 was able to restrain APC/C dependent degradation of the nuclear NLS-CHE-CycB-NT^{285} sensor. However, consistent with this observation nuclear Rca1 was also able to restrain degradation of a cytoplasmic CycB sensor (see 3.4.4.6; Figure 74). A possible explanation for these results could reside in only a partial change in the localization of the different FLAG-tagged Rca1 constructs, as localization of these constructs was not uniformly analyzed by immunostaining. However, strong nuclear accumulation of NLS-4xFLAG-Rca1_204-411 was verified by immunostaining (6 week internship C. Baumgartl 2018) and insertion of the fluorescent protein CHE also displayed strong changes in its localization depending on the different protein tags (data not shown). Thus it can be assumed that the different tags should also cause altered Rca1 localization. Nevertheless, localization of the applied constructs should additionally be tested and quantified to exclude any bias caused by the different FLAG tags.

Thus, two assertions can be made based on the obtained results. First, APC/C^{Fzr} activity is not completely restricted to the nucleus, but occurs also to a minor extent in the cytoplasm in *Drosophila* S2R+ cells. Since cytoplasmic Rca1 and CycB were still destabilized, albeit to a lesser extent as in the nucleus, and Fzr overexpression caused an increased destabilization of NES-CHE-CycB-NT^{285} it must be assumed that the APC/C is also active in the cytoplasm. This would also be consistent with a recent study showing that Fzr localization to the centrioles was essential for efficient degradation of Aurora A (Meghini et al., 2016), also indicating cytoplasmic APC/C activity.

Second, Rca1 can restrain nuclear and cytoplasmic APC/C activity independent of its own localization. The obtained results indicate that Rca1 must be able to restrain both nuclear and cytoplasmic APC/C activity independent of its own localization, by a so far unknown mechanism. The most obvious explanation for this, would be a shuttling of Rca1 between the cytoplasm and the nucleus that is mediated by 14-3-3 binding and dissociation. However, further experiments must be performed to elucidate the spatial regulation of Rca1 function and to prove this hypothesis.

Summarized, it was possible to gain deeper insight into the life cycle of Rca1 in the course of cell cycle progression (Figure 75). However, several questions regarding the distinct molecular mechanism restraining APC/C activity and the conversion of Rca1 from an APC/C inhibitor to substrate remain unanswered. Several initial indications for a complex regulation of Rca1 including phosphorylation and its

localization have been provided in this thesis, but further studies will be required to elucidate the multilayerd molecular mechanisms regulating Rca1 function and degradation in the course of cell cycle progression.

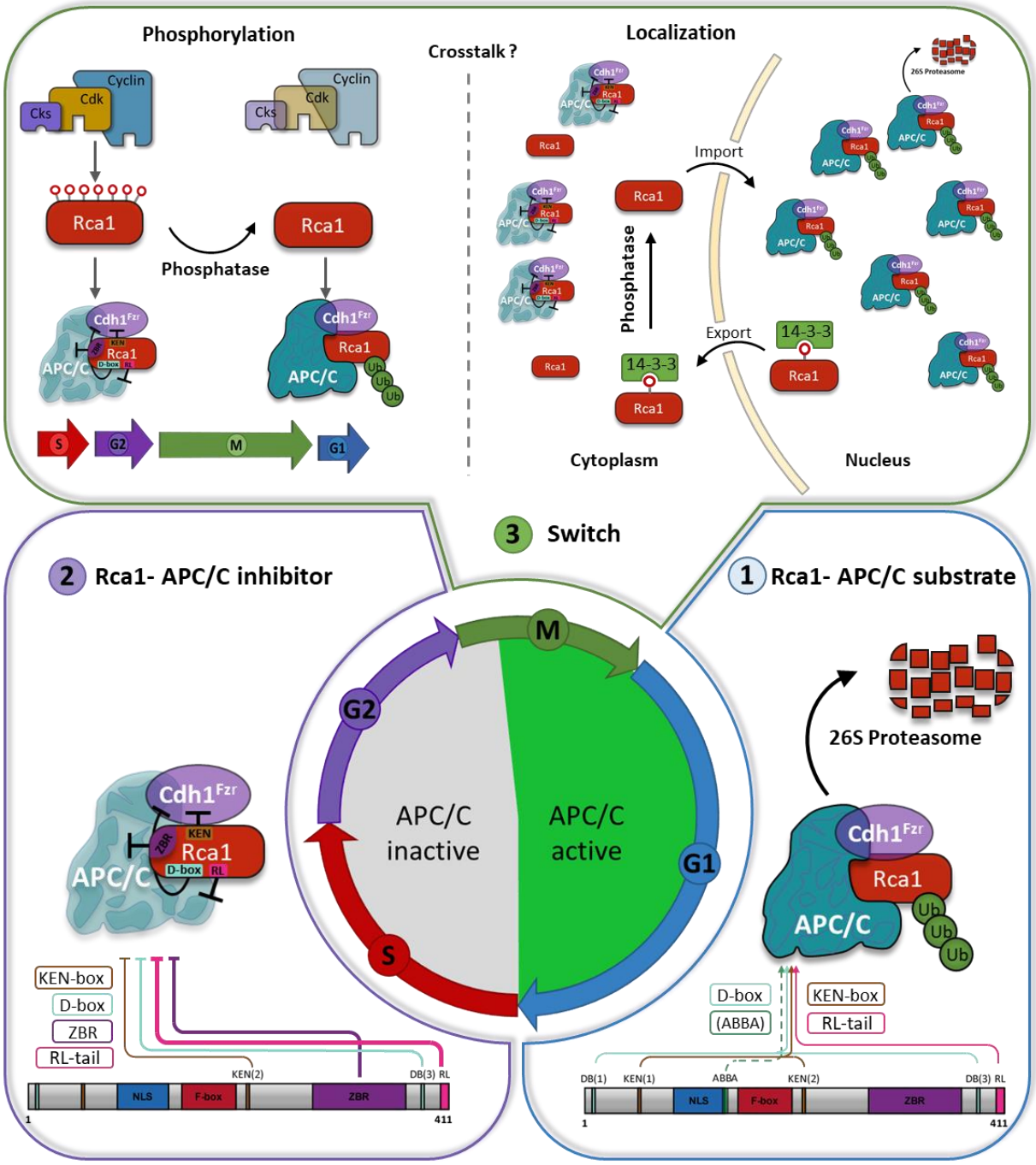

Figure 75| Rca1 life cycle during cell cycle progression

Rca1 life cycle in the course of cell cycle progression. (1) Rca1 destruction during G1-phase is mediated by the APC/C^{Fzr}. Rca1 recruitment is dependent on several APC/C degrons including two D-box and two KEN-box degrons and eventually a ABBA motif together with the C-terminal RL-tail. (2) During S- and G2-phase, Rca1 functions as an APC/C^{Fzr} inhibitor, restraining its activity via several C-terminal domains including a KEN-box, ZBR, D-box, and RL-tail. (3) Conversion of Rca1 from an inhibitor to APC/C substrate is likely to be mediated by a combination of complex molecular mechanisms including its phosphorylation as well as its subcellular localization that is further modulated by a 14-3-3 dependent shuttling mechanism.

5. Material

5.1. Chemicals

Table 1| List of chemicals

Chemical	Distributor
20-Hydroxyecdysone	SelleckChem
Acetic acid (CH_3COOH, HAc)	Merck KGaA
Acrylamide 30%/bisacrylamide	Carl Roth GmbH
Agarose ultra	Invitrogen GmbH
Ampicillin	Carl Roth GmbH
Aphidicolin	Santa Cruz Biotechnology
APS (ammonium persulfate)	Merck KGaA
ATP (100 mM)	New England Biolabs
Bacto Pepton	Becton
Bacto Trypton	Becton
Bacto Yeast Extract	Becton
Beta-Mercaptoethanol	Fluka
Bortezomib	Selleckchem.com
Bromophenol blue	SERVA Electrophoresis
CH_3COOK (potassium acetate)	Merck KGaA
Colchicine	Sigma Aldrich
CTP (100 mM)	New England Biolabs
DMSO (Dimethyl sulfoxide)	Merck KGaA, Sigma-Aldrich Chemie GmbH
dNTP mix (dATP, dCTP, dGTP, dTTP)	New England Biolabs
DTT (1,4-dithiothreitol)	AppliChem GmbH
EDTA (ethylenediaminetetraacetic acid)	Fluka
Ethanol	Carl Roth GmbH
Ethidiumbromide	SERVA Electrophoresis
Euroagar	Becton
FuGENE HD	Promega Corporation
GeneRuler DNA Ladder Mix	ThermoScientific
Glucose	Merck KGaA
Glycerol	Carl Roth GmbH
Glycine	AppliChem GmbH
Glyoxal 40%	Sigma Aldrich
GTP (100mM)	New England Biolabs
HCl (hydrochloric acid)	Merck KGaA
HEPES (2-[4-(2-hydroxyethyl)piperazin-1-yl]ethanesulfonic acid)	AppliChem GmbH
Hoechst 33342	Sigma-Aldrich Chemie GmbH
IPTG (Isopropyl β-D-1-thiogalactopyranoside)	AppliChem GmbH
Liquid nitrogen	AG Schneuwly (University of Regensburg)
L-Mimosin	Cayman Chemical Company
Methanol	Carl Roth GmbH
$MgCl_2$	Merck
NaCl (Sodium chloride)	Carl Roth GmbH, Merck
NaOH (sodiumhydroxide)	Gerbu Trading GmbH
NH_4HCO_3 (ammonium bicarbonate)	AG Deutzmann (University of Regensburg)
N-Hydroxyurea	AppliChem
Phusion GC buffer	Thermo Scientific
Phusion HF buffer	Thermo Scientific
Precision Plus Protein Standard	Bio-Rad Laboratories
Protease inhibitor mix	Bimake
Restriction buffers 10X	New England Biolabs
Schneider`s *Drosophila* medium	Invitrogen, PAN Biotech
SDS (sodium dodecyl sulfate)	Carl Roth GmbH, SERVA Electrophoresis
Skim milk powder Gloria	Nestle
Spermidine	Sigma-Aldrich Chemie GmbH

Chemical	Distributor
Streptomycin 100X	Invitrogen GmbH
T4 ligase Buffer 10X	New England Biolabs
TEMED (tetramethylethylenediamine)	Fluka
Tris (tris(hydroxymethyl)aminomethane)	Carl Roth GmbH
Triton X-100	Fluka
Tween20	Carl Roth GmbH
UTP (100 mM)	New England Biolabs
X-gal	AppliChem GmbH
Xylene cyanol	SERVA Electrophoresis

5.2. Proteins/Enzymes

Table 2| List of proteins and enzymes

Protein/Enzyme	Distributor
BSA (bovine serum albumin)	Sigma-Aldrich Chemie GmbH
FBS (fetal bovine serum)	AG Medenbach
Lambda Protein Phosphatase (LambdaPP)	New England Biolabs
T4 DNA Ligase	Sigma-Aldrich Chemie GmbH
Lysozyme	Boehringer Mannheim, Fluka, Sigma-Aldrich Chemie GmbH
Phusion DNA polymerase	STRATEC Molecular GmbH
Restriction endonucleases	New England Biolabs
RNase A	AppliChem GmbH
RNase Inhibitor	AG Medenbach
Shrimp Alkaline Phosphatase (rSAP)	New England Biolabs
T7 RNA polymerase	New England Biolabs

5.3. Kits

Table 3| List of kits

Kit	Distributor
Invisorb Spin DNA Extraction Kit	STRATEC Molecular GmbH
FastGene Gel/PCR Extraction Kit	Nippon genetics
PureYield Plasmid Midiprep system	Promega
Click-iT™ Plus EdU Alexa Fluor™ 647 Flow Cytometry Assay Kit	Thermo Fisher Scientific

5.4. Oligonucleotides

Oligonucleotides used for molecular cloning and sequencing are not listed but can be accessed from the internal AG Sprenger database.

Table 4| List of Oligos

Name	Sequence	Purpose
SPO_342	TAATACGACTCACTATAGGG	Amplification of DNA for dsRNA production

5.5. Plasmids

Nomenclature of mutations were annotated as suggested by Dunnen and Antonarakis (Den Dunnen et al., 2000). The plasmid maps and the component fragments are deposited in the vector NTI database of the AG Sprenger.

5.5.1. RPS basic expression plasmids

Table 5| List of RPS basic expression plasmids

Number	Name **Nickname**
pFSR-1179	actPro(L)-HA-NLS-BX-CHE-ddT2A-HA-NLS-GFP **RPS-01: HA-NLS-BX-CHE-T2A-HA-NLS-GFP**
pFSR-1180	actPro(L)-HA-NLS-CHE-BX-ddT2A-HA-NLS-GFP **RPS-02: HA-NLS-CHE-BX-T2A-HA-NLS-GFP**
pFSR-1196	actPro(L)-HA-NLS-CHE-ddT2A-HA-NLS-BX-GFP **RPS-03: HA-NLS-CHE-T2A-HA-NLS-B/X-GFP**
pFSR-1197	actPro(L)-HA-NLS-CHE-ddT2A-HA-NLS-GFP-BX **RPS-04: HA-NLS-CHE-T2A-HA-NLS-GFP-B/X**
pFSR-1203	actPro(L)-HA-NLS-BX-GFP-ddT2A-HA-NLS-CHE **RPS-05: HA-NLS-B/X-GFP-T2A-HA-NLS-CHE**
pFSR-1212	actPro(L)-HA-NLS-GFP-BX-ddT2A-HA-NLS-CHE **RPS-06: HA-NLS-GFP-B/X-T2A-HA-NLS-CHE**
pFSR-1214	actPro(L)-HA-NLS-GFP-ddT2A-HA-NLS-BX-CHE **RPS-07: HA-NLS-GFP-T2A-HA-NLS-B/X-CHE**
pFSR-1204	actPro(L)-HA-NLS-GFP-ddT2A-HA-NLS-CHE-BX-myc **RPS-08: HA-NLS-GFP-T2A-HA-NLS-CHE-BX-Myc**
pFSR-1591	actPro(L)-HA-NLS-GFP-ddT2A-CHE-BX-myc **RPS-09: HA-NLS-GFP-T2A-CHE-BX-Myc**
pFSR-1591	actPro(L)-HA-NLS-GFP-ddT2A-HA-NES-CHE-BX-myc **RPS-10: HA-NLS-GFP-T2A-HA-NES-CHE-BX-Myc**
pFSR-1365	actPro(L)-HA-NLS-CHE-ddT2A_G17A_P18A -HA-NLS-GFP-B/X **HA-NLS-CHE-mT2A-HA-NLS-GFP-B/X**

5.5.2. RPS Cyclin B plasmids

Table 6| List of RPS Cyclin B plasmids

Number	Name **Nickname**
pFSR-1217	actPro(L)-HA-NLS-CHE-CycB_Del_286-530-ddT2A-HA-NLS-GFP **CHE-CycB-NT^{285}-T2A-GFP**
pFSR-1218	actPro(L)-HA-NLS-CycB_Del_286-530-CHE-ddT2A-HA-NLS-GFP **CycB-NT^{285}-CHE-T2A-GFP**
pFSR-1221	actPro(L)-HA-NLS-GFP-ddT2A-HA-NLS- CHE-CycB_Del_286-530 **GFP-T2A-CHE-CycB-NT^{285}**
pFSR-1227	actPro(L)-HA-NLS-GFP-ddT2A-HA-NLS-CycB_Del_286-530-CHE **GFP-T2A-CycB-NT^{285}-CHE**
pFSR-1400	actPro(L)-HA-NLS -GFP-ddT2A-HA-NLS-CHE-CycB_Del_286-530_R37A_L40A **GFP-T2A-CHE-CycB-NT^{285}_mDB**
pFSR-1408	actPro(L)-HA-NLS -GFP-ddT2A-HA-NLS-CHE-CycB_248-530 **GFP-T2A-CHE-CycB-NT^{247}_ΔKEN**
pFSR-1409	actPro(L)-HA-NLS -GFP-ddT2A-HA-NLS-CHE-CycB_del_248-530_ R37A_L40A **GFP-T2A-CHE-CycB-NT^{247}_mDB_ΔKEN**
pFSR-1429	actPro(L)-HA-NLS-CHE-ddT2A_G17A_P18A-HA-NLS-GFP-CycB_Del_248-530 **CHE-mT2A-GFP-CycB-NT^{285}**
pFSR-1667	actPro(L)-HA-NLS-GFP-ddT2A-HA-NES-CHE-CycB_Del-286-530 **NLS-GFP-T2A-NES-CHE-CycB-NT^{285}**

5.5.3. RPS Geminin plasmids

Table 7| List of RPS Geminin plasmids

Number	Name **Nickname**
pFSR-1378	actPro(L)-HA-NLS-GFP-ddT2A-HA-NLS-CHE Gem_Del_102-192 **GFP-T2A-CHE-Gem-NT^{101}**
pFSR-1381	actPro(L)-HA-NLS-CHE-Gem_Del_102-192-ddT2A-HA-NLS-GFP **CHE-Gem-NT^{101}-T2A-GFP**
pFSR-1382	actPro(L)-HA-NLS-Gem_Del_102-192-CHE-ddT2A-HA-NLS-GFP **Gem-NT^{101}-CHE-T2A-GFP**
pFSR-1384	actPro(L)-HA-NLS-GFP-ddT2A-HA-NLS-Gem_Del_102-192-CHE **GFP-T2A-Gem-NT^{101}- CHE**
pFSR-1386	actPro(L)-HA-NLS-Gem_Del_102-192_R26A_L29A -CHE-ddT2A-HA-NLS-GFP **Gem-NT^{101}_mDB-CHE-T2A-GFP**
pFSR-1508	actPro(L)-HA-NLS-Gem_Del_102-192_E40A_N41A-CHE-ddT2A-HA-NLS-GFP **Gem-NT^{101}_mKEN-CHE-T2A-GFP**
pFSR-1509	actPro(L)-HA-NLS-Gem_Del_102-192_R26A_L29A_E40A_N41A-CHE-ddT2A-HA-NLS-GFP **Gem-NT^{101}_mDB_mKEN-CHE-T2A-GFP**

5.5.4. RPS Dacapo, E2F1, and Cdt1 plasmids

Table 8| List of RPS Dacapo, E2F1, and Cdt1 plasmids

Number	Name **Nickname**
pFSR-1231	actPro(L)-HA-NLS-CHE-Dap_Del-38-44-RAR_Del-103-105-G-ddT2A-HA-NLS-GFP **CHE-Dap_dCDI-T2A-GFP**
pFSR-1232	actPro(L)-HA-NLS-Dap_Del-38-44-RAR_Del-103-105-G-CHE-ddT2A-HA-NLS-GFP **Dap_dCDI-CHE-T2A-GFP**
pFSR-1237	actPro(L)-HA-NLS-GFP-ddT2A-HA-NLS-Dap-Dap_Del-38-44-RAR_Del-103-105-G-CHE **GFP-T2A-Dap_dCDI-CHE**
pFSR-1238	actPro(L)-HA-NLS-GFP-ddT2A-HA-NLS-CHE-Dap_Del-38-44-RAR_Del-103-105-G **GFP-T2A-CHE-Dap_dCDI**
pFSR-1363	actPro(L)-HA-NLS-GFP-ddT2A-HA-NLS-CHE-Dap_Del-38-44-RAR-_Del-103-150-G_Del-184-188 **GFP-T2A-CHE-Dap_dCDI_dPIPa**
pFSR-1522	actPro(L)-HA-NLS-GFP-ddT2A-HA-NLS-CHE-E2F1_Del_231-805 **GFP-T2A-CHE-E2F1-NT^{230}**
pFSR-1280	actPro(L)-HA-NLS-Cdt1_Del_102-743-CHE-ddT2A-HA-NLS-GFP **Cdt1-NT^{101}-CHE-T2A-GFP**

5.5.5. RPS Rca1 plasmids

Table 9| List of RPS Rca1 plasmids

Number	Name **Nickname**
pFSR-1261	actPro(L)-HA-NLS-GFP-ddT2A-HA-NLS-CHE-Rca1 **GFP-T2A-CHE-Rca1**
pFSR-1484	actPro(L)-HA-NLS-GFP-ddT2A-HA-NLS-CHE-Rca1_Del_1-10_E53A_N54A_E215A_N216A **GFP-T2A-CHE-Rca1_ΔDB(1)_mKEN(1)_mKEN(2)**
pFSR-1528	actPro(L)-HA-NLS-GFP-ddT2A-HA-NLS-CHE-Rca1_Del_1-10_E53A_N54A_L135A_P137A_H138A_E140A_ E215A_N216A **GFP-T2A-CHE-Rca1_ΔDB(1)_mKEN(1)_mABBA_mKEN(2)**
pFSR-1537	actPro(L)-HA-NLS-GFP-ddT2A-HA-NLS-CHE-Rca1_Del_1-10_Del_406-411_E53A_N54A_L135A_P137A_ H138A_E140A_E215A_N216A **GFP-T2A-CHE-Rca1_ΔDB(1)_mKEN(1)_mABBA_mKEN(2)_ ΔRL**

Number	Name Nickname
pFSR-1570	actPro(L)-HA-NLS-GFP-ddT2A-HA-NLS-CHE-Rca1_Del_1-10_Del_406-411_E53A_N54A_L135A_P137A_ H138A_E140A_E215A_N216A **GFP-T2A-CHE-Rca1_ΔDB(1)_mKEN(1)_mABBA_mKEN(2)_C351S_ ΔRL**
pFSR-1630	actPro(L)-HA-NLS-GFP-ddT2A-HA-NLS-CHE-Rca1_Del_1-10_E53A_N54A_L135A_P137A_H138A_E140A_E215A_N216A_R384A_L387A **GFP-T2A-CHE-Rca1_ΔDB(1)_mKEN(1)_mABBA_mKEN(2)_mDB(3)**
pFSR-1631	actPro(L)-HA-NLS-GFP-ddT2A-HA-NLS-Rca1_Del_1-10_Del_406-411_E53A_N54A_L135A_P137A_H138A_ E140A_E215A_N216A_R384A_L387A **GFP-T2A-CHE-Rca1_ΔDB(1)_mKEN(1)_mABBA_mKEN(2)_mDB(3)_ ΔRL**
pFSR-1657	actPro(L)-HA-NLS-GFP-ddT2A-HA-NLS-Rca1_Del_1-10_Del_406-411_E53A_N54A_L135A_P137A_H138A_ E140A_R207A_L210A_E215A_N216A_R384A_L387A **GFP-T2A-CHE-Rca1_ΔDB(1)_mKEN(1)_mABBA_mDB(2)_mKEN(2)_mDB(3)_ ΔRL**
pFSR-1344	actPro(L)-HA-NLS-GFP-ddT2A-HA-NLS-CHE-Rca1_S285R **GFP-T2A-CHE-Rca1_S285R**
pFSR-1256	actPro(L)-HA-NLS-GFP-ddT2A-HA-NLS-CHE-Rca1_A344T **GFP-T2A-CHE-Rca1_A344T**
pFSR-1258	actPro(L)-HA-NLS-GFP-ddT2A-HA-NLS-CHE-Rca1_C351S **GFP-T2A-CHE-Rca1_C351S**
pFSR-1463	actPro(L)-HA-NLS-GFP-ddT2A-HA-NLS-CHE-Rca1_S14A_T43A_T70A_T104A_S123A_S127A_S186A_ S335A_T376A_T388A **GFP-T2A-CHE-Rca1_10A**
pFSR-1613	actPro(L)-HA-NLS-GFP-ddT2A-HA-NLS-CHE-Rca1_S123A_S127A **NLS-GFP-T2A-NLS-CHE-Rca1_S123A_S127A**
pFSR-1579	actPro(L)-HA-NLS-GFP-ddT2A-HA-NLS-CHE-Rca1_S326A **GFP-T2A-CHE-Rca1_S326A**
pFSR-1603	actPro(L)-HA-NLS-GFP-ddT2A-CHE-Rca1 **NLS-GFP-T2A-CHE-Rca1**
pFSR-1604	actPro(L)-HA-NLS-GFP-ddT2A-CHE-Rca1_S326A **NLS-GFP-T2A-CHE-Rca1_S326A**
pFSR-1614	actPro(L)-HA-NLS-GFP-ddT2A-CHE-Rca1_S123A_S127A **NLS-GFP-T2A-CHE-Rca1_S123A_S127A**
pFSR-1609	actPro(L)-HA-NLS-GFP-ddT2A-HA-NES-CHE-Rca1 **NLS-GFP-T2A-NES-CHE-Rca1**
pFSR-1610	actPro(L)-HA-NLS-GFP-ddT2A-HA-NES-CHE-Rca1_S326A **NLS-GFP-T2A-NES-CHE-Rca1_S326A**
pFSR-1615	actPro(L)-HA-NLS-GFP-ddT2A-HA-NES-CHE-Rca1_S123A_S127A **NLS-GFP-T2A-NES-CHE-Rca1_S123A_S127A**

5.5.6. RPS Rca1_1-203 plasmids

Table 10| List of RPS Rca1_1-203 plasmids

Number	Name Nickname
pFSR-1387	actPro(L)-HA-NLS -GFP-ddT2A-HA-NLS-CHE-Rca1_Del_204-411 **GFP-T2A-CHE-Rca1_1-203**
pFSR-1388	actPro(L)-HA-NLS -GFP-ddT2A-HA-NLS-CHE-Rca1_Del_1-10_Del_204-411 **GFP-T2A-CHE-Rca1_1-203_ΔDB(1)**
pFSR-1392	actPro(L)-HA-NLS -GFP-ddT2A-HA-NLS-CHE-Rca1_Del_204-411_R7A **GFP-T2A-CHE-Rca1_1-203_mDB(1)**
pFSR-1410	actPro(L)-HA-NLS -GFP-ddT2A-HA-NLS-CHE-Rca1_Del_204-411_L34A_N38A **GFP-T2A-CHE-Rca1_1-203_mOB(1)**
pFSR-1411	actPro(L)-HA-NLS -GFP-ddT2A-HA-NLS-CHE-Rca1_Del_204-411_R7A_L34A_N38A **GFP-T2A-CHE-Rca1_1-203_mDB(1)_mOB(1)**
pFSR-1426	actPro(L)-HA-NLS -GFP-ddT2A-HA-NLS-CHE-Rca1_Del_204-411_L135A_P137A_H138A_E140A **GFP-T2A-CHE-Rca1_1-203_mABBA**

Number	Name Nickname
pFSR-1435	actPro(L)-HA-NLS-GFP-ddT2A-HA-NLS-CHE-Rca1_Del_1-10_Del_204-411_L135A_P137A_H138A_E140A **GFP-T2A-CHE-Rca1_1-203_ΔDB(1)_mABBA**
pFSR-1443	actPro(L)-HA-NLS-GFP-ddT2A-HA-NLS-CHE-Rca1_Del_204-411_E53A_N54A **GFP-T2A-CHE-Rca1_1-203_mKEN**
pFSR-1444	actPro(L)-HA-NLS-GFP-ddT2A-HA-NLS-CHE-Rca1_Del_1-10_Del_204-411_E53A_N54A_L135A_P137A_H138A_E140A **GFP-T2A-CHE-Rca1_1-203_ΔDB(1)_mKEN_mABBA**
pFSR-1445	actPro(L)-HA-NLS-GFP-ddT2A-HA-NLS-CHE-Rca1_Del_1-10_Del_204-411_E53A_N54A **GFP-T2A-CHE-Rca1_1-203_ΔDB(1)_mKEN**
pFSR-1422	actPro(L)-HA-NLS -GFP-ddT2A-HA-NLS-CHE-Rca1_Del_1-25_Del_204-411 **GFP-T2A-CHE-Rca1_26-203**
pFSR-1425	actPro(L)-HA-NLS -GFP-ddT2A-HA-NLS-CHE-Rca1_Del_1-35_Del_204-411 **GFP-T2A-CHE-Rca1_36-203**
pFSR-1397	actPro(L)-HA-NLS -GFP-ddT2A-HA-NLS-CHE-Rca1_Del_1-50_Del_204-411 **GFP-T2A-CHE-Rca1_51-203**
pFSR-1398	actPro(L)-HA-NLS -GFP-ddT2A-HA-NLS-CHE-Rca1_Del_1-75_Del_204-411 **GFP-T2A-CHE-Rca1_76-203**
pFSR-1462	actPro(L)-HA-NLS-GFP-ddT2A-HA-NLS-CHE-Rca1_Del_204-411_S14A_T43A_T70A_T104A_S123A_S127A_S186A **GFP-T2A-CHE-Rca1_1-203_7A**

5.5.7. RPS Rca1_204-299 plasmids

Table 11| List of RPS Rca1_204-299 plasmids

Number	Name Nickname
pFSR-1286	actPro(L)-HA-NLS -GFP-ddT2A-HA-NLS-CHE-Rca1_Del_1-203_Del_300-411 **GFP-T2A-CHE-Rca1_204-299**
pFSR-1373	actPro(L)-HA-NLS -GFP-ddT2A-HA-NLS-CHE-Rca1_Del_1-210_Del_300-411 **GFP-T2A-CHE-Rca1_210-299_ΔDB(2)**
pFSR-1374	actPro(L)-HA-NLS -GFP-ddT2A-HA-NLS-CHE-Rca1_Del_1-203_Del_300-411_R207A_L210A **GFP-T2A-CHE-Rca1_204-299_mDB(2)**
pFSR-1394	actPro(L)-HA-NLS -GFP-ddT2A-HA-NLS-CHE-Rca1_Del_1-203_Del_300-411_E215A_N216A **GFP-T2A-CHE-Rca1_204-299_mKEN(2)**
pFSR-1395	actPro(L)-HA-NLS -GFP-ddT2A-HA-NLS-CHE-Rca1_Del_1-203_Del_300-411_R207A_L210A_E215A_N216A **GFP-T2A-CHE-Rca1_204-299_mDB(2)_mKEN(2)**

5.5.8. RPS Rca1_100-299 plasmids

Table 12| List of RPS Rca1_100-299 plasmids

Number	Name Nickname
pFSR-1454	actPro(L)-HA-NLS-GFP-ddT2A-HA-NLS-CHE-Rca1_Del_1-99_Del_300-411 **GFP-T2A-CHE-Rca1_100-299**
pFSR-1455	actPro(L)-HA-NLS-GFP-ddT2A-HA-NLS-CHE-Rca1_Del_1-99_Del_300-411_E215A_N216A **GFP-T2A-CHE-Rca1_100-299_mKEN(2)**
pFSR-1457	actPro(L)-HA-NLS-GFP-ddT2A-HA-NLS-CHE-Rca1_Del_1-99_Del_300-411_R207A_L210A **GFP-T2A-CHE-Rca1_100-299_mDB(2)**
pFSR-1458	actPro(L)-HA-NLS-GFP-ddT2A-HA-NLS-CHE-Rca1_Del_1-99_Del_300-411_R207A_L210A_E215A_N126A **GFP-T2A-CHE-Rca1_100-299_mDB(2)_mKEN(2)**
pFSR-1530	actPro(L)-HA-NLS-GFP-ddT2A-HA-NLS-CHE-Rca1_Del_99_Del_300-411_L135A_D137A_H138A_E140A_E215A_N216A **GFP-T2A-CHE-Rca1_100-299_mABBA_mKEN(2)**

Number	Name Nickname
pFSR-1596	actPro(L)-HA-NLS-GFP-ddT2A-HA-NLS-CHE-Rca1_Del_1-133_Del_300-411 **GFP-T2A-CHE-Rca1_134-299**
pFSR-1597	actPro(L)-HA-NLS-GFP-ddT2A-HA-NLS-CHE-Rca1_Del_1-99_Del_300-411_M182T **GFP-T2A-CHE-Rca1_100-299_M182T**

5.5.9. RPS Rca1_221-411 plasmids

Table 13| List of RPS Rca1_221-411 plasmids

Number	Name Nickname
pFSR-1396	actPro(L)-HA-NLS -GFP-ddT2A-HA-NLS-CHE-Rca1_Del_1-220 **GFP-T2A-CHE-Rca1_221-411**
pFSR-1401	actPro(L)-HA-NLS -GFP-ddT2A-HA-NLS-CHE-Rca1_Del_1-220_Del_368-411 **GFP-T2A-CHE-Rca1_221-367**
pFSR-1407	actPro(L)-HA-NLS -GFP-ddT2A-HA-NLS-CHE-Rca1_Del_1-220_R384A_L387A **GFP-T2A-CHE-Rca1_221-411_mDB(3)**
pFSR-1417	actPro(L)-HA-NLS -GFP-ddT2A-HA-NLS-CHE-Rca1_Del_1-220_Del_406-411 **GFP-T2A-CHE-Rca1_221-405_ΔRL**
pFSR-1442	actPro(L)-HA-NLS-GFP-ddT2A-HA-NLS-CHE-Rca1_Del_1-220_S253A_S256A_S257A **GFP_T2A_CHE_Rca1_221-411_mDSGxxS**
pFSR-1452	actPro(L)-HA-NLS-GFP-ddT2A-HA-NLS-CHE-Rca1_Del_1-244 **GFP-T2A-CHE-Rca1_245-411**

5.5.10. RPS Rca1_204-411 plasmids

Table 14| List of RPS Rca1_204-411 plasmids

Number	Name Nickname
pFSR-1246	actPro(L)-HA-NLS-GFP-ddT2A-HA-NLS- CHE-Rca1_Del-1-203 **GFP-T2A-CHE-Rca1_204-411**
pFSR-1567	actPro(L)-HA-NLS-GFP-ddT2A-HA-NLS-CHE-Rca1_Del_1-203_C279G **GFP-T2A-CHE-Rca1_204-411_C279G**
pFSR-1566	actPro(L)-HA-NLS-GFP-ddT2A-HA-NLS-CHE-Rca1_Del_1-203_C281S **GFP-T2A-CHE-Rca1_204-411_C281S**
pFSR-1341	actPro(L)-HA-NLS-GFP-ddT2A_HA-NLS-CHE-Rca1_Del-1-203_S285R **GFP-T2A-CHE-Rca1_204-411_S285R**
pFSR-1569	actPro(L)-HA-NLS-GFP-ddT2A-HA-NLS-CHE-Rca1-Del_1-203_A344T **GFP-T2A-CHE-Rca1_204-411_A344T**
pFSR-1568	actPro(L)-HA-NLS-GFP-ddT2A-HA-NLS-CHE-Rca1-Del-1-203_C351S **GFP-T2A-CHE-Rca1_204-411_C351S**
pFSR-1577	actPro(L)-HA-NLS-GFP-ddT2A-HA-NLS-CHE-Rca1_Del_1-203_Del_291-330 **GFP-T2A-CHE-Rca1_204-411_ΔZBR_loop**
pFSR-1473	actPro(L)-HA-NLS-GFP-ddT2A-HA-NLS-CHE-Rca1_Del_204-411_S335A_T376A_T388A **GFP-T2A-CHE-Rca1_204-411_3A**
pFSR-1576	actPro(L)-HA-NLS-GFP-ddT2A-HA-NLS-CHE-Rca1_Del_204-411_S326A_S335A_T376A_T388A **GFP-T2A-CHE-Rca1_204-411_4A**
pFSR-1573	actPro(L)-HA-NLS-GFP-ddT2A-HA-NLS-CHE-Rca1_Del_1-203_S326A **GFP-T2A-CHE-Rca1_204-411_S326A**
pFSR-1574	actPro(L)-HA-NLS-GFP-ddT2A-HA-NLS-CHE-Rca1_Del_1-203_S326D **GFP-T2A-CHE-Rca1_204-411_S326D**
pFSR-1602	actPro(L)-HA-NLS-GFP-ddT2A-CHE-Rca1_Del_1-203 **NLS-GFP-T2A-CHE-Rca1_204-411**
pFRS-1607	actPro(L)-HA-NLS-GFP-ddT2A-CHE-Rca1_Del_1-203_S326A **GFP-T2A-CHE-Rca1_204-411_S326A**

Number	Name Nickname
pFSR-1611	actPro(L)-HA-NLS-GFP-ddT2A-HA-NES-CHE-Rca1_204-411 **NLS-GFP-T2A-NES-CHE-Rca1_204-411**
pFSR-1612	actPro(L)-HA-NLS-GFP-ddT2A-HA-NES-CHE-Rca1_204-411_S326A **NLS-GFP-T2A-NES-CHE-Rca1_204-411_S326A**

5.5.11. NLS-4xFLAG plasmids

Table 15| List of NLS-4xFLAG plasmids

Number	Name Nickname
pFSR-1464	PubPro-NLS-4xFLAG-Rca1 **NLS-4xFLAG-Rca1**
pFSR-1475	PubPro-NLS-4xFLAG-Rca1_S14A_T43A_T70A_T104A_S123A_S127A_S186A_S335A_T376A_T388A **NLS-4xFLAG-Rca1_10A**
pFSR-1629	PubPro-NLS-4xFLAG-Rca1_S123A_S127A **NLS-4XFLAG_Rca1_S123A_S127A**
pFSR-1529	PubPro-NLS-4xFLAG-Rca1_Del_204-411 **NLS-4XFLAG_Rca1_1-203**
pFSR-1485	PubPro-NLS-4xFLAG-Rca1_Del_204-411_ S14A_T43A_T70A_T104A_S123A_S127A_S186A **NLS-4XFLAG_Rca1_1-203_7A**
pFSR-1658	PubPro-NLS-4xFLAG-Rca1_Del_1-10_Del_204-411_E53A_N54A_ L135A_P137A_H138A_E140A **NLS-4XFLAG_Rca1_1-203_ΔDB(1)_mKEN_mABBA**
pFSR-1421	PubPro-NLS-4xFLAG-Rca1_Del-1-203 **NLS-4XFLAG_Rca1_204-411**
pFSR-1465	PubPro-NLS-4xFLAG-Rca1_Del_1-203_S285R **NLS-4xFLAG-Rca1_204-411_S285R**
pFSR-1472	PubPro-NLS-4xFLAG-Rca1_Del_1-203_A344T **NLS-4xFLAG-Rca1-204-411_A344T**
pFSR-1500	PubPro-NLS-4xFLAG-Rca1_Del_1-203_C351S **NLS-4xFLAG_Rca1_204-411_C351S**
pFSR-1564	PubPro-NLS-4xFLAG-Rca1_Del_1-203_C281S **NLS-4xFLAG_Rca1_204-411_C281S**
pFSR-1565	PubPro-NLS-4xFLAG-Rca1_Del_1-203_C279G **NLS-4xFLAG_Rca1_204-411_C279G**
pFSR-1578	PubPro-NLS-4xFLAG-Rca1_Del_1-203_Del_291-330 **NLS-4xFLAG_Rca1_204-411_ΔZBR_loop**
pFSR-1466	PubPro-NLS-4xFLAG-Rca1_Del_1-203_R384A_L387A **NLS-4xFLAG_Rca1_204-411_mDB(3)**
pFSR-1467	PubPro-NLS-4xFLAG-Rca1_Del_1-203_E215A_N216A **NLS-4xFLAG_Rca1_204-411_mKEN(2)**
pFSR-1474	PubPro-NLS-4xFLAG-Rca1_Del_1-203_Del_406-411 **NLS-4xFLAG-Rca1_204-405_ΔRL**
pFSR-1476	PubPro-NLS-4xFLAG-Rca1_Del_1-203_S335A_T376A_T388A **NLS-4x-FLAG-Rca1_204-411_3A**
pFSR-1563	PubPro-NLS-4xFLAG-Rca1_Del_1-203_Del_369-411 **NLS-4x-FLAG-Rca1_204-368**
pFSR-1575	PubPro-NLS-4xFLAG-Rca1_Del_1-203_S326A **NLS-4x-FLAG-Rca1_204-411_S326A**
pFSR-1571	PubPro-NLS-4xFLAG-Rca1_Del_1-203_S326D **NLS-4x-FLAG-Rca1_204-411_S326D**
pFSR-1572	PubPro-NLS-4xFLAG-Rca1_Del_1-203_ S326A_S335A_T376A_T388A **NLS-4x-FLAG-Rca1_204-411_4A**
pFSR-1598	PubPro-NLS-4xFLAG-Rca1_Del_1-203_E215A_N216A_R384A_L387A **NLS-4xFLAG_Rca1_204-411_mKEN(2) _mDB(3)**

5.5.12. 4xFLAG-NES plasmids

Table 16| List of 4xFLAG-NES plasmids

Number	Name **Nickname**
pFSR-1618	PubPro-4xFLAG-NES-Rca1_Del_1-203 **4xFLAG-NES-Rca1_204-411**
pFSR-1623	PubPro-4xFLAG-NES-Rca1_Del_1-203_S326A **4xFLAG-NES-Rca1_204-411_S326A**

5.5.13. 4xFLAG plasmids

Table 17| List of 4xFLAG plasmids

Number	Name **Nickname**
pFSR-1315	PubPro-4xFLAG-CHE **4xFLAG-CHE**
pFSR-1318	PubPro-4xFLAG-Fzr **4xFLAG-Fzr**
pFSR-0837	PubPro-4xFLAG-Rca1 **4xFLAG-Rca1**
pFSR-1589	PubPro-4xFLAG-Rca1_S326A **4xFLAG-Rca1_S326A**
pFSR-1368	PubPro-4xFLAG-Rca1_Del_1-203 **4xFLAG-Rca1_204-411**
pFSR-1590	PubPro-4xFLAG-Rca1_Del_1-203_S326A **4xFLAG-Rca1_204-411_S326A**

5.5.14. 3xHA plasmids

Table 18| List of 3xHA plasmids

Number	Name **Nickname**
pFSR-1543	PubPro-3xHA-14-3-3 epsilon **3xHA-14-3-3**

5.5.15. Plasmids for IVT or mir1 based knockdown

Table 19| List of plasmids for IVT or mir1 based knockdown

Number	Name **Nickname**
pFSR-0264	T7-Fzr_Del_1-250-T7
pFSR-0856	T7-Cul4-T7
pFSR-0845	T7-hygromycin-T7
pFSR-1545	PubPro-Gal4-Delta
pFSR-1640	UAS-Mir1(Cul4)
pFSR-1616	UAS-Mir1(hygro)

5.5.16. Other plasmids

Table 20| List of Other plasmids

Number	Name **Nickname**
pFSR-0092	pBSII Bluescript KS+ **Bluescript**
pFSR-1253	PubPro-SkpA-ryUTR **SkpA**
pFSR-1184	PubPro-HA-CycE **HA-CycE**
pFSR-0986	PubPro-Cdk2_T18A_Y19F_HA-ryUTR **Cdk2_T18A_Y19F-HA**

5.6. Bacterial strains

Table 21| Bacterial strains

Strain	Genotype	Distributor
DH5 alpha (electrocompetent)	F⁻ *endA1 glnV44 thi-1 recA1 relA1 gyrA96 deoR nupG purB20* ϕ80d*lacZ*ΔM15 Δ(*lacZYA-argF*) U169, hsdR17($r_K^- m_K^+$), λ⁻	AG Sprenger

5.7. Eukaryotic cell lines

Table 22| Eukaryotic cell lines

Strain	Genotype	Distributor
S2R+	-	-

5.8. Antibodies

5.8.1. Primary Antibody

Table 23| Primary antibody

Antigen	Number	Source	Western Blot	co-IP	Distributor
HA	373	Mouse	1:2000	-	Cavance
FLAG	374	Mouse	1:5000	1:500	Sigma

5.8.2. Secondary Antibody

Table 24| Secondary antibody

Antigen	Number	Source	Western Blot	co-IP	Distributor
Mouse	381	Goat	IRDye 680LT	1:10000	Li-Cor

5.9. Solutions and buffers

Table 25| Solutions and buffers

Solution/buffer	Distributor	
Ampicillin stock solution	Ampicillin	50 mg/ml

Solution/buffer	Distributor	
	In 50 % glycerol	
APS solution 10 %	APS In H_2O	10 % (w/v)
Cell Lysis Solution (from PureYield Plasmid Midiprep system)	NaOH SDS In H_2O	0.2 M 1 % (v/v)
Cell Resuspension Solution (from PureYield Plasmid Midiprep system)	Tris, pH 7.5 EDTA RNase A In H_2O	50 mM 10 mM 100 µg/ml
Column Wash Solution	Tris, pH 7.5 Potassium acetate EDTA, pH 8.0 For use dilute 2:5 in 99 % EtOH	22.6 mM 162.8 mM 0.109 mM
DNA/RNA Loading buffer 10X	Bromphenol blue Xylene cyanol EDTA, pH 8.0 Tris, pH 7.8 Glycerol In H_2O For analysis of DNA bands with low molecular weight DNA loading buffer without Bromphenol blue was used.	0.25% (w/v) 0.25% (w/v) 1 mM 10 mM 50% (v/v)
DNA/RNA Loading buffer 6X	Ficoll®-400 EDTA Tris-HCl 0.08% SDS Dye1 (pink/red) Dye2 (blue) pH 8.0	2.5% (w/v) 10mM 3.3mM 0.08% 0.02% 0.0008%
dNTP mix (2 mM each)	dNTP mix In H_2O	2 mM
EasyPrep buffer	Tris, pH 8.0 EDTA, pH 8.0 Sucrose Lysozym RNase A BSA In H_2O	10 mM 1 mM 150 mg/ml 2 mg/ml 0.2 mg/ml 0.1 mg/ml
4% Glyoxal solution	EtOH 40% Glyoxal stock solution Acetic acid In H_2O pH was adjusted to 4-5 with NaOH.	19.725 % (v/v) 7.825 % (v/v) 0.750 % (v/v)
IP Lysis buffer	HEPES, pH 7.5 NaCl EGTA NaF Triton X-100 Glycerol In H_2O For use Protease inhibitor mix is freshly added.	50 mM 150 mM 1 mM 10 mM 1 % (v/v) 10 % (v/v)
IP Washing buffer	HEPES, pH 7.5 NaCl Triton X-100	50 mM 150 mM 1 % (v/v)

<table>
<tr><th>Solution/buffer</th><th colspan="2">Distributor</th></tr>
<tr><td></td><td>Glycerol
In H_2O</td><td>10 % (v/v)</td></tr>
<tr><td>LSB 2X</td><td>Tris, pH 6.8
SDS
Glycerol
Bromphenol blue
Beta-Mercaptoethanol
In H_2O</td><td>120 mM
4 % (w/v)
20 % (v/v)
0.04 % (w/v)
10 % (v/v)</td></tr>
<tr><td>LSB, non-reducing 2X</td><td>Tris, pH 6.8
SDS
Glycerol
Bromphenol blue
In H_2O</td><td>120 mM
4 % (w/v)
20 % (v/v)
0.04 % (w/v)</td></tr>
<tr><td>Lysis buffer for dephosphorylation</td><td>HEPES, pH 7.5
NaCl
Triton X-100
Glycerol
In H_2O
For use Protease inhibitor mix is freshly added.</td><td>50 mM
150 mM
1 % (v/v)
10 % (v/v)</td></tr>
<tr><td>NTP mix (25 mM each)</td><td>ATP
CTP
GTP
UTP</td><td>25 mM
25 mM
25 mM
25 mM</td></tr>
<tr><td>Milk powder solution</td><td>Skim milk powder
Sodium azide
In PBS</td><td>5 % (m/v)
0.01 % (m/v)</td></tr>
<tr><td>Neutralization Solution
(from PureYield Plasmid Midiprep system)</td><td>Guanidine hydrochloride, pH 4.2
Potassium acetate
Glacial acetic acid
In H_2O</td><td>4.09 M
759 mM
2.12 M</td></tr>
<tr><td>PBS</td><td>NaCl
Na_2HPO_4
NaH_2PO_4
pH
In H_2O</td><td>130 mM
7 mM
3 mM
7.2</td></tr>
<tr><td>PBST</td><td>Tween 20
In PBS</td><td>0.1 % (v/v)</td></tr>
<tr><td>Resolving gel (SDS PAGE)</td><td colspan="2">For 10 ml resolving gel:

<table>
<tr><th>Gel</th><th>H_2O (ml)</th><th>Acrylamide 30%/ Bisacrylamide (ml)</th><th>1.5 M Tris/HCl pH 8.8 (ml)</th><th>10 % SDS (ml)</th><th>10 % APS (µl)</th><th>TEMED (µl)</th></tr>
<tr><td>6%</td><td>5.4</td><td>2.0</td><td>2.5</td><td>0.1</td><td>100</td><td>10</td></tr>
<tr><td>7%</td><td>5.1</td><td>2.3</td><td>2.5</td><td>0.1</td><td>100</td><td>10</td></tr>
<tr><td>8%</td><td>4.7</td><td>2.7</td><td>2.5</td><td>0.1</td><td>100</td><td>10</td></tr>
<tr><td>9%</td><td>4.4</td><td>3.0</td><td>2.5</td><td>0.1</td><td>100</td><td>10</td></tr>
<tr><td>10%</td><td>4.1</td><td>3.3</td><td>2.5</td><td>0.1</td><td>100</td><td>10</td></tr>
<tr><td>11%</td><td>3.7</td><td>3.7</td><td>2.5</td><td>0.1</td><td>100</td><td>10</td></tr>
<tr><td>12%</td><td>3.4</td><td>4.0</td><td>2.5</td><td>0.1</td><td>100</td><td>10</td></tr>
<tr><td>13%</td><td>3.1</td><td>4.3</td><td>2.5</td><td>0.1</td><td>100</td><td>10</td></tr>
<tr><td>14%</td><td>2.7</td><td>4.7</td><td>2.5</td><td>0.1</td><td>100</td><td>10</td></tr>
<tr><td>15%</td><td>2.4</td><td>5.0</td><td>2.5</td><td>0.1</td><td>100</td><td>10</td></tr>
</table>

Resolving gels were stored as 50 ml stock solutions without APS and TEMED.</td></tr>
<tr><td>SDS solution 10 %</td><td>SDS
In H_2O</td><td>10 % (w/v)</td></tr>
</table>

<table>
<tr><th>Solution/buffer</th><th colspan="2">Distributor</th></tr>
<tr><td>Stacking gel (SDS PAGE)</td><td colspan="2">For 10 ml stacking gel:
<table><tr><th>Gel</th><th>H_2O (ml)</th><th>Acrylamide 30%/ Bisacrylamide (ml)</th><th>1.5 M Tris/HCl pH 6.8 (ml)</th><th>10 % SDS (ml)</th><th>10 % APS (µl)</th><th>TEMED (µl)</th></tr><tr><td>4%</td><td>6.1</td><td>1.3</td><td>2.5</td><td>0.1</td><td>100</td><td>10</td></tr></table>Stacking gel was stored as 50 ml stock solution without APS and TEMED.</td></tr>
<tr><td>TAE buffer</td><td>Tris, pH 8.0
EDTA
In H_2O</td><td>40 mM
10 mM</td></tr>
<tr><td>Transfer buffer 3 (Western blot)</td><td>Methanol
Tris, pH 7.5
EDTA, pH 8.0
Sodium acetate
SDS
In H_2O</td><td>20 % (v/v)
40 mM
2 mM
20 mM
0.05 % (v/v)</td></tr>
<tr><td>Turbo Laemmli running buffer 10X</td><td>Tris
Glycin
SDS
In H_2O</td><td>250 mM
9,46 M
10 g/l</td></tr>
<tr><td>Transcription buffer 5X (T7)</td><td>HEPES, pH 7.5
Spermidine
DTT
NTPs (ATP, CTP, GTP, UTP)
$MgCl_2$
In H_2O</td><td>80 mM
2 mM
10 mM
3 mM
12 mM</td></tr>
</table>

5.10. Media and Agar plates

Table 26| Media and Agar plates

Medium/Agar plate	Components	
LB agar plate	Euroagar In LB medium (autoclaved) Solution is boiled for casting plates. Before adding any antibiotic, the solution is first cooled down to 50 °C.	1.7 % (w/v)
LB medium (autoclaved)	BactoTrypton Bacto Yeast Extract NaCl pH In H_2O	10 g/l 5 g/l 10 g/l 7.2
Schneider's *Drosophila* complete medium	GIBCO FBS Penicillin Streptomycin In Schneider's *Drosophila* Medium	20 g/l 5 g/l 10 mM 2.5 mM 10 mM 20 mM

5.11. Consumable material

Table 27| Consumable material

Equipment	Manufacturer
12-well plate	Cellstar
6-well plate	Sarstedt
Cell culture flask, 250 ml, 75 cm²	Cellstar
Cell scraper	Sarstedt
Cups (0.5 ml, 1.5 ml, 2 ml)	Eppendorf, Sarstedt
Electroporation cuvettes	Peqlab
Falcons 15 ml, 50 ml	Sarstedt
GIBCO FBS (fetal bovine serum)	Invitrogen GmbH
Glass pasteur pipettes 150 mm	BRAND
Nitrocellulose membrane	Schleicher & Schuell BioScience
Parafilm "M" Laboratory Film	Pechiney
PCR-Cups 200 µl	Sarstedt
Petri dishes 92 X 16 mm	Sarstedt
Pipet tips 10 µl, 200 µl, 1000 µl	Eppendorf, Sarstedt
Trypsin/EDTA solution	PAN Biotech
Tubes 3,5 ml	Sarstedt
Whatman paper	Whatman International Ltd

5.12. Software and online tools

The following software and online tools were used for data analysis:

Table 28| Software

Software	Developer
Axio Vision	Zeiss
Canvas X	ACD Systems International Inc.
FCS Express 6	De Novo Software
Filemaker Pro 15	Filemaker Inc.
ImageJ 1.50i	NIH
Microsoft Office	Microsoft Corp.
NLS Mapper	Kosugi et al.
Origin 2020	OriginLab
Vektor NTI Advance 11	Invitrogen
ImageStudio Light	LI-COR Biosciences
GPS-ARM Prediction of APC/C Recognition motifs	The CUCKOO Workgroup
GPS 5.0 Kinase-specific Phosphorylation prediction	The CUCKOO Workgroup
RStudio	RStudio

Table 29| Online tools

Online tool	Link	Reference
APC/C degron repository	http://slim.icr.ac.uk/apc/index.php	n.a.
14-3-3-Pred	http://www.compbio.dundee.ac.uk/1433pred/	(Madeira et al., 2015)
Eukaryotic Linear Motif (ELM)	http://elm.eu.org/	(Gouw et al., 2018)
Phosphorylation Databases	https://www.flyrnai.org/tools/iproteindb/web/ http://www.phosida.de/	(Hu et al., 2019) (Gnad et al., 2007, 2011)

Online tool	Link	Reference
	http://www.unipep.org/phosphopep/index.php	(Bodenmiller et al., 2007)
Phyre 2.0	http://www.sbg.bio.ic.ac.uk/~phyre2/html/page.cgi?id=index	(Kelley et al., 2015)
NetNES 1.1 Server	http://www.cbs.dtu.dk/services/NetNES/	(La Cour et al., 2004)
E-RNAi (Design of RNAi constructs)	https://www.dkfz.de/signaling/e-rnai3/	(Horn et al., 2010)
cNLS-mapper	http://nls-mapper.iab.keio.ac.jp/cgi-bin/NLS_Mapper_form.cgi	(Kosugi et al., 2008, 2009 a; b)
Scan Prosite	https://prosite.expasy.org/scanprosite/	(de Castro et al., 2006)

5.13. Equipment

Table 30| Equipment

Equipment	Manufacturer
Acrylamide gel apparatus	Bio-Rad Laboratories
Agarose gel electrophoresis apparatus HE33	Hoefer
Axio Observer.Z1 (inverted)	Zeiss
AxioCam MRm Rev3	Zeiss
Beaker 250 ml, 500 ml, 5 L	Schott, VITLAB, VWR
Cell culture incubator	Hereaus
Cell culture roller TC-7	New Brunswick Scientific
Centrifuge 5424	Eppendorf
Centrifuge Heraeus Multifuge 1S	Thermo Scientific
Clean bench	Ceag Schirp Reinraumtechnik
Clean bench Mars Safety Class 2	SCANLAF
Culture roller drum TC-7	New Brunswick Scientific
Electrophoresis power supply EPS 200/600	Pharmacia Biotech
Electroporation apparatus Easyject Prima	Equibio
Erlenmeyer flask	DURAN Group GmbH
FastPette V2 Pipette Controller	Labnet
Flow cytometer CyFlow space	Partec
Freezer	AEG, Bosch, Siemens
Freezer C760	New Brunswick Scientific
Fuchs-Rosenthal Counting chamber (16 mm², 0.2 mm cell depth)	Hausser Scientific
Glass bottle 250 ml, 500 ml, 1 L	Schott
Glass pipettes 1 ml, 5 ml, 10 ml, 25 ml	Hirschmann
Glass tube	Schuett-biotec
Gyrotory Water Bath shaker G76	New Brunswick Scientific
Heating block (Digital Dry Bath, dual position)	Benchmark Scientific
HT 200	ibidi GmbH
I-3020	AppliedScientific Instrumentation
Ice maker MF22	Scotsman
Incubator Heraeus B 5050 E	Heraeus
Incubator Sanyo MIR-153	Sanyo
Incubator WB120K (equipped with culture roller drum TC-7)	Mytron
Incubatorr Innova™ 42	Thermo fischer
Inverted microscope CKX41 (equipped with Reflected Fluorescence System with Light Source X-Cite 120Q)	Olympus
LED Transilluminator	Nippon Genetics
Magnetic stirrer	Heidolph
Measuring cylinder	VITLAB
Microliter syringe 705	Hamilton
Microwave	Vestel
Odyssey Infrared Imaging system	LI-COR

Equipment	Manufacturer
PerfectBlue Semi-Dry Electro Blotter	Peqlab
pH meter 766 Caltimatic	Knick
Plan-APOCHROMAT 20X	Zeiss
Plastic boxes 11 cm x 7 cm x 4 cm (Coomassie/Antibody staining)	-
Protein G Plus-Agarose Beads	Santa Cruz
Refrigerator	AEG, Bosch
Sieve (2 cm² diameter)	Own production
Spectrophotometer / Fluorometer DS-11 FX+	DeNovix
Spinning disk unit (CSU-X1)	Yokogawa
Table centrifuge ROTOFIX 32 A	Hettich
Thermocycler GTC96S	Cleaver Scientific Ltd
Thermocycler UNO II	Biometra
ThermoMixer F1.5	Eppendorf
UV Crosslinker	Stratalinker
UVP ChemStudio	Analytik Jena
Vacuum Blotting Pump, 2016 Vacugene	LKB Bromma
Vacuum gas pump VP86	VWR
Vacuum manifold	Promega
Vornado™ Vortex Mixer	Benchmark Scientific
Vortex-REAX1DR	Heidolph
Water purification system	ELGA
Wide-Field Fluorescence Microscope Excitation Light Source X-Cite 120Q	Excelitas Technologies

6. Methods

6.1. DNA/RNA methods

6.1.1. Molecular cloning

Assembly of recombinant DNA molecules (molecular cloning) was first performed in silico with the software Vector NTI Advance 11 and subsequently carried out in the following order of steps (see Table 31)

Table 31| Molecular cloning protocol

Time	Protocol		Result
Day 1	**Step 1**	Amplification of Insert DNA by PCR (see section 6.1.2).	Digested Vector DNA and Insert DNA
	Step 2	Digestion of Vector DNA and/or amplified PCR Insert by restriction endonucleases (see section 6.1.4)	
	Step 3	Isolation of Insert and Vector DNA by gel electrophoresis (see section 6.1.3) and subsequent DNA isolation	
	Step 4	Quantification of isolated Vector DNA and Insert DNA (see section 6.1.14)	
	Step 5	If necessary, dephosphorylation of vector DNA (see section 0)	
	Step 6	Ligation of vector and insert DNA (see section 0)	
Day 2	Transformation of electrocompetent cells with ligation mix (see section 6.1.8)		LB agar plates coated with transformed *E. coli*
Day 3	a)	**Step 1** Identification of recombinant clones by colony PCR (see section 6.1.9.2).	Screening + Main-cultures
		Step 2 Preparation of main culture with positive pre-culture (see section 6.1.11.2)	Pre-cultures
	b)	Select clones for inoculation of pre-cultures (see 6.1.11.1).	for screening

Time	Protocol	Result
Day 4	a) **Step 1** Midi scale plasmid DNA isolation from main culture (see section 6.1.11.2). **Step 2** Quantification of yield and purity of isolated plasmid DNA Quantification by gel analysis, if vector DNA is used for cell transfection b) **Step 1** Mini scale plasmid DNA isolation from pre-cultures (see section 6.1.10) **Step 2** Identification of recombinant clones by test digestion of isolated plasmid DNA (see section 6.1.9.1) **Step 3** Preparation of main-culture with positive pre-culture (see 6.1.11.2)	Recombinant plasmid DNA Main-culture of recombinant clone
Day 5	**Step 1** Midi scale plasmid DNA isolation from main-culture (see 6.1.11.2). **Step 2** Quantification of yield and purity of isolated plasmid DNA **Step 3** Quantification by gel analysis, if vector DNA is used for cell transfection	

6.1.2. DNA amplification by PCR

Amplification of DNA fragments was conducted by polymerase chain reaction (PCR) according to Mullis et *al*. (Mullis, K; Faloona, F.; Scharf, S.; Saiki, R.; Horn, G.; Erlich, 1986). PCR was catalyzed by Phusion High-Fidelity Polymerase, a *Pyrococcus*-like enzyme fused with a processivity-enhancing domain, in the following reaction mixture (see Table 32)

Table 32| PCR Standard setup

Component	Amount
DNA (template)	100 ng
Forward primer (100mM)	1 µl
Reverse primer (100mM)	1 µl
dNTP mix (2 mM each dNTP)	5 µl
5X Phusion HF/GC buffer	10 µl
Phusion	0.5 µl
H_2O	Ad 50 µl
Total reaction volume	**50 µl**

DNA was amplified with the following PCR-program (see Table 33)

Table 33| PCR-program

Steps	Temperature	Duration	Cycles
Step 1: Initial denaturation	96 °C	30 sec	
Step 2: Denaturation	96 °C	10 sec	30x
Step 3: Primer annealing	65° C	20 sec	
Step 4: Elongation	72 °C	20 sec/1 kb	
Step 5: Final elongation	72 °C	5 min	
Step 6: Hold	4 °C	∞	

PCR product purification was performed using the MSB Spin PCRapace KIT according the manufacturer´s instruction. The amplified DNA was eluted in 30µl ddH_2O.

6.1.3. Agarose gel electrophoresis

Separation of DNA fragments was accomplished through agarose gel electrophoresis, using 1% agarose gel. DNA detection was carried out using ethidium bromide (10 mg/ml). DNA samples were mixed with 6x Purple loading dye and loaded onto the gel. GeneRuler DNA Ladder Mix was used to estimate DNA

fragment size. Electrophoresis was performed with 90 V for 40 min. Gels were documented with a UVP ChemStudio system by visualizing the DNA bands with UV light at 365 nm.

6.1.4. Restriction digestion of DNA

Restriction digest was performed using restriction endonucleases with buffers and temperatures recommended by enzyme manufacturer for a minimum of 1 h and maximally overnight. Depending on the purpose, different reaction mixtures haven been used (see Table 34)

Table 34| Restriction digestion mixtures

Component	Amount			
	Preparative digestion of plasmid DNA for cloning	**Digestion of purified PCR DNA**	**Test digestion of mini prep DNA**	**Test digestion of midi prep DNA**
DNA	1-5 µg	30 µl	5 µl	500 - 1000 ng
10X restriction buffer	4 µl	4 µl	1 µl	2 µl
Restriction enzyme	1 µl each	1 µl each	0.5 µl each	1 µl each
H_2O	Ad 30 µl	Ad 40 µl	Ad 10 µl	Ad 20 µl
Total volume	**30 µl**	**40 µl**	**10 µl**	**20 µl**

6.1.5. Dephosphorylation of DNA ends

Vector DNA ends were dephosphorylated after restriction digestion to prevent self or re-ligation. Dephosphorylation of digested vector DNA ends was catalyzed by the Shrimp Alkaline Phosphatase (rSAP). The reaction was catalyzed by rSAP either during restriction digestion by adding 1µl of rSAP directly into the reaction mixture or after digestion by the following reaction mixture (see Table 35). The reaction was performed at 37°C for 1h and stopped by heat-inactivation at 65°C for 5 min.

Table 35| Vector dephosphorylation using rSAP

Component	Amount
Digested vector DNA (preparative digestion)	1 µg
CutSmart Buffer (10X)	2 µl
rSAP	1 µl
H_2O	to 20 µl
Total volume	**20 µl**

6.1.6. Ligation of DNA fragments

Ligation reaction was performed with a 5:1 molar ratio of insert to vector DNA using a T4 DNA ligase, according the following reaction mixture (see Table 36)

Table 36| Ligation reaction mixture

Component	Amount
Vector DNA	100 ng
Insert DNA	x ng
10X T4 ligase buffer	2 µl
T4 DNA ligase	1 µl
H_2O	to 20 µl
Total volume	**20 µl**

A ligation reaction without insert was used to estimate the background of vector self-ligation. The reaction mixture was incubated at 24°C for 1h to overnight.

6.1.7. Production of dsRNA for RNA interference

Gene knockdown was performed by RNA-interference (RNAi). For this purpose, dsRNA fragments were produced *in vitro*. A PCR product containing the part of the coding sequence of the gene to be silenced flanked by two opposed T7-promotors was used as template. In vitro transcription using a T7 polymerase resulted in two complementary single stranded RNA molecules that hybridize into dsRNA. In vitro transcription was performed according to Gurevich et al. (Gurevich et al., 1991) by the following reaction (see Table 37):

Table 37| IVT reaction mix for the production of dsRNA

Component	Amount
5x Transcription buffer	10 µl
PCR DNA	1000 ng
T7 RNA-polymerase	1.5 µl
RNAse inhibitor (RNAsin)	1 µl
NTP-Mix (ATP/GTP/CTP/UTP 25nM each)	5µl
H_2O	To 50µl
Total volume	**50 µl**

The *in vitro* transcription reaction was incubated for 2h at 37°C. The concentration of the produced dsRNA was quantified by gel quantification (see section 6.1.14.2)

6.1.8. Transformation of electrocompetent cells

Plasmid DNA was transformed in *E. coli* cells (DH5α) by electroporation by following protocol:

Table 38| Protocol for transformation of electrocompetent cells

Steps	Procedure
Step 1	A 100 µl aliquot of electrocompetent DH5α is thawed on ice and diluted with 100 µl ddH_2O
Step 2	100 µl of the suspension are transferred into precooled electroporation cuvettes
Step 3	3 µl of the ligation reaction mixture (see section 0) are added to the cells
Step 4	Electroporation with following settings: 2,5 kV, capacitance 25µF and resistance 200 ohms
Step 5	Cell suspension is transferred into 1ml LB_0 medium
Step 6	If antibiotic other than ampicillin was used, cells were incubated at 37°C for 30 min
Step 7	50 µl of the cell suspension were plated onto LB plate containing the corresponding antibiotic
Step 8	Cultivate plates at 37 °C over-night

6.1.9. Screening for recombinant clone

Screening *E.coli* colonies for recombinant plasmids was conducted by either test digestion of a small size pre-culture or colony PCR.

6.1.9.1. Screening via test digestion of mini prep DNA

For screening via test digestion a small *E.coli* pre-culture was inoculated and the plasmid DNA was isolated on a mini scale level (see 6.1.11.1). The test digestion was set up that a recombinant positive clone could be distinguished from uncut or re-ligated starting plasmid based on the resulting pattern of DNA bands on an agarose gel.

6.1.9.2. Screening via colony PCR

For colony PCR primers were chosen either specific for the insert, specific for the vector flanking the insert or a combination of vector and insert specific primer. A PCR-Master mix was set up as follows (see Table 39):

Table 39| Colony PCR setup (1x)

Component	Amount
Forward primer (100mM)	0.25 µl
Reverse primer (100mM)	0.25 µl
dNTP mix (2 mM each dNTP)	1.5 µl
5X Phusion HF/GC buffer	3 µl
Phusion	0.15 µl
H_2O	10 µl
Total reaction volume	**15 µl**

The colony PCR was conducted after the following procedure (see Table 40):

Table 40| Protocol for Colony PCR

Steps	Procedure
Step 1	Prepare 1.5 ml Eppendorf tubes (labeled in the same way as the PCR tube) with 200 µl of LB-medium with corresponding antibiotic
Step 2	Pick Colony with plastic crystal tip and pipette up and down in PCR tube
Step 3	Transfer the tip into the corresponding 1.5 ml tube with medium
Step 4	include two controls with just the vector and insert plasmid-DNAs (to test for unspecific bands)
Step 5	Run PCR reaction
Step 6	Determine size of the PCR amplicon by electrophoresis
Step 7	Inoculate positive colony from the 1.5 ml tube in 50 ml Medium for Midi prep (see section 6.1.11.2)

6.1.10. Preparation of *E. coli* cultures

E. coli cultures were prepared by inoculating LB-medium (with the corresponding antibiotics for selection) with single colonies grown on LB-agar plates. Depending on the purpose, either 3ml (pre-cultures, test tube) or 50 ml (main cultures, Erlenmeyer flask) cultures were inoculated and rotated overnight at 37 °C.

6.1.11. Isolation of DNA

6.1.11.1. Mini scale isolation of plasmid DNA

Small amounts of DNA were isolated to screen recombinant clones. The applied protocol was a modified version according to Berghammer and Auer (Berghammer et al., 1993) (see Table 41):

Table 41| Protocol for mini scale isolation of plasmid DNA

Steps	Procedure
Step 1	1,5 ml of a 3ml overnight pre-culture is centrifuged for 4 min at 14.000 rpm
Step 2	The supernatant is discarded, and the pellet is resuspended in 50 µl EasyPrep buffer
Step 3	The suspension is incubated at 102°C for 1 min
Step 4	The suspension is cooled in ice for 1min
Step 5	The cell lysate is centrifuged for 15 min at 14.000 rpm

6.1.11.2. Midi scale isolation of plasmid DNA

Larger amounts of DNA were isolated based on the alkaline lysis procedure by Birnboim and Doly (Birnboim et al., 1979), using the Promega PureYield Plasmid Midiprep system. The following protocol according the manufacturer´s instructions was used (see Table 42)

Table 42| Protocol for Midi scale isolation of plasmid DNA

Steps	Procedure
Step 1	50 ml of a main culture is pelletized for 10 min at 4.500 rpm
Step 2	The supernatant is dissolved and resuspend the pellet in 3 ml Resuspension Solution
Step 3	3 ml cell Lysis Solution is added, gently inverted 3 times, and incubated for 3 min at room temperature
Step 4	5 ml of neutralization solution are added and carefully mixed
Step 5	Cell fragments are centrifuged for 25 min at 4.500 rpm
Step 6	The cell lysate was transferred through a sieve into a PureYield Binding Column, placed onto the vacuum manifold
Step 7	Vacuum was applied until the whole liquid passed through and the DNA bound to the PureYield Binding Column
Step 8	Vacuum is continued and 2 x 10 ml of Column Wash Solution is added and washed through the column
Step 9	The membrane is dried by applying vacuum for at least 10 min. The PureYield Binding Column was removed, the tip was pressed on a paper towel to remove the remaining ethanol
Step 10	The PureYield Binding Column is further dried by centrifugation for 6 min at 1.500 rpm
Step 11	The column is placed into a 50-ml falcon tube and 600 µl of Nuclease free water were added and incubated for 2 min
Step 12	The DNA was eluted from the PureYield Binding Column by centrifugation for 2 min at 1.500 rpm

The DNA concentration was photometric quantified, and the DNA was stored at -20°C.

6.1.12. Preparative isolation of DNA fragments from agarose gels

After electrophoretic separation of DNA fragments in agarose gels, the corresponding DNA bands were extracted on a LED transilluminator. DNA purification from the excised agarose gel was performed using the FastGene Gel/PCR Extraction Kit according to the manufacturer´s instructions.

6.1.13. Isolation of DNA fragments generated by PCR

DNA fragments generated by PCR were purified by the MSB Spin PCRapace KIT according to the manufacturer´s instructions.

6.1.14. Quantification of DNA

6.1.14.1. Photometric quantification of purified DNA

Purity and yield of the isolated DNA fragments was quantified using a Fluorometer DS-11 FX+, based on the ration of absorbance at 260nm and 280 nm.

6.1.14.2. DNA quantification by gel analysis

Plasmid DNA used for cell transfection was quantified by gel analysis. Therefore, plasmid DNA was digested with restriction endonucleases (see section 6.1.4), resulting in a linear fragment of approximately 1000 bps and were separated by agarose gel electrophoresis. The amount of loaded DNA was quantified by its intensity. The bands of the DNA ladder, each containing a defined amount of DNA, were used as the reference for quantification calculation. The quantification was performed using the software ImageJ with the calculation formula $\frac{\text{mass band (ng)} \times \text{size of plasmid (kb)}}{\text{size of band (kb)}}$.

6.1.15. Sequencing of Vector DNA

DNA sequencing was performed by the company SeqLab. The following sequencing setup was used (see Table 43)

Table 43| Sequencing setup

Component	Amount
Plasmid DNA	0.5 to 1.2 µg
Primer	30 pmol
H_2O	to 15 µl
Total volume	**15 µl**

6.2. Protein Methods

6.2.1. SDS-PAGE

Separation of proteins according to their molecular weight was accomplished by discontinuous sodium dodecyl sulfate polyacrylamide gel electrophoresis (SDS-PAGE) as developed by Laemmli (Laemmli, 1970). Therefore, 1.5 mm thick polyacrylamide gels, consisting of 2ml stacking gel and 8 ml resolving gel were produced using an acrylamide gel system (BioRad). The gel percentage was chosen depending on the protein size. The protein samples were boiled at 100°C in 2x Laemmli Sample Buffer (2xLSB) for 15 min. Probes were loaded on the gel with a protein ladder as reference. Electrophoresis was performed with a constant current of 200V for 60-90 min.

6.2.2. Phos-tag SDS-PAGE

Separation of phosphorylated proteins was performed by Phos-tag SDS-PAGE according to the manufacturer´s information. Phos-tag gels were prepared by adding Phos-tag and $MnCl_2$ solution in the resolving gel while preparing the SDS-PAGE gels. The gel percentage, the concentration of Phos-tag and MnCl and the running conditions have to be tested experientially for each protein of interest. The protein standard was diluted 1:1 with 10mM $MnCl_2$ solution. After gel electrophoresis the gel was washed three times in transfer buffer containing 10 mM EDTA under gentle rotation for 10 minutes. Afterwards the gel is soaked once in transfer buffer for 10 min with gentle agitation.

6.2.3. Western blot

Proteins separated by SDS-PAGE (see section 6.2.1) were electrophoretic transferred on a nitrocellulose membrane using a semi dry blotting system. A blotting stack consisting of two whatman paper and a nitrocellulose membrane, soaked in transfer buffer 3, and a polyacrylamide gel was assembled in the following order from cathode to anode: Whatman paper, polyacrylamide gel, nitrocellulose membrane, whatman paper. The Blotting procedure was executed with a constant current of 70 mA for 90 min.

6.2.4. Immunostaining of Western blots

Immunostaining was applied for the detection of specific proteins blotted on the nitrocellulose membrane. A combination of a primary antibody directly binding the target protein and a fluorophore-conjugated secondary antibody, recognizing the Fc domain of the primary antibody. Immunostaining of Western blots was performed in the following order of steps:

Table 44| Protocol for Immunostaining of Western blots

Steps	Procedure
Step 1	Nitrocellulose membrane is blocked with milk powder solution for 30 min shaking on a tilting shaker
Step 2	The membrane is washed 3-4 times with PBST
Step 3	The membrane is incubated with 5 ml of primary antibody solution (diluted in PBST) overnight shaking at 4°C
Step 4	The primary antibody solution is removed and stored at 4°C for re-use
Step 5	The membrane is washed 3-4 times with PBST to remove unbound antibodies

Steps	Procedure
Step 6	Incubation with 5 ml secondary antibody solution (diluted in PBST) for 2h, shaking at room temperature with the exclusion of light
Step 7	The membrane is washed 3-4 times with PBST to remove unbound antibodies
Step 8	The membrane is shaken in PBST for 30 min

Antibody labeled proteins were detected with an Odyssey Infrared Imaging System according to the manufacturer´s instructions. Further data-analysis was performed using the software ImageJ and ImageStudio Light.

6.2.5. Analysis of protein interaction partners by co-Immunoprecipitation

Protein-protein interaction was analyzed by protein Co-immunoprecipitation. For this purpose, a FLAG-tagged protein of interest (bait protein) and a HA-tagged putative interaction partner (prey protein) were co-expressed. The protein interaction analysis between these two proteins was performed as follows (see Table 45):

Table 45| Protocol for co-Immunoprecipitation assay

Time	Protocol
Day 1	S2R+ cells are seeded in a 6-well plate (four wells per co-IP experiment, see section 6.3.1.3)
Day 2	Two S2R+ wells are transfected with the plasmid expressing the prey protein (negative control), whereas the remaining 2 wells are additionally co-transfected with the plasmid expressing the bait protein (see section 6.3.2)
Day 4	1) Adherent cells are scratched off the dish in 500 µl PBS using a cell scraper. 2) Cells that were equally transfected (2 wells) are pooled in a 2 ml cup (from now on samples are kept at 4 °C). 3) Samples are centrifuged at 2,000 rpm for 10 min at 4 °C. 4) Cells are resuspended in 1 ml cold IP lysis buffer (containing 10µl protease inhibitors) and incubated for 20 min at 4 °C. 5) Samples are centrifuged at 12,000 rpm for 15 min at 4 °C. 6) 50 µl of supernatant are transferred in a 1.5 ml cup and stored at 4 °C (Input samples). 7) 850 µl of supernatant are transferred in a 1.5 ml cup (IP samples). 8) Co-IP samples are incubated with 1.7 µl anti-FLAG antibodies (#374, 1:500) for 30 min at 4 °C under rotation. 9) PrG-agarose beads are prepared by washing beads twice with 1 ml IP washing buffer in a 1.5 ml cup by centrifugation at 1,000 rpm for 1 min (25 µl beads per IP sample). Supernatant is removed using a Hamilton syringe and beads are resuspended in 25 µl IP washing buffer. 10) IP samples are incubated with 25 µl washed agarose beads overnight at 4 °C under gentle rotation.
Day 5	1) Beads in IP samples are washed three times with 1 ml IP washing buffer by centrifuging at 1,000 rpm for 1 min. After that, supernatant is discarded using the Hamilton syringe and Beads are resuspended in 40 µl 2X LSB. 2) Input samples are mixed with 50 µl 2X LSB. 3) All samples are boiled for 5 min. 4) Samples are centrifuged at 12,000 rpm for 1 min. **Break possible:** Samples can be stored at -20 °C. 5) Samples are separated by SDS-PAGE (see section 6.2.1): 20 µl of input samples and 10 µl of IP samples are loaded twice on different gels. 6) Interaction between bait and prey protein are analyzed by Western blot (see section 6.2.3). Membranes were stained either with anti-FLAG or anti-HA antibodies (see section 6.2.4).

Time	Protocol

6.3. Cell culture methods

6.3.1. Culturing of S2R+ *Drosophila* cells

S2R+ *Drosophila* cells were cultivated in 14 ml complete Schneider´s Drosophila medium in 75 cm^2 tissue flasks. The adherent cells were grown at 27°C in an incubator and split twice a week (see section 6.3.1.1)

6.3.1.1. Splitting of cells

Cells were separated twice a week into tissue flasks with fresh medium to maintain constant cell growth in a sufficient environment. Therefore, cells were treated as follows:

Table 46| Protocol for splitting of cells

Steps	Procedure	25 cm^2 tissue flasks	75 cm^2 tissue flasks
Step 1	The old medium is removed	-	-
Step 2	The adherent cells are washed with PBS	2.5 ml	5 ml
Step 3	Trypsin/EDTA solution is added and incubated for 2 min at room temperature	2 ml	5 ml
Step 4	The adherent cells are dispensed from the tissue flask by pipetting up and down	-	-
Step 5	The cell suspension is transferred to a 15-ml falcon and centrifuged at 2.000 rpm for 2min to remove the Trypsin solution	-	-
Step 6	The supernatant is discarded, and the cells are resuspended in complete Schneider´s medium	4 ml	8 ml
Step 7	Fresh flasks are filled with fresh medium	5 ml	13 ml
Step 8	Cell suspension is added in a 1:4 ratio		

6.3.1.2. Cell number determination

The cell number was determined using a Fuchs-Rosenthal counting chamber consisting of 256 small square chambers (total area: 16 mm^2; depth: 0.2 mm; cubic content: 3.2 µl). To distinguish living from dead cells, 80 µl Trypan-Blue solution (1:1 dilution H_2O: Trypan-Blue) were added to 20 µl of the cell suspension and incubated for 1-2 min. The solution was transferred into the counting chamber and each cell within a small square was counted under the microscope. At least 16 Squares were counted, and the mean value of cells was determined. The total cell number was then calculated with the following formula:

$$\frac{\text{mean value of counted cells} \times \text{dilution factor}}{\text{area}\,[\text{mm}^2] \times \text{depth}\,[\text{mm}]} = \text{X} \times 10^6 [\text{cells/ml}]$$

6.3.1.3. Seeding of cells

Subsequent after splitting (see section 6.3.1.1) cells were seeded in 6-well or in 12-well plates depending on the experimental approach.

Table 47| Protocol for seeding of cells

Microwell plate	Cell number	Amount of medium
6-well plate	450.000	3 ml
12-well plate	125.000	1.5 ml

The inoculation volume was calculated based on the cell number (see section 6.3.1.2).

6.3.2. Transfection of cells

Transient transfection of *Drosophila* S2R+ cells was carried out 24 h after seeding. The following transfection mixture were used for either 6- or 12-well plates:

Table 48| Setup of transfection mixture

Component	Amount	
	6-well plate	12-well plate
Total plasmid DNA	600 ng	200 ng
Schneider´s Drosophila medium	Ad 150 µl	Ad 75µl
Total volume	**150 µl**	**75 µl**
FuGENE HD	**3 µl**	**1 µl**

FuGENE HD transfection reagent was used for transfection as follows:

Table 49| Protocol for transfection of S2R+ cells

Steps	Procedure
Step 1	FuGENE HD is vortexed for 20 sec.
Step 2	After adding the indicated amount of FuGENE HD reagent to the transfection mix, the mix is immediately vortexed for 3 sec.
Step 3	The mixture is incubated for 15 min at room temperature
Step 4	The whole reaction mixture is added to the cells while smoothly rotating the plate

6.3.3. Silencing of genes by RNA-interference

RNA interference was used for specific gene knockdown using either in vitro transcribed long dsRNA molecules that were directly applied into the cell culture medium or by co-transfection of short hairpin plasmids encoding for micro-RNAs.

6.3.3.1. RNAi via long in vitro transcribed dsRNA molecules

Cells were treated with dsRNA produced by *in vitro* transcription (see section 6.1.7) as follows:

Table 50| Timeline for RNAi gene knockdown via long dsRNA molecules

Time	Protocol
Day 1	Seeding of cells in 12-well plates (see section 6.3.1.3)
Day 2	Transfection of cells (see section 6.3.2)
Day 3	Addition of 1000ng dsRNA directly into the cell medium while rotating
Day 5	Analysis by flow cytometry (see section 6.4)

6.3.3.2. RNAi via short-hairpin RNA molecules

Gene knockdown mediated by vector based expression of micro-RNAs was accomplished by co-transfection of short-hairpin plasmids based on the mir-1-shRNA (Nguyen et al., 2006; Haley et al., 2008). The 21nt siRNA sequence for efficient gene knock down was estimated using the E-RNAi online tool. Cells were treated as follows (see Table 51):

Table 51| Timeline for RNAi gene knockdown via shRNA molecules

Time	Protocol
Day 1	Seeding of cells in 12-well plates (see section 6.3.1.3)
Day 2	Co-transfection of cells with short hairpin plasmids (see section 6.3.2)
Day 5	Analysis by flow cytometry (see section 6.4)

6.3.4. Treatment with protease inhibitors

In order to inhibit protein degradation cells were treated with the specific proteasome inhibitor bortezomib with the following procedure (see Table 52):

Table 52| Timeline for treatment of S2R+ cells with proteasome inhibitor

Time	Protocol
Day 1	Seeding of cells in 12-well plates (see section 6.3.1.3)
Day 2	Transfection of cells (see section 6.3.2)
Day 4	**Step 1**: 1.5 ml complete Schneider´s medium is added with 1.5 µl bortezomib stock solution (100µM) to a final concentration of 100nM **Step 2**: Control medium containing 1.5 µl DMSO is prepared the same way **Step 3**: Cell medium is removed from the 12-well plate and replaced with either control medium or medium containing 100nM bortezomib **Step 4**: After 8h incubation cells are analyzed by flow cytometry (see section 6.3.7.1)

6.3.5. Cell cycle arrest of S2R+ cells

Cell cycle arrest of S2R+ cells was induced by treating S2R+ cells for at least 24h with a final concentration of 0.5mM mimosine (G1-phase arrest), 1µM hydroxyurea and 10 µM aphidicolin (S-phase arrest) and 1.7 µM 20-hydroxyecdysone (G2-phase arrest) or 12 h of 30 µM colchicine (M-phase arrest) (Rogers et al., 2009; Brownlee et al., 2011). Cells have been treated according to the following protocol:

Time	Protocol
Day 1	Seeding of cells in 12-well plates or 6-well plates (see section 6.3.1.3)
Day 2	Transfection of cells (see section 6.3.2)
Day 3	**Step 1**: Half of the medium was removed from the cell culture (0.75 ml – 12 well / 1.5 ml – 6 well). **Step 2**: Either 0.75 ml or 1.5 ml fresh complete Schneider´s medium was transferred in a 1.5 ml tube. **Step 3**: Either DMSO (control), mimosine, hydroxyurea and aphidicolin, 20-hydroxyecdysone or colchicine were added as described above and the mixture was vortexed properly. **Step 4**: The mixture was added to the cells.

Time	Protocol
Day 4/5	Cells were used for phosphorylation analysis using Phos-tag SDS-PAGE (see section 6.3.7.3) or co-IP analysis for protein interaction (see section 6.2.5). Cell cycle arrest was confirmed by flow cytometry (see section 6.4). Therefore, a fifth of the cells used for the respective approach were stained with Hoechst and analyzed for the cell cycle profiles.

6.3.6. Edu labeling of S-phase cells

S-phase cells were labeled using the Click-iT™ Edu Flow Cytometry Assay Kit. Cells were treated according to the following protocol based on the manufacturer´s instructions:

Table 53| Timeline for Edu labeling of S-phase cells

Time	Protocol	
Day 1	S2R+ cells are seeded in 6-well plates	
Day 3	1) Half of the medium (1.5 ml) was removed and 1.5 µl of 10 mM EdU solution were added directly into the remaining medium to a final concentration of 10 µM. 2) Cells were incubated for 2 hours	**Label cells with EdU**
	3) Discard the remaining medium and add 500 µl Trypsin/EDTA solution and incubate for 2 min. Dissolve cells by pipetting up and down 4) Add 1 ml 3% glyoxal solution and incubate for 30 min on ice and 30 min at RT under gentle rotation. 5) Transfer the cells into a 2ml cup. 6) Pellet the cells by centrifugation at 2000 rpm for 2 min and remove the supernatant 7) Add 1ml 0.1M NH_2Cl solution and incubate for 30 min 8) Pellet the cells by centrifugation at 2000 rpm for 2 min and remove the supernatant 9) Permeabilize cells in 500 µl 0.2% Tween solution (in PBS) (add RNase A if required) and incubate for 30 min 10) Pellet the cells by centrifugation at 2000 rpm for 2 min and discard the supernatant 11) Resuspend the cells in 100µl of 1x Click-iT™ saponin-based permeabilization and wash reagent	**Fix and permeabilize**
	Click-IT reaction was performed according to the manufacturer's instructions with Alexa Fluor™ 647 picolyl azide	**Click-iT™ reaction**
	12) Add 900 µl of Typsin/EDTA Hoechst 33342 solution to each sample 13) Incubate the samples for 30 min at RT protected from light	**Stain cells for DNA content**
	14) Analyze samples by flow cytometry. Click-iT EdU Alexa Fluor 647 fluorescence was detected with the 635 nM laser and a 675/20 emission bandpass filter.	**Flow cytometry**

6.3.7. Cell preparation

6.3.7.1. Cell preparation for flow cytometry

Relative protein stability analysis of transiently transfected S2R+ cells was determined by flow cytometry after 2-3 days after transfection. The cells were stained with 6µl Hoechst, added directly into the medium, for at least 15 minutes at 27°C. The medium was discarded and the cells were removed from

the well with 1 ml Trypsin/EDTA solution containing 1µl Hoechst per ml. The cell suspension was transferred into a 3.5 ml tube and analyzed by flow cytometry (see 1826.4).

6.3.7.2. Cell preparation for SDS-PAGE

Protein expression of the cells analyzed by flow cytometry was verified by SDS-Page and subsequent Western blot analysis. 100 µl of the cell suspension used for flow cytometry (1:10 of the total suspension) was pelletized by centrifugation 3 min at 3.000 rpm. The pellet was resuspended in 40µl 2x LSB and boiled for 5 min at 100°C. 20µl of the cell culture lysate were used for SDS-PAGE.

6.3.7.3. Cell preparation for Phos-tag SDS PAGE

Analysis of phosphorylation of a protein of interests was analyzed using Phos-tag SDS PAGE. Cells were treated according to the following protocol (see Table 54):

Table 54| Timeline of cell preparation for Phos-tag SDS-PAGE

Time	Protocol
Day 1	S2R+ cells are seeded in 12-well plates (see section 6.3.1.3)
Day 2	S2R+ were transiently transfected with plasmids expressing the protein of interest (see section 6.3.2)
Day 4	1) Adherent cells are detached off the dish in 500 µl PBS using a cell scratcher. 2) Samples are centrifuged at 2,000 rpm for 10 min at 4 °C. 3) Cells are resuspended in 50 µl cold lysis buffer for dephosphorylation containing protease inhibitor and incubated for 20 min at 4 °C. 4) Samples are centrifuged at 12,000 rpm for 15 min at 4 °C. 5) 40 µl of supernatant are transferred in a 1.5 ml cup and mixed with 5µl PMP and 5µl $MnCl_2$ (phosphorylated sample). 6) 40 µl of supernatant are transferred in a 1.5 ml cup and mixed with 5µl PMP and 5µl $MnCl_2$ and 1 µl lambda phosphatase (dephosphorylated sample). 7) Samples are incubated for 60 min at 30°C 8) Samples are mixed with 5 µl 10x LSB 9) All samples are boiled for 5 min. 10) Samples are centrifuged at 12,000 rpm for 1 min

6.3.7.4. Cell preparation for live cell imaging and localization analysis

For live cell imaging and localization analysis cells were treated according to the following procedure:

Table 55| Timeline of cell preparation for live cell imaging

Time	Protocol
Day 1	Seeding of cells in 12-well plates (see section 6.3.1.3)
Day 2	Transfection of cells (see section 6.3.2)
Day 4	Transfer of cells into IBISI µ plates
Day 5	Live cell imaging (see section 6.5) or localization analysis (see section 6.6)

6.4. Flow cytometry of S2R+ cells

6.4.1. Measurement procedure

Flow cytometry analysis of transfected S2R+ cells was conducted with a Sysmex/Partec CyFlow Space cytometer. The following light sources and optical filters were used for the detection of Hoechst, GFP,

CHE and Fx Cycle Far red fluorescence. Forward and side scatter signals (FSC / SSC) were detected after illumination with the 488 nm blue state laser (see Table 56).

Table 56| List of light source and optical filters - CyFlow Space

Fluorophore	Excitation laser	Detection filter
Hoechst 33342	365 nm High Power UV-LED	FL2 – Bandpass filter BP 455/50
GFP	488 nm blue solid state laser	FL1 – Bandpass filter BP 527/30
CHE	561 nm yellow laser	FL3 – Bandpass filter BP 630/75
Fx cycle Far red	635 nm red diode laser	FL3 – Bandpass filter BP 675/20
Scatter parameters		
Forward scatter	488 nm blue solid state laser	Longpass filter IBP 488
Side scatter	488 nm blue solid state laser	Longpass filter IBP 488

6.4.2. Gating of cell population and data export

The data obtained by the CyFlow Space was imported into FCS express software. Single cells were determined by the combination of two gates. First, a "cells" gate based on the FSC and SSC was applied determining cells based on cell size and granularity. Second, a gate "DNA" was selected applying doublet discrimination based on Hoechst signal height and width. Thereby, cell aggregates and smaller fragments were excluded. Finally, single cells were selected by the combination of "cells" and "DNA" gate referred to "cells-DNA" gate (Figure 76). FL1, FL2 and FL3 values of the particles within the "cells-DNA" gate were exported as comma-separated value (csv) files and further analyzed using the software OriginLab (see 6.4.3.)

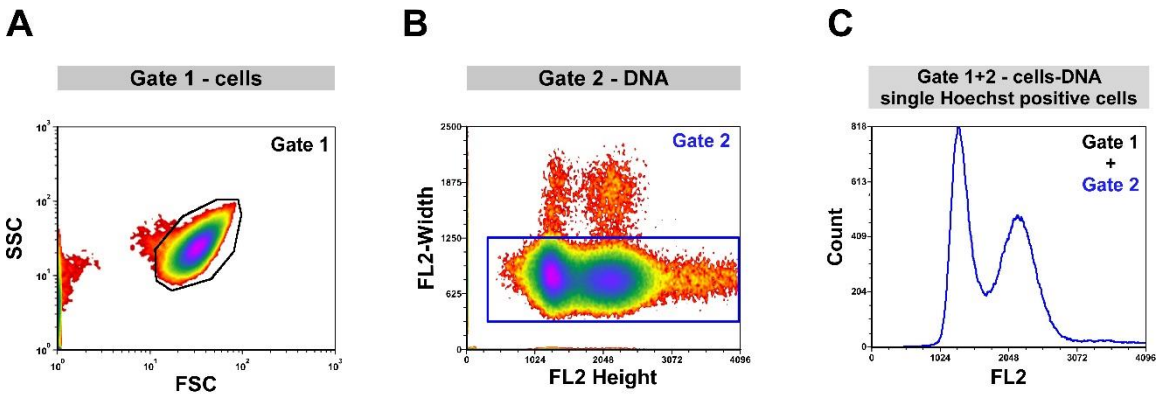

Figure 76| Determination of single cells by the Cells-DNA gate

(**A**) Gate 1 – Cells: Based on FSC and SSC values, cells are selected based on size and granularity in the cells gate (black polygon). (**B**) Plot of Hoechst signal (FL2) peak height against width. Single cells are selected in DNA gate excluding cell aggregates (blue rectangle). (**C**) DNA histogram of cells gated by the combinatorial gate "cells-DNA" displaying the standard distribution of G1-cells with lower DNA content, G2 cells with higher DNA content and S-cells in between.

6.4.3. Data analysis using OriginLab

Data analysis was performed using the software "OriginLab". The exported csv. files containing the FL1, FL2 and FL3 vales of the gated cells were imported to the FACS-template-43.opju file. Subsequent processing was automated using the "all-in-one macro 43" (see section 11.1.1) executing the following commands:

Steps	Procedure
Step 1	GFP or CHE is set as protein of interest (POI) and accordingly the reference protein (RF) is selected.
Step 2	Based on untreated, Hoechst stained cells a threshold for background fluorescence is determined for the signals detected in the FL1 (GFP-signal) and FL3 (CHE-signal) channels. The fluorescent range

Steps	Procedure
	in which 99.5% of these cells reside marked the threshold thereby excluding extreme outlier cells. Cells below this threshold are untransfected "negative" cells and cells above are transfected "positive" cells.
Step 3	Cells are sorted in "positive" and "negative" cells based on the set threshold.
Step 4	Transfection rate is calculated by the percentage of positive cells in relation to the total cell number.
Step 5	For each sample, a DNA histogram of the negative cells is generated, and automatic peak analysis determines the two maxima later used for G1- and G2- determination and the minimum value between the two peaks for S-phase assignment.
Step 6	Calculation of logarithmic FL-POI to FL-RF ratio for each single cell

Using the macro "Analyze different cell cycle populations" (see section 11.1.2) cells were sorted in G1-, S- or G2-phase cells based on defined areas selected from the maxima and minimum values from the DNA histogram.

In a next step, only cells with a certain expression level based on the values of the reference protein were analyzed. Therefore, the macro "Select expression range" was applied (see section 11.1.3).

6.4.4. Data representation

The box represented the interquartile range between the upper (75th percentile) and lower (25th percentile) quartiles. The whiskers represented the last data point of the upper and lower inner fence. These fences were defined as the 75th percentile plus 1.5 times the interquartile range or as the 25th percentile minus 1.5 times the interquartile range, respectively. The average is represented by the square and the median by the line within the box. All stability indices were normalized for reasons of comparability. For relative protein stability analysis, the mean values of the POI were normalized to the respective RPS-control mean value for the respective cell population. In case of the *in vivo* APC/C activity assay all values were normalized to the mean value of Cyclin B (see the result sections for details).

6.5. Live cell imaging

6.5.1. Microscopy system and imaging

Live cell imaging of transfected S2R+ cells was conducted on a Zeiss Cellobserver system equipped with a Yokogawa CSU-X1 spinning disk system using a Plan-Apochromat 20X lens (NA 0.8) and data recorded on an AxioCam MRm camera. Images were taken every 15 and three z-stacks with a distance of 1.25 µm were recorded in three channels: bright-field, GFP- and CHE-fluorescence. The following light sources and optical filters were used (see Table 57):

Table 57| List of light source and optical filters - Zeiss Cellobserver

Fluorophore	Excitation laser	Detection filter
GFP	488 nm OPSL laser	Bandpass filter BP 525/50
CHE	561 diode laser	Bandpass filter BP 630/75

6.5.2. Image processing

Image J was used for image processing. The pixel values of the individual z-stacks at a given position were summed up for the GFP and Cherry channels and projected (average intensity) for the brightfield images. Individual cells undergoing mitosis were selected and traced from 90 min before entry into mitosis and up to 600 min after anaphase onset. A threshold was selected in early telophase cells in which most of NLS-GFP signal was present in the newly formed nuclei and the threshold set to cover the nuclear signal. Only one of the telophase cells after the mitotic division was then followed. The GFP fluorescence signal was quantified in the selected cells and a region of interest (ROI) recorded for

the thresholded signal. Using the same threshold, the GFP signal was similarly quantified and the region of interests recorded in the following time frames. Using the list of ROIs, the CHE-signal was then quantified in the CHE-channel. To determine the GFP and CHE ratios before entry into mitosis, the GFP and CHE signals of three time frames right before nuclear envelope breakdown was quantified in the same manner and with the same threshold as before and an average of these three signal intensities was determined (Figure 77).

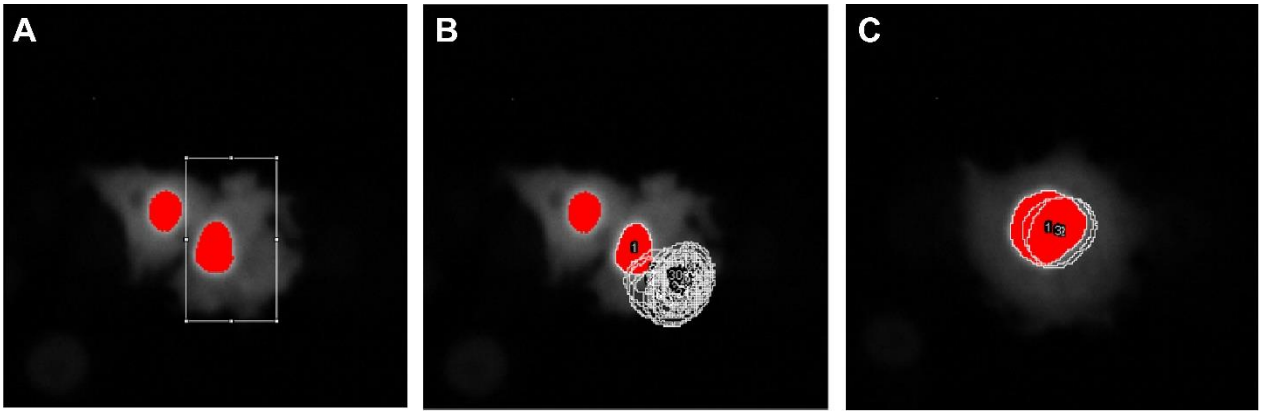

Figure 77| Image processing for live cell imaging

(**A**) A threshold for the NLS-GFP signal was set and one of the daughter cells was marked by a rectangle ROI. (**B**) Using the macro "Analyze-A" the marked cell was automatically traced for 30 time frames and the GFP and CHE values were measured for each time frame. CHE/GFP values were calculated for each time frame to create a degradation curve. (**C**) Mean of CHE/GFP values of three time frames right before nuclear envelop breakdown were used for normalization.

6.5.3. Image analysis and computation

For each time point, a CHE/GFP ratio was calculated and normalized to the CHE/GFP ratio before mitosis in case of G1 degradation or to telophase for degradation in S-phase. Independent cells were analyzed in this way and degradation curves were created from the normalized CHE/GFP ratios at the different time points. A mean curve was calculated from the average CHE/GFP ratios of the analyzed cells at the individual time points.

6.6. Cellular localization analysis

6.6.1. Microscopy system and imaging

Localization analysis of transfected S2R+ cells was conducted on a Zeiss Cellobserver system (see 6.5.1) using a Zeiss Fluor 40X lens (NA 1.3). For each position ten z-stacks with a distance of 0.5 µm were recorded in three channels: bright-field, GFP- and CHE-fluorescence.

6.6.2. Image processing

The software *ImageJ* was used for image processing. One z-section was chosen for each stack that visually appeared to be in the center of the nucleus. Based on nuclear localized GFP signals a threshold was selected in the GFP channel marking the nucleus. Based on this threshold a ROI referred to as "whole nucleus" was defined. A second ROI termed "inner nucleus" was set by decreasing the whole nucleus ROI by the factor 0.5 and a third ROI "nucleus + cytoplasm" increasing the whole nucleus ROI by the factor 1.25 (Figure 78). Subtracting the "whole nucleus" region from the "nucleus + cytoplasm" ROI results in the area "cytoplasm". The defined ROIs were used with the same threshold for analysis of the detected CHE signals.

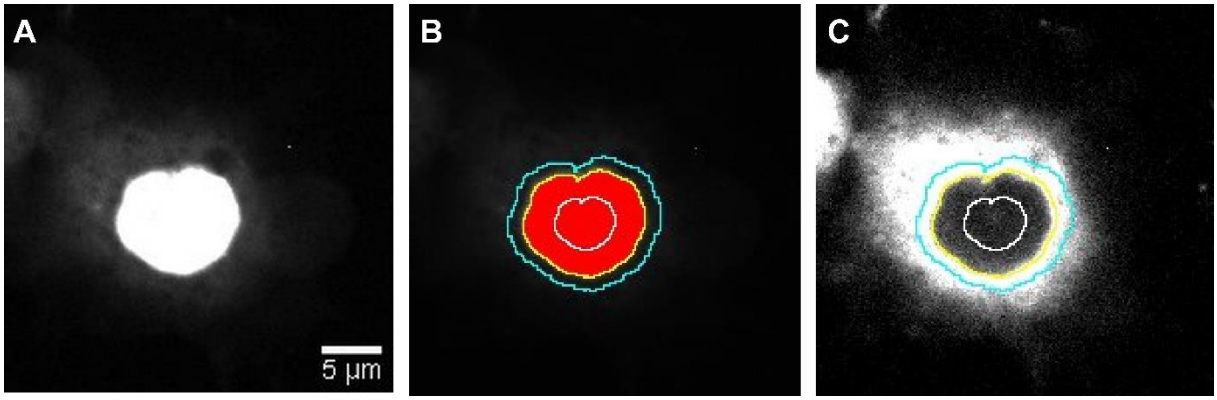

Figure 78| Image processing for localization analysis

The example shows the analysis of NLS-GFP-T2A-NES-Rca1_204-411 (pFSR-1611-actPro(L)-HA-NLS-GFP-ddT2A-HA-NES-CHE-Rca1_Del_1-203). (**A**) A threshold is set in the GFP channel defining the nucleus based on NLS-GFP signal. (**B**) Three ROIs are created after setting the threshold. The "whole nucleus" (yellow), the "inner nucleus" (white = 0.5x"whole nucleus") and the "nucleus + cytoplasm" (cyan = 1.25x"whole nucleus"). Cytoplasm is the Area between the cyan and yellow ROI ("nucleus + cytoplasm" – "whole nucleus"). (**C**) The defined ROIs are used in the CHE-channel with the same threshold set for the GFP channel to analyze CHE signals.

6.6.3. Image analysis and computation

Based on the intensities from the different ROIs, nucleus/cytoplasm ratios can be calculated as a unit for nuclear localization. The calculation was performed as follows (Figure 79):

A

	Area	IntDen	Mean (=IntDen/Area)
whole nucleus	1774	40695	23
inner nucleus	445	2888	6
nucleus + cytoplasm	2773	155540	56
cytoplasm	999	114881	115

B

Calculation of cytoplasm → "nucleus + cytoplasm" – "whole nucleus"

Area (cytoplasm)	2773 - 1774	= 999
IntDen (cytoplasm)	155540 - 40659	= 114881
Mean (cytoplasm)	114881 / 999	= 115

C

Nucleus = inner nucleus

Cytoplasm = (nucleus + cytoplasm) – whole nucleus

Nucleus/cytoplasm = 6/115 =0.05

Figure 79| Calculation of the nucleus/cytoplasm ratio

(**A**) For each ROI the values for Area, Integrated Density (IntDen) and the resulting Mean (IntDen/Area) were calculated using ImageJ. (**B**) Calculation of the "cytoplasm" values for Area and IntDen was accomplished by subtracting "nucleus + cytoplasm" – "whole nucleus" values. Based on these values the cytoplasm Mean was calculated. (**C**) Nucleus/cytoplasm ratios were calculated where "inner nucleus" represents the nucleus value. Equal distribution of a protein into the nucleus and cytoplasm would result in a ratio value of ≈1, values greater than 1 correspond to protein localization in the nucleus and smaller 1 localization in the cytoplasm. In this example the protein is localized in the cytoplasm.

6.7. Statistical analysis

Statistical analysis was performed with R-studio. All data was tested for normal distribution with the Shapiro-Wilk test. If normal distribution was fulfilled, a two-tailed t-test was used for testing of significant differences. If not, the Mann-Whitney U-Test was used instead.

7. List of Figures

8. List of Tables

9. Abbreviation

A	
aa	Amino acid
ABBA	Cyclin **A**,**B**ubR1, **B**ub1, and **A**cm1
Acm1	APC/C-Cdh1 modulator 1
ADP	Adenosine diphosphate
AMP	Adenosine monophosphate
APC/C	Anaphase promoting complex/cyclosome
APS	Ammonium persulphate solution
ATP	Adenosine triphosphate
B	
BF	Brightfield
bp	Base pairs
BRCA1	Breast Cancer 1
BSA	Bovine serum albumin
Bub1	Budding uninhibited by benomyl 1
Bub3	Budding uninhibited by benzimidazoles 3 Homolog
C	
CAK	Cdk-activating kinases
Cdc	Cell division control protein
Cdc20	ell-division cycle protein 20
Cdh1	Cdc20 homologue 1
CDI	Cdk inhibitory domain
Cdk	Cyclin dependent kinase
Cdt1	Chromatin Licensing and DNA Replication Factor 1
Cdt2	Cdc10-dependent transcript 2
CHE	Cherry
CIP/KIP	Cdk interacting protein/kinase inhibitor protein
CKI	Cyclin dependent kinase inhibitor
Cks	Cyclin dependent kinase subunits
Clb	B-type cyclins
co-IP	co-Immunoprecipitation
CP	Core particle
CRL	Cullin Ring ligase
CT	C-terminus
CTD	C-terminal domain
CTP	Cytosine triphosphate
Cul	Cullin
Cut2	Securin S. pombe
Cyc	Cyclin
D	
Dap	Dacapo
DB	D-box
DDB1	DNA damage-binding protein 1
Ddi1	DNA Damage Inducible 1 Homolog 1
Dbf4	Dumbbell former 4 protein
DMSO	Dimethyl sulfoxide
DNA	Deoxyribonucleic acid
dNTP	Deoxynucleotide triphosphate
DTT	Dithiothreitol
DUB	Deubiquitnation enzyme
E	
EDTA	Ethylenediaminetetraacetic acid
E2F1	E2 promotor binding factor 1
EGTA	Ethylene glycol-bis(β-aminoethyl) ether
ELM	Eukaryotic Linear Motif resource
Emi1	Early mitotic inhibitor 1
Emi2	Early mitotic inhibitor 2
END	Emi1-NuMA/Dynein-dynactin
Evi5	Ecotropic viral integration site 5
F	
FACS	Fluorescence-activated cell sorter
FBS	Fetal bovine serum
FL	Fluorescent intensities

FLP	Full-length polyprotein
FSC	Forward Scatter
FUCCI	Fluorescent ubiquitination-based cell cycle indicator
Fzr	Fizzy related
Fzy	Fizzy

G

Gem	Geminin
GFP	Green fluorescent protein
GPS	Group based prediction system
GTP	Guanosine-5'-triphosphate

H

HA	Human influenza epitope
HECT	Homologous to E6-AP Carboxyl Terminus
HEPES	4-(2-hydroxyethyl)-1-piperazineethanesulfonic acid
HURP	Hepatoma up-regulated protein

I

IBR	In-Between-RING
INK4	Inhibitors of Cdk4
IP	Immunoprecipitation
IPTG	Isopropyl β-d-1-thiogalactopyranoside
IQR	Interquartile
IVT	*In vitro* trasncription

K

kb	Kilo base
kDa	kilo Dalton
KIF1C	Kinesin Family Member 1C

L

LB	Lysogeny broth
LED	Light-emitting diode
log	Logarithm
LSB	Laemmli sample buffer

M

Mad1	Mitotic arrest deficient 1
Mad2	Mitotic arrest deficient 2
MAPK	Mitogen-activated protein kinase
MCC	Mitotic checkpoint complex
MCM	Mini-chromosome maintenance complex
MICA	Multiple interval-based curve alignment
mRNA	Messenger RNA

N

NEBD	Nuclear envelope breakdown
Nedd8	Neural-precursor-cell-expressed developmentally down-regulated 8
Nek2A	NIMA-related kinase 2A
NES	Nuclear export signal
NIPA	Nuclear Interaction Partner of Alk kinase
NLS	Nuclear localisation signla
NMR	Nuclear magnetic resonance
NT	N-terminus
NTP	Nucleoside triphosphate
NuSAP	Nucleolar and spindle-associated protein

O

OB	O-box
Orc1	Origin recognition complex subunit 1

P

PAGE	Polyacrylamide gel electrophoresis
PBS	Phosphate buffer saline
PBST	Phosphate buffer saline - tween
PCNA	Proliferating cell nuclear antigen
PCR	Polymerase chain reaction
PDB	Protein database
pFSR	Plasmid Frank Sprenger Regensburg
PIP	PCNA interaction protein
Plk1	Polo-like kinase 1
PMP	Protein Metallo Phosphatases
POI	Protein of interest
PP	Pyrophosphate
pRB	pocket protein retinoblastoma
pre-RC	pre-replicative complex, prereplication complex
PTM	Post-translational modification

R

Rbx1	RING-box protein 1
Rca1	Regulator of Cyclin A1
RING	Really interesting new gene
RISC	RNA-induced silencing complex
RNA	Ribonucleic acid
RNAi	RNA interference
Rnase	Ribonuclease
RNF31	Ring Finger Protein 31
ROI	Region of interest
rpm	Rounds per minute
Rpn1	Ribophorin I
RPS	Relative protein stability
Rpt1	Regulatory particle triple-A protein
rSAP	Shrimp Alkaline Phosphatase
RT	Room temperature
Rux	Roughex

S

SAC	Spindle assembly checkpoint
SCF	Skp/Cullin/F-box complex
SDS	Sodium dodecyl sulfate

Sgo1	Shugoshin 1
Ska3	Spindle and Kinetochore Associated Complex Subunit 3
Skp1	S-phase kinase-associated protein 1
Skp2	S-phase kinase-associated protein 2
Spd2	Spindle-defective protein 2
SPO	Sprenger Oligo
SSC	Side scatter
SUMO	Small Ubiquitin-Related Modifier

T

T2A	*Thosea asigna* virus 2A
TAE	TRIS-Acetat-EDTA
TAME	Tosyl arginine methyl ester
TEMED	N,N,N′,N′-Tetramethylethylendiamin
TPR	tetratricopeptide
TPX2	Targeting protein for Xklp2
TRIP13	Thyroid receptor-interacting protein 13
TTP	Thymidine triphosphate

U

UAS	Upstream activating sequence
Ub	Ubiquitin
UBA	Ubiquitin-associated
UBCH10	Ubiquitin-conjugating Enzyme H10
Ube2S	Ubiquitin-conjugating enzyme E2 S
Ubp6	Ubiquitin carboxyl-terminal hydrolase 6
USP44	Ubiquitin carboxyl-terminal hydrolase 44
UTP	Uridine triphosphat
UTR	Untranslated region
UV	Ultraviolet light

W

Wnt	Wingless + Int1

Z

ZBR	Zinc binding region

*

β-TrCP	β-Transducin repeat-containing protein

10. References

Abbas, T.; Sivaprasad, U.; Terai, K.; Amador, V.; Pagano, M.; Dutta, A., 2008: PCNA-dependent regulation of p21 ubiquitylation and degradation via the CRL4Cdt2 ubiquitin ligase complex. *Genes and Development*., **22**, 2496–2506.

Abbas, T.; Shibata, E.; Park, J.; Jha, S.; Karnani, N.; Dutta, A., 2010: CRL4Cdt2 regulates cell proliferation and histone gene expression by targeting PR-Set7/Set8 for degradation. *Molecular Cell*., **40**, 9–21.

Abbas, T.; Dutta, A., 2011: CRL4 Cdt2 - Master coordinator of cell cycle progression and genome stability. *Cell Cycle*., **10**, 241–249.

Albert, S.; Schaffer, M.; Beck, F.; Mosalaganti, S.; Asano, S.; Thomas, H. F.; Plitzko, J. M.; Beck, M.; Baumeister, W.; Engel, B. D., 2017: Proteasomes tether to two distinct sites at the nuclear pore complex. *Proceedings of the National Academy of Sciences of the United States of America*., **114**, 13726–13731.

Alfieri, C.; Chang, L.; Zhang, Z.; Yang, J.; Maslen, S.; Skehel, M.; Barford, D., 2016: Molecular basis of APC/C regulation by the spindle assembly checkpoint. *Nature*., **536**, 431–436.

Alfieri, C.; Zhang, S.; Barford, D., 2017: Visualizing the complex functions and mechanisms of the anaphase promoting complex/cyclosome (APC/C). *Open Biology*., **7**.

Alfieri, C.; Chang, L.; Barford, D., 2018: Mechanism for remodelling of the cell cycle checkpoint protein MAD2 by the ATPase TRIP13. *Nature*., **559**, 274–278.

Araki, M.; Yu, H.; Asano, M., 2005: A novel motif governs APC-dependent degradation of Drosophila ORC1 in vivo. *Genes and Development*., **19**, 2458–2465.

Arias, E. E.; Walter, J. C., 2006: PCNA functions as a molecular platform to trigger Cdt1 destruction and prevent re-replication. *Nature Cell Biology*., **8**, 84–90.

Aufderheide, A.; Beck, F.; Stengel, F.; Hartwig, M.; Schweitzer, A.; Pfeifer, G.; Goldberg, A. L.; Sakata, E.; Baumeister, W.; Förster, F., 2015: Structural characterization of the interaction of Ubp6 with the 26S proteasome. *Proceedings of the National Academy of Sciences of the United States of America*., **112**, 8626–8631.

Avedisov, S. N.; Krasnoselskaya, I.; Mortin, M.; Thomas, B. J., 2000: Roughex Mediates G 1 Arrest through a Physical Association with Cyclin A, **20**, 8220–8229.

Balleza, E.; Kim, J. M.; Cluzel, P., 2018: Systematic characterization of maturation time of fluorescent proteins in living cells. *Nature Methods*., **15**, 47–51.

Ban, K. H.; Torres, J. Z.; Miller, J. J.; Mikhailov, A.; Nachury, M. V.; Tung, J. J.; Rieder, C. L.; Jackson, P. K., 2007: The END Network Couples Spindle Pole Assembly to Inhibition of the Anaphase-Promoting Complex/Cyclosome in Early Mitosis. *Developmental Cell*., **13**, 29–42.

Bansal, S.; Tiwari, S., 2019: Mechanisms for the temporal regulation of substrate ubiquitination by the anaphase-promoting complex/cyclosome. *Cell Division*., **14**, 1–18.

Barford, D., 2020: Structural interconversions of the anaphase-promoting complex/cyclosome (APC/C) regulate cell cycle transitions. *Current Opinion in Structural Biology*., **61**, 86–97.

Bassermann, F.; Eichner, R.; Pagano, M., 2014: The ubiquitin proteasome system — Implications for cell cycle control and the targeted treatment of cancer. *Biochimica et Biophysica Acta (BBA) - Molecular Cell Research*., **1843**, 150–162.

Benjamin, J. M.; Torke, S. J.; Demeler, B.; McGarry, T. J., 2004: Geminin has dimerization, Cdt1-binding, and destruction domains that are required for biological activity. *Journal of Biological Chemistry*., **279**, 45957–45968.

Berghammer, H.; Auer, B., 1993: 'Easypreps': fast and easy plasmid minipreparation for analysis of recombinant clones in E. coli. *BioTechniques*., **14**, 524, 528.

Bertoli, C.; Skotheim, J. M.; De Bruin, R. A. M., 2013: Control of cell cycle transcription during G1 and S phases. *Nature Reviews Molecular Cell Biology*., **14**, 518–528.

Bhaduri, S.; Pryciak, P. M., 2011: Cyclin-specific docking motifs promote phosphorylation of yeast signaling proteins by G1/S Cdk complexes. *Current Biology*., **21**, 1615–1623.

Bhogaraju, S.; Kalayil, S.; Liu, Y.; Bonn, F.; Colby, T.; Matic, I.; Dikic, I., 2016: Phosphoribosylation of Ubiquitin Promotes Serine Ubiquitination and Impairs Conventional Ubiquitination. *Cell*., **167**, 1636-1649.e13.

Birnboim, H. C.; Doly, J., 1979: A rapid alkaline extraction procedure for screening recombinant plasmid DNA. *Nucleic acids research*., **7**, 1513–1523.

Bischof, C., 2020: *Localisation of Rca1 and the resulting impact on its stability*. University of Regensburg.

Bodenmiller, B.; Malmstrom, J.; Gerrits, B.; Campbell, D.; Lam, H.; Schmidt, A.; Rinner, O.; Mueller, L. N.; Shannon, P. T.; Pedrioli, P. G.; Panse, C.; Lee, H. K.; Schlapbach, R.; Aebersold, R., 2007: PhosphoPep - A phosphoproteome resource for systems biology research in Drosophila Kc167 cells. *Molecular Systems Biology*., **3**, 1–11.

Brand, A. H.; Perrimon, N., 1993: Targeted gene expression as a means of altering cell fates and generating dominant phenotypes. *Development*., **118**, 401–415.

Braten, O.; Livneh, I.; Ziv, T.; Admon, A.; Kehat, I.; Caspi, L. H.; Gonen, H.; Bercovich, B.; Godzik, A.; Jahandideh, S.; Jaroszewski, L.; Sommer, T.; Kwon, Y. T.; Guharoy, M.; Tompa, P.; Ciechanover, A., 2016: Numerous proteins with unique characteristics are degraded by the 26S proteasome following monoubiquitination. *Proceedings of the National Academy of Sciences of the United States of America*., **113**, E4639–E4647.

Brown, Jeremy; Ryan, M. D., 2010: Ribosome "Skipping": "Stop-Carry On" or "StopGo" Translation. *Springer Science and Business Media*., 101–122.

Brown, N. G.; VanderLinden, R.; Watson, E. R.; Qiao, R.; Grace, C. R. R.; Yamaguchi, M.; Weissmann, F.; Frye, J. J.; Dube, P.; Cho, S. E.; Actis, M. L.; Rodrigues, P.; Fujii, N.; Peters, J. M.; Stark, H.; Schulman, B. A., 2015: RING E3 mechanism for ubiquitin ligation to a disordered substrate visualized for human anaphase-promoting complex. *Proceedings of the National Academy of Sciences of the United States of America*., **112**, 5272–5279.

Brown, N. G.; VanderLinden, R.; Watson, E. R.; Weissmann, F.; Ordureau, A.; Wu, K. P.; Zhang, W.; Yu, S.; Mercredi, P. Y.; Harrison, J. S.; Davidson, I. F.; Qiao, R.; Lu, Y.; Dube, P.; Brunner, M. R.; Grace, C. R. R.; Miller, D. J.; Haselbach, D.; Jarvis, M. A. et al., 2016: Dual RING E3 Architectures Regulate Multiubiquitination and Ubiquitin Chain Elongation by APC/C. *Cell*., **165**, 1440–1453.

Brownlee, C. W.; Klebba, J. E.; Buster, D. W.; Rogers, G. C., 2011: The protein phosphatase 2A regulatory subunit Twins stabilizes Plk4 to induce centriole amplification. *Journal of Cell Biology*., **195**, 231–243.

Brunet, A.; Kanai, F.; Stehn, J.; Xu, J.; Sarbassova, D.; Frangioni, J. V.; Dalal, S. N.; Decaprio, J. A.; Greenberg, M. E.; Yaffe, M. B., 2002: 14-3-3 Transits To the Nucleus and Participates in Dynamic Nucleocytoplasmic Transport. *Journal of Cell Biology*., **156**, 817–828.

Burton, J. L.; Solomon, M. J., 2001: D box and KEN box motifs in budding yeast Hsl1p are required for APC-mediated degradation and direct binding to Cdc20p and Cdh1p. *Genes and Development*., **15**, 2381–2395.

Burton, J. L.; Xiong, Y.; Solomon, M. J., 2011: Mechanisms of pseudosubstrate inhibition of the

anaphase promoting complex by Acm1. *EMBO Journal*., **30**, 1818–1829.

Buschhorn, B. A.; Petzold, G.; Galova, M.; Dube, P.; Kraft, C.; Herzog, F.; Stark, H.; Peters, J. M., 2011: Substrate binding on the APC/C occurs between the coactivator Cdh1 and the processivity factor Doc1. *Nature Structural and Molecular Biology*., **18**, 6–14.

Cappell, S. D.; Mark, K. G.; Garbett, D.; Pack, L. R.; Rape, M.; Meyer, T., 2018: EMI1 switches from being a substrate to an inhibitor of APC/CCDH1 to start the cell cycle. *Nature*.

Carroll, C. W.; Morgan, D. O., 2002: The Doc1 subunit is a processivity factor for the anaphase-promoting complex, 1–8.

Castro, A.; Bernis, C.; Vigneron, S.; Labbé, J. C.; Lorca, T., 2005: The anaphase-promoting complex: A key factor in the regulation of cell cycle. *Oncogene*., **24**, 314–325.

Chang, L.; Zhang, Z.; Yang, J.; McLaughlin, S. H.; Barford, D., 2014: Molecular architecture and mechanism of the anaphase-promoting complex. *Nature*., **513**, 388–393.

Chang, L.; Zhang, Z.; Yang, J.; McLaughlin, S. H.; Barford, D., 2015: Atomic structure of the APC/C and its mechanism of protein ubiquitination. *Nature*., **522**, 450–454.

Chao, W. C. H.; Kulkarni, K.; Zhang, Z.; Kong, E. H.; Barford, D., 2012: Structure of the mitotic checkpoint complex. *Nature*., **484**, 208–213.

Chen, X.; Ebelle, D. L.; Wright, B. J.; Sridharan, V.; Hooper, E.; Walters, K. J., 2019: Structure of hRpn10 Bound to UBQLN2 UBL Illustrates Basis for Complementarity between Shuttle Factors and Substrates at the Proteasome. *Journal of Molecular Biology*., **431**, 939–955.

Chiorino, G.; Metz, J. A. J.; Tomasoni, D.; Ubezio, P., 2001: Desynchronization rate in cell populations: Mathematical modeling and experimental data. *Journal of Theoretical Biology*., **208**, 185–199.

Chowdhury, M.; Enenkel, C., 2015: Intracellular Dynamics of the Ubiquitin-Proteasome-System. *F1000Research*., **4**, 1–16.

Ciechanover, A.; Ben-Saadon, R., 2004: N-terminal ubiquitination: More protein substrates join in. *Trends in Cell Biology*., **14**, 103–106.

Clijsters, L.; Ogink, J.; Wolthuis, R., 2013: The spindle checkpoint, APC/CCdc20, and APC/CCdh1 play distinct roles in connecting mitosis to S phase. *Journal of Cell Biology*., **201**, 1013–1026.

Colombo, S. L.; Palacios-Callender, M.; Frakich, N.; De Leon, J.; Schmitt, C. A.; Boorn, L.; Davis, N.; Moncada, S., 2010: Anaphase-promoting complex/cyclosome-Cdh1 coordinates glycolysis and glutaminolysis with transition to S phase in human T lymphocytes. *Proceedings of the National Academy of Sciences of the United States of America*., **107**, 18868–18873.

Cooper, G. M., 2000: *The Cell:A Molecular Approach* 2nd edn. Sinauer Associates Inc.

Cormack, B. P.; Valdivia, R. H.; Falkow, S., 1996: FACS-optimized mutants of the green fluorescent protein (GFP). *Gene*., **173**, 33–38.

Coudreuse, D.; Nurse, P., 2010: Driving the cell cycle with a minimal CDK control network. *Nature*., **468**, 1074–1080.

Crivat, G.; Taraska, J. W., 2012: Imaging proteins inside cells with fluorescent tags. *Trends in Biotechnology*., **30**, 8–16.

Cui, J.; Yao, Q.; Li, S.; Ding, X.; Lu, Q.; Mao, H.; Liu, L.; Zheng, N.; Chen, S.; Shao, F., 2010: Glutamine Deamidation and Dysfunction of Ubiquitin/NEDD8 Induced by a Bacterial Effector Family. *Science*., **329**, 1215–1218.

Da Fonseca, P. C. A.; Kong, E. H.; Zhang, Z.; Schreiber, A.; Williams, M. A.; Morris, E. P.; Barford, D.,

2011: Structures of APC/CCdh1 with substrates identify Cdh1 and Apc10 as the D-box co-receptor. *Nature*., **470**, 274–280.

Dang, F. W.; Chen, L.; Madura, K., 2016: Catalytically active proteasomes function predominantly in the cytosol. *Journal of Biological Chemistry*., **291**, 18765–18777.

Davey, N. E.; Morgan, D. O., 2016: Building a Regulatory Network with Short Linear Sequence Motifs: Lessons from the Degrons of the Anaphase-Promoting Complex. *Molecular Cell*., **64**, 12–23.

De Antoni, A.; Pearson, C. G.; Cimini, D.; Canman, J. C.; Sala, V.; Nezi, L.; Mapelli, M.; Sironi, L.; Faretta, M.; Salmon, E. D.; Musacchio, A., 2005: The Mad1/Mad2 Complex as a Template for Mad2 Activation in the Spindle Assembly Checkpoint. *Current Biology*., **15**, 214–225.

de Castro, E.; Sigrist, C. J. A.; Gattiker, A.; Bulliard, V.; Langendijk-Genevaux, P. S.; Gasteiger, E.; Bairoch, A.; Hulo, N., 2006: ScanProsite: Detection of PROSITE signature matches and ProRule-associated functional and structural residues in proteins. *Nucleic Acids Research*., **34**, 362–365.

De Felipe, P.; Luke, G. A.; Brown, J. D.; Ryan, M. D., 2010: Inhibition of 2A-mediated 'cleavage' of certain artificial polyproteins bearing N-terminal signal sequences. *Biotechnology Journal*., **5**, 213–223.

De Nooij, J. C.; Letendre, M. A.; Hariharan, I. K., 1996: A cyclin-dependent kinase inhibitor, dacapo, is necessary for timely exit from the cell cycle during Drosophila embryogenesis. *Cell*., **87**, 1237–1247.

Den Dunnen, J. T.; Antonarakis, S. E., 2000: Mutation nomenclature extensions and suggestions to describe complex mutations: A discussion. *Human Mutation*., **15**, 7–12.

Deshaies, R. J.; Joazeiro, C. A. P., 2009: RING domain E3 ubiquitin ligases. *Annual Review of Biochemistry*., **78**, 399–434.

Di Fiore, B.; Pines, J., 2007: Emi1 is needed to couple DNA replication with mitosis but does not regulate activation of the mitotic APC/C. *Journal of Cell Biology*., **177**, 425–437.

Di Fiore, B.; Wurzenberger, C.; Davey, N. E.; Pines, J., 2016: The Mitotic Checkpoint Complex Requires an Evolutionary Conserved Cassette to Bind and Inhibit Active APC/C. *Molecular Cell*., **64**, 1144–1153.

Diffley, J. F. X., 2004: Regulation of early events in chromosome replication. *Current Biology*., **14**, 778–786.

DiFiore, B.; Davey, N. E.; Hagting, A.; Izawa, D.; Mansfeld, J.; Gibson, T. J.; Pines, J., 2015: The ABBA Motif binds APC/C activators and is shared by APC/C substrates and regulators. *Developmental Cell*., **32**, 358–372.

Dong, X.; Zavitz, K. H.; Thomas, B. J.; Lin, M.; Campbell, S.; Zipursky, S. L., 1997: Control of G1 in the developing Drosophila eye: rca1 regulates Cyclin A. *Genes & Development*., **11**, 94–105.

Doronina, V. A.; Wu, C.; de Felipe, P.; Sachs, M. S.; Ryan, M. D.; Brown, J. D., 2008: Site-Specific Release of Nascent Chains from Ribosomes at a Sense Codon. *Molecular and Cellular Biology*., **28**, 4227–4239.

Dowdy, S. F.; Hinds, P. W.; Louie, K.; Reed, S. I.; Arnold, A.; Weinberg, R. A., 1993: Physical interaction of the retinoblastoma protein with human D cyclins. *Cell*., **73**, 499–511.

Eifler, K.; Cuijpers, S. A. G.; Willemstein, E.; Raaijmakers, J. A.; El Atmioui, D.; Ovaa, H.; Medema, R. H.; Vertegaal, A. C. O., 2018: SUMO targets the APC/C to regulate transition from metaphase to anaphase. *Nature Communications*., **9**.

Eldeeb, M. A.; Siva-Piragasam, R.; Ragheb, M. A.; Esmaili, M.; Salla, M.; Fahlman, R. P., 2019: A molecular toolbox for studying protein degradation in mammalian cells. *Journal of Neurochemistry*., 1–14.

Eldridge, A. G.; Loktev, A. V; Hansen, D. V; Verschuren, E. W.; Reimann, J. D. R.; Jackson, P. K., 2006: The Evi5 Oncogene Regulates Cyclin Accumulation by Stabilizing the Anaphase-Promoting Complex

Inhibitor Emi1. *Cell*., **124**, 367–380.

Elsasser, S.; Gali, R. R.; Schwikart, M.; Larsen, C. N.; Leggett, D. S.; Müller, B.; Feng, M. T.; Tübing, F.; Dittmar, G. A. G.; Finley, D., 2002: Proteasome subunit Rpn1 binds ubiquitin-like protein domains. *Nature Cell Biology*., **4**, 725–730.

Elsasser, S.; Chandler-Mitilello, D.; Müller, B.; Hanna, J.; Finley, D., 2004: Rad23 and Rpn10 serve as alternate ubiquitin receptors for the proteasome. *Journal of Biological Chemistry*., **279**, 26817–26822.

Enam, C.; Geffen, Y.; Ravid, T.; Gardner, R. G., 2018: Protein Quality Control Degradation in the Nucleus. *Annual Review of Biochemistry*., **87**, 725–749.

Enquist-Newman, M.; Sullivan, M.; Morgan, D. O., 2008: Modulation of the Mitotic Regulatory Network by APC-Dependent Destruction of the Cdh1 Inhibitor Acm1. *Molecular Cell*., **30**, 437–446.

Erpapazoglou, Z.; Walker, O.; Haguenauer-Tsapis, R., 2014: Versatile Roles of K63-Linked Ubiquitin Chains in Trafficking. *Cells*., **3**, 1027–1088.

Ewen, M. E.; Sluss, H. K.; Sherr, C. J.; Matsushime, H.; Kato, J. ya; Livingston, D. M., 1993: Functional interactions of the retinoblastoma protein with mammalian D-type cyclins. *Cell*., **73**, 487–497.

Eytan, E.; Sitry-Shevah, D.; Teichner, A.; Hershko, A., 2013: Roles of different pools of the mitotic checkpoint complex and the mechanisms of their disassembly. *Proceedings of the National Academy of Sciences of the United States of America*., **110**, 10568–10573.

Eytan, E.; Wang, K.; Miniowitz-Shemtov, S.; Sitry-Shevah, D.; Kaisari, S.; Yen, T. J.; Liu, S. T.; Hershko, A., 2014: Disassembly of mitotic checkpoint complexes by the joint action of the AAA-ATPase TRIP13 and p31comet. *Proceedings of the National Academy of Sciences of the United States of America*., **111**, 12019–12024.

Faesen, A. C.; Thanasoula, M.; Maffini, S.; Breit, C.; Müller, F.; Van Gerwen, S.; Bange, T.; Musacchio, A., 2017: Basis of catalytic assembly of the mitotic checkpoint complex. *Nature*., **542**, 498–502.

Fei, C.; Li, Z.; Li, C.; Chen, Y.; Chen, Z.; He, X.; Mao, L.; Wang, X.; Zeng, R.; Li, L., 2013: Smurf1-Mediated Lys29-Linked Nonproteolytic Polyubiquitination of Axin Negatively Regulates Wnt/ -Catenin Signaling. *Molecular and Cellular Biology*., **33**, 4095–4105.

Foley, E.; O'Farrell, P. H.; Sprenger, F., 1999: Rux is a cyclin-dependent kinase inhibitor (CKI) specific for mitotic cyclin-Cdk complexes. *Current biology : CB*., **9**, 1392–1402.

Fonseca, P. C. A.; Kong, E. H.; Zhang, Z.; Schreiber, A.; Mark, A., 2011: Europe PMC Funders Group Structures of APC / C Cdh1 with substrates identify Cdh1 and Apc10 as the D-box co-receptor, **470**, 274–278.

Frank, M., 2013: *Analyse der F-box-Funktion von Rca1 in Drosophila melanogaster*. University of Regensburg.

Frye, J. J.; Brown, N. G.; Petzold, G.; Watson, E. R.; Grace, C. R. R.; Nourse, A.; Jarvis, M. A.; Kriwacki, R. W.; Peters, J. M.; Stark, H.; Schulman, B. A., 2013: Electron microscopy structure of human APC/C CDH1 -EMI1 reveals multimodal mechanism of E3 ligase shutdown. *Nature Structural and Molecular Biology*., **20**, 827–835.

Gardino, A. K.; Yaffe, M. B., 2011: 14-3-3 proteins as signaling integration points for cell cycle control and apoptosis. *Seminars in Cell & Developmental Biology*., **22**, 688–695.

Gatti, M.; Pinato, S.; Maiolica, A.; Rocchio, F.; Prato, M. G.; Aebersold, R.; Penengo, L., 2015: RNF168 promotes noncanonical K27ubiquitination to signal DNA damage. *Cell Reports*., **10**, 226–238.

Geng, Y.; Yu, Q.; Sicinska, E.; Das, M.; Schneider, J. E.; Bhattacharya, S.; Rideout, W. M.; Bronson, R. T.; Gardner, H.; Sicinski, P., 2003: Cyclin E ablation in the mouse. *Cell*., **114**, 431–443.

Giubettini, M.; Asteriti, I. A.; Scrofani, J.; Luca, M. De; Lindon, C.; Lavia, P.; Guarguaglini, G., 2011: Control of Aurora-A stability through interaction with, **1**.

Glotzer, M.; Murray, A. W.; Kirschner, M. W., 1991: Cyclin is degraded by the ubiquitin pathway. *Nature*., **349**, 132–138.

Gmachl, M.; Gieffers, C.; Podtelejnikov, A. V.; Mann, M.; Peters, J. M., 2000: The RING-H2 finger protein APC11 and the E2 enzyme UBC4 are sufficient to ubiquitinate substrates of the anaphase-promoting complex. *Proceedings of the National Academy of Sciences of the United States of America*., **97**, 8973–8978.

Gnad, F.; Ren, S.; Cox, J.; Olsen, J. V.; Macek, B.; Oroshi, M.; Mann, M., 2007: PHOSIDA (phosphorylation site database): Management, structural and evolutionary investigation, and prediction of phosphosites. *Genome Biology*., **8**.

Gnad, F.; Gunawardena, J.; Mann, M., 2011: PHOSIDA 2011: The posttranslational modification database. *Nucleic Acids Research*., **39**, 253–260.

Golan, A.; Yudkovsky, Y.; Hershko, A., 2002: The cyclin-ubiquitin ligase activity of cyclosome/APC is jointly activated by protein kinases Cdk1-cyclin B and Plk. *Journal of Biological Chemistry*., **277**, 15552–15557.

Gouw, M.; Michael, S.; Sámano-Sánchez, H.; Kumar, M.; Zeke, A.; Lang, B.; Bely, B.; Chemes, L. B.; Davey, N. E.; Deng, Z.; Diella, F.; Gürth, C. M.; Huber, A. K.; Kleinsorg, S.; Schlegel, L. S.; Palopoli, N.; Roey, K. V.; Altenberg, B.; Reményi, A. et al., 2018: The eukaryotic linear motif resource - 2018 update. *Nucleic Acids Research*., **46**, D428–D434.

Grant, G. D.; Kedziora, K. M.; Limas, J. C.; Cook, J. G.; Purvis, J. E., 2018: Accurate delineation of cell cycle phase transitions in living cells with PIP-FUCCI. *Cell Cycle*., **17**, 2496–2516.

Grosskortenhaus, R.; Sprenger, F., 2002: Rca1 inhibits APC-Cdh1Fzr and is required to prevent cyclin degradation in G2. *Developmental Cell*., **2**, 29–40.

Guharoy, M.; Bhowmick, P.; Tompa, P., 2016: Design principles involving protein disorder facilitate specific substrate selection and degradation by the ubiquitin-proteasome system. *Journal of Biological Chemistry*., **291**, 6723–6731.

Gurevich, V. V.; Pokrovskaya, I. D.; Obukhova, T. A.; Zozulya, S. A., 1991: Preparative in vitro mRNA synthesis using SP6 and T7 RNA polymerases. *Analytical Biochemistry*., **195**, 207–213.

Haas, a L.; Warms, J. V; Rose, I. a, 1983: Ubiquitin adenylate: structure and role in ubiquitin activation. *Biochemistry*., **22**, 4388–4394.

Hadwiger, J. A.; Wittenberg, C.; Mendenhall, M. D.; Reed, S. I., 1989: The Saccharomyces cerevisiae CKS1 gene, a homolog of the Schizosaccharomyces pombe suc1+ gene, encodes a subunit of the Cdc28 protein kinase complex. *Molecular and Cellular Biology*., **9**, 2034–2041.

Haley, B.; Hendrix, D.; Trang, V.; Levine, M., 2008: A simplified miRNA-based gene silencing method for Drosophila melanogaster. *Developmental Biology*., **321**, 482–490.

Hall, M. C.; Jeong, D. E.; Henderson, J. T.; Choi, E.; Bremmer, S. C.; Iliuk, A. B.; Charbonneau, H., 2008: Cdc28 and Cdc14 control stability of the anaphase-promoting complex inhibitor Acm1. *Journal of Biological Chemistry*., **283**, 10396–10407.

Hamazaki, J.; Iemura, S. I.; Natsume, T.; Yashiroda, H.; Tanaka, K.; Murata, S., 2006: A novel proteasome interacting protein recruits the deubiquitinating enzyme UCH37 to 26S proteasomes. *EMBO Journal*., **25**, 4524–4536.

Hames, R. S.; Wattam, S. L.; Yamano, H.; Bacchieri, R.; Fry, A. M., 2001: APC/C-mediated destruction of the centrosomal kinase Nek2A occurs in early mitosis and depends upon a cyclin A-type D-box. *The*

EMBO journal., **20**, 7117–7127.

Hansen, D. V; Loktev, A. V; Ban, K. H.; Jackson, P. K., 2004: Plk1 Regulates Activation of the Anaphase Promoting Complex by Phosphorylating and Triggering SCF βTrCP -dependent Destruction of the APC Inhibitor Emi1. *Molecular Biology of the Cell*., **15**, 5623–5634.

Harley, M. E.; Allan, L. A.; Sanderson, H. S.; Clarke, P. R., 2010: Phosphorylation of Mcl-1 by CDK1 – cyclin B1 initiates its Cdc20-dependent destruction during mitotic arrest. *The EMBO Journal*., **29**, 2407–2420.

Havens, C. G.; Walter, J. C., 2009: Docking of a Specialized PIP Box onto Chromatin-Bound PCNA Creates a Degron for the Ubiquitin Ligase CRL4Cdt2. *Molecular Cell*., **35**, 93–104.

Havens, C. G.; Walter, J. C., 2011: Mechanism of CRL4Cdt2, a PCNA-dependent E3 ubiquitin ligase. *Genes & development*., **25**, 1568–1582.

Havens, C. G.; Shobnam, N.; Guarino, E.; Centore, R. C.; Zou, L.; Kearsey, S. E.; Walter, J. C., 2012: Direct role for proliferating cell nuclear antigen in substrate recognition by the E3 ubiquitin ligase CRL4Cdt2. *Journal of Biological Chemistry*., **287**, 11410–11421.

Hayashi, A.; Giakoumakis, N. N.; Heidebrecht, T.; Ishii, T.; Panagopoulos, A.; Caillat, C.; Takahara, M.; Hibbert, R. G.; Suenaga, N.; Stadnik-Spiewak, M.; Takahashi, T.; Shiomi, Y.; Taraviras, S.; von Castelmur, E.; Lygerou, Z.; Perrakis, A.; Nishitani, H., 2018: Direct binding of Cdt2 to PCNA is important for targeting the CRL4 Cdt2 E3 ligase activity to Cdt1. *Life Science Alliance*., **1**, e201800238.

Hayles, J.; Beach, D.; Durkacz, B.; Nurse, P., 1986: The fission yeast cell cycle control gene cdc2: isolation of a sequence suc1 that suppresses cdc2 mutant function. *MGG Molecular & General Genetics*., **202**, 291–293.

He, J.; Chao, W. C. H.; Zhang, Z.; Yang, J.; Cronin, N.; Barford, D., 2013: Insights into degron recognition by APC/C coactivators from the structure of an Acm1-Cdh1 complex. *Molecular Cell*., **50**, 649–660.

Hegde, A. N., 2010: The ubiquitin-proteasome pathway and synaptic plasticity. *Learning and Memory*., **17**, 314–327.

Hegemann, B.; Hutchins, J. R. A.; Hudecz, O.; Novatchkova, M.; Rameseder, J.; Sykora, M. M.; Liu, S.; Mazanek, M.; Lénárt, P.; Hériché, J. K.; Poser, I.; Kraut, N.; Hyman, A. A.; Yaffe, M. B.; Mechtler, K.; Peters, J. M., 2011: Systematic phosphorylation analysis of human mitotic protein complexes. *Science Signaling*., **4**, 1–16.

Heidrich, J., 2020: *Analysis of the PIP-degron independent Dap-degradation by Rca1*. University of Regensburg.

Heimbucher, J., 2017: *Untersuchungen von dSkp2 und eines möglichen Substrates des SCF*. University of Regensburg.

Hein, J. B.; Nilsson, J., 2016: Interphase APC/C-Cdc20 inhibition by cyclin A2-Cdk2 ensures efficient mitotic entry. *Nature Communications*., **7**, 1–10.

Hein, M. Y.; Hubner, N. C.; Poser, I.; Cox, J.; Nagaraj, N.; Toyoda, Y.; Gak, I. A.; Weisswange, I.; Mansfeld, J.; Buchholz, F.; Hyman, A. A.; Mann, M., 2015: A Human Interactome in Three Quantitative Dimensions Organized by Stoichiometries and Abundances. *Cell*., **163**, 712–723.

Hellmuth, S.; Böttger, F.; Pan, C.; Mann, M.; Stemmann, O., 2014: PP2A delays APC/C-dependent degradation of separase-associated but not free securin. *EMBO Journal*., **33**, 1134–1147.

Hendrickson, C.; Meyn, M. A.; Morabito, L.; Holloway, S. L., 2001: The KEN box regulates Clb2 proteolysis in G1 and at the metaphase-to-anaphase transition. *Current Biology*., **11**, 1781–1787.

Hendriks, I. A.; Souza, R. C. J. D.; Yang, B.; Vries, M. V. de; Vertegaal, A. C. O., 2015: Uncovering global

SUMOylation signaling networks in a site-specific manner. *Nature Structural and Molecular Biology*., **21**, 927–936.

Herzinger, S., 2019: *SCF-dependent regulation of Dap and CycE / Cdk2 Thesis submitted for the degree Master of Science submitted by*. *Universität Regensburg*. University of Regensburg.

Herzog, F.; Mechtler, K.; Peters, J. M., 2005: Identification of cell cycle-dependent phosphorylation sites on the anaphase-promoting complex/cyclosome by mass spectrometry. *Methods in Enzymology*., **398**, 231–245.

Hicke, L., 2001: Protein regulation by monoubiquitin. *Nature Reviews Molecular Cell Biology*., **2**, 195–201.

Hjerpe, R.; Thomas, Y.; Chen, J.; Zemla, A.; Curran, S.; Shpiro, N.; Dick, L. R.; Kurz, T., 2012: Changes in the ratio of free NEDD8 to ubiquitin triggers NEDDylation by ubiquitin enzymes. *Biochemical Journal*., **441**, 927–936.

Hochegger, H.; Takeda, S.; Hunt, T., 2008: Cyclin-dependent kinases and cell-cycle transitions: does one fit all? *Nature Reviews Molecular Cell Biology*., **9**, 910–916.

Höckner, S.; Neumann-Arnold, L.; Seufert, W., 2016: Dual control by Cdk1 phosphorylation of the budding yeast APC/C ubiquitin ligase activator Cdh1. *Molecular Biology of the Cell*., **27**, 2198–2212.

Hofmann, K.; Bucher, P., 1996: The UBA domain: A sequence motif present in multiple enzyme classes of the ubiquitination pathway. *Trends in Biochemical Sciences*., **21**, 172–173.

Holt, L. J.; Krutchinsky, A. N.; Morgan, D. O., 2008: Positive feedback sharpens the anaphase switch. *Nature*., **454**, 353–357.

Horn, T.; Boutros, M., 2010: E-RNAi: A web application for the multi-species design of RNAi reagents-2010 update. *Nucleic Acids Research*., **38**, 332–339.

Hsu, J. Y.; Reimann, J. D. R.; Sørensen, C. S.; Lukas, J.; Jackson, P. K., 2002: E2F-dependent accumulation of hEmi1 regulates S phase entry by inhibiting APCCdh1. *Nature Cell Biology*., **4**, 358–366.

Hu, Y.; Sopko, R.; Chung, V.; Foos, M.; Studer, R. A.; Landry, S. D.; Liu, D.; Rabinow, L.; Gnad, F.; Beltrao, P.; Perrimon, N., 2019: IProteinDB: An integrative database of drosophila post-translational modifications. *G3: Genes, Genomes, Genetics*., **9**, 1–11.

Huang, H.; Jeon, M. shin; Liao, L.; Yang, C.; Elly, C.; Yates, J. R.; Liu, Y. C., 2010: K33-Linked Polyubiquitination of T Cell Receptor-ζ Regulates Proteolysis-Independent T Cell Signaling. *Immunity*., **33**, 60–70.

Hubner, N. C.; Bird, A. W.; Cox, J.; Splettstoesser, B.; Bandilla, P.; Poser, I.; Hyman, A.; Mann, M., 2010: Quantitative proteomics combined with BAC TransgeneOmics reveals in vivo protein interactions. *Journal of Cell Biology*., **189**, 739–754.

Ji, Z.; Gao, H.; Jia, L.; Li, B.; Yu, H., 2017: A sequential multi-target Mps1 phosphorylation cascade promotes spindle checkpoint signaling. *eLife*., **6**, 1–23.

Jin, J.; Arias, E. E.; Chen, J.; Harper, J. W.; Walter, J. C., 2006: A Family of Diverse Cul4-Ddb1-Interacting Proteins Includes Cdt2, which Is Required for S Phase Destruction of the Replication Factor Cdt1. *Molecular Cell*., **23**, 709–721.

Jin, L.; Williamson, A.; Banerjee, S.; Philipp, I.; Rape, M., 2008: Mechanism of Ubiquitin-Chain Formation by the Human Anaphase-Promoting Complex. *Cell*., **133**, 653–665.

Johnson, A.; Skotheim, J. M., 2013: Start and the restriction point. *Current Opinion in Cell Biology*., **25**, 717–723.

Kalaszczynska, I.; Geng, Y.; Iino, T.; Mizuno, S. ichi; Choi, Y.; Kondratiuk, I.; Silver, D. P.; Wolgemuth, D.

J.; Akashi, K.; Sicinski, P., 2009: Cyclin A Is Redundant in Fibroblasts but Essential in Hematopoietic and Embryonic Stem Cells. *Cell*., **138**, 352–365.

Kelley, L. A.; Mezulis, S.; Yates, C. M.; Wass, M. N.; Sternberg, M. J. E., 2015: The Phyre2 web portal for protein modeling, prediction and analysis. *Nature Protocols*., **10**, 845–858.

Kies, M., 2017: *Dual regulation of APC / C activity by Rca1*. University of Regensburg.

Kim, D. H.; Han, J. S.; Ly, P.; Ye, Q.; McMahon, M. A.; Myung, K.; Corbett, K. D.; Cleveland, D. W., 2018: TRIP13 and APC15 drive mitotic exit by turnover of interphase- and unattached kinetochore-produced MCC. *Nature Communications*., **9**.

Kim, J. H.; Lee, S. R.; Li, L. H.; Park, H. J.; Park, J. H.; Lee, K. Y.; Kim, M. K.; Shin, B. A.; Choi, S. Y., 2011: High cleavage efficiency of a 2A peptide derived from porcine teschovirus-1 in human cell lines, zebrafish and mice. *PLoS ONE*., **6**, 1–8.

Kim, T.; Lara-gonzalez, P.; Prevo, B.; Meitinger, F.; Cheerambathur, D. K.; Oegema, K.; Desai, A., 2017: Kinetochores accelerate or delay APC / C activation by directing Cdc20 to opposing fates, 1089–1094.

Kim, Y.; Starostina, N. G.; Kipreos, E. T., 2008: The CRL4 Cdt2 ubiquitin ligase targets the degradation of p21 Cip1 to control replication licensing. *Genes & Development*., **22**, 2507–2519.

Kimata, Y.; Baxter, J. E.; Fry, A. M.; Yamano, H., 2008: A Role for the Fizzy/Cdc20 Family of Proteins in Activation of the APC/C Distinct from Substrate Recruitment. *Molecular Cell*., **32**, 576–583.

Kirkin, V.; McEwan, D. G.; Novak, I.; Dikic, I., 2009: A Role for Ubiquitin in Selective Autophagy. *Molecular Cell*., **34**, 259–269.

Kito, Y.; Matsumoto, M.; Hatano, A.; Takami, T.; Oshikawa, K.; Matsumoto, A.; Nakayama, K. I., 2020: Cell cycle–dependent localization of the proteasome to chromatin. *Scientific Reports*., **10**, 1–17.

Kliza, K.; Husnjak, K., 2020: Resolving the Complexity of Ubiquitin Networks. *Frontiers in Molecular Biosciences*., **7**.

Klotzbücher, A.; Stewart, E.; Harrison, D.; Hunt, T., 1996: The 'destruction box' of cyclin A allows B-type cyclins to be ubiquitinated, but not efficiently destroyed. *The EMBO journal*., **15**, 3053–3064.

Kõivomägi, M.; Valk, E.; Venta, R.; Iofik, A.; Lepiku, M.; Morgan, D. O.; Loog, M., 2011a: Dynamics of Cdk1 Substrate Specificity during the Cell Cycle. *Molecular Cell*., **42**, 610–623.

Kõivomägi, M.; Valk, E.; Venta, R.; Iofik, A.; Lepiku, M.; Balog, E. R. M.; Rubin, S. M.; Morgan, D. O.; Loog, M., 2011b: Cascades of multisite phosphorylation control Sic1 destruction at the onset of S phase. *Nature*., **480**, 128–131.

Kõivomägi, M.; Örd, M.; Iofik, A.; Valk, E.; Venta, R.; Faustova, I.; Kivi, R.; Balog, E. R. M.; Rubin, S. M.; Loog, M., 2013: Multisite phosphorylation networks as signal processors for Cdk1. *Nature Structural and Molecular Biology*., **20**, 1415–1424.

Komander, D., 2009: The emerging complexity of protein ubiquitination. *Biochemical Society Transactions*., **37**, 937–953.

Komander, D.; Rape, M., 2012: The ubiquitin code. *Annual Review of Biochemistry*., **81**, 203–229.

Kosugi, S.; Hasebe, M.; Entani, T.; Takayama, S.; Tomita, M.; Yanagawa, H., 2008: Design of Peptide Inhibitors for the Importin α/β Nuclear Import Pathway by Activity-Based Profiling. *Chemistry and Biology*., **15**, 940–949.

Kosugi, S.; Hasebe, M.; Tomita, M.; Yanagawa, H., 2009a: Systematic identification of cell cycle-dependent yeast nucleocytoplasmic shuttling proteins by prediction of composite motifs. *Proceedings of the National Academy of Sciences of the United States of America*., **106**, 10171–10176.

Kosugi, S.; Hasebe, M.; Matsumura, N.; Takashima, H.; Miyamoto-Sato, E.; Tomita, M.; Yanagawa, H., 2009b: Six classes of nuclear localization signals specific to different binding grooves of importinα. *Journal of Biological Chemistry*., **284**, 478–485.

Kozar, K.; Ciemerych, M. A.; Rebel, V. I.; Shigematsu, H.; Zagozdzon, A.; Sicinska, E.; Geng, Y.; Yu, Q.; Bhattacharya, S.; Bronson, R. T.; Akashi, K.; Sicinski, P., 2004: Mouse development and cell proliferation in the absence of D-cyclins. *Cell*., **118**, 477–491.

Kraft, C.; Herzog, F.; Gieffers, C.; Mechtler, K.; Hagting, A.; Pines, J.; Peters, J. M., 2003: Mitotic regulation of the human anaphase-promoting complex by phosphorylation. *EMBO Journal*., **22**, 6598–6609.

Kramer, E. R.; Scheuringer, N.; Podtelejnikov, A. V; Mann, M.; Peters, J. M., 2000: Mitotic regulation of the APC activator proteins CDC20 and CDH1. *Molecular biology of the cell*., **11**, 1555–1569.

Kumagai, A.; Yakowec, P. S.; Dunphy, W. G., 1998: 14-3-3 proteins act as negative regulators of the mitotic inducer Cdc25 in Xenopus egg extracts. *Molecular Biology of the Cell*., **9**, 345–354.

La Cour, T.; Kiemer, L.; Mølgaard, A.; Gupta, R.; Skriver, K.; Brunak, S., 2004: Analysis and prediction of leucine-rich nuclear export signals. *Protein Engineering, Design and Selection*., **17**, 527–536.

Laemmli, U. K., 1970: Cleavage of structural proteins during the assembly of the head of bacteriophage T4. *Nature*., **227**, 680–685.

Lahav-Baratz, S.; Sudakin, V.; Ruderman, J. V.; Hershko, A., 1995: Reversible phosphorylation controls the activity of cyclosome-associated cyclin-ubiquitin ligase. *Proceedings of the National Academy of Sciences of the United States of America*., **92**, 9303–9307.

Landis, M. W.; Brown, N. E.; Baker, G. L.; Shifrin, A.; Das, M.; Geng, Y.; Sicinski, P.; Hinds, P. W., 2007: The LxCxE pRb interaction domain of cyclin D1 is dispensable for murine development. *Cancer Research*., **67**, 7613–7620.

Lane, M. E.; Sauer, K.; Wallace, K.; Jan, Y. N.; Lehner, C. F.; Vaessin, H., 1996: Dacapo, a cyclin-dependent kinase inhibitor, stops cell proliferation during Drosophila development. *Cell*., **87**, 1225–1235.

Lara-Gonzalez, P.; Westhorpe, F. G.; Taylor, S. S., 2012: The spindle assembly checkpoint. *Current Biology*., **22**, R966–R980.

Lau, A. W.; Fukushima, H.; Wei, W., 2012: The Fbw7 and betaTRCP E3 ubiquitin ligases and their roles in tumorigenesis. *Frontiers in bioscience (Landmark edition)*., **17**, 2197–2212.

Lee, C. C.; Li, B.; Yu, H.; Matunis, M. J., 2018: Sumoylation promotes optimal apc/c activation and timely anaphase. *eLife*., **7**, 1–26.

Lee, H. O.; Zacharek, S. J.; Xiong, Y.; Duronio, R. J., 2010: Cell type-dependent requirement for PIP box-regulated Cdt1 destruction during S phase. *Molecular Biology of the Cell*., **21**, 3639–3653.

Lee, S. J.; Rodriguez-Bravo, V.; Kim, H.; Datta, S.; Foley, E. A., 2017: The PP2A B56 phosphatase promotes the association of Cdc20 with APC/C in mitosis. *Journal of Cell Science*., **130**, 1760–1771.

Lee, T. V.; Ding, T.; Chen, Z.; Rajendran, V.; Scherr, H.; Lackey, M.; Bolduc, C.; Bergmann, A., 2007: The E1 ubiquitin-activating enzyme Uba1 in Drosophila controls apoptosis autonomously and tissue growth non-autonomously. *Development*., **135**, 43–52.

Leismann, O.; Lehner, C. F., 2003: Drosophila securin destruction involves a D-box and a KEN-box and promotes anaphase in parallel with Cyclin A degradation, **1**.

Leng, F.; Saxena, L.; Hoang, N.; Zhang, C.; Lee, L.; Li, W.; Gong, X.; Lu, F.; Hong Sun, X.; Hui Zhang, X., 2018: Proliferating cell nuclear antigen interacts with the CRL4 ubiquitin ligase subunit CDT2 in DNA

synthesis–induced degradation of CDT1. *Journal of Biological Chemistry*., **293**, 18879–18889.

Leverson, J. D.; Joazeiro, C. A. P.; Page, A. M.; Huang, H. K.; Hieter, P.; Hunter, T., 2000: The APC11 RING-H2 finger mediates E2-dependent ubiquitination. *Molecular Biology of the Cell*., **11**, 2315–2325.

Li, A.; Blow, J., 2004: Non-proteolytic inactivation of geminin requires CDK-dependent ubiquitination. *Nature Cell Biology*., **6**, 260–267.

Li, Q.; Chang, L.; Aibara, S.; Yang, J.; Zhang, Z.; Barford, D., 2016: WD40 domain of Apc1 is critical for the coactivator-induced allosteric transition that stimulates APC/C catalytic activity. *Proceedings of the National Academy of Sciences of the United States of America*., **113**, 10547–10552.

Liess, A. K. L.; Kucerova, A.; Schweimer, K.; Yu, L.; Roumeliotis, T. I.; Diebold, M.; Dybkov, O.; Sotriffer, C.; Urlaub, H.; Choudhary, J. S.; Mansfeld, J.; Lorenz, S., 2019: Autoinhibition Mechanism of the Ubiquitin-Conjugating Enzyme UBE2S by Autoubiquitination. *Structure*., **27**, 1195-1210.e7.

Lin, H. C.; Wu, J. T.; Tan, B. C. M.; Chien, C. T., 2009: Cul4 and DDB1 regulate Orc2 localization, BrdU incorporation and Dup stability during gene amplification in Drosophila follicle cells. *Journal of Cell Science*., **122**, 2393–2401.

Listovsky, T.; Zor, A.; Laronne, A.; Brandeis, M., 2000: Cdk1 is essential for mammalian cyclosome/APC regulation. *Experimental Cell Research*., **255**, 184–191.

Liu, S.; Jiang, M.; Wang, W.; Liu, W.; Song, X.; Ma, Z.; Zhang, S.; Liu, L.; Liu, Y.; Cao, X., 2018: Nuclear RNF2 inhibits interferon function by promoting K33-linked STAT1 disassociation from DNA article. *Nature Immunology*., **19**, 41–50.

Liu, Z.; Yuan, F.; Ren, J.; Cao, J.; Zhou, Y.; Yang, Q.; Xue, Y., 2012: GPS-ARM: Computational analysis of the APC/C recognition motif by predicting D-boxes and KEN-boxes. *PLoS ONE*., **7**, 1–9.

Liu, Z.; Chen, O.; Wall, J. B. J.; Zheng, M.; Zhou, Y.; Wang, L.; Ruth Vaseghi, H.; Qian, L.; Liu, J., 2017: Systematic comparison of 2A peptides for cloning multi-genes in a polycistronic vector. *Scientific Reports*., **7**, 1–9.

Livneh, I.; Cohen-Kaplan, V.; Cohen-Rosenzweig, C.; Avni, N.; Ciechanover, A., 2016: The life cycle of the 26S proteasome: from birth, through regulation and function, and onto its death. *Cell Research*., **26**, 869–885.

Lo, C. A.; Kays, I.; Emran, F.; Lin, T. J.; Cvetkovska, V.; Chen, B. E., 2015: Quantification of Protein Levels in Single Living Cells. *Cell Rep*., **13**, 2634–2644.

Lovejoy, C. A.; Lock, K.; Yenamandra, A.; Cortez, D., 2006: DDB1 Maintains Genome Integrity through Regulation of Cdt1. *Molecular and Cellular Biology*., **26**, 7977–7990.

Lu, D.; Hsiao, J. Y.; Davey, N. E.; van Voorhis, V. A.; Foster, S. A.; Tang, C.; Morgan, D. O., 2014: Multiple mechanisms determine the order of APC/C substrate degradation in mitosis. *Journal of Cell Biology*., **207**, 23–39.

Lu, Y.; Wang, W.; Kirschner, M. W., 2015a: Specificity of the anaphase-promoting complex: A single-molecule study. *Science*., **348**, 1248737–1248737.

Lu, Y.; Wang, W.; Kirschner, M. W., 2015b: Specificity of the anaphase-promoting complex: A single-molecule study. *Science*., **348**, 1248737–1248737.

Machida, Y. J.; Dutta, A., 2007: The APC/C inhibitor, Emi1, is essential for prevention of rereplication. *Genes and Development*., **21**, 184–194.

Madeira, F.; Tinti, M.; Murugesan, G.; Berrett, E.; Stafford, M.; Toth, R.; Cole, C.; MacKintosh, C.; Barton, G. J., 2015: 14-3-3-Pred: Improved methods to predict 14-3-3-binding phosphopeptides. *Bioinformatics*., **31**, 2276–2283.

Mailand, N.; Diffley, J. F. X., 2005: CDKs promote DNA replication origin licensing in human cells by protecting Cdc6 from APC/C-dependent proteolysis. *Cell*., **122**, 915–926.

Malumbres, M., 2014: Cyclin-dependent kinases. *Genome Biology*., **15**, 1–10.

Mann, M.; Kahle, H. P.; Beck, M.; Bender, B. J.; Spiecker, H.; Backofen, R., 2018: MICA: Multiple interval-based curve alignment. *SoftwareX*., **7**, 53–58.

Margottin-Goguet, F.; Hsu, J. Y.; Loktev, A.; Hsieh, H. mei; Reimann, J. D. .; Jackson, P. K., 2003: Prophase Destruction of Emi1 by the SCFβTrCP/Slimb Ubiquitin Ligase Activates the Anaphase Promoting Complex to Allow Progression beyond Prometaphase. *Developmental Cell*., **4**, 813–826.

Marshall, R. S.; Vierstra, R. D., 2019: Dynamic regulation of the 26S proteasome: From synthesis to degradation. *Frontiers in Molecular Biosciences*., **6**.

Martín, R.; Stonyte, V.; Lopez-Aviles, S., 2020: Protein phosphatases in G1 regulation. *International Journal of Molecular Sciences*., **21**, 1–15.

Marzio, A.; Puccini, J.; Kwon, Y.; Maverakis, N. K.; Arbini, A.; Sung, P.; Bar-Sagi, D.; Pagano, M., 2019: The F-Box Domain-Dependent Activity of EMI1 Regulates PARPi Sensitivity in Triple-Negative Breast Cancers. *Molecular Cell*., **73**, 224-237.e6.

Máthé, E.; Kraft, C.; Giet, R.; Deák, P.; Peters, J. M.; Glover, D. M., 2004: The E2-C Vihar Is Required for the Correct Spatiotemporal Proteolysis of Cyclin B and Itself Undergoes Cyclical Degradation. *Current Biology*., **14**, 1723–1733.

Mattiroli, F.; Sixma, T. K., 2014: Lysine-targeting specificity in ubiquitin and ubiquitin-like modification pathways. *Nature Structural and Molecular Biology*., **21**, 308–316.

Maupin-Furlow, J., 2011: Proteasomes and protein conjugation across domains of life. *Nature Reviews Microbiology*., **10**, 100–111.

Mazian, M. A.; Suenaga, N.; Ishii, T.; Hayashi, A.; Shiomi, Y.; Nishitani, H., 2019: A DNA-binding domain in the C-terminal region of Cdt2 enhances the DNA synthesis-coupled CRL4Cdt2 ubiquitin ligase activity for Cdt1. *Journal of Biochemistry*., **165**, 505–516.

McDowell, G. S.; Philpott, A., 2016: *New Insights Into the Role of Ubiquitylation of Proteins*. *International Review of Cell and Molecular Biology*. Elsevier Inc., Vol. 325.

McGarry, T. J.; Kirschner, M. W., 1998: Geminin, an inhibitor of DNA replication, is degraded during mitosis. *Cell*., **93**, 1043–1053.

McGrath, D. A.; Balog, E. R. M.; Kõivomägi, M.; Lucena, R.; Mai, M. V; Hirschi, A.; Kellogg, D. R.; Loog, M.; Rubin, S. M., 2013: Cks confers specificity to phosphorylation-dependent CDK signaling pathways. *Nature Structural & Molecular Biology*., **20**, 1407–1414.

Meghini, F.; Martins, T.; Tait, X.; Fujimitsu, K.; Yamano, H.; Glover, D. M.; Kimata, Y., 2016: Targeting of Fzr/Cdh1 for timely activation of the APC/C at the centrosome during mitotic exit. *Nature Communications*., **7**.

Meyer, H. J.; Rape, M., 2014: Enhanced Protein Degradation by Branched Ubiquitin Chains. *Cell*., **157**, 910–921.

Michelle, C.; Vourc'H, P.; Mignon, L.; Andres, C. R., 2009: What was the set of ubiquitin and ubiquitin-like conjugating enzymes in the eukaryote common ancestor? *Journal of Molecular Evolution*., **68**, 616–628.

Miller, J. J.; Summers, M. K.; Hansen, D. V.; Nachury, M. V.; Lehman, N. L.; Loktev, A.; Jackson, P. K., 2006: Emi1 stably binds and inhibits the anaphase-promoting complex/cyclosome as a pseudosubstrate inhibitor. *Genes and Development*., **20**, 2410–2420.

Min, M.; Mayor, U.; Lindon, C., 2013: Ubiquitination site preferences in anaphase promoting complex/cyclosome (APC/C) substrates. *Open Biology*., **3**.

Minskaia, E.; Luke, G.; Martin, R., 2015: Co-expression Technologies in Eukaryotic cells. *A text book of Biotehnology*., 1–16.

Moore, J. D.; Kirk, J. A.; Hunt, T., 2003: Unmasking the S-phase-promoting potential of cyclin B1. *Science*., **300**, 987–990.

Morgan, D. O., 1997: Cyclin-dependent kinases: engines, clocks, and microprocessors. *Annual review of cell and developmental biology*., **13**, 261–291.

Morgan, D. O., 2007: *The Cell Cycle-Principles of Control*. New Science Press.

Morgenthaler, C., 2013: *Inhibitor und Substrat des Anaphase-Promoting-Komplexes*. University of Regensburg.

Morris, J. R.; Solomon, E., 2004: BRCA1: BARD1 induces the formation of conjugated ubiquitin structures, dependent on K6 of ubiquitin, in cells during DNA replication and repair. *Human Molecular Genetics*., **13**, 807–817.

Moshe, Y.; Boulaire, J.; Pagano, M.; Hershko, A., 2004: Role of Polo-like kinase in the degradation of early mitotic inhibitor 1, a regulator of the anaphase promoting complex/cyclosome. *Proceedings of the National Academy of Sciences*., **101**, 7937–7942.

Moshe, Y.; Bar-On, O.; Ganoth, D.; Hershko, A., 2011: Regulation of the action of early mitotic inhibitor 1 on the anaphase-promoting complex/cyclosome by cyclin-dependent kinases. *Journal of Biological Chemistry*., **286**, 16647–16657.

Mottier, V.; Siaussat, D.; Bozzolan, F.; Auzoux-Bordenave, S.; Porcheron, P.; Debernard, S., 2004: The 20-hydroxyecdysone-induced cellular arrest in G2 phase is preceded by an inhibition of cyclin expression. *Insect Biochemistry and Molecular Biology*., **34**, 51–60.

Mullis, K; Faloona, F.; Scharf, S.; Saiki, R.; Horn, G.; Erlich, H., 1986: Specific enzymatic amplification of DNA in vitro: The Polymerase Chain Reaction. *Cold Spring Harbor Symposia on Quantitative Biology*., **LI**, 263–273.

Murata, S.; Yashiroda, H.; Tanaka, K., 2009: Molecular mechanisms of proteasome assembly. *Nature Reviews Molecular Cell Biology*., **10**, 104–115.

Musacchio, A., 2015: The Molecular Biology of Spindle Assembly Checkpoint Signaling Dynamics. *Current Biology*., **25**, R1002–R1018.

Narbonne-Reveau, K.; Senger, S.; Pal, M.; Herr, A.; Richardson, H. E.; Asano, M.; Deak, P.; Lilly, M. A., 2008: APC/CFzr/Cdh1 promotes cell cycle progression during the Drosophila endocycle. *Development*., **135**, 1451–1461.

Nardozzi, J. D.; Lott, K.; Cingolani, G., 2010: Phosphorylation meets nuclear import: A review. *Cell Communication and Signaling*.

Nguyen, H. T.; Frasch, M., 2006: MicroRNAs in muscle differentiation: lessons from Drosophila and beyond. *Current Opinion in Genetics and Development*., **16**, 533–539.

Nguyen, T. B.; Manova, K.; Capodieci, P.; Lindon, C.; Bottega, S.; Wang, X. Y.; Refik-Rogers, J.; Pines, J.; Wolgemuth, D. J.; Koff, A., 2002: Characterization and expression of mammalian cyclin B3, a prepachytene meiotic cyclin. *Journal of Biological Chemistry*., **277**, 41960–41969.

Ni, J. quan; Perrimon, N., 2006: Cloning hairpins into VALIUM20 and VALIUM22.

Oh, E.; Mark, K. G.; Mocciaro, A.; Watson, E. R.; Prabu, J. R.; Cha, D. D.; Kampmann, M.; Gamarra, N.; Zhou, C. Y.; Rape, M., 2020: Gene expression and cell identity controlled by anaphase-promoting

complex. *Nature*., **579**, 136–140.

Ohta, S.; Bukowski-Wills, J. C.; Sanchez-Pulido, L.; Alves, F. de L.; Wood, L.; Chen, Z. A.; Platani, M.; Fischer, L.; Hudson, D. F.; Ponting, C. P.; Fukagawa, T.; Earnshaw, W. C.; Rappsilber, J., 2010: The Protein Composition of Mitotic Chromosomes Determined Using Multiclassifier Combinatorial Proteomics. *Cell*., **142**, 810–821.

Ohtake, F.; Saeki, Y.; Sakamoto, K.; Ohtake, K.; Nishikawa, H.; Tsuchiya, H.; Ohta, T.; Tanaka, K.; Kanno, J., 2015: Ubiquitin acetylation inhibits polyubiquitin chain elongation. *EMBO reports*., **16**, 192–201.

Ohtake, F.; Saeki, Y.; Ishido, S.; Kanno, J.; Tanaka, K., 2016: The K48-K63 Branched Ubiquitin Chain Regulates NF-κB Signaling. *Molecular Cell*., **64**, 251–266.

Olsen, S. K.; Lima, C. D., 2013: Structure of a Ubiquitin E1-E2 Complex: Insights to E1-E2 Thioester Transfer. *Molecular Cell*., **49**, 884–896.

Örd, M.; Venta, R.; Möll, K.; Valk, E.; Loog, M., 2019a: Cyclin-Specific Docking Mechanisms Reveal the Complexity of M-CDK Function in the Cell Cycle. *Molecular Cell*., **75**, 76-89.e3.

Örd, M.; Loog, M., 2019b: How the cell cycle clock ticks. *Molecular Biology of the Cell*., **30**, 169–172.

Örd, M.; Möll, K.; Agerova, A.; Kivi, R.; Faustova, I.; Venta, R.; Valk, E.; Loog, M., 2019c: Multisite phosphorylation code of CDK. *Nature Structural and Molecular Biology*., **26**, 649–658.

Örd, M.; Puss, K. K.; Kivi, R.; Möll, K.; Ojala, T.; Borovko, I.; Faustova, I.; Venta, R.; Valk, E.; Kõivomägi, M.; Loog, M., 2020: Proline-Rich Motifs Control G2-CDK Target Phosphorylation and Priming an Anchoring Protein for Polo Kinase Localization. *Cell Reports*., **31**, 107757.

Ordureau, A.; Sarraf, S. A.; Duda, D. M.; Heo, J. mi; Jedrykowski, M. P.; Sviderskiy, V.; Olszewski, J. L.; Koerber, J. T.; Xie, T.; Sean, A.; Wells, J. A.; Gygi, S. P.; Schulman, B. A.; Harper, J. W.; Francisco, S.; Core, I. A.; Technologies, S., 2015: HHS Public Access, **56**, 360–375.

Ostapenko, D.; Burton, J. L.; Wang, R.; Solomon, M. J., 2008: Pseudosubstrate Inhibition of the Anaphase-Promoting Complex by Acm1: Regulation by Proteolysis and Cdc28 Phosphorylation. *Molecular and Cellular Biology*., **28**, 4653–4664.

Pack, C. G.; Yukii, H.; Toh-E, A.; Kudo, T.; Tsuchiya, H.; Kaiho, A.; Sakata, E.; Murata, S.; Yokosawa, H.; Sako, Y.; Baumeister, W.; Tanaka, K.; Saeki, Y., 2014: Quantitative live-cell imaging reveals spatio-temporal dynamics and cytoplasmic assembly of the 26S proteasome. *Nature Communications*., **5**.

Panagopoulos, A.; Taraviras, S.; Nishitani, H.; Lygerou, Z., 2020: CRL4 Cdt2 : Coupling Genome Stability to Ubiquitination, 1–13.

Passmore, L. A.; Mccormack, E. A.; Au, S. W. N.; Paul, A.; Willison, K. R.; Harper, J. W.; Barford, D., 2003: Doc1 mediates the activity of the anaphase- promoting complex by contributing to substrate recognition, **22**.

Pavletich, N. P., 1999: Mechanisms of Cyclin-dependent Kinase Regulation : Structures of Cdks , their Cyclin Activators , and Cip and INK4 Inhibitors, 821–828.

Pelzer, C.; Kassner, I.; Matentzoglu, K.; Singh, R. K.; Wollscheid, H. P.; Scheffner, M.; Schmidtke, G.; Groettrup, M., 2007: UBE1L2, a novel E1 enzyme specific for ubiquitin. *Journal of Biological Chemistry*., **282**, 23010–23014.

Pesenti, M. E.; Weir, J. R.; Musacchio, A., 2016: Progress in the structural and functional characterization of kinetochores. *Current Opinion in Structural Biology*., **37**, 152–163.

Pfleger, C. M.; Kirschner, M. W., 2000: The KEN box: An APC recognition signal distinct from the D box targeted by Cdh1. *Genes and Development*., **14**, 655–665.

Pickart, C. M., 2001: Mechanisms Underlying Ubiquitination. *Annual Review of Biochemistry*., **70**, 503–

533.

Pollard, T. D.; Earnshaw, W.; Lippingott-Schwartz, J.; Johnson, G. T., 2017: Cell Biology. *Cell Biology*. Elsevier, pp. 713–726.

Polz, J., 2017: *Establishment of the T2A-system for protein stability analysis of cell cycle proteins by flow cytometry*. University Regensburg.

Potzler, T., 2018: *Analysis of an amino acid exchange mutation at position 285 of Rca1*. University of Regensburg.

Qiao, R.; Weissmann, F.; Yamaguchi, M.; Brown, N. G.; VanderLinden, R.; Imre, R.; Jarvis, M. A.; Brunner, M. R.; Davidson, I. F.; Litos, G.; Haselbach, D.; Mechtler, K.; Stark, H.; Schulman, B. A.; Peters, J. M., 2016: Mechanism of APC/C ^{CDC20} activation by mitotic phosphorylation. *Proceedings of the National Academy of Sciences*., **113**, E2570–E2578.

Qin, L.; Mizrak, A.; Guimarães, D. S. P. S. F.; Tambrin, H. M.; Morgan, D. O.; Hall, M. C., 2019: The pseudosubstrate inhibitor Acm1 inhibits the anaphase-promoting complex/cyclosome by combining high-affinity activator binding with disruption of Doc1/Apc10 function. *Journal of Biological Chemistry*., **53**, jbc.RA119.009468.

Ramachandran, V.; Matzkies, M.; Dienemann, A.; Sprenger, F., 2007: Cyclin A degradation employs preferentially used lysines and a cyclin box function other than Cdk1 binding. *Cell Cycle*., **6**, 171–181.

Rana, A. S. J. B.; Ge, Y.; Strieter, E. R., 2017: Ubiquitin Chain Enrichment Middle-Down Mass Spectrometry (UbiChEM-MS) Reveals Cell-Cycle Dependent Formation of Lys11/Lys48 Branched Ubiquitin Chains. *Journal of Proteome Research*., **16**, 3363–3369.

Rape, M.; Reddy, S. K.; Kirschner, M. W., 2006: The processivity of multiubiquitination by the APC determines the order of substrate degradation. *Cell*., **124**, 89–103.

Reimann, J. D. R.; Freed, E.; Hsu, J. Y.; Kramer, E. R.; Peters, J. M.; Jackson, P. K., 2001a: Emi1 is a mitotic regulator that interacts with Cdc20 and inhibits the anaphase promoting complex. *Cell*., **105**, 645–655.

Reimann, J. D. R.; Gardner, B. E.; Margottin-Goguet, F.; Jackson, P. K., 2001b: Emi1 regulates the anaphase-promoting complex by a different mechanism than Mad2 proteins. *Genes and Development*., **15**, 3278–3285.

Reis, A.; Levasseur, M.; Chang, H. Y.; Elliott, D. J.; Jones, K. T., 2006: The CRY box: A second APCcdh1-dependent degron in mammalian cdc20. *EMBO Reports*., **7**, 1040–1045.

Rodrigo-Brenni, M. C.; Morgan, D. O., 2007: Sequential E2s Drive Polyubiquitin Chain Assembly on APC Targets. *Cell*., **130**, 127–139.

Rogers, G. C.; Rusan, N. M.; Roberts, D. M.; Peifer, M.; Rogers, S. L., 2009: The SCF Slimb ubiquitin ligase regulates Plk4/Sak levels to block centriole reduplication. *Journal of Cell Biology*., **184**, 225–229.

Roskoski, R., 2019: Cyclin-dependent protein serine/threonine kinase inhibitors as anticancer drugs. *Pharmacological Research*., **139**, 471–488.

Rössler, T., 2019: *Identification of substrates of the Drosophila F-Box protein Skp2 by flow cytometric and biochemical assays*. University of Regensburg.

Rotin, D.; Kumar, S., 2009: Physiological functions of the HECT family of ubiquitin ligases. *Nature Reviews Molecular Cell Biology*., **10**, 398–409.

Rudner, A. D.; Murray, A. W., 2000: Phosphorylation by Cdc28 activates the Cdc20-dependent activity of the anaphase-promoting complex. *Journal of Cell Biology*., **149**, 1377–1390.

Saeki, Y.; Kudo, T.; Sone, T.; Kikuchi, Y.; Yokosawa, H.; Toh-e, A.; Tanaka, K., 2009: Lysine 63-linked polyubiquitin chain may serve as a targeting signal for the 26S proteasome. *EMBO Journal*., **28**, 359–

371.

Sakaue-Sawano, A.; Kurokawa, H.; Morimura, T.; Hanyu, A.; Hama, H.; Osawa, H.; Kashiwagi, S.; Fukami, K.; Miyata, T.; Miyoshi, H.; Imamura, T.; Ogawa, M.; Masai, H.; Miyawaki, A., 2008: Visualizing Spatiotemporal Dynamics of Multicellular Cell-Cycle Progression. *Cell*., **132**, 487–498.

Sako, K.; Suzuki, K.; Isoda, M.; Yoshikai, S.; Senoo, C.; Nakajo, N.; Ohe, M.; Sagata, N., 2014: Emi2 mediates meiotic MII arrest by competitively inhibiting the binding of Ube2S to the APC/C. *Nature Communications*., **5**.

Salic, A.; Mitchison, T. J., 2008: A chemical method for fast and sensitive detection of DNA synthesis in vivo. *Proceedings of the National Academy of Sciences of the United States of America*., **105**, 2415–2420.

Santamaría, D.; Barrière, C.; Cerqueira, A.; Hunt, S.; Tardy, C.; Newton, K.; Cáceres, J. F.; Dubus, P.; Malumbres, M.; Barbacid, M., 2007: Cdk1 is sufficient to drive the mammalian cell cycle. *Nature*., **448**, 811–815.

Sedgwick, G. G.; Hayward, D. G.; Di Fiore, B.; Pardo, M.; Yu, L.; Pines, J.; Nilsson, J., 2013: Mechanisms controlling the temporal degradation of Nek2A and Kif18A by the APC/C-Cdc20 complex. *EMBO Journal*., **32**, 303–314.

Shaner, N. C.; Campbell, R. E.; Steinbach, P. A.; Giepmans, B. N. G.; Palmer, A. E.; Tsien, R. Y., 2004: Improved monomeric red, orange and yellow fluorescent proteins derived from Discosoma sp. red fluorescent protein. *Nature Biotechnology*., **22**, 1567–1572.

Shibutani, S. T.; de la Cruz, A. F. A.; Tran, V.; Turbyfill, W. J.; Reis, T.; Edgar, B. A.; Duronio, R. J., 2008: Intrinsic Negative Cell Cycle Regulation Provided by PIP Box- and Cul4Cdt2-Mediated Destruction of E2f1 during S Phase. *Developmental Cell*., **15**, 890–900.

Shindo, N.; Kumada, K.; Hirota, T., 2012: Separase Sensor Reveals Dual Roles for Separase Coordinating Cohesin Cleavage and Cdk1 Inhibition. *Developmental Cell*., **23**, 112–123.

Shteinberg, M.; Protopopov, Y.; Listovsky, T.; Brandeis, M.; Hershko, A., 1999: Phosphorylation of the Cyclosome Is Required for Its Stimulation by Fizzy/cdc20. *Biochemical and Biophysical Research Communications*., **260**, 193–198.

Sigrist, S.; Jacobs, H.; Stratmann, R.; Lehner, C. F., 1995: Exit from mitosis is regulated by drosophila fizzy and the sequential destruction of cyclins A, B and B3. *EMBO Journal*., **14**, 4827–4838.

Sigrist, S. J.; Lehner, C. F., 1997: Drosophila fizzy-related down-regulates mitotic cyclins and is required for cell proliferation arrest and entry into endocycles. *Cell*., **90**, 671–681.

Sivakumar, S.; Daum, J. R.; Tipton, A. R.; Rankin, S.; Gorbsky, G. J., 2014: The spindle and kinetochore-associated (Ska) complex enhances binding of the anaphase-promoting complex/cyclosome (APC/C) to chromosomes and promotes mitotic exit. *Molecular Biology of the Cell*., **25**, 594–605.

Sivakumar, S.; Gorbsky, G. J., 2015: Spatiotemporal regulation of the anaphase-promoting complex in mitosis. *Nature Reviews Molecular Cell Biology*., **16**, 82–94.

Snijder, B.; Pelkmans, L., 2011: Origins of regulated cell-to-cell variability. *Nature Reviews Molecular Cell Biology*., **12**, 119–125.

Song, L.; Rape, M., 2010: Regulated Degradation of Spindle Assembly Factors by the Anaphase-Promoting Complex. *Molecular Cell*., **38**, 369–382.

Spence, J. J.; Sadis, S. S.; Haas, A. L. A. L.; Finley, D. D., 1995: A ubiquitin mutant with specific defects in DNA repair and multiubiquitination. *Molecular and cellular biology*., **15**, 1265–1273.

Spit, M.; Rieser, E.; Walczak, H., 2019: Linear ubiquitination at a glance. *Journal of Cell Science*., **132**.

Stadler, C. B.; Arefin, B.; Ekman, H.; Thor, S., 2019: PIP degron-stabilized Dacapo/p21Cip1 and mutations in ago act in an anti- versus pro-proliferative manner, yet both trigger an increase in Cyclin E levels. *Development (Cambridge)*., **146**.

Steen, J. A. J.; Steen, H.; Georgi, A.; Parker, K.; Springer, M.; Kirchner, M.; Hamprecht, F.; Kirschner, M. W., 2008: Different phosphorylation states of the anaphase promoting complex in response to antimitotic drugs: A quantitative proteomic analysis. *Proceedings of the National Academy of Sciences of the United States of America*., **105**, 6069–6074.

Stegmeier, F.; Rape, M.; Draviam, V. M.; Nalepa, G.; Sowa, M. E.; Ang, X. L.; McDonald, E. R.; Li, M. Z.; Hannon, G. J.; Sorger, P. K.; Kirschner, M. W.; Harper, J. W.; Elledge, S. J., 2007: Anaphase initiation is regulated by antagonistic ubiquitination and deubiquitination activities. *Nature*., **446**, 876–881.

Stern, B.; Nurse, P., 1996: A quantitative model for the cdc2 control of S phase and mitosis in fission yeast. *Trends in genetics : TIG*., **12**, 345–350.

Sudakin, V.; Chan, G. K. T.; Yen, T. J., 2001: Checkpoint inhibition of the APC/C in HeLa cells is mediated by a complex of BUBR1, BUB3, CDC20, and MAD2. *Journal of Cell Biology*., **154**, 925–936.

Sullivan, M.; Morgan, D. O., 2007: A novel destruction sequence targets the meiotic regulator Spo13 for anaphase-promoting complex-dependent degradation in anaphase I. *Journal of Biological Chemistry*., **282**, 19710–19715.

Suryadinata, R.; Sadowski, M.; Sarcevic, B., 2010: Control of cell cycle progression by phosphorylation of cyclin-dependent kinase (CDK) substrates. *Bioscience reports*., **30**, 243–255.

Suzuki, K.; Sako, K.; Akiyama, K.; Isoda, M.; Senoo, C.; Nakajo, N.; Sagata, N., 2015: Identification of non-Ser/Thr-Pro consensus motifs for Cdk1 and their roles in mitotic regulation of C2H2 zinc finger proteins and Ect2. *Scientific Reports*., **5**, 1–9.

Swaffer, M. P.; Jones, A. W.; Flynn, H. R.; Snijders, A. P.; Nurse, P., 2016: CDK Substrate Phosphorylation and Ordering the Cell Cycle. *Cell*., **167**, 1750-1761.e16.

Swan, A.; Barcelo, G.; Schüpbach, T., 2005: Drosophila Cks30A interacts with Cdk1 to target Cyclin A for destruction in the female germline. *Development*., **132**, 3669–3678.

Swanson, C. I.; Meserve, J. H.; McCarter, P. C.; Thieme, A.; Mathew, T.; Elston, T. C.; Duronio, R. J., 2015: Expression of an S phase-stabilized version of the CDK inhibitor Dacapo can alter endoreplication. *Development*.

Swatek, K. N.; Komander, D., 2016: Ubiquitin modifications. *Cell Research*., **26**, 399–422.

Tada, S.; Li, A.; Maiorano, D.; Méchali, M.; Blow, J. J., 2001: Repression of origin assembly in metaphase depends on inhibition of RLF-B/Cdt1 by geminin. *Nature Cell Biology*., **3**, 107–113.

Tang, Z.; Li, B.; Bharadwaj, R.; Zhu, H.; Özkan, E.; Hakala, K.; Deisenhofer, J.; Yu, H., 2001: APC2 cullin protein and APC11 RING protein comprise the minimal ubiquitin ligase module of the anaphase-promoting complex. *Molecular Biology of the Cell*., **12**, 3839–3851.

Teixeira, L. K.; Reed, S. I., 2013: Ubiquitin ligases and cell cycle control. *Annual Review of Biochemistry*., **82**, 387–414.

Thomer, M.; May, N. R.; Aggarwal, B. D.; Kwok, G.; Calvi, B. R., 2004: Drosophila double-parked is sufficient to induce re-replication during development and is regulated by cyclin E/CDK2. *Development*., **131**, 4807–4818.

Tian, W.; Li, B.; Warrington, R.; Tomchick, D. R.; Yu, H.; Luo, X., 2012: Structural analysis of human Cdc20 supports multisite degron recognition by APC/C. *Proceedings of the National Academy of Sciences*., **109**, 18419–18424.

Timney, B. L.; Raveh, B.; Mironska, R.; Trivedi, J. M.; Kim, S. J.; Russel, D.; Wente, S. R.; Sali, A.; Rout, M. P., 2016: Simple rules for passive diffusion through the nuclear pore complex. *Journal of Cell Biology*., **215**, 57–76.

Topacio, B. R.; Zatulovskiy, E.; Cristea, S.; Xie, S.; Tambo, C. S.; Rubin, S. M.; Sage, J.; Kõivomägi, M.; Skotheim, J. M., 2019: Cyclin D-Cdk4,6 Drives Cell-Cycle Progression via the Retinoblastoma Protein's C-Terminal Helix. *Molecular Cell*., **74**, 758-770.e4.

Treier, M.; Seufert, W.; Jentsch, S., 1992: Drosophila UbcD1 encodes a highly conserved ubiquitin-conjugating enzyme involved in selective protein degradation. *EMBO Journal*., **11**, 367–372.

Tsanov, N.; Kermi, C.; Coulombe, P.; Van Der Laan, S.; Hodroj, D.; Maiorano, D., 2014: PIP degron proteins, substrates of CRL4Cdt2, and not PIP boxes, interfere with DNA polymerase g and i focus formation on UV damage. *Nucleic Acids Research*., **42**, 3692–3706.

Tsunematsu, T.; Takihara, Y.; Ishimaru, N.; Pagano, M.; Takata, T.; Kudo, Y., 2013: Aurora-A controls pre-replicative complex assembly and DNA replication by stabilizing geminin in mitosis. *Nature Communications*., **4**.

Uhlmann, F.; Bouchoux, C.; López-Avilés, S., 2011: A quantitative model for cyclin-dependent kinase control of the cell cycle: Revisited. *Philosophical Transactions of the Royal Society B: Biological Sciences*., **366**, 3572–3583.

Van Roey, K.; Uyar, B.; Weatheritt, R. J.; Dinkel, H.; Seiler, M.; Budd, A.; Gibson, T. J.; Davey, N. E., 2014: Short linear motifs: Ubiquitous and functionally diverse protein interaction modules directing cell regulation. *Chemical Reviews*., **114**, 6733–6778.

Varetti, G.; Guida, C.; Santaguida, S.; Chiroli, E.; Musacchio, A., 2011: Homeostatic control of mitotic arrest. *Molecular Cell*., **44**, 710–720.

Verma, R.; Aravind, L.; Oania, R.; McDonald, W. H.; Yates, J. R.; Koonin, E. V.; Deshaies, R. J., 2002: Role of Rpn11 metalloprotease in deubiquitination and degradation by the 26S proteasome. *Science*., **298**, 611–615.

von Klitzing, C.; Huss, R.; Illert, A. L.; Fröschl, A.; Wötzel, S.; Peschel, C.; Bassermann, F.; Duyster, J., 2011: APC/C Cdh1-mediated degradation of the F-box protein NIPA is regulated by its association with Skp1. *PLoS ONE*., **6**, 1–8.

Walden, H.; Rittinger, K., 2018: RBR ligase-mediated ubiquitin transfer: A tale with many twists and turns. *Nature Structural and Molecular Biology*., **25**, 440–445.

Walker, J. M., 2016: *Cell Cycle Oscillators*. (Coutts, A. S. & L. Weston, Eds.)Methods in Molecular Biology. Springer New York, New York, NY, Vol. 1342.

Walters, K. J.; Kleijnen, M. F.; Goh, A. M.; Wagner, G.; Howley, P. M., 2002: Structural studies of the interaction between ubiquitin family proteins and proteasome subunit S5a. *Biochemistry*., **41**, 1767–1777.

Wang, C.; Xu, H.; Lin, S.; Deng, W.; Zhou, J.; Zhang, Y.; Shi, Y.; Peng, D.; Xue, Y., 2020: GPS 5.0: An Update on the Prediction of Kinase-specific Phosphorylation Sites in Proteins. *Genomics, Proteomics and Bioinformatics*., **18**, 72–80.

Wang, J.; Dye, B. T.; Rajashankar, K. R.; Kurinov, I.; Schulman, B. A., 2009: Insights into anaphase promoting complex TPR subdomain assembly from a CDC26-APC6 structure. *Nature structural & molecular biology*., **16**, 987–989.

Wang, Q.; Liu, X.; Cui, Y.; Tang, Y.; Chen, W.; Li, S.; Yu, H.; Pan, Y.; Wang, C., 2014: The E3 Ubiquitin ligase AMFR and INSIG1 bridge the activation of TBK1 kinase by modifying the adaptor STING. *Immunity*., **41**, 919–933.

Wang, W.; Kirschner, M. W., 2013: Emi1 preferentially inhibits ubiquitin chain elongation by the anaphase-promoting complex. *Nature Cell Biology*., **15**, 797–806.

Watson, E. R.; Grace, C. R. R.; Zhang, W.; Miller, D. J.; Davidson, I. F.; Rajan Prabu, J.; Yu, S.; Bolhuis, D. L.; Kulko, E. T.; Vollrath, R.; Haselbach, D.; Stark, H.; Peters, J. M.; Brown, N. G.; Sidhu, S. S.; Schulman, B. A., 2019a: Protein engineering of a ubiquitin-variant inhibitor of APC/C identifies a cryptic K48 ubiquitin chain binding site. *Proceedings of the National Academy of Sciences of the United States of America*., **116**, 17280–17289.

Watson, E. R.; Brown, N. G.; Peters, J. M.; Stark, H.; Schulman, B. A., 2019b: Posing the APC/C E3 Ubiquitin Ligase to Orchestrate Cell Division. *Trends in Cell Biology*., **29**, 117–134.

Weinert, B. T.; Schölz, C.; Wagner, S. A.; Iesmantavicius, V.; Su, D.; Daniel, J. A.; Choudhary, C., 2013: Lysine succinylation is a frequently occurring modification in prokaryotes and eukaryotes and extensively overlaps with acetylation. *Cell Reports*., **4**, 842–851.

Wen, W.; Meinkotht, J. L.; Tsien, R. Y.; Taylor, S. S., 1995: Identification of a signal for rapid export of proteins from the nucleus. *Cell*., **82**, 463–473.

Wenzel, D. M.; Lissounov, A.; Brzovic, P. S.; Klevit, R. E., 2011: UBCH7 reactivity profile reveals parkin and HHARI to be RING/HECT hybrids. *Nature*., **474**, 105–108.

Whittaker, S. R.; Mallinger, A.; Workman, P.; Clarke, P. A., 2017: Inhibitors of cyclin-dependent kinases as cancer therapeutics. *Pharmacology and Therapeutics*., **173**, 83–105.

Wild, T.; Budzowska, M.; Hellmuth, S.; Eibes, S.; Karemore, G.; Barisic, M.; Stemmann, O.; Choudhary, C., 2018: Deletion of APC7 or APC16 Allows Proliferation of Human Cells without the Spindle Assembly Checkpoint. *Cell Reports*., **25**, 2317-2328.e5.

Wilkinson, C. R. M.; Seeger, M.; Hartmann-Petersen, R.; Stone, M.; Wallace, M.; Semple, C.; Gordon, C., 2001: Proteins containing the UBA domain are able to bind to multi-ubiquitin chains. *Nature Cell Biology*., **3**, 939–943.

Wilkinson, K. D.; Tashayev, V. L.; O'Connor, L. B.; Larsen, C. N.; Kasperek, E.; Pickart, C. M., 1995: Metabolism of the Polyubiquitin Degradation Signal: Structure, Mechanism, and Role of Isopeptidase T. *Biochemistry*., **34**, 14535–14546.

Williamson, A.; Banerjee, S.; Zhu, X.; Philipp, I.; Iavarone, A. T.; Rape, M., 2011: Regulation of Ubiquitin Chain Initiation to Control the Timing of Substrate Degradation. *Molecular Cell*., **42**, 744–757.

Wohlschlegel, J. A.; Dwyer, B. T.; Dhar, S. K.; Cvetic, C.; Walter, J. C.; Dutta, A., 2000: Inhibition of eukaryotic DNA replication by geminin binding to Cdt1. *Science*., **290**, 2309–2312.

Xu, P.; Duong, D. M.; Seyfried, N. T.; Cheng, D.; Xie, Y.; Robert, J.; Rush, J.; Hochstrasser, M.; Finley, D.; Peng, J., 2009: Quantitative Proteomics Reveals the Function of Unconventional Ubiquitin Chains in Proteasomal Degradation. *Cell*., **137**, 133–145.

Yamaguchi, M.; VanderLinden, R.; Weissmann, F.; Qiao, R.; Dube, P.; Brown, N. G.; Haselbach, D.; Zhang, W.; Sidhu, S. S.; Peters, J. M.; Stark, H.; Schulman, B. A., 2016: Cryo-EM of Mitotic Checkpoint Complex-Bound APC/C Reveals Reciprocal and Conformational Regulation of Ubiquitin Ligation. *Molecular Cell*., **63**, 593–607.

Yamano, H., 2013: EMI1, a three-in-one ubiquitylation inhibitor. *Nature Structural and Molecular Biology*., **20**, 773–774.

Yamano, H., 2019: APC/C: current understanding and future perspectives. *F1000Research*., **8**, 1–15.

Yang, C. song; Jividen, K.; Spencer, A.; Dworak, N.; Ni, L.; Oostdyk, L. T.; Chatterjee, M.; Kuśmider, B.; Reon, B.; Parlak, M.; Gorbunova, V.; Abbas, T.; Jeffery, E.; Sherman, N. E.; Paschal, B. M., 2017: Ubiquitin Modification by the E3 Ligase/ADP-Ribosyltransferase Dtx3L/Parp9. *Molecular Cell*., **66**, 503-

516.e5.

Yau, R. G.; Doerner, K.; Castellanos, E. R.; Haakonsen, D. L.; Werner, A.; Wang, N.; Yang, X. W.; Martinez-Martin, N.; Matsumoto, M. L.; Dixit, V. M.; Rape, M., 2017: Assembly and Function of Heterotypic Ubiquitin Chains in Cell-Cycle and Protein Quality Control. *Cell*., **171**, 918-933.e20.

Ye, Q.; Rosenberg, S. C.; Moeller, A.; Speir, J. A.; Su, T. Y.; Corbett, K. D., 2015: TRIP13 is a protein-remodeling AAA+ ATPase that catalyzes MAD2 conformation switching. *eLife*., **2015**, 1–44.

Ye, Q.; Kim, D. H.; Dereli, I.; Rosenberg, S. C.; Hagemann, G.; Herzog, F.; Tóth, A.; Cleveland, D. W.; Corbett, K. D., 2017: The AAA + ATP ase TRIP 13 remodels HORMA domains through N-terminal engagement and unfolding . *The EMBO Journal*., **36**, 2419–2434.

Yuan, J.; Eckerdt, F.; Bereiter-Hahn, J.; Kurunci-Csacsko, E.; Kaufmann, M.; Strebhardt, K., 2002: Cooperative phosphorylation including the activity of polo-like kinase 1 regulates the subcellular localization of cyclin B1. *Oncogene*., **21**, 8282–8292.

Yuan, W. C.; Lee, Y. R.; Lin, S. Y.; Chang, L. Y.; Tan, Y. P.; Hung, C. C.; Kuo, J. C.; Liu, C. H.; Lin, M. Y.; Xu, M.; Chen, Z. J.; Chen, R. H., 2014: K33-Linked Polyubiquitination of Coronin 7 by Cul3-KLHL20 Ubiquitin E3 Ligase Regulates Protein Trafficking. *Molecular Cell*., **54**, 586–600.

Zee, B. M.; Garcia, B. A., 2012: Discovery of lysine post-translational modifications through mass spectrometric detection. (Scott, I., Ed.)*Essays in Biochemistry*., **52**, 147–163.

Zhang, S.; Chang, L.; Alfieri, C.; Zhang, Z.; Yang, J.; Maslen, S.; Skehel, M.; Barford, D., 2016: Molecular mechanism of APC/C activation by mitotic phosphorylation. *Nature*., **533**, 260–264.

Zhang, S.; Tischer, T.; Barford, D., 2019: Cyclin A2 degradation during the spindle assembly checkpoint requires multiple binding modes to the APC/C. *Nature Communications*., **10**.

Zheng, N.; Shabek, N., 2017: Ubiquitin ligases: Structure, function, and regulation. *Annual Review of Biochemistry*., **86**, 129–157.

Zhou, Z.; He, M.; Shah, A. A.; Wan, Y., 2016: Insights into APC/C: From cellular function to diseases and therapeutics. *Cell Division*., **11**, 1–18.

Zielke, N.; Querings, S.; Grosskortenhaus, R.; Reis, T.; Sprenger, F., 2006: Molecular dissection of the APC/C inhibitor Rca1 shows a novel F-box-dependent function. *EMBO reports*., **7**, 1266–1272.

Zielke, N., 2006: *Functional analysis of the cell cycle regulator Rca1 in Drosophila melanogaster*. University Köln.

Zielke, N.; Querings, S.; Rottig, C.; Lehner, C.; Sprenger, F., 2008: The anaphase-promoting complex/cyclosome (APC/C) is required for rereplication control in endoreplication cycles. *Genes and Development*., **22**, 1690–1703.

Zielke, N.; Korzelius, J.; Straaten, M. Van; Bender, K.; Schuhknecht, G. F. P.; Dutta, D.; Xiang, J.; Edgar, B. A., 2014: Resource Fly-FUCCI : A Versatile Tool for Studying Cell Proliferation in Complex Tissues, **1**.

Zur, A.; Brandeis, M., 2001: Securin degradation is mediated by fzy and fzr, and is required for complete chromatid separation but not for cytokinesis. *EMBO Journal*., **20**, 792–801.

11. Supplements

11.1. Origin macros

11.1.1. Macro: “all in one macro 43”

```
/////////all-in-one-2018-11-21
page.active$ = "BG";
fpprot = 2;
getn (which is your protein of interest?) fpprot
   (select protein of interest(POI);
;
for CHE as POI (GFP as reference protein) type 3;
;
for GFP as POI (CHE as reference protein) type 1;
;
if you have only CHE, select GFP(1) as POI;
if you have only GPF, select CHE(3) as POI);
cell(1,3)=fpprot;
fp=fpprot;
switch (fp)
   case 1:
      type -b "Your protein of interest is GFP-tagged";
      break;
   case 3:
      type -b "Your protein of interest is CHE-tagged";
      break;
   case 2:
      type -b "Your have not indicated if you are using a CHE or GFP tagged protein, press escape to exit and insert a 1 or 3 in sheeet BG third column";
      wcellcolor (3[4]) color(yellow);
      break;
                              sec -w 30;
                              default:
  }
wcellcolor (3[6]) color(orange);
type -b "This is the all-in-one macro /n wait for the o.k.popup to continue (5-10 min)";
////rr is the number of entries
page.active$ = "all";
ss = wks.ncols;
rr=ss/3;
tt=rr+1;
uu=ss+1;
////duplicate FL2 column for later xIndex function
for (ww = 1; ww<tt; ww++)
{
wks.addCol(x$(ww))
}
hh=4;
for (ww = 1; ww<tt; ww++)
{
range ra = col(x$(ww));
/////ra.index: set column index, places the empty columns in every 4th column
ra.index = $(hh);
hh=hh+4;
}
ss = wks.ncols;
uu=ss+1;
for (ww = 2; ww<uu; ww++)
{
hh=ww+2;
////copy DNA columns;
copydata                irng:=[data]all!col($(ww))
orng:=[data]all!col($(hh))[1];
ww=ww+3;
}
////set FL1 (1) or FL3(as X (type 4);
if (fp == 1)  fx=3;
else fx=1;
///xxx
ss = wks.ncols;
for (ww = fx; ww<ss; ww++)
{
wks.col = ww;
wks.col.type=4;
ww=ww+3;
}
/////sorted by FL (Column 2, 5, etc.) descending and include Column 1(c1)-3(c2)etc.
page.active$ ="all";
if (fp == 1) xx = 3;
 else xx=1;
 for (ii = 1, jj = xx, kk = 4; ii<uu; ii++)
 {
wsort descending:=0 bycol:=$(jj) c1:=$(ii) c2:=$(kk);
ii=ii+3;
jj=jj+4;
kk=kk+4;
}
/////find Background levels: CHE
page.active$ = "all";
wsort descending:=0 bycol:=3 c1:=1 c2:=4;
get col(3) -e numpoints1;
int bba =numpoints1*99.5/100;
range BGCHE = [data]all!col(3)[$(bba)];
range BGCHE1 = [data]BG!col(1)[2];
BGCHE1 = BGCHE;
page.active$ = "BG";
cc= cell(2,1);
dd=cc*5/100+cc;
cell(5,1)=dd;
/////find Background levels: GFP
page.active$ = "all";
//sorted by FL1  (Column 1) descending and include Column 1(c1)-4(c2)etc.
wsort descending:=0 bycol:=1 c1:=1 c2:=4;
get col(1) -e numpoints2;
int bba =numpoints2*99.5/100;
range BGGFP = [data]all!col(1)[$(bba)];
range BGGFP1 = [data]BG!col(2)[2];
BGGFP1 = BGGFP;
page.active$ = "BG";
cc= cell(2,2);
dd=cc*5/100+cc;
cell(5,2)=dd;
/////sorted by FL (Column 2, 5, etc.) descending and include Column 1(c1)-3(c2)etc.
page.active$ ="all";
if (fp == 1) xx = 3;
 else xx=1;
 wsort descending:=0 bycol:=$(xx) c1:=1 c2:=4;
page.active$ = "BG";
wcellcolor (3[7]) color(orange);
////////////////////////////////////////////////////////////////////////////////////
type -a "Sort positive and negative cells";
///rr is the number of entries
page.active$ = "all";
ss = wks.ncols;
rr=ss/4;
tt=rr+1;
uu=ss+1;
page.active$ ="pos";
wks.ncols = rr*3;
/////////Get background, positive and max  levels, for GPF-tagged (fp=1) this will be the first column (CHE-levels), for CHE-tagged, column 2
if (fp == 1)  fx=1;
else fx=2;
///get the background level
range daback = [data]BG!col($(fx))[2];
///get the positive level
range dbpos = [data]BG!col($(fx))[5];
///get the max level
range dcmax = [data]BG!col($(fx))[8];
////sort-code
page.active$ = "all";
aa=1;
bb=2;
cc=3;
dd=1;
ee=2;
ff=3;
gg=1;
/////////GFP or CHE
if (fp == 1)  hh=4;
else hh=2;
uu=rr*4+1;
for (ww = 1; ww<uu; ww++)
{
get col($(ww)) -e endcol;
range rb = [data]all!col($(hh));
mm=xindex($(dbpos),rb);
nn=xindex($(dcmax),rb);
copydata      irng:=[data]all!col($(aa))[$(mm):$(nn)]
orng:=[data]pos!col($(dd))[1];
copydata      irng:=[data]all!col($(bb))[$(mm):$(nn)]
orng:=[data]pos!col($(ee))[1];
copydata           irng:=[data]all!col($(bb))[1:$(mm)]
orng:=[data]neg!col($(gg))[1];
copydata      irng:=[data]all!col($(cc))[$(mm):$(nn)]
orng:=[data]pos!col($(ff))[1];
aa=aa+4;
bb=bb+4;
cc=cc+4;
dd=dd+3;
ee=ee+3;
ff=ff+3;
ww=ww+3;
hh=hh+4;
gg=gg+1;
}
page.active$ = "pos";
hh=1;
for (ww = 1; ww<tt; ww++)
{
wks.col = hh;
wks.col.comment$ = "$(ww)";
wks.col.lname$ = "$(ww)-FL1";
hh=hh+1;
wks.col = hh;
wks.col.comment$ = "$(ww)";
wks.col.lname$ = "$(ww)-FL2";
wks.col.type=4;
hh=hh+1;
wks.col = hh;
wks.col.comment$ = "$(ww)";
wks.col.lname$ = "$(ww)-FL3";
hh=hh+1;
}
page.active$ = "neg";
hh=1;
for (ww = 1; ww<tt; ww++)
{
wks.col = hh;
wks.col.comment$ = "$(ww)";
wks.col.lname$ = "$(ww)-FL2";
hh=hh+1;
}
page.active$ = "BG";
wcellcolor (3[8]) color(orange);
////////////////////////////////////////////////////////////////////////////////////
type -a "This will determine the transfecton rate: number of positive cells (in sheet pos) compared to all cells (in sheet all) \n it will then calculate DNA-frequencies and will give suggestions for for G1, S and G2";
type -a "Be patient, this will take up to 5 minutes to complete /n but you will get a very good estimations of G1 and G2 peaks";
///nothing to change for CHE to GFP
///rr is the number of entries
page.active$ = "pos";
ss = wks.ncols;
rr=ss/3;
tt=rr+1;
page.active$ ="all";
///cell number from sheet all
kk=1;
uu=rr*4;
```

```
for (ii = 1; ii<uu; ii++)
{
int dd=count(col($(ii)),1);
range ab=[data]all1!Col(Txrateall)[kk];
ab=dd;
ii=ii+3;
kk=kk+1;
}
page.active$ ="pos";
//positive cells
//loop through the different FL2 colums (start=2 then add 3 (ii+2 plus one ii (ii++)
//count number of entries, place into sheet all1
kk=1;
for (ii = 2;  ii<ss;  ii++)
{
int dd=count(col($(ii)),1);
range ab=[data]all1!Col(Txratepos)[kk];
ab=dd;
ii=ii+2;
kk=kk+1;
}
type -a "Calculate transfection effiency";
///sets (reset) the calculation of the transfection effiency
page.active$ = "all1";
csetvalue col:=[data]all1!col(Txratio) formula:="Col(Txratepos)*100/Col(Txrateall)";
page.active$ = "all1";
range txrate = [data]all1!col(Txratio)[2:12];
da1 = mean(txrate);
db1=da1*25/100;
ddc1=da1-db1;
wcellsel rng:=txrate cond:=le val:=ddc1;
wcellcolor c:=color(red);
///////type -b "Next it will calculate DNA-frequencies and will give estimates for G1, S and G2";
page.active$ = "neg";
ss = wks.ncols;
uu=ss+1;
page.active$ = "negDNAfreq2";
for (ii = ss; ii>0; ii--)
{
type -a "Calculates cell cycle distribution of negative cells";
range rng = [data]neg!Col($(ii));
stats rng;
int n = stats.n;
double dX;
dX = 200;
double scale = n*dX;
double dw;
dw = kernelwidth(rng);
col($(uu)) = ksdensity(wcol(1), rng, dw) * scale;
uu=uu-1;
}
page.active$ = "negDNAfreq2";
wks.col1.lname$ = "HOECHST";
wks.col1.type=4;
for (ii = 2; ii<=uu; ii++)
{
wks.col$(ii).format=1;
ll=ii-1;
wks.col$(ii).lname$ = "DNA$(ll)";
}
page.active$ = "neg";
ss = wks.ncols;
uu=ss+1;
type -a "finds G1 and G2 maximal values";
page.active$ = "negDNAfreq2";
for (ii = 2; ii<=uu; ii++)
{
mmG1 = list(max(col($(ii))[1:290]),col($(ii)));
mmG100=mmG1+mmg1/2;
mmG100r=round(mmG100,0);
mmG2 = list(max(col($(ii))[mmG100r:900]),col($(ii)));
mmS1 = list(min(col($(ii))[$(mmG1):$(mmG2)]),col($(ii)));
kk=ii-1;
mmG1=;
range rG1 = col(1)[$(mmG1)];
range rG1n = negDNA!col($(kk))[1];
rG1n=round(rG1,0);
mmS1=;
range rS1 = col(1)[$(mmS1)];
range rS1n = negDNA!col($(kk))[2];
rS1n=round(rS1,0);
mmG2=;
range rG2 = col(1)[$(mmG2)];
range rG2n = negDNA!col($(kk))[3];
rG2n=round(rG2,0);
}
type -a "draws curves";
for (ii = 1; ii<tt; ii++)
{
page.active$ = "negDNA";
range G1 = [data]negDNA!col(DNA$(ii))[1];
range S = [data]negDNA!col(DNA$(ii))[2];
range G2 = [data]negDNA!col(DNA$(ii))[3];
page.active$ = "negDNAfreq2";
ll=ii+1;
dd=max(col($(ll)));
ee=dd+dd*0.1;
window -a DNA$(ii);
layer.y.from = 0;
layer.y.to = $(ee);
layer.x.from = 400;
layer.x.to = 3000;
addline value:=$(G1) format:=.0 name:="lineG1";
addline value:=$(S) format:=.0 name:="lineS";
addline value:=$(G2) format:=.0 name:="lineG2";
window -ch 1;
}
page.active$ = "negDNA";
sec -w 10;
page.active$ = "neg";
aa=wks.maxRows;
////////wks.deleteRows(1, $(aa));
page.active$ = "negDNA";
window -s ctn;
wcellcolor (2[8]) color(orange);
wcellcolor (3[8]) color(orange);
////////////////////////////////////////////////////////////////////////////////////
type -a "This will split your positive cells into cell cycle stages according to your set limits for G1, S and G2 \n be patient an wait for next message";
////nothing to change for CHE to GFP
type -a "step-1: determine number of entries and set number of columns";
page.active$ = "pos";
ss = wks.ncols;
rr=ss/3;
tt=rr+1;
page.active$ ="G1";
wks.ncols = rr*3;
page.active$ ="S";
wks.ncols = rr*3;
page.active$ ="G2";
wks.ncols = rr*3;
type -a "step-2: sort positive cells by FL2";
uu=ss+1;
page.active$ = "pos";
for (ii = 1, jj = 2, kk = 3; ii<uu; ii++)
{
//sorted by FL2 (Column 2, 5, etc.) descending and include Column 1(c1)-3(c2)etc.
wsort descending:=0 bycol:=$(jj) c1:=$(ii) c2:=$(kk);
ii=ii+2;
jj=jj+3;
kk=kk+3;
}
type -a "step-3: Get G1, S , G2 (DNA) values";
page.active$ = "pos";
gg=1;
hh=1;
for (ww = 2; ww<ss; ww++)
{
//Read the values from the negDNA sheet
range pG1 = [data]negDNA!col(DNA$(hh))[1];
range pS = [data]negDNA!col(DNA$(hh))[2];
range pG2 = [data]negDNA!col(DNA$(hh))[3];
//Set Range for G1: 300 minus peak, S: 300 around button, G2: 500 after peak
da = pG1-300;
db = pG1;
dc = pS-200;
dd = pS+100;
de = pG2;
df = pG2+500;
type -a "step-4: Split positive cells into G1, S and G2 -$(hh)";
type -a "step-4: Split positive cells into G1 $(hh)";
//G1-code
get col($(ww)) -e numpoints;
for(ll = 1 ; ll <= numpoints ; ll++)
{
  if (Col($(ww))[ll] > da)  break;
}
for(mm = ll ; mm <= numpoints ; mm++)
{
  if (Col($(ww))[mm] > db)  break;
}
op=mm;
if (op >= numpoints)  mm=numpoints;
op=ll;
if (op >= numpoints)  ll=numpoints;
copydata  irng:=[data]pos!col($(gg))[$(ll):$(mm)] orng:=[data]G1!col($(gg))[1];
gg=gg+1;
copydata  irng:=[data]pos!col($(gg))[$(ll):$(mm)] orng:=[data]G1!col($(gg))[1];
gg=gg+1;
copydata  irng:=[data]pos!col($(gg))[$(ll):$(mm)] orng:=[data]G1!col($(gg))[1];
gg=gg+1;
type -a "step-4: Split positive cells into S-$(hh)";
//S-code
for(ll = mm ; ll <= numpoints ; ll++)
{
  if (Col($(ww))[ll] > dc)  break;
}
for(mm = ll ; mm <= numpoints ; mm++)
{
  if (Col($(ww))[mm] > dd)  break;
}
op=mm;
if (op >= numpoints)  mm=numpoints;
op=ll;
if (op >= numpoints)  ll=numpoints;
//gg variable needs to be reset by 3
gg=gg-3;
copydata  irng:=[data]pos!col($(gg))[$(ll):$(mm)] orng:=[data]S!col($(gg));
gg=gg+1;
copydata  irng:=[data]pos!col($(gg))[$(ll):$(mm)] orng:=[data]S!col($(gg));
gg=gg+1;
copydata  irng:=[data]pos!col($(gg))[$(ll):$(mm)] orng:=[data]S!col($(gg));
gg=gg+1;
type -a "step-4: Split positive cells into G2-$(hh)";
//G2-code
for(ll = mm ; ll <= numpoints ; ll++)
{
  if (Col($(ww))[ll] > de)  break;
}
for(mm = ll ; mm <= numpoints ; mm++)
{
  if (Col($(ww))[mm] > df)  break;
}
op=mm;
if (op >= numpoints)  mm=numpoints;
op=ll;
if (op >= numpoints)  ll=numpoints;
gg=gg-3;
copydata  irng:=[data]pos!col($(gg))[$(ll):$(mm)] orng:=[data]G2!col($(gg))[1];
gg=gg+1;
copydata  irng:=[data]pos!col($(gg))[$(ll):$(mm)] orng:=[data]G2!col($(gg))[1];
gg=gg+1;
copydata  irng:=[data]pos!col($(gg))[$(ll):$(mm)] orng:=[data]G2!col($(gg))[1];
gg=gg+1;
ww=ww+2;
hh=hh+1;
}
type -a "step-5: delete missing values from pos-Columns";
uu=ss+1;
```

```
for (ii = 1,; ii<uu; ii++)
{
wxt "col($(ii))[i]==0/0" c1:=$(ii) c2:=$(ii) sel:=1;
menu -e 36442;
type -a "step-5: delete missing values-$(ii)";
}
type -a "step-6: sort G1 and G2 negative cells";
page.active$ = "neg";
for (ii = 1; ii<tt; ii++)
 {
wsort descending:=0 bycol:=$(ii) c1:=$(ii) c2:=$(ii);
}
page.active$ ="G1neg";
wks.ncols = rr;
page.active$ ="G2neg";
wks.ncols = rr;
page.active$ ="Sneg";
wks.ncols = rr;
///Set DNA-limits
gg=1;
hh=1;
for (ww = 1; ww<tt; ww++)
{
//Read the values from the negDNA sheet
type -a "step-6 sort negative cells-$(hh)";
range pG1 = [data]negDNA!col(DNA$(hh))[1];
range pS = [data]negDNA!col(DNA$(hh))[2];
range pG2 = [data]negDNA!col(DNA$(hh))[3];
//Set Range for G1: 200 minus peak, S: 200 around
button, G2: 300 after peak
da = pG1-200;
db = pG1;
dc = pS-100;
dd = pS+100;
de = pG2;
df = pG2+300;
page.active$ = "neg";
//G1-code
type -a "step-6: sort negative cells-G1-$(hh)";
get col($(ww)) -e numpoints;
for(ll = 1 ; ll <= numpoints ; ll++)
{
  if (Col($(ww))[ll] > da)  break;
}
for(mm = ll ; mm <= numpoints ; mm++)
{
  if (Col($(ww))[mm] > db)  break;
}
copydata      irng:=[data]neg!col($(gg))[$(ll):$(mm)]
orng:=[data]G1neg!col($(gg))[1];
//S-code
type -a "step-6: sort negative cells S-$(hh)";
for(ll = mm ; ll <= numpoints ; ll++)
{
  if (Col($(ww))[ll] > dc)  break;
}
for(mm = ll ; mm <= numpoints ; mm++)
{
  if (Col($(ww))[mm] > dd)  break;
}
copydata      irng:=[data]neg!col($(gg))[$(ll):$(mm)]
orng:=[data]Sneg!col($(gg))[1];
//G2-code
type -a "step-6: sort negative cells G2-$(hh)";
for(ll = mm ; ll <= numpoints ; ll++)
{
  if (Col($(ww))[ll] > de)  break;
}
for(mm = ll ; mm <= numpoints ; mm++)
{
  if (Col($(ww))[mm] > df)  break;
}
copydata      irng:=[data]neg!col($(gg))[$(ll):$(mm)]
orng:=[data]G2neg!col($(gg))[1];
gg=gg+1;
hh=hh+1;
}
type -a "step-7: delete missing values from neg-col-
umns";
for (ii = 1,; ii<tt; ii++)
{
wxt "col($(ii))[i]==0/0" c1:=$(ii) c2:=$(ii) sel:=1;
menu -e 36442;
type -a "step-7: delete missing values from neg-col-
umns-$(ii)";
}
type -a "step-8: Calculate FL ratios";
type -a "step-8: Calculate FL ratios-G1";
page.active$ = "logG1";
mm=1;
for (ii = 1; ii<tt; ii++)
{
range FL1 = [data]G1!col($(mm));
kk=mm+2;
range FL3 = [data]G1!col($(kk));
if (fp == 1)  col($(ii))=log(FL1)/log(FL3);
else col($(ii))=log(FL3)/log(FL1);
mm=mm+3;
}
type -a "step-8: Calculate FL ratios-S";
page.active$ = "logS";
mm=1;
for (ii = 1; ii<tt; ii++)
{
range FL1 = [data]S!col($(mm));
kk=mm+2;
range FL3 = [data]S!col($(kk));
if (fp == 1)  col($(ii))=log(FL1)/log(FL3);
else col($(ii))=log(FL3)/log(FL1);
mm=mm+3;
}
type -a "step-8: Calculate FL ratios-G2";
page.active$ = "logG2";
mm=1;
for (ii = 1; ii<tt; ii++)
{
range FL1 = [data]G2!col($(mm));
kk=mm+2;
range FL3 = [data]G2!col($(kk));
if (fp == 1)  col($(ii))=log(FL1)/log(FL3);
else col($(ii))=log(FL3)/log(FL1);
mm=mm+3;
}
type -a "step-8: Calculate FL ratios-all-all-log";
page.active$ = "all-log";
mm=1;
for (ii = 1; ii<tt; ii++)
{
range FL1 = [data]pos!col($(mm));
kk=mm+2;
range FL3 = [data]pos!col($(kk));
if (fp == 1)  col($(ii))=log(FL1)/log(FL3);
else col($(ii))=log(FL3)/log(FL1);
mm=mm+3;
}
type -a "step-8: Calculate FL ratios-all-logall";
page.active$ = "logall";
mm=1;
vv=rr+1;
uu=rr*2+1;
for (ii = vv; ii<uu; ii++)
{
range FL1 = [data]pos!col($(mm));
kk=mm+2;
range FL3 = [data]pos!col($(kk));
if (fp == 1)  col($(ii))=log(FL1)/log(FL3);
else col($(ii))=log(FL3)/log(FL1);
mm=mm+3;
}
type -a "step-9: copy logFL (for scatter plots)";
uu=rr*3+1;
vv=rr*2+1;
mm=1;
for (ii = vv; ii<uu; ii++)
{
range FL1 = [data]pos!col($(mm));
mm=mm+2;
range FL3 = [data]pos!col($(mm));
mm=mm+1;
if (fp == 1)
                col($(ii))=log(FL3);
else
                col($(ii))=log(FL1);
}
type -a "step-10: copy the DNA-columns into sheet
logall (for scatter plots)";
page.active$ = "pos";
kk=1;
uu=rr*3+2;
for (ii = 2; ii<uu; ii++)
{
copydata                irng:=[data]pos!col($(ii))
orng:=[data]logall!col($(kk));
kk=kk+1;
ii=ii+2;
}
type -a "step-11: determine G1/G2 ratios of positive
cells";
page.active$ = "G1";
//G1-cells
kk=1;
for (ii = 2; ii<ss ; ii++)
{
int dd=count(col($(ii)),1);
range ab=[data]all1!Col(G1)[kk];
ab=dd;
kk=kk+1;
ii=ii+2;
}
//G2-cells
page.active$ = "G2";
kk=1;
for (ii = 2; ii<ss ; ii++)
{
int dd=count(col($(ii)),1);
range ab=[data]all1!Col(G2)[kk];
ab=dd;
kk=kk+1;
ii=ii+2;
}
//S-cells
page.active$ = "S";
kk=1;
for (ii = 2; ii<ss ; ii++)
{
int dd=count(col($(ii)),1);
range ab=[data]all1!Col(S)[kk];
ab=dd;
kk=kk+1;
ii=ii+2;
}
type -a "step-12: determine G1/G2 ratios of nega-
tive cells";
page.active$ = "G1neg";
//G1-cells
kk=16;
for (ii = 1; ii<tt ; ii++)
{
int dd=count(col($(ii)),1);
range ab=[data]all1!Col(G1)[kk];
ab=dd;
kk=kk+1;
}
//G2-cells
page.active$ = "G2neg";
kk=16;
for (ii = 1; ii<tt ; ii++)
{
int dd=count(col($(ii)),1);
range ab=[data]all1!Col(G2)[kk];
ab=dd;
kk=kk+1;
}
//S-cells
page.active$ = "Sneg";
kk=16;
for (ii = 1; ii<tt ; ii++)
{
int dd=count(col($(ii)),1);
range ab=[data]all1!Col(S)[kk];
ab=dd;
kk=kk+1;
}
page.active$ = "all1";
csetvalue      col:=[data]all1!col(G1G2ratio)      for-
mula:="Col(G1)/Col(G2)";
type -a "step-18: Determine the log frequencies of
FL1/FL3";
type -a "step-18: Determine the log frequencies of
FL1/FL3-G2";
page.active$ = "logG2";
```

```
for (ii = rr; ii>0; ii--)
{
freqcounts irng:=col($(ii)) inc:=0.01 freq:=0 bin:=ends min:=0 max:=1.3 cumulcount:=0 center:=0 rd:=G2freq!col($(ii));
}
//////////////rename and format
page.active$ = "G2freq";
if (fp == 1) wks.col1.lname$ = "FL1/FL3";
else wks.col1.lname$ = "FL3/FL1";
wks.col1.type=4;
//clear comment in all columns
for (int nn = 1; nn <= wks.ncols; nn++) { wcol(nn)[C]$=""; }
uu=rr+2;
for (ii = 2; ii<uu; ii++)
{
wks.col$(ii).format=1;
ll=ii-1;
wks.col$(ii).lname$ = "G2$(ll)";
}
type -a "step-18: Determine the log frequencies of FL1/FL3-S";
page.active$ = "logS";
for (ii = rr; ii>0; ii--)
{
freqcounts irng:=col($(ii)) inc:=0.01 freq:=0 bin:=ends min:=0 max:=1.3 cumulcount:=0 center:=0 rd:=Sfreq!col($(ii));
}
page.active$ = "Sfreq";
if (fp == 1) wks.col1.lname$ = "FL1/FL3";
else wks.col1.lname$ = "FL3/FL1";
wks.col1.type=4;
for (int nn = 1; nn <= wks.ncols; nn++) { wcol(nn)[C]$=""; }
for (ii = 2; ii<uu; ii++)
{
wks.col$(ii).format=1;
ll=ii-1;
wks.col$(ii).lname$ = "S$(ll)";
}
type -a "step-18: Determine the log frequencies of FL1/FL3-all";
page.active$ = "logall";
kk=rr;
uu=rr*2;
vv=rr-1;
for (ii = uu; ii>vv; ii--)
{
freqcounts irng:=col($(ii)) inc:=0.01 freq:=0 bin:=ends min:=0 max:=1.3 cumulcount:=0 center:=0 rd:=allfreq!col($(kk));
kk=kk-1;
}
page.active$ = "allfreq";
if (fp == 1) wks.col1.lname$ = "FL1/FL3";
else wks.col1.lname$ = "FL3/FL1";
wks.col1.type=4;
for (int nn = 1; nn <= wks.ncols; nn++) { wcol(nn)[C]$=""; }
for (ii = 2; ii<tt; ii++)
{
wks.col$(ii).format=1;
ll=ii-1;
wks.col$(ii).lname$ = "G1$(ll)";
}
type -a "step-18: Determine the log frequencies of FL1/FL3-G1";
page.active$ = "logG1";
for (ii = rr; ii>0; ii--)
{
freqcounts irng:=col($(ii)) inc:=0.01 freq:=0 bin:=ends min:=0 max:=1.3 cumulcount:=0 center:=0 rd:=G1freq!col($(ii));
}
page.active$ = "G1freq";
if (fp == 1) wks.col1.lname$ = "FL1/FL3";
else wks.col1.lname$ = "FL3/FL1";
wks.col1.type=4;
for (int nn = 1; nn <= wks.ncols; nn++) { wcol(nn)[C]$=""; }
for (ii = 2; ii<tt; ii++)
{
wks.col$(ii).format=1;
ll=ii-1;
wks.col$(ii).lname$ = "G1$(ll)";
}

type -a "step-19: Determine maximal frequencie values";
uu=rr+2;
page.active$ = "G2freq";
for (ii = 2; ii<uu; ii++)
{
///finds maximal value in frequency count and places into all1
mm = list(max(col($(ii))),col($(ii)));
range r1 = col(1)[$(mm)];
kk=ii-1;
range r2 = all1!col(logG2)[$(kk)];
r2=r1;
}
page.active$ = "G1freq";
for (ii = 2; ii<uu; ii++)
{
mm = list(max(col($(ii))),col($(ii)));
range r1 = col(1)[$(mm)];
kk=ii-1;
range r2 = all1!col(logG1)[$(kk)];
r2=r1;
}
page.active$ = "Sfreq";
for (ii = 2; ii<uu; ii++)
{
mm = list(max(col($(ii))),col($(ii)));
range r1 = col(1)[$(mm)];
kk=ii-1;
range r2 = all1!col(logS)[$(kk)];
r2=r1;
}
page.active$ = "allfreq";
for (ii = 2; ii<uu; ii++)
{
mm = list(max(col($(ii))),col($(ii)));
range r1 = col(1)[$(mm)];
kk=ii-1;
range r2 = all1!col(logall)[$(kk)];
r2=r1;
}
if (fp == 1) type -a "step-20: determine cell cycle profile of the GFP positive cells";
else type -a "step-20: determine cell cycle profile of the CHE positive cells";
type -a "step-20: sort";
page.active$ ="pos";
uu=rr*3+1;
if (fp == 1)
{
for (ii = 1, jj = 1, kk = 3; ii<uu; ii++)
{
wsort descending:=0 bycol:=$(jj) c1:=$(ii) c2:=$(kk);
ii=ii+2;
jj=jj+3;
kk=kk+3;
type -a "sort by GFP";
}
}
else
{
for (ii = 1, jj = 3, kk = 3; ii<uu; ii++)
{
wsort descending:=0 bycol:=$(jj) c1:=$(ii) c2:=$(kk);
ii=ii+2;
jj=jj+3;
kk=kk+3;
type -a "sort by CHE";
}
}
type -a "step-21: get BG-level";
////get the background level
page.active$ ="BG";
if (fp == 1)
bgd=cell(2,1);
else
bgd=cell(2,2);
type -a "step-22: determine cell cycle profile of positive cells-search through the values";
page.active$ ="pos";
kk=2;
uu=rr*3+1;
if (fp == 3)
{
for (ii = 3; ii<uu; ii++)
{
get col($(ii)) -e numpoints;
for(ll = 1 ; ll < numpoints ; ll++)
{
  if (Col($(ii))[ll] > bgd) break;
}
ii=ii-1;
copydata
irng:=[data]pos!col($(ii))[$(ll):$(numpoints)]
orng:=[data]DNA!col($(kk));
ii=ii+3;
kk=kk+1;
}
}
else type -a "GFP-tagged";
kk=2;
if (fp == 1)
{
for (ii = 1; ii<uu; ii++)
{
get col($(ii)) -e numpoints;
for(ll = 1 ; ll < numpoints ; ll++)
{
  if (Col($(ii))[ll] > bgd) break;
}
ii=ii+1;
copydata
irng:=[data]pos!col($(ii))[$(ll):$(numpoints)]
orng:=[data]DNA!col($(kk));
ii=ii+1;
kk=kk+1;
}
}
else type -a "CHE-tagged";
page.active$ = "logall";
kk=1;
uu=rr+1;
vv=rr*2+1;
for (ii = uu; ii<vv; ii++)
{
wks.col = ii;
if (fp == 1) wks.col.lname$ = "FL1FL3";
else wks.col.lname$ = "FL3FL1";
if (fp == 1) wks.col.comment$ = "$(kk)-FL1/FL3";
else wks.col.comment$ = "$(kk)-FL3/FL1";
kk=kk+1;
}
kk=1;
for (ii = 1; ii<tt; ii++)
{
wks.col = ii;
wks.col.type=4;
wks.col.lname$ = "DNA";
if (fp == 1) wks.col.comment$ = "$(kk)-DNA-CHE-pos";
else wks.col.comment$ = "$(kk)-DNA-GFP-pos";
kk=kk+1;
}
kk=1;
uu=rr*3+1;
for (ii = vv; ii<uu; ii++)
{
wks.col = ii;
wks.col.lname$ = "FL1";
wks.col.comment$ = "$(kk)-FL1";
kk=kk+1;
}
page.active$ = "logG1";
for (ii = 1; ii<tt; ii++)
{
wks.col = ii;
if (fp == 1) wks.col.comment$ = "FL1/FL3";
else wks.col.comment$ = "FL3/FL1";
}
page.active$ = "logG2";
for (ii = 1; ii<tt; ii++)
{
wks.col = ii;
```

```
if (fp == 1)  wks.col.comment$ = "FL1/FL3";
else wks.col.comment$ = "FL3/FL1";
}
page.active$ = "logS";
for (ii = 1; ii<tt; ii++)
{
wks.col = ii;
if (fp == 1)   wks.col.comment$ = "FL1/FL3";
else wks.col.comment$ = "FL3/FL1";
}
page.active$ = "all-log";
for (ii = 1; ii<tt; ii++)
{
wks.col = ii;
if (fp == 1)   wks.col.comment$ = "FL1/FL3";
else wks.col.comment$ = "FL3/FL1";
}
page.active$ = "allfreq";
wks.col = 1;
wks.col.comment$ = "freqFLs";
kk=1;
uu=tt+1;
for (ii = 2; ii<uu; ii++)
{
wks.col = ii;
wks.col.comment$ = "$(kk)";
kk=kk+1;
}
page.active$ = "G1freq";
wks.col = 1;
wks.col.comment$ = "freqFLs";
kk=1;
for (ii = 2; ii<uu; ii++)
{
wks.col = ii;
wks.col.comment$ = "$(kk)";
kk=kk+1;
}
page.active$ = "G2freq";
wks.col = 1;
wks.col.comment$ = "freqFLs";
kk=1;
for (ii = 2; ii<uu; ii++)
{
wks.col = ii;
wks.col.comment$ = "$(kk)";
kk=kk+1;
}
page.active$ = "Sfreq";
wks.col = 1;
wks.col.comment$ = "freqFLs";
kk=1;
for (ii = 2; ii<uu; ii++)
{
wks.col = ii;
wks.col.comment$ = "$(kk)";
kk=kk+1;
}
page.active$ = "all1";
type -a "step-27: find cells in background";
page.active$ = "pos";
ss = wks.ncols;
rr=ss/3;
tt=rr+1;
uu=rr*3+1;
/////This will take the background level in sheet BG
\nand will check how many positive cells have value
at or below this background level";
//Determine how many data points, ss in number of
columns in page pos, rr is the number of entries;
page.active$ = "pos";
ss = wks.ncols;
rr=ss/3;
tt=rr+1;
uu=rr*3+1;
//background-level
page.active$ = "BG";
if (fp==1) bg = cell(2,2);
else bg = cell(2,1);
bg=bg+0.01;
if (fp==1) bb=1;
else bb=3;
//G1
page.active$ = "G1";
for (ii = 1, jj = $(bb); ii<tt && jj<uu; ii++)
{
get col($(jj)) -e np;
range ab=[data]all1!Col(G1-BGA)[ii];
ab=np;
range rFL3=$(jj);
string strCond$="rFL3<$(bg)";
wxt test:=strCond$  num:=nExtRows;
range ab=[data]all1!Col(G1B)[ii];
ab=nExtRows;
  jj=jj+3;
}

//G2
page.active$ = "G2";
for (ii = 1, jj = $(bb) ; ii<tt && jj<uu; ii++)
{
get col($(jj)) -e np;
range ab=[data]all1!Col(G2BGA)[ii];
ab=np;
range rFL3=$(jj);
string strCond$="rFL3<$(bg)";
wxt test:=strCond$  num:=nExtRows;
range ab=[data]all1!Col(G2B)[ii];
ab=nExtRows;
  jj=jj+3;
}
//S
page.active$ = "S";
for (ii = 1, jj = $(bb) ; ii<tt && jj<uu; ii++)
{
get col($(jj)) -e np;
range ab=[data]all1!Col(SBGA)[ii];
ab=np;
range rFL3=$(jj);
string strCond$="rFL3<$(bg)";
wxt test:=strCond$  num:=nExtRows;
range ab=[data]all1!Col(SB)[ii];
ab=nExtRows;
  jj=jj+3;
}
//all
page.active$ = "pos";
for (ii = 1, jj = $(bb) ; ii<tt && jj<uu; ii++)
{
get col($(jj)) -e np;
range ab=[data]all1!Col(allBGA)[ii];
ab=np;
range rFL3=$(jj);
string strCond$="rFL3<$(bg)";
wxt test:=strCond$  num:=nExtRows;
range ab=[data]all1!Col(allB)[ii];
ab=nExtRows;
jj=jj+3;
}
page.active$ = "all1";
csetvalue col:=[data]all1!col(allPer) for-
mula:="Col(allB)*100/Col(allBGA)";
csetvalue col:=[data]all1!col(G1Per) for-
mula:="Col(G1B)*100/Col(G1BGA)";
csetvalue col:=[data]all1!col(SPer) for-
mula:="Col(SB)*100/Col(SBGA)";
csetvalue col:=[data]all1!col(G2Per) for-
mula:="Col(G2B)*100/Col(G2BGA)";
csetvalue col:=[data]all1!col(G1G2) for-
mula:="Col(G1)+Col(G2)";
////////////////////////////////////////////////////
////////////////////////////////////////////////////
//////////////////
page.active$ ="BG";
wcellcolor (3[5]:[10]) color(white);
page.active$ = "all1";
page.active$ = "pos";
ss = wks.ncols;
rr=ss/3;
tt=rr+1;
type -a "step-28: Box Plots";
page.active$ = "logG1";
for (ii = 1,; ii<tt; ii++)
{
wxt "col($(ii))[i]==0/0" c1:=$(ii) c2:=$(ii) sel:=1;
menu -e 36442;
}
kk=4;
oo=18;
for (ii = 1; ii<tt; ii++)
{
aa=mean(Col($(ii)));
[data]Boxes!Cell($(kk),2)=aa;
bb=count(Col($(ii)));
[data]Boxes!Cell($(oo),2)=bb;
kk=kk+1;
oo=oo+1;
}
window -a BoxG1;
layer.y.from = 0;
layer.y.to = 1.5;
layer.x.from = 0.5;
layer.x.to = 12.9;
if (fp == 1)  label -y1l log(FL1) / log(FL3);
else label -y1l log(FL3) / log(FL1);
legendbox box:=0 whisker:=0 mdl:=0 mean:=1;
window -ch 1;
////////////////////////////////////////////////////
///S
page.active$ = "logS";
for (ii = 1,; ii<tt; ii++)
{
wxt "col($(ii))[i]==0/0" c1:=$(ii) c2:=$(ii) sel:=1;
//Delete rows with no values
menu -e 36442;
}
kk=4;
oo=18;
for (ii = 1; ii<tt; ii++)
{
aa=mean(Col($(ii)));
[data]Boxes!Cell($(kk),3)=aa;
bb=count(Col($(ii)));
[data]Boxes!Cell($(oo),3)=bb;
kk=kk+1;
oo=oo+1;
}
window -a BoxS;
layer.y.from = 0;
layer.y.to = 1.5;
layer.x.from = 0.5;
layer.x.to = 12.9;
if (fp == 1)  label -y1l log(FL1) / log(FL3);
else label -y1l log(FL3) / log(FL1);
legendbox box:=0 whisker:=0 mdl:=0 mean:=1;
window -ch 1;
////////////////////////////////////////////////////
///G2
page.active$ = "logG2";
for (ii = 1,; ii<tt; ii++)
{
wxt "col($(ii))[i]==0/0" c1:=$(ii) c2:=$(ii) sel:=1;
//Delete rows with no values
menu -e 36442;
}
kk=4;
oo=18;
for (ii = 1; ii<tt; ii++)
{
aa=mean(Col($(ii)));
[data]Boxes!Cell($(kk),4)=aa;
bb=count(Col($(ii)));
[data]Boxes!Cell($(oo),4)=bb;
kk=kk+1;
oo=oo+1;
}
window -a BoxG2;
layer.y.from = 0;
layer.y.to = 1.5;
layer.x.from = 0.5;
layer.x.to = 12.9;
if (fp == 1)  label -y1l log(FL1) / log(FL3);
else label -y1l log(FL3) / log(FL1);
legendbox box:=0 whisker:=0 mdl:=0 mean:=1;
window -ch 1;
////////////////////////////////////////////////////
///all
page.active$ = "all-log";
for (ii = 1,; ii<tt; ii++)
{
wxt "col($(ii))[i]==0/0" c1:=$(ii) c2:=$(ii) sel:=1;
//Delete rows with no values
```

```
menu -e 36442;
}
kk=4;
oo=18;
for (ii = 1; ii<tt; ii++)
{
aa=mean(Col($(ii)));
[data]Boxes!Cell($(kk),5)=aa;
bb=count(Col($(ii)));
[data]Boxes!Cell($(oo),5)=bb;
kk=kk+1;
oo=oo+1;
}
window -a Boxall;
layer.y.from = 0;
layer.y.to = 1.5;
layer.x.from = 0.5;
layer.x.to = 12.9;
if (fp == 1)  label -y1l log(FL1) / log(FL3);
else label -y1l log(FL3) / log(FL1);
legendbox box:=0 whisker:=0 mdl:=0 mean:=1;
window -ch 1;
page.active$ = "Boxes";
sec -p 5;
win -a data;
page.active$ = "neg";
ss = wks.ncols;
page.active$ = "BG";
cell(20,3)=ss;
//////////FLxFLy
type -a "FLxFLy";
win -a data;
page.active$ = "BG";
fp= cell(1,3);
ss = cell(20,3);
uu=ss*2;
tt=ss*2;
win -a data;
newsheet name:=FLxFLy cols:=uu;
wks.index = 4;
page.active$ = "FLxFLy";
mm=1;
nn=1;
for (ii = 1; ii<tt; ii++)
{
range FL1 = [data]pos!col($(mm));
kk=mm+2;
range FL3 = [data]pos!col($(kk));
if (fp == 1)  col($(ii))=log(FL3);
else col($(ii))=log(FL1);
wks.col = ii;
if (fp == 1) wks.col.lname$ = "$(nn)-logFL3";
else wks.col.lname$ = "$(nn)-FL1";
wks.col.type=4;
ii=ii+1;
if (fp == 1)  col($(ii))=log(FL1);
else col($(ii))=log(FL3);
wks.col = ii;
if (fp == 1) wks.col.lname$ = "$(nn)-logFL1";
else wks.col.lname$ = "$(nn)-FL3";
wks.col.type=1;
mm=mm+3;
nn=nn+1;
}
layer -d "DNA";
layer -d "G1neg";
layer -d "Sneg";
layer -d "G2neg";
page.active$ = "BG";
////////////////////////////////////////////////////////
//////////////////////////////////
//////////G1
/////tt is the number of entries
win -a data;
page.active$ = "pos";
tt = wks.ncols;
ss=tt/3;
page.active$ = "BG";
cell(20,3)=ss;
sminus=ss-1;
mm=ss*2+5;
newbook name:="curves" sheet:=1 option:=lsname;
newsheet name:=G1align cols:=1;
newsheet name:=freqs cols:=46;
win -a "curves";
page.active$ = "freqs";
wks.nCols = wks.nCols + tt;
colcopy irng:=[data]BG!Col(5) orng:=[curves]freqs!Col($(mm));
win -a "curves";
page.active$ = "freqs";
wks.nCols = wks.nCols + tt;
///////positive cells
kk=1;
for (ii = 5; ii<tt; ii++)
{
range rng = [data]pos!Col($(ii));
stats rng;
int n = stats.n;
double dX;
dX = 200;
double scale = n*dX;
double dw;
dw = kernelwidth(rng);
col($(kk)) = ksdensity(wcol($(mm)), rng, dw) * scale;
kk=kk+2;
ii=ii+2;
}
///column number where values are put
tt=ss*2-1;
urow=tt+3;
rr=1;
///find maximum number G1-range
range g1ra = [data]negDNA!Col(DNA1)[1];
g1rangestart=mmg1-100;
g1rangestop=mmg1+100;
for (ii = 1; ii<tt; ii++)
{
dd = list(max(col($(ii))[$(g1rangestart) : $(g1rangestop)]),col($(ii)));
cell($(rr),$(urow))= dd;
dd=;
max1=cell($(dd), $(ii));
cell($(rr),$(tt))=max1;
ii=ii+1;
rr=rr+1;
}
///rows
uu=ss-1;
///column number with max values in rows
vv=tt+1;
/////find maximum number in row
dd = list(max(col($(tt))[1:$(uu)]),col($(tt)));
dd=;
max1=cell($(dd), $(tt));
cell(1,$(vv))=max1;
ww=vv+1;
for (ii = 1; ii<ss; ii++)
{
cell($(ii),$(ww))=cell($(ii),$(tt))/cell(1,vv);
}
ll=1;
tt=ss*2-1;
for (ii = 1; ii<tt; ii++)
{
kk=ii+1;
xx=cell($(ll), $(ww));
xx=;
csetvalue col:=[curves]freqs!col($(kk)) formula:="Col($(ii))/ xx";
ii=ii+1;
ll=ll+1;
}
for (ii = 1; ii<tt; ii++)
{
wks.col$(ii).digitMode=1;
wks.col$(ii).digits=0;
}
win -a "curves";
page.active$ = "freqs";
////////////////////////////////////////////////////////
////////////////////////////////////////////
urow=ss*2+2;
urowplus=urow+1;
dd = list(max(col($(urow))[1:$(sminus)]),col($(urow)));
dd=;
ee = list(min(col($(urow))[1:$(sminus)]),col($(urow)));
ee=;
max1=cell($(dd), $(urow));
cell(1,$(urowplus))=max1;
min1=cell($(ee), $(urow));
cell(2,$(urowplus))=min1;
urowplusplus=urowplus+1;
for (ll = 1; ll<ss; ll++)
{
cell($(ll),$(urowplusplus))=cell(1,$(urowplus))-cell($(ll),$(urow));
}
//////////////////realign
oo=2;
pp=urowplusplus+2;
for (ll = 1; ll<ss; ll++)
{
nn=cell($(ll),$(urowplusplus));
nn=;
for (ii = 1000; ii>0; ii--)
{
mm=ii+nn;
cell($(mm),$(pp))=cell($(ii),$(oo));
}
oo=oo+2;
pp=pp+1;
}
for (ii = urowplus; ii<pp; ii++)
{
wks.col$(ii).digitMode=1;
wks.col$(ii).digits=0;
}
win -a "curves";
page.active$ = "G1align";
mm=ss*2+5;
nn=mm+ss;
tt=ss+1;
colcopy irng:=[curves]freqs!Col($(mm)):Col($(nn)) orng:=[curves]G1align!Col(1);
for (ii = 2; ii<tt; ii++)
{
wks.col$(ii).lname$ = Pos-$(ii);
}
win -a data;
page.active$ = "BG";
cell(20,3)=ss;
sminus=ss-1;
mm=ss*2+5;
splusplus=ss+2;
win -a "curves";
newsheet name:=negfreqs cols:=46;
page.active$ = "negfreqs";
///////negative cells
kk=1;
for (ii = 3; ii<splusplus; ii++)
{
kk=;
colcopy irng:=[data]negDNAfreq2!Col($(ii)) orng:=[curves]negfreqs!Col($(kk));
kk=kk+2;
}
///column number where values are put
tt=ss*2-1;
urow=tt+3;
rr=1;
///find maximum number G1-range
for (ii = 1; ii<tt; ii++)
{
dd = list(max(col($(ii))[1:223]),col($(ii)));
cell($(rr),$(urow))=dd;
dd=;
max1=cell($(dd), $(ii));
cell($(rr),$(tt))=max1;
ii=ii+1;
rr=rr+1;
}
///rows
uu=ss-1;
///column number with max values in rows
vv=tt+1;
/////find maximum number in row
dd = list(max(col($(tt))[1:$(uu)]),col($(tt)));
dd=;
```

```
max1=cell($(dd), $(tt));
cell(1,$(vv))=max1;
ww=vv+1;
for (ii = 1; ii<ss; ii++)
{
cell($(ii),$(ww))=cell($(ii),$(tt))/cell(1,vv);
}
ll=1;
tt=ss*2-1;
for (ii = 1; ii<tt; ii++)
{
kk=ii+1;
xx=cell($(ll), $(ww));
xx=;
csetvalue col:=[curves]negfreqs!col($(kk)) formula:="Col($(ii))/ xx";
ii=ii+1;
ll=ll+1;
}
for (ii = 1; ii<tt; ii++)
{
wks.col$(ii).digitMode=1;
wks.col$(ii).digits=0;
}
urow=ss*2+2;
urowplus=urow+1;
dd = list(max(col($(urow))[1:$(sminus)]),col($(urow)));
dd=;
ee = list(min(col($(urow))[1:$(sminus)]),col($(urow)));
ee=;
max1=cell($(dd), $(urow));
cell(1,$(urowplus))=max1;
min1=cell($(ee), $(urow));
cell(2,$(urowplus))=min1;
urowplusplus=urowplus+1;
for (ll = 1; ll<ss; ll++)
{
cell($(ll),$(urowplusplus))=cell(1,$(urowplus))-cell($(ll),$(urow));
}
//////////////////realign
oo=2;
pp=urowplusplus+2;
for (ll = 1; ll<ss; ll++)
{
nn=cell($(ll),$(urowplusplus));
nn=;
for (ii = 1000; ii>0; ii--)
{
mm=ii+nn;
cell($(mm),$(pp))=cell($(ii),$(oo));
}
oo=oo+2;
pp=pp+1;
}
mm=2*sminus+7;
colcopy irng:=[data]negDNAfreq2!Col(1) orng:=[curves]negfreqs!Col($(mm));
win -a "curves";
newsheet name:=freqs2 cols:=46;
colcopy irng:=[curves]freqs!Col(1):Col($(mm)) orng:=[curves]freqs2!Col(1);
pp=mm-1;
colcopy irng:=[curves]negfreqs!Col($(pp)) orng:=[curves]freqs2!Col($(pp));
//////////////////realign
oo=2;
pp=urowplusplus+2;
for (ll = 1; ll<ss; ll++)
{
nn=cell($(ll),$(urowplusplus));
nn=;
for (ii = 1000; ii>0; ii--)
{
mm=ii+nn;
cell($(mm),$(pp))=cell($(ii),$(oo));
}
oo=oo+2;
pp=pp+1;
}
for (ii = urowplus; ii<pp; ii++)
{
wks.col$(ii).digitMode=1;
wks.col$(ii).digits=0;
}
win -a "curves";
newsheet name:=G1align_base_neg cols:=13;
page.active$ = "G1align_base_neg";
mm=ss*2+5;
nn=mm+ss;
tt=ss+1;
colcopy irng:=[curves]freqs2!Col($(mm)):Col($(nn)) orng:=[curves]G1align_base_neg!Col(1);
for (ii = 2; ii<tt; ii++)
{
wks.col$(ii).lname$ = Pos-$(ii);
}
////////////////////////////////////
type -a "copy FLx/FLy columns for G1, S and G2";
type -a "sorted by cell cycle stage for Box-Plots";
type -a " into new Sheet CCBoxes";
tt = ss+1;
ww=ss-1;
uu=ww*3;
win -a curves;
newsheet name:=CCBoxes cols:=uu;
nn=1;
for (ii = 2; ii<=ss; ii++)
{
copydata irng:=[data]logG1!col($(ii)) orng:=[curves]CCBoxes!col($(nn));
nn=nn+1;
}
for (ii = 2; ii<=ss; ii++)
{
copydata irng:=[data]logS!col($(ii)) orng:=[curves]CCBoxes!col($(nn));
nn=nn+1;
}
for (ii = 2; ii<=ss; ii++)
{
copydata irng:=[data]logG2!col($(ii)) orng:=[curves]CCBoxes!col($(nn));
nn=nn+1;
}
type -a " 200";
page.active$ = "CCBoxes";
mm=2;
for (ii = 1; ii<ss; ii++)
{
wks.col = ii;
wks.col.lname$ = "$(mm)-G1";
if (fp == 1)  wks.col.comment$ = "FL1/FL3";
else wks.col.comment$ = "FL3/FL1";
mm=mm+1;
}
type -a " 212";
uu=ss*2-1;
mm=2;
for (ii = ss; ii<uu; ii++)
{
wks.col = ii;
wks.col.lname$ = "$(mm)-S";
if (fp == 1)  wks.col.comment$ = "FL1/FL3";
else wks.col.comment$ = "FL3/FL1";
mm=mm+1;
}
type -a " 224";
vv=ss*3-2;
mm=2;
uu=ss*2-1;
for (ii = uu; ii<vv; ii++)
{
wks.col = ii;
wks.col.lname$ = "$(mm)-G2";
if (fp == 1)  wks.col.comment$ = "FL1/FL3";
else wks.col.comment$ = "FL3/FL1";
mm=mm+1;
}
range st= [data]BG!Col(3)[20:20];
st = ss;
tt=ss+1;
plotxy [curves]G1align_base_neg!2 plot:=200 ogl:=<new template:=curves-all>;
page.longname$= "DNA-curves";
for(ii = 3 ; ii <tt ; ii++)
{
plotxy [curves]G1align_base_neg!$(ii) plot:=200 rescale:=1 color:=ii ogl:=!1;
}
layer.y.from = 0;
layer.x.from = 450;
layer.x.to = 3500;
label -xl Hoechst;
label -yl number of cells;
win -a data;
page.active$ ="BG";
fp=col(C)[1];
/////sorted by FL  (Column 2, 5, etc.) descending and include Column 1(c1)-3(c2)etc.
page.active$ ="pos";
ss = wks.ncols;
uu=ss+1;
if (fp == 1) xx = 1;
 else xx=3;
 for (ii = 1, jj = xx, kk = 3; ii<uu; ii++)
 {
wsort descending:=0 bycol:=$(jj) c1:=$(ii) c2:=$(kk);
ii=ii+2;
jj=jj+3;
kk=kk+3;
}
page.active$ ="BG";
if (fp == 1) xc = col(2)[5];
 else xc = col(1)[5];

page.active$ ="CHE-GFP-posDNA";
pp=uu*2;
wks.ncols = pp;
page.active$ ="pos";
tt = wks.ncols+1;
gg=2;
for (ww = xx; ww<tt; ww++)
{
get col($(ww)) -e numpoints;
for(ll = 1 ; ll <= numpoints ; ll++)
{
  if (Col($(ww))[ll] > xc)  break;
}
ww=;
if (fp == 1) vv = ww+1;
 else vv = ww-1;

mm=ll;
copydata irng:=[data]pos!col($(vv))[mm:numpoints] orng:=[data]CHE-GFP-posDNA!col($(gg))[1];
gg=gg+1;
ww=ww+2;
numpoints=;
ll=;
mm=;
}
colcopy irng:=[data]BG!Col(5) orng:=[data]CHE-GFP-posDNA!Col(1);
page.active$ ="BG";
xe = col(3)[20];
xee=xe+1;
xf=xe+2;
xg=xf;
page.active$ = "CHE-GFP-posDNA";
for (ii = 2; ii<xf; ii++)
{
type -a "Calculates cell cycle distribution";
ii=;
range rng = [data]CHE-GFP-posDNA!Col($(ii));
stats rng;
int n = stats.n;
double dX;
dX = 200;
double scale = n*dX;
double dw;
dw = kernelwidth(rng);
col($(xg)) = ksdensity(wcol(1), rng, dw) * scale;
xg=xg+1;
}
win -a data;
page.active$ ="BG";
numexp=col(C)[20];
tt = numexp *2-1;
```

```
tt=;
win -a curves;
newsheet name:="GFPCHEfreqs" cols:=tt;
mm=1;
nn=numexp+3;
for(ll = 2 ; ll <= tt; ll++)
{
  colcopy irng:=[curves]freqs2!Col($(mm)) orng:=[data]DNAfreqs!Col($(ll));
  ll=ll+1;
  colcopy irng:=[data]CHE-GFP-posDNA!Col($(nn)) orng:=[data]DNAfreqs!Col($(ll));

mm=mm+2;
nn=nn+1;
}
win -a data;
page.active$ ="BG";
fp=col(C)[1];
if (fp == 3) POI$="-GFPpos";
 else POI$="-CHEpos";

 if (fp == 3) RP$="-CHEpos";
 else RP$="-GFPpos";

page.active$ ="all";
ss = wks.ncols;
uu=ss+1;


kk=2;
ll=3;
for (ii = 5; ii<uu; ii++)
 {

range r1 = [data]all!col($(ii)); // Point to the source column
range r2 = [data]DNAfreqs!col($(kk)); // Point to the target column
range r3 = [data]DNAfreqs!col($(ll)); // Point to the target column
r2[L]$ = r1[L]$; // Copy the LongName
strln1$=r1[C]$;
strln2$=strln1.left(2)$ + POI$;
strln2$=;
strln3$=strln1.left(2)$ + RP$;
r2[L]$ = strln2$;
r3[L]$ = strln3$;
r2[C]$ = strln2$;
r3[C]$ = strln3$;
ii=ii+3;
kk=kk+2;
ll=ll+2;
}
win -a data;
page.active$ ="BG";
numexp=col(C)[20];
tt = numexp+1;
for (ii = 2; ii<tt; ii++)
{
page.active$ = "DNAfreqs";
window -a $(ii)-DNAs;
Rescale;
layer.y.from = 0;
layer.x.from = 650;
layer.x.to = 3500;
label -xl Hoechst;
label -yl number of cells;
window -ch 1;
}
type -b "o.k. All done-save your project as....";
```

11.1.2. Macro: “Analyze different cell cycle populations”

```
// First, declare the variables to be used:
string ccphases$="G1, S, G2 or pos";
getn
(G1, S, G2 or pos) ccphases$
(Select which cell cycle phase to analyze);
win -a data;
page.active$ = "%(ccphases$)";
ss = wks.ncols;
rr=ss/3;
tt=rr+1;
page.active$ = "BG";
fp= cell(1,3);
//////new book
newbook name:=exlevels%(ccphases$) sheet:=1 option:=1;
exlevels$=page.name$;
win -a %(exlevels$);
newsheet name:=FLs cols:=$(ww);
for (ii = 1; ii<tt; ii++)
{
newsheet name:=s0$(ii) cols:=1;
}
//////get FLs and perform FLx/FLy
mm=1;
for (ii = 1; ii<tt; ii++)
{
range FL1 = [data]%(ccphases$)!col($(mm));
range logFL1 = [%(exlevels$)]FLs!col($(mm));
logFL1 = log(FL1);
mm=mm+3;
}
mm=3;
for (ii = 1; ii<tt; ii++)
{
range FL3 = [data]%(ccphases$)!col($(mm));
range logFL3 = [%(exlevels$)]FLs!col($(mm));
logFL3 = log(FL3);
mm=mm+3;
}
mm=1;
kk=3;
ll=2;
for (ii = 1; ii<tt; ii++)
{
range logFL1 = [%(exlevels$)]FLs!col($(mm));
range logFL3 = [%(exlevels$)]FLs!col($(kk));
range logFLxFLy = [%(exlevels$)]FLs!col($(ll));
if (fp == 1)  logFLxFLy = logFL1/logFL3;
else logFLxFLy = logFL3/logFL1;
mm=mm+3;
kk=kk+3;
ll=ll+3;
}
page.active$ = "Fls";
uu=rr*3+1;
kk=3;
if (fp == 1)  jj=3;
else jj=1;
for (ii = 1; ii<uu; ii++)
{
//sort by FLx (Column 1, 1, etc.) acending and include Column 1(c1)-3(c2)etc.
wsort descending:=0 bycol:=$(jj) c1:=$(ii) c2:=$(kk);
ii=ii+2;
jj=jj+3;
kk=kk+3;
}
aa = 0.5;
ab = 0.75;
if (fp == 1)  qq=3;
else qq=1;
rb=1;
for(ds = 1; ds<tt; ds++)
{
aa = 0.5;
ab = 0.75;
uu=1;
op=1;
for(ww = 1 ; ww < 16 ; ww++)
{
page.active$ = "FLs";
get col($(qq)) -e numpoints;
for(ll = op ; ll <= numpoints ; ll++)
{
  if (Col($(qq))[ll] > aa)  break;
}
for(mm = ll ; mm <= numpoints ; mm++)
{
  if (Col($(qq))[mm] > ab)  break;
}
op=mm;
op=;
if (mm == ll)
{ll=1;
mm=1;}
//////if (op >= numpoints )  break;
copydata
irng:=[%(exlevels$)]FLs!col($(rb))[$(ll):$(mm)]
orng:=[%(exlevels$)]s0$(ds)!col($(uu))[1];
uu=uu+1;
rb=rb+1;
copydata
irng:=[%(exlevels$)]FLs!col($(rb))[$(ll):$(mm)]
orng:=[%(exlevels$)]s0$(ds)!col($(uu))[1];
uu=uu+1;
rb=rb+1;
copydata
irng:=[%(exlevels$)]FLs!col($(rb))[$(ll):$(mm)]
orng:=[%(exlevels$)]s0$(ds)!col($(uu))[1];
uu=uu+1;
rb=rb-2;
aa=aa+0.25;
ab=ab+0.25;
}
qq=qq+3;
rb=rb+3;
}
for (jj = 1; jj<tt; jj++)
{
aa = 0.5;
ab = 0.75;
page.active$ = "s0$(jj)";
sr = wks.ncols;
for (ii = 1; ii<=sr; ii++)
{
wks.col = ii;
wks.col.lname$ = "logFL1";
ii=ii+1;
wks.col = ii;
wks.col.lname$ = "$(aa)-$(ab)";
if (fp == 1)  wks.col.comment$ = "FL1/FL3";
else wks.col.comment$ = "FL3/FL1";
ii=ii+1;
wks.col = ii;
wks.col.lname$ = "logFL3";
aa=aa+0.25;
ab=ab+0.25;
}
}
win -a data;
page.active$ = "%(ccphases$)";
ss = wks.ncols;
rr=ss/3;
tt=rr+1;
win -a %(exlevels$);
if (fp == 1)  qw=3;
else qw=1;
qp=1;
qr=2;
qs=2;
for(ll = 1; ll < tt ; ll++)
{
copydata irng:=[%(exlevels$)]FLs!col($(qw)) orng:=[%(exlevels$)]Sheet1!col($(qp));
copydata irng:=[%(exlevels$)]FLs!col($(qr)) orng:=[%(exlevels$)]Sheet1!col($(qs));
qw=qw+3;
qp=qp+2;
qr=qr+3;
qs=qs+2;
}
page.active$ = "Sheet1";
uu=rr*2;
mm=1;
for(ll = 1; ll <= uu ; ll++)
{
wks.col = ll;
if (fp == 1)  wks.col.comment$ = "$(mm)-FL3";
```

```
else wks.col.comment$ = "$(mm)-FL1";
wks.col$(ll).type = 4;
ll=ll+1;
wks.col = ll;
if (fp == 1)  wks.col.comment$ = "$(mm)-FL3/FL1";
else wks.col.comment$ = "$(mm)-FL1/FL3";
wks.col$(ll).type =1;
mm=mm+1;
}
type -a "185";
for (ii = 1; ii<tt; ii++)
{
newsheet name:=sFL0$(ii) cols:=1;
page.active$ = "s0$(ii)";
st = wks.ncols;
rt = st/3;
ru = rt+1;
dg=2;
ia=1;
for (ia = 1; ia<ru; ia++)
{
colcopy irng:=[%(exlevels$)]s0$(ii)!col($(dg))
orng:=[%(exlevels$)]sFL0$(ii)!col($(ia)) data:=1 for-
mat:=1 lname:=1 units:=1 comments:=1;
dg=dg+3;
}
}
page.active$ = "FLs";
mm=1;
sr = wks.ncols;
for (ii = 1; ii<sr; ii++)
{
wks.col = ii;
wks.col.lname$ = "logFL1";
ii=ii+1;
wks.col = ii;
wks.col.lname$ = "$(mm)";
if (fp == 1)  wks.col.comment$ = "FL1/FL3";
else wks.col.comment$ = "FL3/FL1";
ii=ii+1;
wks.col = ii;
wks.col.lname$ = "logFL3";
mm=mm+1;
}
newsheet name:=FL3FL1 cols:=24;
uu=(rr*3);
co=2;
for (ia = 1; ia<=uu; ia++)
{
colcopy irng:=[%(exlevels$)]FLs!col($(ia))
orng:=[%(exlevels$)]FL3FL1!col($(co)) data:=1 for-
mat:=1 lname:=1 units:=1 comments:=1;
ia=ia+2;
co=co-1;
colcopy irng:=[%(exlevels$)]FLs!col($(ia))
orng:=[%(exlevels$)]FL3FL1!col($(co)) data:=1 for-
mat:=1 lname:=1 units:=1 comments:=1;
co=co+3;
}
mm=1;
sr = wks.ncols;
for(ll = 1; ll <= sr ; ll++)
{
wks.col = ll;
wks.col$(ll).type = 4;
wks.col.comment$ = "$(mm)";
ll=ll+1;
wks.col$(ll).type = 1;
mm=mm+1;
}
for (ii = 1; ii<tt; ii++)
{
page.active$ = "sFL0$(ii)";
st = wks.ncols;
ru = st+1;
ia=1;
for (ia = 1; ia<ru; ia++)
{
wks.col = ia;
get col($(ia)) -e np;
wks.col.unit$ = $(np);
}
}
for (ii = 1; ii<tt; ii++)
{
layer -d "s0$(ii)";
}
layer -d "FLs";
page.active$ = "Sheet1";
wks.name$ = "FLx_FLxFLY";
newsheet name:= "number-cells" cols:=13;
page.active$ = "number-cells";
aa = 0.5;
ab = 0.75;
for (kk = 1; kk<15; kk++)
{
string sh$="$(aa)" + "-" + "$(ab)";
Cell($(kk),1)$=sh$;
aa=aa+0.25;
ab=ab+0.25;
}
for (ii = 1; ii<tt; ii++)
{
page.active$ = "sFL0$(ii)";
st = wks.ncols;
ru = st+1;
ia=1;
for (ia = 1; ia<ru; ia++)
{
wks.col = ia;
get col($(ia)) -e np;
wks.col.unit$ = $(np);
mm=ii+1;
range rc1 = number-cells!Col($(mm))[$(ia)];
rc1=np;
}
}
page.active$ = "sFL02";
type -b "O.K. have fun analyzing your data";
```

11.1.3. Macro: “Select expression level range”

```
// First, declare the variables to be used:
type -b "look at the name of the sheet with the ex-
pressio level range. It might look like this. Exlevel-
G4 - exlevel-G1. Select the first G-numer, for G1 you
would then need to type G4 in the next window";
string ccphases$="G1, S, G2 or pos";
double yf =  0.75;
double yt = 2;
getn
(G1, S, G2 or Pos) ccphases$
(Expression-from) yf
(Expression-to) yt
(Select which cell cycle phase and expression level
range);
win -a data;
page.active$ = "pos";
ss = wks.ncols;
rr=ss/3;
tt=rr+1;
page.active$ = "BG";
fp= cell(1,3);
win -a exlevels%(ccphases$);
newsheet name:=sel cols:=$(rr);
page.active$ = "FLx_FLxFLY";
aa = yf;
ab = yt;
qq=1;
rb=2;
ds=1;
uu=1;
for(ww = 1 ; ww < tt ; ww++)
{
page.active$ = "FLx_FLxFLY";
get col($(qq)) -e numpoints;
for(ll = 1 ; ll <= numpoints ; ll++)
{
  if (Col($(qq))[ll] > aa)  break;
}
for(mm = ll ; mm <= numpoints ; mm++)
{
  if (Col($(qq))[mm] > ab)  break;
}
if (mm == ll)
{ll=1;
mm=1;}
//////if (op >= numpoints )  break;
copydata
irng:=[exlevels%(ccphases$)]FLx_FLxFLY!col($(rb))[
$(ll):$(mm)]
orng:=[exlevels%(ccphases$)]sel!col($(uu))[1];
rb=rb+2;
uu=uu+1;
qq=qq+2;
}
page.active$ = "sel";
for(ww = 1 ; ww < tt ; ww++)
{
wks.col = ww;
wks.col.lname$ = "0$(ww)";
}
wks.name$ = "sel_$(yf)-$(yt)";
type -b "O.K. selected"
```

11.2. Supplementary Tables

Table S 1| Single and three letters for amino acids

One letter code	Three letter code	Amino acid
A	Ala	Alanine
C	Cys	Cysteine
D	Asp	Aspartate
E	Glu	Glutamate
F	Phe	Phenylalanine
G	Gly	Glycine
H	His	Histidine
I	Ile	Isoleucine
K	Lys	Lysine
L	Leu	Leucine
M	Met	Methionine
N	Asn	Asparagine
P	Pro	Proline
Q	Gln	Glutamine
R	Arg	Arginine
S	Ser	Serine
T	Thr	Threonine
V	Val	Valine
W	Trp	Tryptophan
Y	Tyr	Tyrosine

Table S 2| APC/C subunits and their structural domains

Subunit	Stoichi-ometry	Location	Domain 1	Domain2	Domain 3
Apc1	1	Scaffolding module platform	WD 40 domain	mid-N mid-C	PC domain
Apc2	1	Catalytic module	NTD cullin repeats	CTD including WHB domain	-
Apc3/ 3A	2	Scaffolding module TPR lobe	TPR dimer interface TPR motif 1-7	TPR superhelix TPR motif 8-14	-
Apc4	1	Scaffolding module platform	WD 40 domain	-	-
Apc5	1	Scaffolding module platform	NTD	TPR superhelix TPR motif 1-13	-
Apc6A/ 6B	2	Scaffolding module TPR lobe	TPR dimer interface TPR motif 1-7	TPR superhelix TPR motif 8-14	-
Apc7A/ 7B	2	Scaffolding module TPR lobe	TPR dimer interface TPR motif 1-3	TPR dimer interface TPR motif 4-7	TPR superhelix TPR motif 8-14
Apc8A/ 8B	2	Scaffolding module TPR lobe	TPR dimer interface TPR motif 1-7	TPR superhelix TPR motif 8-14	-
Apc10	1	Substrate recognition module	Doc homology	IR tail	-
Apc11	1	Catalytic module	β-strand	RING domain	-
Apc12A/ 12B	2	Scaffolding module TPR lobe	N-term extended chain, short α-helix	-	-
Apc13	1	Scaffolding module	Extended chain	-	

Subunit	Stoichi-ometry	Location	Domain 1	Domain2	Domain 3
Apc15	1	TPR lobe Scaffolding module platform	Extended chain and α-helix	-	-
Apc16	1	Scaffolding module TPR lobe	α-helix	-	-
Cdc20/ Cdh1	1	Substrate recognition module	NTD	WD40 domain	IR tial

Table based on Alfieri et al., 2017

Table S 3| Amino acid and nucleotide sequence of WT-T2A, ddT2A, and mT2A

WT T2A sequence

Glu (E)	Gly (G)	Arg (R)	Gly (G)	Ser (S)	Leu (L)	Leu (L)	Thr (T)	Cys (C)	Gly (G)	Asp (D)	Val (V)	Glu (E)	Glu (E)	Asn (N)	Pro (P)	Gly (G)	Pro (P)	Gly (G)	Ser (S)
GAA	GGA	CGC	GGC	AGC	CTA	CTG	ACT	TGC	GGA	GAT	GTC	GAA	GAG	AAC	CCT	GGC	CCT	GGT	TCC

ddT2A sequence

Glu (E)	Gly (G)	Arg (R)	Gly (G)	Ser (S)	Leu (L)	Leu (L)	Thr (T)	Cys (C)	Gly (G)	Asp (D)	Val (V)	Glu (E)	Glu (E)	Asn (N)	Pro (P)	Gly (G)	Pro (P)	Gly (G)	Ser (S)
GAA	GG**C**	CGC	GG**G**	AG**T**	CTA	CT**A**	ACT	TG**T**	GG**G**	GA**C**	GT**A**	GAA	GA**A**	AA**T**	CCT	GG**G**	CCT	GG**G**	TC**T**

mT2A sequence

Glu (E)	Gly (G)	Arg (R)	Gly (G)	Ser (S)	Leu (L)	Leu (L)	Thr (T)	Cys (C)	Gly (G)	Asp (D)	Val (V)	Glu (E)	Glu (E)	Asn (N)	Pro (P)	Ala (A)	Ala (A)	Gly (G)	Ser (S)
GAA	GGA	CGC	GGC	AGC	CTA	CTG	ACT	TGC	GGA	GAT	GTC	GAA	GAG	AAC	CCT	**GCA**	**GCC**	GGT	TCC

Table S 4| Identification of Rca1 interaction partners by mass spectrometry

Protein	Biological process (related to GO term "cell cycle")	Score	No. of peptides	SC [%]
14-3-3 epsilon	DNA damage checkpoint regulation of mitotic nuclear division mitotic cell cycle checkpoint mitotic G2 DNA damage checkpoint	1438.6	23	53.4
14-3-3 zeta	Mitotic cell cycle, embryonic	769.0	9	41.9

*SC = sequence coverage

4XFLAG-Rca1 precipitate from S2R+ cells was analyzed by LC-MS/MS. Raw MS data were searched against the Drosphila UniProtKB database. Identified proteins were restricted to proteins involved in cell cycle regulation using the gene ontology browser QuickGo (GO-term "cell cycle"/GO:0007049, releationship settings: is_a, part_of, occurs_in, regulates, positively_regulates and negatively_regulates). Data from Kies, 2017.

11.3. Supplementary Figures

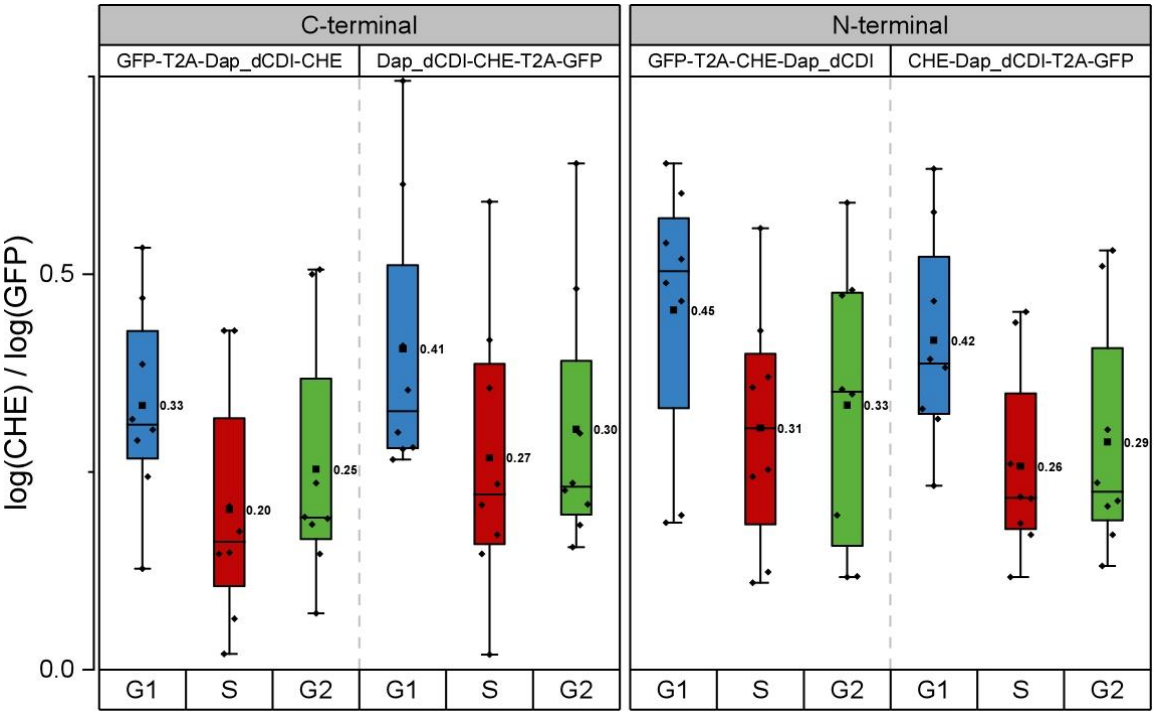

Figure S 1| Flow cytometric analysis of N- and C-terminal tagged Dap_dCDI

Comparison of N- and C-terminal reporter fusions of CycB-NT[285]. Box plot (exp.lvl. 1.0 - 1.75) summarizing the mean quantification of CHE/GFP ratios of independent replicates normalized to the RPS control values. Increase of CHE-Dap_dCDI proteins levels is detected in S-phase for all four RPS variants.

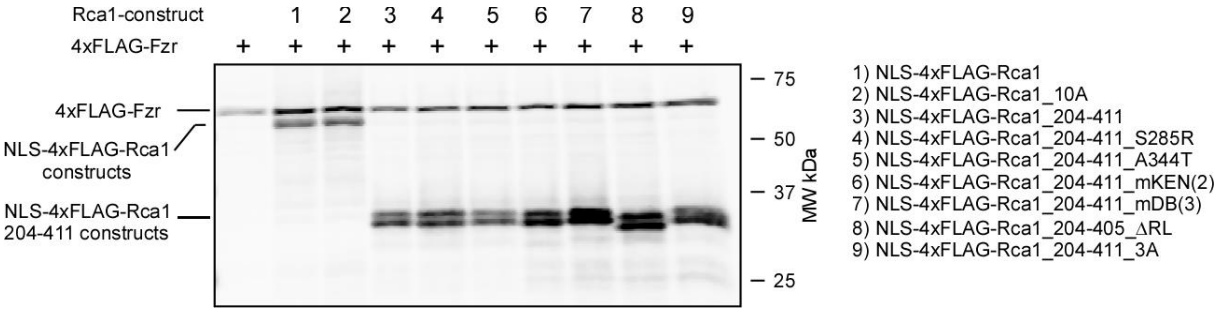

Figure S 2| Western blot of cell lysates of APC/C inhibition assay

Western blot analysis of cell lysates from APC/C activity assay. Protein expression of 4xFLAG-Fzr and NLS-4xFLAG-Rca1 was analyzed via Western blot analysis using an anti-FLAG-antibody. Protein expression after transient transfection resulted in relatively comparable amounts of the FLAG-tagged proteins.

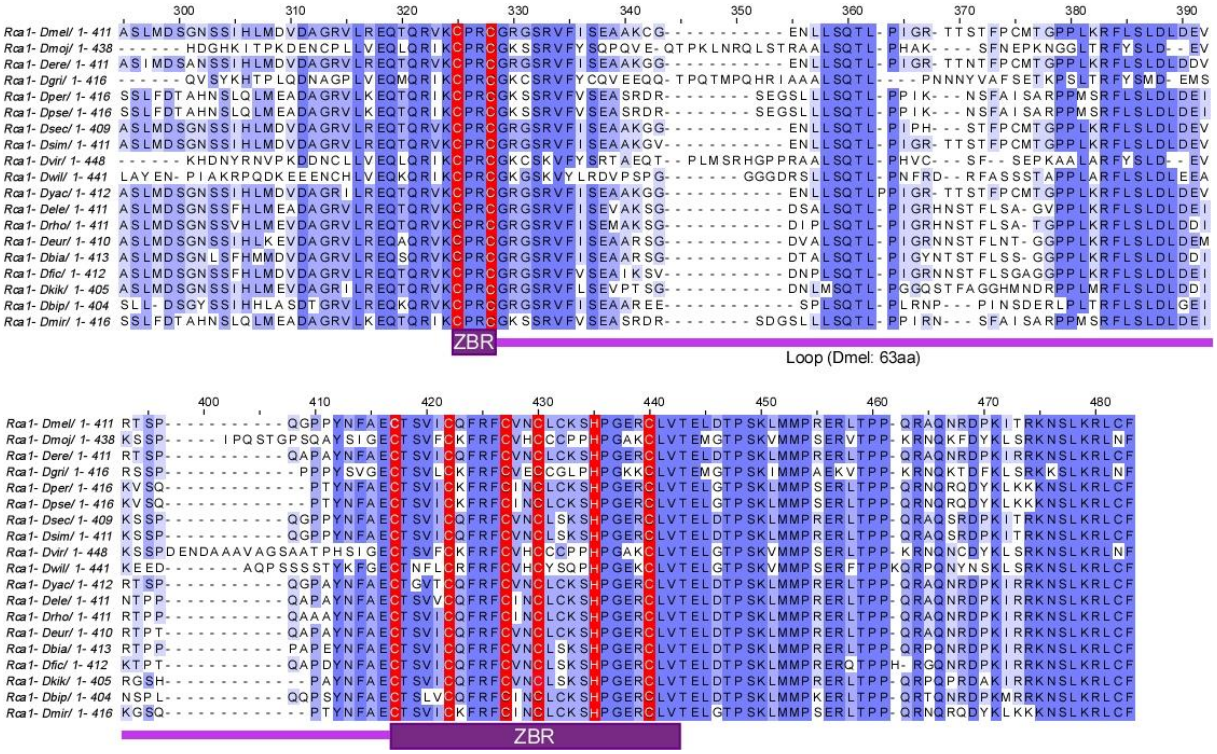

Figure S 3| Rca1 ZBR sequence alignment

Sequence alignment of Rca1 zinc binding region (ZBR) among different *Drosophila* species. The seven cysteine and the histidine residue of the C6HC IBR consensus pattern are highly conserved. Cysteine and histidine residues are highlighted in red. The first part of the ZBR containing the first two cysteine residues is separated from the second ZBR part by a 63 amino acid long loop (pink line).

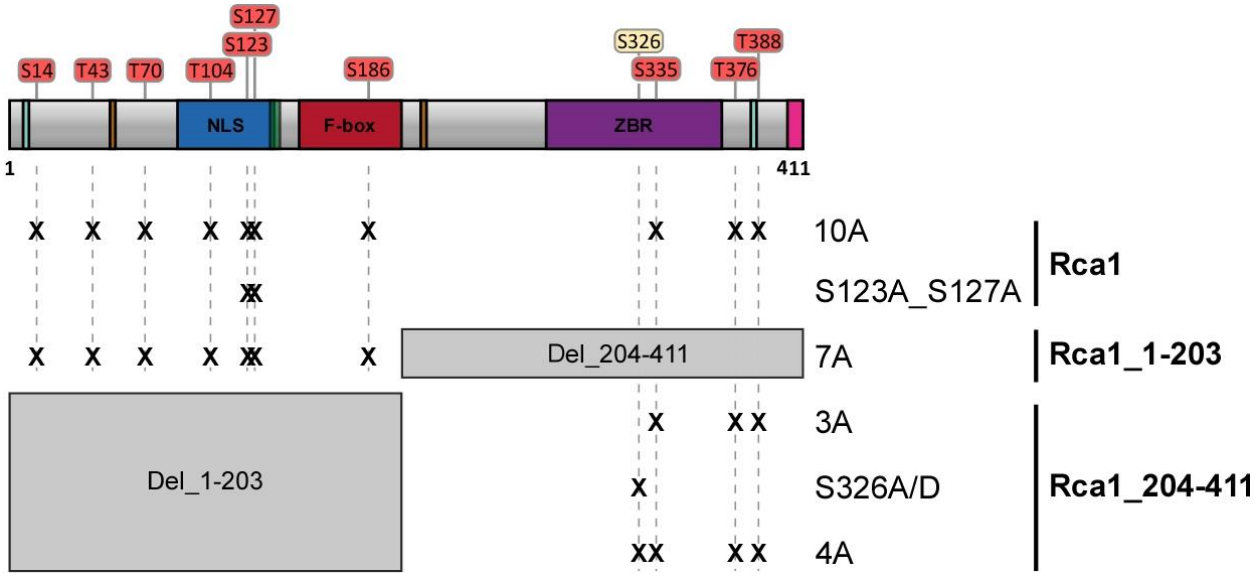

Figure S 4| Summary of Rca1 phosphorylation site mutants

Illustrtaion of the positions of the ten S/T-P Cdk phosphorylatin sites and phosphorylation site S326 in Rca1. Substitution of the amino acid residue is marked with an “x”. Deletions of Rca1 are shown by the grey boxes.

12. Zusammenfassung

Der durch E3 -Ubiquitin -Ligasen vermittelte proteolytische Abbau von Proteinen zu genau definierten Zeitpunkten ist ein zentraler Bestandteil der Regulation des Zellzyklus. Der APC/C-Komplex (Anaphase-Promoting-Complex/Cyclosome) ist verantwortlich für den strikt geregelten Abbau einer Vielfalt von regulatorischen Proteinen während der Mitose und der G1-Phase. Eine Inaktivierung des APC/C in der S- und G2-Phase, die eine erneute Akkumulierung der für die Mitose benötigten Proteine ermöglicht, erfolgt durch inhibitorische Phosphorylierung des Co-Aktivators Cdh1/Fzr und die Interaktion mit spezifischen APC/C- Inhibitoren. In *Drosophila*, fungiert das Protein „Regulator of Cyclin A1“ (Rca1) als spezifischer APC/C -Inhibitor, welches selbst während der G1-Phase abgebaut wird und somit eine vollständige Aktivierung des APC/C-Komplexes ermöglicht. Im Fokus dieser Dissertation lag es den Abbau von Rca1 in der G1-Phase, den inhibitorischen Mechanismus und die Regulation von Rca1 im Verlauf des Zellzyklus zu untersuchen. Um den Abbau von Proteinen in *Drosophila* Zellkulturzellen untersuchen zu können, wurde ein Durchflusszytometrie basierte Hochdurchsatzmethode zur Analyse von relativen Proteinstabilitäten in asynchronen Zellpopulationen etabliert. Mit dem als „Relative Protein Stability“ (RPS) System bezeichneten Verfahren konnte gezeigt werden, dass der Abbau von Rca1 in der G1-Phase dem Abbau des APC/C-Substrates Geminin ähnelt. Im weiteren Verlauf konnte aufgezeigt werden, dass die Degradation von Rca1 von der Aktivität des APC/C abhängig ist und durch spezifische APC/C-Erkennungssequenzen und einer weiteren RL-tail Domäne vermittelt wird. Somit handelt es sich bei Rca1 sowohl um einen APC/C-Inhibitor als auch -Substrat.

Im weiteren Verlauf konnten mittels eines *in vivo* APC/C- Aktivitäts-Assay mehrere für die APC/C-Inhibition notwendige C-terminale Proteindomänen identifiziert werden. Hierbei handelte es sich, ähnlich zum Vertebraten APC/C Inhibitor Emi1, unter anderem um ein KEN-box und D-box Degron, eine Zink-Binde-Region (ZBR) und eine RL-tail Domäne. Die Verwendung ähnlicher struktureller Domänen lässt auf einen vergleichbaren inhibitorischen Mechanismus für Rca1 schließen und widerspricht der bisherigen Annahme einer hauptsächlichen Inhibition als Pseudosubstrat.

Da Rca1 abhängig von der entsprechenden Phase des Zellzyklus als ein APC/C Inhibitor oder Substrat fungiert, wurden verschiedene regulatorische Mechanismen für die Funktion und den Abbau von Rca1 untersucht. Hierbei konnte gezeigt werden, dass die Phosphorylierung von Rca1 in der C-terminalen Region einen verstärkenden Effekt auf die APC/C Inhibition hat und Rca1 gleichzeitig durch N-terminale Phosphorylierung stabilisiert wird. Auch die Lokalisation von Rca1 in den Zellkern war essenziell für die Degradation von Rca1 während der G1-Phase. In weiteren Experimenten wurde eine bisher unbekannte phosphorylierungs-abhängige Interaktion mit einem 14-3-3 Protein entdeckt, die den Export von Rca1 aus dem Zellkern in das Zytoplasma verstärkt. Diese Ergebnisse geben erste Hinweise auf einen komplexen Regulationsmechanismus von Rca1, der auf synergetischen Effekten von Veränderungen der Phosphorylierung und zellulärer Lokalisation von Rca1 beruhen könnte.

13. Danksagung

Meiner erster Dank gilt meinem Doktorvater Prof. Dr. Frank Sprenger, der mir die Möglichkeit gegeben hat, meine Dissertation in seiner Arbeitsgruppe anzufertigen. Besonders möchte ich mich für die stets offene Tür, die große Hilfsbereitschaft bei Problemen und das entgegengebrachte Vertrauen bedanken, welches mir eine sehr unabhängige und freie Gestaltung meiner Doktorarbeit ermöglicht hat. Auch bei meinen Mentoren Prof. Dr. Gernot Längst und Dr. Peter Gallant möchte ich mich für ihr tolles Mentoring und die vielen konstruktiven Vorschläge bedanken.

Ein ganz besonderer Dank gilt unserer „Labormutti“ Christiane Sprenger. Neben der vielen Hilfestellungen im Labor und in der Zellkultur, möchte ich mich für die unzähligen lustigen Gespräche und deine große Anteilnahme bei jeglichen Höhen und Tiefen im Privatleben und Laboralltag bedanken. Unsere lustigen Pläuschchen werden mir sehr fehlen. Auch bei meinen Doktoranden-Kollegen Manuel Saller möchte ich mich für seine ruhige und entspannte Art bedanken, die es sehr angenehm gemacht hat mit ihm im gleichen Büro und Labor zusammenzuarbeiten. Ein weiterer Dank gilt meinen Hefe-Kolleginnen Franziska Wojciech , Simone Fabian und Lea Neumann- Arnold zwei Zimmer weiter. Es war mir immer eine Freude euch kleine Streiche zu spielen, Franzis Kaffee zu schnorren und mit euch im Büro ausgediegen zu tratschen. Ein großer Dank geht auch an meinen guten Freund und Vorgänger Matthias Kies, der mir auch nach seiner Zeit in der AG Sprenger immer mit Rat, Tat und einem Bierchen zur Seite stand. Ich werde unsere Chemie-Cafetensitzungen am Mittwoch Abend wirklich vermissen. Auch bei Phillip Girke möchte ich mich für die vielen netten Gespräche und seine große Hilfsbereitschaft bei allen Fragen, die ich ihm in den letzten 3 Jahren gestellt habe, bedanken. Der guten Seele des Lehrstuhl, Arlett Hirsch, möchte ich Danke sagen, dass Sie sich immer in Windeseile um alle Anliegen, mit denen ich mal eben zu ihr ins Sekretariat gestolpert bin, gekümmert hat. Danke auch für den guten Tipp mit dem Primitivo, das ein oder andere Glas hat mir durch die langen Abende des Schreibens geholfen.Bei Andrea Brücher möchte ich mich für die vielen dummen Sprüche, die wir uns immer liebevoll an den Kopf geworfen haben, bedanken, das hat die allgemeine Stimmung immer sehr aufgelockert. Im gleichen Zug möchte ich mich bei Antje Machetanz-Morokane, Adelheid Weissgerber und Wolfgang Mages für ihre große Hilfsbereitschaft bei allen Anliegen im Labor bedanken.Des Weiteren möchte ich mich bei den vielen StudentInnen, die während meiner Zeit am Lehrstuhl waren bedanken, die immer frischen Wind ins Labor gebracht haben: Timo Reitinger, Serena Herzinger, Tobias Potzler, Kerstin Tremmel, Andreas Schmidbauer, Jonathan Schiller, Jana Heidrich, Conradin Baumgartl und Catharina Bischof. Hierbei möchte ich mich besonders bei Kerstin für die große Hilfe mit der dsRNA, bei Catherina für die tolle Arbeit zu den Lokalisationsanalysen von Rca1 und bei Jana für die vielen Live cell imaging- Daten bedanken.

Ein Dank, der sich nur schwer in Worte fassen lässt, gilt meiner Frau Verena, die mich immer durch alle Höhen und Tiefen der letzten Jahre begleitet hat und mich nach jedem Rückschlag im Labor oder beim

Schreiben wieder aufs Neue ermutigt hat weiterzumachen. Ohne deine unfassbare Unterstützung, gerade in den letzten Monaten, wäre das alles nicht möglich gewesen. Auch bei unserem Sohn Ferdinand möchte ich mich bedanken, der mich mit seinem sonnigen Gemüt immer wieder auf den Boden der Tatsachen zurückgeholt hat und mir zeigt, was wirklich wichtig im Leben ist. Als letztes möchte ich mich noch bei meinen Eltern bedanken, die es mir erst ermöglicht haben, Biologie zu studieren und mich immer bei allen Anliegen unterstützt haben.

14. Eidesstattliche Erklärung

Ich erkläre hiermit an Eides statt, dass ich die vorliegende Arbeit ohne unzulässige Hilfe Dritter und ohne Benutzung anderer als der angegebenen Hilfsmittel angefertigt habe. Die aus anderen Quellen direkt oder indirekt übernommenen Daten und Konzepte sind unter Angabe des Literaturzitats gekennzeichnet. Die Arbeit wurde bisher weder im In- noch im Ausland in gleicher oder ähnlicher Form einer anderen Prüfungsbehörde vorgelegt. Ich versichere an Eides statt, dass ich nach bestem Wissen die reine Wahrheit gesagt und nichts verschwiegen habe.

Regensburg, den 17.03.2021

_____

Jan Polz